Examination of IpLITR-mediated control of the phagocytic process

by

Dustin Martin Ernest Lillico

A thesis submitted in partial fulfillment of the requirements for the degree of

Doctor of Philosophy
in
Physiology, Cell, and Developmental Biology

Department of Biological Sciences
University of Alberta

ABSTRACT

The ability of immune cells to perform a range of potent antimicrobial effector responses is tightly regulated by intracellular signaling events. These signals are transduced via distinct sets of membrane expressed proteins termed immunoregulatory receptors that translate extracellular cues (e.g. ligand binding) into immunological responses. Such effectors are vital for the elimination of invading microbes and the removal of cellular debris and dying cells from the body. One such effector response is the engulfment and destruction of extracellular targets such as microbes, cellular debris, and necrotic or apoptotic cells by the process known as phagocytosis. Phagocytosis evolved from a nutrient acquisition process in primitive unicellular organisms into a dynamic, complex and fundamental component of innate immunity. The ability of phagocytic cells to recognize and internalize large extracellular particulates is dependent on the expression of specialized immunoregulatory receptors on the cell surface. Phagocytic receptors relay their engagements with extracellular targets to promote filamentous (F)-actin (F-actin) polymerization events that induce dynamic remodelling and reshaping of the plasma membrane through specialized intracellular signaling events.

Channel catfish (*Ictalurus punctatus*) leukocyte immune-type receptors (IpLITRs) are a polygenic and polymorphic immunoregulatory receptor family that share basic structural and distant phylogenetic relationships with several immunoregulatory proteins within the mammalian immunoglobulin super family (IgSF). IpLITRs exist as both stimulatory and inhibitory sub-types, which regulate several innate effector responses via classical as well as unique biochemical signaling networks. The focus of my thesis was to utilize IpLITRs as a receptor

model system for better understanding the control of innate effector responses in teleost. Previously, it was demonstrated that the stimulatory IpLITR 2.6b directly associated with ITAM-encoding adaptors (e.g IpFcRγ-L) and induced cellular degranulation and phagocytosis when expressed in mammalian myeloid cell-line. Alternatively, the inhibitory receptor IpLITR 1.1b abrogated NK cell-mediated killing via SHP-dependent and SHP-independent mechanisms, which was revealed after transfection and expression in primary mouse NK cells. Since catfish myeloid cells express both stimulatory and inhibitory IpLITR types, the signaling and functional potential of IpLITR 1.1b in myeloid cells was examined and activities were compared to that of the stimulatory IpLITR 2.6b/IpFcRγ-L receptor. Surprisingly, IpLITR 1.1b when expressed in myeloid cells exhibited phagocytic activities. However, the mechanism surrounding IpLITR 1.1b's stimulatory capabilities remained unclear. Therefore, the overall objective of my thesis was on the examination of the regulatory capabilities of IpLITRs. Specifically, my research aims were; (1) to characterize the ITAM-independent phagocytic pathway facilitated by IpLITR 1.1b; (2) to confirm that the surface expression of IpLITR 1.1b was necessary for the unique target acquisition and engulfment phenotype; (3) to examine IpLITR 1.1b selective induction of F-actin dynamics; (4) to examine the recruitment of Syk and Nck during IpLITR 1.1b-induced filopodia and the capture and internalization of targets.

My research demonstrates IpLITRs can selectively activate distinct components of the phagocytic process. Specifically, I show that IpLITR 1.1b uses an alternative phagocytic pathway that is functionally distinct from the classical ITAM-mediated response. I further show trypsin selectively reduced IpLITR 1.1b cell surface expression levels and phagocytic activity. I also observed a significant alteration of the IpLITR 1.1b phagocytic phenotype post-trypsin exposure while IpLITR 2.6b//IpFcRγ-L-mediated target engulfment phenotype was unchanged,

indicating the presence of IpLITR 1.1b on the cellular surface effects the way in which cells engage in target-cell interactions through the formation of membranous protrusions. In addition, I show that during the early stages of the IpLITR 1.1b-mediated phagocytic process, filopodia-like structures retract after target contacts to secure captured microspheres to the cell surface. I identified IpLITR 1.1b endogenously colocalizes with Nck in filopodia-like plasma membrane structures and suggesting IpLITR 1.1b-Nck interactions play a pivotal role in the receptor-specific formation of filopodia. Lastly, I demonstrate IpLITR 1.1b recruits Syk and Nck to sites of bead-cell interfaces providing new mechanistic details regarding ITAM-independent phagocytosis. Overall, these results offer new insights regarding the capability of immunoregulatory receptors to initiate filopodia formation and provide new understandings into the cellular events surrounding alternative transduction dynamics that regulate F-actin polymerization and membrane remodelling events. Therefore, IpLITRs as a receptor model system serve to extend our understanding of how other vertebrate immunoregulatory receptor-types may link with intracellular signaling components to regulate effector responses such as phagocytosis.

PREFACE

This thesis is the original work by Dustin Martin Ernest Lillico. No animal ethics committee approval was required for this work as this research was completed without the use of animals.

Chapter IV of this thesis has been published in part as Dustin M. E. Lillico, Myron A. Zwozdesky, Joshua G. Pemberton, Julianna M. Deutcher, Lena O. Jones, John P. Chang, James L. Stafford., 2015. Teleost leukocyte immune-type receptors activate distinct phagocytic modes for target acquisition and engulfment. *J Leukoc Biol*. 98(2):235-248. Chapter V of this thesis has been published in part as Dustin M. E. Lillico, Joshua G. Pemberton, James L. Stafford., 2016., Trypsin Differentially Modulates the Surface Expression and Function of Channel Catfish Leukocyte Immune-Type Receptors. *Dev Comp Immunol*. 65: 231-244. Chapter VI was in part published as Dustin M. E. Lillico, Joshua G. Pemberton, James L. Stafford., 2018., Selective Regulation of Cytoskeletal Dynamics and Filopodia Formation by Teleost Leukocyte Immune-Type Receptors Differentially Contributes to Target Capture During the Phagocytic Process. *Front. Immunol*. 9; 1144.

I was responsible for the data collection and analysis, as well as manuscript writing. Dr James Stafford (supervisor) provided conceptual and technical guidance as well as help in manuscript writing. Dr. Joshua Pemberton provided conceptual and technical guidance as well as help in manuscript writing. I supervised and helped many undergraduate students; Julianna Deutcher (399 and 499 student), Rikus Niemand (298 and 499 student), Emily Sugars (298 and 498 student), Thilini Mudiyanselage (298 and 398 student), Milton Chan (499), and Sharon Rao (499 student).

ACKNOWLEDGEMENTS

I would first like to thank Dr. James Stafford. As a graduate student I could not asked for a better supervisor. Without his mentorship I do not believe I would have been able to achieve this. Not only was he a great mentor but also a great friend. I will miss all of our laughs and ridiculous conversations. I am sorry for all the headaches I know I caused, but I really appreciated all the things you did for me, and from the bottom of my heart I want to truly say thank you. You are my blue boy.

I would like to thank all the lab members of the Stafford lab, current and past. I would like to thank Herman Cortes for helping me when I first started in the lab. I would like to thank Juilanna Deuchter for being a great first undergrad under my wing and also a great friend. I also would like to thank the current lab members, Hima, Myron and Harry for all the support, ideas and laughs.

I would like to thank my committee members Dr. Brad Magor and Dr. Norman Neuman for all their suggestions, ideas and support for the past seven years. Dr. Dan Barreda and Dr. Kevin Kane for being apart of my candidacy exam. I would like to also thank Dr. Rob Ingham for being apart of my defense. I would also like to thank Dr. Mike Belosevic for our morning meetings and all his great advice.

I would like to give a big thank you to Dr. Stephanie DeWitte-Orr for taking the time to be my external examiner. I hope you like it!

I need to give the biggest thank you to my family. To my mom and dad; thank you for all your love and support throughout the last twelve years of my life as I went on this crazy adventure. You always had my back and were always willing to help me whenever I needed it. Your constant support and love are one the biggest reasons I got as far I have. Without you this truly would not be possible. To my sister and brother; thank you for always being a phone call away when I needed it. Although I know I was not around very much over the past seven years, that did not keep us from being the best of friends. To my friends Jerret, Brendan, Brad, Dave and Kevin; thank you for constantly reminding me that as a scientist all I do is make volcanoes. Oh, the correct ratio of vinegar to baking powder is 4:1 and blue coloring. Also, thank you for being great friends. Our conversations everyday made this journey a lot easier. To my friend Josh; I would not have made it this far without you. Our time late in the lab listening to old school rap will be some of the greatest moments I remember about this journey. Your support and guidance kept my head in the game and I truly thank you for being an ear to talk to.

To my most patient and understanding girlfriend Elecia. Honestly, I cannot thank you enough for all your love and support over the last two years. Your constant craziness and love made everyday brighter and more worthwhile. Thank you for giving me balance and making me a better person. I truly cannot express how you have helped me through the past few years. You were always in my corner and for that I thank you.

TABLE OF CONTENTS

CHAPTER I
INTRODUCTION

CHAPTER II
LITERATURE REVIEW

CHAPTER IV

TELEOST LEUKOCYTE IMMUNE-TYPE RECEPTORS ACTIVATE DISTINCT PHAGOCYTIC MODES FOR TARGET ACQUISITION AND ENGULFMENT

CHAPTER V

TRYPSIN DIFFERENTIALLY MODULATES CHANNEL CATFISH LITR EXPRESSION LEVELS AND PHAGOCYTIC FUNCTIONS

CHAPTER VI

SEM AND LIVE-CELL IMAGING ANALYSIS OF CHANNEL CATFISH LITR-INDUCED PLASMA MEMBRANE DYNAMICS DURING THE PHAGOCYTIC PROCESS

CHAPTER VII

EXAMINATION OF SYK AND NCK RECRUITMENT BY CHANNEL CATFISH IpLITRS DURING FILOPODIA-MEDIATED TARGET CAPTURE AND ENGULFMENT

CHAPTER VIII

GENERAL DISCUSSION AND FUTURE DIRECTIONS

REFERENCES

LIST OF TABLES

LIST OF FIGURES

LIST OF ABBREVATIONS

- ADCC — Antibody dependent cell-mediated cytotoxicity
- Akt — Protein kinase B
- AMPS — Antimicrobial peptides
- Arp 2/3 — Actin-related protein 2/3 complex
- APC — Antigen presentation cell
- ASB — Antibody staining buffer
- BAI1 — Brai specific angiogenesis inhibitor
- BAR — Bin/Amphiphsyin/Rvsp
- BSA — Bovine serum albumin
- BB — Blue beads
- BCR — B cell receptor
- BNI1P — *Saccharomyces cerevisiae* BNI 1 gene product
- Cdc42 — Cell division control protein 42 homolog
- CLR — C-type lectin
- CREB — cAMP response binding protein
- CD — Cluster differentiation
- CTLD — C-type lectin-like domains
- CR3 — Complement receptor 3
- CTL — Cytotoxic T lymphocyte
- CEACAM3 — Carcinoembryonic antigen-related cell adhesion molecule 3
- CYT — Cytoplasmic tail

- C-Abl Tyrosine kinase ableson murine leukemia mammalian oncogene-1
- D Domains
- Dok1 Docking protein 1
- DAMP Damaged associated molecular pattern
- DC Dendric Cell
- EGFR Epidermal growth factor receptor
- EGF Epidermal growth factor
- EST Expressed sequence tag
- FcR Fc-receptors
- FBS Fetal bovine serum
- F-actin Filamentous (F)-actin
- FITC Fluorescein
- FAK Focal adhesion kinase
- G-actin Globular actin
- GAP GTPase-activating protein
- GEF Guanine nucleotide exchange factor
- GIALT Gill-associated lymphoid tissue
- GFP Green fluorescent protein
- GALT Gust-associated lymphoid tissue
- GST Glutathione-s-transferase
- Grb2 Growth factor receptor-bound protein 2
- GSK Glycogen synthase kinase
- HA Hemagglutinin

- HEPES N-2-hydroxyethylpiperazine-N'-2-ethansulfonic acid
- HRP Horseradish peroxidase
- Ig Immunoglobulin
- IgG Immunoglobulin G
- IgSF Immunoglobulin superfamily
- IRSp53 inverse-BAR protein insulin receptor substrate protein of 53 kDa
- IpLITR Ictalurus punctatus leukocyte immune-type receptor
- ITAM Immunoreceptor tyrosine-based activation motif
- ITIM Immunoreceptor tyrosine-based inhibitory motif
- JNK c-jun N-terminal kinase
- KIR Killer Ig-like receptors
- LITR Leukocyte immune-type receptor
- LPS Lipopolysaccharide
- LCI Live cell imaging
- LRC Leukocyte receptor complex
- MLC Mixed leukocyte culture
- LITR Leukocyte immune-type receptor
- LILR Leukocyte Ig-like receptors
- mAb Monoclonal antibody
- MALT Mucosal associated lymphoid tissue
- MARCO Macrophage receptor with collagenous structure
- MAPK Mitogen activated kinase
- mDia Mammalian diaphanous-related formins

- MEM Minimal essential media
- MEK Extracellular signal-regulated kinase kinase
- MFI Mean fluorescent intensity
- MMP Matrix metalloproteinases
- MPO Myeloperoxidase
- MR Mannose receptor
- MSK Mitogen-stress activated kinase
- NALT Nasopharynx-associated lymphoid tissue
- NCC Nonspecific cytotoxic cell
- NCCRP-1 NCC receptor protein 1
- Nck Non-catalytic region of tyrosine kinase
- NK Natural Killer
- NKR Natural killer receptor
- NO Nitric Oxide
- NET Neutrophil extracellular trap
- NPF Nucleation promoting factor
- NSP Neutrophil serine proteases
- N-WASP Neural Wiskott-Aldrich Syndrome protein
- PAR Protease activated receptor
- PAK p21-kinase
- PAMP Pathogen associated molecular pattern
- PBL Peripheral blood leukocyte
- PBS Phosphate buffered saline

- PCD Programmed cell death
- PCC Pearsons Correlation Coefficient
- PDK1 Phosphoinositide-dependent kinase-1
- PDGF Platelet derived growth factor
- PFA Paraformaldehyde
- PECAM-1 Platelet endothelial cell adhesion molecule
- PI3K Phosphoinositide 3-kinase
- PKC Protein kinase C
- PMA Phorbol myristate acetate
- PLC Phospholipase C
- ProS1 Protein S1
- PRR Pathogen recognition receptor
- PtdIns(3,4,5)P_3 Phosphatidylinositol 3,4,5-trisphosphate
- PtdIns(4,5)P_3 Phosphatidylinositol 4,5-trisphosphate
- PtdSer Phosphatidylserine
- PSR PtdSer receptor
- Rac Ras-related C3 botulinum toxin substrate 1
- ROS Reactive oxygen species
- ROSi Reactive oxygen species intermediates
- RhoA Ras homolog gene family member A
- RBL-2H3 Rat basophilic leukemia-2H3
- SA Streptavidin
- Src Proto-oncogene tyrosine-protein kinase src

- Syk — Spleen tyrosine kinase
- SHP — Src homology region 2 domain (SH2) containing phosphatase-1/2
- SHIP — SH2 domain containing inositol-5 phosphatase
- SAP-130 — Sin3-aossciated protein 130
- SALT — Skin-associated lymphoid tissue
- SEM — Scanning electron microscopy
- SFK — Src-family kinases
- SRBC — Sheep red blood cells
- TAM — Tyro3, Axl, MER
- TIM — T cell immunoglobulin mucin
- TLR — Toll-like receptor
- Tks5 — Tyrosine kinase substrate 5
- TNF — Tumor necrosis factor
- Vav — Proto-oncogene vav
- VASP — Ena/vasodilator-stimulated phosphoprotein
- VEGEF — Vascular endothelial growth factor
- VLR — Variable lymphocyte receptor
- WASP — Wiskott-Aldrich syndrome protein
- WAVE2 — WASP-family verprolin-homologous protein
- YG — Yellow green
- ZAP-70 — Zeta associated protein

CHAPTER I
INTRODUCTION

1.1 Introduction

Innate immunity consists of complex and highly specialized cells capable of inducing potent effector responses that are important for the destruction of microbes. For example, innate cellular responses such as phagocytosis, degranulation, and cell-mediated cytotoxicity have all been characterized in both mammals and fish, representing vertebrates that diverged more than 450 million years ago [1]. This suggests that components of vertebrate innate cellular immunity are conserved among endothermic and ectothermic vertebrates. Furthermore, examining such vital processes in a range of model systems will offer unique opportunities to study the convergent and divergent aspects of vertebrate innate immune responses.

One highly conserved effector response in vertebrates is the ability for specialized immune cells to recognize, bind, and engulf extracellular targets. This process, termed phagocytosis, was initially utilized by simple cellular organisms for the acquisition of nutrients, but over the course of evolution has become a vital process in both host defense and tissue homeostasis [2]. The engagement of surface expressed receptors by pathogens or other targets such as dead/dying cells trigger receptor-specific intracellular signaling events in phagocytes that ultimately leads to the internalization of a diverse range of targets [2]. Although different phagocytic receptor-types often use similar signaling components to induce phagocytosis, recent studies have also identified several alternative phagocytic mechanisms that rely on receptor-specific signaling components to coordinate the regulation of the phagocytic machinery [3]. However, detailed examination of the cellular mechanisms associated with the dynamic regulation of various modes of phagocytosis are not well understood.

Phagocytosis has been mostly studied using mammalian receptor model systems [4–8]. Although phagocytic uptake of targets has been identified and studied in fish [9], much less is known about the receptor-types that regulate this process, and therefore my research focused on the regulation of phagocytosis by the channel catfish IpLITR receptor family. IpLITRs are a polymorphic teleost immunoregulatory receptor family, which share phylogenetic and structural characteristics with other receptors in mammals. IpLITRs have been shown to control immune-effector responses when transfected into mammalian immune cell lines using both prototypical stimulatory and inhibitory signaling mechanisms. Specifically, the putative stimulatory chimeric receptor IpLITR 2.6b/IpFcRγ-L has been shown to induce degranulation, cytokine secretion and phagocytosis in an immunoreceptor tyrosine-based activation motif (ITAM)-dependent manner [10,11]. In contrast, IpLITR 1.1b, a putative inhibitory receptor, abrogated NK cell-mediated killing response through both immune receptor tyrosine-based inhibitory motif (ITIM)-dependent and -independent mechanisms [12,13]. More recently IpLITR 1.1b has been shown to exhibit functional plasticity by inducing phagocytosis when expressed in myeloid cells, representing the first demonstration of functional plasticity for an ITIM-containing teleost immunoregulatory receptor. Characterization of this functional plasticity may reveal the conserved nature of innate signaling events among vertebrate immunoregulatory receptors. Furthermore, the conservation of functional plasticity among the ITIM and immunoreceptor tyrosine-based switch motif (ITSM)-containing vertebrate immunoregulatory proteins is unknown. By understanding the plasticity of certain teleost immunoregulatory receptors, we may also uncover new cellular mechanisms responsible for the control of important innate immune cell effector functions that may be conserved throughout the vertebrate linage. Therefore, to

advance our understanding of the induction and regulation of phagocytosis in vertebrates my thesis research focused on the facilitation of phagocytosis by IpLITRs.

1.2 Objective of thesis

The overall objective of this thesis was to examine the regulatory capabilities of IpLITRs. The specific aims of my research were: (1) to characterize the unique ITAM-independent phagocytic pathway regulated by IpLITR 1.1b; (2) to confirm that the surface expression of IpLITR 1.1b was a requisite for the unique target acquisition and engulfment phenotype; (3) to examine IpLITR 1.1b selective regulation of F-actin dynamics, and; (4) to examine the recruitment of spleen tyrosine kinase (Syk) and non-catalytic region of tyrosine kinase (Nck) during IpLITR 1.1b-induced formation of filopodia and the capture and engulfment of targets

1.3 Outline of thesis

Chapter II is an overview of the literature related to my thesis work. In this chapter I first provide a brief overview of teleost innate immunity with an emphasis on teleost cellular effector responses. I then review information surrounding phagocytosis including its evolution as a process and discuss phagocytosis as a receptor-mediated F-actin dependent response. Then I will discuss information on key examples of phagocytic receptors in mammals. Next, I will review and discuss the phagocytic cell-types and phagocytic receptors in fish. Lastly, I will give a comprehensive overiew of the recent characterization of IpLITRs with an emphesis on their phagocytic capabilities. Chapter III contains the detailed descriptions of the procedures and methods I used during the completion of my thesis. In Chapter IV I tested the hypothesis that ITAM-dependent and ITAM-independent phagocytic pathways are engaged by different sub-types of the IpLITR family. I provide a kinetic and pharmacological profile of IpLITR 1.1b- and IpLITR 2.6b/IpFcRγ-L-induced phagocytosis in addition to a detailed phenotypic analysis of the

phagocytic responses activated by these immunoregulatory receptors using confocal microscopy. Overall my results show that IpLITR 1.1b uses an alternative phagocytic pathway that is functionally distinct from the classical ITAM-mediated response. In Chapter V I examined the effects of the serine protease trypsin on IpLITR-mediated phagocytosis. Using flow cytometry, I show trypsin potently inhibited IpLITR 1.1b-mediated phagocytosis, which closely correlated with a reduction in the surface expression of this protein. In comparison, cell surface expression and phagocytic activity of IpLITR 2.6b/IpFcRγ-L was trypsin-insensitive. My confocal microscopy results revealed trypsin-treated IpLITR 1.1b-expressing cells rarely displayed fully internalized beads and they had a significant reduction in the number of beads captured in phagocytic cups or at the ends of membranous protrusions. Overall, my results show that the presence of IpLITR 1.1b on the cellular surface influences the way in which cells engage in target-cell interactions through the formation of unique membranous protrusions. In Chapter VI I tested the hypothesis that IpLITR 1.1b-expressing cells selectively induce the formation of F-actin dense protrusions, also known as filopodia. I used a combination of live cell imaging (LCI) and high-resolution scanning electron microscopy (SEM) to provide detailed new information regarding IpLITR 1.1b-induced plasma membrane dynamics during the phagocytic process. I show that expression of IpLITR 1.1b, but not IpLITR 2.6b/IpFcRγ-L, specifically triggers filopodia formation in the absence of any known stimuli. In addition, I show during the early stages of the IpLITR 1.1b-mediated phagocytic process, these filopodia-like structures retract after target contact to secure the captured microspheres to the cell surface. Overall, my results show IpLITR 1.1b can selectively regulate filopodia formation over a range of incubation temperatures for target capture and engulfment. In Chapter VII I wanted to develop immunofluorescence-based imaging protocols to directly examine the recruitment of Syk and

Nck during IpLITR 1.1b-induced formation of filopodia and the capture and engulfment of targets. I show Nck but not Syk colocalize with IpLITR 1.1b within constitutively generated filopodia structures. Furthermore, during the various phases of IpLITR 1.1b-mediated target binding, capture, and engulfment, both Syk and Nck were found to specifically accumulate at cell-target interfaces. Overall, these results provide a first look at the unique dynamics of IpLITR 1.1b-mediated molecular recruitments during F-actin-dependent membrane dynamics and provide new details regarding Syk and Nck recruitments during ITAM-dependent and independent phagocytic modes. In summary, my research provides new information about the mechanism(s) facilitating unique F-actin dependent membrane dynamics during IpLITR 1.1b-mediated phagocytosis. Finally, in Chapter VIII I provide an overview of my findings and describe how these findings relate to the current understanding of both phagocytic signaling as well as filopodia formation by immunoregulatory receptors. Chapter IX lists all the references used in this thesis.

CHAPTER II
LITERATURE REVIEW

2.1 Overview

Comparative immunology is the study of immunity across a wide spectrum of animals ranging from invertebrates to vertebrates. While a great understanding of immune mechanisms has come from focused studies using mammalian models (e.g. humans, mice, and rats), significant advancements in our understanding of immune protection mechanisms, and the evolution of immunity, has also come from research focused on exploring immune processes in ectothermic vertebrate (e.g. amphibians and fish) and invertebrate (e.g. insects, arthropods, and echinoderms) animal models. For example, comparative immunological studies using teleost (boney) fishes has provided seminal insights into our understanding of vertebrate immunity and a broader understanding of the evolution of antimicrobial mechanisms. Select examples include the identification of phagocytic B cells in fish [14], the discovery of novel subtypes of fish antibodies [15], and the description of several large and diverse teleost multigene immunoregulatory receptor-types belonging to both the immunoglobulin and c-type lectin superfamily's [16,17]. Beyond bony fishes, research in lamprey and hagfish has revealed a completely divergent mechanism of adaptive immunity, which is independent of the generation of classical antibody proteins through the production of variable lymphocyte receptor (VLR) proteins in these primitive jawless vertebrates [18–20].

Teleost represent the most diverse class of extant vertebrates that contain both adaptive and innate immune components. Fish live in diverse aquatic environments and are constantly bathed in waters populated with numerous bacterial, viral and parasitic pathogens. Consequently,

fish are armed with a robust innate antimicrobial defense system that begins with their natural barriers to infection (e.g. skin, scales, and mucus) that if breached then requires engagement of potent immune cell effector responses such as degranulation and phagocytosis. Importantly, teleost represent one of the earliest vertebrates to have adaptive immune system components (e.g. T cells, B cells, and antibodies) like those found in mammals and thus comparative studies in fishes offers a unique opportunity to study the evolution of immunological mechanisms of higher vertebrates. Fish are also of interest in immunological studies since they are heavily relied on in aquaculture practices throughout the world. Therefore, an understanding of fish immunity is vital for maintaining healthy and thriving populations of fish for both economical reasons as well as to ensure aquatic farms remain a sustainable source of food.

Over the past few decades, immunological studies in fish have disproportionately focused on the cloning, sequencing, and molecular characterization of fish cytokines, chemokines, and several immunoregulatory receptor-types. While aided by the availability of several completed genome sequencing projects in fish and advancements in DNA and RNA sequencing technologies, the known inventory of teleost genes exponentially exceeds our understanding of their functions. Therefore, a return to the biochemical and functional assessments of teleost immune proteins is required to fully appreciate the mechanisms underlying fish immune cell mediated effector responses.

The research described in this thesis represents a series of studies focused on understanding the regulatory capabilities of a specific immunoregulatory receptor family identified in the channel catfish termed (*Ictalurus punctatus*) leukocyte immune-type receptors (IpLITRs). In this review I first provide a brief overview of teleost innate immunity with an importance on teleost cellular effector responses. I will then review in brief evolutionary origins

of phagocytosis as well as phagocytosis as a cellular process. I next review major phagocytic receptors that have been characterized in mammals involved with the phagocytic uptake of microbes and dead/dying cells. I then review information surrounding the characterization of the cell-types in fish associated with phagocytosis as well as the limited information surrounding phagocytic receptors in fish. Lastly, I will discuss recent research surrounding the functional characterization of the channel catfish leukocyte immune-type receptor (IpLITR) family with a focus on their ability to regulate the phagocytic process.

2.1.1 Overview of innate immunity in fish: physical barriers

The separation of the extracellular environment from the internal tissues of an organism represents a fundamental feature of innate immunity that functions to block pathogen entry [21,22]. In general, vertebrate skin contains two major cellular layers, the dermis and the epidermis, which provides a formidable anatomical barrier that acts as the first line of defense against pathogens [21,22]. Since teleost live in aquatic habitats they have evolved a robust epidermal layer, which is protected by ossified scales and rigid actin-rich filaments. This unique histology helps protect this anatomical barrier from injury, which if breached would provide a portal of entry for potential pathogens [22]. Teleost also have diverse array of lymphoid tissues located within their epithelial tissues that help combat infection. These consist of immune cell rich areas such as the mucosal associated lymphoid tissue (MALT), gust-associated lymphoid tissue (GALT), skin-associated lymphoid tissue (SALT), nasopharynx-associated lymphoid tissue (NALT), and the gill-associated lymphoid tissue (GIALT) [23,24]. [23,24]. These sites contain site-specific variations of resident immune cells, and include in some combination B cells, T cells, melano-macrophages, dendritic cells (DC), nonspecific cytotoxic cells (NCCs), and neutrophils (Reviewed in [23,24]). With such large collections of immune cell-types, these sites

are important for the interplay between the innate and adaptive arms of teleost immunity. For example, macrophages and DCs act as antigen presentation cells for tissue resident B and T cells, thereby inducing the activation of adaptive immune responses [23,25,26]. Another important innate immunological barrier in fish is their generation of mucus. Mucus is composed of high molecular weight glycoproteins and is secreted by specialized cells known as the globlet cell [27]. Fish mucus plays a major role in antimicrobial responses. For example, mucosal layers within the gills of fishes represents a main contact point with microbes and therefore it contains numerous antimicrobial peptides (AMPs), a low pH, hydrolytic enzymes, and resident immune cells [22,26–28]. If these initial barriers fail to keep pathogens from invading, the next line of defense is the induction of cellular effector responses by the various innate immune cell-types found throughout the body.

2.1.2 Overview of innate immunity in fish: cellular effector responses

Innate immune cell effector responses are critical to the health of an organism as these are facilitated by immune cells at sites of infection. In mammals, the major contributors to innate effector responses are monocytes, macrophages, granulocytes (e.g. neutrophils, basophils, and eosinophils), natural killer (NK)-like cells, and the recently discovered phagocytic B cells. These cells perform a wide variety of immunological responses such as degranulation, phagocytosis, cytokine production, antigen presentation, and cytotoxicity. The specific effector response(s) of these cell-types are in part associated with the type(s) of surface receptors they express that mediates their ability to interact with various binding partners (e.g. ligands).

In mammals, one major antimicrobial effector response is the release of destructive molecules from intracellular stores termed degranulation. One major inducer of degranulation is the binding of IgE antibodies to the Fc epsilon receptor (FcεR) expressed on the surface of

specific granulocyte-types such as eosinophils and basophils, which when triggered by antigen, induces the release of granule contents vial exocytosis [29]. In teleost, two major pathways of basophilic degranulation have been identified. For example, basophils extracted from the blood of fugu (*Takifugu rubripes*) can be induced to release two distinct types of granules after the addition of IgM [30]. A secondary degranulation pathway was also induced by stimulating the cells with the protease enzyme papain, revealing both antibody-dependent and independent degranulation mechanisms in fish [30]. A secondary degranulation pathway was also induced by stimulating the cells with the protease enzyme papain, revealing both antibody-dependent and independent degranulation mechanisms in fish [30]. The first identification of neutrophils in fish were from gilthead seabream (*Sparus aurata*) head kidney and peripheral blood leukocytes (PBLs) that positively stained for both alkaline phosphatase and peroxidase; hallmark identifiers of neutrophil granules [31–33], which showed specific cell-types in the head kidney and peripheral blood leukocytes (PBLs) that positively stained for both alkaline phosphatase and peroxidase; hallmark identifiers of neutrophil granules [32,33]. These granules have basophilic-like stores of antimicrobial molecules similar to those found in mammalian neutrophils such as proteinase-3, cathepsin-G, elastase, and azurocidin [34]. Neutrophils are routinely classified as the first cellular responders to infection, and upon arriving at inflammatory sites they elicit a variety of immunological effector responses including degranulation, production of reactive oxygen species (ROS), and phagocytosis to help combat invading pathogens. Fish neutrophils represent a larger portion of circulating leukocytes under homeostatic conditions compared to mammals [35,36] and have been identified as major inducers of degranulation upon stimulation with zymosan, *Aeromonas salmonicida,* and mitogens [35,37,38]. Interestingly, recent studies have identified that neutrophil migration is bi-directional as *in vivo* imaging studies have shown

zebrafish neutrophils migrating back towards the vasculature post inflammation, suggesting a novel resolution role in inflammatory processes. This alters the general view of neutrophils during inflammation, which after completing their pro-inflammatory roles during early stages of inflammation are believed to undergo rapid cell-death. Interestingly, recent studies have identified that neutrophil migration is bi-directional as *in vivo* imaging studies have shown zebrafish neutrophils migrating back towards the vasculature post inflammation, suggesting a novel resolution role in inflammatory processes [39]. This alters the general view of neutrophils during inflammation, which after completing their pro-inflammatory roles during early stages of inflammation are believed to undergo rapid cell-death. Finally, neutrophils have also been shown to promote a unique mechanism for pathogen destruction by forming and releasing neutrophil extracellular traps (NETs). Like mammals, generation of NETs by fish neutrophils has been shown in several species including carp (*Cyprinus carpio*), fathead minnows (*Pimephales promelas*), zebrafish (*Danio rerio*), and the smooth tongue sole (*Cynoglossus semilaevis*) [35,40–43]. NETs represent nuclear DNA-containing filaments mixed with granular proteins (e.g. elastase) that are expelled from the intracellular space of the cell acting as a potent antimicrobial substance [35]. NETs have been shown to specifically degrade bacterial and viral virulence factors and the ability to bind, trap, and kill pathogens directly [35,40–43].

NK cells and cytotoxic T lymphocytes (CTLs) are important immune cells that survey the health of host cells by monitoring the body for signs of infection, stress, or transformation. NK cells and CTLs are able to recognize unhealthy cells using three major mechanisms; 1) non-self recognition (e.g. recognition of pathogen induced molecules), 2) missing self (e.g. recognition of reduced self markers on healthy cells), and 3) induced self (e.g. recognition of self stress markers) [44]. If NK cells and CLTs recognize any of the above-mentioned scenarios, then NK

cells and CLTs facilitate cell death of these unhealthy cells in a process known as cytotoxicity. The induction of cytotoxicity by NK cells and CTLs in mammals is facilitated by granule exocytosis and FasL/Fas interactions [45], which also have been verified to occur in fish[46,47]. The two main types of non-specific cytotoxic cells identified in fish are known as nonspecific cytotoxic cells (NCC) and NK-like cells [48–50]. NCCs were first identified in channel catfish as small agranular lymphocytes, which are characterized by the expression of the NCC receptor protein 1 (NCCRP-1) These cells induce spontaneous cytotoxicity for a variety of xenogeneic targets and virally infected autologous cells without the need for prior stimulation .[51–53]. Since fish NCCs facilitate similar effector responses to mammalian NK-cells, they are thought to be the evolutionary pre-cursors of these innate killers [46,54]. The second major non-specific cytotoxicity cell in fish are referred to as NK-like cells and unlike NCCs, these cells kill allogenic but not xenogeneic targets spontaneously [48,53,55,56]. NK-like cells are also distinct from NCCs as these cells express a putative FcμR and are negative for classical markers of other teleost immune cell-types [51]. Another differentiating feature of NK-like and NCC teleost cells is their origins within the fish. NK-like cells are found within PBL while NCCs are derived in the head kidney [52]. Recently, the antimicrobial peptide NK-lysin, an ortholog to mammalian granulysin, was identified in the tilapia [57]. Granulysin is a cytolytic and pro-inflammatory molecule that is a major component in CTL and NK cell-mediated cytotoxicity against infected host cells [58]. Overexpressing NK-lysin tilapia had significantly lower bacterial load post challenge compared to control fish, indicating NK-lysin to function similar to that of mammalian granulysin [57]. Interestingly, flatfish turbot (*Scopthalmus maximus*) red blood cells (RBCs) also contain NK-lysin when undergoing autophagy [59]. Expression of NK-lysin in turbot RBCs was shown to increase upon viral infection prior to the induction of autophagy and if autophagy was

blocked viral replication was significantly higher compared to controls [59]. This identified a novel role of teleost RBCs in anti-viral immunity.

Phagocytosis is another vital innate immune cell effector response. This cellular engulfment process is performed by specialized cells known as phagocytes that can recognize, bind, and then internalize extracellular targets such as microbes, cellular debris, and dying/dead host cells [2,60]. Initially a process utilized for nutrient acquisition by single cell organisms, phagocytosis has evolved as a major process in immunity across evolution [2]. The recognition of pathogens by phagocytes is elicited by specialized surface expressed phagocytic receptor proteins that when bound to their respective ligands, induce intracellular signaling events that lead to F-actin polymerization and dynamic remodelling of the plasma membrane. In mammals, many phagocytic receptors have been identified with the most well characterized of these being the Fc receptor (FcR), dectin-1, and complement receptor 3 [2,61–63]. In teleost, the main phagocytic effectors are macrophage, monocytes [24,37,64–69], DCs [70], and neutrophils [35–37,71,72]. These cells elicit destructive intracellular responses such as ROS and nitric oxide (NO) production during the binding and internalization of extracellular targets. An interesting aspect of phagocytic activities in fish was the recently discovered ability for sub populations of teleost B cells to perform phagocytosis [14]. First identified for rainbow trout and catfish B cell populations [14], IgM+B cells were shown as potent inducers of phagocytosis of both IgM-opsonized bacteria and IgM-opsonized latex beads. [14]. The importance of these phagocytic B cells was further demonstrated as IgM+B cells with phagocytic abilities were subsequently identified in other teleost species including Atlantic salmon (*Salmo salar*) [72] and zebrafish [73]. Following the discovery of phagocytic B cells in teleost, research began searching for this

unique cell-type in other vertebrates and to date, most vertebrate species (fish, amphibians, mammals) have been identified to contain phagocytic B cells [74].

In mammals, the receptors that initiate and regulate the innate immune cell effector responses described above have been well-studied and in general they represent two major classes of receptor-types; PRRs and other immunoregulatory receptor-types such as those belonging to the immunoglobulin superfamily (IgSF). In contrast, although fish immune cells generally elicit the same overall repertoire of antimicrobial responses (e.g. degranulation, cytotoxicity, and phagocytosis) very little is known about the receptor-types and associated mechanisms that regulate these important protective actions in fish. However, representatives of both PRRs and immunoregulatory receptor-type genes belonging to the IgSF have been identified in fish. Unfortunately, despite this large molecular inventory of immunoregulatory receptor-types, most have yet to be functionally examined. In the next sections of this review, I will provide a more in-depth examination of phagocytosis as an evolutionarily conserved process and give some details of phagocytosis in both mammals and fish.

2.2 Phagocytosis

2.2.1 Introduction

The emergence of multicellular organisms in evolution offered a new opportunity for the generation of specialized cells with specific cellular functions. This division of labour allowed for the formation of specific types of tissues, organs and systems within multicellular organisms. The immune system is a fundamental component to any organism as a means of defending against possible infectious agents. One cellular process within the immune system that existed prior to the emergence of complex cell-types is the ability for immune cells to dynamically

regulate their membranes during internalization of extracellular targets. This process is termed phagocytosis.

2.2.2 Evolution of phagocytosis

Mitochondria and related organelles exist in all eukaryotes studied to date, suggesting that early unicellular organisms possessed these structures very early on in evolutionary history [75,76]. The rise of such a diverse array of cellular structures is believed to have occurred due to an endosymbiosis event whereby an autotrophic bacterium was engulfed by a larger primitive heterotrophic eukaryotic cell [75]. This event lead to the formation of a cell with both a mitochondria-like organelle as well as other intracellular structures we observe today in more complex eukaryotic cells. Known as the archezoan hypothesis, this suggests that the internalization of a simple single cell organism by a larger and more complex cell gave rise to the complexity and organization of cells that we see today [77]. The ability to internalize large extracellular particulate targets via phagocytosis was utilized by simple unicellular organisms for a variety of functions such as the internalization of nutrients from the extracellular environment to the internalization of whole organisms such as bacterium as a food source [75,77]. Consequently, phagocytosis has evolved into a fundamental component of innate immune defense and tissue homeostasis in all animals.

2.2.3 The phagocytic process

Formally, phagocytosis is defined as the ability of specialized cells called phagocytes to recognize and engulf large insoluble particles greater than 0.5 μm in diameter [2]. Also a receptor-mediated process, phagocytosis is important for food acquisition, removal of apoptotic cells, tissue remodeling, and in more complex organism's host defense against invading

microbes [78]. Phagocytosis has been demonstrated in unicellular organisms such as amoebas, plants, and has been described in numerous invertebrates and vertebrate animal species [78]. As a cellular process, phagocytosis consists of a series of connected stages, which includes: (i) detection and recognition of extracellular targets through surface expressed phagocytic receptors; (ii) attachment of particles to the surface of phagocytes; (iii) internalization of particles into a phagosome via F-actin polymerization; (iv) fusion of the phagosome with the lysosome generating the destructive phagolysosome; (v) the intracellular killing and degradation of the ingested particle, and; (vi) the presentation of degraded antigens to adaptive immune cells [2,65,79]. Professional phagocytes consist of neutrophils, macrophages, monocytes and DCs. Epithelial and fibroblast cells have also been shown to contain phagocytic abilities and are considered non-professional phagocytes that regulate routine homeostatic clearance of dead/dying cells [65]. The distinction between professional and non-professional phagocytes is the types of molecules these cells can recognize as well as their ability to facilitate secondary signaling events for the promotion of target destruction [80]. In general, professional phagocytes are capable of engaging a broader array of extracellular molecules while non-professional phagocytes have limited recognition capabilities [81]. Secondly, professional phagocytes can generate additional signaling events, which facilitate the destruction of an internalized target, while most non-professional phagocytes cannot [79,81]. Given the importance of the ability of phagocytes to recognize potentially harmful targets, much interest in understanding the phagocytic process comes from trying to understand the relationship between phagocytes and their abilities to recognize microbial targets. Specifically, the two major classes of molecules recognized by phagocytes as potentially harmful to a host are apoptotic/necrotic (altered self) molecules and microbes (non-self) [2,78,79,82]. How phagocytes distinguish altered self versus

non-self is due to the presence of surface expressed proteins on their membranes known as phagocytic receptors. These phagocytic receptors recognize extracellular targets via direct interactions (e.g dead/dying cell or microbe) or through indirect interactions via host-derived proteins or opsonin's, which include antibodies and complement proteins that are often pre-bound to targets in the extracellular environment [2,79,82].

One specific phagocytic receptor-type known as Dectin-1, recognizes pathogens directly by its ability to bind carbohydrate motifs located on the outer portions of fungal pathogens [63,83]. This engagement stimulates intracellular signaling events in the cell terminating in F-actin polymerization that induces remodeling of phagocytic membranes as they bind and then fungal targets [63]. Indirect recognition of pathogens is facilitated by host-derived antibodies, which bind to a diverse array of microbes, essentially tagging them for phagocytic uptake [2,82]. This is induced by antibody recognizing receptors known as Fc-receptors (FcRs), which bind to the conserved regions of antibodies causing intracellular signaling events that also promote F-actin controlled plasma membrane dynamics required for target capture and enfulfment [2,78,84]. F-actin polymerization is a fundamental and distal event during the phagocytic process. In general, activation of F-actin polymerization is a receptor-mediated process that induces the formation of pseudopods [2,85], which extend outwards from the membrane to form a phagocytic cup at the target-cell interface [2,82,85]. As the process progresses this cup begins to fully engulf the target as the membrane flows over the outer surfaces of the target by the extension of pseudopods until it becomes completely sealed, eventually forming the phagosome [2,84,85]. Once a target is completely internalized, the fusion of the phagosome with intracellular lysosomes generates the destructive phagolysosome, which will facilitate the degradation of the internalized target [79,86]. Recently, imaging studies of the phagocytic

process have identified F-actin polymerization events that occur prior to the initial binding phase of the target to the cell surface. This represents an early capturing mechanism via formation of F-actin dense membranous protrusions [87,88]. These protrusions extend well beyond the cell surface and are used by phagocytes to increase the likelihood that they will encounter a potential extracellular target. Once engaged with a target, extended protrusions retract back towards the cell body facilitating phagocytic receptor engagements [87,88]. Overall, the accumulation of all of the above-mentioned events are considered as the phagocytic process. Moreover, target binding, pseudopod formation, engulfment, as well as protrusion formations are all facilitated by the spatial-temporal regulation of F-actin polymerization events. In the next section I will discuss the regulatory properties of F-actin polymerization in the context of receptor-induced phagocytosis.

2.2.4 F-actin polymerization

Actin is one of the most abundant proteins in all eukaryotic cells and it is highly conserved [77]. Recently, this protein was also identified within prokaryotes, suggesting that actin is one of the most ancient proteins identified to date [75,77]. Actin exists in two physical states, a monomeric form (G-actin) and a filamentous form (F-actin) allowing this protein to dynamically regulate a variety of cellular processes including phagocytosis [89]. A characteristic feature of all these processes is the conversion of G-actin monomers into long extensions of F-actin via the joining of G-actin to the barbed growing end of a cellular filament [90–92]. Cytoskeletal dynamics are tightly regulated by the homeostatic balance of actin between these two forms, and this balance can be polarized in the presence of extracellular stimuli and/or the activation of surface expressed receptors [90,92]. The reorganization of the actin cytoskeleton during processes like phagocytosis is regulated spatially and temporally by many factors, one of

the most important is the activation of small Rho family GTPases that act as molecular switches [62,90,91]. Within the family of Rho GTPases are Cdc42, Rac, and Rho, which are important facilitators of actin assembly [4,92,93]. GTPases are activated via another set of proteins known as guanine nucleotide exchange factors (GEFs), which induce the release of the non-energetic GDP for the activate form GTP on small GTPases [62,90,92–94]. This activation of small GTPases is relatively poor, however, through their engagement of GTPase-activating proteins (GAPs), small GTPase activity can be significantly enhanced [2,82,90]. GTPases activate other important components of the actin polymerization machinery, specifically effector proteins known as nucleation promoting factors (NPFs) such as Wiskott-Aldrich syndrome protein (WASP), neural WASP (N-WASp), and WASP-family verprolin homologous protein (WAVE) [2,82]. When activated by GTPases directly, NPFs activate the actin polymerization protein Arp 2/3 complex by inducing a conformational change within the protein complex [82,90]. The Arp 2/3 complex consist of seven proteins including Arp2, Arp3 and subunits ARPC1-5, which upon activation via NPFs facilitate the generation of F-actin filaments that induce membranal changes needed for cellular processes like phagocytosis [90–92]. The binding of the Arp2/3 complex to actin within the cell initiates new actin filaments to form from already existing actin branches thereby generating the highly branched F-actin filaments needed to facilitate membrane remodeling events [92]. To facilitate the internalization of extracellular targets, phagocyte membranes must be able to extend beyond the already existing structure of the plasma membrane. In part, this is induced by a class of proteins known as formins [90]. A variety of formins have been identified, including mammalian diaphanous-related formin 1 (mDia1) and *Saccharomyces cerevisiae* BNI 1 gene product (Bni1p) [90,92]. These proteins are important for a variety of cytoskeletal changes involved in phagocytosis such as regulation and dimerization of

actin during nucleation events induced by Arp 2/3 complex and elongation of the plasma membrane [90,92]. Another major protein-type involved in F-actin polymerization events are actin crosslinking proteins, which are made up of α-actinin, spectrin, and dystrophin [90]. These proteins are localized to the submembrane of the cytoskeleton at the leading edges of the membrane extending around cell-bound targets during phagocytosis [90–92]. Actin crosslinking proteins anchor newly polymerized F-actin to the extracellular matrix and therefore act as scaffolds for newly polymerized F-actin [90]. Lastly, due to the spatiotemporal nature of the membrane dynamics associated with F-actin polymerization and phagocytosis, there must be ways in which these events are regulated as the phagocytic process occurs. This in part is regulated by Bin/Amphiphsyin/Rvsp (BAR) domain-containing proteins, which connect intracellular signaling pathways to the dynamics of F-actin polymerization events [90]. In general, BAR-containing proteins are regulated by directly associating with the above mentioned small GTPases, which generates localized F-actin polymerization events at specific sites at the plasma membrane causing curvature changes of the membrane as engulfment of targets proceeds [2,82,90]. These BAR-containing proteins also facilitate the recruitment of other signaling molecules to the sites of F-actin polymerization, thereby connecting extracellular stimuli to the F-actin machinery such as the Arp 2/3 complex [2]. Interestingly, recent proteomic studies have identified some of the above-mentioned F-actin polymerization associated molecules back to early archaeon's, and therefore suggests that the ability for cells to change their shape has been a fundamental component of almost every single cell since the earliest known single cell organisms existed [75].

2.2.5 Evasion of phagocytosis

Since phagocytosis is important for host defense, pathogenic microbes have evolved mechanisms to evade capture and destruction by phagocytes. One of the most common mechanisms by which pathogens can avoid being detected by phagocytes is through the ability to inhibit host-derived proteins from opsonizing [2,95]. Bacteria and fungal pathogens can produce polysaccharide-based coatings that prevent the ability for antibodies and complement proteins from binding to their surfaces, thus reducing their chances of being targeted by phagocytic receptors such as FcR and CR3 [2,95]. Pathogens also use host-derived molecules to down regulate receptor binding. Specifically, group A *Streptocci* generates M proteins, which recruit host-derived C4-b complement proteins to their cell surfaces [2]. C4-b acts as an inhibitor of complement activation and downregulates complement-mediated phagocytic uptake [2]. The ability to employ host-derived opsonin's for avoiding detection has been identified for other microbes as well. For example, *Staphylococcus aureus* secretes Protein A onto its surface, which has a very high binding affinity for the Fc region of the antibody IgG [2,95]. This interection prevents IgG from being able to bind and activate FcRs on the surface of phagocytes [2,95]. Even more complex mechanisms have been evolved by microbes to utilize a host's immune cells for their own advantage. For example, *Pseudomonas aeruginosa* injects into immune cells, via a type-3 secretion system, bacteria-derived GAPs [2,95]. As mentioned earlier, GAPs stimulate the activation of small GTPases, which regulate F-actin polymerization events for membrane remodeling processes like phagocytosis. The injection of *P. aeruginosa* GAP molecules ExoT and ExoS causes immune cells to become more phagocytic and thereby internalize the pathogen, which allows its entry into host cells [2,95]. This is wanted by *P. aeruginosa* in order to utilize intracellular compartments of cells as a mechanism for protection against extracellular

antimocribal responses and for replication purposes [2,95]. Alternatively, some microbes directly inhibit the phagocytic process to prevent their internalization and destruction. For example, *Escherichia coli* injects EspB and EspH into cells, which act as GEF inhibitors and therefore block F-actin polymerization phagocytosis [2,95]. Lastly, HIV-1 blocks membrane exocytosis during phagocytosis via the release of the viral molecule Nef and therefore abrogates the ability for phagocytes to remodel their plasma membranes [2]. Overall, pathogens have evolved unique capabilities to alter or utilize a host's immune system for their own benefit. However, host defenses have also co-evoled to combat pathogen infection mechanisms. One example is the evolution of a diverse array of phagocytic receptors that can recognize pathogens using a variety of mechanisms and can facilaite phagocytic uptake of microbes using converget and diverget intracellular signaling pathways. In the next section I will discuss some phagocytic receptors that have been characterized in mammals.

2.3 Phagocytic receptors

2.3.1 Introduction

In mammals, a diverse array of phagocytic receptor-types has been identified for both the phagocytic uptake of microbes as well as dead/dying host cells. Most of our understanding of phagocytosis has been uncovered using two major phagocytic receptors in mammals, namely FcRs and CR3 However, there are several other phagocytic receptor-types that utilize overlapping yet distinct signaling mechanisms from the FcR and CR3 receptors such as Dectin-1 and CEACAM3. In the following sections I will discuss the functions and signaling mechanisms identified for Rs, CR3, Dectin-1, and CEACAM3. I will also discuss details surrounding the phagocytic uptake of dead/dying host cells via a related engulfment process known as efferocytosis.

2.3.2 Fc-receptors (FcRs)

FcR-mediated phagocytosis occurs via the binding of surface expressed FcR proteins to antibody opsonized targets [2,79,96]. Phagocytic FcRs in humans include FcγRI, FcγRIIa, FcγRIIc, FcγRIIIa, FcεRI, FcαRI, and FcRn [2,97,98]. These receptors recognize and bind their respective antibody types (IgG, IgE, IgA and IgG) and initiate spatial and temporal intracellular signaling events that activates effector proteins that in turn, stimulate F-actin polymerization leading to membrane remodeling [2,97–99]. FcR signaling is induced by the clustering of the receptors through their lateral movements within the membrane to contact sites of bound targets causing signaling events, the first of which is the phosphorylation of an ITAM[2,99] . This activation motif is characterized by a tandem YxxI/L amino acid sequence [100], which acts as a substrate for phosphorylation events facilitated by Src family kinases [2,100,101]. ITAMs can be directly contained in the FcR cytoplasmic tail (CYT), as is the case for FcγRIIa and FcγRIIc [2]. Alternatively, FcRs can associate with ITAM-containing cytosolic adaptor proteins through transmembrane electrostatic interactions such as the case with FcγRI and FcγRIIIa [2,100,102]. Following receptor clustering, these ITAMs become phosphorylated, causing them to become docking sites for other intracellular signaling proteins, specifically spleen tyrosine kinase (Syk) [2,103,104]. Syk contains two Src homology 2 (SH2) domains which it uses to bind the tandem tyrosine's located within the ITAM motif and once bound to an ITAM Syk itself becomes phosphorylated and activated [2,101,105]. Interestingly, it has been shown in knock-out studies that in the absence of Src kinases, Syk may also facilitate the phosphorylation of nearby ITAMs, which augments other stimulatory signaling cascades during phagocytosis [2]. Syk recruitment to ITAM induces the activation and recruitment of a large variety of other intracellular signaling molecules to promote F-actin polymerization during the engulfment stages of targets. For

example, the activation of Syk leads to the phosphorylation and recruitment of adaptor proteins including the transmembrane protein linker of activated T cells (LAT) that acts as a scaffold for the recruitment of additional intracellular signaling molecules to the site of receptor activation [106,107]. The adaptor protein non-catalytic region of tyrosine kinase (Nck) has also been identified as a major scaffolding protein associated with the induction of FcR-mediated phagocytosis [108–110]. Due to the recruitment of LAT or Nck to receptor-activated sites, new signaling molecules including growth factor receptor-bound protein 2 (Grb2), docking protein 1 (Dok1), and Grb2-associated binder (Gab2) are brought into close proximity of the activated Syk kinase, which in turn can phosphorylate and activate the above-mentioned molecules amplifying further downstream signaling events [2,108,109,111,112]. Syk also activates the GEF Vav, which is important for the activation of small GTPases including Rho, Cdc42, Rac and RhoA [4,93,94,111,113]. The activation of these GTPases induces the activation of NPFs including WAVE, N-WASP, and WASP, which all directly initiate Arp 2/3 activation, causing the polymerization of F-actin and the remodeling of the plasma during target engulfment [2,5,108,111,114]. Another major contributor to FcR-mediated phagocytosis is phosphatidylinositol 3-kinase (PI3K) [2,94,111,115]. PI3K is activated by Syk kinase activity and it is localized to the inner membrane leaflet of the plasma membrane [2,94,111,115]. As a lipid kinase, PI3K promotes the phosphorylation of lipid molecules at the plasma membrane [111]. Specifically, PI3K converts phosphatidylinositol 4,5-tris-phosphate ($PI(4,5)P_2$) to phosphatidylinositol 3,4,5-tris-phosphate ($PI(3,4,5)P_{3)}$ which is then used by the cell as an anchor for the recruitment of other intracellular signaling proteins such as Rac and Cdc42 [116]. Dynamic lipid compositions during receptor-mediate signaling creates docking sites for small GTPases, among other protein-protein interactions such as the stabilization of Gab2, causing the

localized generation of F-actin polymerization at receptor-target sites [112,116]. FcR-stimulated membrane remodeling dynamics during antibody-coated target engulfment is considered the classical model of phagocytosis, which when observed via microscopy lead to the description of its zipper-like internalization of extracellular targets [2,111,116]. Activation of FcRs facilitates the generation and extension of pseudopodia from the cell-target interface, which are propelled around the outer edges of a bound target causing it to become enveloped within the plasma membrane [79,86,111]. As the membrane surrounds the bound target, newly formed FcR-target interactions are generated, which propagates the activation of intracellular signaling and promotes the elongation of the membrane around a target until it becomes completely internalized by the phagocyte [2,111].

In contrast to stimulatory FcR-types, inhibitory FcRs also exist within the FcR receptor family, namely FcRγBII1 and FcγRBII2. These FcR-types contain ITIMs within their long CYT regions, a motif that consists of the amino acid sequence S/I/VLxYxxI/V/L [102,117]. Inhibitory FcRs abrogate the activation of downstream signaling molecules such as Src and Syk kinases as well as modulate lipid compositions at the sites of inhibitory receptor engagement [102,117]. This is promoted by the binding of inhibitory FcRs to antibodies, which induces the phosphorylation of the tyrosine's found within the ITIMs, leading to the recruit of cytoplasmic phosphatases such as Src homology 2 phosphatase (SHP)-1/2 and Src homology 2 (SH2) domain-containing inositol phosphatase (SHIP)-1/2 [102,117]. These phosphatases deactivate intracellular signaling proteins or induce lipid compositional changes, which abrogate stimulatory signaling through de-phosphorylation events [102]. Overall, inhibitory FcRs block the activation of immunological responses including phagocytosis and downregulate immune cell activation thereby dampening the activation state of the cell [111]. A tight balance between

stimulatory and inhibitory FcR signaling dictates the activation state of an immune cell in response to antibody-opsonized extracellular targets.

2.3.3 Complement receptor 3 (CR3)

Another well characterized phagocytic receptor in mammals is the integrin CR3 receptor, which recognizes complement protein (iC3b)-opsonized extracellular targets [2,111,118]. CR3 is involved in multiple cellular processes including adhesion, diapedesis, as well as phagocytosis [2,79,118]. Unlike the zipper-like model of phagocytosis associated with FcR-mediated engulfment of targets, CR3-mediated phagocytosis has been described as an invagination event whereby targets 'sinks' into the cell during the engulfment process [2]. A major difference between CR3-mediated and FcR-mediated phagocytosis is the spatial-temporal nature of CR3-mediated signaling of F-actin polymerization. For example, CR3-mediated phagocytosis is largely regarded as an ITAM-independent process and it requires priming in order to effectively promote phagocytosis [119,120]. This unique receptor activation event has been termed 'outside-in' signaling whereby CR3 changes its conformation intracellularly post extracellular stimulation in order to facilitate a response such as phagocytosis [120]. Unlike what has been shown for FcR-mediated phagocytosis, CR3-mediated phagocytosis is largely independent of Syk recruitment and signaling [2]. F-actin polymerization and localization events during CR3-mediated phagocytosis appears to rely solely on the small GTPase RhoA [113], unlike FcR-mediated phagocytosis, which requires both Rac and Cdc42 [4]. During CR3-mediated phagocytosis, RhoA facilitates F-actin polymerization via two distinct intracellular signaling mechanisms. First, RhoA can induce the activation of Rho kinase causing the phosphorylation and stimulation of myosin II, which is important for the recruitment of Arp 2/3 complex at sites of surface bound targets [2,86,121]. RhoA also facilitates the recruitment of the formin mDia1,

which associates with the microtubule protein CLIP-70, indicating that unlike FcR-mediated phagocytosis, microtubules play an important role in CR3-mediated events [122]. Ultimately these signaling events induce F-actin polymerization at localized sites of bound targets, which facilitates membrane dynamics that are required to accommodate internalization of extracellular targets [2,111,119]. Overall, the characterization of CR3 indicates that the distal stimulation of F-actin polymerization is vital, however this phagocytic process is facilitated by unique and receptor-specific events that are distinguishable from FcR-mediated phagocytosis. This concept is further reinforced in the next section with the descriptions of Dectin-1 and CEACAM3-mediated specific phagocytic events.

2.3.4 Dectin-1 and CEACAM3

Dectin-1 is an ITAM-containing phagocytic receptor-type that recognizes carbohydrate motifs on the surfaces of fungal pathogens [63,123]. Like FcR-mediated phagocytosis, Dectin-1 signals phagocytosis via phosphorylation of a single ITAM-like motif recruitments Syk at sites of receptor-target interactions [2,63,124]. However, since Syk requires both of its SH2 domains to be engaged to be optimally activated, it is necessary that two Dectin-1 receptors dimerize to accommodate Syk recruitment, activation, and downstream signaling [2]. From the initial associations of Syk to Dectin-1, a similar set of signaling events to that of FcR-mediated phagocytosis progresses, with the activation of PI3K, Cdc42, and Rac leading to WAVE2 activation and F-actin polymerization [2]. Similarly, CEACAM3 contains an ITAM-like motif within its CYT region that it uses to stimulate the phagocytic uptake of *Neisseria gonorrhea* in humans [8]. However, CEACAM3 stimulates a novel intracellular signaling mechanism to facilitate F-actin polymerization during the engulfment process. Specifically, CEACAM3 directly recruits Nck to its CYT region, which directly associates with the WAVE2 NPF

complex [3]. Nck and WAVE engagement with CEACAM3 in conjunction with activated Syk, Vav, and Rac directly activates F-actin polymerization leading to the induction of phagocytosis [3,8]. Therefore, compared with other phagocytic receptors, CEACAM3 uses a short-circuited minimal F-actin polymerization mechanism to facilitate the rapid uptake of CEACAM3-bound *Neisseria gonorrhea [3,8]*. Overall, these phagocytic receptor-induced processes reveal convergent and divergent aspects of signaling events that ultimately terminate at the induction of F-actin polymerization during phagocytic processes required for the uptake of various microbial targets.

2.3.5 Efferocytosis

Phagocytes are also important for the removal of dead/dying host cells via a process termed efferocytosis [125,126]. Programmed cell death (PCD) or apoptosis is an important aspect for multicellular organisms as the induced death of old or infected cells is vital for tissue homeostasis [125,126]. During apoptosis, host cells begin to undergo changes in shape including blebbing (cell fragmentation) and become smaller in size, making apoptotic cells easier for phagocytic cells to ingest. [125] This changing of the cellular membrane of apoptotic cells alters the types of molecules found on their surfaces, which serve as ‘eat me’ signals to phagocytes [127]. The most common of these ‘eat me’ signals is phosphatidylserine (PS), which for healthy cells is generally found in the inner leaflet of the plasma membrane making it not readily accessible [125,127]. However, during apoptosis, PS is translocated to the outer leaflet of the plasma membrane where it acts as a signal for initiation of efferocytosis by phagocytes [125,127]. To facilitate efferocytosis, phagocytes must express unique phagocytic receptor-types which can recognize the distinct signatures of apoptotic cells death (e.g. PS exposure) [127]. Examples of these include the PS receptor (PSR), T cell immunoglobulin mucin 1 (TIM-1),

TIM-4, brain specific angiogenesis inhibitor 1 (BAI1), αvβ3, αvβ5, TAM (Tyro3, Axl, MER), and CD300f [125,127]. BAI1 as a phagocytic receptor is restricted to gastric and intestinal phagocytes and induces the uptake of dying cells via the recognition of PS [128] . TIM-1/TIM-4 also bind PS, however TIM-4, unlike TIM-1, has only been shown to bind PS but not to stimulate efferocytosis. [129–131] TAM receptors also bind PS, however they first require the binding of PS to PS-binding proteins GAS6 and Protein S1 (ProS1) to recognize apoptotic cells [125]. Ax1 and Mer are expressed on both macrophages and DCs and elicit the phagocytic uptake of apoptotic bodies by the recognition of PS [125,132,133]. Similar to the TAM receptors, αvβ3 and αvβ5 facilitate efferocytosis uptake of apoptotic cells through first binding to PS-binding proteins MFG-E8, CCN1, GAS6 and ProS1 [125]. Lastly, CD300f recognizes PS but uniquely it can activate and inhibit efferocytosis depending on the cell-type it is expressed by [125,134,135]. Whether or not CD300f acts as an inhibitor or stimulator of efferocytosis is due to variations in the levels of inhibitory molecules like SHP-1/2 across different cell-types [125,134,136]. Another aspect of efferocytosis that differs from microbial phagocytosis is the coordination of multiple receptors in order to effectively undergo the internalization of apoptotic cells. This coordination, termed the tethering and tickling model, requires an individual receptor to facilitate the binding of the apoptotic cell to the surface of the phagocyte (tethering receptor), while another receptor is necessary for the induction of intracellular signaling to promote the actual internalization of the target (tickling receptor) [137]. For example, αvβ3 and αvβ5 facilitate the binding of apoptotic cells to the surface of phagocytes, but alone this interaction does not induce internalization [138]. However, when αvβ3/αvβ5 and PSR are engaged on the surface of a cell, the internalization of apoptotic cells is initiated by the phagocyte [137,138]. This system exists as cells can transiently express PS on the cell surface, and therefore in order to

negate unwanted internalization of healthy cells, efferocytosis requires strong avidity from both the tethering and the tickling receptor to stimulate uptake [137]. Overall, it is the accumulation of these two events that effectively allows phagocytes to remove apoptotic cells from the body.

Imaging studies have shown that the uptake of apoptotic bodies via efferocytosis occurs via a wave-like membranous structure, which extends across one side of the cell and flows across through the extracellular fluid towards the opposing side [139,140], effectively sweeping across the cell to capture and engulf a bound target. This process, similar to FcR-mediated phagocytosis, requires key F-actin polymerization signaling components including small Rac, Cdc42, RhoA, PI3K, and WASP that terminate with the activation of Arp 2/3 complex to facilitate F-actin polymerization [125–127]. Activation of αvβ5 expressed on non-professional phagocytes causes the recruitment of p130, CrkII and Dock180 [137], which triggers Rac GTPases [137] activity suggesting that cell-specific and receptor-specific types of signaling also exist during efferocytosis, as described earlier for the various phagocytic receptor-types. Once an apoptotic body has been internalized, intracellular signaling pathways are activated that are usually associated with the release of anti-inflammatory molecules such as IL-10 and vascular endothelial growth factor (VEGF) [125,141] and reduced generation of pro-inflammatory molecules such as tumor necrosis factor (TNF) and IL-2 [125] to prevent further host cell destruction.

2.5 Phagocytosis in fish

2.5.1 Introduction

Initial studies of phagocytosis in fish were done using *in vivo* assays. This work identified that fish immune cells could facilitate the phagocytic uptake of particles such as bacteria or

opsonized targets, but the identification of the cell-types responsible for these functions was unknown. With the development of new techniques for the isolation and culturing of fish immune cells, *in vitro* assays began to address many of the unanswered questions surrounding phagocytosis and the cell-types which facilitated it in fish. The following sections will discuss the characteristics of phagocytic cell-types in fish and the known but limited information regarding fish phagocytic receptor-types.

2.4.2 Fish macrophages

The development of fish immune cell isolation techniques and the establishment of fish macrophage cell-lines have led to the functional characterization of fish. One of the first fish macrophage culturing techniques developed to assess their functional capabilities was the isolation of pronephros macrophages from both salmon and trout. Specifically, these studies isolated macrophages via density gradient centrifugation [142]. The phagocytic abilities of these cells were the examined by incubations with fixed sheep red blood cells (SRBC), carbon particles, live/dead yeast, and *Vibrio anguillarum* [142]. These studies demonstrated that both salmon and trout macrophages were capable of phagocytic uptake of all the above-mentioned targets, indicating fish macrophages are potent phagocytes. Further development of fish macrophage culturing techniques established long-term macrophage cell lines which were instrumental in the study of fish macrophage functions. Specifically, goldfish kidney macrophages were isolated in a similar manner to the previously mentioned trout macrophages through the isolation from mixed cell cultures by density gradient centrifugation [143]. Combined with the generation of a specialized culture media formula consisting of N-2-hydroxyethylpiperazine-N'-2-ethansulfonic acid (HEPES), 10% FBS and 5% goldfish serum, these cells were capable of surviving extensive periods in culture [143]. These cells were also

shown to have morphological similarities to mammalian macrophages, were capable of living up to two years in culture and were positive for non-specific esterase's (marker for mononuclear phagocytes) [143,144]. Functionally, these cells elicited antimicrobial responses including the phagocytic uptake of SRBC, generation of ROS intermediates and the production of NO [143,144].

The ability to isolate and culture fish macrophages also lead to further characterization of these cell-types in other fish species. For example, salmon head kidney macrophages performed complement-dependent phagocytic uptake of human CR3b and C3bi opsonized latex beads [145], indicating the presence of a complement-like receptor on the surface of these cells. Furthermore, salmon pronephric macrophages phagocytosed yeast generated glucan particles [146] and carp pronephros macrophages internalized bacteria as well as yeast cells, which both induced the generation of ROS production [147]. Channel catfish macrophages also perform phagocytosis and interestingly can do so at temperatures as low as 4°C [148]. This was identified when catfish peritoneal macrophages internalized *E. icaluri* when incubated together at 4°C [149]. This contrasts with what has been observed for the phagocytic abilities of zebrafish macrophages that are unable to internalize *E. ictaluri* at 4°C, suggesting that species-specific regulation of phagocytosis exists among teleost [150]. It has also been shown that fish macrophages can be sub-divided into two phenotypes, M1 and M2 [151,152]. Goldfish M1 macrophages can rapidly kill pathogens through the induction of phagocytosis and the formation of toxic reactive intermediates and the acidification of a phagolysosome [66]. In goldfish, M2 macrophages can be induced through the stimualation of recombinant fish IL-4/IL-3 [153]. Goldfish kidney macrophages stimulated by recombinant fish IL-4/IL-3 were shown to have reduced NO responses and increased mRNA levels of arginase-2 (marker of M2 macrophages in

mammals) post parasite challegenes, suggesting that like in mammals IL-4/IL-3 can facilaite macrophage polarization in fish [154]. Recent studies using translucent zebrafish larvae and whole organism live imaging observed macrophages migrating towards sterile wound sites using thin pseudopod membrane extensions [155]. Once these macrophages reached wound sites they internalized tissue debris, indicating that fish macrophages also play important roles in homeostasis and wound healing [155]. Lastly, like mammalian macrophages, trout macrophages have been shown to potentially play roles in antigen presentation. Specifically, the trout monocyte/macrophage cell-line RTS11 has been shown to contain and assemble the MHC-I peptide loading complex [156]. Further studies using RTS11 have also shown that upon poly I:C or viral exposures a major contributor to the peptide loading complex Tapasin, is significantly upregulated along with the MHC-I heavy chain [156], indicating that antigen presentation capabilities of macrophages likely exist in fish. This concept is further reinforced by studies involving melano-macrophages in catfish. Melano-macrophages are found in clusters in the spleen and kidney of catfish [157], which are thought to represent the early forms of germinal centers found in mammals. Melano-macrophages have the capability of retaining antigen on or near their surfaces for long periods of time following vacation [157], indicating their abilities to act as APC. Taken together, all these discoveries have led to the conclusion that macrophages in fish can facilitate the same fundamental immune functions as they do in mammals.

2.4.3 Fish neutrophils

Neutrophils represent one of the first immune cell-types to migrate towards sites of infections and are armed with many antimicrobial capabilities [35]. Their functional roles are similar to those of macrophages, which includes recognition, internalization, and destruction of invading microbes [35]. Neutrophils also have cell-specific antimicrobial mechanisms such

degranulation and the release of neutrophil extracellular traps (NETs) [158], which facilitate extracellular killing of microbes. NETs contain nuclear DNA filaments along with granular proteins such as elastase that are expelled from the intracellular space of the cell acting as a potent antimicrobial substance which facilitates the degradation of virulence factors, direct killing bacteria, as well as restricting microbial dissemination during infection [35]. The release of NETs is stimulated by the activation of neutrophils by pathogens or pathogen related molecules, which induces the break down of the plasma membrane allowing for the release of its intracellular components, causing pathogens to be trapped in the NETs and within a localized area of antimicrobial molecules [158].

Recent culturing techniques have been able to generate long-term primary kidney-derived neutrophil-like cells from goldfish [159]. These cells stained positive for sudan black and acid phosphatase (neutrophil markers), expressed myeloperoxidase (MPO), and performed degranulation and respiratory burst when exogenously stimulated with mitogens or in the presence of pathogens (zymosan, *A.salmonicida*) [159,160]. Moreover, when exposed to live or heat killed *Mycobacterium marinum*, gold fish neutrophils exhibited phagocytic abilities, increased mRNA levels of pro-inflammatory cytokines including IL-1β1, IL-1β2, TNFα-1 and TNFα-2, and significant increases in their production of ROS [160]. Taken together these studies identified that fish neutrophils facilitate antimicrobial responses akin to those attributed to mammalian neutrophils. Continued studies of gold fish neutrophils also identified their abilities to facilitate the phagocytic uptake of apoptotic bodies [37]. In these studies, activated goldfish neutrophils, but not activated mouse neutrophils, were capable of the phagocytic uptake of apoptotic bodies [37]. The internalization of apoptotic bodies by goldfish neutrophils generated reduced ROS production, suggesting fish neutrophilic roles in the resolution phase of

inflammation [37]. This was further identified *in vivo* when goldfish neutrophils were shown to participate in both pro- and anti-inflammatory responses. After injection with zymosan, neutrophils were isolated during the pro-inflammatory phase and the resolution phase of the infection [36]. Neutrophils isolated during the pro-inflammatory phase demonstrated neutrophilic antimicrobial responses such as respiratory burst and the release of pro-inflammatory molecules such as leukotriene B(4) [36]. Those neutrophils isolated during the resolving phase of the infection had reduced respiratory activity and released anti-inflammatory molecules such as lipoxin A(4) [36], suggesting that fish neutrophils are important at both the initiaton and resolution stages of an inflammatory response. This concept was reinforced by zebrafish *in vivo* studies through whole organism live imaging which demonstrated zebrafish neutrophils migrating away from sites of inflammation during the resolution phase of infection [39]. These neutrophils had an activated-state morphology and when tested against a secondary infection of *Staphylococcus aureus* were capable of mounting effective antimicrobial responses, indicating that experienced neutrophils, which migrate back to circulation do not have altered cellular behaviour [39]. Goldfish neutrophils can also facilitate protection against *Aeromonas veronii* in both *in vivo* and *in vitro* [38]. This study identified that post *Aeromonas veronii* infection, neutrophils were important for the removal of bacteria infected macrophages which had died due to infection [38]. Interestingly, these neutrophils were also capable of generating antimicrobial responses such as ROS production after infected macrophage uptake, indicating that the phagocytic uptake of infected dead/dying cells maintains the pro-inflammatory state of the neutrophils instead of switching to an anti-inflammatory role [38].

Aside from goldfish, other fish species neutrophils have been functionally characterized. For example, trout neutrophils can internalize *Staphylococcus aureus* over a range of

temperatures [161] and catfish neutrophils have been shown to phagocytose *Ewardsiella ictalurid*, *Aeremonas hydrophilla*, and *Micrococcus luteus* but not *Ewardsiella tarda* [162,163]. During phagocytosis of these bacteria, catfish neutrophils facilitated extracellular microbe killing through the release of antimicrobial complexes into their surrounding environment [162]. Continued studies of catfish neutrophils showed that similar to catfish macrophages, these cells performed phagocytic responses at reduced temperatures. Specifically, it was demonstrated that catfish anterior kidney derived neutrophils incubated at both 18°C and 10°C were capable of phagocytosing *Aeromonas hydrophilia* [164]. The ability for fish immune cells to facilitate defense mechanisms like phagocytosis at reduced temperatures likely is an evolutionary adaption to the diversity in environmental temperatures that fish inhabit. This also suggests that fish have adapted intracellular signaling mechanisms to generate F-actin polymerization events to induce the phagocytic uptake of extracellular microbes over a wide-range of environmental temperatures.

As mentioned above, one cell-specific response of neutrophils is the release of antimicrobial NETs into the surrounding extracellular environment. Recent studies of zebrafish, fathead minnow, and carp have identified that like mammalian neutrophils, fish neutrophils can clearly facilite the release of antimicrobial NETs. For example, kidney-derived zebrafish neutrophils were shown to generate MPO and release NETs upon stimulation with ionophore, phorbol myristate acetate (PMA), and β-glucan [40]. These NETs were identified to contain DNA fibers along with intracellular granular proteins, similar to that identified for NETs in mammals [40]. In carp, NETs were shown to be released by neutrophils when stimulated with bacteria, fungi or viral pathogens, which also consisted of DNA fibers, MPO, and multiple antimicrobial proteases [165]. Neutrophils isolated from the kidney of fathead minnows were

also shown to release NETs post stimulation with PMA, β-glucan, and zymosan [166]. As these studies show, it is apparent that neutrophils in fish can elicit a range of potent pro- and anti-inflammatory processes.

2.4.5 Fish Dendritic cells

DCs in mammals play a pivotal role in bridging the innate and adaptive immune systems through the phagocytic uptake and subsequent presentation of antigens to lymphocytes [167]. In mammals, DCs have distinct cellular characteristics which include; (i) cellular morphology consisting of membranous spines; (ii) high mobility; and, (iii) lack of adhesion to substrates [65,168,169]. Through the utilization of mammalian DC cell culturing techniques and conserved aspects of DC morphology/behavior, DC-like cells from trout hematopoietic tissues were discovered [170]. These were identified as DC-like due to similar cellular characteristics to those associated with mammalian DCs such as non-adherent properties and having a tree branch-like morphology. Trout DCs were also shown to express MHC-II on their surfaces and therefore it was suspected that like mammalian DCs [171], fish DCs may also facilitate antigen presentation. The ability of fish DCs to act as APC was identified when DCs from zebrafish immunized against keyhole limpet hemocyanin (KLH) were incubated with native T cells [172]. In this study, these T cells experienced increased levels of proliferation that could be modulated in an antigen-dependent manner [172]. These studies demonstrate that the evolution of DC antigen presentation to activate adaptive immune responses emerged early on in vertebrate evolution. Further characterization of trout and salmon DCs demonstrated their capabilities to phagocytosis trout serum-opsonized beads, expressed the mammalian DC cell marker CD207 and could be activated via toll-like receptor ligands [65], all of which are characteristics of mammalian DCs.

Overall, it appears that DC exist within fish and like DC in mammals they play important roles in the phagocytosis and presentation of antigens.

2.4.6 Fish Thrombocytes

Thrombocytes are nucleated hemostatic blood cells in non-mammals and are the functional equivalents to mammalian platelets [65]. In mammals' platelets facilitate a variety of cellular roles including a central role in inflammatory and immune responses, including phagocytosis [173]. In fish, some evidence suggests that these cells can facilitate immunological processes such as phagocytosis. Specifically, it was shown that thrombocytes isolated from carp were capable of ingesting live bacteria and carp serum-opsonized latex beads both *in vivo* and *in vitro* [174]. The internalization of bacteria by carp thrombocytes induced intracellular killing responses determined by bacterial colony formation post thrombocyte lysing, suggesting carp thrombocytes are capable of antibacterial responses [174]. Further studies in other fish species are needed to confirm if function of thrombocytes is conserved across fish species.

2.4.7 Phagocytic B cells in fish

Up until the early21st century the concept that B cells had phagocytic properties was not identified. This paradigm was changed in 2006 when phagocytic IgM^{+}B cell populations in both trout and catfish were identified [14]. Specifically, these cells were shown to phagocytose both bacteria and salmon IgM opsonized-beads *in vitro* [14]. Initial studies identified small cells in trout PBLs which contained phagocytosed trout-opsonized beads [14]. This led to the use of a mAb which specifically recognized IgM on trout B cells and not serum IgM. These small cells, which internalized opsonized beads stained positive for the B cell specific IgM antibody, indicating that these were B cells which facilitated a phagocytic response [14]. Further tests

using bacteria showed that the internalization of bacteria coincided with the IgM^{+}B cells activating degradation pathways which facilitated bacterial killing [14], indicating for the first time that subsets of B cells could perform phagocytosis. A similar study was conducted in trout examining IgT+B cells. Like trout IgM+ B cells, IgT+B cells could also facilitate the phagocytic uptake of IgT-opsonized targets [175]. These studies also concluded that IgT+ B cells when incubated with bacteria can facilitate intracellular killing, indicating the presence of antibody-dependent receptor-mediated phagocytosis in fish [175]. Interestingly, zebrafish phagocytic B cells have also been shown capable of performing antigen presentation. Specifically, it was shown that phagocytic B cells presented both soluble antigens and bacterial particles to naïve CD4(+) T cells causing T cell activation [176]. This is a similar process identified for phagocytic APC B cell population in mammals, known as B-1 cells [177]. It is likely that similar APC functions of phagocytic B cells in zebrafish are conserved across fish species, however more studies will need to be conducted to confirm this notion. Based on these studies it is clear that a phagocytic antibody-dependent pathway is utilized by fish phagocytes, however the receptor(s) that facilaite this response remains unclear. Overall, the identification of phagocytic B cells in fish lead to the discovery of a new subset of immune cell-types which exist across the vertebrate lineage that play important roles in both antimicrobial responses as well as the stimulation of the adaptive immune system.

2.5 Phagocytic receptors in fish

Identification and characterization of phagocytic receptors in fish is limited. In the next sections I will discuss current information surrounding what is known regarding fish phagocytic receptor-types.

2.5.1 Evidence for a CR3-like receptor in fish

As mention previously, complement receptors facilitate the phagocytic uptake of C3 and C3bi-osponzied targets. To date, no functional homolog of the mammalian CR3 receptor has been identified in fish, however evidence does suggest that they exist. Specifically, it has been shown that human complement proteins C3b and C3bi can bind salmon macrophages directly [145]. It has also been shown that salmon macrophages, when incubated with targets coated in human C3b and C3bi or salmon serum, are readily phagocytosed, suggesting that a complement-like receptor(s) is/are expressed on the surface of salmon macrophages [145]. Further studies showed that carp C3-coated beads are phagocytosed by carp peritoneal neutrophils [178]. Treatment of carp neutrophils with the serine protease trypsin to remove surface-bound receptors significantly reduced the phagocytic uptake of C3-opsonized targets; further suggesting the presence of C3 receptors on the surface of fish phagocytes [178]. Evidence for the presence of a CR3-like receptor has also come from studies in trout, which identified a CR3-like sequence [179]. Whether or not this protein facilitates CR3-mediated phagocytosis remains to be determined. Therefore, based on these studies it is likely that a CR3-like receptor is expressed and utilized by fish phagocytes.

2.5.2 Evidence for FcR-like receptor(s) in fish

The induction of phagocytosis in an antibody-dependent manner is facilitated by the IgSF receptor family of FcRs in mammals. In fish, multiple antibody-types have been identified including IgM, IgD and the fish specific IgT/Z [180]. Evidence for the presence of antibody-associating receptors in fish aside from the previous work mentioned on phagocytic B cells is

demonstrated by the description of antibody-dependent cell-mediated cytotoxicity (ADCC) by catfish NK-like cells [181]. Specifically, catfish PBLs were identified to have sub populations of cells which were positive for F and G IgL chain isotypes [181], suggestive that these cells could passively acquire serum derived IgM through an unknown FcμR. Cells which were positive for F and G IgL isotypes were capable facilitating the spontaneous killing of allogenic targets [181]. Long-term viable alloantigen stimulated PBLs were further shown to contain both IgM^+ and IgM^- cell populations that expressed a catfish homolog of the FcεR chain [181]. Co-immunoprecipitation studies from lysates of NK-like IgM+ cells identified the presence of a putative FcμR [181]. Lastly, removal of IgM from NK-like IgM+ cells, which were subsequently given an anti-hapten antibody, were capable of killing hapten-expressing targets but unable to kill using a non-specific IgM control [181]. These results indicate that a putative FcμR is likely expressed by these NK-like cells for ADCC. Other studies in catfish identified a putative FcR homolog, termed IpFcR. This was identified through the mining of catfish expressed sequence tag (EST) databases, which used mammalian FcR sequences as a query [182]. IpFcR is phylogenetically and structurally related to mammalian FcRs [182]. Qualitative PCR and Northern blot analysis identified that IpFcR is primarily expressed in IgM- catfish leukocytes isolated from lymphoid kidney tissues [182]. When expressed in insect cell lines, IpFcR was generated as a secreted protein and as a recombinant protein it bound catfish IgM [182]. Although it appears that FcRs exist within teleost, their functional roles associated with antibody-dependent effector responses remains unclear.

2.5.3 Mannose receptor (MR) in fish

In mammals, the mannose receptor (MR) is a well-characterized macrophage-expressed phagocytic receptor [86,183]. As its name suggests, mammalian MR receptor recognizes

microbes (bacteria, yeast, and select protozoa) through the detection of carbohydrates such as mannose and fructose in a Ca^{2+}dependent manner [183,184]. Recent studies in the blunt snout bream (*Megalobrama amblycephala*) identified a putative MR receptor (termed MaMR) [69]. Functional studies identified that the blocking of MaMR via antibodies on the surface of blunt snout bream macrophages inhibited the phagocytic uptake of GFP-expressing *E. coli* [69]. Further studies demonstrated that the uptake of the *E. coli* was Ca^{2+} dependent [69], suggesting that MR function and activity has been conserved between fish and mammals.

2.5.4 MARCO receptors in fish

In mammals, the macrophage receptor with collagenous structure (MARCO) acts as a PRR receptor, which is important for the recognition and induction of phagocytosis for a variety of pathogens including mycobacterium, gram-positive, and gram-negative bacteria [6]. Recently, two variants of the scavenger receptor MARCO in rainbow trout were identified (rtMARCO-1 and rtMARCO-2) [185]. When rtMARCO-1 and rtMARCO-2 were overexpressed in fish CHSE-214 cells, a cell line with known low bacterial binding capabilities, both receptors showed significant binding capabilities of both gram-positive and gram-negative bacteria [185]. This response was specific to bacteria, as no binding was identified for rtMARCO-expressing cells that were treated with either zymosan or dsRNA [185]. Interestingly, the expression of both rtMARCO-1 and rtMARCO-2 in CHSE-214 cells appeared to have altered cellular morphology of some transfected cells [185]. Specifically, it was shown that these cells generated F-actin protrusions or spikes from the cell surface when expressing rtMARCOs [185]. Although the function of these protrusions was not identified, it could possibly be that the expression of rtMARCOs may influence the membrane dynamics of the cell for extracellular target binding through protrusion-target interactions [185]; an early stage event important in phagocytosis.

Further studies of MARCO in ayu fish (*Plecoglossus altivelis)* (termed PaMARCO) showed both binding and phagocytic uptake of gram-positive and gram-negative bacterial strains indicating that similar to mammalian MARCO [186], this fish receptor plays an important role in the removal of bacterial pathogens.

2.6 Channel catfish leukocyte-immune type receptors (IpLITRs)

2.6.1 Introduction

There is a large diversity of receptor-types found within the IgSF and these interact with a variety of ligands consisting of microbial and viral antigens, host derived proteins (e.g. antibodies, complement, adhesion molecules), and altered or damaged host cells (e.g. viral-infected and necrotic cells) [187,188]. Often IgSF receptor-types are members of large gene families, which are highly polymorphic and polygenic [187]. The expansion of germline encoded receptor families is likely due to rapidly evolving ligands or pathogen products that these proteins are known to engage. IgSF receptors influence a variety of immunological responses such as phagocytosis, antibody-dependent cytotoxicity, antigen presentation, degranulation, cytokine production, and cytotoxicity [98,189]. Structurally, IgSF immunoregulatory receptor-types consist of extracellular ligand-binding regions containing one or more Ig-like domains, a hydrophobic TM segment, and a variable length CYT region [98,189]. These CYT regions often contain one or more tyrosine residues, which following phosphorylation facilitates intracellular signing events that regulator a vast array of immune cell effector responses such as those mentioned above [98,189]. The number of tyrosine residues situated within the CYT often dictates the signaling possibilities of immunoregulatory receptor-types and can vary between individual receptors. For example, inhibitory immunoregulatory receptor-types abrogate immune cell functions through recruitment of cellular phosphatases to ITIMs, whereas stimulatory

immunoregulatory receptor-types often promote immune cell effector responses via kinases-driven signaling initiated through ITAMs [102,117]. Overall, the activation of an immune cell is regulated through a delicate balance of stimulatory and inhibitory signaling pathways [102,117]. In teleost, many large IgSF receptor families have been recently identified, but only a few have been functionally characterized [187]. The next sections will discuss one of these major IgSF receptor, the channel catfish (*Ictalurus punctatus*) leukocyte immune-type receptors (IpLITRs).

2.6.2 Overview of IpLITRs

IpLITRs were first identified in the channel catfish (*Ictalurus punctatus*) and share distant phylogenetic relationships with numerous other IgSF families in mammals. This includes the previously mentioned FcRs, FcR-like proteins (FcRL), and a variety of NK receptors (NKRs) found within the leukocyte receptor complex (LRC) [190]. The IpLITR gene complex is polymorphic, polygenic, and is separated between multiple homologous loci [190]. Initial IpLITR prototypes were identified to have variable numbers of extracellular C2-like Ig domains, a charged or uncharged TM segment, and either long or short CYT regions that in some instances contained tyrosine-based signaling motifs (e.g. ITIMs and ITAMs) [190]. In general, IpLITRs that contain short CYT and a positively charged TM segment were predicted to be stimulatory in nature, as the positively charged TM of immunoregulatory receptors facilitate associations with stimulatory ITAM adaptor proteins as described previously for FcRs [190]. IpLITRs with long CYT regions were identified to contain inhibitory ITIMs and/or ITSMs, indicating that these receptor-types may abrogate immune cell responses [190]. In the following sections I will describe recent work associated with the functional characterization of stimulatory and inhibitory IpLITR-types as a first step towards understanding their overall immunoregulatory potentials.

2.6.3 Stimulatory IpLITRs

IpLITR 2.6b is a putative stimulatory receptor containing a positively charged lysine residue and a short CYT region lacking tyrosine-based signaling motifs that was predicted to require the recruitment of intracellular adaptor proteins for surface expression and to facilitate immune responses [190,191]. This was tested using HEK 293T cells co-transfected with hemagglutinin (HA)-tagged IpLITR 2.6b and results showed the co-immunoprecipitation of IpLITR 2.6b with the catfish ITAM-containing IpFcRγ, IpFcRγ-L, and IpCD3ζ-L signaling adaptors, but not with IpDAP12 [191]. The engagement of IpLITR 2.6b with both IpFcRγ-L and IpFcRγ also coincided with increased levels of surface expression, but not when co-expressed with IpCD3ζ-L, IpDAP10 or IpDAP12 [191]. Site-directed mutagenesis studies converting the lysine residue within the TM segments of IpLITR 2.6b to arginine or alanine residues did not affect surface expression or adaptor recruitment of IpLITR 2.6b, indicating that a charged residue within its TM was not required for receptor-signaling adaptor engagement [191]. Additionally, the neutralization of the TM segment of IpLITR 2.6b caused the acquisition of binding of IpLITR DAP12 [191]. These results suggested that unlike what is characterized for immunoregulatory receptor-adaptor molecule associations in mammals, a positively charged TM segment is not always required to facilitate these interactions. The functional activities of IpLITR 2.6b associated with IpFcRγ-L were further examined using an N-terminal HA-tagged chimeric receptor construct consisting of the extracellular domains of IpLITR 2.6b fused with the TM segment and ITAM-containing CYT region of IpFcRγ-L (Fig 2.1; left side) [10]. This construct was transfected and stably-expressed in the rat basophilic leukemia (RBL-2H3) cell line, where it then could be activated by αHA mAbs. This led to the

identification that IpLITR 2.6b/IpFcRγ-L activated intracellular signaling and was capable of stimulating degranulation in RBL-2H3 cells [10]. IpLITR 2.6b/IpFcRγ-L was further examined using a mitogen activated protein kinase (MAPK) signaling array and a cytokine secretion profile [10]. Crosslinking of IpLITR 2.6b/IpFcRγ-L using αHA mAb increased phosphorylation of extracellular regulated-kinase (ERK1/2), glycogen synthase kinase (GSK)-3α/β, RSK1 (ribosomal S6 kinase-1), cAMP-response element binding protein (CREB), c-jun N-terminal kinase (JNK), extracellular signal-regulated kinase kinase (MEK)6, mitogen-stress -activated protein kinase (MSK)2, p38δ, and protein kinase b (Akt2) [10]. Furthermore, pharmacological inhibition of PI3K, MAPK kinase (MEK)1/2, and protein kinase C (PKC) caused significant reduction in IpLITR 2.6b/IpFcRγ-L-mediated degranulation [10]. A cytokine profiling assay also showed that cross-linked IpLITR 2.6b/IpFcRγ-L facilitated the secretion of multiple cytokines such as IL-3, IL-4, IL-6, and TNF-α [11]. IpLITR 2.6b/IpFcRγ-L phagocytic abilities were then examined using yellow-green (YG) 4.5 μm αHA mAb-opsonized beads that showed for the first time the phagocytic activity potential of IpLITR 2.6b/IpFcRγ-L-expressing cells [11]. IpLITR 2.6b/IpFcRγ-L-mediated phagocytosis was dependent on both F-actin polymerization and extracellular Ca^{2+} [11]. Overall, these studies demonstrated that IpLITR 2.6b in association with an ITAM containing adaptor protein stimulated the activation of several innate immune cell effector responses, including phagocytosis.

2.6.4 Inhibitory IpLITRs

Initial studies of inhibitory IpLITR-types were performed to determine if these receptors recruited inhibitory cellular phosphatases, specifically SHP-1 and/or SHP-2 [13]. To do this, the inhibitory prototypes, IpLITR 1.1b and IpLITR 1.2a, were expressed as chimeric

constructs containing the extracellular regions and TM segments of the human NK cell receptor KIR2DL3 fused with the tyrosine-containing CYT regions of the IpLITR 1.1b or IpLITR 1.2a [13]. The KIR2DL3 extracellular domains were specifically chosen for these studies as this human inhibitory receptor is known to bind human leukocyte antigen (HLA)-Cw3 found on the target cells used in killing assays [13]. KIR_{ED}-LITR receptor constructs were first examined using transient expression experiments in HEK 293T cells. Post tyrosine phosphorylation, the CYT segments of IpLITR 1.1b and IpLITR 1.2a recruited both SHP-1 and SHP-2 to their CYT ITIMs. IpLITR 1.1b also had a unique tyrosine containing TM proximal CYT region lacking classic inhibitory or stimulatory tyrosine-based signaling motifs that did not bind SHP-1 or SHP-2 [13]. To examine IpLITR-mediated inhibitory signaling these constructions were transfected into mammalian NK cells and incubated with HLA-Cw3-positive targets to activate the chimeric proteins. These experiments identified that IpLITR-mediated signaling events were capable of manipulating cytotoxic activities and that the engagement of IpLITRs facilitated the abrogation of NK cell-mediated killing responses [12]. Inhibitory functions of IpLITRs were additionally examined using a vaccinia virus system to express KIR_{ED}-LITR $1.2a_{CYT}$ and KIR_{ED}-LITR $1.1b_{CYT}$ in mouse spleen-derived cytotoxic lymphocytes to identify directly IpLITR-induced inhibitory signaling associated with both IpLITR 1.1b and IpLITR 1.2a [12]. These experiments showed that IpLITR 1.2a and IpLITR 1.1b can both facilitate the inhibition of NK cytotoxicity. Specifically, it was shown that IpLITR 1.2a-mediated inhibition occurred through a SHP-dependent mechanism [12]. Surprisingly, the inhibitory ability of IpLITR 1.1b persisted when co-expressed with an inactivate SHP-1 recombinant protein [12], indicating that IpLITR 1.1b's inhibitory response was not solely facilitated by SHP-1 phosphatase activity.

The IpLITR 1.1b (Fig 2.1; right side) CYT region contains six tyrosine residues, among its membrane proximal (Y_{433}, Y_{453}, and Y_{463}) and distal (Y_{477}, Y_{499}, and Y_{503}) regions [13]. Specifically, the CYT distal region contains two ITIMs located at Y^{477} and Y^{499} and one overlapping ITSM (Y_{503}) (Fig 2.1; right side). When tested as a separate construct, IpLITR 1.1b CYT_{DISTAL} induced effective inhibitory activity that was dependent on recruitment of SHP-1 [12]. A construct encoding only the proximal region of IpLITR 1.1b CYT was also generated and when tested it unexpectedly also abrogated NK cell-mediated killing responses in the absence of any ITIM or ITSM motifs [12]. This study indicated that a SHP-independent inhibitory pathway was engaged by IpLITR 1.1b that likely required a tyrosine within its proximal region. Further analysis of IpLITR 1.1b's proximal region didentified an amino acid sequence, which closely resembled the consensus-binding motif for c-terminal Src kinase (Csk) [12]. In mammals, Csk facilitates inhibition of Src-mediated intracellular signaling causing the downregulation of cellular responses [12]. Using site-directed mutagenesis and co-immunoprecipitation assays, Csk was shown to bind IpLITR 1.1b [12], suggesting it as a possible reason for the ITIM-independent inhibitory activity observed for IpLITR 1.1b.

2.6.5 IpLITR 1.1b functional plasticity

The complexity of IpLITR 1.1b, aside from its unique ability to facilitate inhibition using two distinct signaling mechanisms, was further demonstrated when it was identified as an effective stimulatory of the phagocytic response. This was shown by the stable expression of an N-terminal HA-tagged construct of IpLITR 1.1b in rat basophilic leukemia (RBL)-2H3 cells [11]. This suggested that the differential recruitment of signaling mediators by IpLITR 1.1b in different cell-types (e.g. lymphoid vs. myeloid) may facilitate a context-dependent plasticity during the receptor-mediated control of cellular processes. It was further demonstrated that

activated IpLITR 1.1b induced phosphorylation of ERK1/2 and Akt with distinct kinetics from those observed for IpLITR 2.6b/IpFcRγ-L and that its phagocytic response was not dependent on the presence of extracellular Ca^{2+} [11]. Generation of a truncated CYT IpLITR 1.1b construct showed that although IpLITR 1.1b remained expressed on the cell surface, it did not phagocytose target beads, indicating that the signal to initiate phagocytosis was induced by its tyrosine-containing CYT region [11].

IpLITR 1.1b-mediated phagocytosis was further characterized using imaging flow cytometry-based phagocytic assays and glutathione-s-transferase (GST) pulldowns [192]. These studies were performed to examine what portion(s) of the IpLITR 1.1b CYT region were important for generating signals required for inducing phagocytosis. To test whether signaling from the IpLITR 1.1b CYT proximal and distal segments also differentially regulated phagocytosis, as was observed for the previously mentioned NK killing experiments, expression constructs were generated encoding these CYT regions and their phagocytic activity and biochemical recruitment potential were independently examined [192]. This was done via expression of HA-tagged IpLITR constructs in the non-myeloid AD293 cell line and these studies supported that teleost receptors activate distinct phagocytic modes for target acquisition and engulfment [192]. Specifically, AD293 stables expressing IpLITRs with an ITAM-containing CYT region completely engulfed αHA mAb-coated beads while those expressing the full-length CYT region of IpLITR 1.1b displayed a capture and tethering phenotypic response with an overall reduced ability to fully engulf beads [192]. Two additional constructs containing IpLITR 1.1b CYT proximal or distal segments only were also examined. These constructs both showed target capture and engulfment responses akin to the originally described IpLITR

1.1b wild-type (WT) phagocytic response [192]. These results suggested that IpLITR 1.1b may use two distinct signaling mechanisms for the initiation of the phagocytic process [192].

This hypothesis was further examined through qualitative assessment of the recruitment capabilities of various CYT regions of IpLITRs in GST pulldown assays. In these studies, phosphorylated constructs were generated containing a GST domain fused to different CYT regions to examine possible intracellular-CYT binding interactions of IpLITRs [192]. Specifically, GST-expressing constructs were generated containing the CYT of IpLITR 1.1b wild type (GST-IpLITR-WT), IpLITR 1.1b proximal (GST-IpLITR 1.1b-PRX), IpLITR 1.1b distal (GST-IpLITR 1.1b-DST), IpFcRγ-L (GST-ITAM) and a construct consisting of the human CEACAM3 CYT (GST-CEACAM3) [192]. These constructs were used as 'bait' recombinant proteins in AD293 cellular lysates expressing C-terminal FLAG-tagged versions of various SH2-domain containing 'prey' signaling molecules [192]. After pulldowns were conducted, αFLAG mAb Western blots were performed to identify which constructs associated with each of the tested signaling proteins which included SHP2, Csk, Syk, Grb2, Nck, PI3K, p85α, and Vav1/3 [192]. These studies showed that GST-IpLITR WT associated with Csk, Syk, Grb2, Nck, SHP2, PI3K, p85α and Vav1 [192]. In comparison, GST-IpLITR 1.1b-PRX did not recruit SHP-2, Syk or Vav3 but did associate with Csk, Grb2, Nck and Vav1 [192]. Furthermore, GST-IpLITR 1.1b-DST recruited SHP-2, Syk, PI3K and p85α only [192]. The GST-ITAM construct recruited Syk, PI3K, p85α and Vav1 and finally, the positive control for Nck binding GST-CEACAM3 interacted with Nck as wel las PI3K, p85α, and both Vav1/3 [192]. Taken together, these studies supported hypothesis that IpLITR 1.1b has a unique ability to differential recruit signaling molecules to its CYT regions that may affect its control of various effector responses. This work also showed that both the proximal and distal regions of IpLITR 1.1b CYT can independently

activate the phagocytic process and identified some potential signaling molecules that may be associated with its activity.

Overall these studies revealed that IpLITRs have potent immunoregulatory potentials for the control of selected immune cell effector responses and that IpLITR 1.1b is a versatile immunoregulatory protein with both inhibitory and stimulatory abilities via distinct CYT region-mediated mechanisms. Furthermore, the differential recruitment capabilities of each individual region of IpLITR 1.1b CYT region for key intracellular signaling molecules associated with F-actin polymerization, indicates that distinct signaling mechanisms may facilitate IpLITR 1.1b-mediated phagocytosis. To further examine the control of phagocytosis by IpLITR 1.1b, the research aims of my thesis were to; (1) further characterize IpLITR 1.1b's ITAM-independent response through pharmacological profiling and kinetic studies; (2) identify that IpLITR 1.1b-expression was fundamental to its unique capture and engulfment phenotype; (3) examine IpLITR 1.1b selective induction of F-actin dynamics; and (4) determine the recruitment of hypothesized intracellular signaling molecules to IpLITR 1.1b during its induced phagocytic events. The examination of alternative signaling mechanisms associated with F-actin polymerization and membrane dynamics offers novel insights into the regulation of phagocytosis overall. Morever, this research expands our understanding of how immunoregulatory receptors network with intracellular signaling to promote immunological responses across vertebrate evolution.

FIGURE 2.1

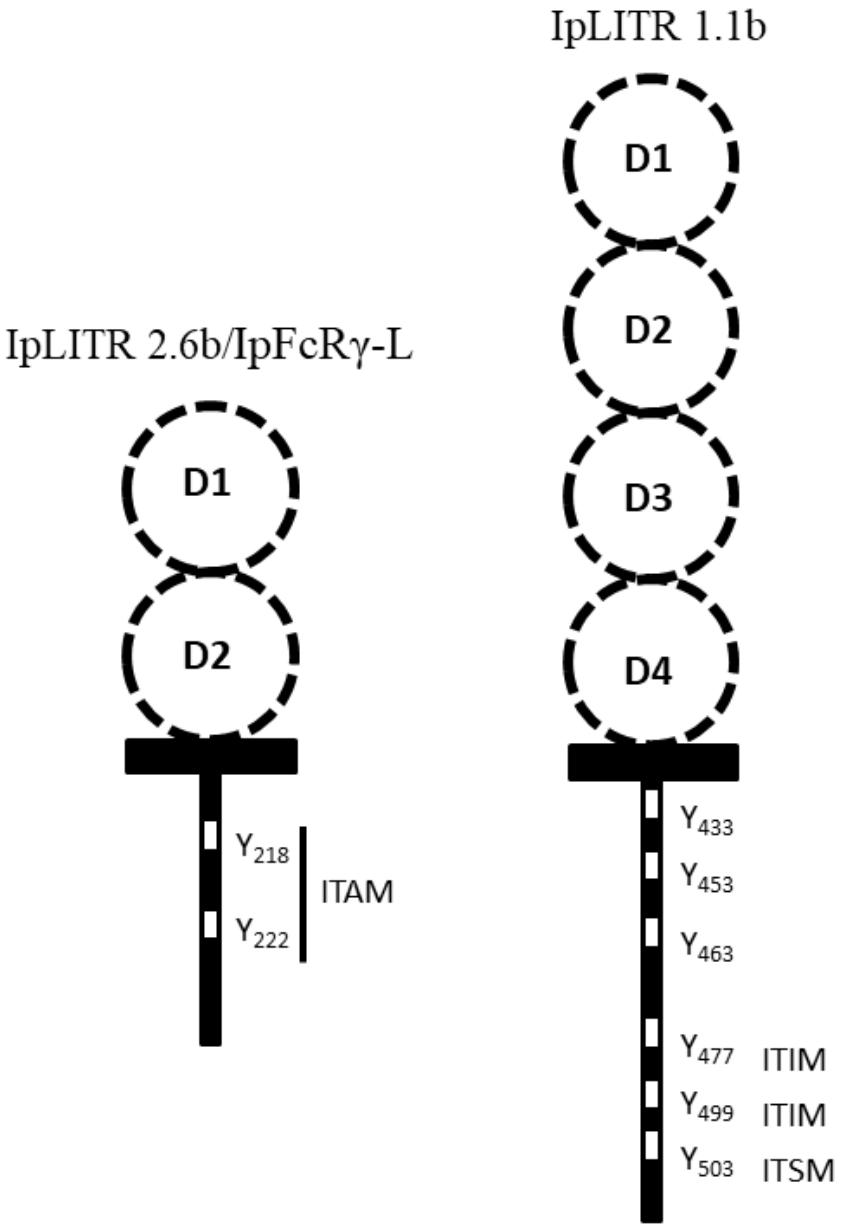
IpLITR 1.1b
D1
D2
D3
D4
Y433
Y453
Y463
Y477 ITIM
Y499 ITIM
Y503 ITSM
IpLITR 2.6b/IpFcRγ-L
D1
D2
Y218
Y222
ITAM

FIGURE 2.1 Schematic of IpLITR 2.6b/IpFcRγ-L and IpLITR 1.1b. Representative diagrams of IpLITR 2.6b/IpFcRγ-L (left) and IpLITR 1.1b (right). IpLITR 2.6b/IpFcRγ-L (left) contains two extracellular domains (D1 D2) and is a chimeric protein fused with the channel catfish adaptor protein IpFcRγ-L which contains an ITAM motif. IpLITR 1.1b (right) contains four extracellular domains (D1-D4) and has a long CYT which contains two ITIM motifs and an ITSM motif. For experiments conducted in RBL-2H3 cells both IpLITR 2.6b/IpFcRγ-L and IpLITR 1.1b were expressed with the addition of a HA-epitope tag located on the D1 of each receptor in order to induce receptor activation for functional and mechanistic studies.

CHAPTER III
MATERIALS AND METHODS

3. Material and Methods

3.1 Cells, Pharmacological Drugs and Antibodies

3.1.1 Cells

Rat basophilic leukemia-2H3 (RBL-2H3) cells were grown at 37°C and 5% CO_2 in minimal essential medium (MEM) supplemented with 2mM L-glutamine (Life sciences), 100 units/mL penicillin (Life sciences), 100 mg/mL streptomycin (Life Sciences) and 10% heat-inactivated fetal bovine serum (Hyclone).

3.1.2 Pharmacological Drugs

The following drugs were used in this thesis: Latrunculin B (Calbiochem), Akt Inhib VII (Calbiochem), Bis II (Calbiochem), ML 141 (Tocris Bioscience), PP2 (Tocris Bioscience), LY294002 (Tocris Bioscience), EHT 1864 (Tocris Bioscience), ER 27391 (Tocris Bioscience), U0126 (Tocris Bioscience), KB SRC4 (Tocris Bioscience), nocodazole (Tocris Bioscience), GSK 233470 (Tocris Bioscience), Go6976 (EMD Biosciences), and Wortmannin (Sigma-Aldrich)

3.1.3 Antibodies

The following antibodies were used in this thesis: αHA mAb IgG3 clone HA. C5 (Abcam), αIgG3 goat αmouse (Abcam), goat αmouse IgG (H+L)-PE pAb (Jackson Immuno Research), HRP-conjugated goat αHA pAb (GenSript Corp), HRP-conjugated streptavidin antibody (Sigma-Aldrich), rabbit αNck mAb (Cell Signaling Technologies), rabbit α-pSyk mAb (Cell Signaling Technologies).

3.2 Cloning and expression in RBL-2H3 cells

3.2.1 Transfections of IpLITRs in RBL-2H3 cells

Transfection and selection of RBL-2H3 cells stably expressing N-terminal (extracellular domains) hemagglutinin (HA)-tagged IpLITRs has already been described in detail within previous work [11]. pDISIPLAY IpLITR 2.6b/FcRγ-L is a chimeric receptor which encodes two extracellular Ig-like domains (GenBank Accession: ABI23577) fused with the endogenously associated immunoreceptor tyrosine-based activation motif (ITAM)-containing signaling adaptor IpFcRγ-L. IpLITR 1.1b (GenBank Accession: ABI16050) encodes the full length TS32.17 L1.1b sequence containing a cytoplasmic tail (CYT) that contains multiple immunoreceptor tyrosine-based inhibitory motifs (ITIMs). Xfect (Takarabio) transfected RBL-2H3 cells were grown at 37°C and 5% CO_2 in complete culture media (minimal essential media (MEM) with Earl's balance salt solution (GE Healthcare), 2 mM L-Glutamine (Life Technologies), 100 Units/mL Penicillin (Life Technologies, Inc.), 100 μg/mL Streptomycin (Life Technologies, Inc.), 400 μg/mL G418 disulfate salt solution (Sigma-Aldrich) and 10% heat inactivated fetal bovine serum (FBS; Sigma-Aldrich). Surface expression of IpLITRs was monitored by flow cytometry using an α-hemagglutinin (HA) monoclonal antibody (mAb; Cedarlane Laboratories Ltd) as described previously [11,193].

3.2.2 Generation of Stable RBL-2H3 expressing IpLITRs with LifeAct-GFP F actin Probe

In order to visualize IpLITR-mediated phagocytosis and membrane dynamics in real time, I generated LifeAct-GFP expressing IpLITR cells to observe F-actin regulation by IpLITR-types. Stable IpLITR expression was continuously examined throughout the studies and stably expressing IpLITR RBL-2H3 cells were transfected with LifeAct-GFP. LifeAct-GFP is a C-

terminal conjugated GFP probe which binds specifically to F-actin molecules within the intracellular spaces when transfected into cells [194] (A generous gift from Dr. Nicholas Touret, University of Alberta). RBL-2H3 expressing IpLITRs were transfected with LifeAct-GFP by using a nucleofection technique specific for RBL-2H3 cell lines according to the manufactures protocol (Amaxa Cell Line Nucleofector Kit T, RBL-2H3). IpLITR- expressing cells (either IpLITR 2.6b/IpFcRγ-L or IpLITR 1.1b) were grown to confluency (~ $2.6x10^6$ cells) in a 6-well tissue culture plate (Fisher Scientific Company) and were subsequently harvested using RBL-2H3 harvest buffer, washed with PBS, and then given 100 µL of Cell Line Nucleofector Solution T (Amaxa) and 5 µg of LifeAct-GFP plasmid. Samples were transferred into a nucleofection cuvette and transfected using the Nucleofector II Device (Amaxa) using the program designated for RBL-2H3 cell line specifically (Program X-001). After transfection, cells were placed into pre-warmed selection media (complete MEM supplemented with 400 µg of G418) and allowed to grow to confluency. Once confluent, cells were harvested and sorted based upon GFP expression (high FL-1 intensities). The top 15% FL-1 expressing cells were sorted into a new cell population via the FACS flow cytometer Canto II (BD Bioscience) and further cultured. Sorted cells were then plated and allowed to reach confluency. Cells were once again harvested and IpLITR expression along with LifeAct-GFP expression was assessed via flow cytometry (FL-2 and FL-1 intensities respectively as previously described [11,193].

3.3 Flow cytometric analysis of IpLITR phagocytic activities

3.3.1 IpLITR-phagocytic responses analyzed by flow cytometry

In order to determine quantifiable differences between IpLITR 2.6b/IpFcRγ-L and IpLITR 1.1b-mediated phagocytosis I performed flow cytometric population-based assays under various conditions (time course (kinetics), temperature sensitives, susceptibility to

pharmacological drugs). Flow cytometric analysis of phagocytosis was performed as previously described [11]. For IpLITR-mediated phagocytosis experiments, target beads included 10 µg/mL of αHA monoclonal antibody (mAb; Cedarlane Laboratories Ltd) to specifically ligate surface expressed IpLITRs or 10 µg/mL of mouse IgG3 (Beckman Coulter) as an isotype control which were adsorbed onto protein A (from *Staphylococcus aureus*; Sigma-Aldrich) pre-coated 4.5 µm YG beads (Fluoresbrite™ Carboxy YG microspheres; Polysciences). Testing the activation of endogenous phagocytic pathways in RBL-2H3 cells was accomplished via 4.5 µm YG beads opsonized with 20% (v/v) non-heated fetal bovine serum (FBS; Sigma-Aldrich) diluted in Dulbecco's phosphate buffered saline (PBS) or non-opsonized (i.e. 0% FBS) beads incubated with PBS alone were used. FBS was used in these studies to activate the endogenously expressed receptors on RBL-2H3 cells. For each standard phagocytosis experiment, $1x10^5$ cells in phagocytosis buffer (1:1 mixture of 1X PBS containing 2 mg/mL BSA and 1X OptiMEM reduced serum medium; Gibco) were incubated with either Ab- or FBS-opsonized beads ($3x10^5$ beads) for 1 hr at 37ºC. Cells were centrifuged at 5000xg for 1 min and the supernatant aspirated, cell pellet was then gently agitated, and cells were re-suspended in ice-cold PBS/EDTA containing 0.05% trypsin (Hyclone) and 1 mM EDTA to remove non-specifically bound targets. After a 15 min incubation on ice, ice-cold PBS containing 2 mM EDTA and 0.5% BSA was then added to each tube and the cells were centrifuged at 5000xg for 1 min and then re-suspended in 1% paraformaldehyde (PFA) dissolved in PBS. Samples were analyzed via flow cytometry (Cell Lab Quanta; Beckman Coulter) using FL-1 intensities to distinguish between cells with and without beads as done previously here [11].

3.3.2 Assessment of IpLITR phagocytic activity with respect to their kinetics, temperature and pharmacological sensitivities.

To identify functional and mechanistic differences among IpLITR-types I performed time course, temperatre and pharmacological sensitivity I used population-based based flow cytometric studies. For kinetic studies of IpLITR-mediated phagocytosis cells were incubated at 37ºC with target beads (either αHA or IgG3-coated (isotype control beads)) for 15, 30, 60, and 90 min prior to analysis. For temperature sensitivity studies cells were incubated at the reduced temperatures of 27, 22, 17, 12, or 4ºC with 4.5 μm beads opsonized with either αHA mAb or mouse IgG3 isotype control prior to analysis. Additionally, phagocytosis experiments were also performed with FBS-opsonized 4.5 μm beads at incubation temperatures of 37, 22, or 4ºC. To examine the effects of selected pharmacological inhibitors (listed in 3.1.3) on RBL-2H3 endogenous pathway or IpLITR-induced phagocytic activity cells were first pre-treated for 1 hr at 37ºC with each drug tested or with 0.1% dimethyl sulfoxide (DMSO) as the vehicle control. Phagocytosis was then performed for 1 h4 min at 37ºC using the indicated target beads (αHA, IgG3 or FBS-coated) in phagocytosis buffer supplemented with the pharmacological inhibitor.

3.4 Confocal imaging analysis of IpLITR phagocytic phenotypes

3.4.1 IpLITR-specific phagocytic phenotypes examined using confocal imaging and 3D renders

To examine phenotypic and quantitative differences among IpLITR-types at the individual cell level I performed confocal imaging and 3D rendering of IpLITR-mediated phagocytosis. In brief, $5x10^5$ cells of either Parental RBL-2H3 cells or those stably expressing IpLITRs were seeded into 6-well tissue culture plates (Fisher Scientific Company) containing 3

mL of complete MEM and a sterile microscope glass coverslip. RBL-2H3 cells were allowed to attach and grow overnight at 37ºC (~75% confluence over the coverslip). After incubation, growth media was removed, coverslips washed twice with PBS and live cells were stained using the membrane stain CellMask Orange™ (Life Technologies Inc) at 1:1000 v/v dilution in phagocytosis buffer for 10 min at 37ºC. Membrane stain was then aspirated from the well and cells washed with PBS. Once washed cells were given 1.25 mL of phagocytosis buffer containing 15 µl of target beads at the same target-to-bead ratio (i.e. 3 beads per cell) as described in the phagocytosis assay protocol from Section 2.2. Culture plates containing cells and beads were then centrifuged for 1 min at 1500 rpm and then incubated at either 37ºC or 22ºC for 1 hr. Supernatants were then removed and cells were washed with PBS prior to fixation using 4% PFA at room temperature for 10 min. After a final PBS wash, coverslips were placed on a glass slide containing a drop of ImmunoMount™ Mounting Media (GeneTex, Inc) and sealed. Samples were viewed with a Laser Scanning Confocal Microscope (LSCM; Zeiss LSM 710, objective 40X and 60X 1.3 oil plan-Apochromat; Cross Cancer Institute Microscopy Facility, Edmonton, AB). All images were collected and analyzed using Zen 2009 or 2011 software and 3D rendering was performed using Imaris 9.2.1 (Bitplane).

3.5 Examination of trypsin-induce alteration of IpLITR-mediated phagocytic phenotypes

3.5.1 Receptor-specific effects of trypsin on IpLITR expression and phagocytic activity

To test the possibility of receptor-specific sensitives of IpLITRs to the enzymatic activity of trypsin, I performed flow cytometric analysis of both IpLITR-expression and IpLITR-function post trypsin exposure. Prior to incubation with target beads, IpLITR-expressing RBL-2H3 cells were pre-treated for 15 min at 4ºC in a PBS/EDTA (1 mM) solution containing various concentrations (e.g. 0.03125, 0.0625, 0.125, 0.25, 0.5, 1.0, 2.0, and 20 µM) of porcine trypsin

(Gibco), which cleaves at the C-terminal side of lysine and arginine residues. Phagocytosis assays were then performed as described above. BLAST searches using the UniProt porcine trypsinogen (TRYP_PIG) sequence (ID: P00761) show that teleost trypsin's are ~75% similar to the mammalian enzymes. Trypsin is also a member of a large family of serine proteases with highly conserved enzymatic mechanisms that require a catalytic triad composed of serine, histidine, and aspartic acid residues. Although the sequences can vary among vertebrates, at the ideal temperate for a given trypsin, their proteolytic processing activities are likely highly conserved. To determine the effects of trypsin pre-treatment on IpLITR surface staining, FL-2 intensities were translated to mean fluoresce intensity (MFI) values via FlowJo 7.2 software (Treestar Inc). Fold-changes in receptor expression for IpLITR 2.6b/IpFcRγ-L and IpLITR 1.1b were then calculated as follows: [MFI value for untreated cells (i.e. 0 μM Trypsin) / MFI values for enzyme-treated cells (i.e. 0.03125 to 20 μM trypsin)]. In some experiments, cells were allowed to recover for 2 hrs at 37ºC in complete MEM after trypsin exposure, prior to performing phagocytosis assays and surface expression analysis.

3.5.2 Immunoprecipitation and western blot assessment of the effects of trypsin on IpLITR surface expression

In order to identify at the protein level the receptor-specific effects of trypsin on IpLITR-expression and IpLITR-mediated phagocytosis I performed whole cell lysate immunoprecipitation assays post trypsin exposure. IpLITR 2.6b/IpFcRγ-L- and IpLITR 1.1b-expressing RBL-2H3 cells ($4x10^6$) were harvested as described [193] and washed twice with ice-cold PBS. Surface proteins were biotinylated by the addition of 5 mg/mL of biotin (Thermo Fisher Scientific) for 30 min at 4°C according to the protocol described in [195]. Excess biotin was quenched by washing the cells with ice-cold 100 mM glycine. Surface biotinylated cells

were then centrifuged at 5000xg for 1 min and re-suspended in 400 µL lysis buffer (50mM Tris-HCl, 150mM NaCl, 1% Triton X-100) and sonicated. Lysates were incubated on ice for 30 min with intermittent vortexing. Cellular debris was removed by centrifuging samples at 16,000xg for 10 min. Whole cell lysates (400 µl) were then mixed with 25 µL of αHA coated microspheres (Thermo Fisher Scientific) and incubated at 4°C for 14 hours. Beads were washed three times with lysis buffer and proteins were eluted by the addition of 100 µL of 2x SDS-PAGE reducing buffer (Bio-Rad) and boiled at 95°C for 10 min. Immunoprecipitated samples were separated using a 10% SDS-PAGE gel, transferred to a nitrocellulose membrane (Bio-Rad), and then probed with either a horseradish peroxidase (HRP)-conjugated goat αHA polyclonal antibody (1:1000; GenScript Corp. Piscataway, NJ, USA) or streptavidin (SA)-HRP (1:1000; Sigma-Adrich) as previously described [13,191]. Detection of immunoreactive bands using the Super Signal West Pico Chemiluminescent Substrate kit (Pierce Biotechnology) have been previously described [13]. Receptor glycosylation was examined by treatment of IpLITR 1.1b-expressing cells with an endoglycosidase and by treating the immunopurified IpLITR 1.1b protein with endoglycosidase directly. Briefly, cells $2.5x10^6$ were harvested, washed with PBS (1X), and then treated with 50 U of Neuraminidase (New England Bio Labs Inc.) and then either 0 U or 40,000 U of O-Glycosidase (New England Bio Labs Inc.) for 3hrs at 37°C. Cells were then lysed and immunoprecipitated as previously described prior to Western blot detection. Another approach was to first immunopurify the IpLITR 1.1b protein and then treat it with 50 U of Neuraminidase and either 0 U or 40,000 U of O-Glycosidase for 1hr at 37°C as outlined in the manufactures protocol (New England Bio Labs Inc.) prior to the detection of immunoreactive bands by Western blot as described above.

3.5.3 Examination of the effects of trypsin on IpLITR surface expression and phagocytic phenotypes by confocal imaging

To examine the nature by which trypsin effected IpLITR 1.1b-mediated phagocytosis specifically, I examined IpLITR-expressing cells exposed to trypsin and then incubated with target beads and visualized phenotypic differences between IpLITR-types. For visualization of phagocytosis, IpLITR 2.6b/IpFcRγ-L- and IpLITR 1.1b-expressing RBL-2H3 cells were plated overnight and then trypsin-treated as described above. Target beads ($15x10^6$) suspended in phagocytosis buffer were added to each well and centrifuged at 400xg for 6 min in order to initiate bead-cell contacts. Cell solutions were then incubated for 1 h3 at 37°C and then washed with PBS to remove any beads not associated with cells. Coverslips were fixed with 4% PFA and mounted onto microscope slides (Thermo Fisher Scientific). Phagocytosis of target beads was analyzed as previously described by staining the cellular membranes of the cells with CellMask™ [193]. Three-dimensional reconstructions of cell-bead interactions were generated from the z-stacks using the Imaris 9.2.1. To visualize the translocation of IpLITR 1.1b into the cell after trypsin treatment IpLITR 1.1b-expresing cells were plated onto 18mm diameter #1 ½ circular coverslips at a cell density of $2x10^5$ and allowed to adhere overnight. The following day these cells were treated with 2 μm trypsin for 15min at 4°C, fixed with 4% PFA for 10min at 37°C and then stained for receptor presence as previously above. After receptor staining was done these coverslips were mounted and imaged using a Zeiss LSM 710 laser scanning confocal microscope (Objective 60x, 1.3 oil plan-Apochromat) located at the Cross Cancer Institute Microscopy Facility (Faulty of Medicine & Dentistry; University of Alberta) and analysis was performed using Zen 2011 software (Carl Zeiss).

3.5.4 Flow cytometry and confocal analysis of intracellular IpLITR 1.1b proteins

To further examine the possibility that IpLITR 1.1b was being internalized post trypsin exposure, I used a modified surface staining protocol for both flow cytometric analysis and confocal imaging of IpLITR 1.1b-expressing cells. IpLITR 1.1b-expressing cells were either grown on a coverslip (for confocal imaging) or harvested from a 6-well plate and subsequently were pre-treated with trypsin at either 0 or 2 μM for 15 min at 4°C. Trypsin enzymatic activity was then inhibited by the addition of 1% BSA/PBS solution. Post trypsin treatment IpLITR 1.1b-expressing cells were then immediately stained with a αHA mAb and subsequently stained with either a goat αmouse IgG (H+L)-PE pAb for flow cytometric analysis or a secondary goat αmouse Alexa-488 immunofluorescence for confocal imaging. For assessing the intracellular localization of IpLITR 1.1b proteins after trypsin treatment these cells were first fixed with 4% PFA for 10 min at 37°C (induces small level of permeabilization) and then stained for the presence of IpLITR 1.1b either with a goat αmouse IgG (H+L)-PE pAb for assessing the relative levels of IpLITR 1.1b after permeabilization and trypsin treatment or a secondary goat αmouse Alexa-488 immunofluorescence for assessing the localization of IpLITR 1.1b post trypsin treatment.

3.6 SEM and live cell imaging analysis of IpLITR phagocytic responses

3.6.1 SEM imaging of IpLITR-mediated phagocytosis

To better resolve the membrane dynamics of IpLITR-mediated phagocytosis I performed high resolution scanning electron (SEM) microscopy. Briefly, RBL-2H3 cells expressing either IpLITR 2.6b/IpFcRγ-L or IpLITR 1.1b were plated onto a sterile 18mm diameter #1 ½ circular coverslip (Electron Microscopy Sciences) at a cell density of $3x10^5$ and cultured overnight at

37°C and 5% CO_2 in a 6-well tissue culture plate (Fisher Scientific Company). The following day cells were washed with phosphate buffered saline (PBS) and then given phagocytosis buffer (1:1 mixture of 1X PBS containing 2 mg/mL bovine serum albumin (BSA); (Sigma Aldrich) and 1X Opti-MEM reduced serum medium; Fisher Scientific Company) containing $9x10^5$ 4.5 μm target microspheres (beads) (Polybead® Carboxylate YG microspheres) that were either opsonized with 10 μg/mL of αHA monoclonal antibody (mAb; Cedarlane Laboratories Ltd.) to ligate specifically surface expressed IpLITRs via their extracellular HA-epitopes or 10 μg/mL of mouse IgG3 (Beckman Coulter) as an isotype control. Both IgG3 and αHA opsonisation occurred by absorbing them onto beads pre-coated with protein A (isolated from *Staphylococcus aureus*; Sigma-Aldrich). Plates containing cells and beads were centrifuged at 1500 rpm for 1 min to synchronize cell-bead interactions and then incubated for 1hr at either 37°C, 27°C or 37°C after pre-treatment with Latrunculin B to demonstrate F-actin polymerization involved in the processes I previously observed. Finally, for SEM preparation cells were fixed with 2.5% Glutaraldehyde/ 2% paraformaldehyde (PFA) in a 0.1 M phosphate buffer solution. Dehydration of cells was then done by sequential treatments with ethanol and hexamethyldisilazane (HMDS) according to the procedure outlined in [196,197]. After dehydration, coverslips were mounted onto round metal double sided sticky stubs and coated with an ultrathin coating of gold/plutonium via a Hummer 6.2 Sputter Coater (Anatech USA) and coverslips were then imaged using a Philips/FEI XL30 SEM microscope (FEI: Hillsboro) and analysis was done using Scandium 5.0 software (Emsis).

3.6.2 Live cell imaging of LifeAct-GFP expressing IpLITR RBL-2H3

To observe IpLITR-mediated membrane dynamics during phagocytic events I used my previous mentioned LifeAct-GFP/IpLITR-expressing RBL-2H3s in live cell imaging studies.

IpLITR-expressing and LifeAct GFP positive RBL-2H3 stables were plated onto 50mm µ-dishes (Ibidi; Madison, Wisconsin, USA) at a density of $3x10^5$ the day prior to use. Cells were washed with PBS and then incubated in phagocytosis buffer containing $9x10^5$ αHA mAb-opsonized target 4.5 µm non-fluorescent beads (previously used in section 2.2) or αHA mAb-opsonized 4.5 µm blue beads (Fluoresbrite™ Carboxy BB microspheres; Polysciences) and placed into a microscope stage chamber which was supplied with 5% CO_2 and heated to 37°C or 27°C. Immediately after the addition of target beads, images were collected at 10 sec intervals for ~8 min in a single plane. The use of 10 sec intervals was based on the shortest period of time allowed by the software to obtain an image based on the scanning speed and imaging speed of the microscope itself for an individual color (i.e. GFP). Images were obtained using a Zeiss LSM 710 laser scanning confocal microscope (Objective 60x, 1.3 oil plan-Apochromat) located at the Cross Cancer Institute Microscopy Facility (Faulty of Medicine & Dentistry; University of Alberta) and analysis was performed using Zen 2011 software (Carl Zeiss). Subsequently analyzed using both Zen 2011 software (Carl Zeiss) and ImageJ (ImageJ version 1.51p; Rasband, 1997–2017).

3.7 Examination of IpLITR recruitment of Nck and pSYK during filopodia formation and receptor activation during phagocytosis

3.7.1 Examination of Syk and Nck colocalization with IpLITR surface expression

In order to determine if Syk ad Nck are associated with IpLITR 1.1b during filopodia formation I performed cell staining of IpLITRs and both Syk and Nck to identify their colocalization at various regions of cells. RBL-2H3 cells stably expressing IpLITR 2.6b/IpFcRγ-L or IpLITR 1.1b were plated onto a sterile 18mm diameter #1 ½ circular coverslip (Electron Microscopy Sciences) at a cell density of $3x10^5$ and cultured overnight at 37°C and 5% CO_2 in a

6-well tissue culture plate (Fisher Scientific Company). The following day cells were washed with pre-warmed 37°C PBS twice, fixed with 4% PFA warmed to 37°C and then were washed with antibody staining buffer (0.5% sodium azide; Sigma, 1% BSA in PBS) (ASB). Coverslips were then transferred to a slip of parafilm containing 50 µL of 5 µg/mL mouse αHA in ASB and incubated at 4°C for 30 min. Coverslips and cells were then washed with ASB twice and then placed onto parafilm containing 20 µg/mL goat αmouse Alexa-647 (Molecular Probes) secondary antibody and again incubated at 4°C for 30 min. After secondary antibody staining cells were washed with ASB again and then given 1X permeabilization buffer (Biolegend) for 15min at room temperature. Once permeabilized cells were washed with cell staining buffer (CSB) (Biolegend) and then were then placed onto parafilm containing either 1:50 (pSyk) or 1:100 (Nck) v/v of rabbit primary mAb in CSB for specifically probed intracellular protein and were incubated at room temperature for 30 min. After primary antibody staining samples were washed with CSB, blocked for 30min in 1%BSA/PBS and then coverslips were transferred to parafilm containing 20 µg/mL goat αrabbit Alex-488 (Molecular Probes) for 30 min at room temperature. For a positive control sample, IpLITR 1.1b-expressing cells were first incubated with a αHA mAb followed by the incubation with two goat αmouse secondary antibodies; one conjugated to Alexa-657 and another conjugated to Alexa-488 which was done sequentially. By using the same specificity of antibody (ie. αmouse) these two fluorescent antibodies should double stain surface IpLITRs and therefore have a significantly high level of colocalization observationally as well as when analyzed via software. Finally, cells were washed again with CSB, blocked with 1% BSA/PBS for 30min and then placed onto microscope slides containing a small droplet of Prolong® Gold antifade (Molecular Probes) mounting media and left overnight to solidify. Immunofluorescent images were obtained using a Zeiss LSM 710 laser scanning

confocal microscope (Objective 60x, 1.3 oil plan-Apochromat) located at the Cross Cancer Institute Microscopy Facility (Faulty of Medicine & Dentistry; University of Alberta) and analysis was performed using Zen 2011 software (Carl Zeiss) along with Imaris 9.2.1. For colocalization analysis via Imaris 9.2.1, individual cells were isolated from captured z-stack images using Zen 2011 along with the chosen regions of interest on each cell. These newly produced z-stack images for each region of the cell were then ran through the Imaris 9.2.1 colocalization analysis tool for the entire 3D volume of the selected region. Analysis of colocalization was done on the top 10% intensities for both channels (red; IpLITR, green; pSyk/Nck) to reduce false positives from low intensity signals and the measure of colocalization used within these studies was the Pearsons Correlation Coefficient (PCC). PCC values indicate whether two separate signals are distinctly associated with one another more so then due to random chance. A PCC value of +1 indicates complete colocalization while a PCC value of -1 indicates perfect exclusion. A PCC value <0.5 is considered inconclusive if the overlap of two signals is greater then random chance. This was done for three individual cells for each cell-type tested and three regions of interest were used for each cell (total of 9 regions in all). Statistical significance between cell-types for a given intracellular protein (i.e RBL-2H3 pSyk values vs IpLITR 1.1b pSyk values) was done by a student t-test using a two-tailed paired analysis.

3.7.2 Imaging analysis of the recruitment of pSyk and Nck to sites of IpLITR-induced phagocytosis

In order to examine if Nck and Syk are recruited to regions of IpLITR 1.1b-target interfaces (or IpLITR 1.1b activation) I performed a variety of staining procedures and utilized confocal imaging and imaging analysis software. To assess the associations between IpLITR ligation activity and intracellular signaling, cells were incubated with target beads and

localization of specific intracellular signaling proteins (ie. Nck, pSyk) was assessed via immunofluorescence. Like the protocol detailed in section 3.4 and 3.6, RBL-2H3 IpLITR-expressing cells were grown on a sterile 18mm diameter #1 ½ circular coverslip at a cell density of $3x10^5$ in a 6-well tissue culture plate and allowed to adhere overnight. Coverslips were then washed with PBS and given 1mL of phagocytosis buffer containing $9x10^5$ αHA coated beads, centrifuged at 1500rpm for 1 min and then incubated at either 15, 30 or 60 min. After each time point cells were washed with PBS and then give 4% PFA pre-warmed to 37°C for 10 min for fixation. Once cells were fixed beads were stained for inside-outside discrimination as described here [192], which consisted of placing coverslips onto parafilm containing 2 μg/mL of goat αmouse Alexa-647 (Molecular Probes) which binds to exposed regions of the target beads. This was done for 30 min at 4°C. After staining of the beads, coverslips were washed with ASB and then given 1X permeabilization buffer (Biolegend) for 15 min at room temperature. Once permeabilized, cells were washed with CSB and placed onto parafilm containing either 1:50 or 1:100 v/v dilution of primary rabbit mAb in CSB for each respective intracellular protein target depending on the recommended concentration by the manufactures protocol (Nck, 1:50, pSyk, 1:100). Cells were incubated at room temperature with these primary rabbit mAb for 30 min. After primary antibody incubation, cells were washed with CSB and then stained on parafilm with 20 μg/mL of goat αrabbit Alexa-550 secondary antibody in CSB for 30 min at room temperature. Lastly, coverslips were washed with CSB and mounted onto microscope slides containing a small droplet of Prolong® Gold antifade mounting media and allowed to solidify overnight at room temperature. Imaging was done as previously described [193,198,199] using a Laser Scanning Confocal Microscope (LSCM; Zeiss LSM 710, objective 60X 1.3 oil plan-Apochromat). All images were collected and analyzed using Zen 2009 or 2011 software as well

as Imaris 9.2.1 software for the generation of 3D renders. Individual cellular events were then isolated from obtained z-stack images and the mean fluorescence interties (MFIs) for both bead staining as well as for the intracellular molecule being studied (i.e pSyk or Nck). MFIs were obtained by using an analysis line which was placed onto a chosen z-stack image. This analysis line collects the MFIs for all intensities that are present along the line.

CHAPTER IV

TELEOST LEUKOCYTE IMMUNE-TYPE RECEPTORS ACTIVATE DISTINCT PHAGOCYTIC MODES FOR TARGET ACQUISITION AND ENGULFMENT

A version of this chapter has been published:

Lillico et al. 2015. Teleost leukocyte immune-type receptors activate distinct phagocytic modes for target acquisition and engulfment. *J Leukoc Biol*. 98(2):235-248

4.1 INTRODUCTION

Specialized cells called phagocytes can directly or indirectly recognize a range of microbes- and/or host apoptotic cells, using different phagocytic receptor-types [2]. These interactions selectively control intracellular signaling pathways that regulate a specialized engulfment process called phagocytosis, which facilitates the destruction of invading pathogens or orchestrates the quiescent clearance of dying cells from the body [2]. Although different phagocytic receptor-types use shared signaling components during the engulfment process, several distinct cellular modes of phagocytosis have also been identified that rely on receptor-specific structural and signaling components to coordinately regulate the phagocytic machinery [61–63,200]. The two classical models of phagocytosis that have been extensively described involve either FcRs for IgG or CR3 (also known as integrin $\alpha_M\beta_2$ or the iC3b receptor) [2] and these display key differences in the cellular mechanisms controlling target acquisition as well as engulfment [2,62,200,201]. Despite these differences, the CR3- and FcR-dependent phagocytic pathways both converge at the recruitment of the actin-related protein (Arp) 2/3 complex, which is a key nucleator of F-actin polymerization [202]. However, there are recognizable differences in how F-actin polymerization and associated membrane remodeling culminates in target engulfment that further differentiates the FcR- and CR3-mediated phagocytic modes. Early

observations of CR3-mediated phagocytosis demonstrated that target particles appeared to sink into the phagocyte membrane [203] without generating pseudopod extensions or membrane ruffles that are often observed during FcR-mediated phagocytosis [62]. The general pattern of actin polymerization during CR3-mediated phagocytosis also featured discrete foci of F-actin that were associated with the RhoA-dependent assembly of contractile actomyosin filaments [62,200] and limited filopodia-like extensions [86]. This is markedly different from the continuous pattern of F-actin polymerization that generates the lamellipodial and filopodial membrane protrusions induced by FcR [2,201]. Versatility in phagocytic receptor functions is further appreciated by the recent description of the cellular actions of carcinoembryonic antigen-related cell adhesion molecule 3 (CEACAM3) [3,8]. The CEACAM3 receptor is expressed by human neutrophils and activates a unique short-circuited mode of phagocytosis through a minimal set of molecules that effectively trigger rapid actin-dependent pathogen internalization [3,8]. Whether other vertebrate immunoregulatory receptor-types can activate a similar repertoire of phagocytic modes is largely unknown.

To gain a greater understanding of the induction and regulation of the phagocytic process in vertebrates, my research is focused on members of the polymorphic family of teleost immunoregulatory receptors: IpLITRs [16,190]. These teleost receptors share phylogenetic and structural relationships with a wide range of immunoregulatory receptors in humans, including FcRs, FcR-like proteins, and CEACAMs [187]. Predictably, IpLITRs also control immune cell effector responses in transfected mammalian cells using prototypical stimulatory and inhibitory signaling pathways. For example, the putative stimulatory receptor IpLITR 2.6b associates with the ITAM-containing catfish adaptor signaling protein IpFcRγ-L, and when fused together as a receptor chimera, IpLITR 2.6b/IpFcRγ-L promoted protein tyrosine kinase (PTK)-mediated

signaling and induced ITAM-dependent degranulation, cytokine secretion, and phagocytosis in transfected RBL-2H3 cells [10]. In comparison, IpLITR 1.1b abrogated NK cell-mediated killing responses via the recruitment of intracellular phosphatases to its ITIM-containing CYT region [12]. Surprisingly, IpLITR 1.1b also induced the engulfment of extracellular targets when stably RBL-2H3 cell line [38]: a commonly used mammalian cell model for characterizing receptor-mediated control of innate effector responses, including phagocytosis [4,115,204–207]. Taken together, the ability to regulate stimulatory and inhibitory immune cell actions revealed the signaling versatility of IpLITR 1.1b and suggested that this receptor may utilize a unique phagocytic mechanism different from the prototypical ITAM-mediated pathway represented by IpLITR 2.6b/IpFcRγ-L.

The main research objective of this thesis chapter was to further characterize the unique ITAM-independent phagocytic pathway regulated by IpLITR 1.1b. Specifically, I performed detailed kinetic and pharmacological profile of IpLITR 1.1b- and IpLITR 2.6b/IpFcRγ-L-induced phagocytosis in addition to phenotypic analyses of the phagocytic responses activated by these different IpLITR-types. My results show that IpLITR 1.1b uses an alternative phagocytic pathway that is functionally distinct from the classical ITAM-mediated response represented by IpLITR 2.6b/IpFcRγ-L. Examination of IpLITR 1.1b-mediated phagocytosis provides new information about immunoregulatory receptor-mediated target acquisition and internalization mechanisms that regulate distinct modes of target engulfment. Furthermore, my data provides the basis for formulating mechanistic hypotheses regarding how an ITIM-containing immunoregulatory receptor can uniquely promote F-actin-mediated plasma membrane remodeling events during the capture and engulfment of extracellular targets.

4.2 RESULTS

4.2.1 Flow cytometric examinations of IpLITR-mediated phagocytosis

When IpLITR 2.6b/IpFcRγ-L-expressing cells were incubated with αHA mAb-opsonized 4.5 μm bead targets, I observed 13.7% phagocytosis at 15 min, which increased to 23.2%, 35.5%, and 44.1% after 30, 60, and 90 min, respectively (Fig. 4.1A). Over the same time course, values obtained using the control IgG3-opsonized beads ranged from 7.4%-12.8% phagocytosis, which were significantly lower than the corresponding αHA mAb opsonized bead values ($p \leq 0.05$). IpLITR 1.1b-expressing cells also phagocytosed 4.5 μm αHA beads with values of 39.6%, 64.2%, 75.2%, and 83.2% phagocytosis after 15, 30, 60, and 90 min, respectively (Fig. 4.1B). These % phagocytosis values were all significantly higher ($p \leq 0.05$) than those observed for IpLITR 2.6b/IpFcRγ-L at each time point. Importantly, as seen for IpLITR 2.6b/IpFcRγ-L-expressing cells, no significant change in phagocytosis by IpLITR 1.1b-expressing cells was observed using the control IgG3-opsonized 4.5 μm beads at any of the incubation periods (Fig. 4.1B).

To identify that IpLITR-mediated phagocytosis was an activate process, I tested IpLITR-expressing cells abilities to induce phagocytosis at reduced incubation temperatures. At reduced incubation temperatures, IpLITR 2.6b/IpFcRγ-L-mediated phagocytosis was significantly abrogated (Fig. 4.1C). For example, compared to 43% phagocytosis values at 37ºC, IpLITR 2.6b/IpFcRγ-L-expressing cells incubated at 27, 22, 17, 12, and 4ºC all demonstrated significantly reduced phagocytic responses ranging from 20% at 27ºC to 8% at 4ºC. In comparison, IpLITR 1.1b-mediated phagocytosis was less sensitive to these lower incubation temperatures (Fig. 4.1D). In fact, at 27ºC, IpLITR 1.1b-mediated phagocytosis (61%) was not significantly different than its 70% phagocytic activity at 37ºC; and although IpLITR 1.1b-

mediated phagocytosis (55%) at 22ºC was significantly lower than its phagocytic activity at 37ºC, this was not significantly different compared to its activity at 27ºC. Only when the incubation temperatures were dropped below 22ºC did IpLITR 1.1b fail to induce a significant increase in phagocytosis compared with cells treated with IgG3-opsonized control beads (Fig. 4.1D), whereas IpLITR 2.6b/IpFcRγ-L-mediated phagocytosis was abolished at 22ºC (Fig. 4.1C). An overview of the comparative differences in the temperature-dependent inhibition of IpLITR 2.6b/IpFcRγ-L- and IpLITR 1.1b-mediated phagocytosis are summarized in Figure 4.1E.

To test if the IpLITR transfection protocol affected the endogenous phagocytic responses of RBL-2H3 cells, I also examined their phagocytic activity using FBS-opsonized beads (Fig. 4.2). When incubated at 37ºC for 60 min, parental RBL-2H3 cells (empty vector; Fig. 4.2A) as well as the IpLITR-expressing cells (Fig. 4.2B and 4.2C) had similar overall phagocytic activities (i.e. ~50% phagocytosis) when using FBS-opsonized as targets. In comparison, RBL-2H3 cells did not effectively phagocytose non-opsonized targets (0% FBS) regardless of whether they were transfected with empty vectors or IpLITR 2.6b/IpFcRγ-L or IpLITR 1.1b. At 22ºC, empty vector-expressing cells (Fig. 4.2A), IpLITR 2.6b/IpFcRγ-L-expressing cells (Fig. 4.2B), and IpLITR 1.1b-expressing cells (Fig 4.2 C) all exhibited significantly reduced phagocytic responses. Similar inhibitory effects (93.7%, 100.4%, and 99.8% inhibition of phagocytosis) were also observed at 4ºC for all the cells tested.

4.2.2 Confocal imaging of IpLITR-mediated phagocytosis

To examine the ratio of captured-to-engulfed extracellular targets, I also examined IpLITR-mediated phagocytosis using confocal microscopy. At 37ºC, cells transfected with an empty vector did not associate with targets (Fig. 4.3A). In comparison, IpLITR-expressing RBL-2H3 cells were shown to associate with multiple αHA target beads when incubated at 37ºC (Fig.

4.3B and 4.3C, left columns). At 22ºC, most IpLITR 2.6b/IpFcRγ-L-expressing cells failed to associate with any beads (Fig. 4.3B; right column) whereas, at this temperature, IpLITR 1.1b-expressing cells consistently interacted with one or more targets (Fig. 4.3C; right column). This further reinforced that unlike IpLITR 2.6b/IpFcRγ-L-expressing cells, which only phagocytosed beads at 37ºC, IpLITR 1.1b-expressing cells readily interacted with beads at both 37ºC and 22ºC.

4.2.3 Assessment of the phagocytic phenotypes of IpLITR-expressing RBL-2H3 cells

Using images collected by confocal microscopy (Fig 4.3), I generated three-dimensional (3D) renderings of phagocytic cells using representative z-stacks. These images detail the main phenotypic differences between IpLITR 2.6b/IpFcRγ-L- and IpLITR 1.1b-mediated phagocytosis. Notable features of IpLITR 2.6b/IpFcRγ-L-mediated phagocytosis were that phagocytic cells consumed three or more beads and each of these beads were completely engulfed by the plasma membrane (Fig. 4.4A and 4.4B). In comparison, of the IpLITR 1.1b-expressing cells that had successfully internalized beads at 37ºC, only one completely engulfed bead was usually observed per cell (Fig. 4.4C and 4.4D). Strikingly, the majority of IpLITR 1.1b-expressing cells had beads attached to their plasma membrane unlike IpLITR 2.6b/IpFcRγ-L-expressing cells (Fig. 4.3). In general, these captured beads were firmly embedded in the plasma membrane in what often resembled phagocytic cup-like structures (Fig. 4.4D). Another definable feature for the IpLITR 1.1b-expressing cells was the attachment of beads at the ends of extended membranous protrusions; which, in some cases resulted in the beads being shared between multiple isolated cells (Fig. 4.4D). Interestingly IpLITR 1.1b-expressing cells still actively captured beads at 22ºC (Fig. 4.4C). Visually, the captured beads were indistinguishable from those observed at 37ºC; displaying a mixture of beads that were either contained within

phagocytic cups or embedded between the plasma membranes of two or more cells via membranous extensions (Fig. 4.4E and Fig. 4.4F).

Next, I quantified the cell-bead interaction observed in the confocal images by counting and then categorizing cells as either: i) cells with no associated or internalized beads (% No beads); ii) cells with at least one partially internalized bead contained within a phagocytic cup-like structure but with no completely engulfed beads (% Captured); and iii) cells that had at least one completely engulfed bead (% Phagocytosed; Fig. 4.5). Often, cells categorized as phagocytic also had beads attached to their surface in phagocytic cup-like structures, but these cells were still considered phagocytic due to the complete engulfment of at least one target bead. Based on these analyses, the majority (i.e. ~95%) of empty vector-transfected RBL-2H3 cells did not associate with or engulf any target beads (Fig. 4.5A). However, 62% of the IpLITR 2.6b/IpFcRγ-L-transfected cells completely engulfed at least one bead with very few cells (i.e. 3%) displaying captured beads on their surfaces when incubated at 37ºC (Fig. 4.5B). In agreement with my flow cytometry data (Fig 4.1C), when IpLITR 2.6b/IpFcRγ-L-expressing cells were incubated at 22ºC, a significant reduction in their ability to engulf opsonized targets was observed as 81% of the cells did not associate with any beads (Fig. 4.5B). Examination of IpLITR 1.1b-mediated phagocytosis revealed a completely different phagocytic phenotype. Unlike IpLITR 2.6b/IpFcRγ-L-expressing cells, 70% of IpLITR 1.1b-expressing cells associated with αHA mAb-opsonized beads with an overall distribution of 32% engulfed to 44% captured beads at 37ºC (Fig. 4.5C). Furthermore, at 22ºC, IpLITR 1.1b-mediated phagocytosis was reduced from 32% to 11% but the proportion of cells with captured beads was not significantly different to that observed at 37ºC (~ 46%; Fig. 4.5C).

4.2.4 Pharmacological profiling of IpLITR-mediated phagocytic activities

Selective pharmacological inhibitors of intracellular signaling molecules and cytoskeletal components were profiled for their effects on RBL-2H3 cell phagocytosis. Intracellular signaling molecules tested using pharmacological blocking were selected based on an ITAM-induced phagocytic response. This was done to utilize IpLITR 2.6b/IpFcRγ-L-expressing cells as a positive control for the effectiveness of the blockers tested to identify their roles in IpLITR 1.1b-mediated phagocytosis. The compound names, doses tested [μM], and intracellular targets of each pharmacological inhibitor are listed in Table 4.1. I report the efficacy of these blockers as % inhibition of phagocytosis and the corresponding pharmacological profiles generated from these results are shown in Figure 4.6 and Figure 4.7. These data were all generated using the flow cytometry-based phagocytosis assay and the raw data, including statistical analysis, from these experiments are provided in Figure 4.8 and Figure 4.9.

Overall, three levels of drug efficacy (defined as 25, 50, and 75% inhibition of phagocytosis) were selected and are indicated on each of the profiles in Fig. 4.6. The inhibitors tested are listed on the x-axis and they are ordered from left-to-right based on the general trend of most-to-least effective at reducing phagocytosis of the empty vector transfected cells using the FBS-opsonized beads (Fig. 4.6A). Overall, the pharmacological profiles for RBL-2H3 (empty vector), IpLITR 2.6b/IpFcRγ-L-, and IpLITR 1.1b-expressing cells (Fig. 4.6A, 4.6B, and 4.6C, respectively) are similar when the FBS-opsonized bead targets were used. For example, the most effective small molecule inhibitors of phagocytosis for all cells (i.e. ~70-100% inhibition) were Latrunculin B (F-actin polymerization), GSK2334470 (phosphoinositide-dependent kinase 1), and ML 141 (cell division control protein 42 homolog (Cdc42) GTPase). Approximately 50-60% inhibition of phagocytosis was then observed using drugs that targeted Src kinases (PP2;

selectivity for Lck and Fyn), PI3Ks (wortmannin and LY294002), and the Rho GTPases ras-related C3 botulinum toxin substrate (Rac)1/2/3 (EHT 1864). Lower efficacy (i.e. ~15-30% inhibition of phagocytosis) was observed using blockers of protein kinase B (Akt Inhibitor VIII), conventional and novel protein kinase Cs (Gö6976 and BisII), Syk (ER 27391), and extracellular signal-regulated kinase kinase (MEK1/2; U0126). Nocodazole, which targets microtubules, had little effect on RBL-2H3 cell-mediated phagocytosis of FBS-opsonized 4.5 μm beads (<10% inhibition for all three cell groups).

Using the same panel of pharmacological inhibitors, I then examined their efficacy against IpLITR-mediated phagocytosis by switching to the αHA mAb-opsonized beads. The pharmacological inhibitory profiles for these experiments are shown in Figure 4.7, and the raw data, including the statistical analysis, from these experiments are provided in Figure 4.8. To facilitate direct comparisons with the FBS-opsonized bead results, the same 25%, 50%, and 75% inhibition markers are indicated on the graphs and the drugs listed on the x-axis remain in the same order as described above. Since RBL-2H3 cells transfected with the pDisplay empty vector did not phagocytose αHA mAb-opsonized beads, no pharmacological profile data was generated for these cells.

Results from these experiments show that relative to the endogenous RBL-2H3 phagocytic pathway, induction of IpLITR 2.6b/IpFcRγ-L-mediated phagocytosis with αHA mAb-opsonized beads generated a distinct inhibition profile (Fig. 4.7A). The major differences were observed for the increased sensitivity of IpLITR 2.6b/IpFcRγ-L-mediated phagocytosis to the inhibitors Gö6976 (conventional PKCs), ER 27391 (Syk), Akt Inhibitor VIII (protein kinase B), wortmannin (PI3K), KB SRC4 (c-Src), and PP2 (Src kinases; compare Fig. 4.7A vs Fig. 4.6A). Latrunculin B (F-actin), Nocodazole (microtubules), and EHT 1864 (Rac1/2/3) were also

modestly more effective when used to block IpLITR 2.6b/IpFcRγ-L-mediated phagocytosis (Fig. 4.7A). The inhibitory effects of ML 141 (Cdc42), LY294002 (PI3K), U0126 (MEK1/2), and BisII (novel PKC isoforms) were similar between the endogenous and IpLITR-dependent phagocytic pathways and the only drug that was less effective at blocking IpLITR 2.6b/IpFcRγ-L-mediated phagocytosis compared to the endogenous phagocytic activity was the PDK1 inhibitor GSK2334470 (63.4% inhibition of IpLITR 2.6b/IpFcRγ-L-mediated phagocytosis vs. 84.6% inhibition of endogenous phagocytic activity; -21.2% difference). When ten-fold reduced concentrations of each inhibitor were used (Fig. 4.7C; black bars), a significant reduction in the efficacy was observed and only Latrunculin B, PP2, wortmannin, and Gö6976 achieved ~25% inhibition of phagocytosis (i.e. 87.5%, 24.9%, 23.8%, and 38%, respectively).

Differences in the pharmacological profiles between IpLITR 2.6b/IpFcRγ-L- and IpLITR 1.1b-expressing cells are revealed when comparing Figure. 4.7A and 4.7B. Unlike what I observed for IpLITR 2.6b/IpFcRγ-L-expressing cells, the majority of the inhibitors tested did not effectively block the IpLITR 1.1b-mediated phagocytic response (Fig. 4.7B). Latrunculin B (83.5% inhibition), ER 27391 (30% inhibition), and PP2 (23.7% inhibition) were the only drugs that caused >25% inhibition of IpLITR 1.1b-mediated phagocytosis. The remaining eleven inhibitors used all demonstrated <25% inhibitory effects that ranged from 1.5-16.1% inhibition (Fig. 4.7B). As described above, when the drug concentrations were reduced ten-fold, a precipitous drop in their inhibitory activities against IpLITR 1.1b-mediated phagocytosis was observed (Fig. 4.7C). However, the relative magnitude of the reduction was minimal when compared to IpLITR 2.6b/IpFcRγ-L, due in large part to the general ineffectiveness of the higher doses of each inhibitor against the IpLITR 1.1b-dependent pathway.

4.3 DISCUSSION

In this thesis chapter, my major objective was to characterize the unique ITAM-independent phagocytic pathway regulated by IpLITR 1.1b. Here, I show that IpLITR 2.6b/IpFcRγ-L and IpLITR 1.1b execute different intracellular mechanisms for activating the phagocytic machinery. These experiments were performed using the heterologous expression of fish immunoregulatory proteins in the well characterized and representative mammalian myeloid immune cell line, RBL-2H3 cells. By using N-terminal epitope-tagged (e.g. HA) IpLITR constructs that allow for the expression of IpLITRs in mammalian immune cells, I have taken advantage of commercially available antibodies to easily engage and activate these receptors. In the absence of identified ligands combined with challenges associated with expressing these proteins in fish cells, this experimental strategy has assisted in defining the fundamental cellular mechanisms that contribute to the stimulatory and inhibitory actions of IpLITRs and has outlined their important regulatory roles in diverse innate cell effector responses, including: cytotoxicity, degranulation, cytokine secretion, and phagocytosis [10–12,187]. However, I cannot exclude the possibility that miscommunication between the transfected teleost receptors and the RBL-2H3 signaling machinery resulted in the unique phenotype of target acquisition and engulfment displayed by IpLITR 1.1b-expressing cells, however due to the lack of available experimental reagents for fish cell lines a mammalian cell-line offers more diversity in the ways to study IpLITR functional capabilities. However, the data obtained using IpLITR 2.6b/IpFcRγ-L-transfected RBL-2H3 cells strongly suggest that the IpLITR-overexpression approach does allow for the engagement of conserved signaling effectors that are involved in ITAM-dependent phagocytic responses. Consequently, while this experimental strategy is not adequate for drawing direct comparisons between the actions of IpLITRs observed in RBL-2H3 cells and the

potential *in vivo* activities of these receptors in fish, my findings do allow for the examination of IpLITR-mediated phagocytosis in an innate immune cell-type and provides important new information regarding the signaling potential of two different teleost immunoregulator-types. Overall based on my findings the phagocytic phenotype for IpLITR-expressing cells is best described as two separate outputs: i) activation of the phagocytic process refers to cells that have captured their targets by initiating the formation of actin-dependent phagocytic cups, and ii) completion of the phagocytic process refers to any cell that has fully engulfed at least one bead. Using these two stages of the phagocytic process I was able to comprehensively detail a classical ITAM-mediated pathway initiated by IpLITR 2.6b/IpFcRγ-L and a unique ITAM-independent pathway regulated by IpLITR 1.1b using flow cytometry and confocal microscopy.

The ITAM-dependent phagocytic response of IpLITR 2.6b/IpFcRγ-L-expressing cells was abrogated at reduced incubation temperatures and was sensitive to known pharmacological inhibitors of FcR-mediated phagocytosis. Interestingly, unlike its ITAM-containing counterpart, IpLITR 1.1b-expressing cells were able to trigger a likely actin-dependent phagocytic process at depressed temperatures as low as 22ºC and were refractory to pharmacological inhibitors of the classical signaling steps involved in FcR-mediated phagocytosis. Detailed analysis of IpLITR-mediated target interactions also revealed that IpLITR 1.1b-expressing cells have a unique target acquisition and engulfment phenotype. This phenotype featured the formation of extended membranous protrusions that captured targets within phagocytic cup-like structures but were overall less capable of completing the engulfment process. This was remarkably different than the phagocytic mode utilized by the ITAM-containing IpLITR 2.6b/IpFcRγ-L construct, which was similar to the classical FcR-mediated target engulfment pathway described extensively in mammals [2,61,62,200,201].

The similarities in the pharmacological profiles generated for empty vector-transfected and IpLITR-expressing cells using FBS-opsonized beads suggest that the endogenous phagocytic response of RBL-2H3 cells was not affected by my transfection protocols or by the stable expression of IpLITRs in these cells. Pharmacological profiling also indicated that the potency (% inhibition of phagocytosis) of each selective inhibitor was dependent on the receptor-types engaged (i.e. the engagement of endogenous receptors for various serum components using FBS-opsonized beads [29,208] vs. the receptor specific engagement of IpLITRs using αHA mAb-opsonized beads). Regardless of these differences, if an inhibitor consistently abrogated the phagocytic responses >25% when compared to their vehicle controls, I considered that the target of the inhibitor was likely involved in the intracellular network controlling the phagocytic response. In most cases, this chosen level of effectiveness (i.e. >25% inhibition of phagocytosis) also correlated with statistically significant differences between the vehicle control and the inhibitor treatments (Fig. 4.6). Based on these criteria, my data provides the first biochemical details describing the phagocytic pathway activated by IpLITR 2.6b/IpFcRγ-L; which, was shown to be similar to the ITAM- and PTK-dependent mode of phagocytosis utilized by mammalian FcRs [103,209,210]. Specifically, inhibition of proximal (Src and Syk), intermediate (PI3K, PKCα/β1, Cdc42, and Rac1/2/3), and distal (F-actin) mediators of the classical FcR-dependent phagocytic pathway all effectively abrogated (i.e. >25% inhibition; ranging from 45-100%) the IpLITR 2.6b/IpFcRγ-L-mediated phagocytic response (Fig. 4.7A). As previously reported, IpLITR 2.6b/IpFcRγ-L-mediated phagocytosis was also inhibited at incubation temperatures below 37ºC [36], as was the endogenous pathway used for the engulfment of FBS-opsonized beads. These results suggest that the ITAM-dependent mode of signaling, as well as one or more of the signaling steps leading to activation of actin polymerization and membrane

remodeling, is/are temperature-sensitive. In addition, the marked similarities observed between IpLITR 2.6b/IpFcRγ-L-mediated phagocytosis and the endogenous pathway elicited within the same mammalian myeloid cell-type indicates that ITAM-dependent phagocytosis in vertebrates may represent a conserved signaling mode for target engulfment.

In this chapter, I also characterized a unique ITAM-independent pathway for the activation of phagocytosis that was both phenotypically and pharmacologically distinct from the ITAM-mediated mode described above. In particular, the IpLITR 1.1b-mediated phagocytic pathway was only significantly blocked by treatment with Latrunculin B (prevents F-actin assembly; 83.5% inhibition), PP2 (targets Src-family kinases Lck and Fyn; 24% inhibition), and ER 27391 (targets Syk; 30% inhibition) (Fig. 4.7B). These results indicate that the IpLITR 1.1b phagocytic process is actin-dependent and possibly requires the activity of common membrane-proximal PTKs; strongly suggesting that tyrosine phosphorylation of the IpLITR 1.1b CYT is required for the induction of this pathway. However, despite the convergence of IpLITR-mediated phagocytic processes at the control of actin polymerization dynamics, IpLITR 1.1b clearly operates independently of several of the key components of the ITAM-dependent signaling machinery. That said, at this time, I cannot exclude the possibility that IpLITRs share other signaling molecules that have not been targeted in these pharmacological profiles. Specifically, other known effectors of the ITAM-independent phagocytic pathway utilized by CR3 include RhoA, Rho-associated protein kinase, mDia, and myosin II [113,122,211]. Whether and how these and other molecules may influence the induction and regulation of IpLITR 1.1b-mediated phagocytosis remain to be tested.

In addition to pharmacological profiling of the intracellular signaling networks involved, phenotypic assessments of IpLITR-mediated phagocytic phenotypes were also performed using

confocal microscopy imaging. The flow cytometry-based phagocytosis assay can accurately differentiate beads that are non-specifically associated with cell membranes from those actively captured by the membrane using trypsin treatments prior to analysis. Without the trypsin treatment step, phagocytic outputs increased ~15-20% suggesting that a proportion of beads are non-specifically associated with cell membranes; these are likely not captured within active membrane structures such as phagocytic cups. However, since the trypsin treatment step does not remove beads that are actively captured and/or partially engulfed by cells, the positive phagocytic events I reported using flow cytometry represents a mixture of completely internalized beads and/or those that are actively captured in phagocytic cups. Therefore, accurately quantifying the numbers of captured vs. engulfed beads is not possible using my standard flow cytometry protocol. Therefore, to more accurately enumerate the ratio of captured-to-engulfed extracellular targets, I also examined IpLITR-mediated phagocytosis using confocal microscopy. In general, IpLITR 2.6b/IpFcRγ-L-expressing cells contained three or more fully engulfed beads per cell (Fig. 4.3B and Fig. 4.5B). In comparison, significantly fewer IpLITR 1.1b-expressing cells had completely internalized their targets and, when they did, only a single bead was found in each cell (Fig. 4.3C and Fig. 4.5D). Interestingly, many IpLITR 1.1b-expressing cells interacted with beads by extending their membranes around targets and forming phagocytic cup-like structures, but many of these captured beads were not internalized. Incomplete target engulfment is indicative of a stalled phagocytic phenotype and was observed for ~44% of the IpLITR 1.1b-expressing cells examined, but rarely observed for IpLITR 2.6b/IpFcRγ-L-dependent target interactions. IpLITR 1.1b-expressing cells also captured some of the beads along or at the ends of extended membranous protrusions that often resulted in a single bead being captured/shared by two or more cells. Again, this unique target acquisition

phenotype was not observed for IpLITR 2.6b/IpFcRγ-L-expressing cells. When combined with my temperature-dependency and pharmacological studies, the discrepancies observed in the phagocytic phenotypes provides additional evidence that IpLITR 2.6b/IpFcRγ-L and IpLITR 1.1b activate distinct cellular modes of phagocytosis. The ITAM-independent IpLITR 1.1b target acquisition and engulfment pathway may represent a new mode of immunoregulatory receptor-mediated membrane remodeling required for immune cell-target interactions and reinforces previous studies demonstrating that certain IpLITRs exhibit functional plasticity [38].

At present, the mechanism(s) controlling an ITAM-independent target acquisition pathway activated by IpLITR 1.1b are not understood. However, I hypothesize that the proximal and distal regions of the IpLITR 1.1b CYT may differentially participate in the recruitment and activation of select phagocytic effectors. Although the specific molecules recruited are not yet known, this mechanism may be similar to previous findings suggesting that distinct regions of the IpLITR 1.1b CYT can differentially regulate NK cell killing responses by selective recruitment of intracellular signaling effectors [12]. Furthermore, in mammals, CR3-mediated phagocytosis also requires that various adaptors and signaling molecules are recruited to either the proximal or distal CYT regions in order to facilitate the ITAM-independent recruitment and activation of RhoA [119].

The distal CYT region of IpLITR 1.1b encodes three tyrosines (Y_{477}, Y_{499}, and Y_{503}) that are embedded within two ITIMs and one immunoreceptor tyrosine-based switch motif [11,13]. The proximal CYT region also contains three more tyrosine residues (Y_{433}, Y_{453}, and Y_{463}) but these are not found within ITIMs, ITAMs, or switch motifs. Therefore, for IpLITR 1.1b to activate phagocytosis, my results suggest that it must stimulate actin polymerization and may require the catalytic activity of the Src and Syk families of intracellular kinases. Furthermore, I

hypothesize that IpLITR 1.1b may exist in a primed state causes the facilitating basal or constitutive coupling to the machinery requisite for target acquisition and phagocytic cup extension. This could be due to constitutive association with effectors of actin dynamics, which would be similar to the novel short-circuited phagocytic pathway recently described for CEACAM3 that required the non-ca Nck [3,8]. In this model of phagocytosis Nck serves as a cytosolic adaptor that couples ligand-occupied/bound receptors with a range of intracellular effectors that influence actin dynamics [212–214]. The recruitment of Nck to CEACAM3 occurred within the proximal CYT region at a phosphorylated tyrosine [3] and was responsible for recruiting the WAVE2 complex; a highly conserved multimolecular protein complex that is vital component of the actin polymerization machinery [215]) to the vicinity of the ligand-bound receptor. In addition to Nck and WAVE2, the CYT region of CEACAM3 also recruits the GEF Vav, which is a known activator of the Rho family GTPase, Rac1 [94]. Activation of Rac1 serves as the trigger for the induction of actin polymerization downstream of the Nck-associated WAVE2 complex [3]. This alternative CEACAM3-mediated phagocytic signaling pathway efficiently couples target recognition to a rapid phagocytic mode using a minimal set of intracellular mediators [3] and a similar scenario may exist for IpLITR 1.1b.

The control of actin-driven pseudopod protrusions and phagocytic cup formation by IpLITR 1.1b illustrates, for the first time, a unique ITAM-independent mechanism for the activation of phagocytosis by a non-mammalian immunoregulatory receptor. Outside the detailed examinations of the classical phagocytic receptors FcR and CR3, the knowledge regarding the dynamic control of intracellular effectors responsible for actin-dependent membrane remodeling events by immunoregulatory receptors is still limited. Furthermore, how the growing repertoire of known phagocytic receptors and their associated signaling pathways contribute to the

conserved innate cellular activities of target capture and engulfment is largely unexplored across vertebrates. Interestingly, the phagocytic events for IpLITR 1.1b-mediated phagocytosis detailed here are reminiscent of the known tethering functions described for other mammalian immunoregulatory receptors [216,217]. Tethering of extracellular targets to the cell surface assists in the rapid and efficient immobilizing of captured targets by phagocytes, making them more susceptible to antimicrobial products and/or increasing the likelihood they will be engulfed. Capturing mobile pathogens may also prevent their dissemination and make them prone to subsequent engagement by other phagocytic receptors that use robust internalization pathways such as the ITAM-dependent phagocytic mode described for IpLITR 2.6b/IpFcRγ-L. Such a system by which one receptor is used for efficiently securing targets to the cell surface while another receptor triggers the phagocytic machinery, would provide a cooperate mechanism for the capture and engulfment of extracellular targets. This may also be an operational scenario for IpLITR 2.6/IpFcRγ-L and IpLITR 1.1b as their membrane distal and putative ligand binding Ig-like domains share 91% aa identity. It is therefore possible that, when co-expressed by immune cells that these two receptor-types serve to tether extracellular targets (IpLITR 1.1b) and subsequently trigger the internalization process (IpLITR 2.6/IpFcRγ-L). However, whether this process requires opsonin's such as Ig or direct interactions with extracellular targets cannot be determined until the ligands of IpLITRs are identified. Nonetheless, multi-receptor systems further compound the complexity of understanding phagocytic modes by taking into account the integration of signals from different immunoregulatory receptors during the binding and internalization of targets. This is an emerging theme that will be important for understanding the complexity of innate cell phagocytosis, in mammals and across vertebrates.

FIGURE 4.1

A.

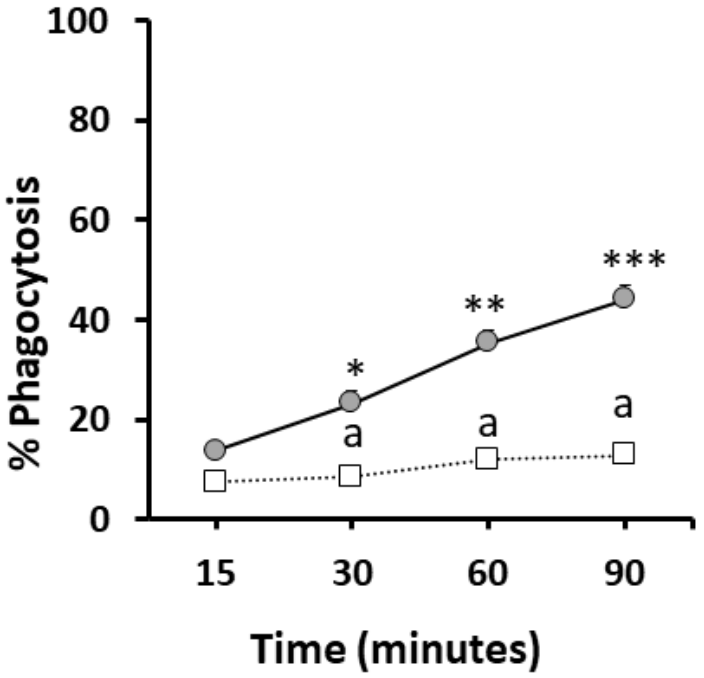
100
80
60
40
20
0
% Phagocytosis
*
**
***
a
a
a
15
30
60
90
Time (minutes)

B.

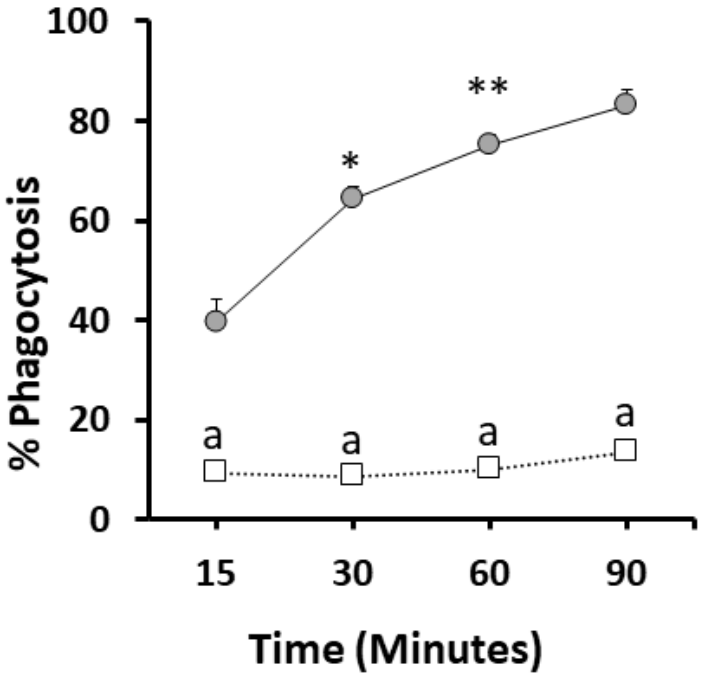
100
80
60
40
20
0
% Phagocytosis
*
**
a
a
a
a
15
30
60
90
Time (Minutes)

FIGURE 4.1

C.

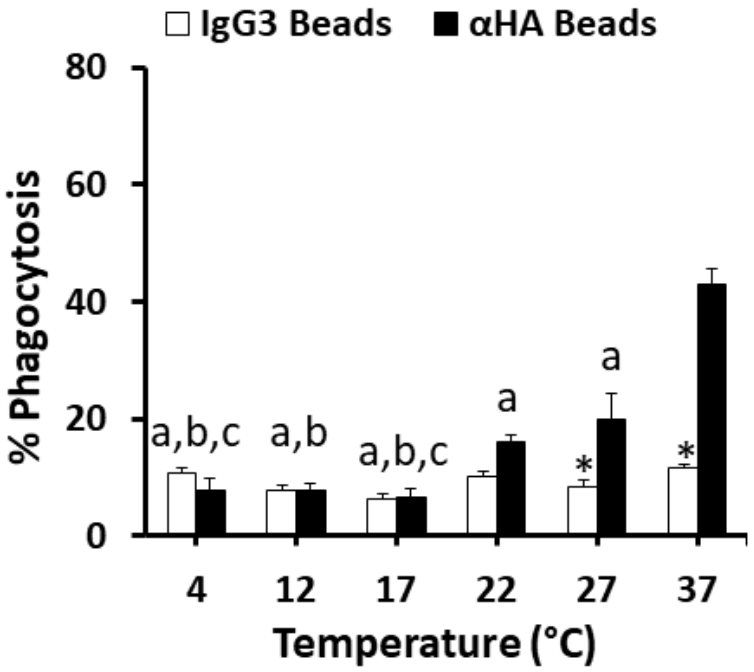
IgG3 Beads
αHA Beads
% Phagocytosis
80
60
40
20
0
a,b,c
a,b
a,b,c
a
a
*
*
4
12
17
22
27
37
Temperature (°C)

D.

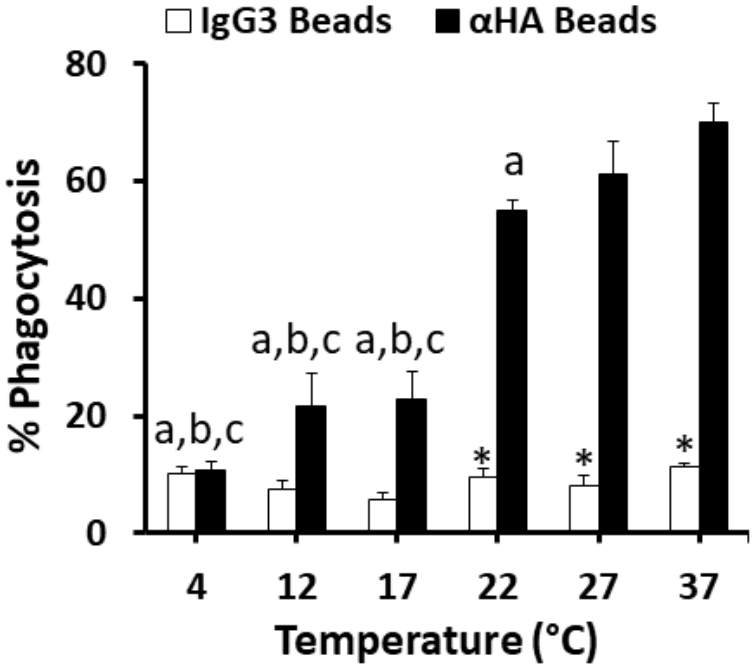
IgG3 Beads
αHA Beads
% Phagocytosis
80
60
40
20
0
a,b,c
a,b,c
a,b,c
a
*
*
*
4
12
17
22
27
37
Temperature (°C)

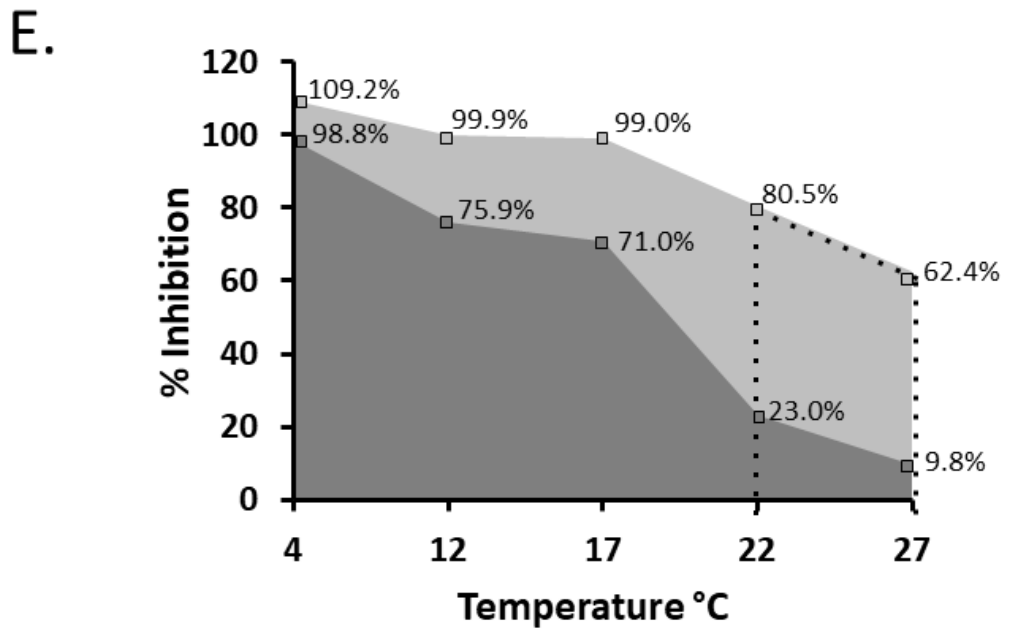

FIGURE 4.1 Kinetic and temperature dependency of IpLITR-induced phagocytosis. Phagocytosis assays were performed by incubating $1x10^5$ IpLITR 2.6b/IpFcRγ-L- (A) or IpLITR 1.1b-expressing cells (B) with 4.5-μm YG polystyrene beads ($3x10^5$) pre-opsonized with αHA mAb (grey circles) or mouse IgG3 (open squares) for 15, 30, 60, and 90 minutes at 37^oC. Samples were then analyzed by flow cytometry and gated to determine the percentage of phagocytic cells as previously described [36, 38]. $^a p\leq0.05$ when comparing αHA mAb-opsonized bead and IgG3-opsonized bead phagocytosis at each time-point examined. $^* p\leq0.05$ when comparing 15 min to 30 min αHA mAb-opsonized bead phagocytosis values; $^{**} p\leq0.05$ when comparing 30 min to 60 min αHA mAb-opsonized bead phagocytosis values, and $^{***} p\leq0.05$ when comparing 60 min to 90 min αHA mAb-opsonized bead phagocytosis values. Grey circles and open squares represent the mean ± SEM of four independent time-course phagocytosis experiments performed. Phagocytosis assays were also performed by incubating $1x10^5$ IpLITR 2.6b/IpFcRγ-L- (C) or IpLITR 1.1b- (D) expressing cells with 4.5-μm YG polystyrene beads ($3x10^5$) pre-opsonized with αHA mAb (black bars) or mouse IgG3 (white bars) for 60 min at 37^oC, 27^oC, 22^oC, 17^oC, 12^oC, and 4^oC. $^a p\leq0.05$ when comparing αHA mAb-opsonized bead phagocytosis values at reduced incubation temperatures to control incubations (i.e. 37^oC). $^b p\leq0.05$ when comparing αHA mAb-opsonized bead phagocytosis values to the phagocytosis values obtained at 27^oC, $^c p\leq0.05$ when comparing αHA mAb-opsonized bead phagocytosis values to the phagocytosis values obtained at 22^oC, and $^* p\leq0.05$ when comparing the αHA mAb-opsonized bead phagocytosis values to the IgG3-opsonized values at the same temperature. Each bar represents the mean ± SEM of eight independent time-course phagocytosis experiments performed. A percent summary graph is also shown (E) demonstrating the differential effects of incubation temperature on IpLITR 2.6b/IpFcRγ-L - and IpLITR 1.1b-mediated phagocytosis.

FIGURE 4.2

A.

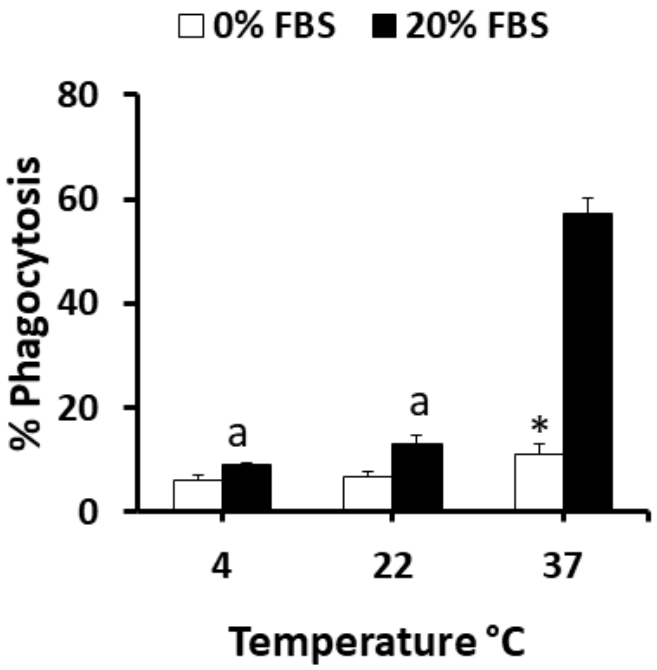
0% FBS
20% FBS
% Phagocytosis
80
60
40
20
0
a
a
*
4
22
37
Temperature °C

B.

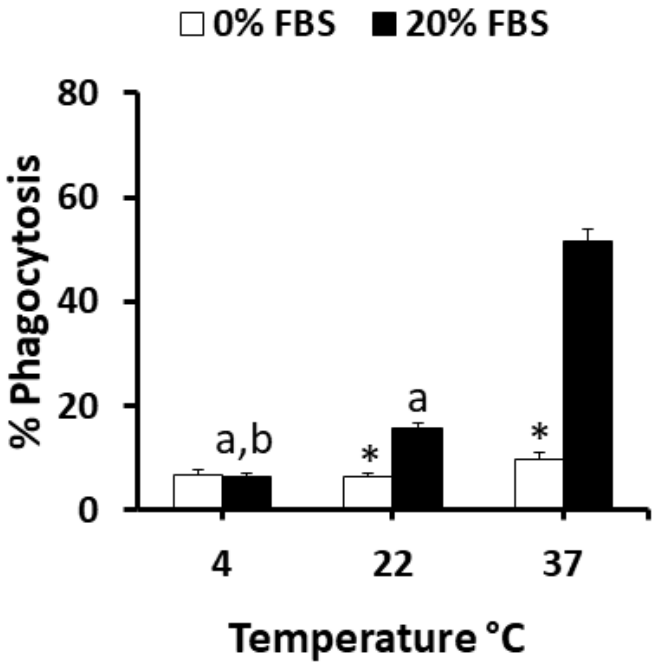
0% FBS
20% FBS
% Phagocytosis
80
60
40
20
0
a,b
*
a
*
4
22
37
Temperature °C

C.

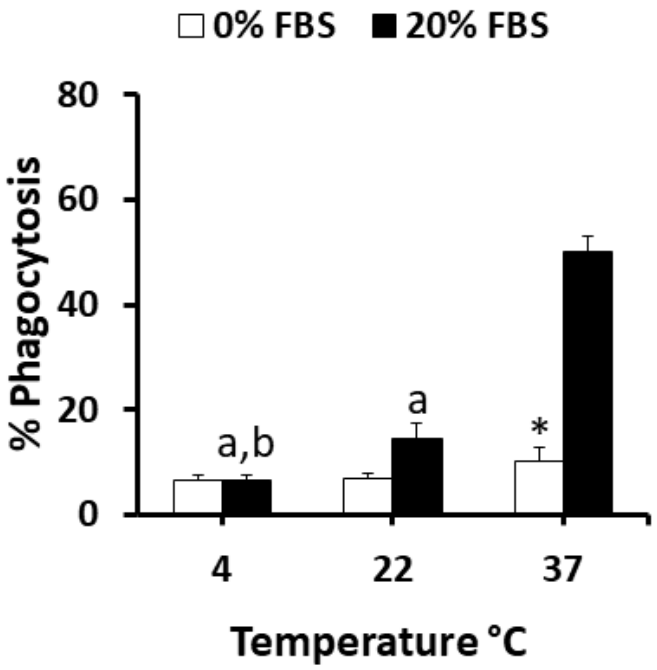

FIGURE 4.2 Flow cytometric examination of endogenous RBL-2H3 FBS-induced phagocytosis. RBL-2H3 endogenous phagocytic activity was assessed through incubation of FBS-opsonized beads. Either empty vector (A), IpLITR 2.6b/IpFcRγ-L (B), or IpLITR 1.1b-expressing (C) cells were incubated with FBS-opsonized beads (black bars) or non-opsonized beads (white bars) at either 37°C, 22°C or 4°C and their phagocytic responses were measured as %phagocytosis. Data shown here is the result of three independent experiment and each bar represents the mean ±SEM.

FIGURE 4.3

A.

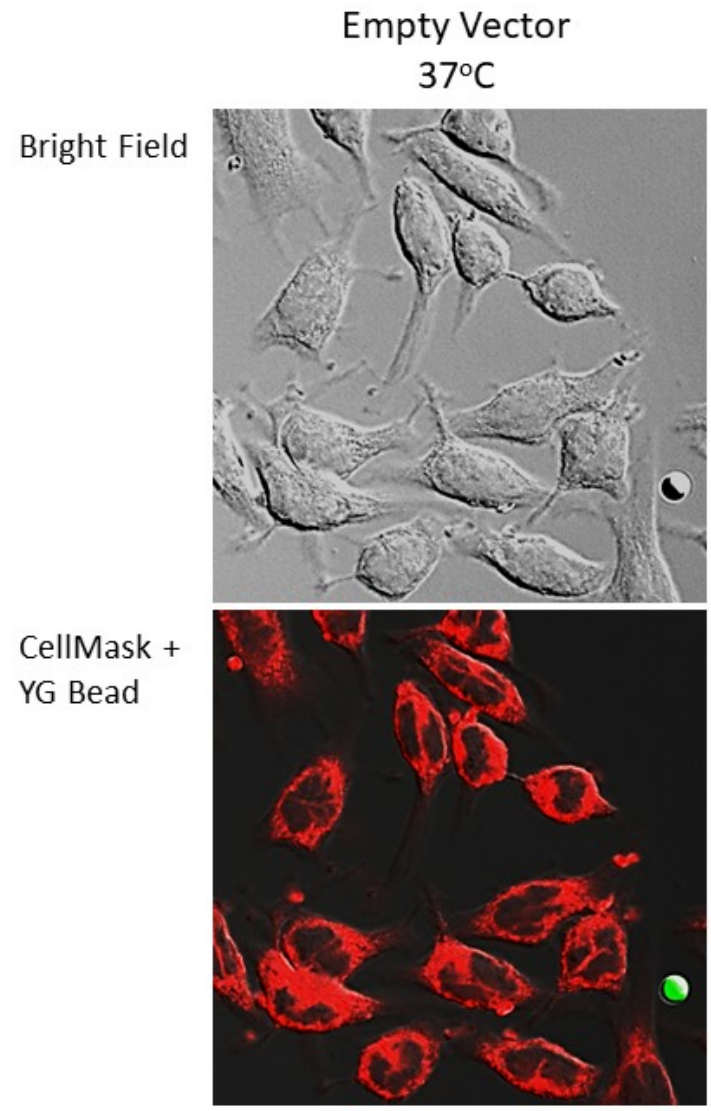

FIGURE 4.3

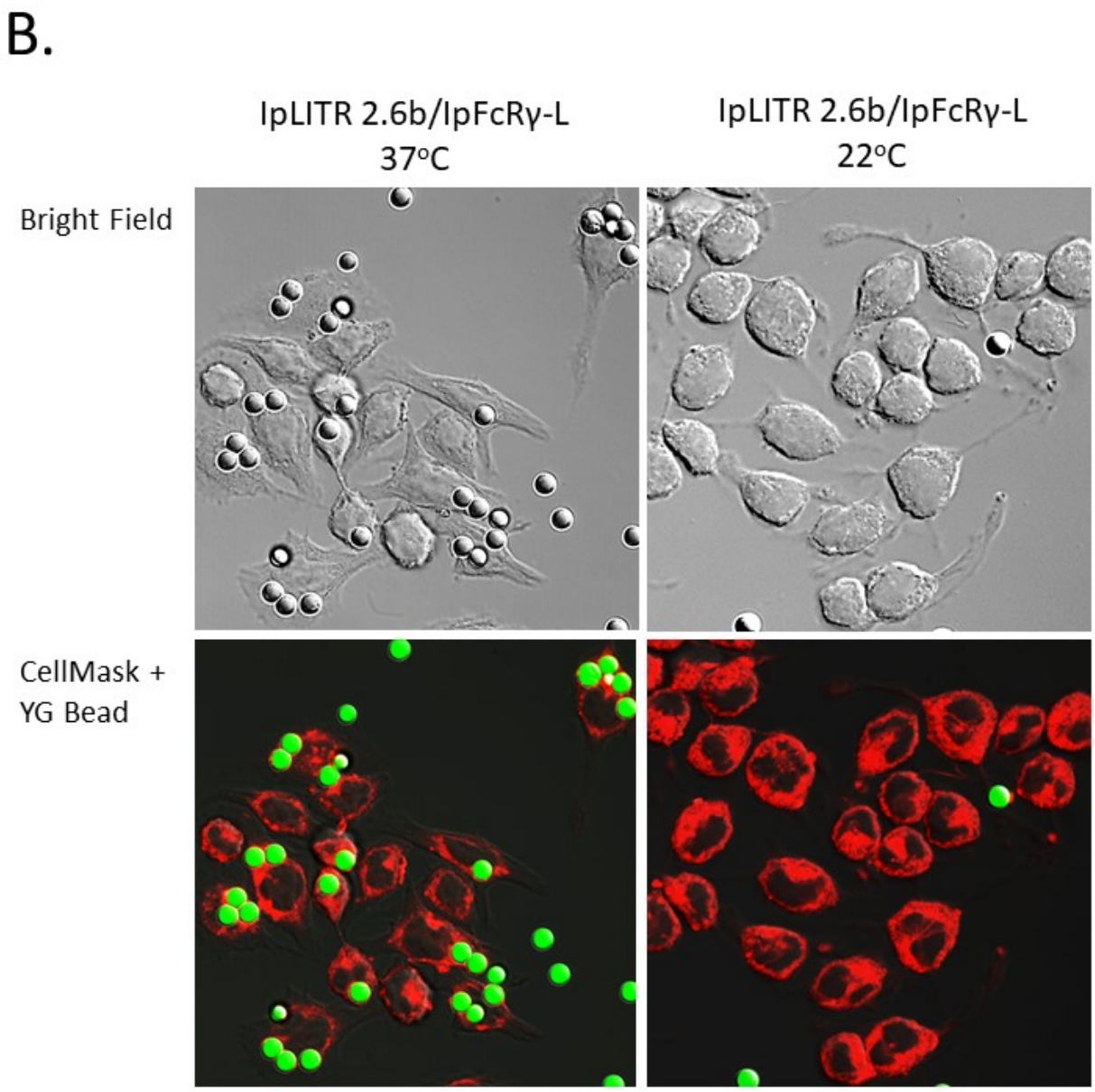
B.
IpLITR 2.6b/IpFcRγ-L
37°C
IpLITR 2.6b/IpFcRγ-L
22°C
Bright Field
CellMask +
YG Bead

FIGURE 4.3

C.

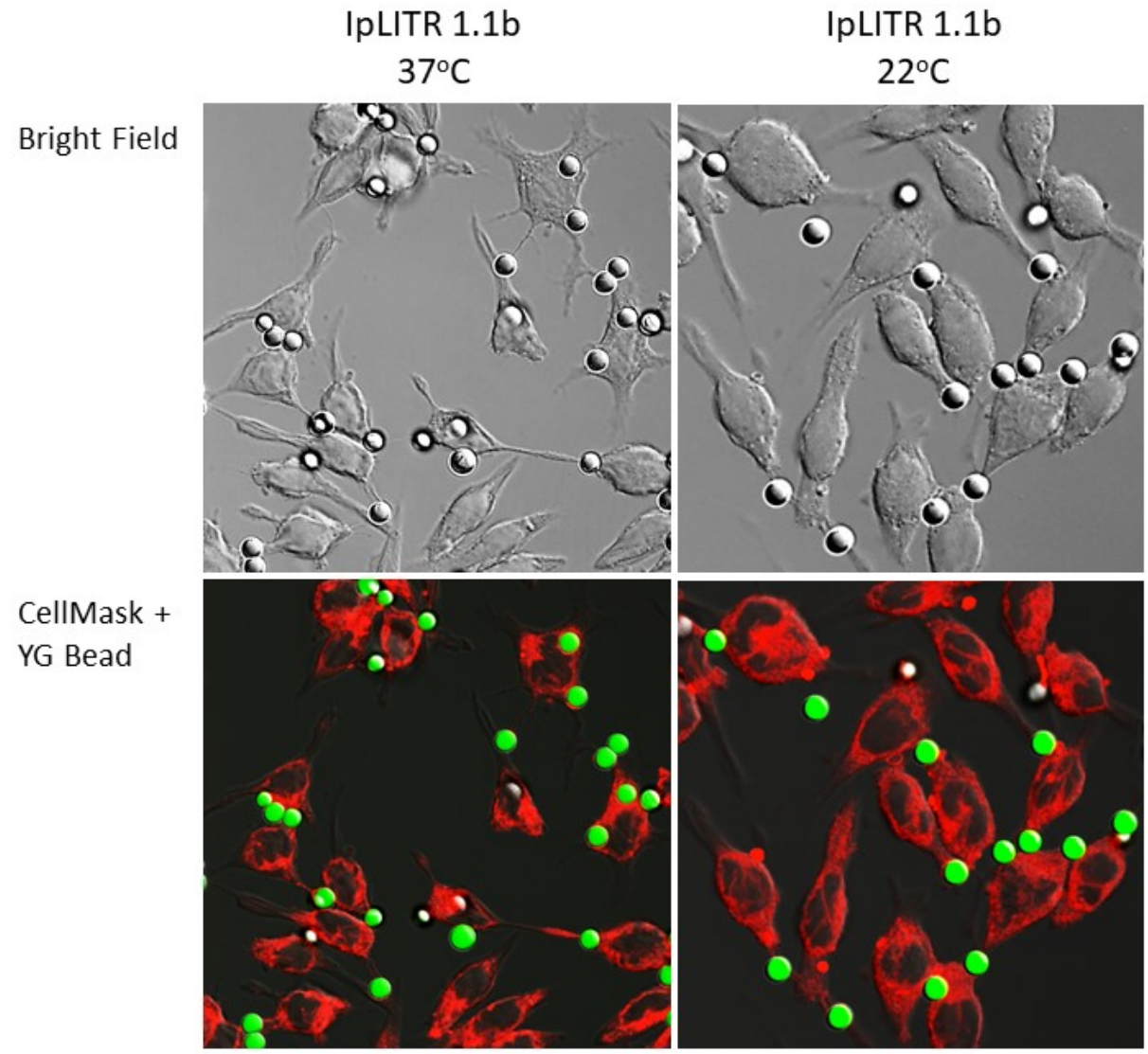

FIGURE 4.3 Confocal imaging analysis of IpLITR-mediated phagocytosis Empty vector-transfected RBL-2H3 cells (A) and cells expressing IpLITR 2.6b/IpFcRγ-L (B) or IpLITR 1.1b (C) were grown on glass coverslips and stained using CellMask™ membrane stain (Life Techologies). Phagocytosis was then performed as described for the flow cytometric assay for 60 min at 37^{o}C or 22^{o}C, and the cells were washed with PBS, fixed using 4% PFA, and then mounted onto glass slides. Cells were imaged with a Laser Scanning Confocal Microscope (LSCM): Zeiss LSM 710, objective 40X and 60X 1.3 oil plan-Apochromat (Cross Cancer Institute Microscopy Facility, University of Alberta). Selected images from z-stack acquisitions are shown as bright field images, merged fluorescence images showing membrane (red) and YG bead (green spheres) staining. For each column, selected images from the experimental groups are shown, and these are representatives of three independent staining experiments performed.

FIGURE 4.4

A.

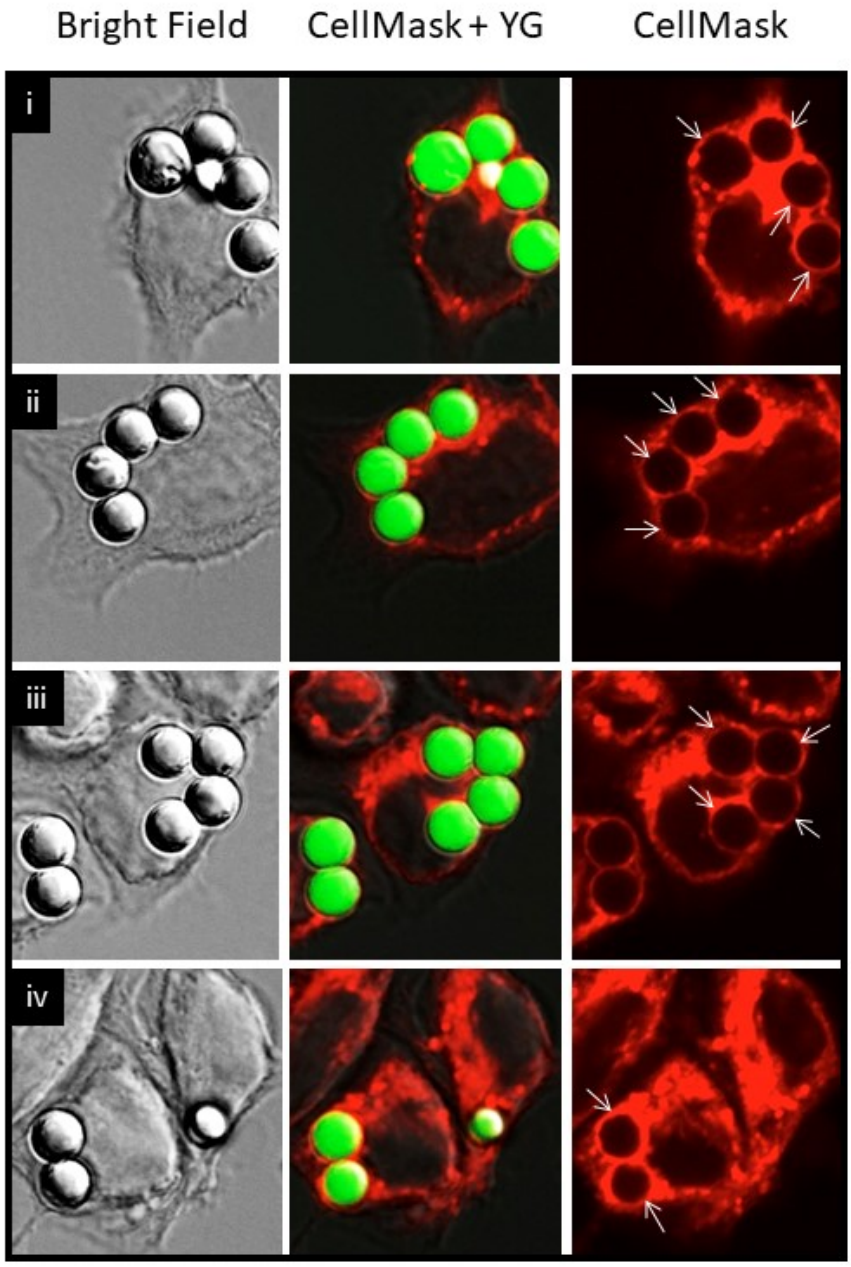

FIGURE 4.4

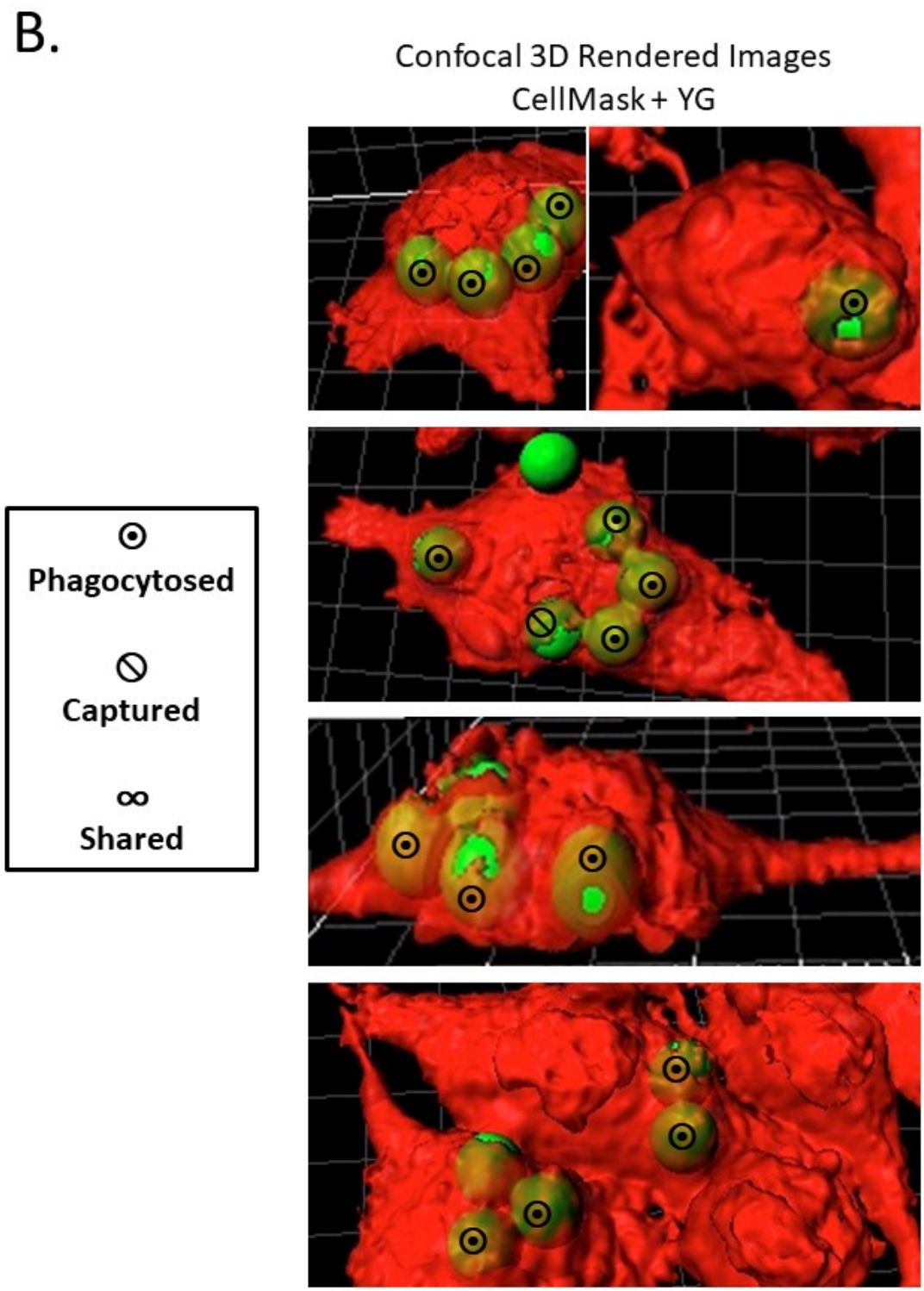
B.
Confocal 3D Rendered Images
CellMask + YG
⊙
Phagocytosed
⊘
Captured
∞
Shared

FIGURE 4.4

C.

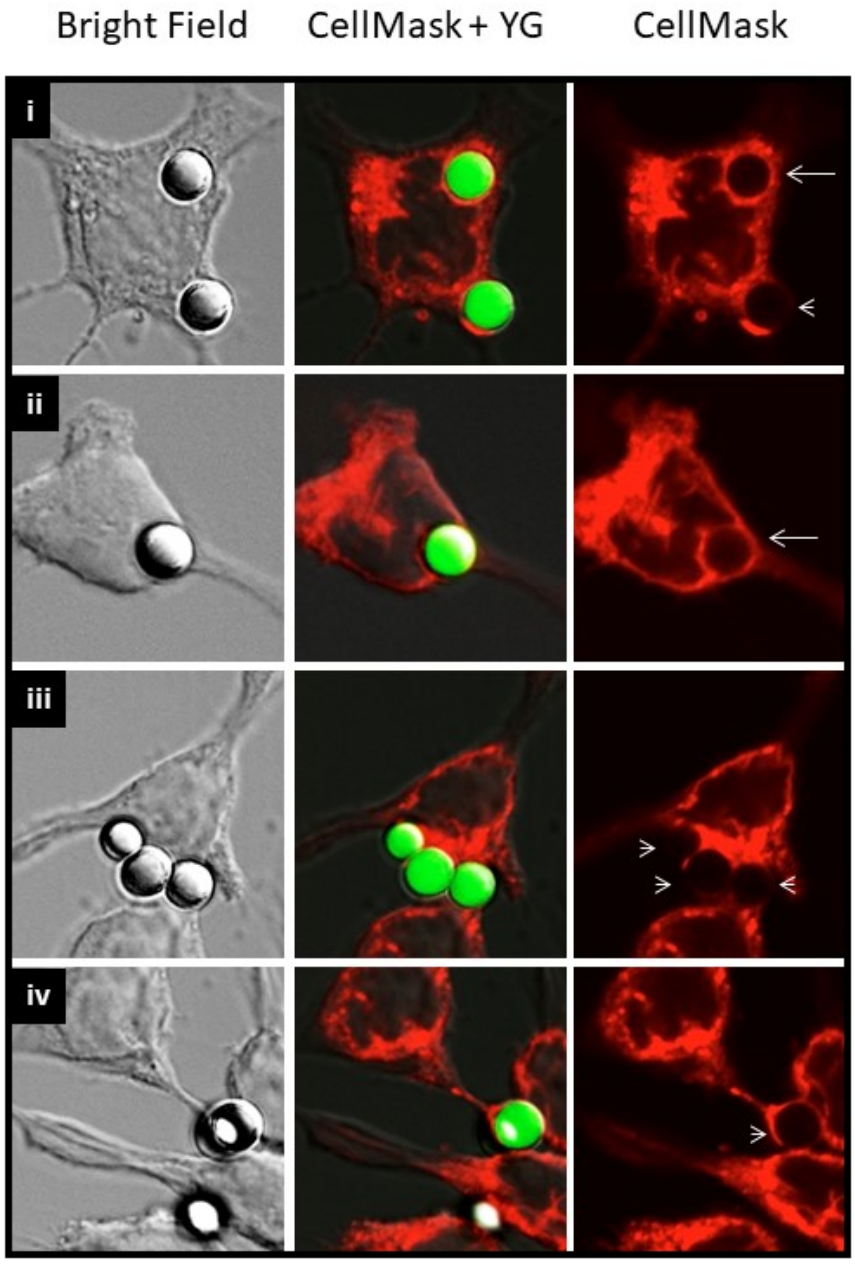

FIGURE 4.4

D.

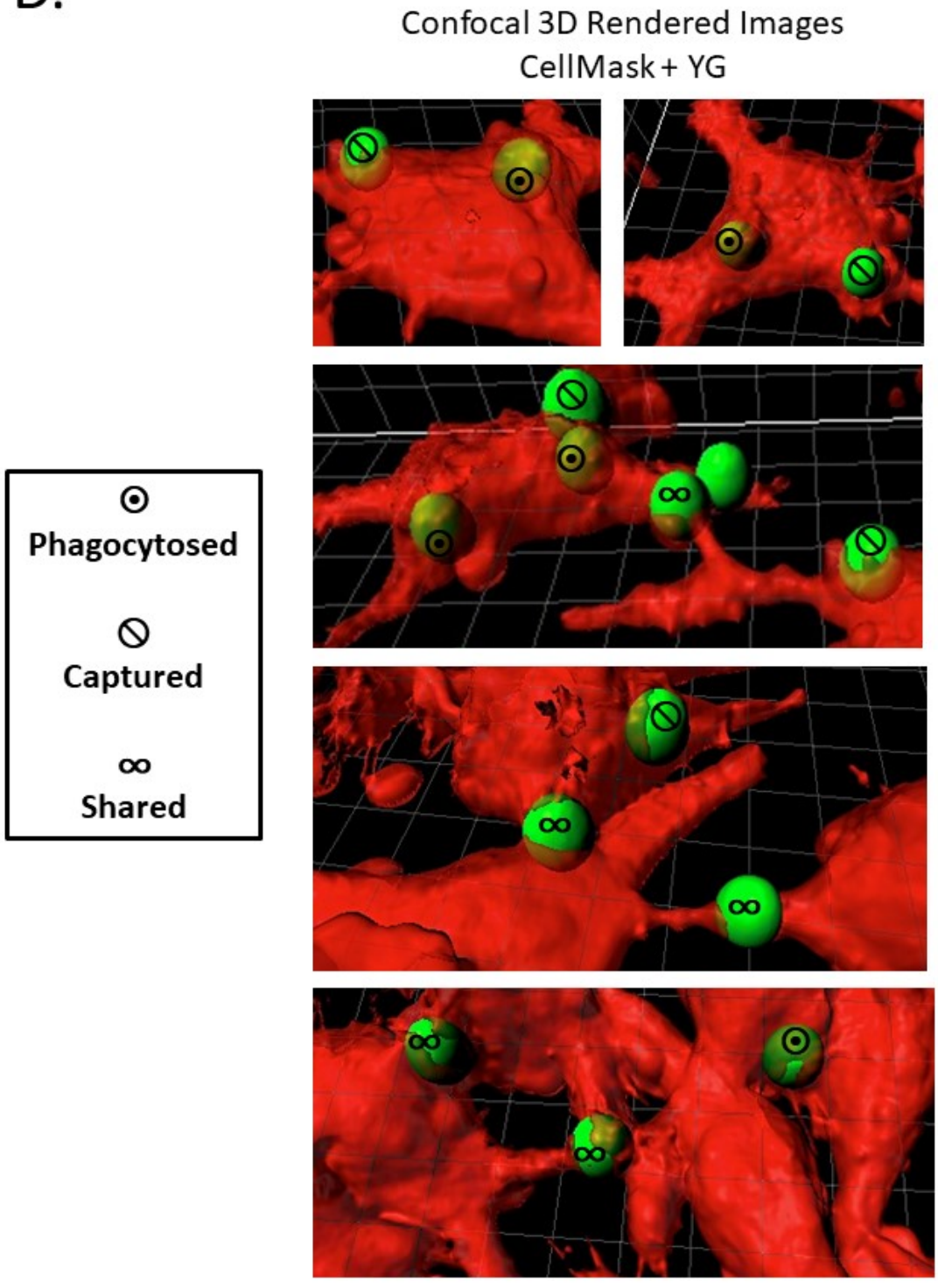
Confocal 3D Rendered Images
CellMask + YG
Phagocytosed
Captured
Shared

FIGURE 4.4

E.

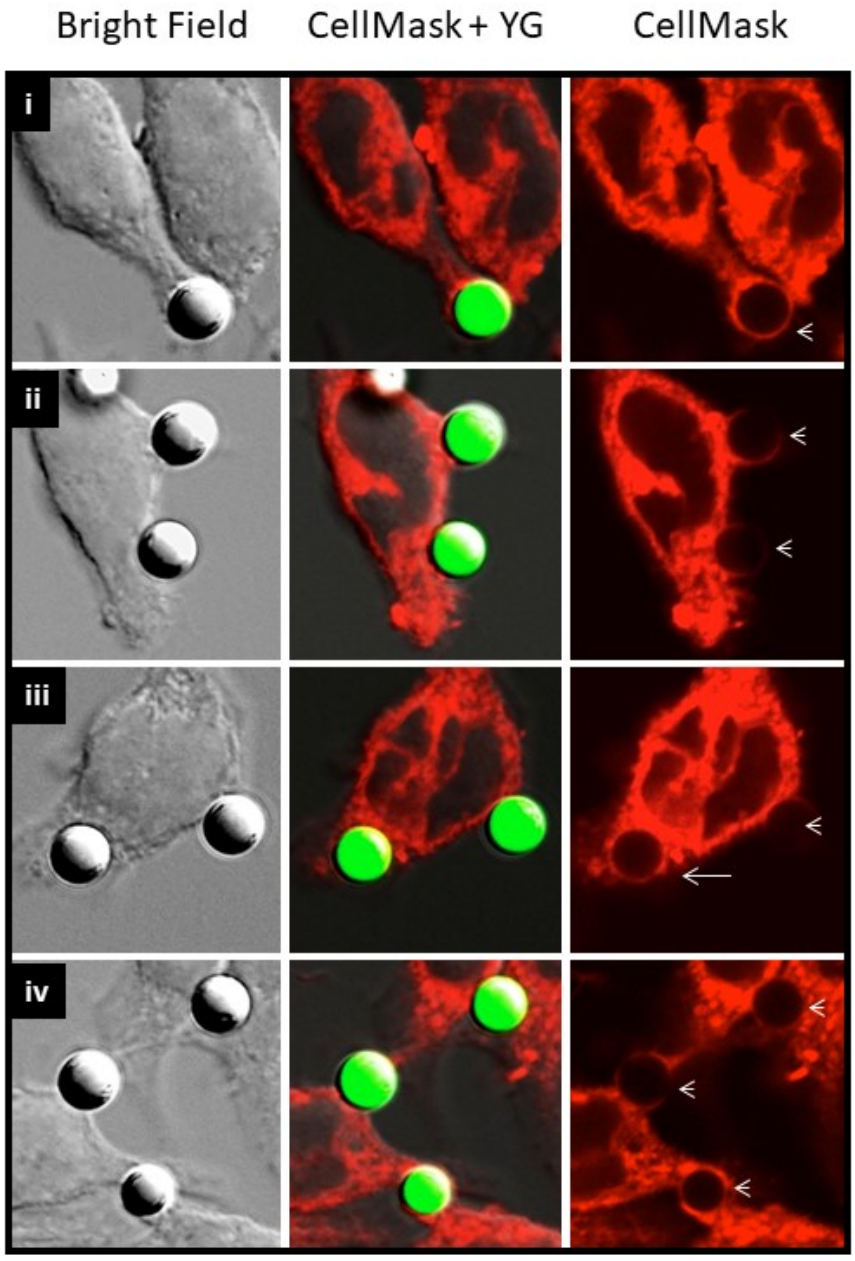

FIGURE 4.4

F.

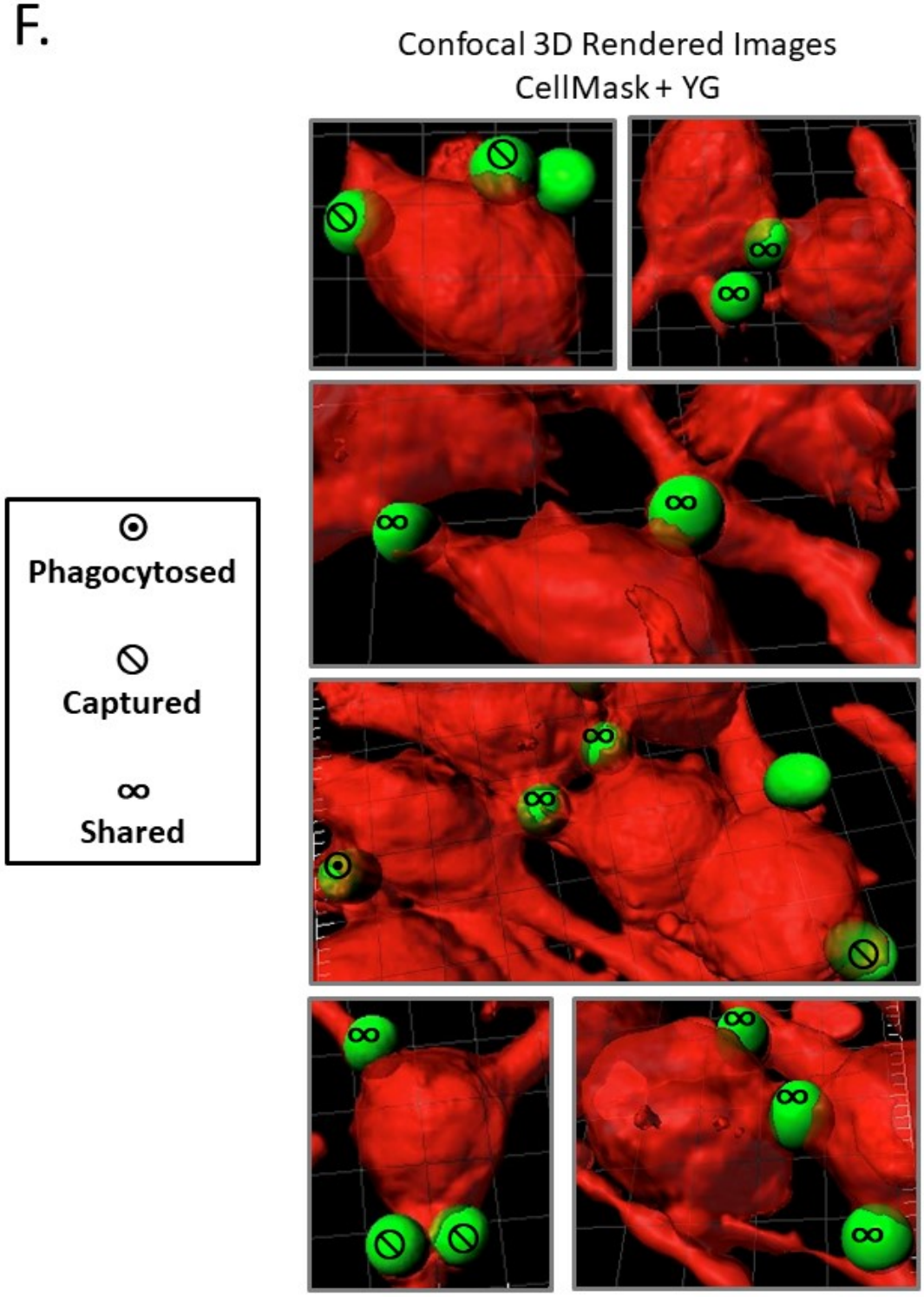
Confocal 3D Rendered Images
CellMask + YG
⊙
Phagocytosed
⊘
Captured
∞
Shared

FIGURE 4.4 Confocal Imaging and 3D rendering of IpLITR 2.6b/IpFcRγ-L and IpLITR 1.1b phagocytic phenotypes. Representative z stack images obtained from Figure 4.3 were used to assess individual cell-bead interactions by generating 3D renders. IpLITR 2.6b/IpFcRγ-L-expressing cells were incubated at 37°C (A) or IpLITR 1.1b-expressing cells were incubated at 37°C (C) or at 22°C (E) with αHA-opsonized beads and cell-bead interactions for individual cells were examined. These associations were designated into two categories; phagocytosed beads (arrows) and captured beads (arrowheads). Renders were generated for IpLITR 2.6b/IpFcRγ-L (B) and IpLITR 1.1b-expressing cells (37°C; D, 22°C; F) from the same experiments from Figure 4.3 and Figure 4.5. In these 3D renders YG beads (green) that are completely engulfed within the membrane (red) are marked as ⊙, YG beads capture are marked as ⊘, and those YG beads shared between one or more cells are marked as ∞. Beads devoid of symbols indicate an undetermined association with the cell based on the angle of the rendered image displayed. Not all cells shown in the 3D renders are those found within the same images shown in Figure 4.3 or Figure 4.4 but were from the same experiment.

FIGURE 4.5

A.

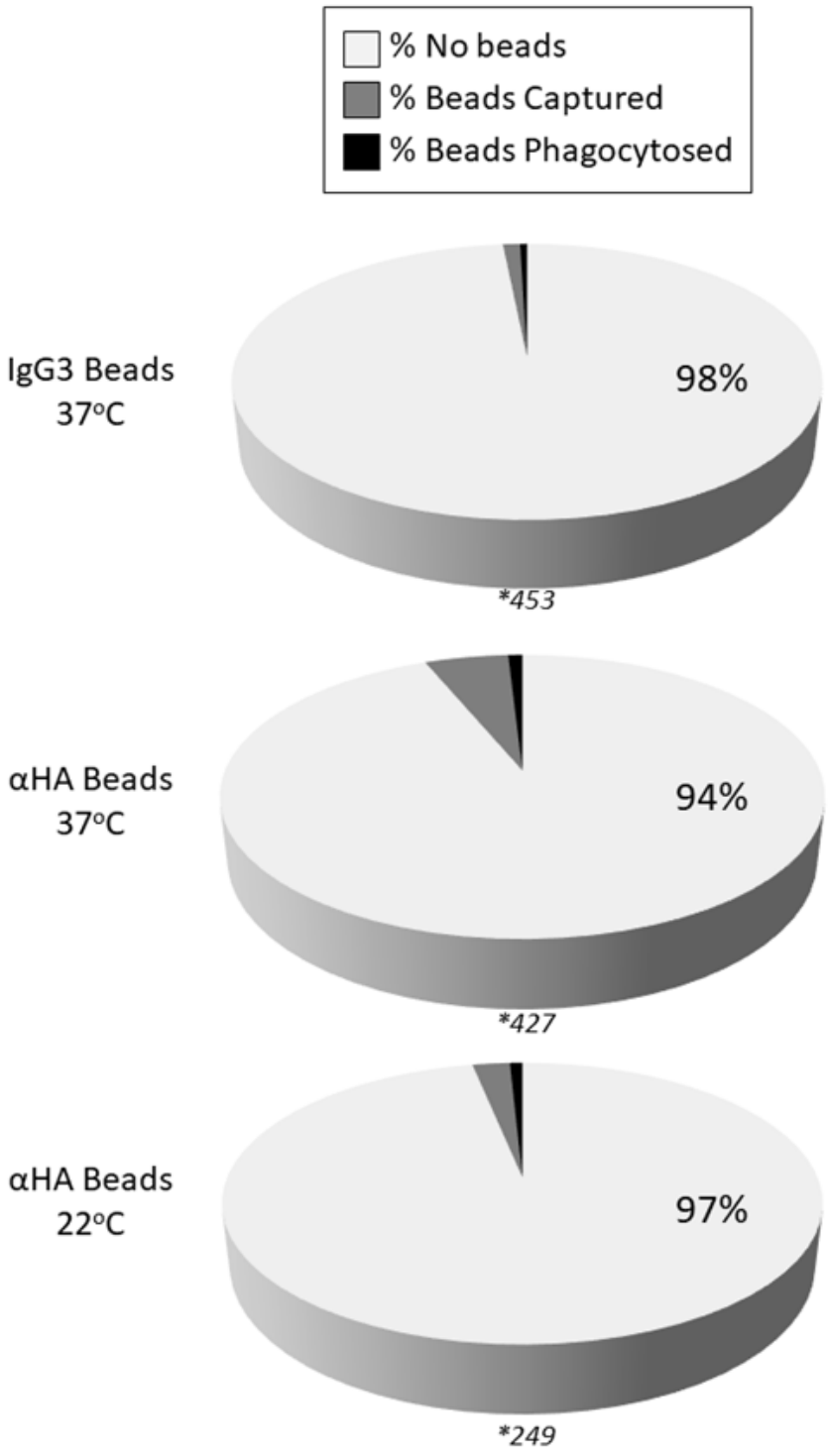
% No beads
% Beads Captured
% Beads Phagocytosed
IgG3 Beads
37°C
98%
*453
αHA Beads
37°C
94%
*427
αHA Beads
22°C
97%
*249

FIGURE 4.5

B.

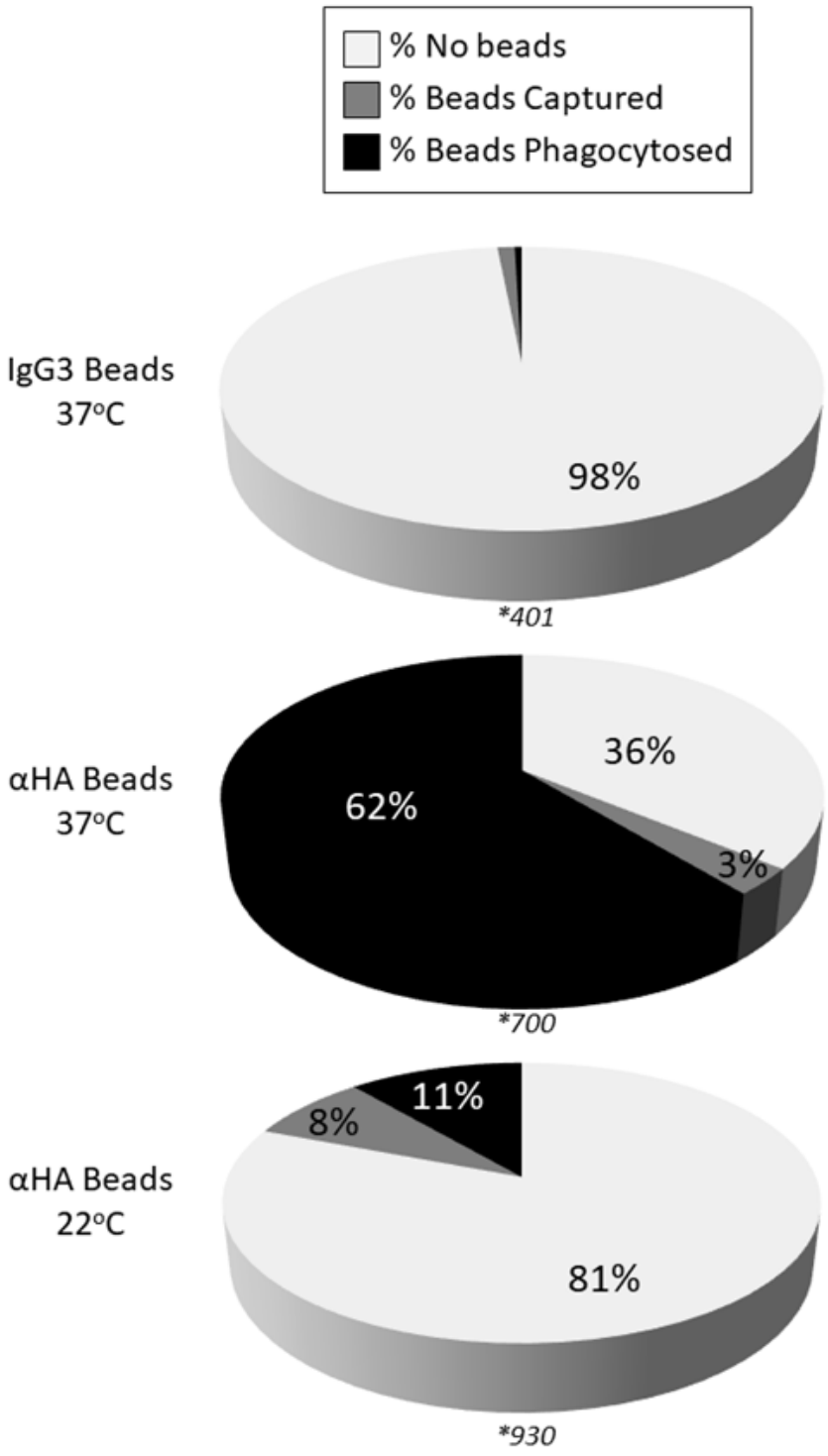
% No beads
% Beads Captured
% Beads Phagocytosed
IgG3 Beads
37°C
98%
*401
αHA Beads
37°C
36%
62%
3%
*700
αHA Beads
22°C
11%
8%
81%
*930

FIGURE 4.5

C.

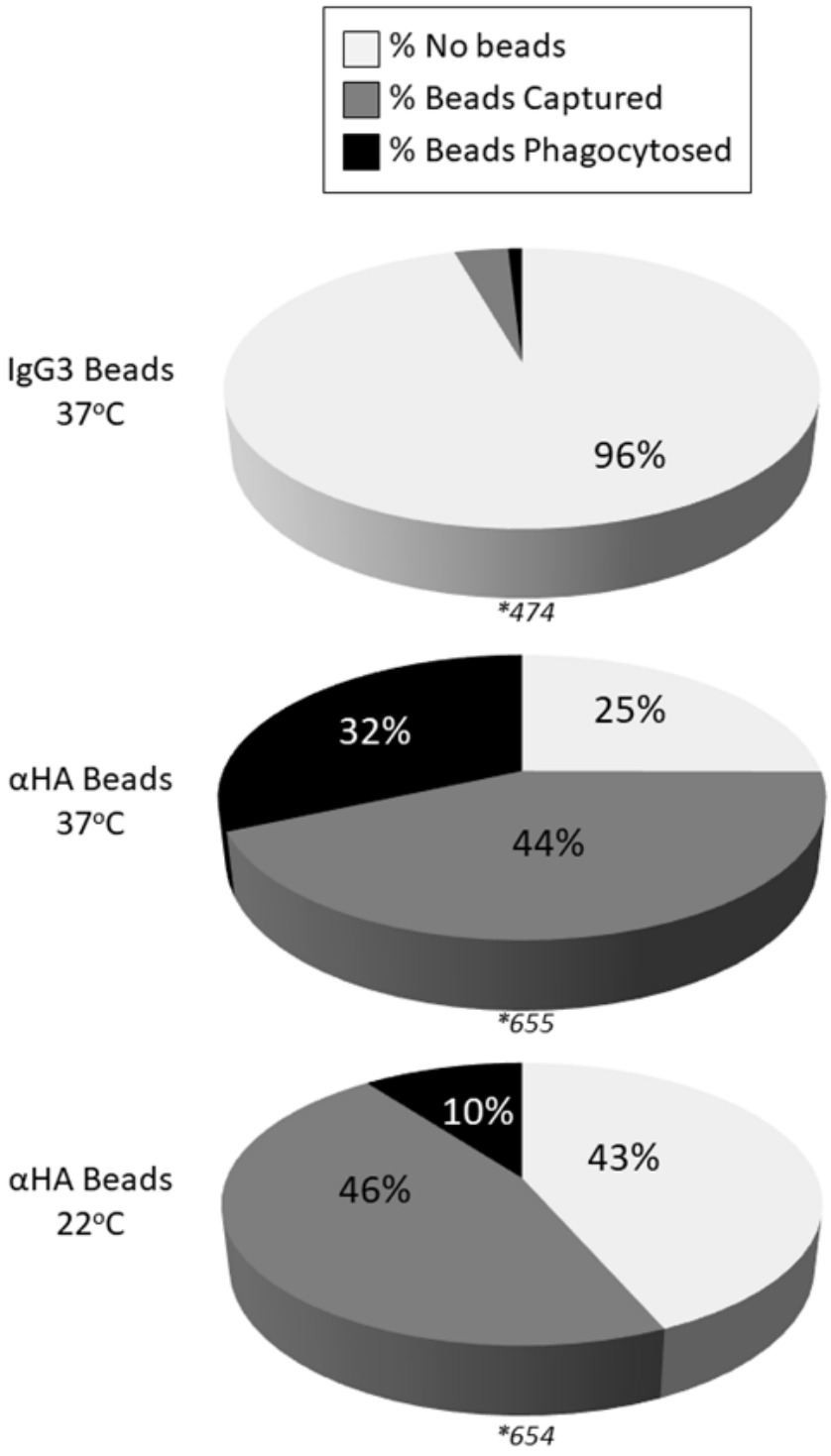
% No beads
% Beads Captured
% Beads Phagocytosed
IgG3 Beads
37°C
96%
*474
αHA Beads
37°C
32%
25%
44%
*655
αHA Beads
22°C
10%
43%
46%
*654

FIGURE 4.5 Assessment of the phagocytic phenotypes of IpLITR-expressing RBL-2H3 cells. Confocal images obtained in Figure 4.3 were used to enumerate the percentages of phagocytosed or captured beads for each cell-type. Confocal images of either Empty vector expressing cells (A), IpLITR 2.6b/IpFcRγ-L (B), or IpLITR 1.1b-expressing cells (C) were used to count the number of cells which had one of three designated bead associates; %beads phagocytosed (black), %beads captured (grey) or %no beads (white). * References the number of cells that were enumerated to obtain the percent shown.

FIGURE 4.6

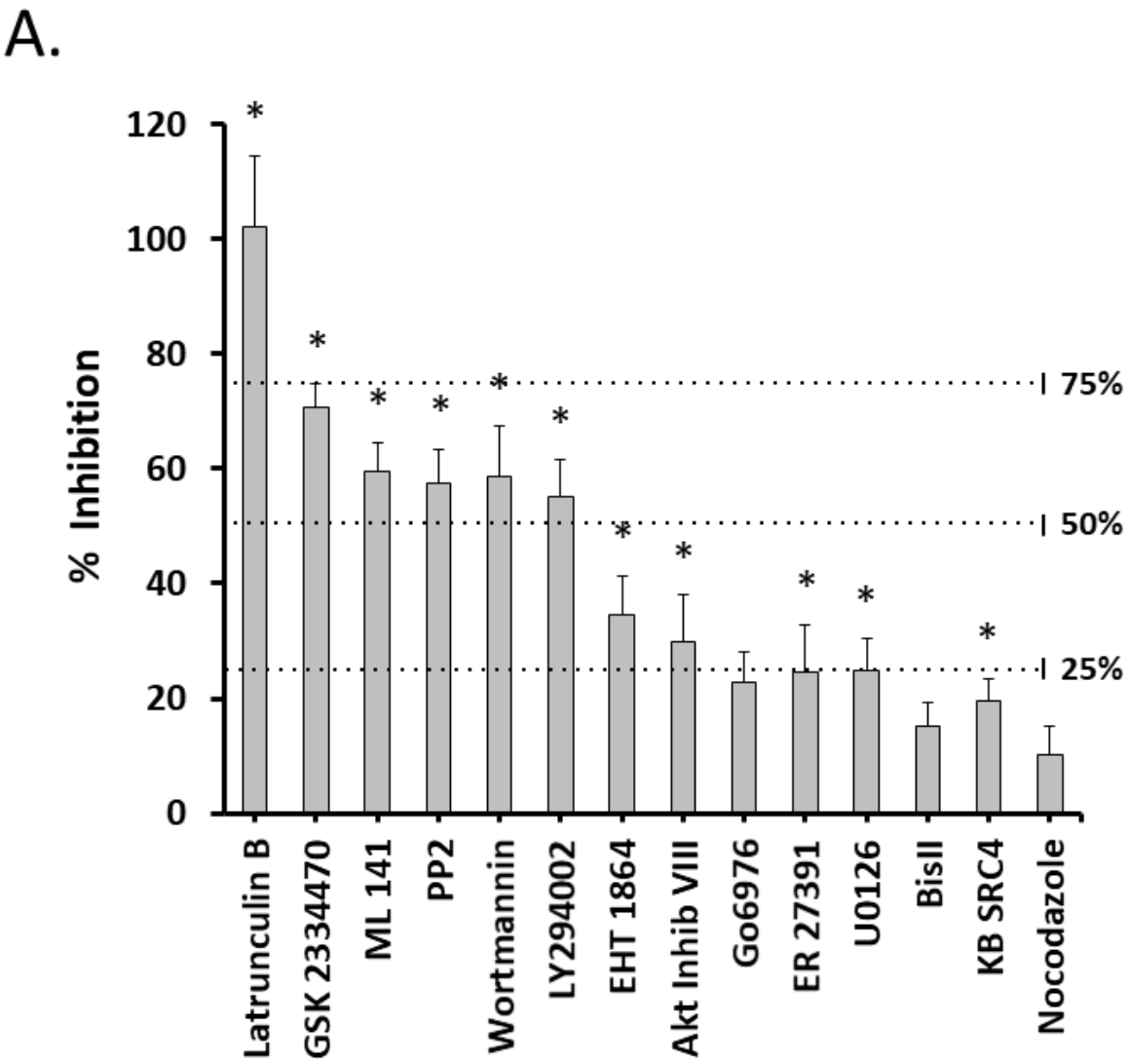
A.
% Inhibition
120
100
80
60
40
20
0
75%
50%
25%
*
Latrunculin B
GSK 2334470
ML 141
PP2
Wortmannin
LY294002
EHT 1864
Akt Inhib VIII
Go6976
ER 27391
U0126
BisII
KB SRC4
Nocodazole

FIGURE 4.6

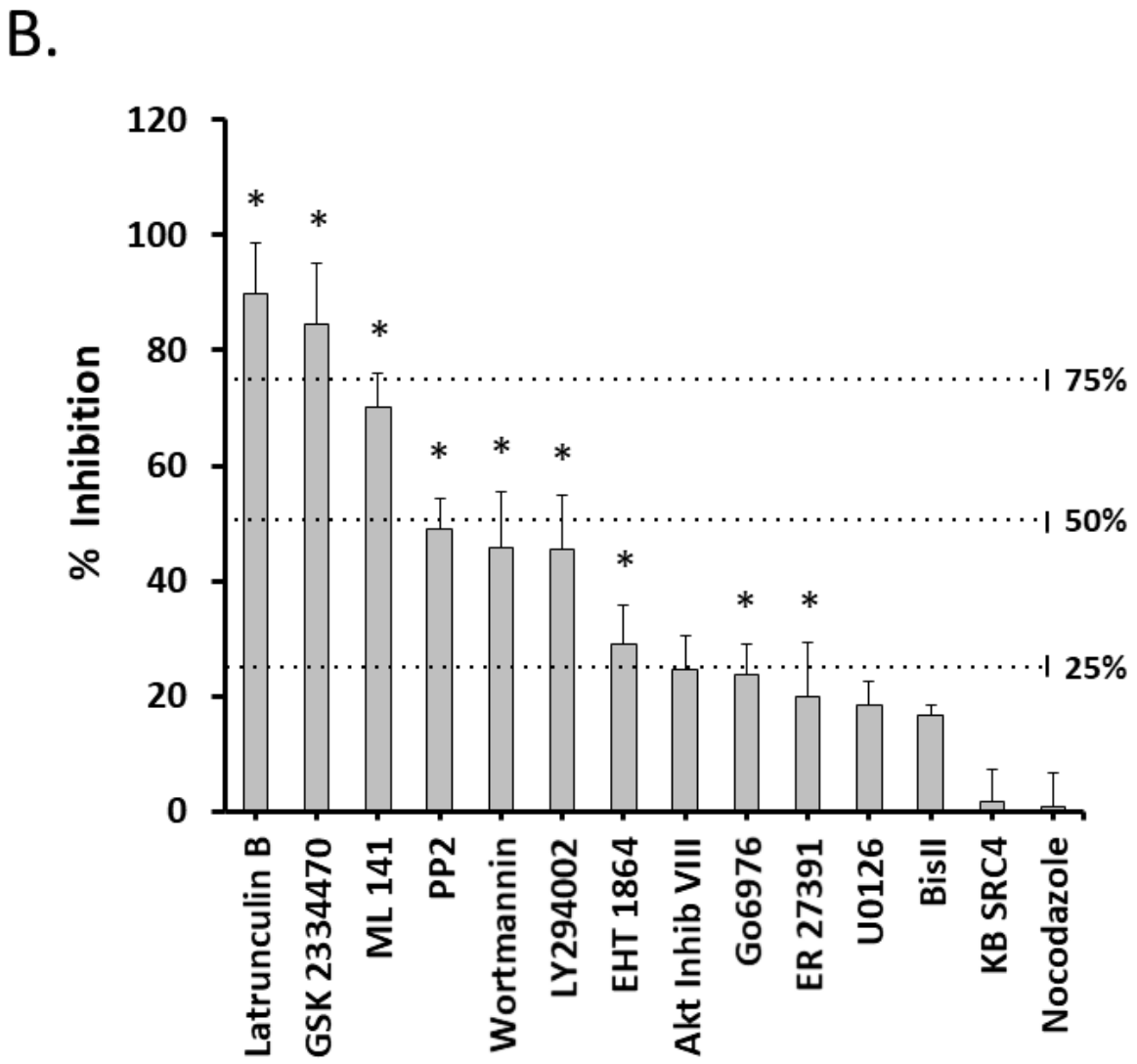
B.
% Inhibition
120
100
80
60
40
20
0
75%
50%
25%
*
Latrunculin B
GSK 2334470
ML 141
PP2
Wortmannin
LY294002
EHT 1864
Akt Inhib VIII
Go6976
ER 27391
U0126
BisII
KB SRC4
Nocodazole

FIGURE 4.6

C.

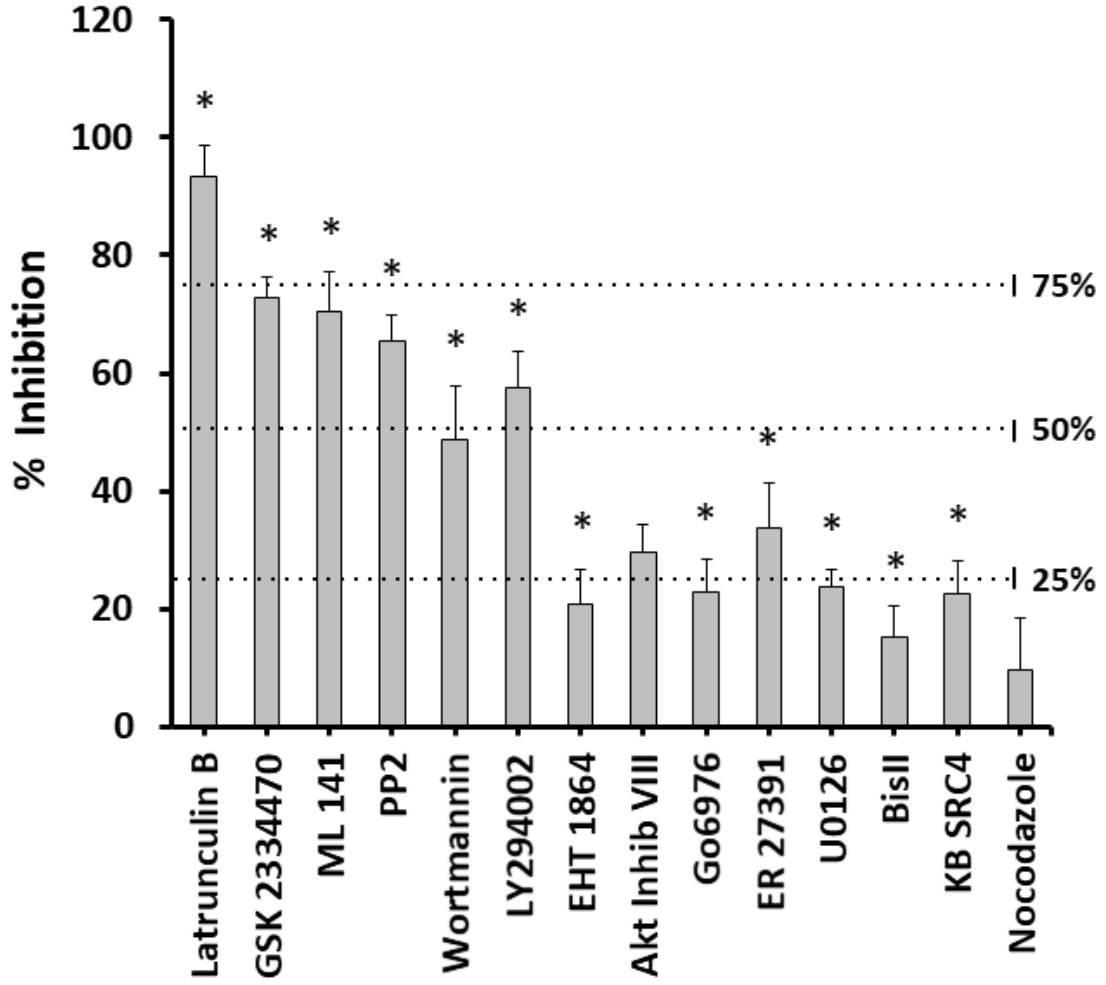
120
100
80
60
40
20
0
% Inhibition
75%
50%
25%
Latrunculin B
GSK 2334470
ML 141
PP2
Wortmannin
LY294002
EHT 1864
Akt Inhib VIII
Go6976
ER 27391
U0126
BisII
KB SRC4
Nocodazole

FIGURE 4.6 Pharmacological profiling of endogenous RBL-2H3 FBS-induced phagocytosis. To examine the endogenous phagocytic activities of the cells used in this study, $1x10^5$ empty-vector transfected RBL-2H3 cells (A), IpLITR 2.6b/IpFcRγ-L-expressing cells (B), or IpLITR 1.1b-expressing cells (C) were incubated with 20% FBS-opsonized 4.5-μm YG polystyrene beads ($3x10^5$) or non-opsonized PBS treated beads (i.e. 0% FBS) for 60 min at 37°C. In general, prior to incubating the cells with target beads they were pre-treated for 60 min at 37°C with 0.1% v/v DMSO in phagocytosis buffer (vehicle control) or with the indicated drugs dissolved in DMSO and the drugs were present throughout the entire phagocytic assay. After 60 min of phagocytosis, cells were treated with ice-cold trypsin (0.05%) for 15 min, washed, and fixed in 1% PFA. Samples were then analyzed by flow cytometry. For each pharmacological profile graph the y-axis represents percent inhibition of phagocytosis. Three levels of drug effectiveness (e.g. 25, 50, and 75% Inhibition of phagocytosis) are indicated on the graphs with dashed lines.

FIGURE 4.7

A.

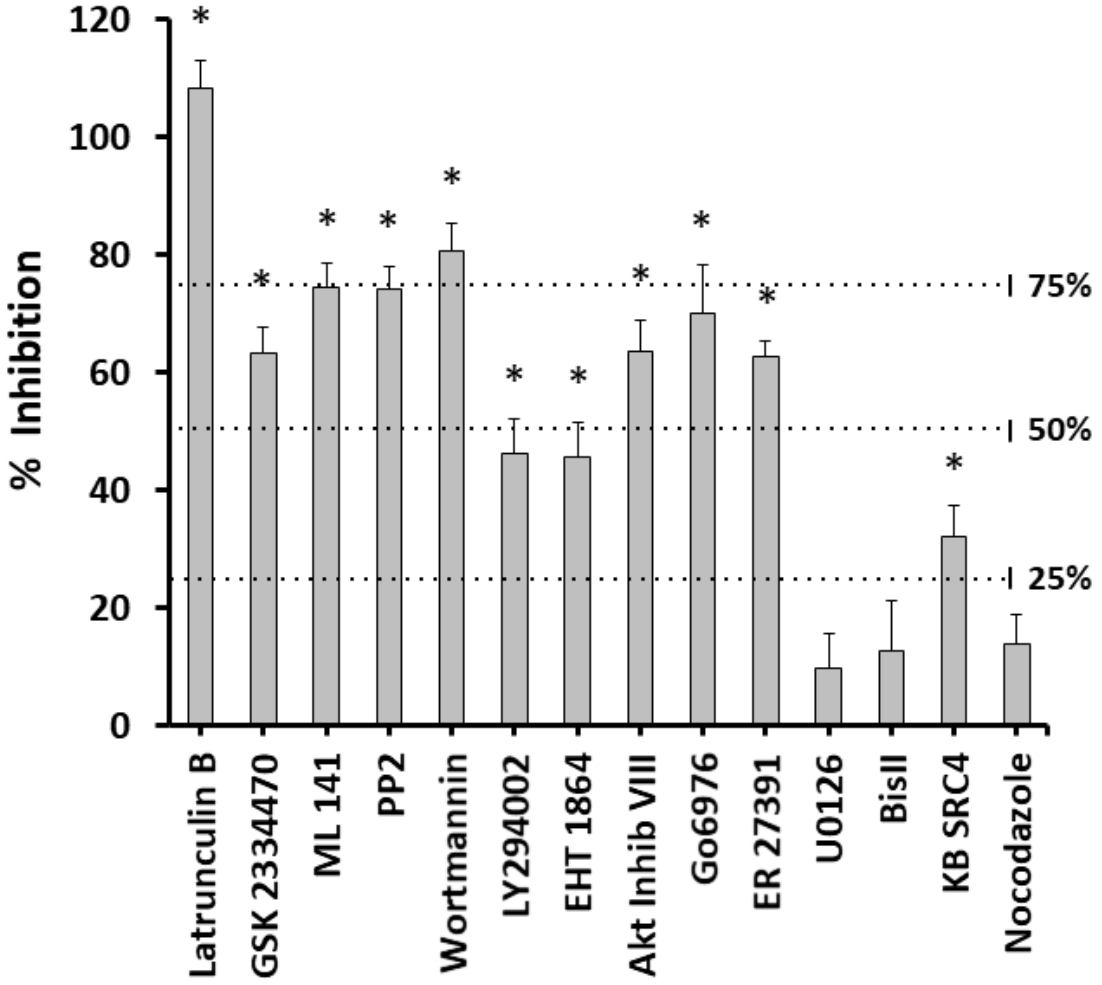
% Inhibition
120
100
80
60
40
20
0
75%
50%
25%
Latrunculin B
GSK 2334470
ML 141
PP2
Wortmannin
LY294002
EHT 1864
Akt Inhib VIII
Go6976
ER 27391
U0126
BisII
KB SRC4
Nocodazole

FIGURE 4.7

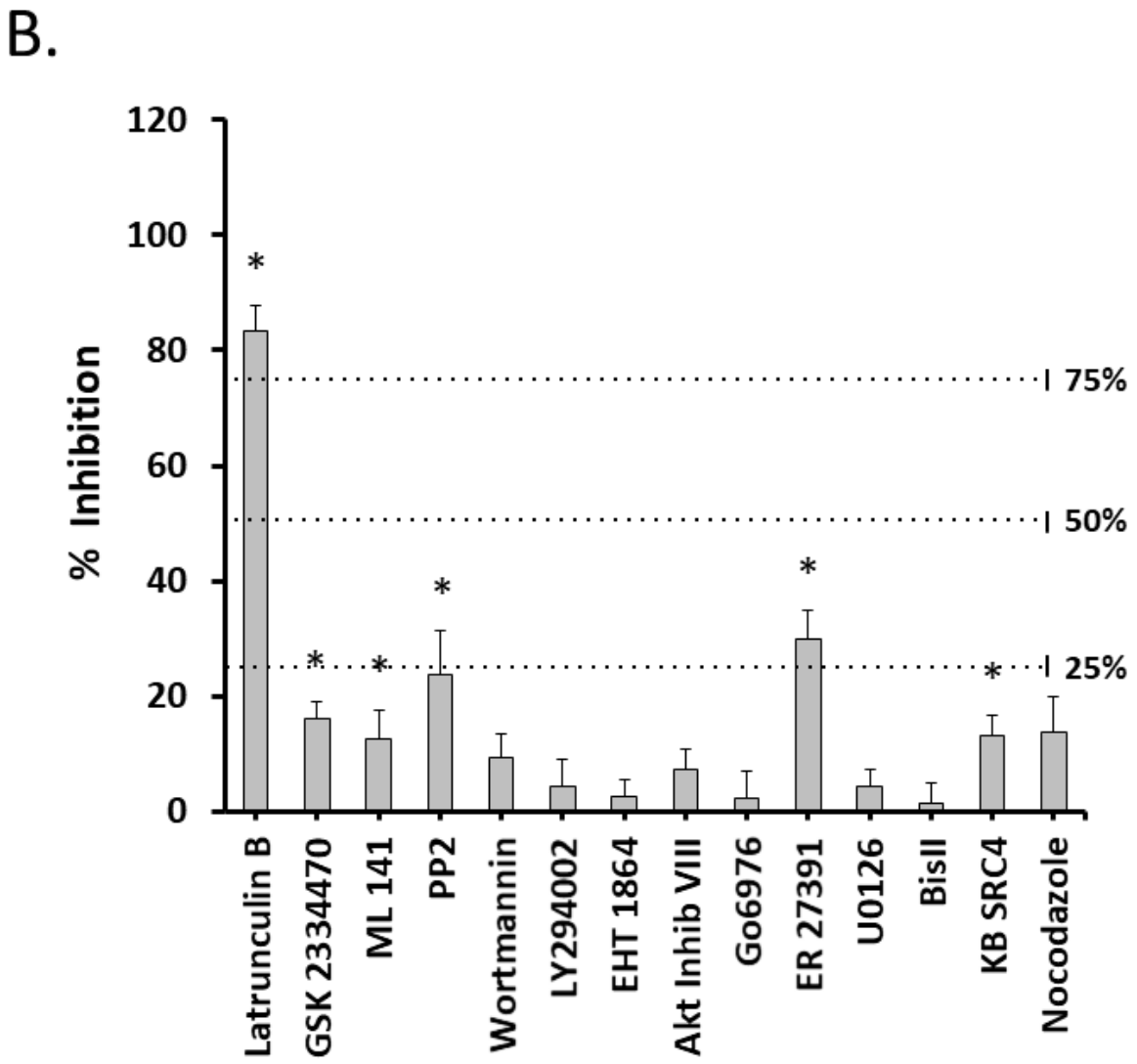
B.
% Inhibition
120
100
80
60
40
20
0
75%
50%
25%
*
Latrunculin B
GSK 2334470
ML 141
PP2
Wortmannin
LY294002
EHT 1864
Akt Inhib VIII
Go6976
ER 27391
U0126
BisII
KB SRC4
Nocodazole

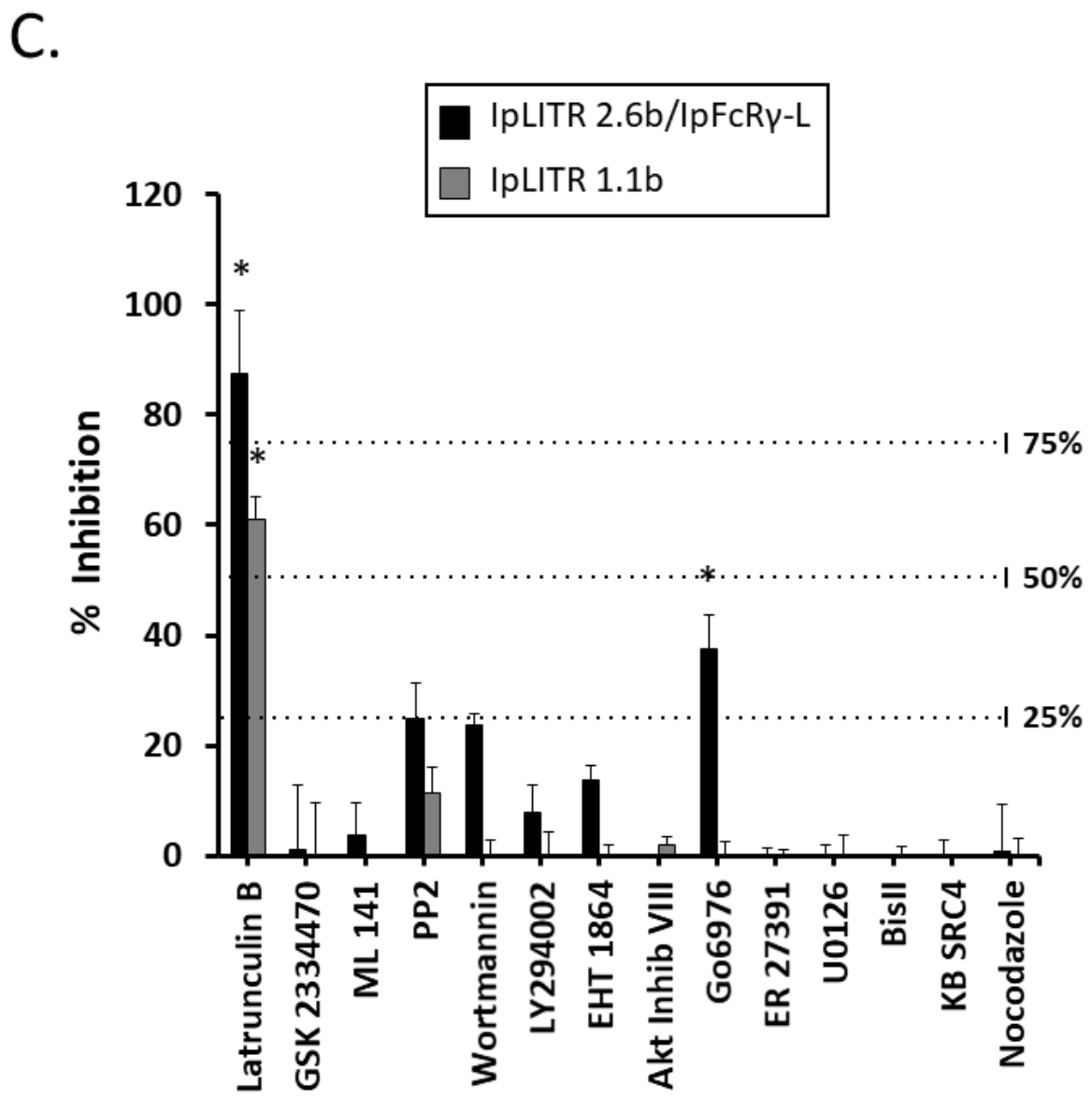

FIGURE 4.7 Pharmacological profiling of IpLITR-specific phagocytosis.
Pharmacological profiling of IpLITR-mediated phagocytosis was also examined by incubating $1x10^5$ IpLITR 2.6b/IpFcRγ-L cells (A) or IpLITR 1.1b cells (B) in the presence of the same doses of pharmacological blockers used in Figure 4.7 or by using ten-fold reduced inhibitor concentrations (low dose) (C). For these assays the cells were incubated with either αHA mAb- or mouse IgG3-opsonized 4.5 μm YG polystyrene beads ($3x10^5$) for 60 min at 37^oC in the presence of each drug.

FIGURE 4.8

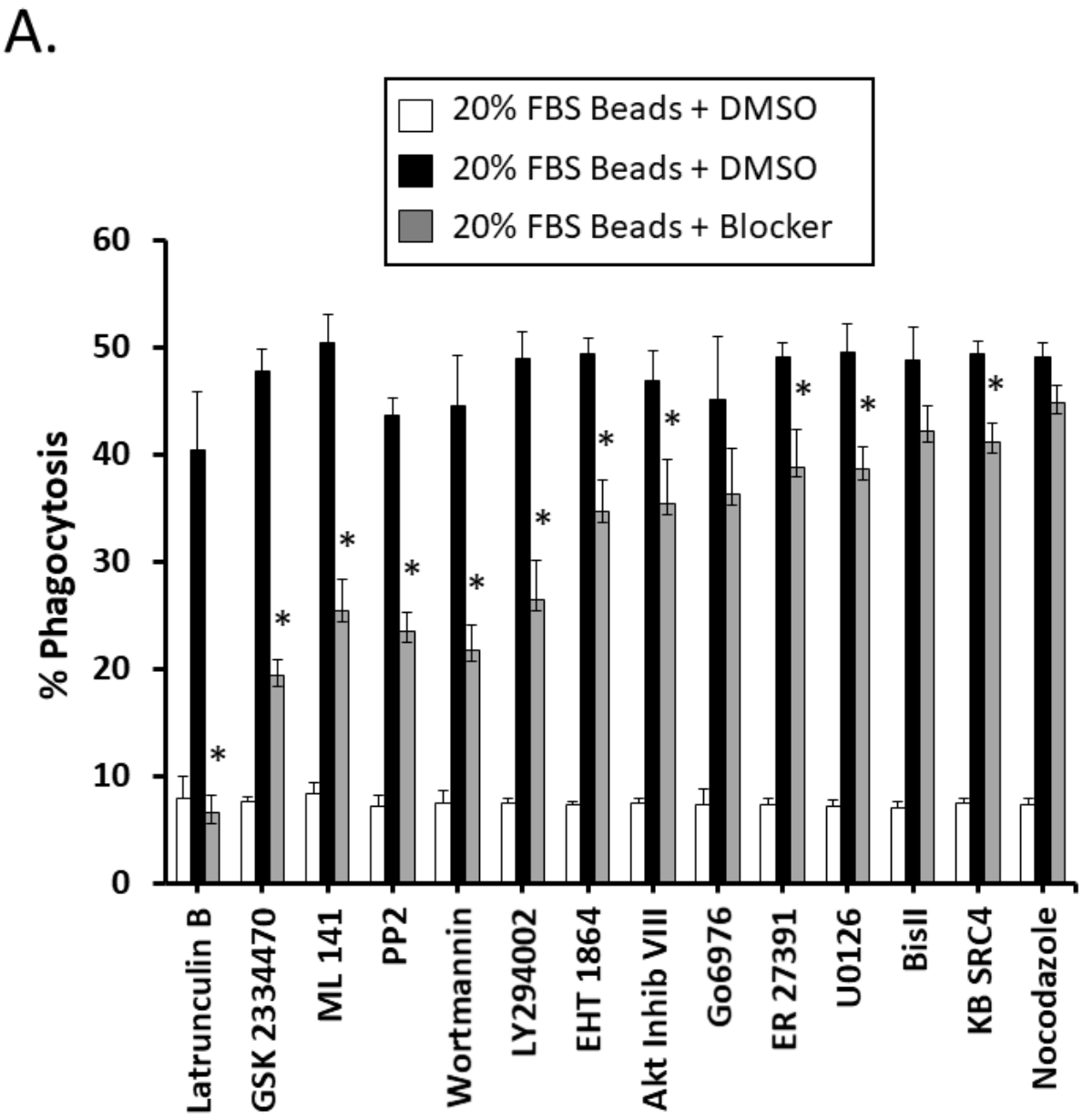
A.
20% FBS Beads + DMSO
20% FBS Beads + DMSO
20% FBS Beads + Blocker
% Phagocytosis
60
50
40
30
20
10
0
Latrunculin B
GSK 2334470
ML 141
PP2
Wortmannin
LY294002
EHT 1864
Akt Inhib VIII
Go6976
ER 27391
U0126
BisII
KB SRC4
Nocodazole

FIGURE 4.8

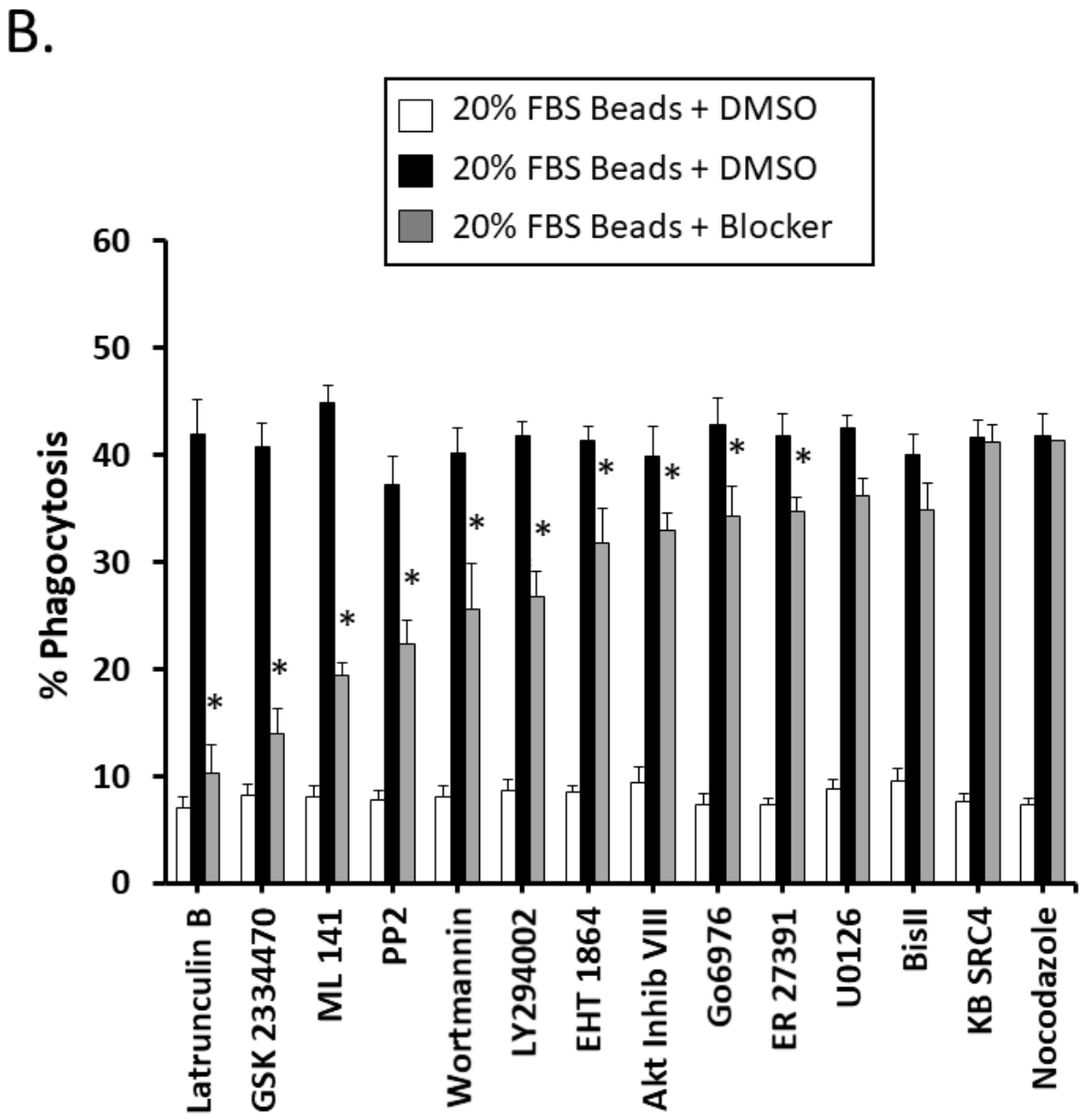
B.
20% FBS Beads + DMSO
20% FBS Beads + DMSO
20% FBS Beads + Blocker
% Phagocytosis
0
10
20
30
40
50
60
*
Latrunculin B
GSK 2334470
ML 141
PP2
Wortmannin
LY294002
EHT 1864
Akt Inhib VIII
Go6976
ER 27391
U0126
BisII
KB SRC4
Nocodazole

FIGURE 4.8

C.

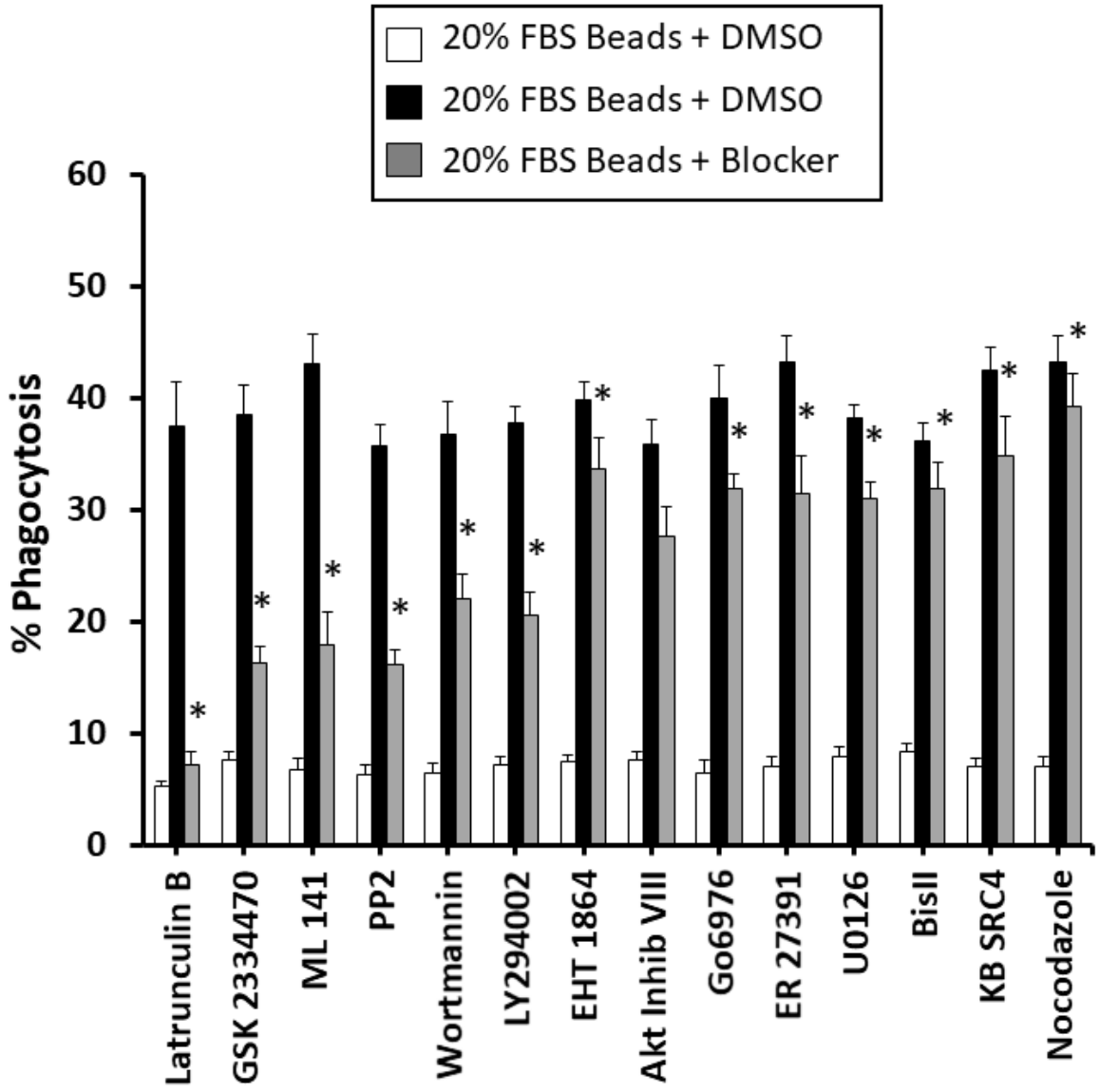
20% FBS Beads + DMSO
20% FBS Beads + DMSO
20% FBS Beads + Blocker
% Phagocytosis
0
10
20
30
40
50
60
Latrunculin B
GSK 2334470
ML 141
PP2
Wortmannin
LY294002
EHT 1864
Akt Inhib VIII
Go6976
ER 27391
U0126
BisII
KB SRC4
Nocodazole

FIGURE 4.8 Standard flow cytometry-based assays for pharmacological profiling of endogenous RBL-2H3 phagocytic activity using serum-opsonized beads. Percent phagocytosis data for empty vector-transfected RBL-2H3 cells (A), IpLITR 2.6b/IpFcRγ-L-expressing cells (B), and IpLITR 1.1b-expressing cells are shown (C). For each experiment, transfected cells were pre-incubated for 1 hr at 37^{o}C with 0.1% DMSO (vehicle control) or with the indicated drug dissolved in DMSO at the concentrations listed in Table 4.1. Pre-treated cells were then incubated with non-opsonized beads (i.e. 0% FBS) or with serum-opsonized beads (i.e. 20% FBS) for 1 hr at 37^{o}C in the presence of the indicated drugs. Cells were then washed, treated with trypsin, and then fixed prior to examination by flow cytometry as described (36, 38). Each bar represents the mean ± SEM of at least four individual blocker studies performed for each drug tested and $^{*}p \leq 0.05$ when comparing blocker treated cells (grey bars) to vehicle control cells (black bars) for each drug.

FIGURE 4.9

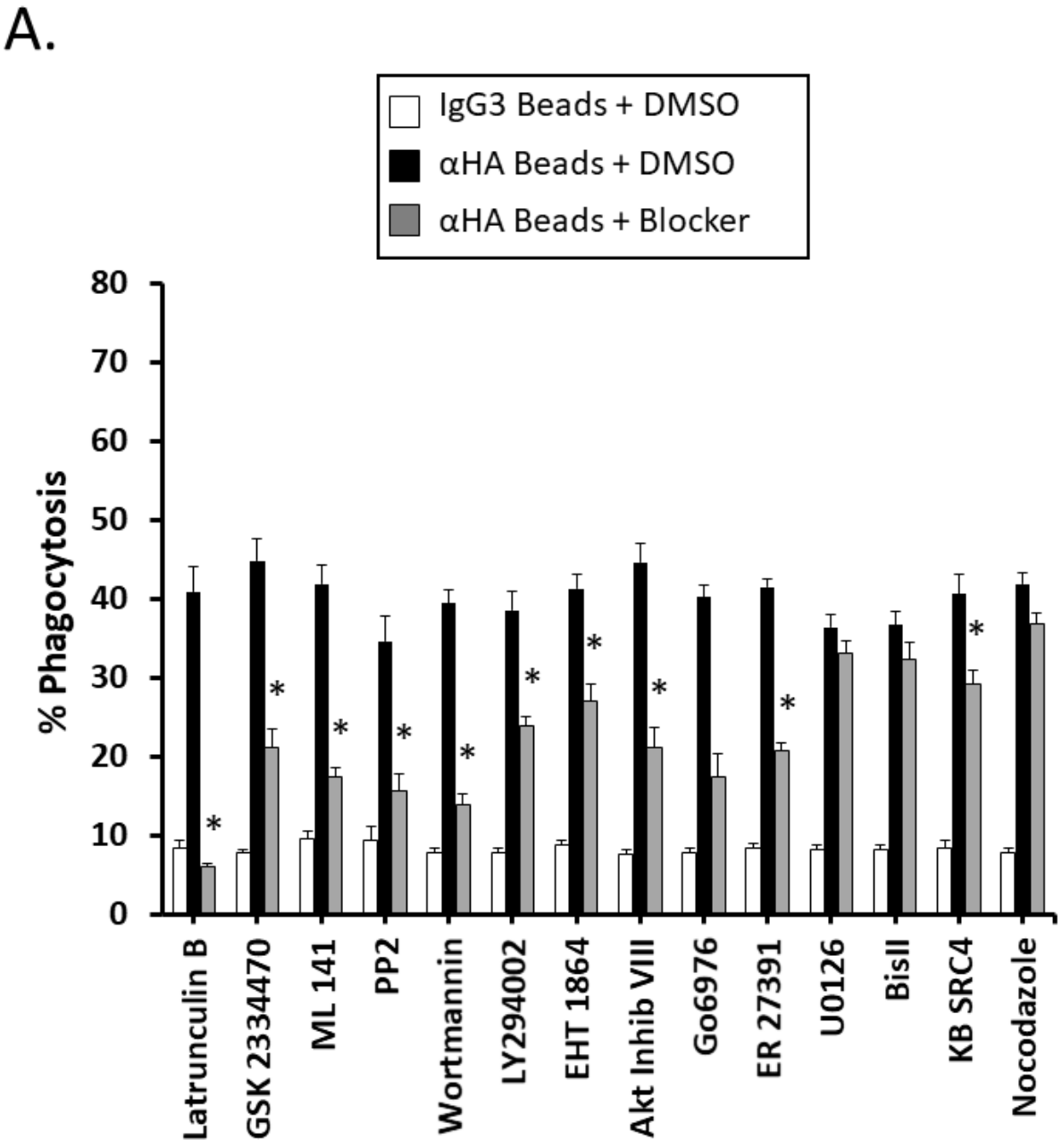
A.
IgG3 Beads + DMSO
αHA Beads + DMSO
αHA Beads + Blocker
% Phagocytosis
0
10
20
30
40
50
60
70
80
Latrunculin B
GSK 2334470
ML 141
PP2
Wortmannin
LY294002
EHT 1864
Akt Inhib VIII
Go6976
ER 27391
U0126
BisII
KB SRC4
Nocodazole

FIGURE 4.9

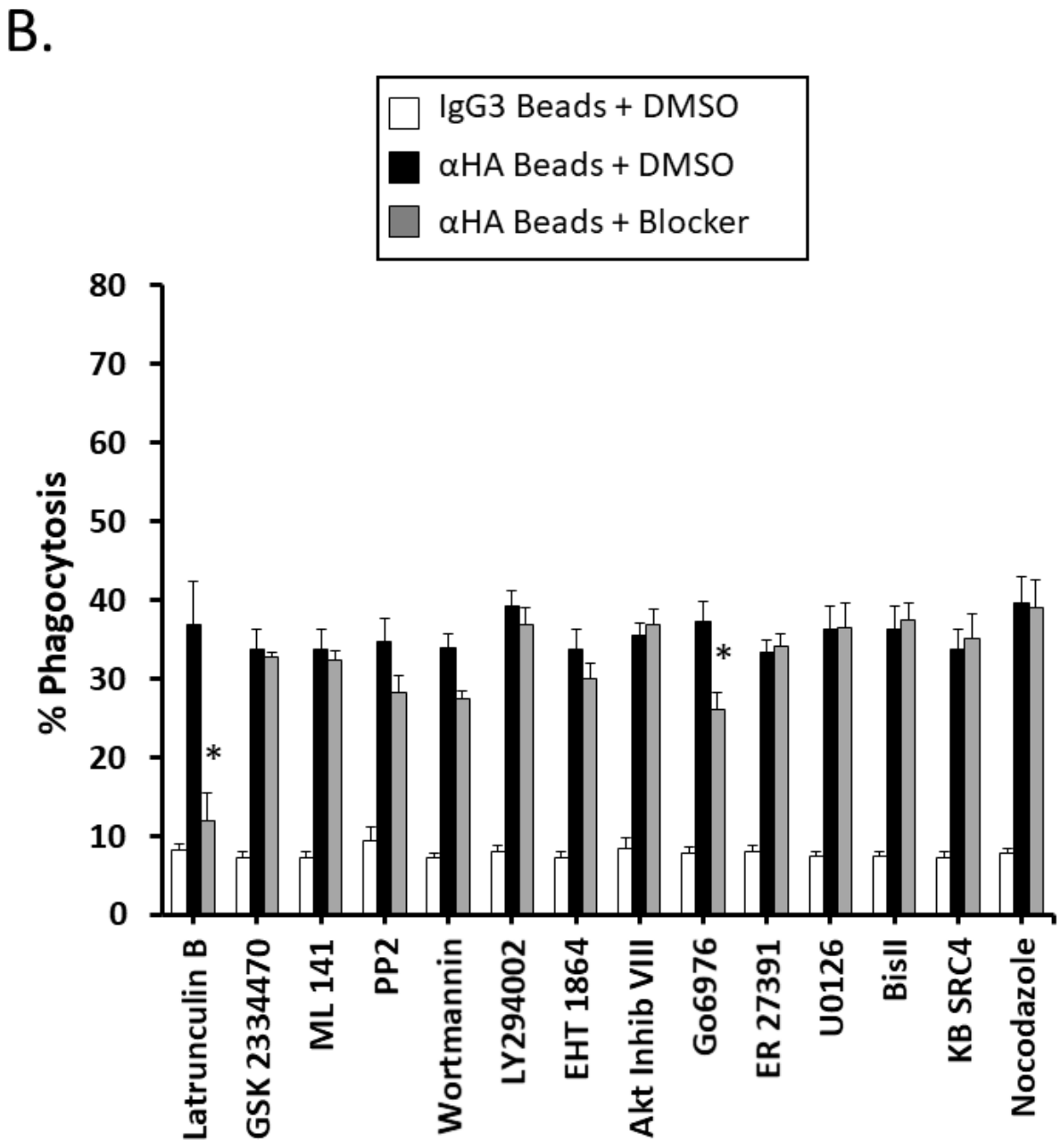
B.
IgG3 Beads + DMSO
αHA Beads + DMSO
αHA Beads + Blocker
% Phagocytosis
0
10
20
30
40
50
60
70
80
*
*
Latrunculin B
GSK 2334470
ML 141
PP2
Wortmannin
LY294002
EHT 1864
Akt Inhib VIII
Go6976
ER 27391
U0126
BisII
KB SRC4
Nocodazole

FIGURE 4.9

C.

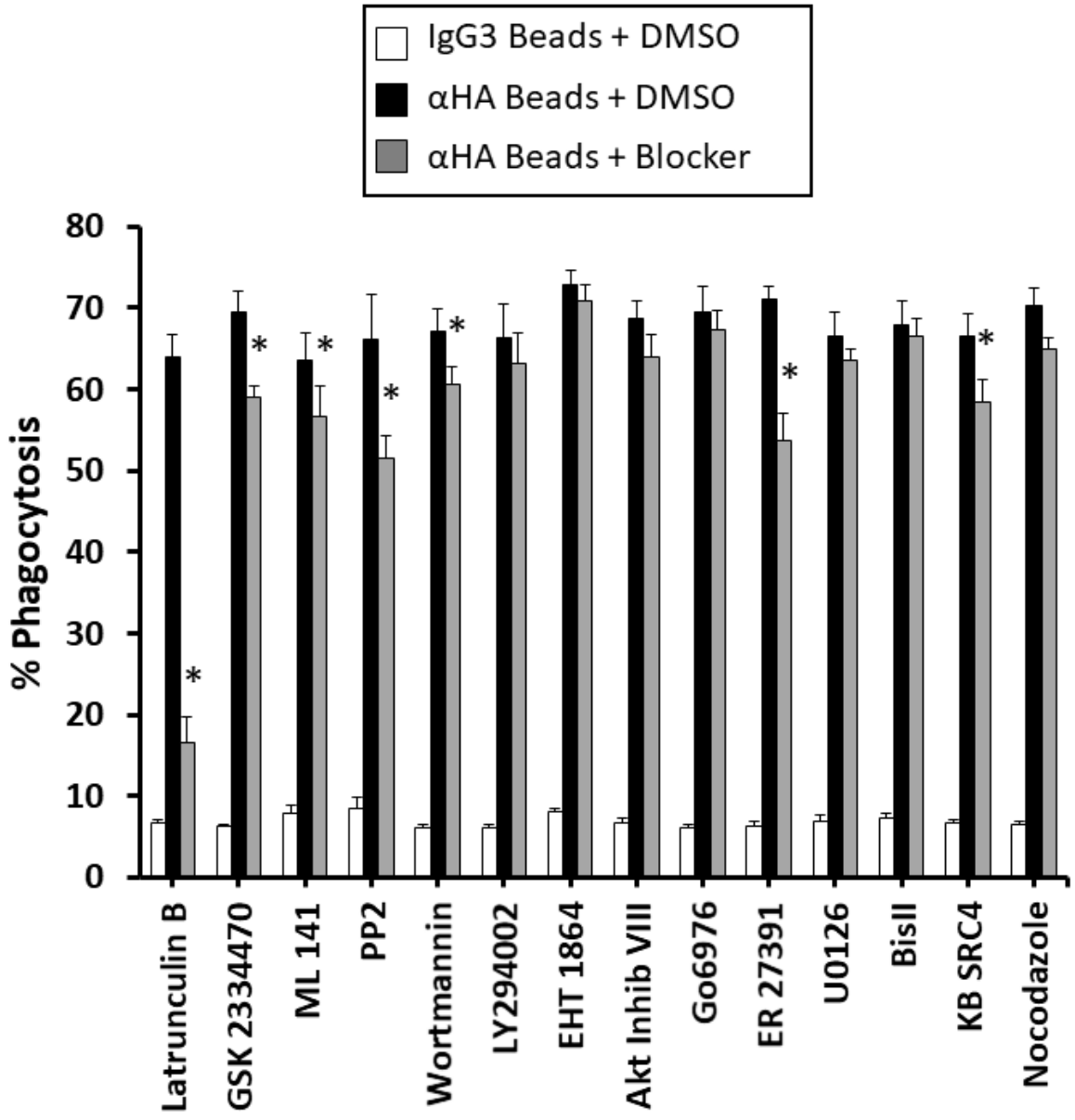
IgG3 Beads + DMSO
αHA Beads + DMSO
αHA Beads + Blocker
% Phagocytosis
0
10
20
30
40
50
60
70
80
*
Latrunculin B
GSK 2334470
ML 141
PP2
Wortmannin
LY294002
EHT 1864
Akt Inhib VIII
Go6976
ER 27391
U0126
BisII
KB SRC4
Nocodazole

FIGURE 4.9

D.

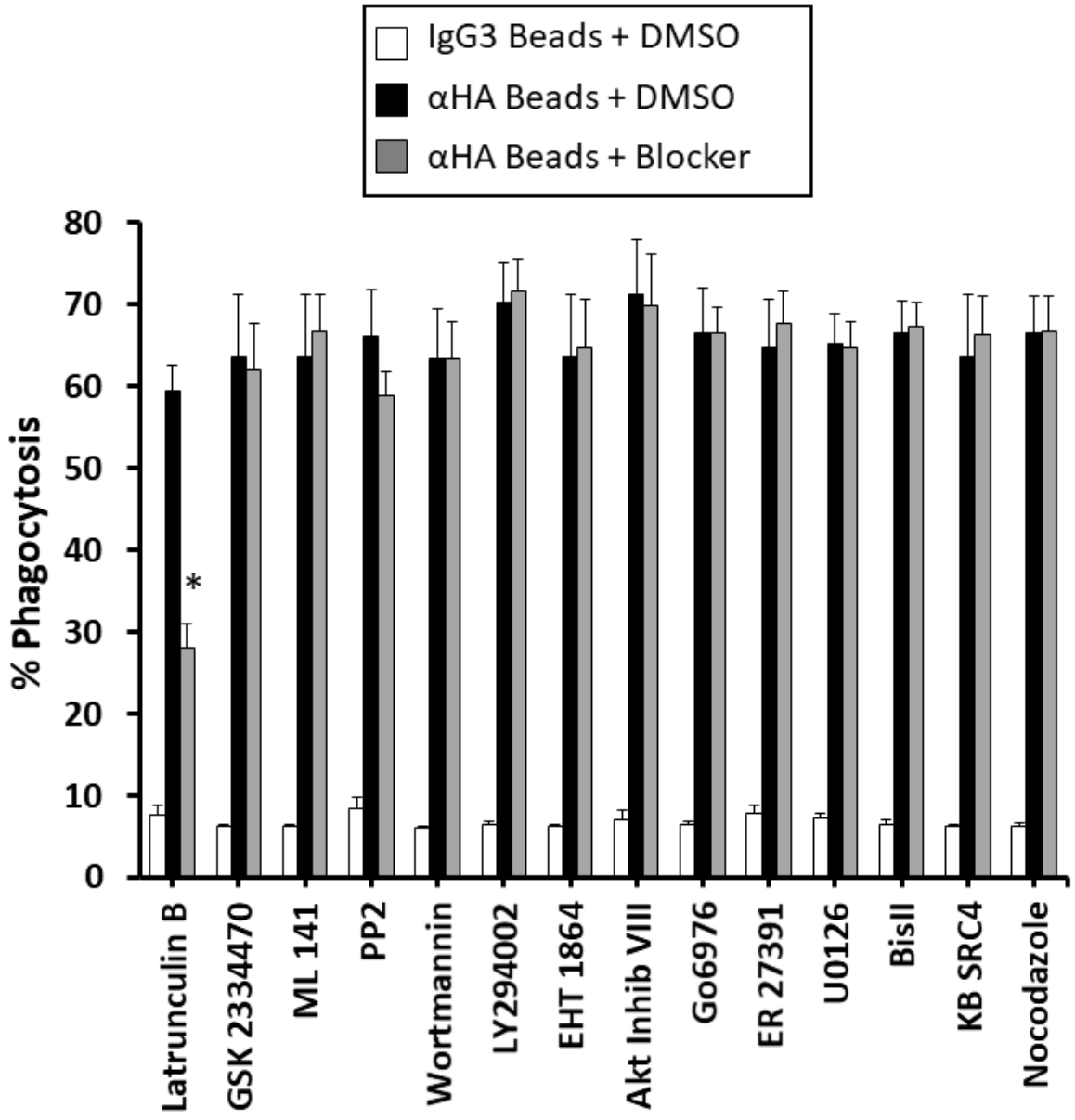
IgG3 Beads + DMSO
αHA Beads + DMSO
αHA Beads + Blocker
% Phagocytosis
80
70
60
50
40
30
20
10
0
*
Latrunculin B
GSK 2334470
ML 141
PP2
Wortmannin
LY294002
EHT 1864
Akt Inhib VIII
Go6976
ER 27391
U0126
BisII
KB SRC4
Nocodazole

FIGURE 4.9 Standard flow cytometry-based assays for pharmacological profiling of IpLITR-induced phagocytosis using αHA mAb-opsonized beads. The percent phagocytosis data for IpLITR 2.6b/IpFcRγ-L-expressing cells treated with standard (A) and low doses of selective pharmacological blockers (B), and for IpLITR 1.1b-expressing cells treated with standard (C) and low doses of blockers (D) are shown. Standard drug concentrations refer to the same doses used in the FBS bead assays and low doses are ten-fold reductions of these concentrations as listed in Table 4.1. For each experiment, IpLITR-expressing cells were pre-incubated for 1 hr at 37^{o}C with 0.1% DMSO (vehicle control) or with the indicated drug dissolved in DMSO. Pre-treated cells were then incubated with αHA mAb-opsonized beads or with IgG3-opsonized beads for 1 hr at 37^{o}C in the presence of the indicated drugs. Cells were then washed, treated with trypsin, and then fixed prior to examination by flow cytometry as described (36, 38). Each bar represents the mean ± SEM of at least three individual blocker studies performed for each drug tested and $^{*}p \leq 0.05$ when comparing blocker treated cells (grey bars) to vehicle control cells (black bars) for each drug.

			% Inhbition of Phagocytosis			% Inhbition of Phagocytosis	
Drug	Intracellular Target	dose [μM]	IpLITR 2.6b	IpLITR 1.1b	dose [μM]	IpLITR 2.6b	IpLITR 1.1b
Latrunculin B	*Actin polymerization*	25	108.4 ± 4.5	83.5 ± 4.3	2.5	87.5 ± 11.5	61.1 ± 3.9
GSK 2334470	*3-phsophoinositide-dependent protein kinase (PDK1)*	30	63.4 ± 4.4	16.1 ± 2.8	3.0	1.2 ± 11.7	-0.4 ± 10.0
ML 141	*Cdc42 GTPase*	50	74.6 ± 4.2	12.6 ± 5.1	5.0	3.9 ± 5.8	-8.6 ± 8.0
PP2	*Src-family tyrosine kinases*	10	74.1 ± 4.0	23.7 ± 7.7	1.0	24.9 ± 6.6	11.4 ± 4.7
Wortmannin	*phosphatidylinositol 3-kinase (PI 3-kinase), MLCK, DNA-PK*	0.1	80.7 ± 4.8	9.2 ± 4.1	0.01	23.8 ± 2.1	-1.4 ± 4.3
LY294002	*phosphatidylinositol 3-kinase (PI 3-kinase), mTOR, DNA-PK*	10	46.2 ± 6.1	4.2 ± 4.9	1.0	8.0 ± 4.9	-4.0 ± 8.4
EHT 1864	*Inhibitor of Rac family GTPases*	50	45.7 ± 5.8	2.5 ± 3.1	5.0	13.7 ± 2.8	-4.2 ± 6.1
Akt Inhib VIII	*Inhibitor of Akt1, Akt2, and Akt3*	20	63.5 ± 5.4	7.3 ± 3.6	2.0	-5 ± 2.7	2.0 ± 1.4
Go6976	*Conventional Protein kinase C (PKC) inhibitor; PKCα and PKCβ1*	1.0	70.2 ± 8.0	2.2 ± 4.6	0.2	38.0 ± 6.1	-1.8 ± 4.3
ER 27391	*Syk kinase*	50	62.7 ± 2.8	30.0 ± 4.8	5.0	-3.7 ± 5.2	-7.7 ± 8.7
U0126	*MAP kinase kinase; inhibits MEK-1 and MEK-2*	10	10.0 ± 5.7	4.3 ± 3.1	1.0	-0.6 ± 2.8	-0.5 ± 4.2
BisII	*Novel (δ, ϑ, η, ε) and conventional (α, β1) PKC isoforms*	0.5	12.9 ± 8.3	1.5 ± 3.4	0.05	-5.4 ± 4.4	-2.3 ± 4.0
KB SRC4	*cSrc-family tyrosine kinases*	10	32.2 ± 5.2	13.2 ± 3.6	1.0	-5.5 ± 8.5	-7.3 ± 5.8
Nocodazole	*Microtubules*	0.1	14.0 ± 4.9	13.6 ± 6.2	0.01	-0.7 ± 8.5	-1.7 ± 4.8

Table 4.1 List of pharmacological drug names, targets, doses and %inhibition of IpLITR-mediated phagocytosis.

CHAPTER V

TRYPSIN DIFFERENTIALLY MODULATES CHANNEL CATFISH LITR EXPRESSION LEVELS AND PHAGOCYTIC FUNCTIONS

A version of this chapter has been published:

Lillico et al. 2016., Trypsin Differentially Modulates the Surface Expression and Function of Channel Catfish Leukocyte Immune-Type Receptors. *Dev Comp Immunol*. 65: 231-244.

5.1 INTRODUCTION

Results from chapter IV of this thesis showed that IpLITRs appear to selectively engage distinct components of the phagocytic process resulting in unique target capture and engulfment phenotypes. Specifically, when stably expressed in RBL-2H3 cells, the ITAM-containing construct IpLITR 2.6b/IpFcRγ-L stimulated phagocytic activities that were abrogated at sub-optimal incubation temperatures and by pharmacological inhibitors of the classical signaling components of the mammalian FcR-dependent phagocytic pathway. In comparison, although the ITIM-containing receptor IpLITR 1.1b also induced phagocytosis through an actin-dependent mechanism, this process was insensitive to most of the pharmacological inhibitors tested and remained functional at temperatures as low as 22ºC. IpLITR 1.1b also elicited a unique target acquisition phenotype that consisted of complex membranous protrusions that captured targets in phagocytic cup-like structures but often failed to completely engulf them. These findings suggest IpLITRs that associate with ITAM-containing adaptors can engage conserved components of the phagocytic machinery to engulf extracellular targets; whereas, IpLITR 1.1b displays a stalled phagocytic phenotype that is likely dependent on the selective recruitment of the minimal molecular machinery required for target capture. Overall, this provides new information

regarding the target acquisition and internalization mechanisms involved in controlling the vertebrate phagocytic response.

Since IpLITR 1.1b-phagocytosis was not affected using a range of pharmacological blockers or at reduced incubation temperatures, it was not possible to selectively inhibit its ability to induce target capture and engulfment. In this chapter I used the protease trypsin to selectively cleave IpLITR 1.1b from the cell surface. I also tested the hypothesis that the shorter construct IpLITR 2.6b/IpFcRγ-L (two extracellular Ig-like domains) would be resistant to trypsin-mediated cleavage whereas the four Ig-domain containing IpLITR 1.1b protein would be sensitive to this enzyme. Selective removal of IpLITR 1.1b from the surface of stably transfected RBL-2H3 cells using trypsin would then allow me to specifically block and subsequently verify that the surface expression of IpLITR 1.1b is requisite for the unique target acquisition and engulfment phenotype that I reported in chapter IV.

Proteolysis has already been shown to selectively influence the phagocytic activity of innate immune cells through targeting of immunoregulatory receptor proteins. For example, in humans the high-affinity IgG receptor (FcγRI; CD64) is cleaved from the surface of macrophages by trypsin, whereas the low-affinity IgG receptor (FcγRII; CD32) is insensitive to trypsin-mediated processing [218,219]. FcγRIIb is also shed from the surface of activated human neutrophils [220–222], although the enzymes required for these cleavage events vary depending on the agonists used and can involve both metalloproteinases as well as serine proteases [223]. Trypsin has also been shown to inhibit mannose receptor (MR)-mediated phagocytosis due to targeted cleavage of the receptor ectodomains, resulting in the rapid internalization and degradation of MR. This process is suggested to down-regulate receptor activation in the protease-rich environment produced at inflammatory sites [224]. During the chronic

inflammation associated with cystic fibrosis and bronchiectasis, neutrophil-derived elastases selectively cleave phosphatidylserine receptors, but not CD32, to significantly reduce the ability of macrophages to clear apoptotic bodies [225]. Reduced clearance of apoptotic cells also occurs in damaged heart tissue due to the unique ability of human cardiomyocytes to directly influence macrophage phagocytic activities via the secretion of proteases [226]. Altogether, these examples illustrate the important role that endogenous proteases play in the regulation of receptor-mediated phagocytosis. However, the cellular mechanisms underlying the potent immunomodulatory properties of proteases, and in particular selectivity for immunoregulatory receptor subtypes, are not well understood.

In this chapter, I examined the effects of the serine protease trypsin on IpLITR-mediated phagocytosis. The ectodomains of IpLITRs are distantly related to a variety of mammalian Ig superfamily members, including those that belong to the FcR family [16,187,190,227]. Like mammalian FcR proteins, IpLITR 2.6b/IpFcRγ-L and IpLITR 1.1b also vary in their ectodomain compositions: IpLITR 2.6b/IpFcRγ-L has two Ig-like domains (D1 and D2), while IpLITR1.1b contains four Ig-like domains (D1, D2, D3, and D4). Early studies of mammalian FcR subtypes determined that protease sensitivities varied considerably depending on FcR ectodomain compositions [228]. Specifically, FcγRI is cleaved by trypsin due to its unique membrane proximal D3 region, whereas the low affinity FcγRII contains only D1 and D2 and is not sensitive to trypsin [228]. Therefore, I predict that IpLITR 1.1b will be selectively cleaved by trypsin treatments resulting in reduced surface expression levels of this protein. Using this approach, I will be able to show for the first time that IpLITR 1.1b-mediated control of a unique phagocytic phenotype can be altered using trypsin as a surrogate and selective ‘inhibitory’ reagent when compared to IpLITR 2.6b/IpFcRγ-L-expressing cells.

In this chapter I present results showing that trypsin selectively reduced IpLITR 1.1b cell surface expression levels and phagocytic activity in a dose-dependent manner. I also observed a significant alteration of the IpLITR 1.1b phagocytic phenotype post-trypsin exposure; whereas, the IpLITR 2.6b//IpFcRγ-L-mediated target engulfment phenotype was unchanged. Trypsin recovery experiments also show that trypsin-induced inhibition of IpLITR 1.1b-dependent phagocytosis was reversible and that the re-establishment of phagocytic function was associated with re-expression of IpLITR 1.1b on the cell surface. Taken together, these results reveal a unique role for trypsin as a selective modulator of IpLITR-mediated phagocytosis and also demonstrate how receptor-specific regulation of immunological responses can be differentially controlled by extracellular proteases using a fish model receptor model of phagocytosis.

5.2 RESULTS

5.2.1 Effects of trypsin treatment on IpLITR cell surface expression and function

In the absence of a trypsin pre-treatment (i.e. 0 μM), IpLITR 1.1b- and IpLITR 2.6b/IpFcRγ-L-expressing RBL-2H3 cells demonstrated 72.2% and 30.7% phagocytic activity, respectively (Fig. 5.1A and 5.1B). Trypsin exposures prior to incubations with target beads caused a striking reduction in the % phagocytosis for IpLITR 1.1b-expressing cells (Fig. 5.1B). Specifically, 20 μM, 2 μM, 1 μM, 0.5 μM, and 0.25 μM trypsin exposures resulted in a dose-dependent inhibition of the IpLITR 1.1b-mediated phagocytic responses, ranging from 85.6% to 28.1% inhibition respectively; but lower doses of trypsin (i.e. 0.125-0.03125 μM) had no significant effect. Conversely, when IpLITR 2.6b/IpFcRγ-L-expressing cells were pre-treated with the same trypsin doses, no significant inhibition of phagocytosis was observed (Fig. 5.1A). Trypsin treatments also had no effect on the phagocytic activity of RBL-2H3 cells when FBS-opsonized beads were used as targets to trigger endogenous engulfment pathways (Fig. 5.1C).

The expression of IpLITRs was also differently affected by trypsin treatments (Fig. 5.2A). Specifically, the surface staining profile for IpLITR 1.1b was significantly reduced after a 2 μM trypsin exposure due to an apparent loss of IpLITR 1.1b surface expression (Fig. 5.2A). These data were quantified as a reduction in the αHA MFI staining values of IpLITR 1.1b from ~614 (0 μM) to ~27 (2 μM); and although the control αHA MFI (~144) for IpLITR 2.6b/IpFcRγ-L was significantly lower than IpLITR 1.1b, it was not affected by trypsin pre-treatments (Fig. 5.2A). To directly compare the MFI values and the associated effects of trypsin, the fold change in MFI for both receptors are reported in Figure 5.2B. This shows that the surface expression levels of IpLITR 1.1b were reduced from ~36-fold to ~5-fold at trypsin concentrations ranging from 20 μM to 0.5 μM (Fig. 5.2B; grey bars). However, lower trypsin concentrations (i.e. 0.25-0.03125 μM) had no significant effect on IpLITR 1.1b expression levels (Fig. 5.2B; grey bars). Finally, imaging of the αHA stained cells at the representative trypsin pre-treatment dose of 2 μM confirmed that IpLITR 1.1b-expressing RBL-2H3 cells displayed an observable reduction in IpLITR 1.1b surface staining when compared to IpLITR 2.6b/IpFcRγ-L, which was not affected (Fig. 5.2C and 5.2D). It is important to note that for microscopy, the 20 μM dose of trypsin was not examined since this concentration readily removed cells from the coverslips.

5.2.2 IpLITR 1.1b-mediated target capture and engulfment phenotype is significantly altered by trypsin

As I have described in chapter IV, IpLITR 1.1b-expressing cells display a unique phagocytic phenotype that consists of few fully internalized targets, but many more cells with captured beads at the ends of extended membranous protrusions and/or associated with the plasma membrane in stalled phagocytic cup-like structures. An overview of this phenotype is shown in Figure 5.3A (top panel) for IpLITR 1.1b-expressing cells that were not pre-exposed to

the trypsin enzyme (0 μM). Individual cells (c1-c6) are indicated in this single representative z-stack image showing several cell (red) and target bead (green) interactions. In Figure 5.3A (bottom four panels), cell-bead interactions are also shown as 3D reconstructed images that were rendered from individual z-stacks. In these images it is shown for example that cell #1 (c1) has internalized three target beads. This cell has also captured a bead at the end of a membranous extension, and two other targets (green) are shared with c2; which itself has also completely engulfed two beads, along with an individual bead captured on its surface (Fig. 5.3A). Phagocytic cup-like structures are evident for c5, whereas c3 and c4 display a unique target capture and engulfment phenotype that features extended membranous protrusions. When compared to these control images, IpLITR 1.1b-expressing RBL-2H3 cells pre-treated with 2 μM trypsin, demonstrated a dramatic alteration in their overall phagocytic phenotype (Fig. 5.3B). In the representative z-stack image (Fig. 5.3B, top panel), most target beads appear in close proximity to the cells (c1-c5), with only c3 appearing to have fully phagocytosed a single bead. Furthermore, the general lack of extended membrane protrusions is evident. As described above, 3D renders were examined to precisely visualize each cell-bead interaction after enzyme exposure (Fig. 5.3B; bottom panels). In the examples provided, c1 has no internalized beads but five targets are present on its surface, while c2 has two visible membranous extensions but the beads are not captured at their ends and another bead appears to be partially engulfed. c3 has engulfed one bead completely, with two others on its surface, and c4 as well as c5 have only surface-attached beads. Overall, for IpLITR 1.1b there are visually discernable differences between the phagocytic phenotype of untreated control cells when compared with trypsin-treated cells. IpLITR 2.6b/IpFcRγ-L-expressing RBL-2H3 cells were also imaged after a 2 μM trypsin pre-treatment (Fig. 5.3C). In comparison, these images detailing several cell-bead interactions

(c1-c11) show no alteration in the overall phagocytic phenotype for this IpLITR-type as the majority of the IpLITR 2.6b/IpFcRγ-L-expressing cells have completely engulfed three or more target beads. This reinforces that trypsin treatment does not alter IpLITR 2.6b/IpFcRγ-L-mediated phagocytic activity.

5.2.3 Trypsin-mediated effects on IpLITR 1.1b expression and function are reversible

To examine if the loss of IpLITR 1.1b surface expression following trypsin treatment was reversible, I examined cells immediately after trypsin treatment and compared them with cells 2 hrs post-trypsin exposures. As shown in Figure 5.4, IpLITR 1.1b-expressing RBL-2H3 cells examined immediately after trypsin treatment (i.e. 0 hrs recovery) displayed a dose-dependent decrease in IpLITR 1.1b surface staining (Fig. 5.4A). However, when IpLITR 1.1b-expressing cells were incubated in trypsin-free media for 2 hrs, a significant recovery of IpLITR 1.1b surface expression was observed (Fig. 5.4B). Although complete recovery of IpLITR 1.1b surface staining was not achieved, there was clearly a rebound of IpLITR 1.1b surface expression when trypsin was removed.

Post-recovery, the phagocytic activity of IpLITR 1.1b-expressing cells was also tested to determine if the recovery of IpLITR 1.1b surface expression correlated with a gain-of-function. As shown in Figure 5.4C, IpLITR 1.1b-expressing cells that were incubated for 2 hrs after enzyme exposures demonstrated a significant recovery in their phagocytic activity when compared to cells tested immediately following trypsin treatments. Notably, cells treated with 2 μM trypsin showed the greatest recovery in phagocytic function (69.5% increase in phagocytic activity); whereas, 1 μM and 0.5 μM trypsin-treated cells had 39.5% and 26% increases in their phagocytic activities, respectively, relative to controls (Fig. 5.4C).

5.2.4 Biochemical examination of trypsin-exposed RBL-2H3 cells reveals receptor-selective modification of IpLITR 1.1b

RBL-2H3 whole cell lysates prepared from trypsin-treated cells were immunoprecipitated with the αHA mAb in order to examine the relative amounts of IpLITR proteins across trypsin treatment regimes. As expected, when αHA immunoprecipitations were performed from empty vector control RBL-2H3 cells no specific protein bands were observed (Fig. 5.5A). However, immunoprecipitations from IpLITR 1.1b-expressing RBL-2H3 control lysates (i.e. 0 μM trypsin) produced an immunoreactive band at ~70 kDa as well as a smaller protein band at ~60 kDa (Fig. 5.5B; 0 μm lane). The ~70 kDa band identified at 0 μM trypsin samples is suspected to be the mature form of IpLITR 1.1b which includes likely post-translational modifications as based on amino acid sequence alone IpLITR 1.1b should be ~60 kDa. The ~60 kDa bad identified I suspect to be the un-modified or immature form of IpLITR 1.1b as this size correlates with the predicited size of IpLITR 1.1b based on amino acid sequence prior to any modifications during occurring during surface expression. Following treatment with 0.5 μM trypsin, a similar banding pattern was observed, but with relatively more of the ~60 kDa band appearing (Fig. 5.5B; lane 2; 0.5 μm lane). When IpLITR 1.1b-expressing cells were treated with 1 μM or 2 μM of trypsin the 70 kDa band was no longer detected while the 60 kDa band was still clearly visible (Fig. 5.5B; 1 μm and 2 μM lanes). If the IpLITR 1.1b-expressing cells were allowed to recover for 2 hrs after trypsin exposures, the major band observed in all lanes was the 70 kDa protein with very little of 60 kDa detected (Fig. 5.5C). In addition, the relative amount of the 70 kDa protein appeared to decrease at increasing trypsin concentrations. In complementary experiments, I also tested the effects of trypsin digestion directly on the IpLITR 1.1b recombinant protein by first purifying the receptor by immunoprecipitation and then treating it with 2 μM trypsin (Fig. 5.5D). Results of

this experiment showed that the effect of trypsin on the cell surface expressed IpLITR 1.1b (Fig. 5.5B) was no different than what I observed for the purified recombinant protein, which converted from a 70 kDa to a 60 kDa form after enzyme treatment (Fig. 5.5D). I then assessed whether or not the apparent difference in sizes of the IpLITR 1.1b immunoreactive bands were due to a post-translational modification. In particular, I examined the O-linked glycosylation status of IpLITR 1.1b to determine if the mature receptor modification observed for trypsin could be similarly achieved using an endoglycosidase. Both IpLITR 1.1b-expressing cells (Fig. 5.5E) as well as immunoprecipitated IpLITR 1.1b protein (Fig. 5.5F) were treated with O-glycosidase, which showed that targeted removal of putative O-linked sugars on IpLITR 1.1b did not cause a size shift of the protein unlike what was observed following trypsin exposures (Fig 5.5B and 5.5D). However, based on these results alone I am unable to definitively identify if O-linked or perhaps some other form of post-translational modification is associated with the effects observed for IpLITR 1.1b-expression when exposed to trypsin. Finally, when immunoprecipitations were performed from the IpLITR 2.6b/IpFcRγ-L-expressing RBL-2H3 cellular lysates, an ~30 kDa band was detected with a slightly smaller and fainter band observed just slightly below (Fig. 5.5G). Unlike what was shown for IpLITR 1.1b, trypsin did not appear to alter the banding pattern observed in IpLITR 2.6b/IpFcRγ-L-expressing cells (Fig. 5.5G). Combined with the relative insensitivity of IpLITR 2.6b/IpFcRγ-L-mediated phagocytosis to trypsin treatment, recovery experiments were not performed for this IpLITR protein.

5.2.5 Immunoprecipitation of IpLITR 1.1b from trypsin-exposed RBL-2H3 cells identifies a mature cell surface protein and a putative intracellular form

Since immunoprecipitations performed using whole cell lysates cannot differentiate between cell surface and intracellular IpLITR 1.1b protein forms, I repeated the αHA

immunoprecipitations using IpLITR 1.1b-expressing cells that had their surface proteins selectively biotinylated (Fig. 5.6). Subsequently, following the αHA pull-downs, streptavidin (SA)-HRP reagent was then used to differentiate cell-surface biotinylated proteins from non-biotinylated intracellular proteins. First, control experiments using empty vector RBL-2H3 cells revealed one major surface protein at ~50 kDa (indicated by the asterisk; Fig. 5.6A). Importantly, this unidentified protein is very close in size to the ~60 kDa immunoreactive IpLITR 1.1b species described above; however, in relationship to the ~60 kDa IpLITR 1.1b form, this non-specific surface protein could easily be tracked as it consistently migrated below the 55 kDa marker. Several other cell-surface proteins were also detected from the control RBL-2H3 cell lysate, but these bands, along with the 50 kDa protein were not detectable when the cells were treated with trypsin above 0.5 μM (Fig. 5.6A). In addition to the 50 kDa non-specific protein (identified by an asterisk), a 70 kDa biotinylated protein was also immunoprecipitated from the surface of IpLITR 1.1b-expressing cells (Fig. 5.6B; 0 μM). Although the non-specific 50 kDa band disappears following treatment with 0.5 μM trypsin, the 70 kDa biotinylated protein remains and no smaller IpLITR 1.1b species are detectable. Interestingly, the higher trypsin concentrations of 1 μM and 2 μM completely eliminated the 70 kDa biotinylated protein. Once again, unlike whole cell lysates immunoprecipitated with αHA mAb, I did not detect an immunoreactive 60 kDa band in biotinylated protein lysates. When the IpLITR 1.1b-expressing RBL-2H3 cells were allowed to recover for 2 hrs after enzyme treatments, the biotinylated 70 kDa protein, as well as several other proteins, were observed in all lanes (Fig. 5.6C). Overall, these results provide evidence for the possible translocation of IpLITR 1.1b into cells following exposure to trypsin

5.2.6 Flow cytometry and confocal imaging experiments further reinforce that trypsin treatment promotes the translocation of IpLITR 1.1b into the cell

To determine if the loss of IpLITR 1.1b surface expression following trypsin treatment was in fact due to its internalization, I once again used αHA mAb staining to detect surface expressed IpLITR 1.1b using flow cytometry. As shown in Figure 5.7A, without a permeabilization step, IpLITR 1.1b levels are significantly reduced following treatment of the cells with 2 μM trypsin. In this scenario, the loss of surface expression could be due to cleavage of the receptor from the cell surface and/or its translocation into the cell. Since my biochemical findings suggest that trypsin appears to induce IpLITR 1.1b internalization, flow cytometry was then also performed on permeabilized cells to allow for the detection of both surface expressed and intracellular HA-tagged IpLITR proteins. As shown in Figure 5.7B, this approach shows that the observed reduction in IpLITR 1.1b surface staining using non-permeabilized cells (Fig. 5.7A) is significantly mitigated when intracellular IpLITR 1.1b is made available by permeabilization. Overall, this suggests that increased intracellular translocation of IpLITR 1.1b following trypsin exposure, leads to the higher staining levels following permeabilization (Fig. 5.7B). Then using confocal imaging, I also observed that without permeabilization, trypsin treatment (2 μM) caused significant reduction in the surface expression levels of IpLITR 1.1b, which can be readily observed as the loss of green staining around the periphery of the cells (Fig. 5.7C). However, when the cells were permeabilized prior to confocal imaging, I observed a dramatic alteration in the staining pattern in cells that were exposed to 2 μM trypsin. This featured an apparent translocation of the intense peripheral IpLITR 1.1b staining to a more diffuse intracellular pattern (Fig. 5.7D). Overall, this provides further evidence that IpLITR 1.1b may be translocated internally following exposure of the cells to trypsin.

5.3 DISCUSSION

Proteases are important regulators of inflammation through both direct and indirect modulation of cell surface immunoregulatory receptors. In this chapter, I examined the effects of trypsin on the surface expression and function of two teleost phagocytic immunoregulatory receptor-types, IpLITR 2.6b/IpFcRγ-L and IpLITR 1.1b. My results demonstrate that these representative IpLITR subtypes are differentially susceptible to trypsin-dependent proteolysis, which is likely dependent on unique features of their extracellular receptor ectodomains. Specifically, trypsin potently inhibited IpLITR 1.1b-mediated phagocytosis, which closely correlated with a reduction in the surface expression of this protein. In comparison, cell surface expression and phagocytic activity of IpLITR 2.6b/IpFcRγ-L was trypsin-insensitive at all of the doses tested. Demonstrating that a serine protease can selectively alter the ability of two closely related immunoregulatory receptor variants to couple with the phagocytic signaling machinery represents an interesting aspect of enzyme-mediated and receptor-selective regulation of innate immune cell effector response.

Following trypsin exposures, I did not observe non-specific effects on RBL-2H3 cell viability, morphology, or any other general perturbations of phagocytic signaling ability. The RBL-2H3 cells used in my studies effectively internalized serum-opsonized beads after trypsin treatments, demonstrating that their endogenous phagocytic functions remained intact. Furthermore, the selective inhibition of IpLITR 1.1b-mediated phagocytosis by trypsin was reversible and correlated with the recovery of receptor expression on the cell surface. Trypsin-sensitive and IgM-selective FcRs on human T-cells require 12 hrs recovery before receptor expression levels return to control levels; however, increases in FcR mRNA expression were observed as early as 2 hrs post-protease treatment [229]. For FcRs, recovery of their functions

was completely abolished by treatment with general inhibitors of protein translation; indicating that de novo synthesis of FcR was the major source of the newly expressed receptors. Unlike IgM-binding FcRs, the phagocytic activity of MRs expressed by human macrophages rapidly recovers within 10 min post-trypsin treatment [183]**.** However, the majority of the cell surface MRs expressed following enzyme exposure were derived from recycling endosomes rather than as a result of newly synthesized receptor proteins [183]. In comparison to the time course established from these studies, my results suggest that the recovery of IpLITR 1.1b surface expression and associated function at 2 hrs likely relies in part on receptor trafficking from within the endomembrane system, however, since complete recovery of surface expression and phagocytic activity was not achieved, my findings do not exclude a role for de novo receptor synthesis. Understanding the precise cellular mechanisms involved in IpLITR 1.1b re-sensitization following trypsin treatments will require further experiments.

My confocal microscopy results revealed a dramatic alteration in how IpLITR 1.1b-expressing cells interacted with target beads following trypsin treatment (Fig. 5.3A and 5.3B). Specifically, trypsin-treated IpLITR 1.1b-expressing cells rarely displayed fully internalized beads and they had a significant reduction in the number of beads captured in phagocytic cups or at the ends of membranous protrusions; in fact, most of the beads appeared to be located adjacent to cells but not bound in membrane-based structures (Fig. 5.3B). However, unlike IpLITR 1.1b-expressing cells, the phagocytic phenotype did not change for IpLITR 2.6b/IpFcRγ-L-expressing cells exposed to the highest concentration of trypsin (Fig. 5.3C); reinforcing the specificity of trypsin-mediated effects on IpLITR 1.1b-mediated phagocytic activity. These findings suggest that extracellular proteases can selectively alter the ability of IpLITRs to uniquely alter the remodeling of cellular membranes during the process of extracellular target capture and

engulfment. This also indicates that the yet to be deciphered IpLITR 1.1b-mediated phagocytic signaling pathway(s) promote the formation of extended cellular protrusions not readily observed for IpLITR 2.6b/IpFcRγ-L.

Trypsin treatment also significantly reduced IpLITR 1.1b surface expression, suggesting that the proteolytic activity of trypsin may cleave IpLITR 1.1b from the cell surface. However, my data clearly show that IpLITR 2.6b/IpFcRγ-L is resistant to trypsin-dependent cleavage. This demonstrates a novel aspect of immunoregulatory receptor regulation; especially considering that both IpLITRs have multiple predicted trypsin-sensitive cleavage sites throughout their ectodomains [230]. However, the extracellular compositions of these two receptors are not identical as IpLITR 2.6b consists of only two extracellular Ig-like domains, D1 and D2, whereas IpLITR 1.1b has four, D1-D4. Since the membrane-distal D1 and D2 domains of these receptors share ~95% amino acid identity, I hypothesize that trypsin may target the unique membrane proximal D3 and/or D4 regions of IpLITR 1.1b to remove this protein from the cell surface, however, repeated attempts to detect soluble forms of IpLITR 1.1b after immunoprecipitation with αHA antibodies from the cellular supernatants of trypsin-exposed cells were unsuccessful. These data suggest that trypsin may not actually cleave this receptor from the cell surface, but that trypsin may induce a conformational change in IpLITR 1.1b structure that stimulates removal of the receptor from cell surface through regulated endocytosis. It has already been reported that IpLITRs are rapidly internalized after antibody-mediated cross-linking due to classical endocytic events [12]. My data provides no direct evidence that the trypsin-mediated reduction in cell surface IpLITR 1.1b expression occurs due to clathrin-dependent or -independent endocytosis. However, based on the lack of degradation products in my co-immunoprecipitation assays (would be indicitative of multiple cleavage sites on IpLITR 1.1b), I

support the alternative perspective that proteases may also selectively modulate immunoregulatory receptor functions by inducing signaling events from within the endomembrane system.

The hypothesis that trypsin triggers the endocytosis but not cleavage of IpLITR 1.1b is further supported by my immunoprecipitation and cell-surface biotinylation experiments. Specifically, I showed that increasing concentrations of trypsin altered the co-immunoprecipitation profile of IpLITR 1.1b, which was not observed for IpLITR 2.6b/IpFcRγ-L. Specifically, without typsin exposures IpLITR 1.1b predominantly appears as an ~70 kDa band when immunoprecipitated from cellular lysates, with a minor band also evident at ~60 kDa. Since the predicted size of the IpLITR 1.1b construct is 57.5 kDa, I propose that the smaller 60 kDa form detected on the blots is most likely the native version of the receptor whereas the ~70 kDa form represents the modified and surface-expressed mature receptor form. A plausible, however yet to be completely tested, explanation for the ~10 kDa size difference between the immature and mature versions of this receptor is due to the post-translational modification of the receptor through glycosylation events [231]. However, the electrophoretic mobility of the mature ~70 kDa form of IpLITR 1.1b was not changed when cells (Fig. 5E) or the immunoprecipitated receptor (Fig. 5F) were treated with O-glycosidase suggesting that IpLITR 1.1b glycosylation is not likely responsible for the ~10 kDa size difference observed. In addition, if IpLITR 2.6b/IpFcRγ-L is also glycosylated, the extent of these post-translational modifications does not significantly adjust the size of the protein as the native IpLITR 2.6b/IpFcRγ-L protein is predicted at ~30 kDa, which closely matches the predominant size observed following immunoprecipitations from control and trypsin-exposed cells.

Based on the observed protein banding patterns of IpLITR 1.1b forms pre- and post-trypsin treatments it is possible that a trypsin-sensitive post-translation modification may be selectively removed from the receptor. For example, when IpLITR 1.1b-expressing RBL-2H3 cells were treated with 0.5 μM trypsin, I observed a 70 kDa band as well as a relative increase in the intensity of the 60 kDa band. At doses of 1 and 2 μM trypsin, the 70 kDa band is dramatically reduced while the 60 kDa band remained as the major immunoreactive protein. This suggests that increasing concentrations of trypsin modify the IpLITR 1.1b protein from a mature 70 kDa form to a native 60 kDa form possibly via the selective removal of a functionally-relevant post-translational modification, which as described above, is unlikely to be O-linked glycosylation. Interestingly, when the cells were allowed to recovery for 2 hrs following trypsin exposure, the predominant product that was immunoprecipitated from the cellular lysates was one again located at 70 kDa. This occurred at all trypsin doses tested but the relative amounts of IpLITR 1.1b detected per lane were proportionately reduced at increasing enzyme concentrations. Overall, these results show a clear correlation between the presence of the mature IpLITR 1.1b protein band at 70 kDa with optimal surface expression as well as phagocytic function. Furthermore, as demonstrated by the recovery of IpLITR 1.1b-mediated phagocytic function, trypsin removal facilitates the re-emergence of IpLITR 1.1b on the cell surface, a gain of phagocytic activity, and the reappearance of the 70 kDa mature protein.

In support of my hypothesis, immunoprecipitation of IpLITR 1.1b from cellular lysates after trypsin exposure indicates that this receptor is likely associated with internal membranes and not likely shed into the supernatant by proteolysis. To further differentiate cell-surface from internalized receptors, I selectively biotinylated proteins on the cell surface of IpLITR 1.1b-expressing RBL-2H3 and repeated the immunoprecipitation experiments (Fig. 5.6). Using

streptavidin-based detection, cell surface (i.e. biotinylated) and intracellular IpLITR 1.1b forms (i.e. non-biotinylated) could be differentiated before and after trypsin exposures. These experiments support that the predominant surface form of IpLITR 1.1b is the mature 70 kDa protein, which is clearly present in the control (0 μM) and 0.5 μM trypsin-exposed cells (Fig. 5.6B). However, the mature receptor form was not detected within the biotinylated fraction after the cells were exposed to trypsin doses of 1 μM and 2 μM (Fig. 5.6B). The putative immature IpLITR 1.1b protein (60 kDa) was also not detected as a biotinylated protein in all treatment groups, including cells that were not exposed to trypsin (Fig. 5.6B). By comparing the biotinylation results with the banding patterns from immunoprecipitation experiments using the whole cell lysates shown in Figure 5.5B, my results suggest that the immature form (60 kDa) of IpLITR 1.1b is not present on the cell surface. Overall, these data indicate that IpLITR 1.1b exists as trypsin-sensitive cell surface 70 kDa protein that is likely internalized following exposure to concentrations of trypsin ranging from 0.5 μM to 2 μM. However, this intracellular form of IpLITR 1.1b was not detected in my initial flow cytometric and confocal experiments. Therefore, I used a different fixation/staining approach to determine if trypsin induced IpLITR 1.1b internalization. This was performed by simply PFA fixing the trypsin-exposed cells prior to αHA staining, which causes increased permeability of the cells compared to staining for IpLITR-expression using non-fixed live cells. Comparatively, by performing fixation first, trypsin-exposed IpLITR 1.1b cells showed significantly more αHA staining compared to cells that were stained first and then fixed (Fig. 5.7A vs 5.7B; dashed lines). This result suggests that the increased staining of the cells may be due to increased intracellular translocation of the protein following trypsin exposure. To further explore this hypothesis, I also used confocal imaging to visualize the approximate cellular location of IpLITR 1.1b using cells that were fixed and then

stained. These confocal imaging results correlated with my flow cytometric data (Fig. 5.7A vs 5.7B) and showed a previously un-detected IpLITR 1.1b protein that seemed to translocate from a peripheral staining pattern (without trypsin) to one with diffuse intracellular staining (after trypsin treatment). Taken together, these results further support my hypothesis that trypsin induces the receptor specific translocation of the mature IpLITR 1.1b surface protein into an immature intracellular form. This loss of IpLITR 1.1b surface expression directly affects IpLITR 1.1b-mediated phagocytic capabilities, in particular the generation of extended membranous protrusions that facilitated target binding and capture.

As mentioned earlier, the trypsin-sensitivity of the mammalian MR phagocytic activity parallels my own observations for IpLITR 1.1b. However, in contrast to my findings, the MR is proteolytically processed into a surface-expressed form that is smaller than the native protein [224]. The trypsin-generated MR is internalized and degraded, which supports the hypothesis that trypsin can provide a trigger for the regulated internalization of surface proteins. However, since I did not observe any protein fragments <60 kDa after trypsinization of IpLITR 1.1b-expressing cells, I suggest that trypsin modulates this receptor by selectively removing a post-translational modification and not by cutting the polypeptide backbone; which coincides with an apparent reduction in the size of IpLITR 1.1b and the movement of the receptor from the plasma membrane into internal endomembranes. I also favored the idea that trypsin targets O-linked glycosylation of IpLITR 1.1b to convert it from a mature to an immature form since glycosylation prediction software identified only O-linked glycosylation possibilities for IpLITR 1.1b, but my data is suggestive that this may not be the case as treatment with O-glycosidase failed to shift the size IpLITR 1.1b. However, I only tested one O-glycosidase under one condition and therefore these studies only superficially suggest this and therefore more extensive

studies are required to truly identify this idea. Therefore, how trypsin modulates IpLITR 1.1b remains unknown at this time but my data reinforces the idea that the trafficking and associated functions of certain IpLITR-types are dependent upon a trypsin-sensitive post-translational processing event that remains to be deciphered

In summary, serine proteases function as potent immunoregulatory factors through in part their ability to rapidly modify the primary structure and function of surface proteins. Collectively, my data provides a detailed conceptual framework for exploring the unique ability of trypsin to selectively modulate IpLITR structure and trafficking. Importantly, I have identified that the presence of IpLITR 1.1b on the cellular surface influences the way in which cells engage in target-cell interactions through the formation of unique membranous protrusions. Combined with the results presented in Chapter IV, it is now evident that IpLITR 1.1b-induced phagocytic activity is a receptor-specific event that differentially modulates the actin-dynamics of RBL-2H3 cells using a mechanism that is distinct from the classical ITAM-induced response of IpLITR 2.6b/IpFcRγ-L. This study identifies IpLITRs as an excellent model for investigating emergent concepts involved in the coordination of complex and highly-conserved effector responses, such as phagocytosis, during innate defense mechanisms that are often performed in a protease-rich inflammatory environment.

FIGURE 5.1

A.

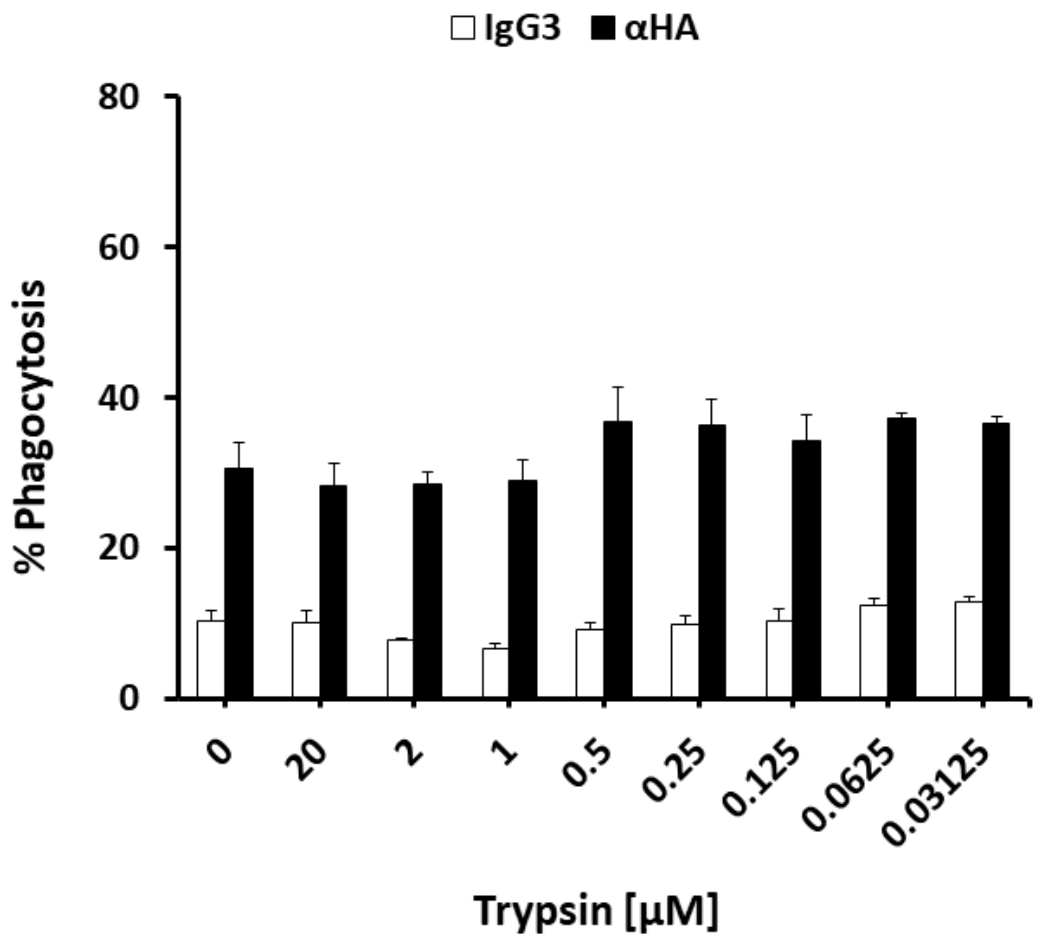
IgG3
αHA
80
60
40
20
0
% Phagocytosis
0
20
2
1
0.5
0.25
0.125
0.0625
0.03125
Trypsin [µM]

FIGURE 5.1

B.

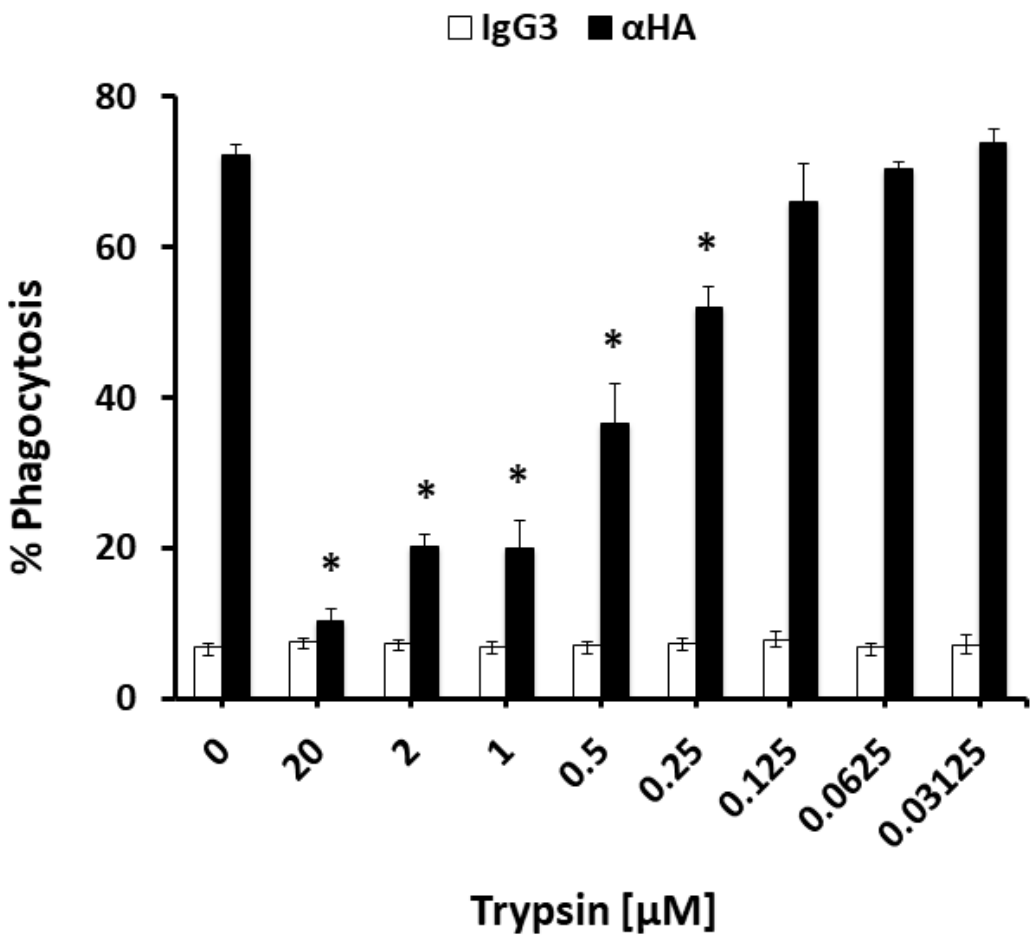
IgG3
αHA
% Phagocytosis
80
60
40
20
0
*
0
20
2
1
0.5
0.25
0.125
0.0625
0.03125
Trypsin [μM]

FIGURE 5.1

C.

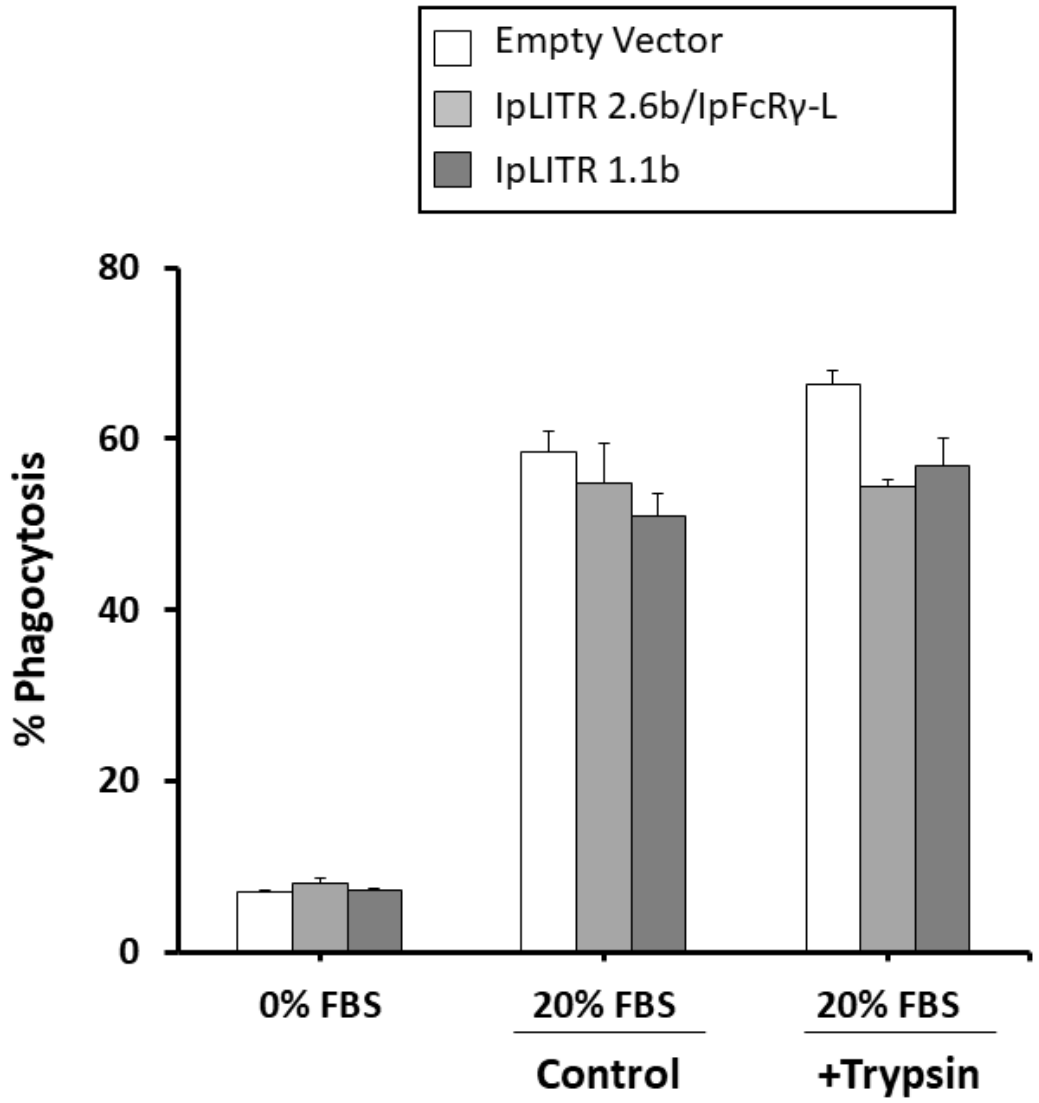
Empty Vector
IpLITR 2.6b/IpFcRγ-L
IpLITR 1.1b
% Phagocytosis
80
60
40
20
0
0% FBS
20% FBS
Control
20% FBS
+Trypsin

FIGURE 5.1 Effects of trypsin treatment on IpLITR cell surface expression and function. (A) IpLITR 2.6b/IpFcRγ-L- and (B) IpLITR 1.1b-expressing RBL-2H3 cells were pre-treated for 15 min with serial dilutions of ice-cold trypsin ranging in doses from 0.03125 μM to 20 μM. Cells were incubated for 60 min at 37^{o}C with either IgG3 isotype opsonized 4.5 μm YG beads (white bars) or αHA mAb opsonized beads (black bars) and IpLITR-mediated phagocytosis was analyzed by flow cytometry as previously described (Lillico et al., 2015). The effects of trypsin on the endogenous phagocytic response of RBL-2H3 cells was also assessed in the same manner as previously described. Empty vector-expressing cells (white bars), IpLITR 2.6b/IpFcRγ-L-expressing cells (light gray bars), and IpLITR 1.1b-expressing cells (dark gray bars) were pre-treated with either 20 or 0 μM tryspin prior to being incubated for 1 hr at 37° in the presence of FBS-opsonized beads (C). Each bar represents the mean ± SEM of three independent experiments and * indicates $p < 0.05$ when comparing the % phagocytosis values (i.e. the proportion of cells in the population that have associated with at least on target bead) of trypsin-pretreated cells vs. the untreated (i.e. 0 μM) control group.

FIGURE 5.2

A.

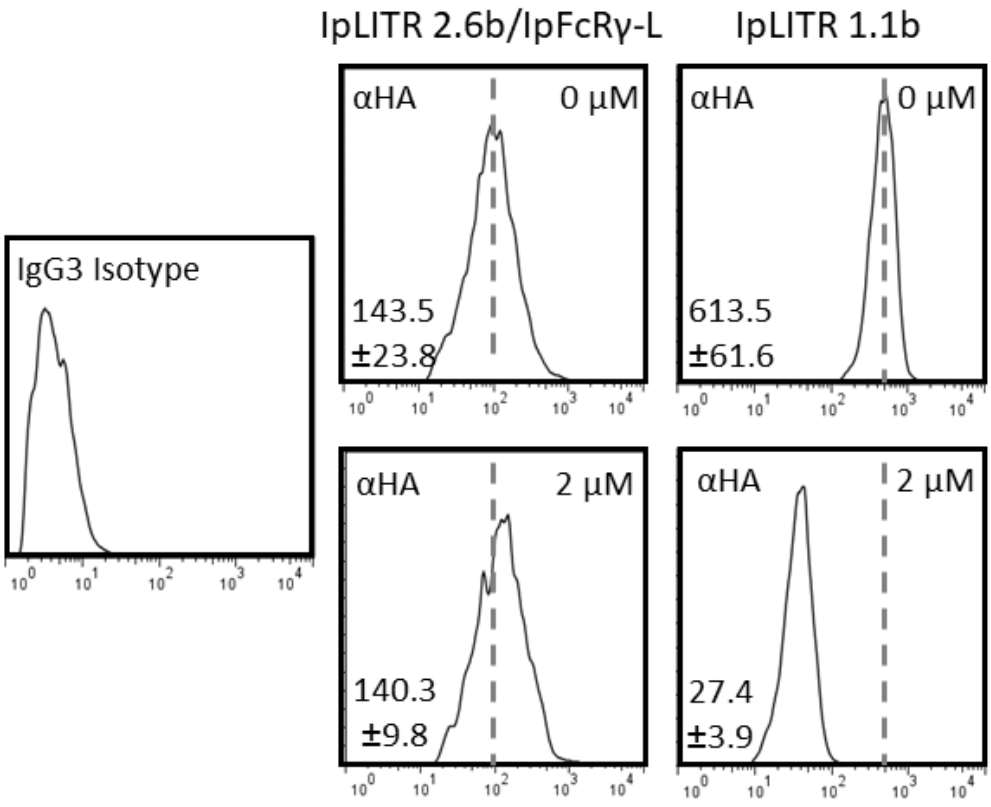
IpLITR 2.6b/IpFcRγ-L
IpLITR 1.1b
IgG3 Isotype
αHA
0 μM
143.5
±23.8
αHA
0 μM
613.5
±61.6
αHA
2 μM
140.3
±9.8
αHA
2 μM
27.4
±3.9

FIGURE 5.2

B.

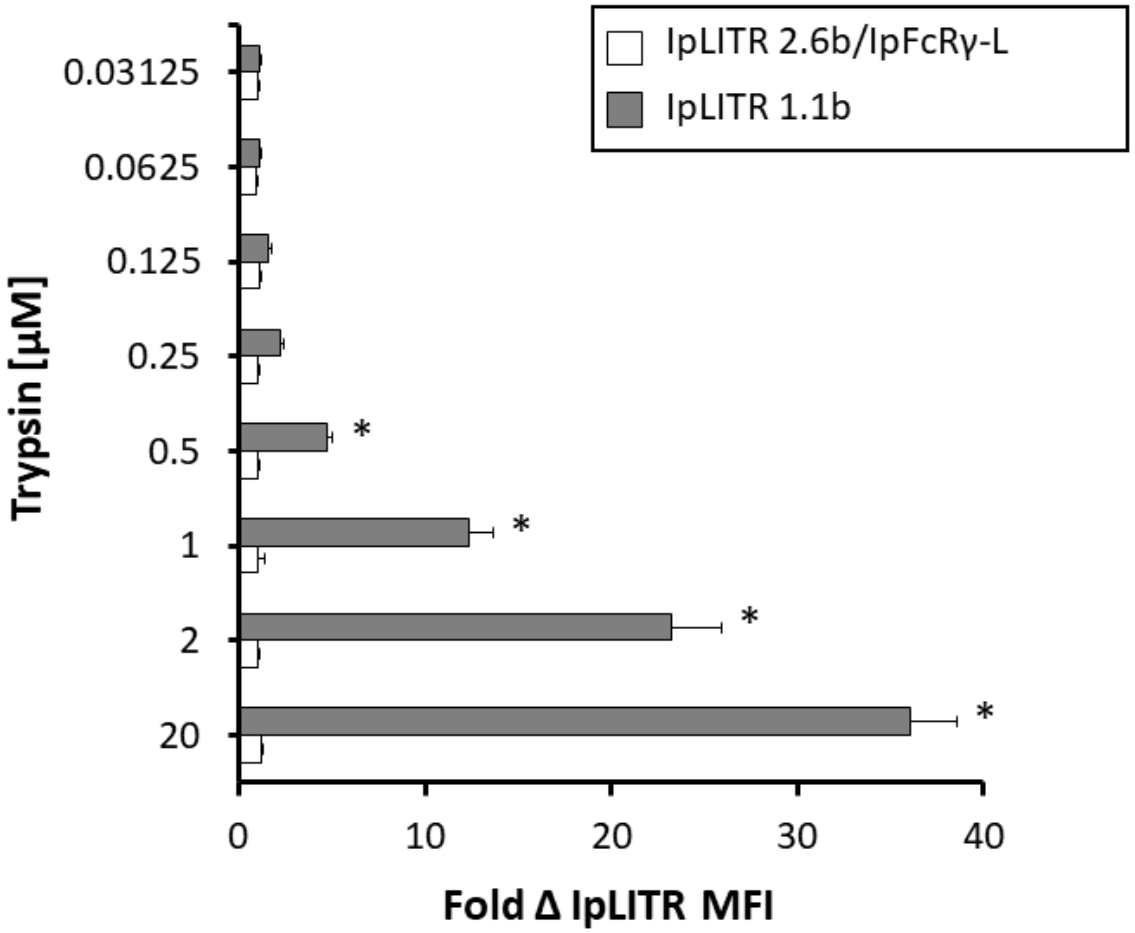
IpLITR 2.6b/IpFcRγ-L
IpLITR 1.1b
Trypsin [µM]
0.03125
0.0625
0.125
0.25
0.5
1
2
20
*
*
*
*
0
10
20
30
40
Fold Δ IpLITR MFI

FIGURE 5.2

C.

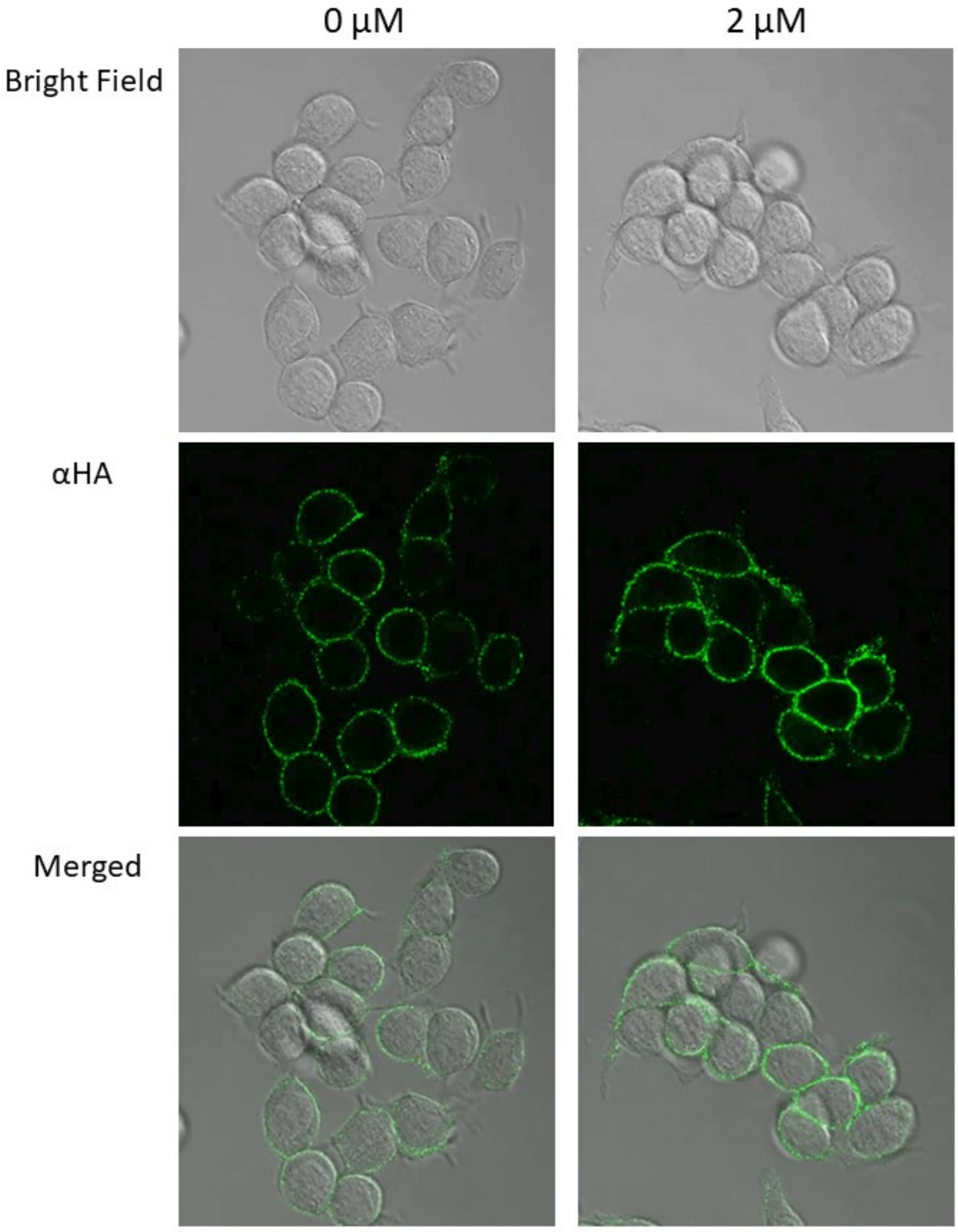

FIGURE 5.2

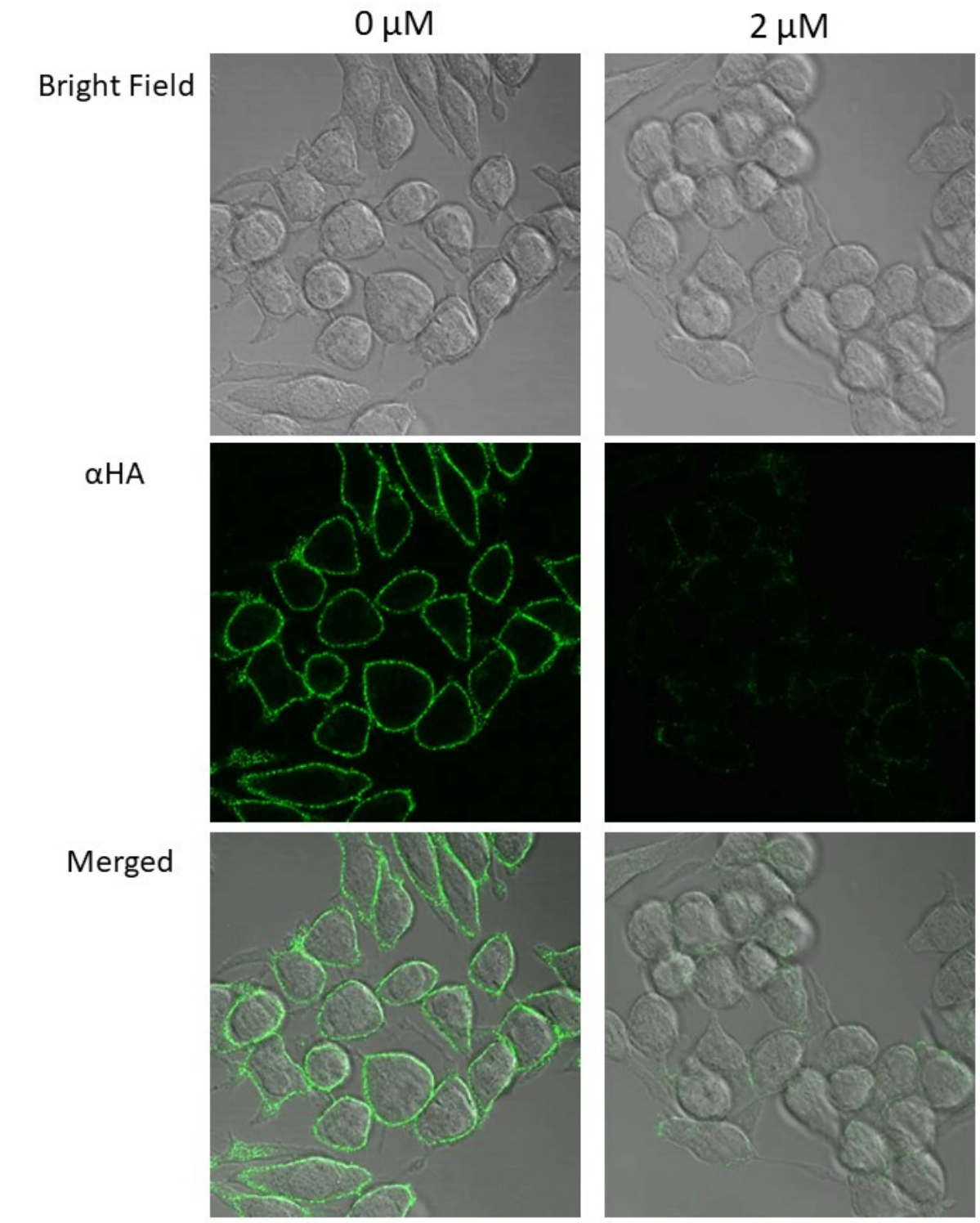

FIGURE 5.2 IpLITR 1.1b but not IpLITR 2.6b/IpFcRγ-L surface expression is altered by trypsin treatment. (A) Flow cytometric histograms show the surface staining profiles for IpLITR 2.6b/IpFcRγ-L- and IpLITR 1.1b-expressing RBL-2H3 cells before (0 μM) and after (2 μM) 15 min trypsin pre-treatments. Also shown is the IgG3 isotype staining level for IpLITR 1.1b-expressing cells. Numbers in the bottom left of each histogram represent the mean ± SEM of the MFI calculated from three independent experiments. (B) The fold-change (Δ) of IpLITR 2.6b/IpFcRγ-L- (white bars) and IpLITR 1.1b (grey bars) surface staining following trypsin pretreatments were calculated from the MFI values as described in the methods section. Each bar represents the mean ± SEM of three independent experiments and * indicates $p < 0.05$ when comparing the Δ MFI values of trypsin-pretreated cells vs. the untreated (i.e. 0 μM) control group. (C) IpLITR 1.1b and (D) IpLITR 2.6b/IpFcRγ-L- cell surface staining levels were also examined by confocal microscopy following 15 min trypsin pre-treatment (2 μM) of RBL-2H3 cells. In these images, the relative αHA mAb staining is visualized using an Alexa-488 conjugated goat αmouse IgG3 and compared with control IpLITR-expressing cells (i.e. 0 μM trypsin). Statistical significance for changes in IpLITR expression in the presence of trypsin doses was done using a student-t test using a two tailed paired analysis.

FIGURE 5.3

A.

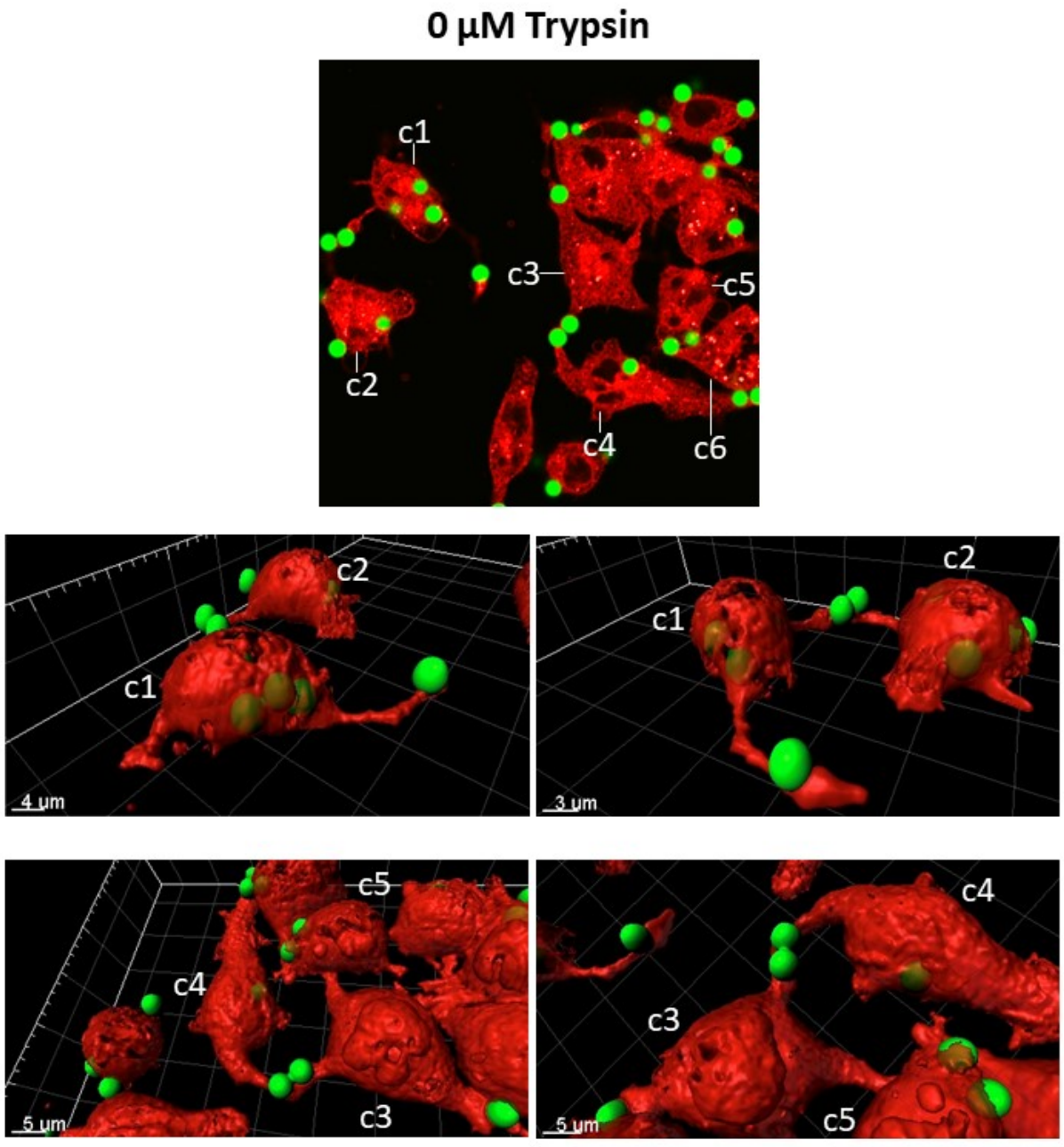
0 µM Trypsin
c1
c2
c3
c4
c5
c6
c1
c2
4 µm
c1
c2
3 µm
c3
c4
c5
5 µm
c3
c4
c5
5 µm

FIGURE 5.3

B.

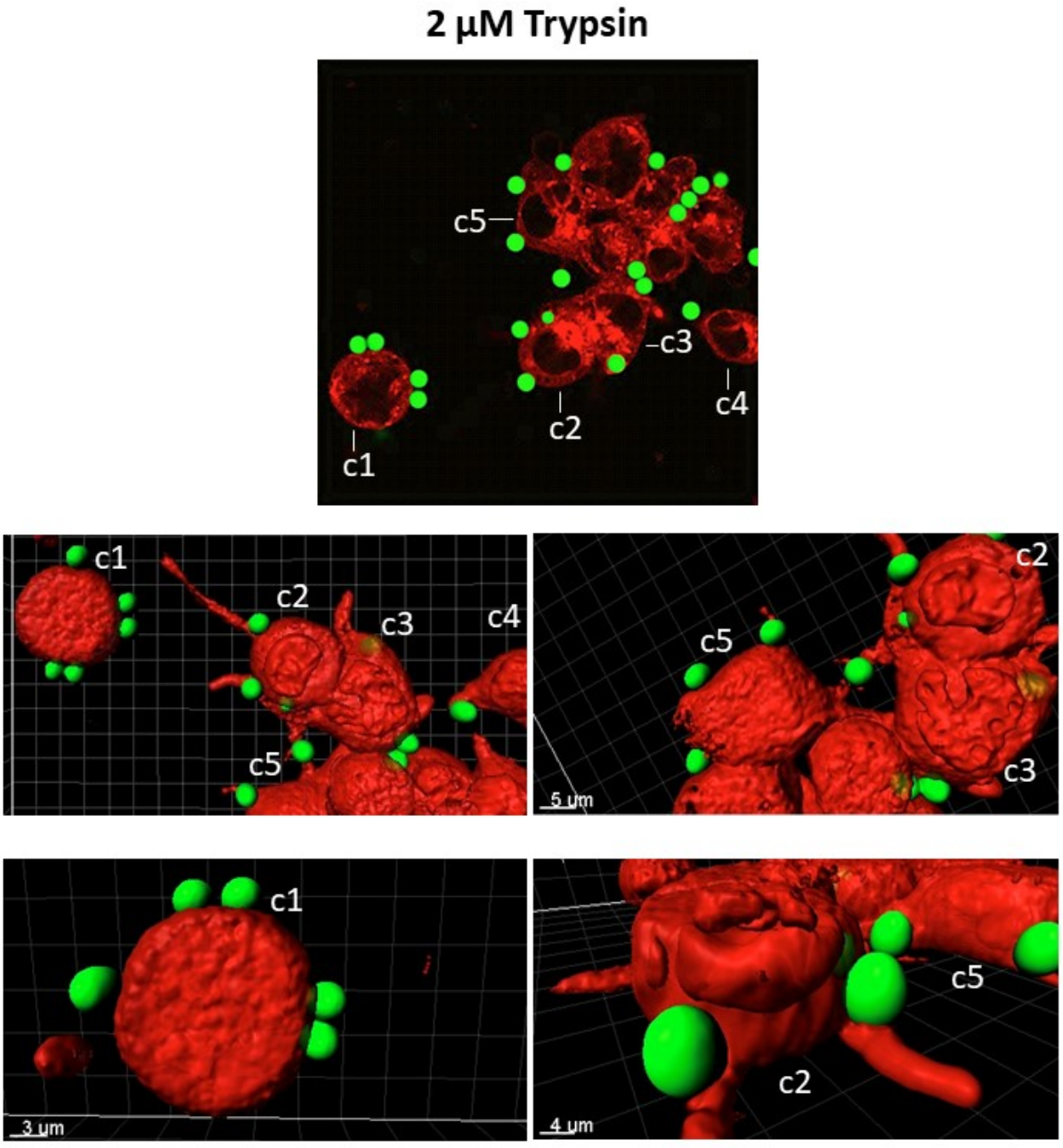
2 µM Trypsin
c5
c3
c4
c2
c1
c1
c2
c3
c4
c5
c2
c5
c3
5 µm
c1
3 µm
c5
c2
4 µm

FIGURE 5.3

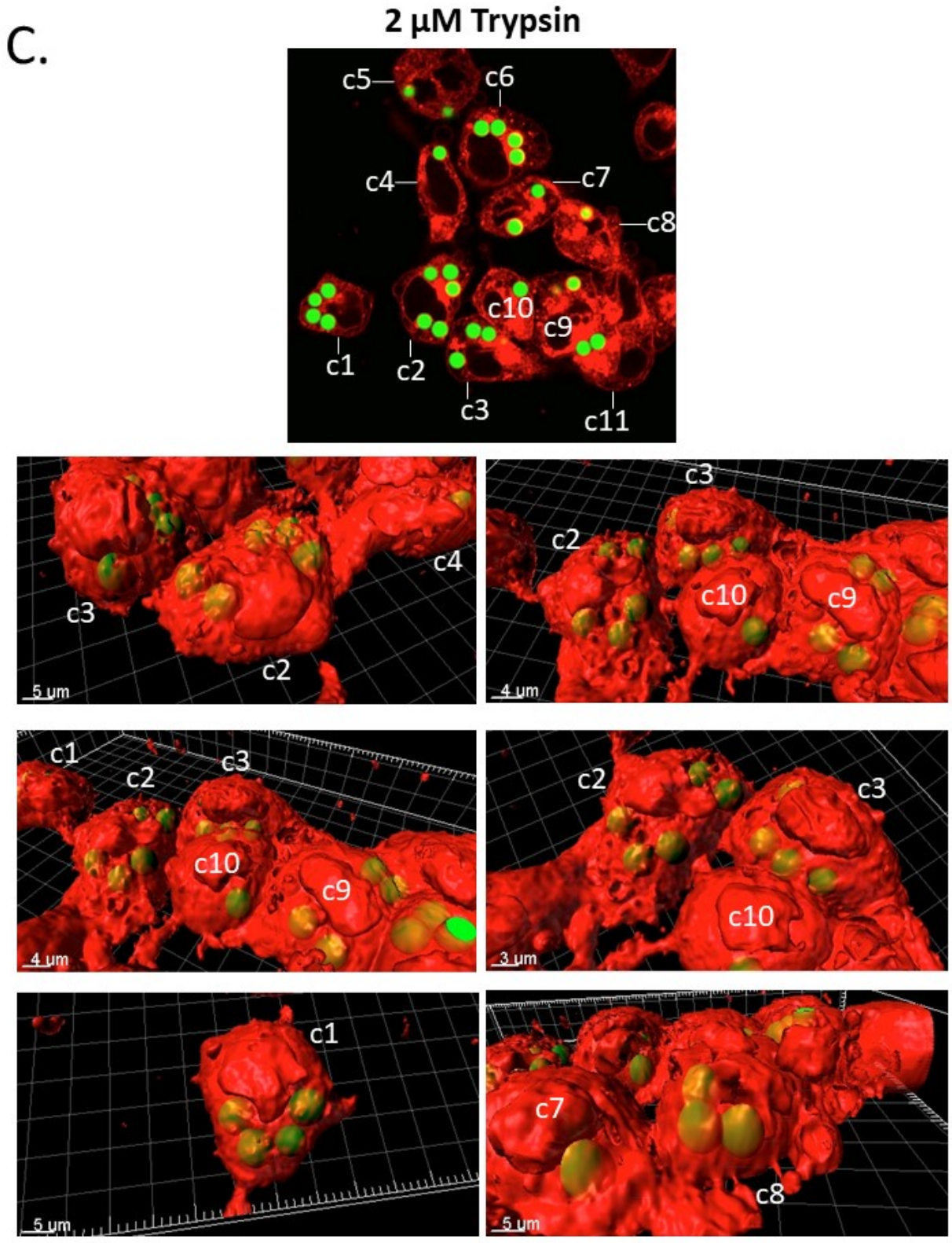
C.
2 µM Trypsin
c5
c6
c4
c7
c8
c10
c9
c1
c2
c3
c11
c3
c4
c2
5 µm
c3
c2
c10
c9
4 µm
c1
c2
c3
c10
c9
4 µm
c2
c3
c10
3 µm
c1
5 µm
c7
c8
5 µm

FIGURE 5.3 IpLITR 1.1b-mediated target capture and engulfment phenotype is significantly altered by trypsin. (A) Untreated (i.e 0 μM) and (B) trypsin pre-treated (i.e. 2 μM) IpLITR 1.1b-expressing RBL-2H3 cells were plated overnight on sterile coverslips, stained with CellMask Orange and then incubated with 4.5 μm αHA mAb-opsonized YG beads for 60 min at 37^{o}C. Cells were then fixed with 4% PFA and then analyzed by confocal microscopy. Representative z-stack images demonstrating the cell (red) and bead (green) interactions are shown. Individual cells (c) are identified on the images. (A) Untreated (i.e. 0 μM) and (B) trypsin pre-treated (i.e. 2 μM trypsin) IpLITR 1.1b-expressing RBL-2H3 cells are represented as a series of 3D reconstructions to visualize cell-bead interactions. (C) A representative z-stack (top image) and a 3D reconstruction (bottom image) are shown for 2 μM trypsin pre-treated IpLITR 2.6b/IpFcRγ-L- -expressing cells and a series of 3D reconstructions are shown.

FIGURE 5.4

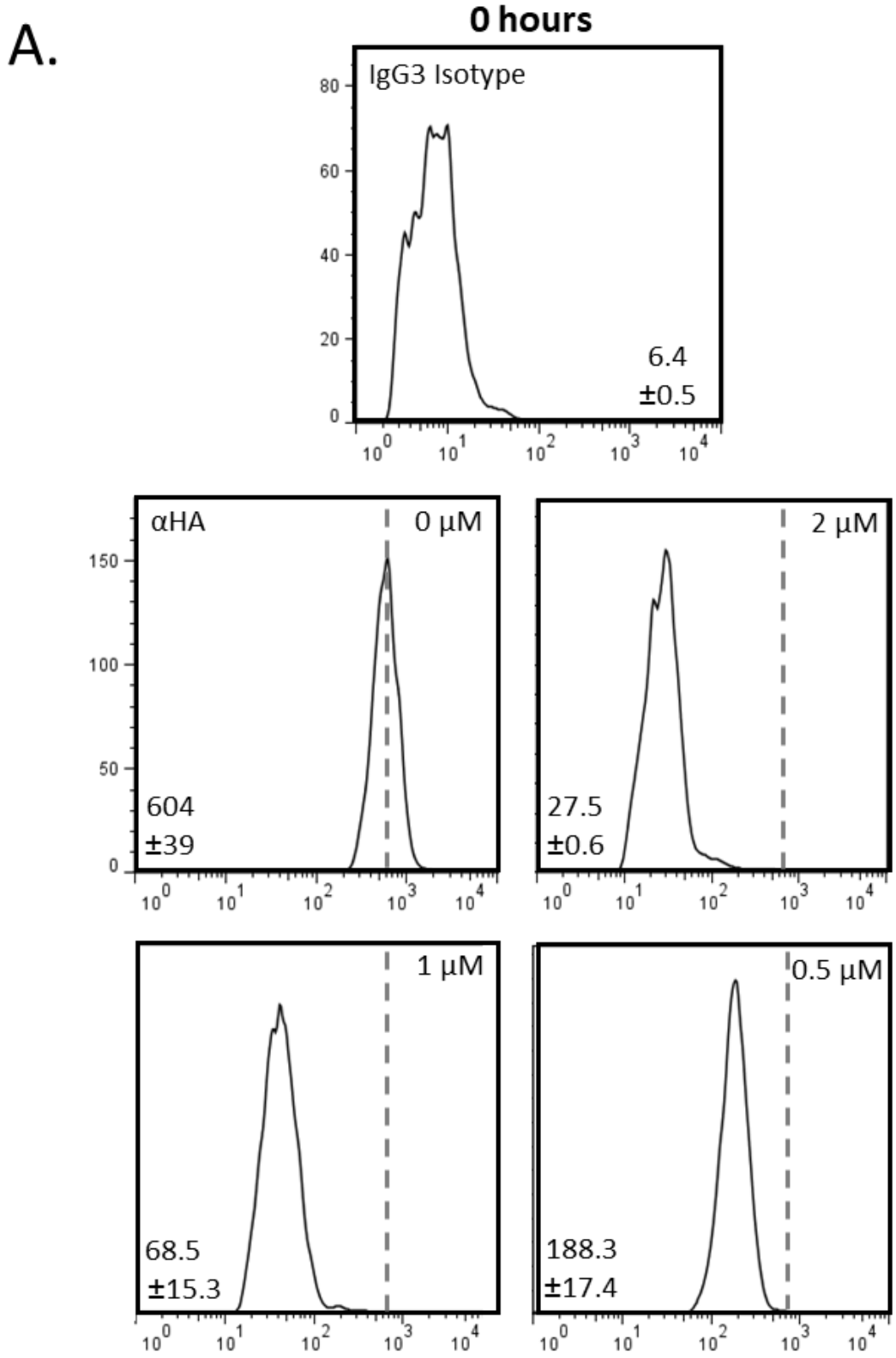
A.
0 hours
IgG3 Isotype
6.4
±0.5
αHA
0 µM
604
±39
2 µM
27.5
±0.6
1 µM
68.5
±15.3
0.5 µM
188.3
±17.4

FIGURE 5.4

B.

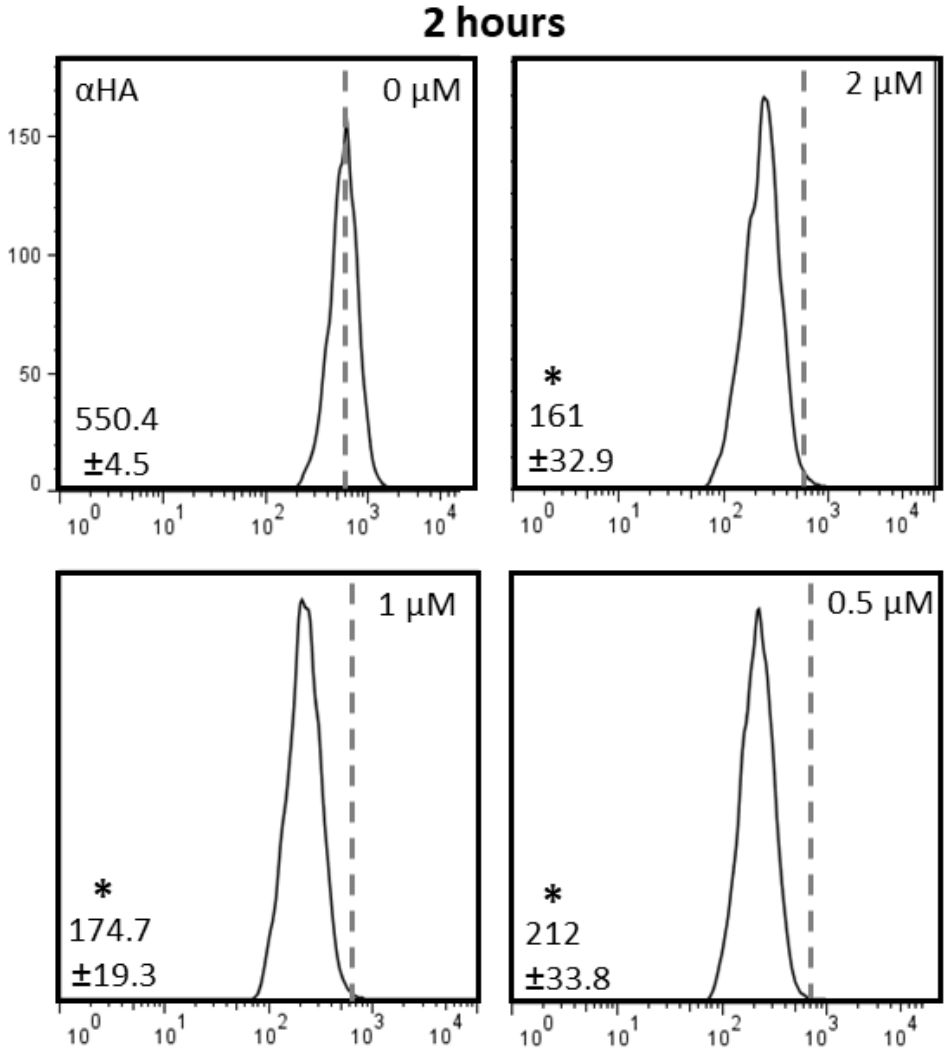
2 hours
αHA
0 µM
550.4
±4.5
2 µM
*
161
±32.9
1 µM
*
174.7
±19.3
0.5 µM
*
212
±33.8
150
100
50
0
10^0
10^1
10^2
10^3
10^4

FIGURE 5.4

C.

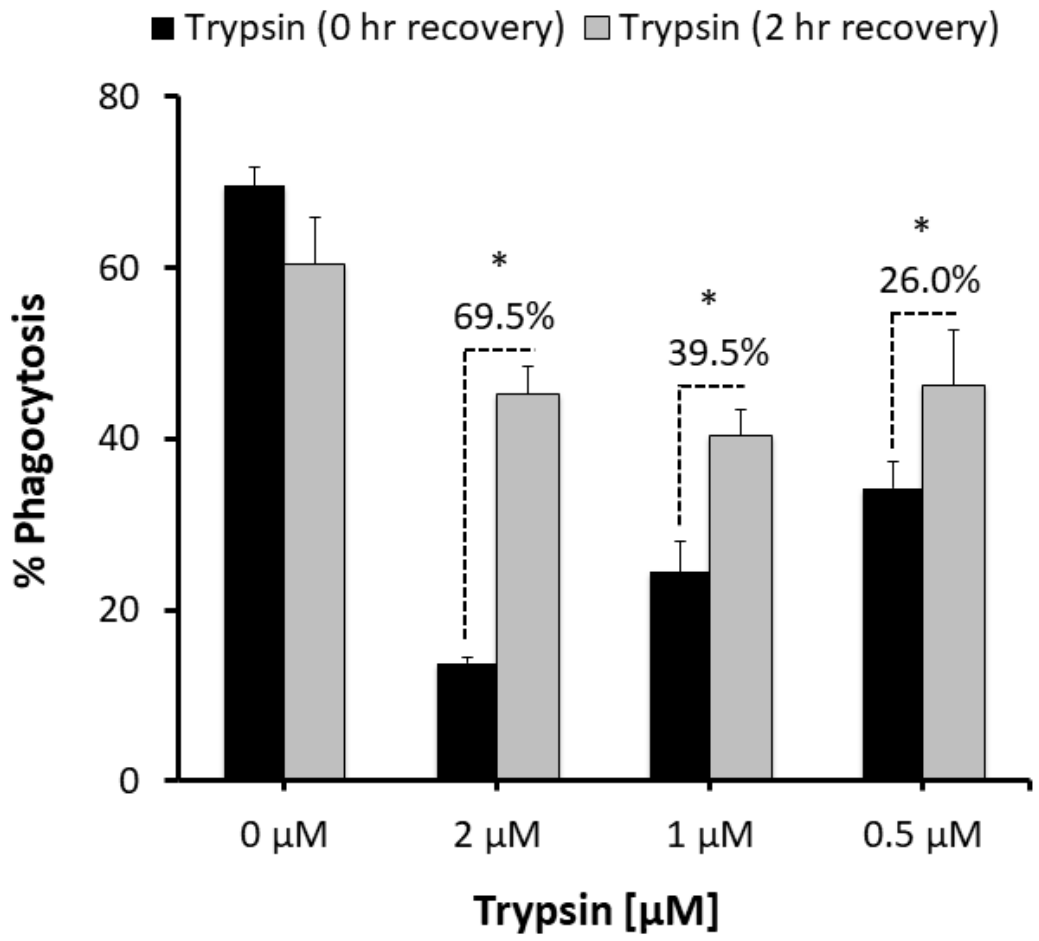
Trypsin (0 hr recovery)
Trypsin (2 hr recovery)
% Phagocytosis
80
60
40
20
0
*
69.5%
*
39.5%
*
26.0%
0 µM
2 µM
1 µM
0.5 µM
Trypsin [µM]

FIGURE 5.4 Trypsin-induced effects on IpLITR 1.1b-expressing cells are reversible. Flow cytometric histograms show the surface staining profiles for IpLITR 1.1b-expressing RBL-2H3 cells immediately following 0 hours (A) or 2 hrs after (B) pre-treatment of the cells with 2 μM, 1 μM, or 0.5 μM trypsin. Also shown is the IgG3 isotype staining level for IpLITR 1.1b-expressing cells (top panel; A). Numbers in the bottom left of each histogram represent the mean ± SEM of the MFI calculated from three independent experiments and * indicates $p < 0.05$ when comparing the Δ MFI values at each trypsin pre-treatment dose between cells allowed to recover for 2 hrs vs. those that had no recovery period (i.e. 0 hrs). (C) The phagocytic activity of IpLITR 1.1b-expressing cells was also determined by flow cytometry using 4.5 μm αHA mAb-opsonized YG beads. Cells pre-treated with 2 μM, 1 μM, or 0.5 μM trypsin all had significantly increased phagocytic activities when compared with cells that did not have a recovery period (i.e. 0 hrs). Each bar represents the mean ± SEM of three independent experiments and * indicates $p < 0.05$ when comparing the phagocytic values after 0 hrs and 2 hrs recovery post-trypsin treatments. The % value indicated on the graphs represents the % increase of the phagocytic activity after 2 hrs post-trypsin exposure. Statistical significance for changes in phagocytosis in the presence of trypsin doses was done using a student-t test using a two tailed paired analysis.

FIGURE 5.5

A.

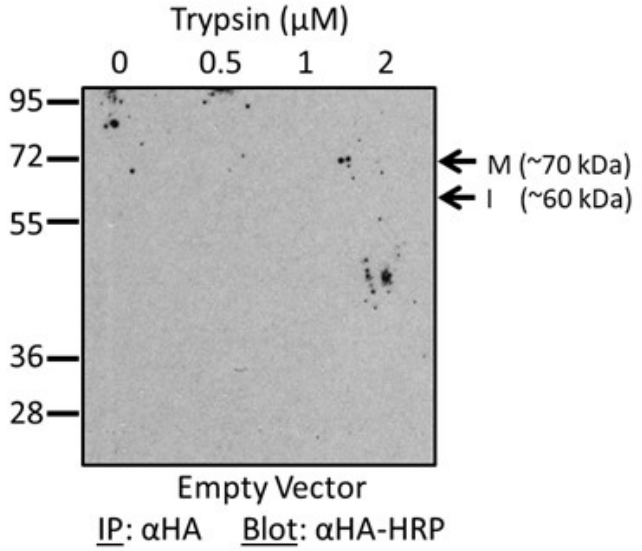
Trypsin (μM)
0
0.5
1
2
95
72
55
36
28
M (~70 kDa)
I (~60 kDa)
Empty Vector
IP: αHA Blot: αHA-HRP

B.

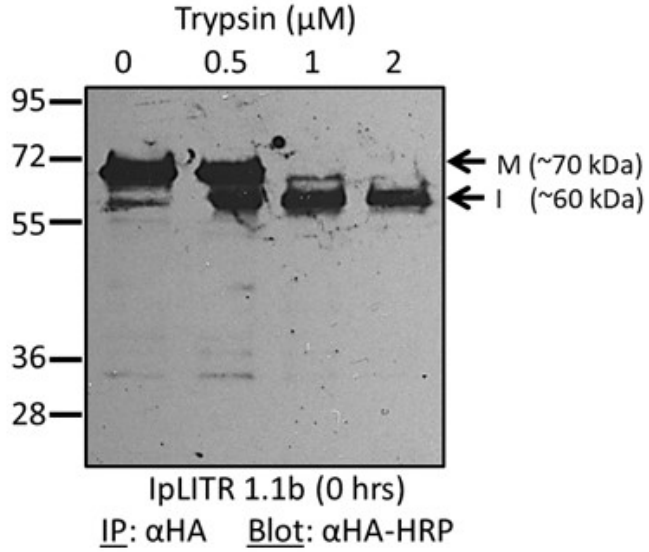
Trypsin (μM)
0
0.5
1
2
95
72
55
36
28
M (~70 kDa)
I (~60 kDa)
IpLITR 1.1b (0 hrs)
IP: αHA Blot: αHA-HRP

FIGURE 5.5

C.

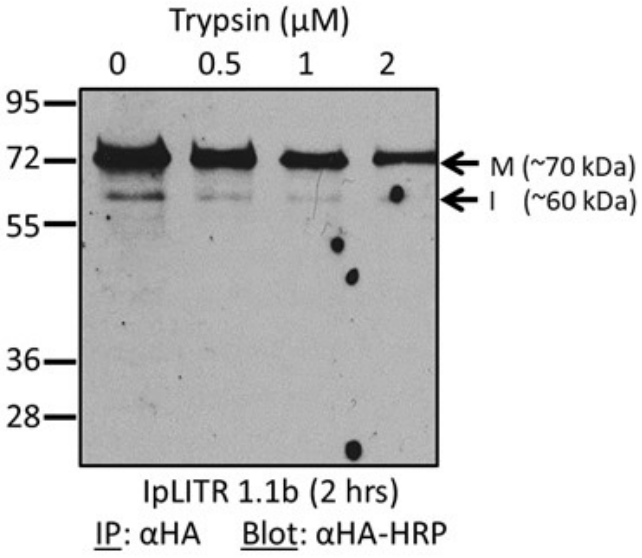
Trypsin (μM)
0
0.5
1
2
95
72
55
36
28
M (~70 kDa)
I (~60 kDa)
IpLITR 1.1b (2 hrs)
IP: αHA Blot: αHA-HRP

D.

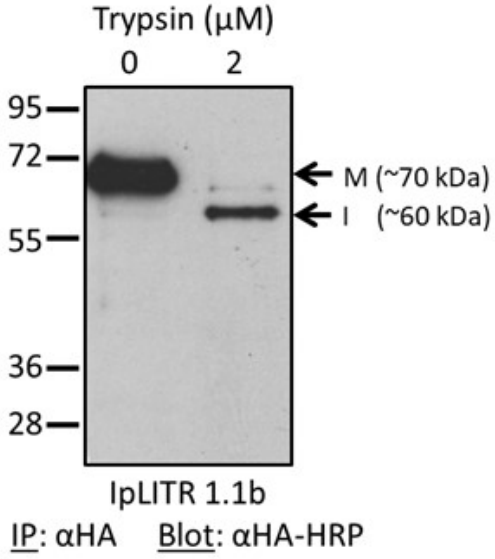
Trypsin (μM)
0
2
95
72
55
36
28
M (~70 kDa)
I (~60 kDa)
IpLITR 1.1b
IP: αHA Blot: αHA-HRP

FIGURE 5.5

E.

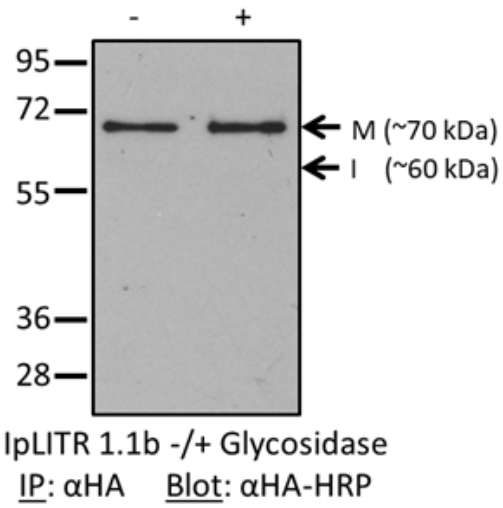

IpLITR 1.1b -/+ Glycosidase
IP: αHA Blot: αHA-HRP

F.

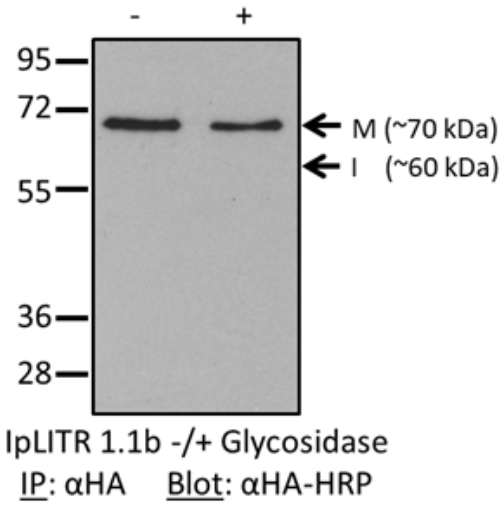

IpLITR 1.1b -/+ Glycosidase
IP: αHA Blot: αHA-HRP

G.

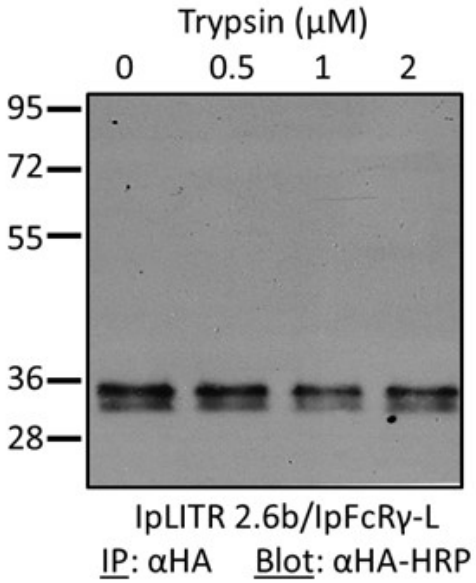

FIGURE 5.5 Biochemical examination of trypsin-exposed RBL-2H3 cells reveals receptor-selective modification of IpLITR 1.1b. (A) Empty-vector transfected RBL-2H3 cells, (B) trypsin-treated IpLITR 1.1b-expressing RBL-2H3 cells without a recovery period, and (C) trypsin-treated IpLITR 1.1b-expressing RBL-2H3 cells with a 2 hr recovery period were lysed and then immunoprecipitated (IP) using the αHA mAb. Immunoreactive proteins were detected using an HRP-conjugated goat αHA polyclonal antibody. Values at the top of each lane represent doses of trypsin (μM). Size markers in kDa are indicated on the left side of each blot and the arrows on the right side of the blots in (B) and (C) identify the putative mature (M) and immature (I) forms of the IpLITR 1.1b protein at ~70 kDa and ~60 kDa, respectively. (D) IpLITR 1.1b-expressing RBL-2H3 cells were lysed and immunoprecipitated using αHA mAb microspheres. The purified receptor was then treated with either 0 or 2 μM trypsin and immunoreactive proteins were detected using αHA HRP-conjugated antibody. For the receptor deglycosylation experiments, RBL-2H3 cells expressing IpLITR 1.1b were either directly treated (E) or the IpLITR 1.1b protein was first immunoprecipitated from whole cell lysates (F) and then treated with 0 U (-) or 40,000 U (+) of O-Glycosidase. (E) cells were incubated for 3 hrs at 37°C with O-Glycosidase and then immunoprecpipitated as previously described. Alternatively, immunoprecipitated samples (F) were first denatured and then treated with O-Glycosidase for 1 hr at 37°C. All samples prepared in (E, F) were eluted and immunoreactive proteins were detected using the αHA HRP-conjugated antibody protocol previously described. (G) IpLITR 2.6b/IpFcRγ-L-expressing cells were pre-treated with trypsin and then immunoprecipitated using the same protocol as described for IpLITR 1.1b above.

FIGURE 5.6

A.

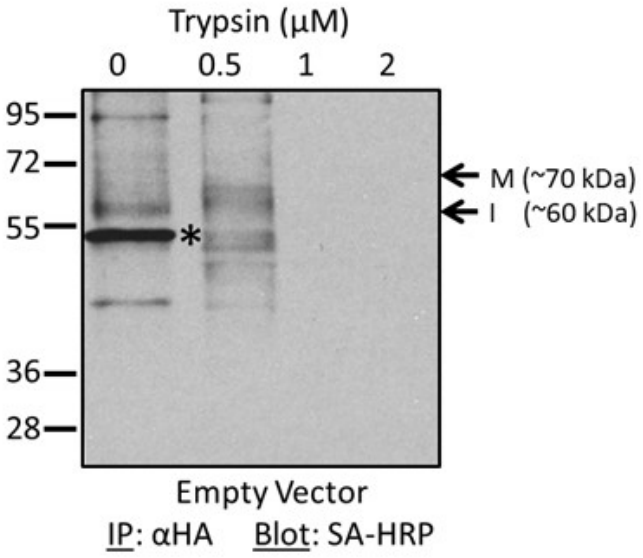
Trypsin (μM)
0
0.5
1
2
95
72
55
36
28
*
M (~70 kDa)
I (~60 kDa)
Empty Vector
IP: αHA Blot: SA-HRP

B.

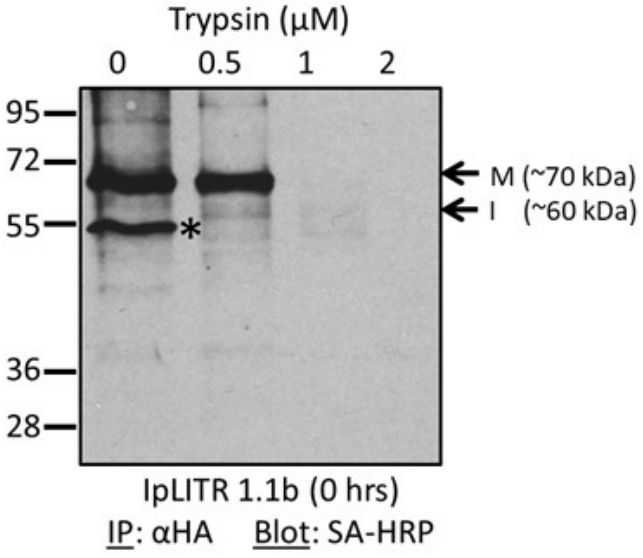
Trypsin (μM)
0
0.5
1
2
95
72
55
36
28
*
M (~70 kDa)
I (~60 kDa)
IpLITR 1.1b (0 hrs)
IP: αHA Blot: SA-HRP

C.

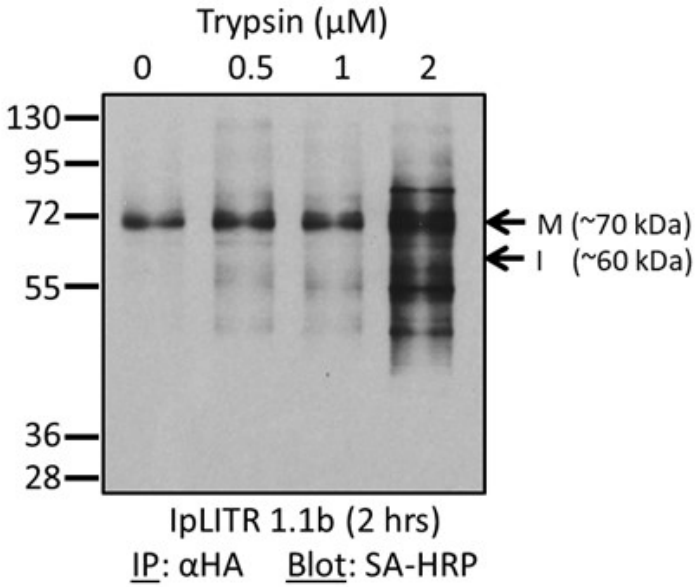

FIGURE 5.6 Immunprecipitation of IpLITR 1.1b from trypsin-exposed RBL-2H3 cells identifies a mature cell surface protein and a putative intracellular form. (A) Empty-vector transfected RBL-2H3 cells, (B) trypsin-treated IpLITR 1.1b-expressing RBL-2H3 cells without a recovery period, and (C) trypsin-treated IpLITR 1.1b-expressing RBL-2H3 cells with a 2 hr recovery period were lysed and then immunoprecipitated (IP) using the αHA mAb. Immunoreactive proteins were detected by probing with HRP-conjugated streptavidin (SA). Values at the top of each lane represent doses of trypsin (μM). Size markers in kDa are indicated on the left side of each blot and the arrows on the right side of the blots in (B) and (C) identify the putative mature (M) and immature (I) forms of the IpLITR 1.1b protein at ~70 kDa and ~60 kDa, respectively. * indicates the presence of a non-specific surface protein at ~50 kDa.

FIGURE 5.7

A.

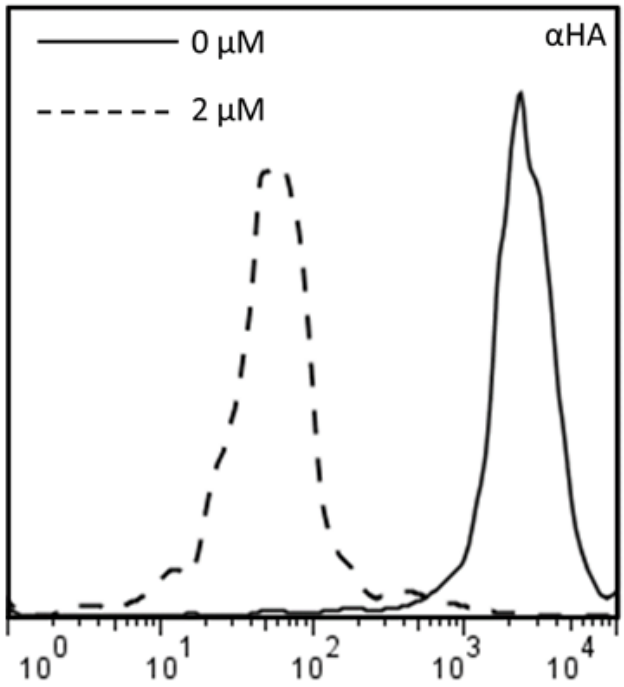

B.

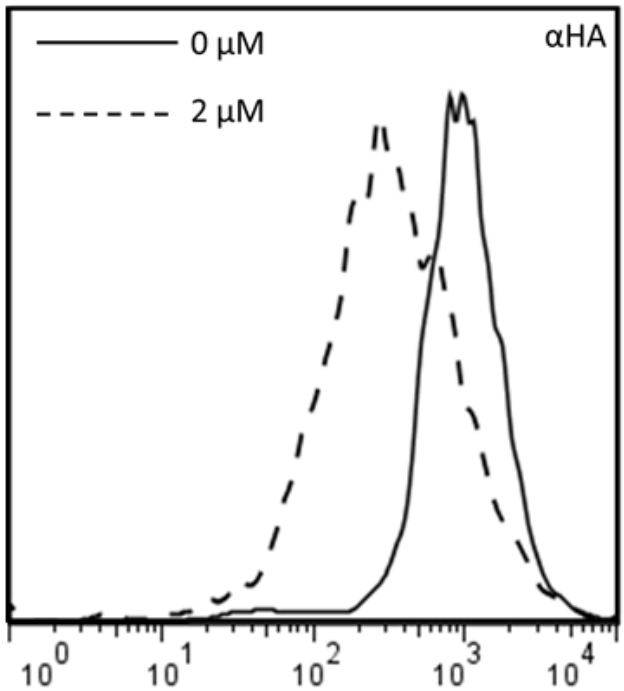

FIGURE 5.7

C.

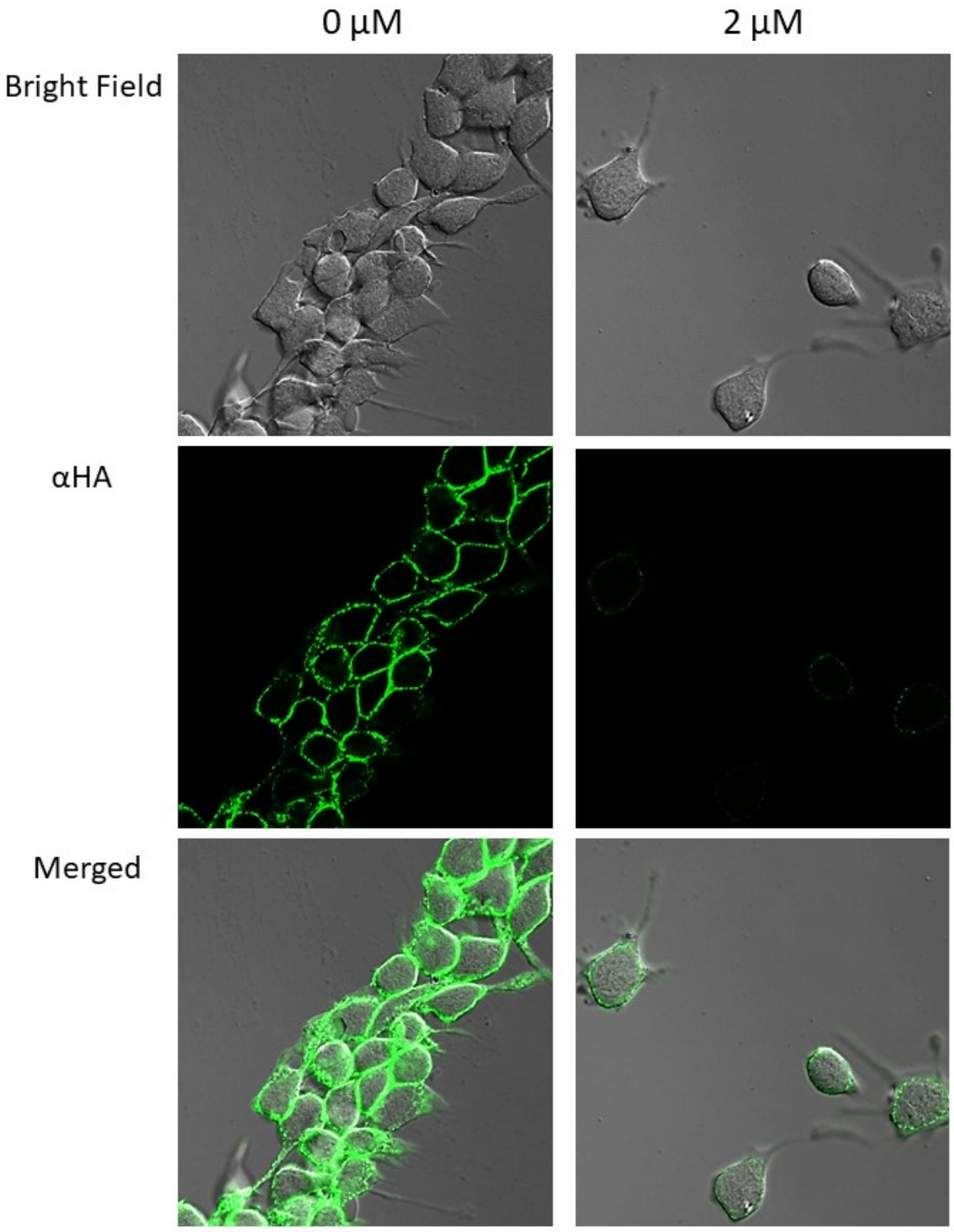

FIGURE 5.7

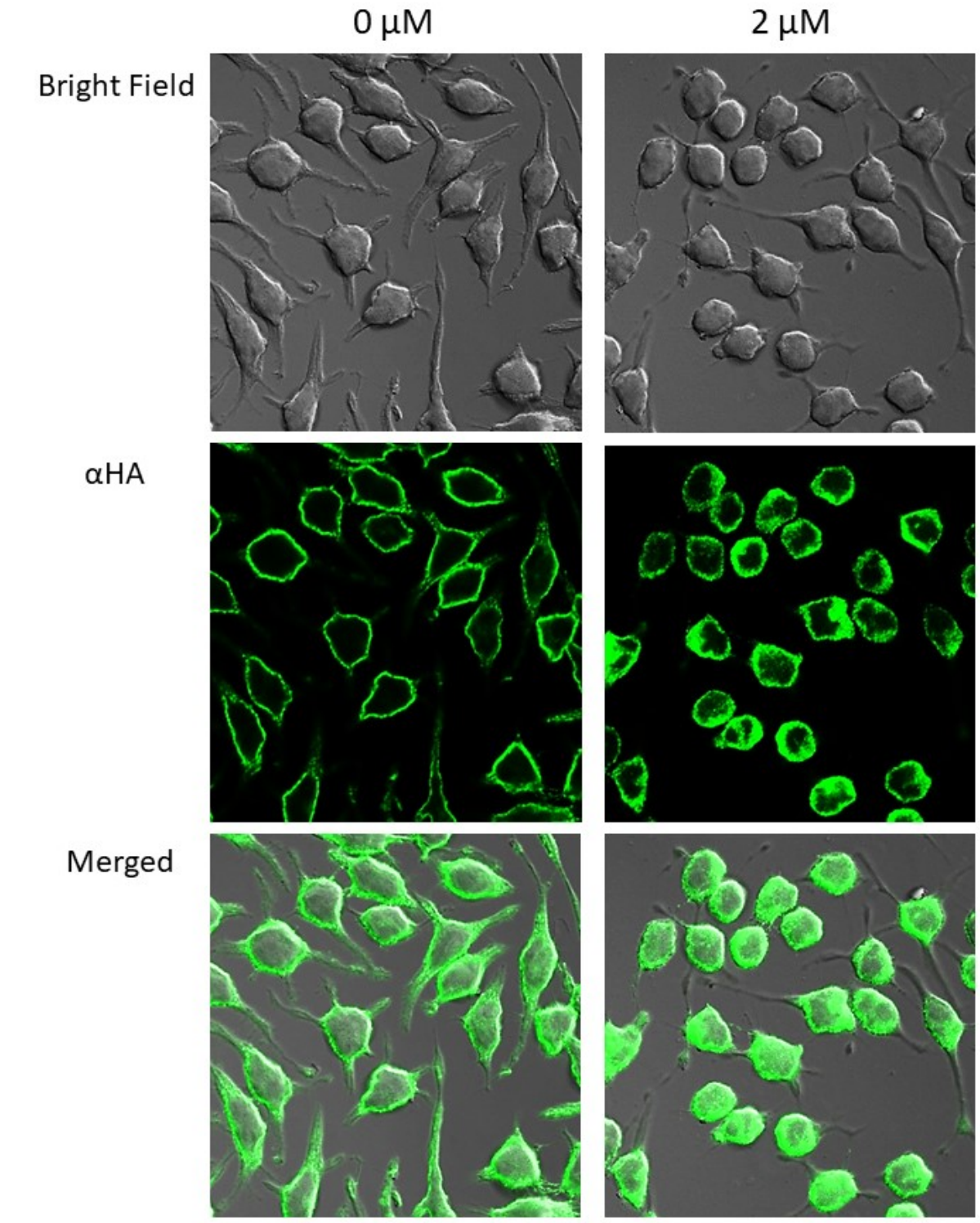

FIGURE 5.7 Flow cytometry and confocal imaging experiments further reinforce that trypsin treatment promotes the translocation of IpLITR 1.1b into the cell.
Flowcytometry histograms of non-permeabilized (A) or permeabilized (B) IpLITR 1.1b-expressing cells stained treated with 2 μM trypsin (dashed line) or untreated (solid line) Represented histograms are one of three independent experiments done. Similarly, non permeabilized (C) or permeabilized (D) IpLITR 1.1b-expressing cells were plated onto coverslips and then treated with 2 μM trypsin or untreated (0 μM) and αHA mAb stained followed by secondary staining with an Alexa 488 goat αmouse secondary antibody for confocal imaging.

CHAPTER VI

SEM AND LIVE-CELL IMAGING ANALYSIS OF CHANNEL CATFISH LITR-INDUCED PLASMA MEMBRANE DYNAMICS DURING THE PHAGOCYTIC PROCESS

A version of this chapter has been published:

Lillico et al. 2018., Selective Regulation of Cytoskeletal Dynamics and Filopodia Formation by Teleost Leukocyte Immune-Type Receptors Differentially Contributes to Target Capture During the Phagocytic Process. *Front. Immunol*. 9; 1144

6.1 INTRODUCTION

The unique ability of phagocytic cells to recognize and engulf large particulate targets depends on the surface expression of specialized immunoregulatory receptors. Well known mammalian phagocytic receptor-types include complement receptors [2,200,232,233], members of the Fc receptor (FcR) family [2,200,232], and dectin-1 [63,83,123,234]. Studies using these model immune proteins have shown that phagocytosis is a multifaceted process that tightly regulates the active capture, ingestion, and subsequent destruction of various microbial targets [2,63,200,232,233]. Phagocytic receptors relay their interactions with extracellular targets into dynamic F-actin remodelling events that reshape the plasma membrane through specialized intracellular signaling events [2,61,82,86,203]. Generally, each of these phagocytic pathways requires localized phospholipid metabolism and the engagement of actin nucleation and regulatory factors that link surface receptor activation with the cytoskeletal machinery to facilitate target engulfment [2,61,82,86,203].

Interactions between phagocytic receptors and extracellular targets is not always reliant on passive binding events; rather, phagocytes actively increase the incidence of target-binding events through the formation of unique finger-like extensions of the plasma membrane called filopodia [235–238]. These membrane protrusions are composed of un-branched filaments of

polymerized F-actin that vary greatly in length (1-100 μm), thickness (0.1-0.3 μm), molecular composition, and geometry [235–238]. Early studies using SEM have revealed that mouse peritoneal macrophages formed cord-like extensions that arose from the plasma membrane to tether extracellular targets to the cell surface [239]. In addition, the formation of filopodia following bacterial lipopolysaccharide stimulation of macrophages occurs through the phosphorylation of various intracellular signaling mediators [240,241]. Following the initial contact with extracellular targets, filopodia quickly retract back towards the cell body, resulting in the immobilization and tethering of targets to the plasma membrane [87,88,237–240]. This action allows for additional surface receptor-target interactions to occur that reinforce the transduction events responsible for the temporal activation of the phagocytic process [87,237,238]. While the ability of phagocytes to actively deploy filopodia has been demonstrated, and some of the molecular components controlling their formation have been described, relatively little is known about the specific intracellular molecules that participate in filopodial dynamics within innate immune cells. Furthermore, much less is known about what specific cell surface receptor-types trigger the formation of these structures and whether the functional ability of specific immunoregulatory receptor-types to control membrane dynamics are conserved in basal vertebrates.

My work has shown that when expressed in the RBL-2H3 cell-line, IpLITR 2.6b/IpFcRγ-L activates phagocytosis using a characteristic intracellular transduction response that is reminiscent of the prototypical mammalian ITAM-dependent FcR phagocytic pathway (chapter IV) [193]. Subsequently, I also described an alternative phagocytic mechanism mediated by IpLITR1.1b. As described in chapter IV, this unique IpLITR1.1b-mediated mechanism exhibited reduced overall target engulfment but featured a significantly enhanced ability to capture

extracellular beads [30]. While this atypical pathway requires active engagement of the actin polymerization machinery, I showed that IpLITR 1.1b-expressing cells were insensitive to pharmacological inhibitors that blocked the classic signaling components of ITAM-dependent phagocytosis. Furthermore, the ability of IpLITR 1.1b-expressing RBL-2H3 cells to capture beads was not affected at 27ºC, an incubation temperature that completely inhibited IpLITR 2.6b/IpFcRγ-L phagocytosis [193]. My static imaging experiments using fixed IpLITR 1.1b-expressing cells also showed that these cells produced extended plasma membrane structures that participated in the capture and tethering of microsphere targets to the cell surface; a phagocytic phenotype that was not observed for IpLITR 2.6b/IpFcRγ-L-expressing cells [193]. In chapter V, I also showed that trypsin selectively modulated IpLITR 1.1b surface expression levels, revealing that this IpLITR-type directly influenced the production of dynamic membranous filopodial-like protrusions that facilitated extracellular target capture and engulfment. However, whether or not IpLITR 1.1b was directly controlling the formation of filopodia during the various stages of the phagocytic process (i.e. binding, capturing, and engulfment) and how these structures were utilized for target interactions could not be conclusively deciphered from fixed cell imaging techniques.

In this thesis chapter I used a combination of LCI and high-resolution SEM to provide detailed new information regarding IpLITR 1.1b-induced plasma membrane dynamics during the phagocytic process. My results support the hypothesis that IpLITR 1.1b-expressing cells selectively induce the formation of F-actin dense protrusions (i.e filopodia). In addition, I show that during the early stages of the IpLITR 1.1b-mediated phagocytic process, these filopodia-like structures retract after target contacts to secure the captured microspheres to the cell surface. This unique target-capturing phenotype is followed by the formation of phagocytic cup-like

structures at the membrane interface and, in some cases, the eventual engulfment of the immobilized microspheres. At the reduced incubation temperature of 27ºC, I also show that although the membrane structures had repressed mobility, dynamic filopodia structures were still generated by IpLITR 1.1b expressing cells and that these continued to facilitate sustained cell-target interactions. Conversely, no F-actin dynamics or any associated membrane activity was seen in IpLITR 2.6b/IpFcRγ-L-expressing cells at this lower temperature; likely due to an inability of this receptor to promote or maintain F-actin polymerization events below 37ºC. Interestingly, in the absence of extracellular targets, the unique dynamic membranous behaviour observed for IpLITR 1.1b-expressing cells at both 37ºC and 27ºC using LCI provides compelling evidence that expression of this specific IpLITR sub-type is directly responsible for inducing filopodia production. Overall, results from this chapter show that IpLITR 1.1b can selectively regulate filopodia formation over a range of incubation temperatures. This also reinforces the use of IpLITRs as an alternative vertebrate model for investigating the integration of immune cell membrane and cytoskeletal dynamics during the coordinate control of the phagocytic process.

6.2 RESULTS

6.2.1 Examination of IpLITR-mediated phagocytosis using SEM

When IpLITR 2.6b/IpFcRγ-L-expressing RBL-2H3 cells were incubated with isotype control IgG3 beads, no internalized or surface-bound targets were observed (Fig. 6.1A; top left panel). Comparatively, when incubated with αHA-opsonized beads (1 hr at 37ºC), these cells displayed a characteristic flattened morphology and had multiple internalized beads with few surface-bound targets (Fig. 6.1A; top right panel). Pre-treatment of the cells with the selective inhibitor of actin polymerization, Latrunculin B abrogated bead internalization; although many of the beads remained associated with the cell surface (Fig. 6.1A; bottom left panel). Not

surprisingly, cells treated with Latrunculin B also had a rounded morphology (compare Fig. 6.1A; top right panel with Fig. 6.1A; bottom left panel). When IpLITR 2.6b/IpFcRγ-L-expressing cells were incubated with target beads for 1 hr at the reduced temperature of 27ºC, engulfment was abrogated, and the target microspheres appeared to be loosely associated with the plasma membrane (Fig. 6.1A; bottom right panel). Notably, when IpLITR 2.6b/IpFcRγ-L-expressing cells were incubated at 27ºC they also had an overall rounded appearance. To capture additional representative images during the early stages of the IpLITR 2.6b/IpFcRγ-L phagocytic process, SEM was performed using cells incubated with the αHA-opsonized beads for shorter time periods at 37ºC (i.e. 4, 8, 16, and 32 min). Characteristic stages of IpLITR 2.6b/IpFcRγ-L phagocytosis, beginning with cell-bead contacts through to complete target internalization are shown as representative images (Fig. 6.1B (panels i-iv)). For example, phagocytic cup formation (Fig.6.1B; panel i, beads b1 and b2) occurs after initial contact of the target beads with the cell membrane. The cup progresses as extended pseudopod-like structures (Fig. 6.1B; panel ii, b3 and b4) around the outer edges of the beads, which then continues over the beads (Fig. 6.1B; panel iii, b5 and b6) until the targets are internalized (Fig.6.1B; panel iv). Overall, this high-resolution imaging details the standard steps that occur during a prototypical (i.e. ITAM-dependent) phagocytic process and serves as the basis for comparison with the unique IpLITR 1.1b phenotype described below.

I also performed SEM analysis of the IpLITR 1.1b-mediated phagocytic process (Fig. 6.1C to 6.1E). Similar to observations for IpLITR 2.6b/IpFcRγ-L, when incubated with isotype control IgG3 beads, no internalized or surface-bound beads were observed (Fig. 6.1C; top left panel). However, when IpLITR 1.1b-expressing cells were incubated with αHA-opsonized beads (1 hr at 37°C), SEM revealed that most of the targets appeared to be firmly secured to the cell

surface but often they were not completely engulfed (Fig.6.1C; top right panel). Pre-treatment of the cells with the F-actin inhibitor Latrunculin B significantly altered their morphology and also caused the beads to remain loosely tethered to the cell surface by disorganized plasma membrane structures (Fig. 6.1C; bottom left panel). When the IpLITR 1.1b-expressing cells were incubated with targets at 27ºC for 1hr, the beads remained secured at the cell surface (Fig. 6.1C; bottom right panel), but the cells displayed a more rounded appearance compared to when they were incubated at 37ºC. SEM imaging was also performed at 37ºC for shorter time periods (i.e. 4, 8, 16, and 32 min) and shown in representative images (Fig. 6.1D to Fig. 6.1E) are the temporal stages of IpLITR 1.1b-mediated target interactions starting from initial cell-bead contacts (Fig. 6.1D; panels i-iv, Fig 6.1E; panels v-viii) through target capture and their eventual tethering to the cell membrane and occasional engulfment (Fig. 6.1D; panels v-viii). Specifically, during the early stages of target interactions most IpLITR 1.1b-expressing cells produced thin elongated membrane protrusions with beads tethered at their ends (Fig. 6.1D; panels i-iv; beads (b1-b5)). Some cells also generated thicker cellular extensions (Fig. 6.1E; panels v and vi), which also participated in bead capture (b6-b9). I also consistently observed what appeared to be membrane ruffling (Fig. 6.1E; vii), which contributed to the tethering of target beads to the plasma membrane (b10, b11). At later stages, stalled phagocytic cup-like structures (Fig. 6.1E; panel viii) could be seen interacting with multiple beads (b12, b13) on the cell surface, and occasionally targets that were almost completely surrounded by the plasma membrane (b14).

6.2.2 LCI of membrane dynamics in IpLITR-expressing stables

Although SEM provided high-resolution static images showing distinct phenotypic differences between IpLITR 2.6b/IpFcRγ-L and IpLITR 1.1b-mediated responses, I next wanted to observe these membrane dynamic events in real time. To do this I co-transfected IpLITR-

expressing RBL-2H3 stables with LifeAct-GFP (marker for F-actin). As shown in Figure 6.2A, the levels of IpLITR 2.6b/IpFcRγ-L expression were not affected after stable transfection with the LifeAct-GFP probe (Fig. 6.2A; top panel; dashed vs. dotted line). The bottom panel of Figure 6.2A shows increased GFP signal (FL1-intensity) in the co-transfected IpLITR 2.6b/IpFcRγ-L-expressing cells confirming the expressing of LifeAct (Fig. 6.2A; bottom graph; dashed vs. dotted line). IpLITR 1.1b-expressing cells were also co-transfected with LifeAct-GFP and as shown in Figure 6.2B, this did not affect their surface expression of (top panel; dashed line) but did cause an increase in their FL1-intensity indicating LifeAct-GFP was expressed (Fig. 6.2B; bottom panel; dashed vs dotted line). With the creation of IpLITR/LifeAct-GFP co-transfected RBL-2H3 cells, I first observed them using LCI without extracellular beads to establish the imaging protocols. I also tested the hypothesis that IpLITR 1.1b-expressing cells would uniquely generate filopodia whereas IpLITR 2.6b/IpFcRγ-L-expressing cells would not. This was visualized by examining the F-actin-mediated plasma membrane dynamics in the GFP channel by confocal microscopy. As shown in Figure 6.2C, time-stamped images demonstrate IpLITR 1.1b-expressing cells clearly have increased membrane dynamics associated with the formation of F-actin rich (green) filopodia-like structures when compared to IpLITR 2.6b/IpFcRγ-L-expressing cells at 37ºC (Fig. 6.2A; left panels vs right panels). When LCI was performed at 27ºC, a stark difference in the plasma membrane behaviors of the cells was also clearly evident revealing that IpLITR 2.6b/IpFcRγ-L-expressing cells were ovoid in shape and had little to no membrane dynamics (Fig. 6.2D; left panels). In comparison, IpLITR 1.1b-expressing cells at the lower temperature appeared amorphous with clearly visible F-actin rich plasma membrane structures extending from their plasma membranes (Fig. 6.2D; left panels). This was the first live

cell evidence showing clear phenotypic difference in the plasma membrane behaviors of IpLITR-expressing cells.

6.2.3 Examination of IpLITR 2.6b/IpFcRγ-L-mediated phagocytosis at 37°C and 27°C

SEM provided high-resolution static images of the IpLITR 2.6b/IpFcRγ-L-mediated phagocytic process. However, to observe the dynamic membrane remodelling events that occur during cell-target interactions I imaged live cells. To achieve this, I used IpLITR 2.6b/IpFcRγ-L-expressing RBL-2H3 cells stably expressing the fluorescent probe LifeAct-GFP. This allowed me to visualize and track distinct F-actin polymerization events (green) and associated membrane dynamics that occur starting from initial target contacts through to the engulfment of individual microspheres.

My LCI clearly shows that IpLITR 2.6b/IpFcRγ-L mediates the internalization of αHA-opsonized target beads through a series of distinctive phases of F-actin dependent plasma membrane remodelling events. These F-actin polymerization dynamics are shown in a series of time-stamped static images extracted from the LCI video. Specifically, in Figure 6.3A and 6.3B both brightfield images merged with LifeAct-GFP (top panels) as well as the LifeAct-GFP signal alone (bottom panels) are displayed with the non-fluorescent target microspheres clearly visible in the brightfield panels, which are indicated with an asterisk. During the initial stages of IpLITR 2.6b/IpFcRγ-L-mediated phagocytosis, actin polymerization (green) is clearly visible at the cell surface-target interface in what appears as a phagocytic cup-like structure (Fig. 6.3A; asterisk, 0-40 sec). As the phagocytic process proceeds, polymerization of F-actin is visible along the leading edges of extended pseudopods (Fig. 6.3A; 40-70sec). The accumulated F-actin behind the bead then depolymerizes as the pseudopods seal together and the microsphere sinks into the cell (Fig. 6.3A; 120-140sec). Another representative LCI time-lapse video showing IpLITR

2.6b/IpFcRγ-L-mediated phagocytic behaviour is show in Figure 6.3B. Shown here are the binding of the bead (Fig. 6.3B; 0-40 sec), the extension of pseudopods around the bead, and the subsequent closure of the phagosome (Fig. 6.3B; 40-180 sec) followed by a secondary burst of actin, which indicates the engulfment of the bead as F-actin polymerization proceeds up and around the target (Fig. 6.3B; 180-250 sec).

I next compared the phagocytic activities of IpLITR 2.6b/IpFcRγ-L-expressing cells incubated at 37ºC vs. 27ºC. For these experiments, αHA-opsonized 4.5μm blue beads (BB) were used as targets instead to allow for simultaneous visualization of both the target beads (blue) and F-actin dynamics (green). As shown in the time-stamped still images (Fig. 6.3C; asterisk), a microsphere target (blue) contacts the cell membrane (between 70-120 sec) and is then progressively engulfed through a series of F-actin-mediated plasma membrane dynamic events similar to the temporal events described above. From initial contact to internalization, the entire process is completed in ~400 sec at 37ºC (Fig. 6.3C). Although multiple beads are present in these images, for clarity I selected the target bead that could be resolved from its initial contact with the cell through to engulfment. In comparison, when IpLITR 2.6b/IpFcRγ-L-expressing RBL-2H3 cells were incubated with αHA-opsonized 4.5μm BB at 27ºC, no apparent target contacts or F-actin-mediated membrane dynamic events were observed (Fig. 6.3D). In this example IpLITR 2.6b/IpFcRγ-L-expressing cells were examined over the span of 560 sec starting from the time when the targets were first introduced to the cells, and although numerous extracellular beads were observed in the field of view, none of these targets established contacts with the cell membrane.

6.2.4 Examination of IpLITR 1.1b-mediated target interactions at 37ºC

Using IpLITR 1.1b-expressing cells co-transfected with LifeAct-GFP, a variety of unique F-actin polymerization-dependent membrane remodelling events could be observed. Specifically, LCI imaging shows that IpLITR 1.1b-expressing cells generated F-actin rich filopodia-like structures that extend out from the cell surface, attached to beads, and then rapidly withdrew back towards the cell membrane. For example, as shown Figure 6.4A (target marked with an asterisk), an IpLITR 1.1b-expressing cell can be seen producing a thick actin-rich extension (green) that reaches out and attaches to the target bead (Fig. 6.4A; 410-480 sec panels). After ~10 sec of contact with the target, the bead is then rapidly retracted back towards the cell surface, which correlates with the disappearance of the F-actin-rich extension as shown in the time-stamped panels at 480-490 sec (Fig. 6.4A). Following ~100 sec of sustained contact between the target bead and the plasma membrane, a second F-actin rich pseudopod-like extension (Fig. 6.4A; 600 sec) can be seen crawling up and then over the outer edge of bead until it returns towards the cell surface; momentarily wrapping the target in the plasma membrane (Fig. 6.4A; 600-610 sec). Subsequently, the filopodia then retracts away from the bead before rapidly disappearing with the bead now tethered at the cell surface (Fig. 6.4A; 660-690 sec). An alternative mode of filopodia-mediated capture of targets displayed by IpLITR 1.1b-expressing RBL-2H3 cells is shown in the time-stamped images presented in Figure 6.4B. Here, the formation of a thin F-actin containing membrane protrusion (green) rapidly extends out from the cell surface and makes contact with a bead (Figure 6.4B; 60-110 sec). After initial contact with the target (indicated with an asterisk), the membrane protrusion rapidly retracts back towards the cell surface (Figure 6.4B; 110-140 sec), thus pulling the bead towards the cell and tethering it to the membrane. This is then followed by the transient generation of actin-dense pseudopod-like

structures that appear to surround the bead (Figure 6.4B; 150-170 sec). Another representative cell-target interaction phenotype that I uniquely observed for IpLITR 1.1b-expressing cells using LCI was the generation of an F-actin rich extended membranous stalk that formed after initial contact with the bead (Fig. 6.4C; target bead indicated with an asterisk; at 40 sec). Following target contact, this extended stalk exhibited probing behaviour for ~700 sec during which time there were variable levels of F-actin polymerization observed along the edges and around the surface of the bead (Fig. 6.4C; 40-740 sec). The plasma membrane stalk also appeared to both elongate and thicken over the course of its contact with the bead and, unlike what I described earlier, the target remained at a distance from the cell body as it was not rapidly retracted back towards the membrane surface during the duration of the video. Of note, this IpLITR 1.1b-expressing cell also contained one internalized bead as well as one tethered bead in addition to the target bead documented here.

While IpLITR 1.1b-expressing cells commonly generated and used extended membranous F-actin containing structures to capture and tether extracellular targets, other dynamic interaction behaviours were also observed, and representatives of these behaviours are shown in Figures 6.4D to 6.4F. For example, IpLITR 1.1b-expressing cells were capable of generating complex membranous ruffles (Fig. 6.4D). Here two extracellular beads are captured by actin-dense membrane ruffles generated at the cell surface (Fig. 6.4D; asterisk and ⊙; 130-270 sec). After being captured, the formation of a second F-actin rich membrane ruffle is observed, which encapsulates one of the beads (Fig. 6.4D; ⊙; 290-320 sec) along the outer edge of the cell before depolymerizing as the bead is tethered to the cell surface (Fig. 6.4E; 340 sec). I also observed situations where a thin F-actin-dense protrusion captures a target bead at its outer most end (Fig. 6.4E). As the time-lapse progresses, polymerized actin accumulates around the

bead as it is contracted down onto the cell surface (Fig. 6.4E; 0-60 sec). After this initial tethering, actin-dense membrane structures begin to surround the bead (Fig. 6.4E; 110 sec) initially from the left side and then from the right side of the target (Fig. 6.4E; 170-200 sec). Over the next 300 sec, the F-actin depolymerizes leading to the apparent internalization of the bead (Fig. 6.4E; 310-500 sec). Lastly, as shown in Figure 6.4F, multiple cell-bead interactions could be seen for an individual IpLITR 1.1b-expressing cell (Fig. 6.4F; asterisk, ⊙ and ⭘). As the cell moves within the field of view from the top left, one bead had already begun to be internalized (Fig. 6.4F; asterisk; 160 sec) and another bead was actively tethered to the cell surface (Fig. 6.4F; 200-260 sec). The generation of an F-actin-rich membrane protrusion then actively extended towards and contacted a third bead (Fig. 6.4F; red x; 290-320 sec). After this initial contact, a phagocytic-cup like structure rapidly formed around the edges of the bead (Fig. 6.4F; ⊙; 370sec), which was subsequently retracted back towards the cell surface (Fig. 6.4F; 470 sec). Overall, these results provide a representative summary of the diverse F-actin mediated plasma membrane remodelling events uniquely observed for IpLITR 1.1b- but not IpLITR 2.6b/IpFcRγ-L-expressing cells. Notably, most IpLITR 1.1b-mediated target interactions involved the formation of dynamic membranous extensions.

6.2.5 Examination of IpLITR 1.1b-mediated target interactions at 27ºC

After documenting several unique phagocytic phenotypes for IpLITR 1.1b-expressing RBL-2H3 cells, experiments were then performed to compare IpLITR 1.1b-mediated target interactions at 37ºC vs. 27ºC. The rationale for these experiments was based on my previous results showing the ability of IpLITR 1.1b-expressing cells to facilitate target interactions at lower incubation temperatures (chapter IV). Here, again, αHA-opsonized 4.5μm BB were used to allow for simultaneous visualization of target beads (blue) and F-actin dynamics (green). As

shown in the still images extracted from LCI videos (Fig. 6.5A; asterisk), at 37ºC an extracellular bead is located at a distance from the cell membrane until a series of F-actin rich membrane structures (green) extend towards (Fig. 6.5A; 350-360 sec) and then contacts the target (Fig. 6.5A; 370-380 sec). The bead is then rapidly pulled towards the cell membrane during which time distinct actin polymerization events appear to mediate extension of pseudopods around the entire bead (Fig. 6.5A; 390-400 sec). The actin-rich pseudopod immediately retracts away from the bead as evidenced by the gradual depolymerization of F-actin from around the outer surface of the bead (Fig. 6.5A; 410-440 sec). Over the remainder of the time series, the captured bead remains tethered on the cell surface but is not engulfed (Fig. 6.5A; 450-510 sec). There are two other targets in the frame that are similarly captured by this IpLITR 1.1b-expressing RBL-2H3 cell at 37ºC, which are shown in Figures 6.5B and 6.5C. In another representative cell-target interaction phenotype, I observed an IpLITR 1.1b-expressing cells that continuously probed and then repeatedly attempted to pull a pre-tethered microsphere away from another cell in the frame. As shown in Figure 6.5D, a target bead has already been captured, and is visible at the top left of the image. As the time series progresses, a second cell visible in the center of the image projects an F-actin containing membrane ruffle towards this target (Fig. 6.5D; asterisk; 130-180 sec), which is already tethered to the other cell (Fig. 6.5D; red arrow; 130 sec). After the ruffle makes initial contact with this bead, it appears to then withdraw back towards the cell leaving an extended membrane structure attached to the target with a detectable F-actin rich area at the point of contact with the bead (Fig. 6.5D; 190-260 sec). Subsequently, following the cells initial failed attempt to pull the bead back towards the cell, a secondary F-actin rich membrane ruffle projects out towards the secured target (Fig. 6.5D; 270-300 sec). As this ruffle subsides and the F-actin depolymerizes, the cell has again failed to retract the target towards its surface, although

contact with this bead remains (Fig. 6.5D; 310-490 sec). When viewed in its entirety, three separate F-actin rich membrane ruffles are actively projected toward the target in what may be repeated attempts to capture the tethered target. Ultimately, these events leave the bead remaining attached to two separate cells. Of note, this cell also appears to have engulfed two other targets (Fig. 6.5D; 430 sec).

Unlike the inhibition of phagocytic responses observed for IpLITR 2.6b/IpFcRγ-L at lower incubation temperatures, IpLITR 1.1b-expressing cells continued to display active target capture phenotypes at 27ºC. However, at this lower incubation temperature the overall activity of the F-actin mediated membrane dynamics was markedly slower. For example, as shown in Figure. 6.6A an extracellular target (asterisk) is initially contacted by the cell between 420-430 sec, which promotes the extension of plasma membrane around the left side of the target (430-470 sec). This contact leads to the formation of a thin F-actin rich structure that extends beyond the surface of the attached bead and into the extracellular space (480-500 sec). At this stage, the membrane protrusion appears to momentarily probe the environment before collapsing back towards the cell, which coincides with the disappearance of the F-actin signal (520-550 sec). At the conclusion of this time series, the bead remains tethered at the cell surface, but it is not engulfed (590 sec). Another example shows an IpLITR 1.1b-expressing cells that first uses an F-actin containing membrane ruffle to attach to a bead at 27ºC, which is then followed by the formation of a thin F-actin containing membrane structure that partially surrounds the tethered target (Fig. 6.6B). At 650 sec, the bead remains attached to the cell surface and is partially surrounded by an F-actin rich membranous structure. Further representative examples of the unique F-actin-mediated capture of extracellular targets using filopodia-like structures are shown for IpLITR 1.1b-expressing cells in Figure 6.6C to 6.6E. Overall, these examples all demonstrate

that unlike what I observed for IpLITR 2.6b/IpFcRγ-L, IpLITR 1.1b uniquely promotes the formation of dynamic membrane structures at 27ºC, which function to bind and capture extracellular targets.

6.3 DISCUSSION

Using high resolution SEM and real-time LCI, the results of this chapter provide new evidence regarding IpLITR-mediated production of dynamic cytoskeletal and membrane remodelling events. I show for the first time using live cells that IpLITR 1.1b-expressing RBL-2H3 cells uniquely generate filopodia-like extensions composed of long filaments of polymerized F-actin and reveal that these plasma membrane structures are actively used for extracellular target binding and capture. Considering that very little is known regarding the ability of immunoregulatory receptor-types to induce filipodia formation in other vertebrates, including mammals, these functional studies set the stage for future studies targeted at understanding how the dynamic control of intracellular transduction events controlled by IpLITR 1.1b selectively contribute to diverse innate cell effector responses across vertebrates. It is likely that IpLITR-mediated responses in mammalian cells feature similar signaling components that would be present in representative fish immune cell-types [227]. Further exploration of these mechanisms will assist in uncovering the functional versatility for ITIM- and ITAM-encoding receptors that can eventually be used to explore teleost immunoregulatory receptor networks in homologous systems.

Filopodia are dynamic membrane structures that can vary in length and thickness but rely on the cytoskeletal machinery and actin-binding proteins for their formation [235,237,238,242]. Filopodia also play many important physiological roles in health and disease and have been shown to participate in a range of cellular processes including cell migration, morphogenesis,

neurite outgrowth, metastasis, and wound healing [235,238,242–245]. For example, SEM analysis has shown that prior to the initiation of phagocytosis, bacteria are tethered to phagocyte surfaces by long and thin membranous protrusions [87,88,236–239]. Importantly, these plasma membrane extensions provide phagocytes with the ability to dynamically explore their extracellular environments as the rapid elongation and subsequent retraction of filopodia assists in the active capture of microbes by increasing the functional radius available for pathogen contact beyond the circumference of the cell [2,82,87,236–239]. While this shows that immune cells can actively deploy filopodia to capture targets, very little is known regarding the specific receptor-types and associated intracellular dynamics that participate in the formation and regulation of these membrane structures. Previously, I demonstrated that IpLITR 1.1b-expressing RBL-2H3 cells displayed a unique target acquisition and engulfment phenotype associated with the formation of extended membranous protrusions [193]. The results of this chapter further support a role for this specific immunoregulatory receptor-type in the control of cytoskeletal dynamics and filopodia formations during the initial contact with and then capture of extracellular targets over a range of temperatures. Taken together, these findings show, for the first time, that active capture and tethering of extracellular targets to the cell surface might represent a conserved function for certain members of the IpLITR family via their unique ability to transmit signals that affect F-actin polymerization and associated plasma membrane dynamics. Comparatively, for IpLITR 2.6b/IpFcRγ-L-expressing cells, filopodia-like structures were not specifically used to capture targets, as in these cells sustained contact time between the plasma membrane and microspheres was required to trigger the IpLITR 2.6b/IpFcRγ-L-mediated phagocytic process. In addition, phagocytic activity and membrane dynamics were both completely abolished at 27ºC in IpLITR 2.6b/IpFcRγ-L-expressing cells; likely due to an

inability of IpLITR 2.6b/IpFcRγ-L to promote or facilitate F-actin polymerization events at temperatures below 37ºC in RBL-2H3 cells.

Filopodia are regulated by mechanisms instigated in part by constitutive intracellular signaling events that involve several conserved transductions [86,242,246–251]. Overall, constitutively generated filopodia allow phagocytes to constantly probe their extracellular environments as these membranous probes also contain phagocytic receptors located along their edges, a process that depends on an unknown mechanism for the loading of phagocytic receptors into the protrusions [2,87,252]. Any stochastic phagocytic receptor-target interactions that may occur would facilitate the attachment of specific targets to the extended membranes. Extracellular targets would then be pulled back towards the cell surface during filopodial retractions due to the retrograde flow of actin back towards the cell body and the contractile forces generated by myosins [235]. Once in close contact with the plasma membrane, newly established target-receptor interactions could activate additional intracellular signaling pathways to reinforce tethering or subsequently trigger target engulfment [82,87].

While constitutively generated filopodia facilitates continuous sampling of the environment by phagocytes, it has been shown that these structures are also produced in responses to specific stimuli. For example, LPS-induced activation of TLR4 increases the production of filopodia-like structures [240,241]. Receptor-induced filopodia formation has also been characterized in cancer cells, which use these inducible pathways to produce invasive membrane protrusions [244,245]. Termed invadopodia, these extensions are formed by the selective stimulations of tumour cell-expressed platelet-derived growth factor (PDGF) and epidermal growth factor (EGF) [244]. Upon growth factor stimulation, the local recruitment and activation of kinases such as focal adhesion kinase (FAK) and Src occurs early in the process of

invadopodia formation that initiate phosphorylation of downstream signaling proteins [244,245]. Unlike the receptor-specific production of filopodia or invadopodia described above, IpLITR 1.1b-expressing cells were not stimulated by any known endogenous ligands. Therefore, it seems that the stable expression of IpLITR 1.1b alone was sufficient to support filopodia generation. These results suggest that IpLITR 1.1b can uniquely network with intracellular components requisite for the production of F-actin containing filopodia-like structures. Based on the results obtained in chapters IV and V, I hypothesize that IpLITR 1.1b-controlled signaling events induce formation of macromolecular complexes with its CYT that pre-assemble prior to receptor engagement; effectively priming the receptor for subsequent interactions with extracellular targets [11,193,227]. Pre-associations of IpLITR 1.1b with intracellular effectors capable of modulating the cytoskeletal machinery would allow for dynamic membrane remodelling events prior to the formation of stable receptor-ligand interactions [29,30,31].

The unique target acquisition and engulfment pathways facilitated by IpLITR 1.1b likely requires the differential participation of the proximal and distal regions of its CYT in the recruitment and activation of select intracellular effectors [12,192]. Specifically, for IpLITR 1.1b to constitutively trigger filopodia formation in RBL-2H3 cells without ligand engagements, this receptor may exist in a primed state, facilitating its basal coupling to effectors of actin dynamics. In this model (Fig. 6.7), Nck serves as a cytosolic adaptor that could couple surface expressed IpLITR 1.1b with the intracellular effector WAVE2. Interestingly, this Nck-dependent mechanism closely aligns with the short-circuited phagocytic pathway recently described for human CEACAM 3 [3]. In addition, I have shown in chapter IV that IpLITR 1.1b-mediated activity is partially dependent upon the catalytic activity of Src and Syk [193]. Although yet to be confirmed, sustained activation of these kinases in the absence of agonist stimulation would

likely require pre-aggregation of IpLITR 1.1b on the cell surface. This would maintain basal Src-dependent tyrosine phosphorylation of the IpLITR 1.1b CYT region facilitating constitutive coupling of IpLITR 1.1b to select components of the cytoskeletal machinery. In mammalian cells, activation of WAVE2 requires state-specific phosphorylation as well as interactions with GTP-bound Rho superfamily proteins, most commonly Rac [253]. As a result, the assembly of the Nck-WAVE2 complex within the proximal CYT region of IpLITR 1.1b would most likely be coupled to the recruitment of cytoplasmic guanine nucleotide exchange factors, including Vav. Recent biochemical studies showed that Syk might be preferentially recruited to the distal region of the IpLITR 1.1b CYT [192]. Therefore, I suspect that recruitment and activation of Vav by Syk would provide the necessary catalyst for Rac 1/2 activation and the stimulation of actin-driven membrane protrusions via the Nck-recruited WAVE2. Overall, this predicted model encompasses the minimal machinery required for a constitutive IpLITR 1.1b-dependent deployment of filopodia in the absence of agonist stimulation and is supported by our recent biochemical studies (new Fig. 6.7) [187,192,193]. Lastly, if IpLITR 1.1b is indeed basally phosphorylated and pre-associated with intracellular components linking it to F-actin dynamics, then this would in part explain why IpLITR 1.1b continues to capture targets at suboptimal incubation temperatures due to pre-assembly of these components with the receptor. The reduced plasma membrane dynamics for IpLITR 1.1b-expressing RBL-2H3 cells at 27ºC are likely due to specific affects on phospholipid dynamics and membrane mobility at this lower temperature [254–256], but likely not from an inability of IpLITR 1.1b to associate with signalling complexes, which would have previously occurred prior to the cooling of the cells.

Following filopodia-mediated capture of extracellular targets, I frequently observed the generation of secondary waves of F-actin polymerization after the target was secured at the cell

surface. These events may be triggered by aggregations of IpLITR 1.1b at the newly established contact sites formed between the plasma membrane and the captured target. In some cases, the immobilized targets remained firmly tethered on the cell surface and occasionally the beads were completely internalized. This phenotype is reminiscent of efferocytosis, a process responsible for phagocyte-mediated clearance of apoptotic bodies through the recognition of phosphatidylserine (PtdSer) on dying cells [253]. However, unlike linear filopodia that extend perpendicular to the cell surface, efferocytosis typically involves membrane dynamics that form extended but laterally moving arcs or wave-like structures that flow along the cell surface [139,253,257]. Functionally, these structures reach out into the extracellular space to make contact with apoptotic cells and their sweeping motion augments trapping of distant targets. This brings dying cells into close proximity to the plasma membrane, where they are tethered and eventually cleared by secondary activated phagocytic processes [253,257]. Rac 1/2, Cdc42, and WAVE2 have all been identified as key players during the control of efferocytosis [126,139,253,257,258], which occurs in two discrete receptor-specific steps known as the tethering and tickling [216,253,258,259] that participate in the step-wise capture and engulfment of apoptotic bodies. For example, engagement of receptors that bind apoptotic cells, including CD36, CD14, CD68, αvβ3, and αvβ5, promotes the tethering of specific targets on macrophages [259]. Uptake of targets then occurs when tethering receptors are co-engaged with the phagocytic PSR [259]. Interestingly, incubation of the cells with PtdSer-coated erythrocytes was insufficient for both tethering and phagocytic uptake by the PSR; indicating that both tethering and phagocytic signals are required for effective apoptotic cell removal [259]. In agreement with this dual mode for target capture and engulfment, my observations support a model that involves constitutive mechanisms for IpLITR 1.1b-mediated deployment of filopodia to tether targets to the cell

surface. Subsequently, captured targets can trigger additional IpLITR 1.1b-dependent pathways, which may be distinct from the constitutive mechanism that regulates resting filopodia production. The results of this chapter combined with previous chapters provide the necessary framework for deciphering how IpLITR 1.1b variably controls the actin polymerization machinery.

Taken together, my results show that the expression of IpLITR 1.1b, but not IpLITR 2.6b/IpFcRγ-L, specifically triggers RBL-2H3 cells to induce filopodia formation in the absence of any known stimuli. The receptor-specific nature of IpLITR 1.1b-indcued filopodia is clear when both IpLITR-expressing cell-types were incubated at depressed temperatures (e.g. 27ºC). This also appears to be the first study to suggest that expression of a specific immunoregulatory receptor can promote the constitutive formation of filopodia without the need for an exogenous ligand. IpLITR 1.1b-mediated signaling also initiates secondary waves of actin polymerization events that are associated with the internalization and membrane tethering of extracellular targets, which I propose to be a distinct event from those involved in the initial generation of filopodia. These responses are likely due to the unique structure and signaling potential associated with the IpLITR 1.1b CYT; thereby allowing for diversity in the integrated control of cytoskeletal and membrane remodelling associated with IpLITR 1.1b expression. Overall, these results offer novel information regarding the ability of immunoregulatory receptors to initiate filopodia formation and provide new insights into the temporal organization of cellular events surrounding the unique transduction dynamics that regulate F-actin polymerization and membrane remodelling events.

FIGURE 6.1

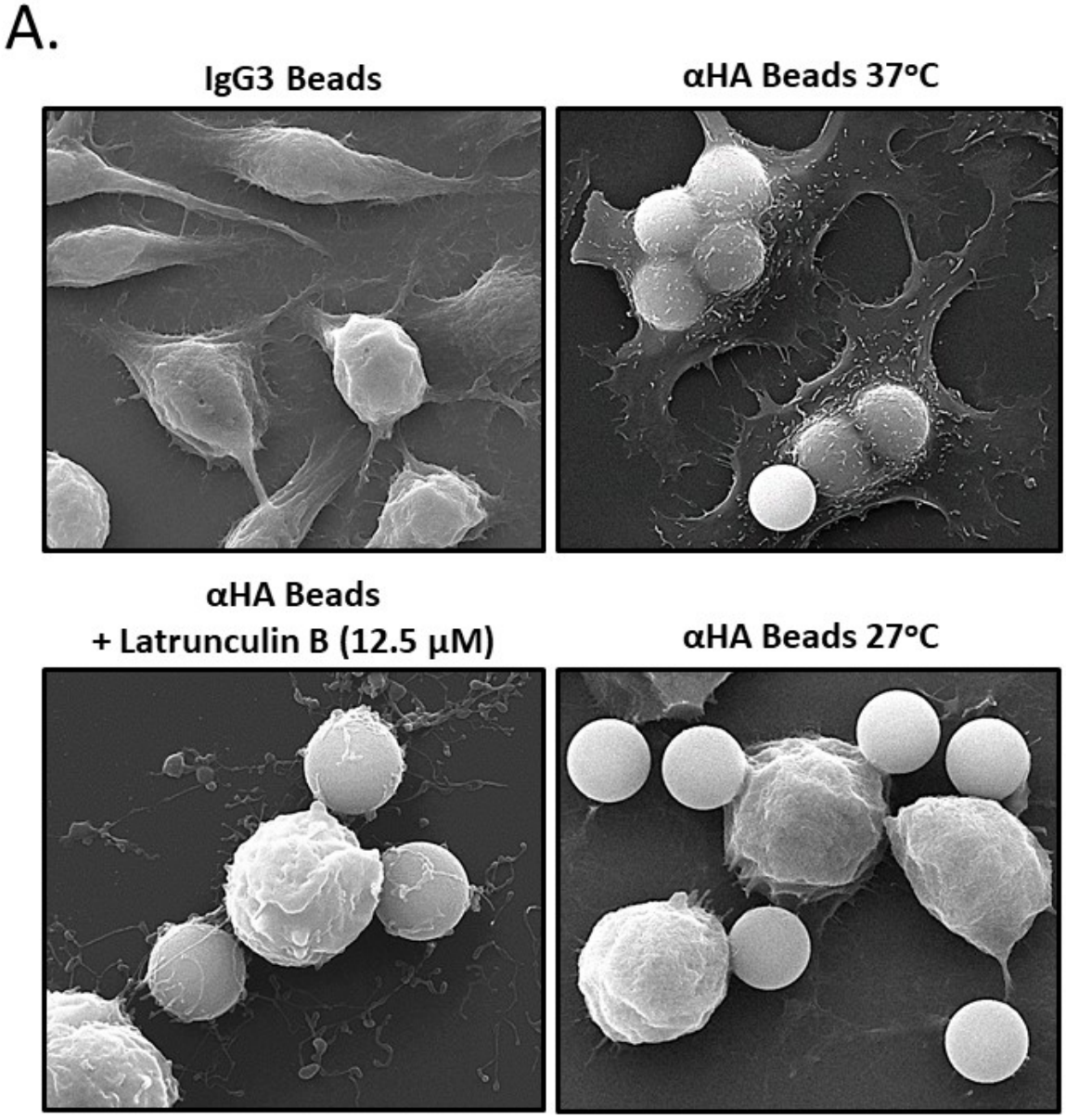
A.
IgG3 Beads
αHA Beads 37°C
αHA Beads
+ Latrunculin B (12.5 µM)
αHA Beads 27°C

FIGURE 6.1

B.

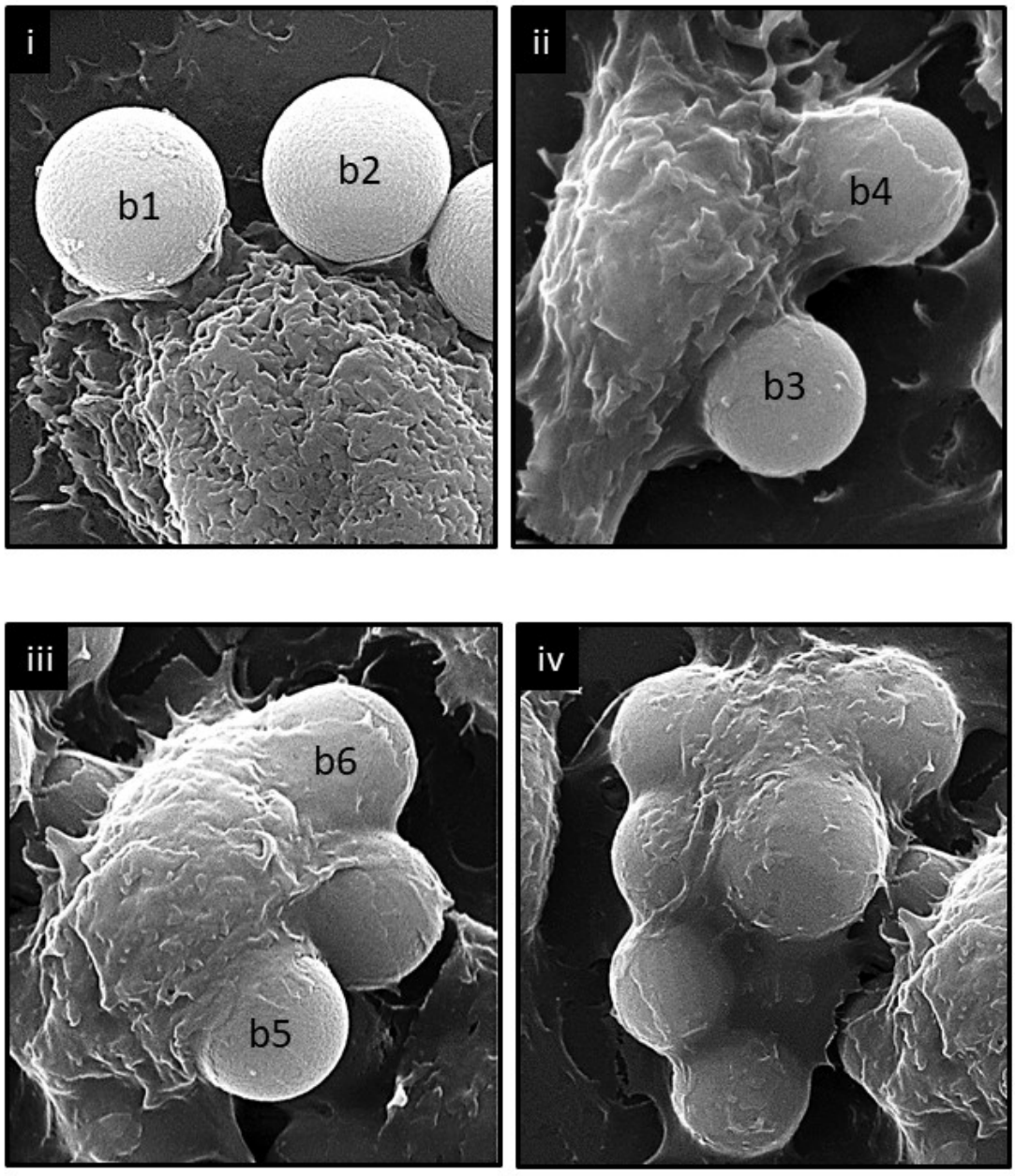

FIGURE 6.1

C.

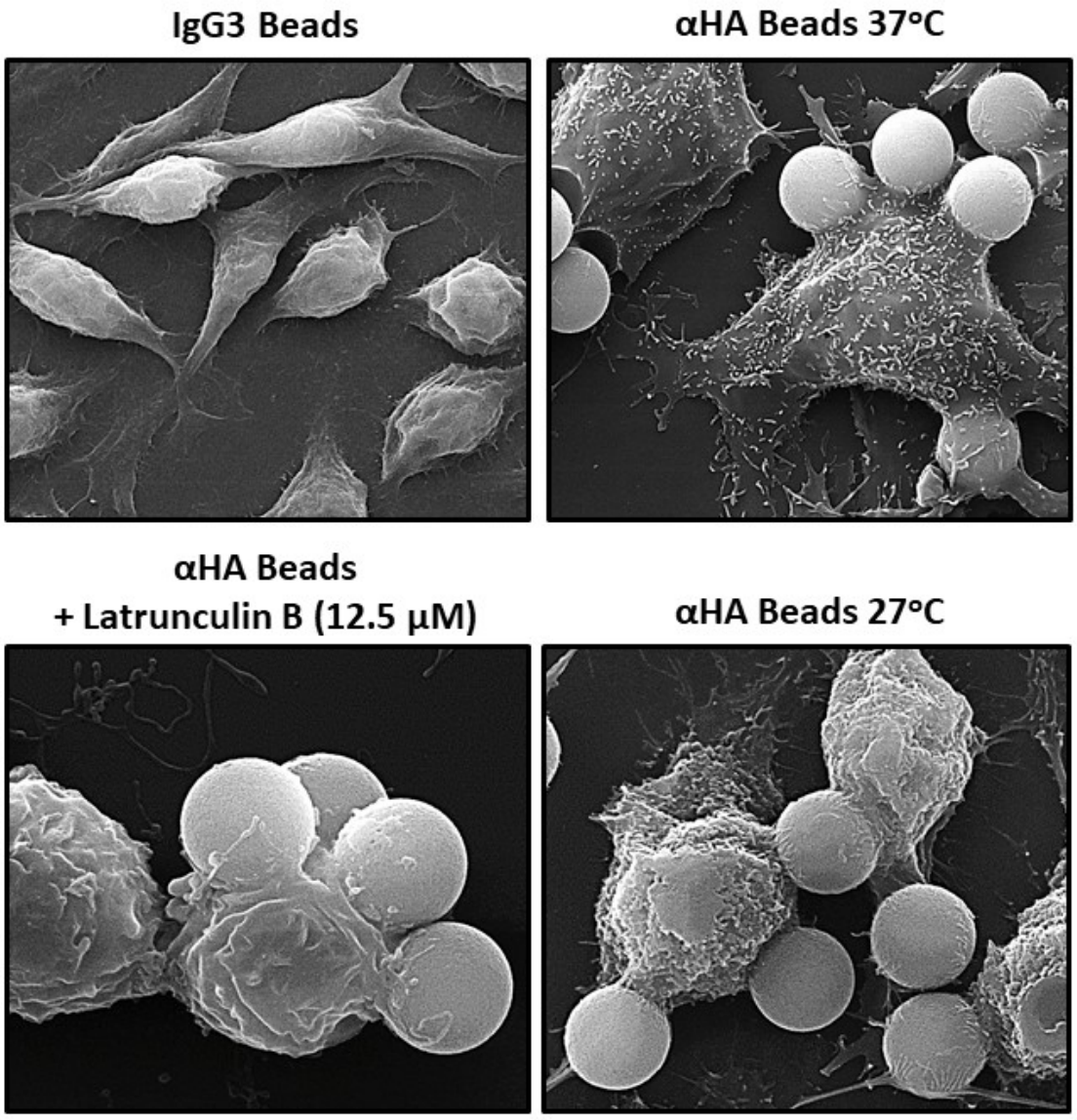
IgG3 Beads
αHA Beads 37°C
αHA Beads
+ Latrunculin B (12.5 µM)
αHA Beads 27°C

FIGURE 6.1

D.

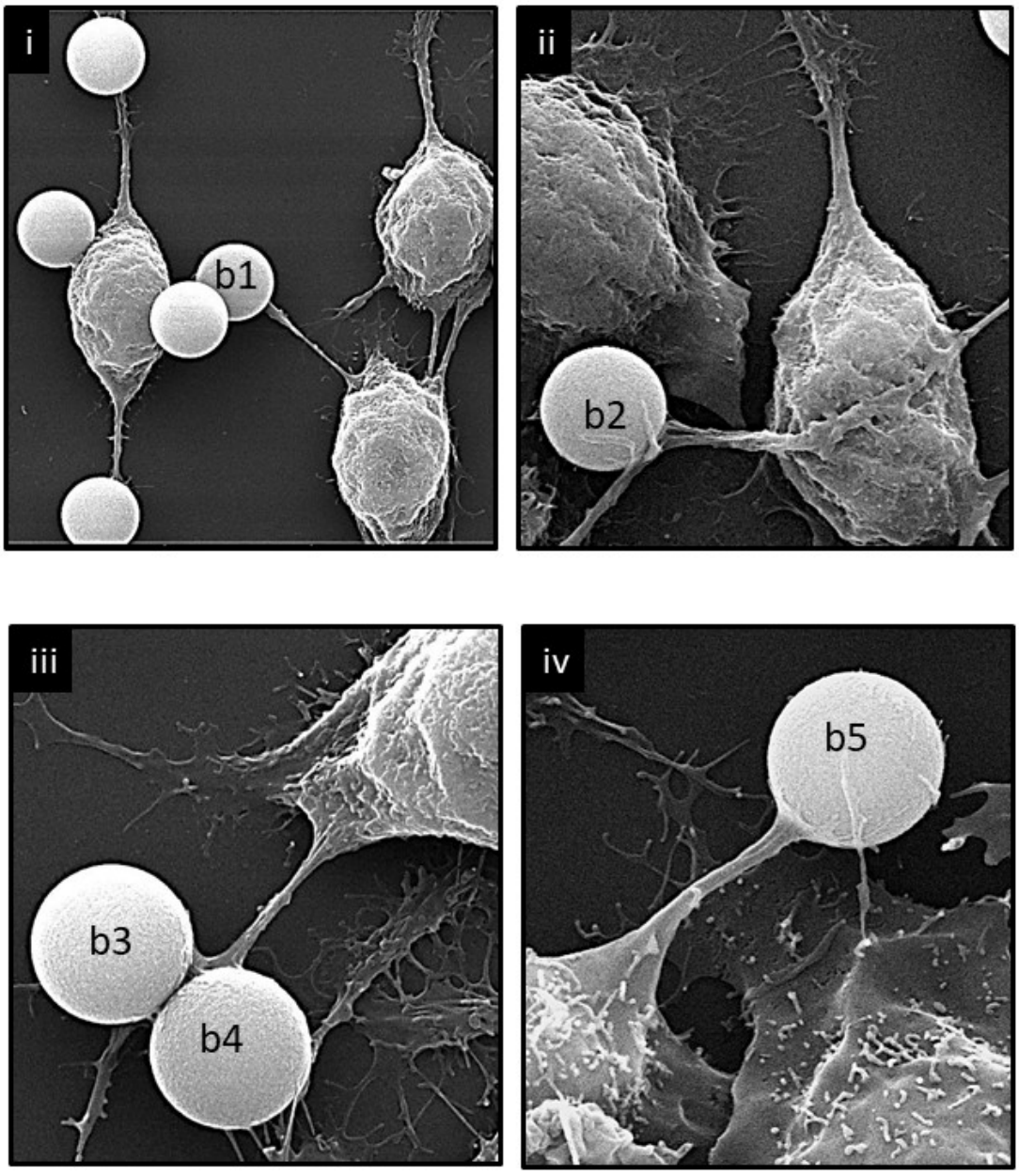

FIGURE 6.1

E.

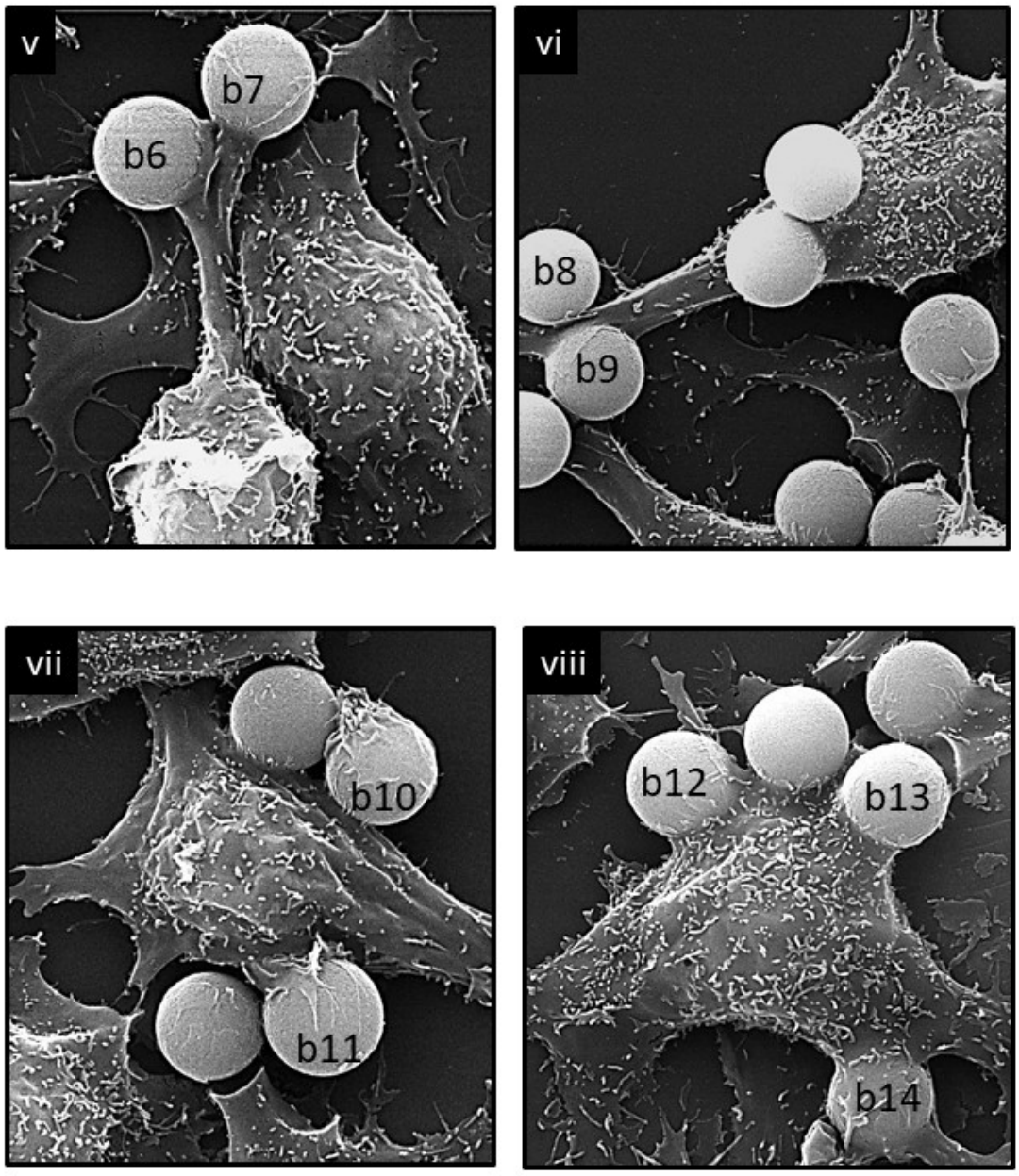

FIGURE 6.1 Examination of IpLITR-mediated phagocytosis using SEM. SEM of IpLITR 2.6b/IpFcRγ-L (A and B) or IpLITR 1.1b (C-E)-mediated phagocytosis. IpLITR 2.6b/IpFcRγ-L-expressing RBL-2H3 cells ($3x10^5$) were incubated at 37^oC for 1 h with $9x10^5$ IgG3-coated 4.5 μm microspheres or with $9x10^5$ αHA mAb-coated 4.5 μm microspheres prior to imaging using a Philips/FEI XL30 SEM microscope (FEI: Hillsboro, Oregon, USA). Cells ($3x10^5$) were also pre-treated for 1 h with 12.5 μM of the F-actin inhibitor Latrunculin B prior to their incubation with $9x10^5$ αHA mAb-coated 4.5 μm microspheres or incubated at 27^oC for 1 h with $9x10^5$ αHA mAb-coated 4.5 μm microspheres prior to imaging. IpLITR-expressing cells ($3x10^5$) were also incubated at 37^oC for various times (e.g. 4 min, 8, min, 16 min, and 32 min) with $9x10^5$ αHA mAb-coated 4.5 μm microspheres and representative SEM images of the progressive stages of IpLITR-mediated phagocytosis and specific beads are labeled (b) as described in the results section.

FIGURE 6.2

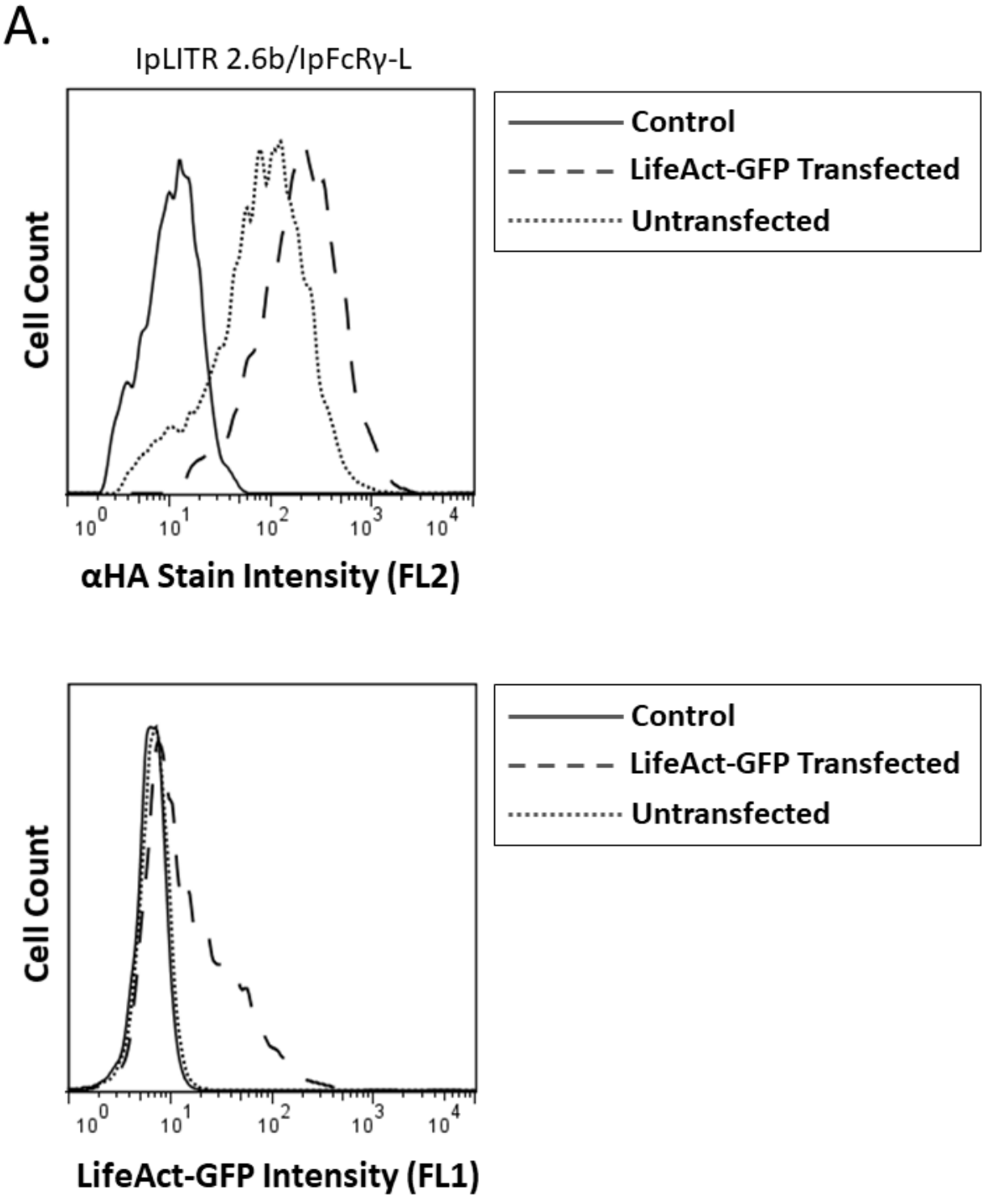
A.
IpLITR 2.6b/IpFcRγ-L
Cell Count
Control
LifeAct-GFP Transfected
Untransfected
10^0 10^1 10^2 10^3 10^4
αHA Stain Intensity (FL2)
Cell Count
Control
LifeAct-GFP Transfected
Untransfected
10^0 10^1 10^2 10^3 10^4
LifeAct-GFP Intensity (FL1)

FIGURE 6.2

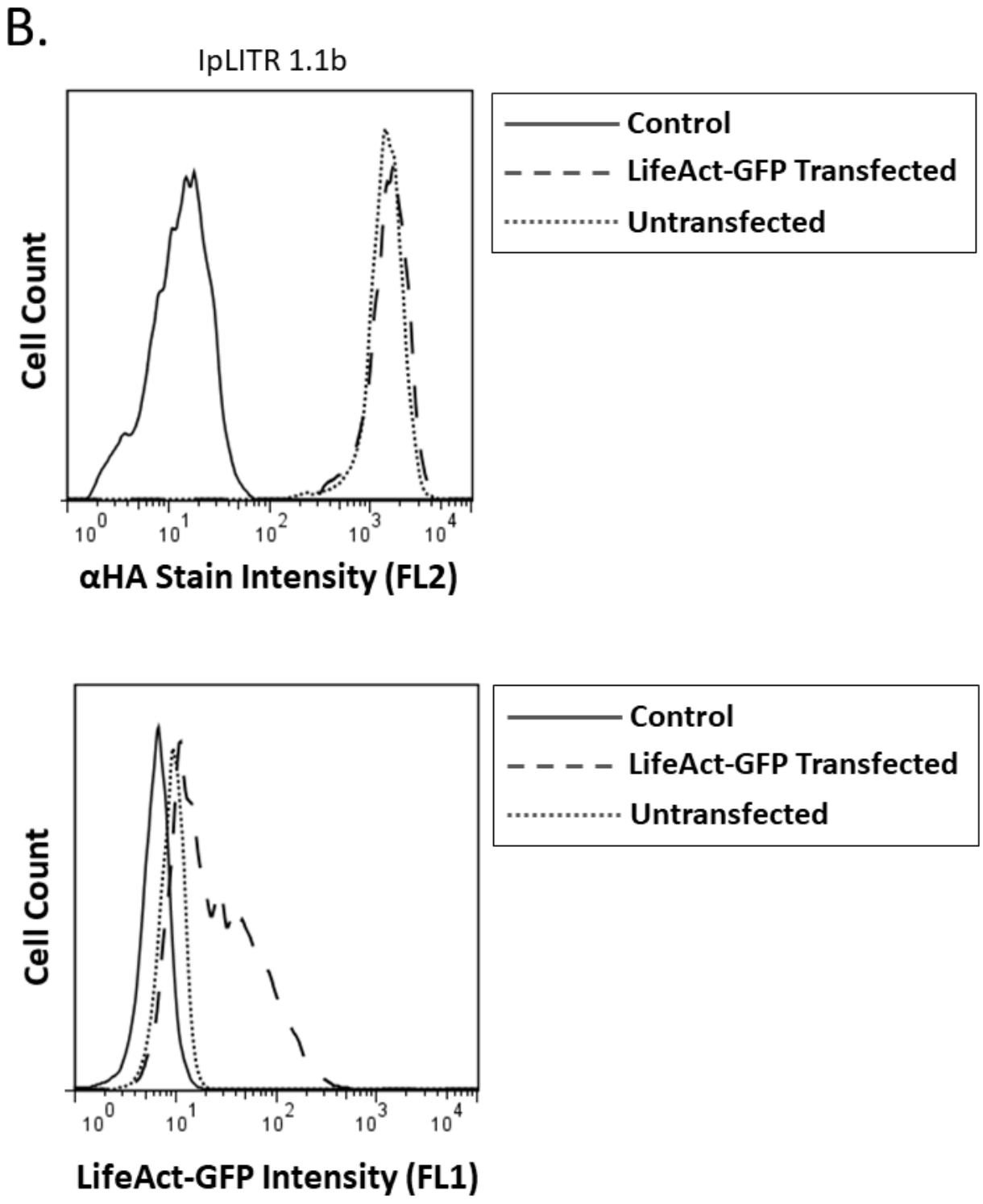
B.
IpLITR 1.1b
Cell Count
Control
LifeAct-GFP Transfected
Untransfected
10^0 10^1 10^2 10^3 10^4
αHA Stain Intensity (FL2)
Cell Count
Control
LifeAct-GFP Transfected
Untransfected
10^0 10^1 10^2 10^3 10^4
LifeAct-GFP Intensity (FL1)

FIGURE 6.2

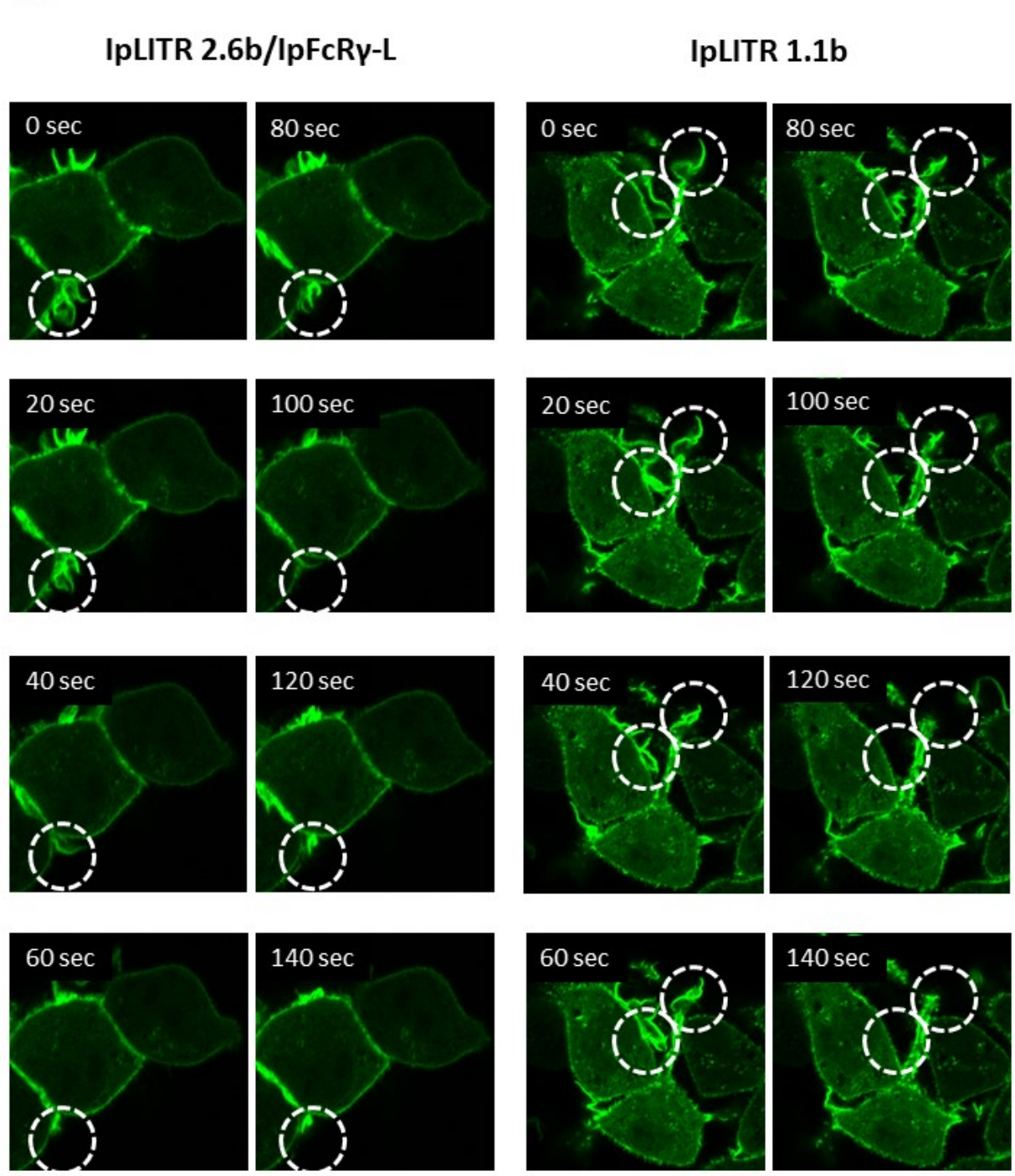
C.
IpLITR 2.6b/IpFcRγ-L
IpLITR 1.1b
0 sec
80 sec
0 sec
80 sec
20 sec
100 sec
20 sec
100 sec
40 sec
120 sec
40 sec
120 sec
60 sec
140 sec
60 sec
140 sec

FIGURE 6.2

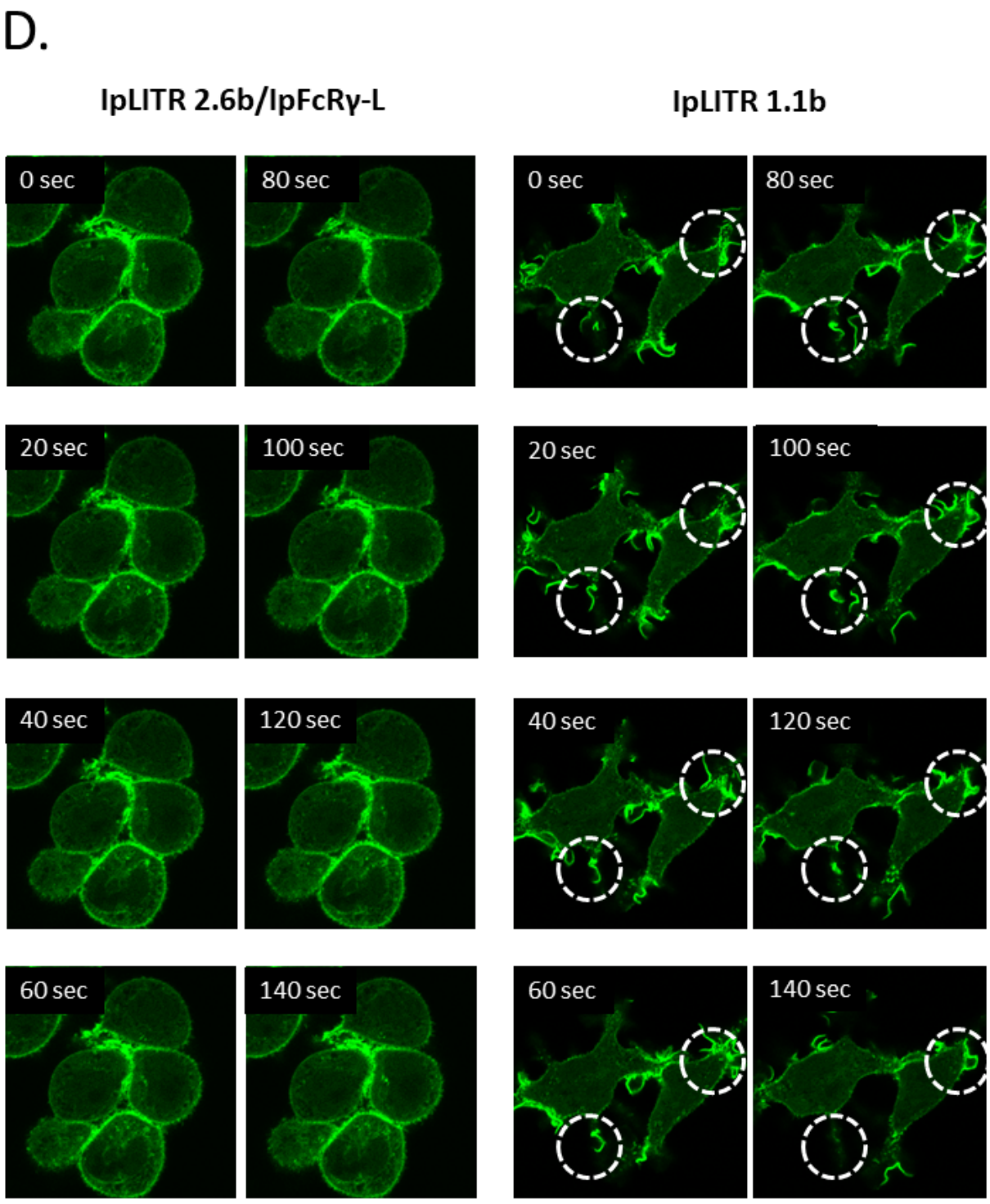
D.
IpLITR 2.6b/IpFcRγ-L
IpLITR 1.1b
0 sec
80 sec
0 sec
80 sec
20 sec
100 sec
20 sec
100 sec
40 sec
120 sec
40 sec
120 sec
60 sec
140 sec
60 sec
140 sec

FIGURE 6.2 LCI of membrane dynamics in IpLITR-expressing stables. Already stable expressing IpLITR RBL-2H3 cells were transfected with the F-actin probe LifeAct-GFP via the use of a nucleofection system designed specifically for the RBL-2H3 cell line as recommended by the company. Confluent cells expressing IpLITR 2.6b/IpFcRγ-L or IpLITR 1.1b were harvested and placed into a nucleofection cuvette, given 5 μg of LifeAct-GFP plasmid and transfected using the recommended nucleofection settings designed for RBL-2H3 cells specifically. These cells were then sorted via flowcytometry for their IpLITR/LifeAct-GFP expression and further cultured. Expression of IpLITR 2.6b/IpFcRγ-L (A; top histogram) and IpLITR 1.1b (B; top histogram) along with the levels of LifeAct-GFP expression (bottom histograms) was assessed via flowcytometry. The level of IpLITR-expression in cells transfected with LifeAct-GFP (dashed line) vs non-transfected cells (dotted line) was assessed for both IpLITR 2.6b/IpFcRγ-L-expressing cells (A) and IpLITR 1.1b-expressing cells (B) via their FL2-intensities which were obtained through the use of a αHA mAb to measure IpLITR-expression. Validation of LifeAct-GFP transfection was determined by assessing changes in non-transfected cells vs transfected cells via changes in the FL1-intensities of cells tested. IpLITR-specific membrane dynamics were assessed using LCI and overview representative images are shown for IpLITR-expressing cells at either 37^{o}C (C) or at 27 ^{o}C (D). Dashed circles indicate observed filopodia.

FIGURE 6.3

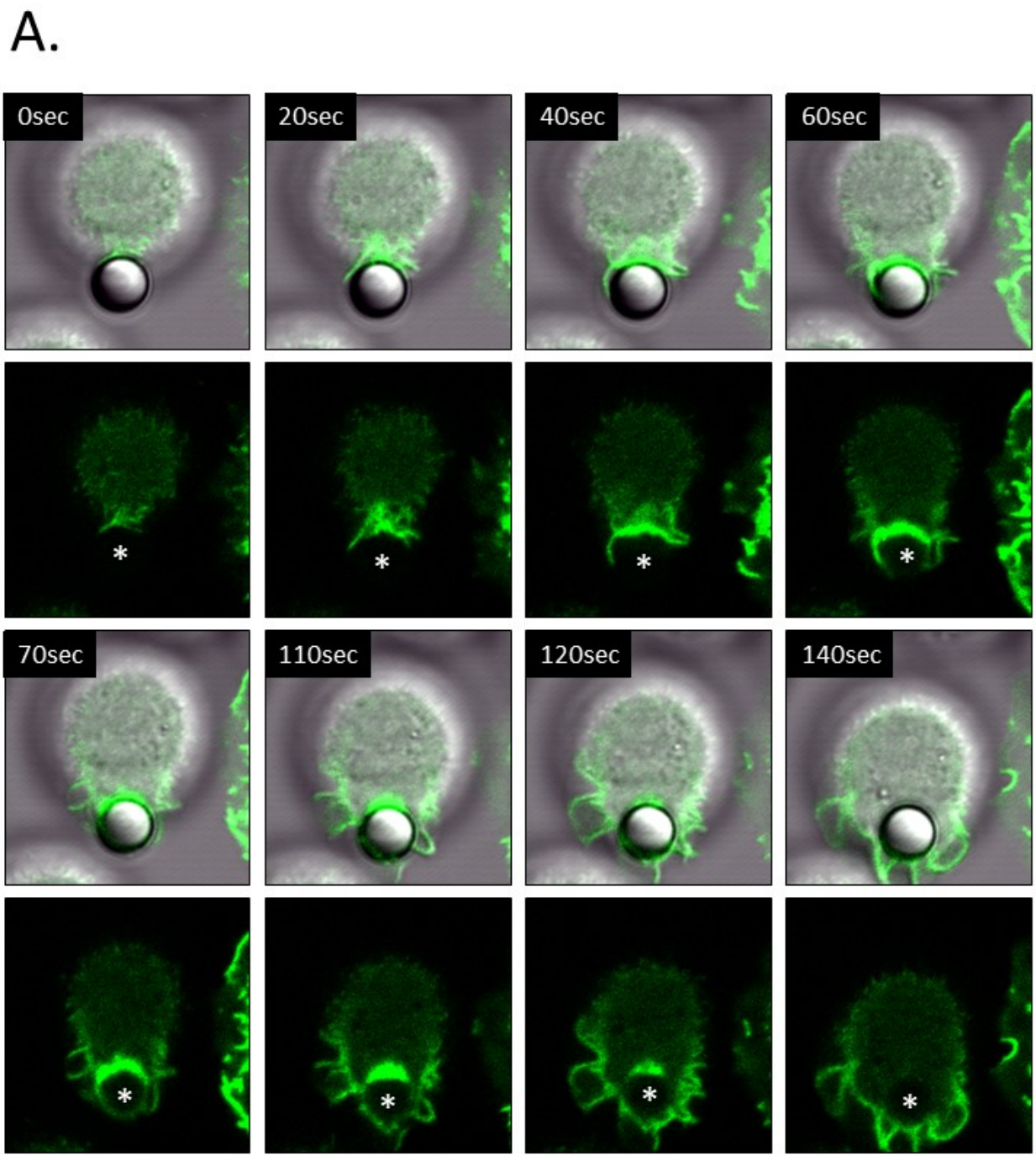

FIGURE 6.3

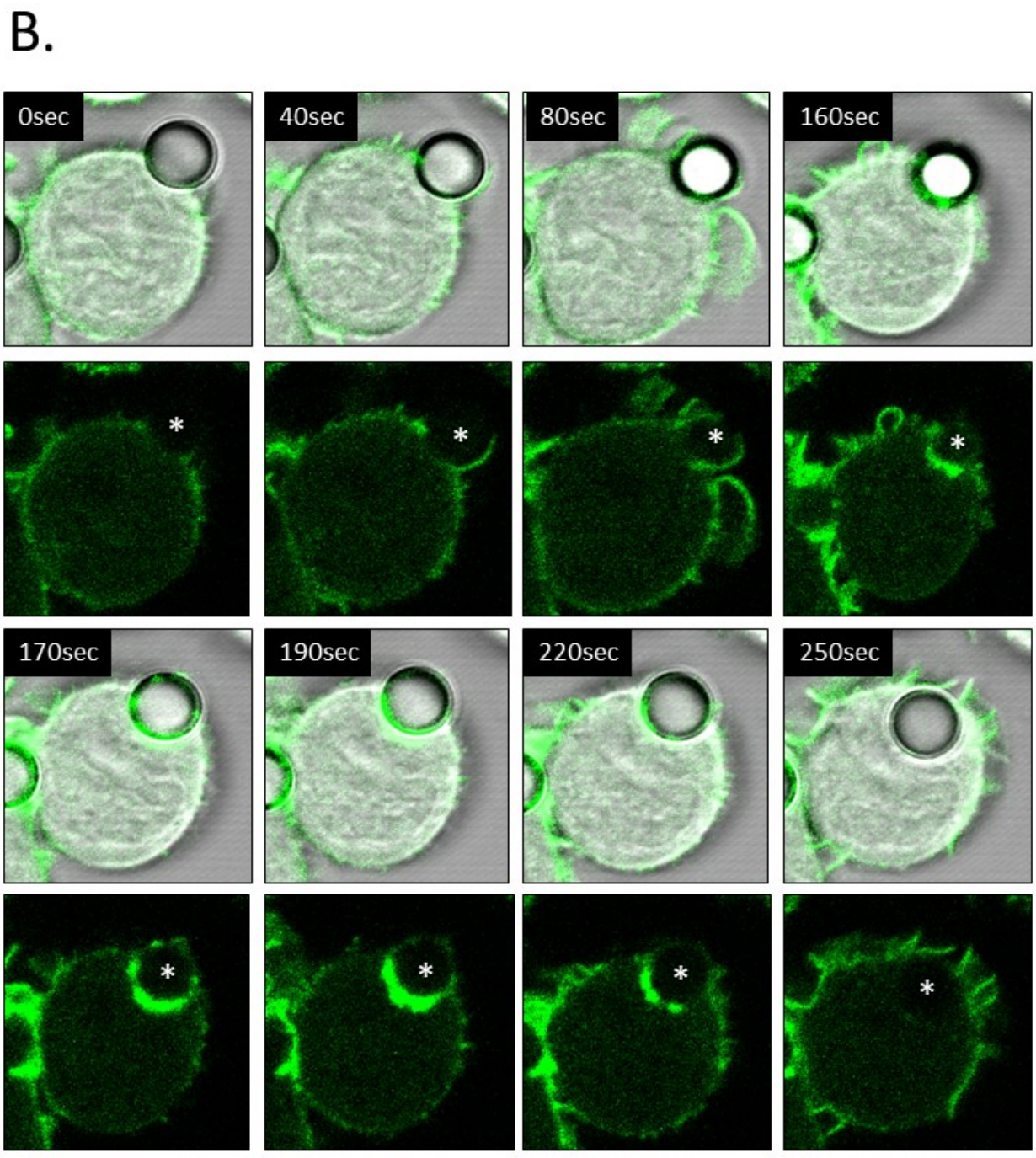

C.

FIGURE 6.3

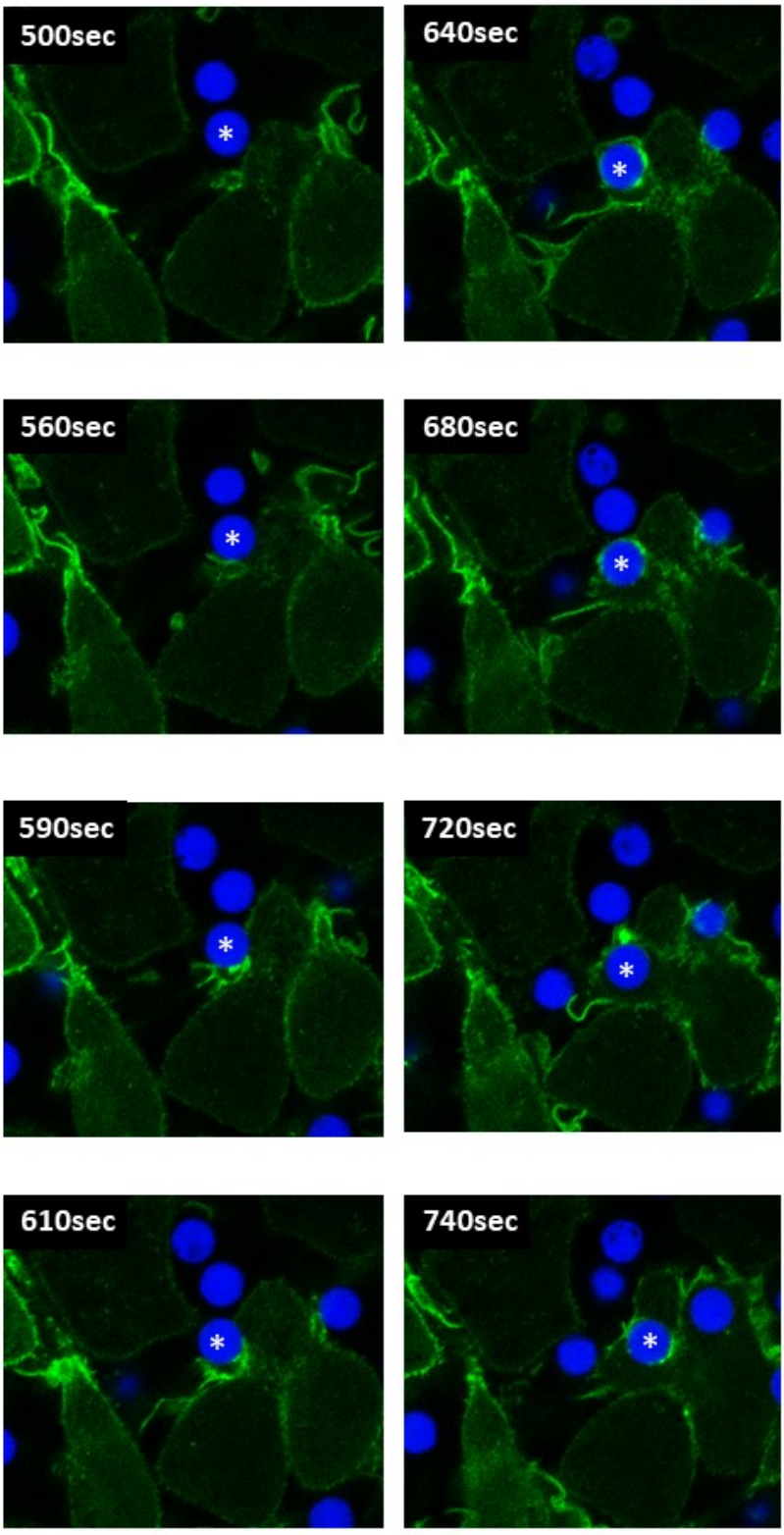

FIGURE 6.3

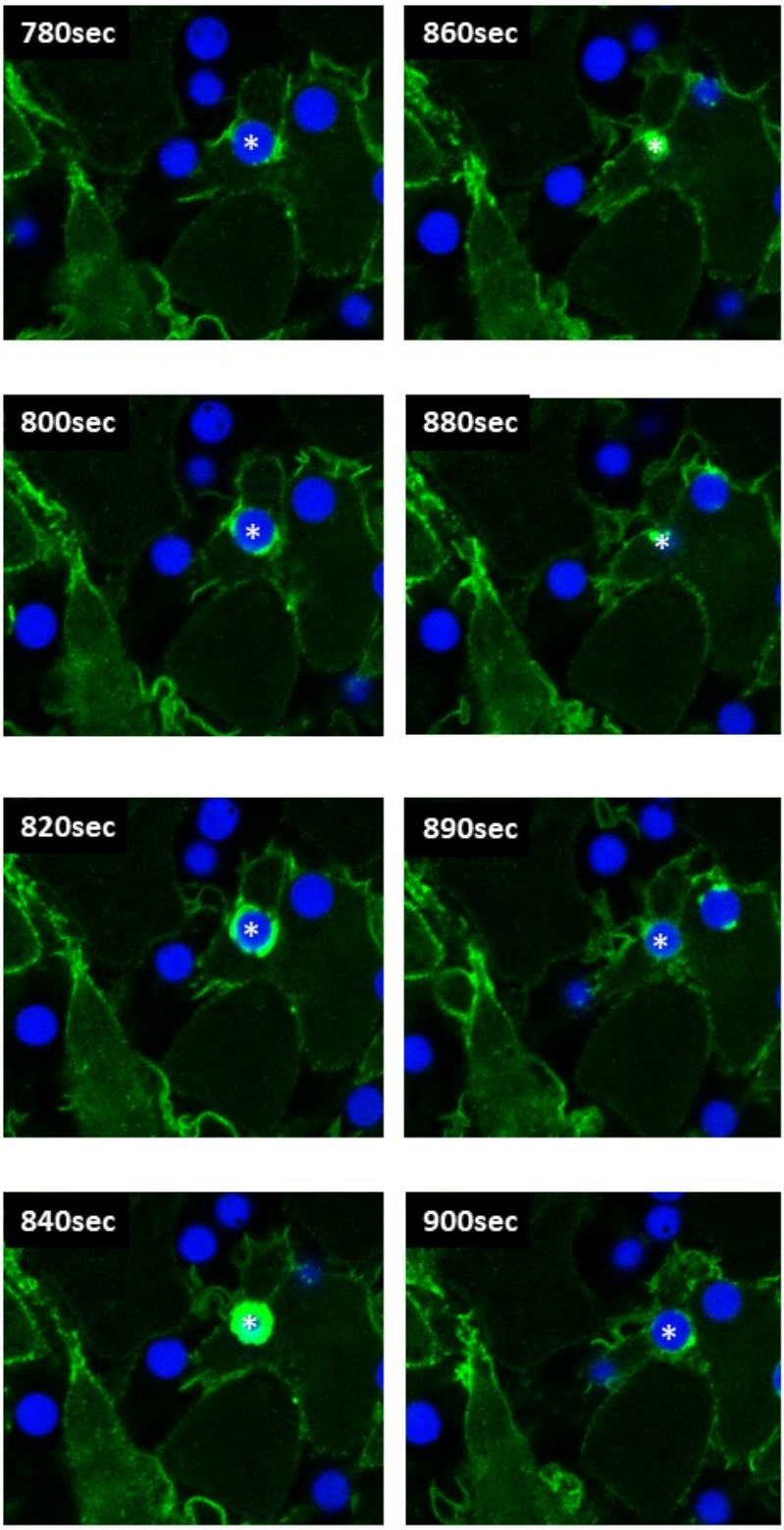

FIGURE 6.3

D.

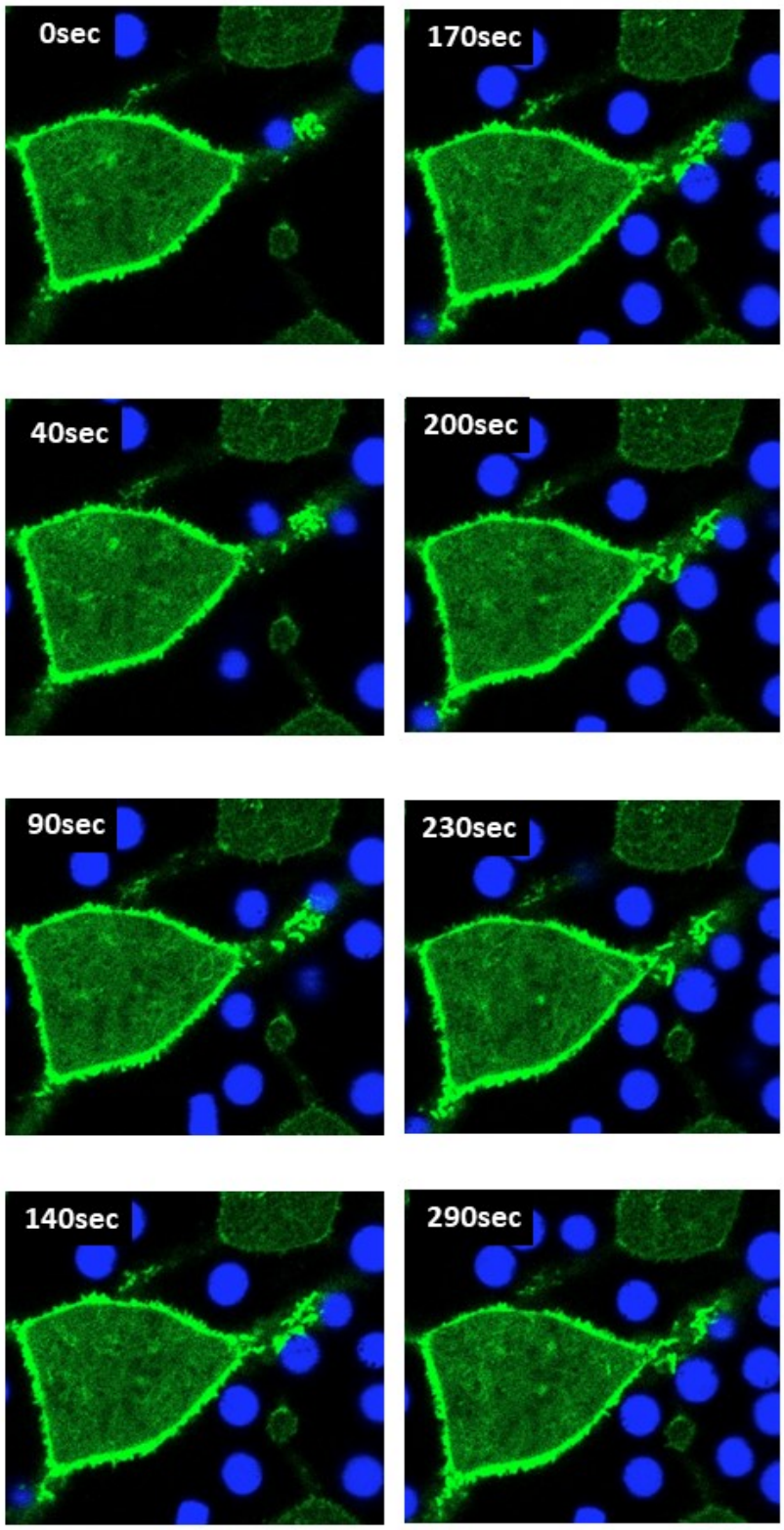

FIGURE 6.3

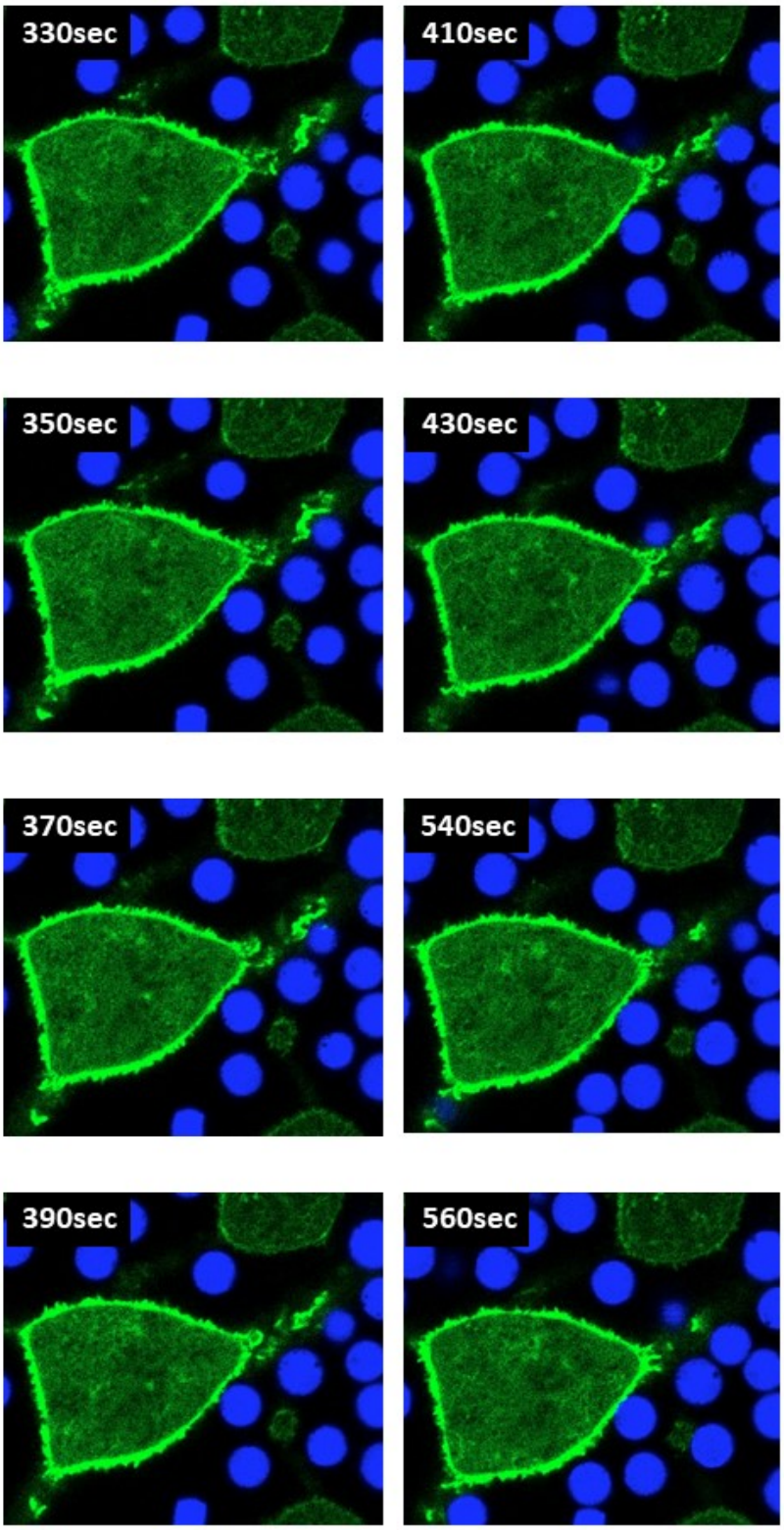

FIGURE 6.3 Examination of IpLITR 2.6b/IpFcRγ-L-mediated phagocytosis at 37°C and 27°C. LCI of IpLITR 2.6b/IpFcRγ-L-mediated phagocytosis. RBL-2H3 cells ($3x10^5$) stably co-expressing IpLITR 2.6b/IpFcRγ-L and LifeAct-GFP were incubated at 37°C (A and B) with $9x10^5$ αHA mAb-coated 4.5 μm microspheres. Immediately after the addition of target beads, images were collected at 10 sec intervals for ~8 min using a Zeiss LSM 710 laser scanning confocal microscope (Objective 60x, 1.3 oil plan-Apochromat; Munich, Germany). Both the brightfield-LifeAct-GFP merged views (top panels) and the LifeAct-GFP views alone (bottom panels) are shown with the location of the target microsphere indicated with an asterisk (A and B). IpLITR 2.6b/IpFcRγ-L-mediated phagocytosis at different incubation temperatures. RBL-2H3 cells ($3x10^5$) stably co-expressing IpLITR 2.6b/IpFcRγ-L and LifeAct-GFP were incubated at 37°C (C) or at 27°C (D) with $9x10^5$ αHA mAb-coated 4.5 μm bright blue microspheres. Immediately after the addition of target beads, images were collected at 10 sec intervals for ~8 min using a Zeiss LSM 710 laser scanning confocal microscope. Arrows indicate beads of interest. Representative time-stamps were extracted from LCI videos.

FIGURE 6.4

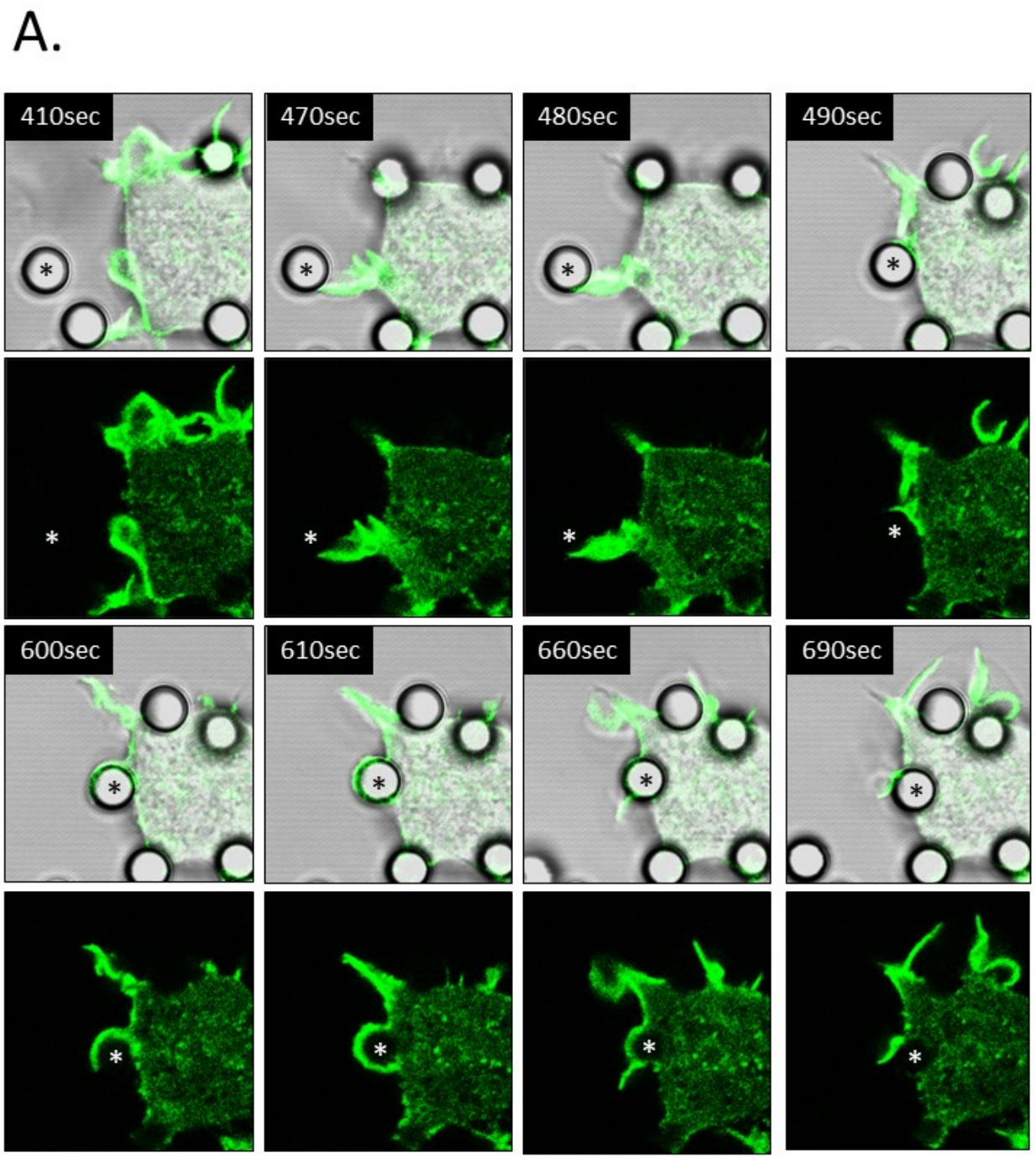

FIGURE 6.4

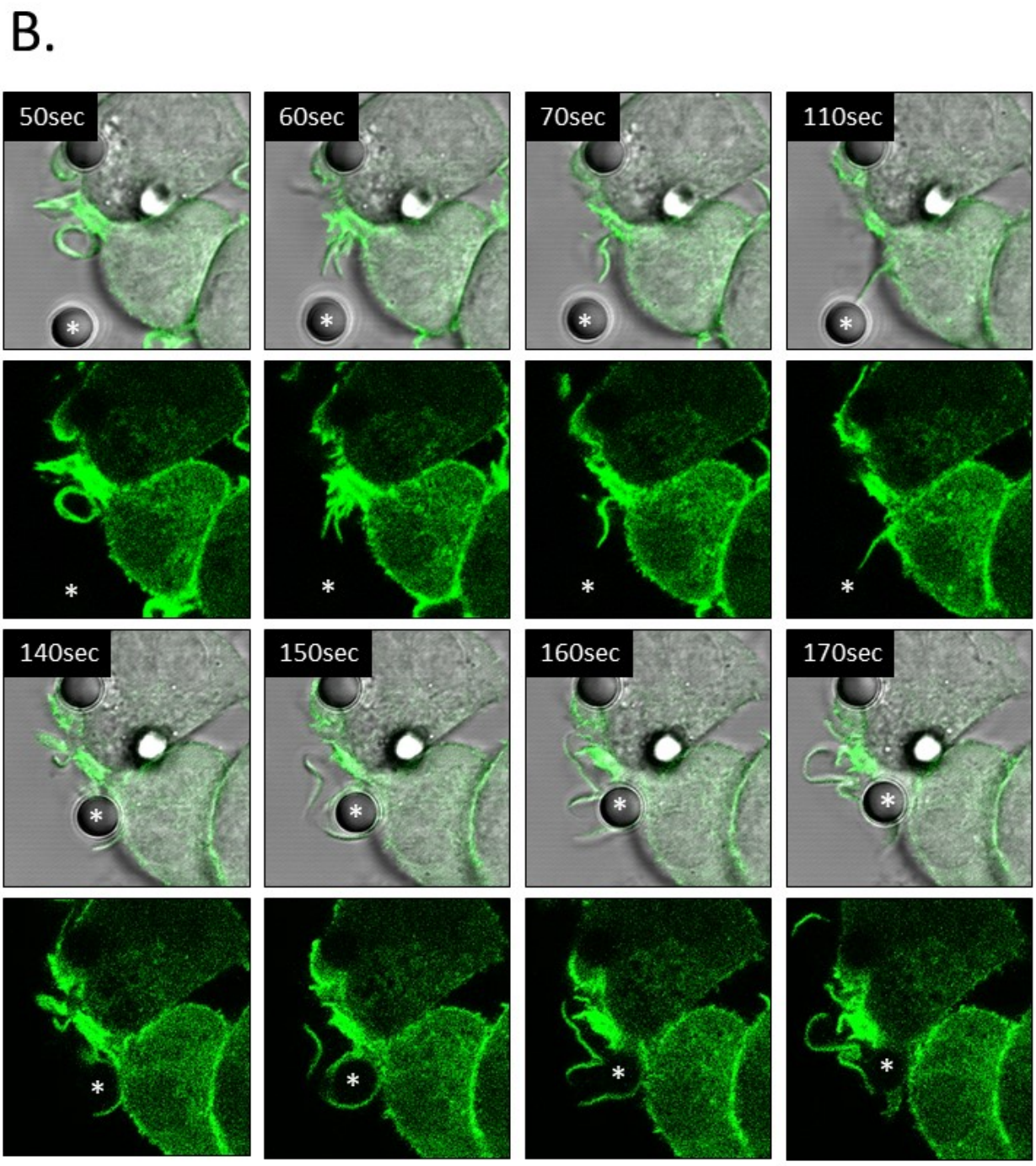

FIGURE 6.4

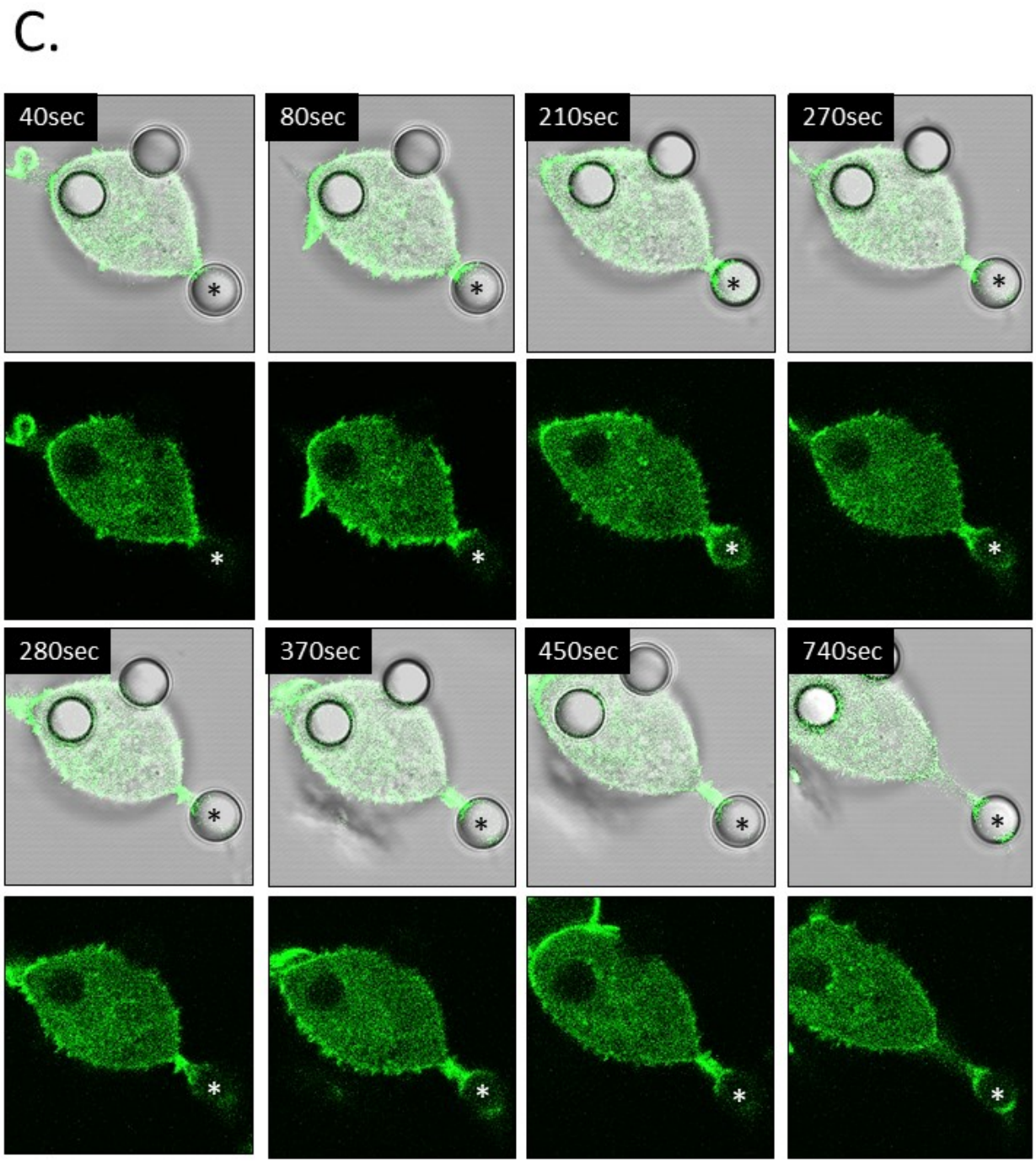

FIGURE 6.4

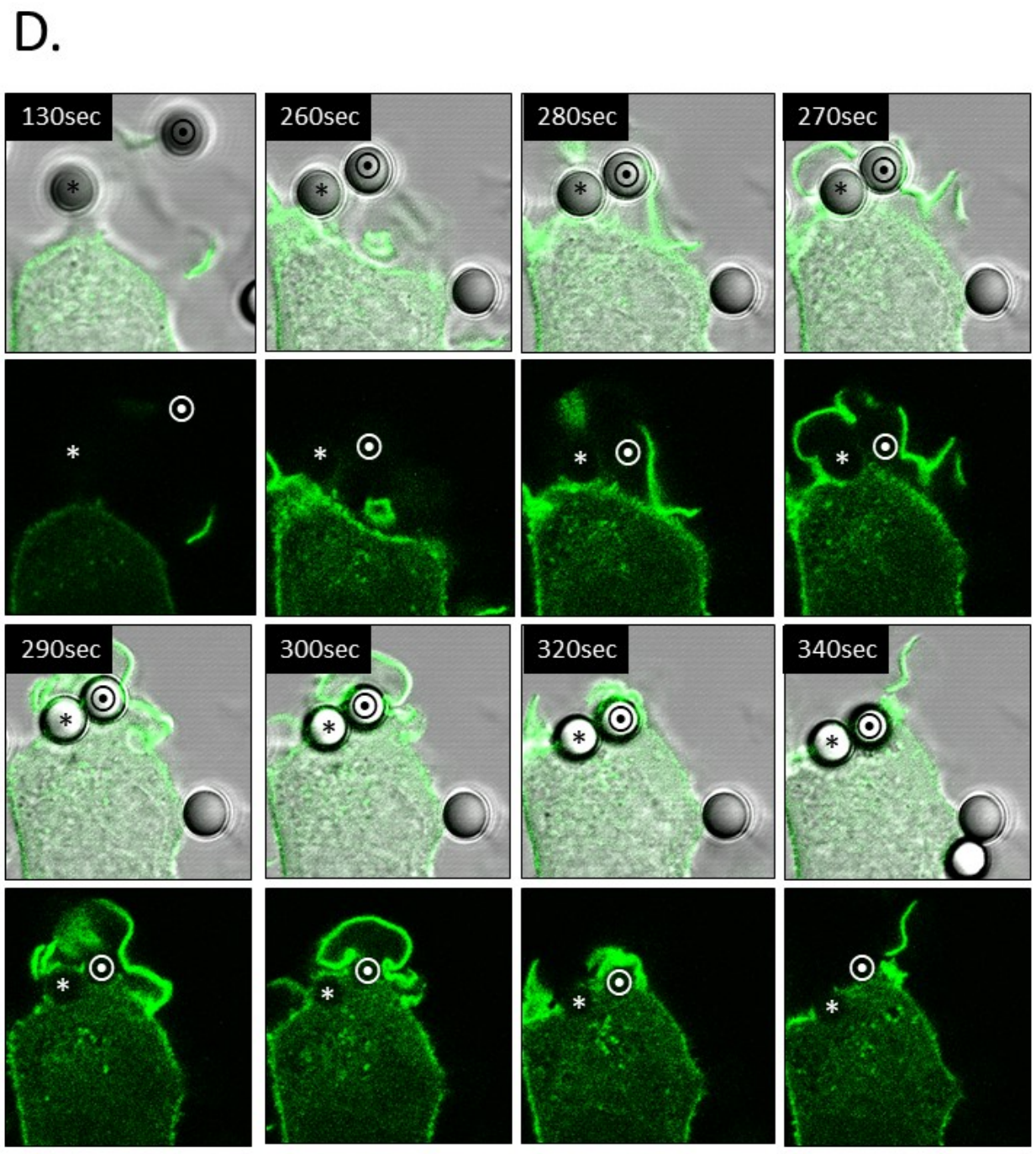

FIGURE 6.4

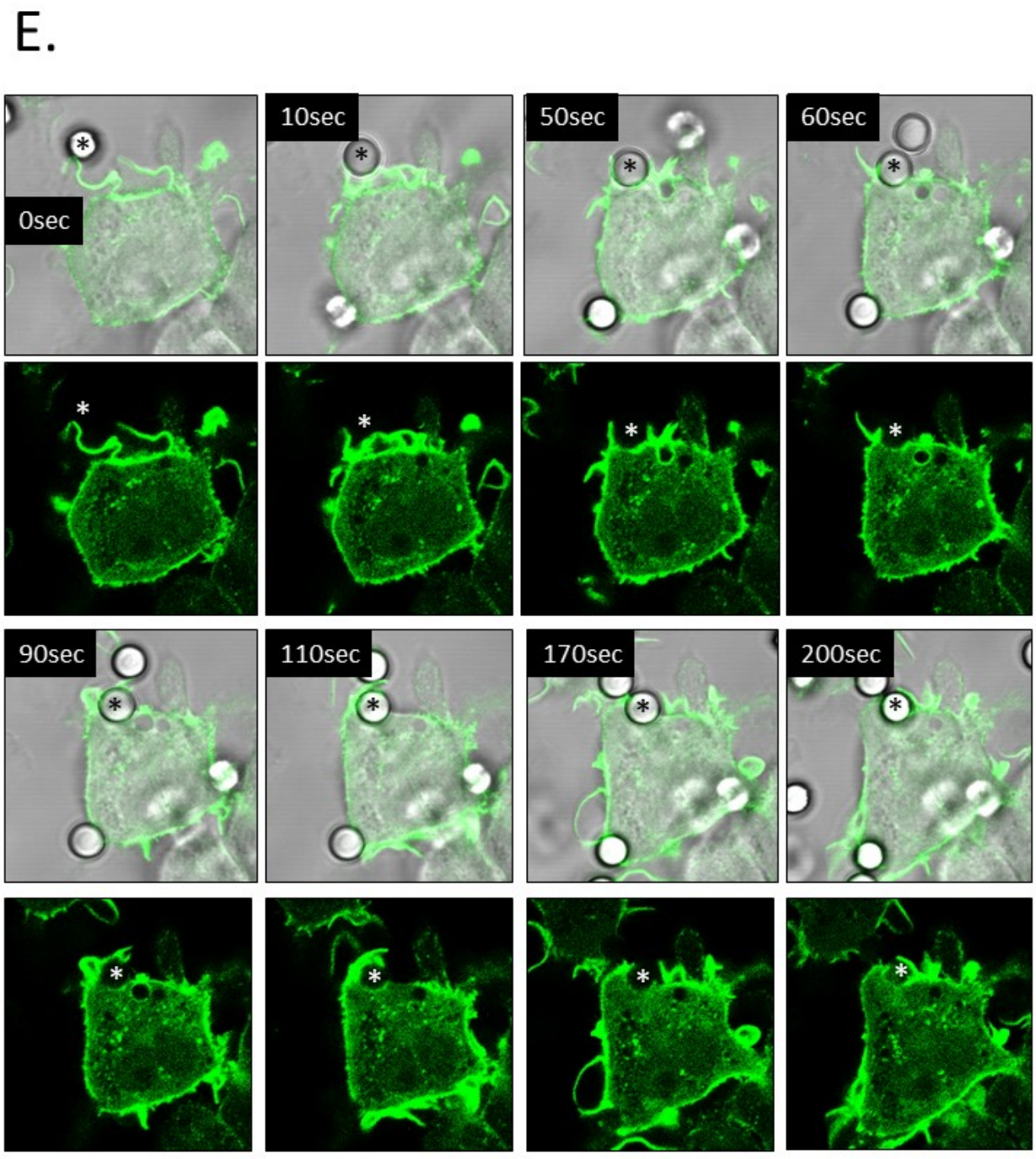

FIGURE 6.4

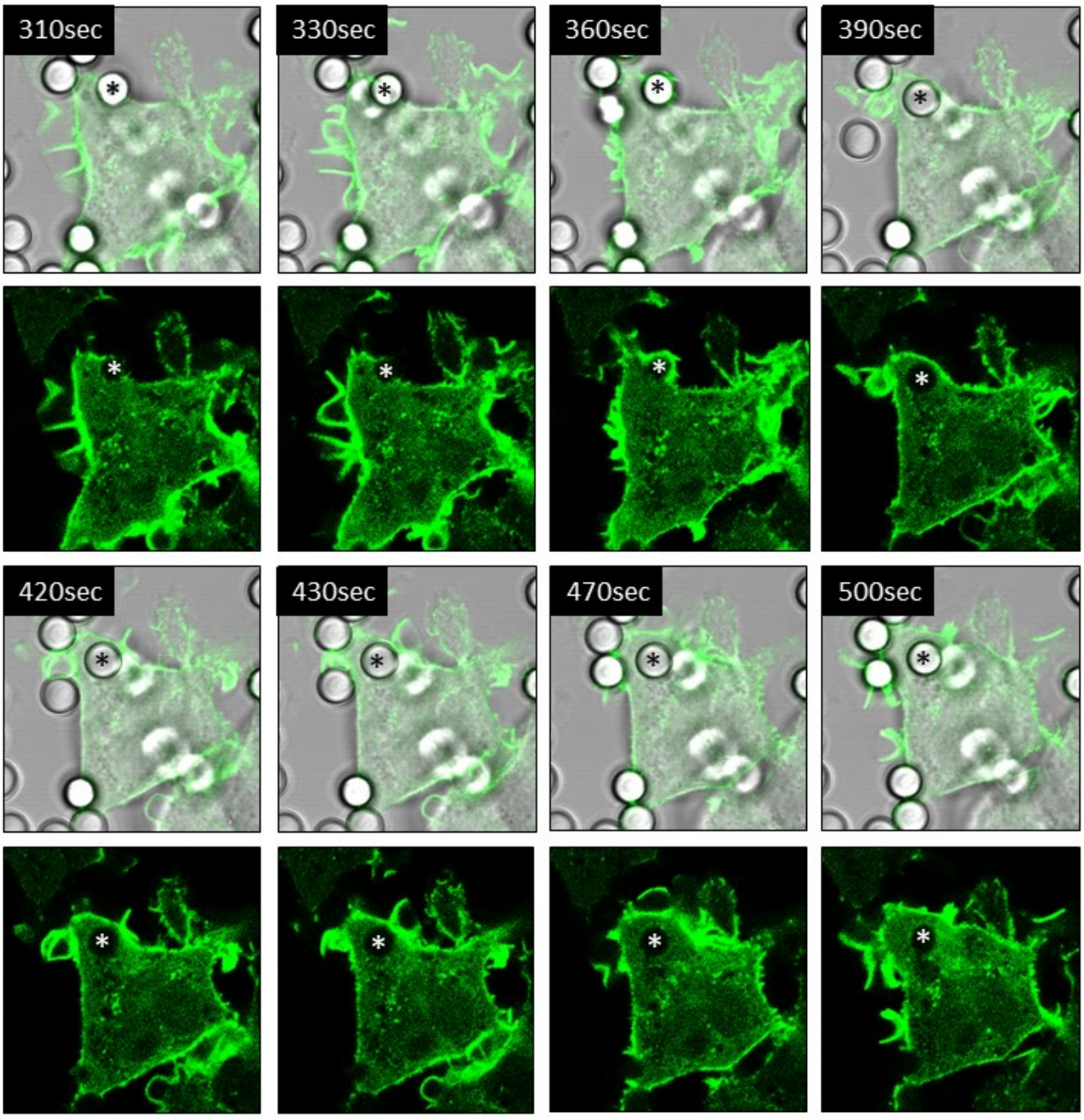

FIGURE 6.4

F.

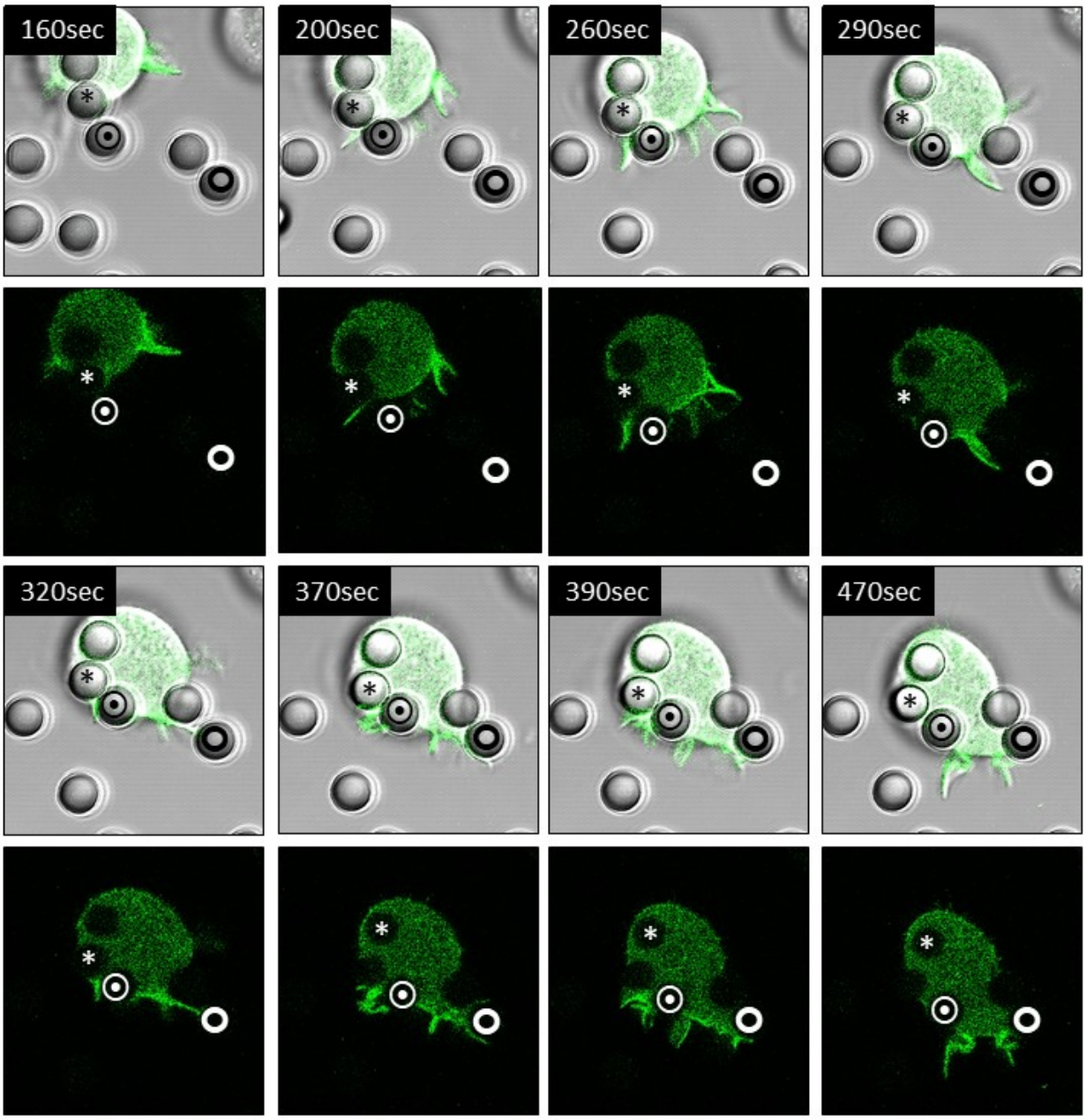

FIGURE 6.4 Examination of IpLITR 1.1b-mediated target interactions at 37^{o}C. LCI of IpLITR 1.1b-mediated phagocytosis. RBL-2H3 cells ($3x10^{5}$) stably co-expressing IpLITR 1.1b and LifeAct-GFP were incubated at 37^{o}C with $9x10^{5}$ αHA mAb-coated 4.5 μm microspheres. Immediately after the addition of target beads, images were collected at 10 sec intervals for ~8 min using a Zeiss LSM 710 laser scanning confocal microscope (Objective 60x, 1.3 oil plan-Apochromat; Munich, Germany). Both the brightfield-LifeAct-GFP merged views (top panels) and the LifeAct-GFP views alone (bottom panels) are shown for a series of representative phenotypes in A-F. The location of the target microsphere are indicated in the images by an asterisk or with the symbols ⊙ and ❍ when multiple beads were being tracked.

FIGURE 6.5

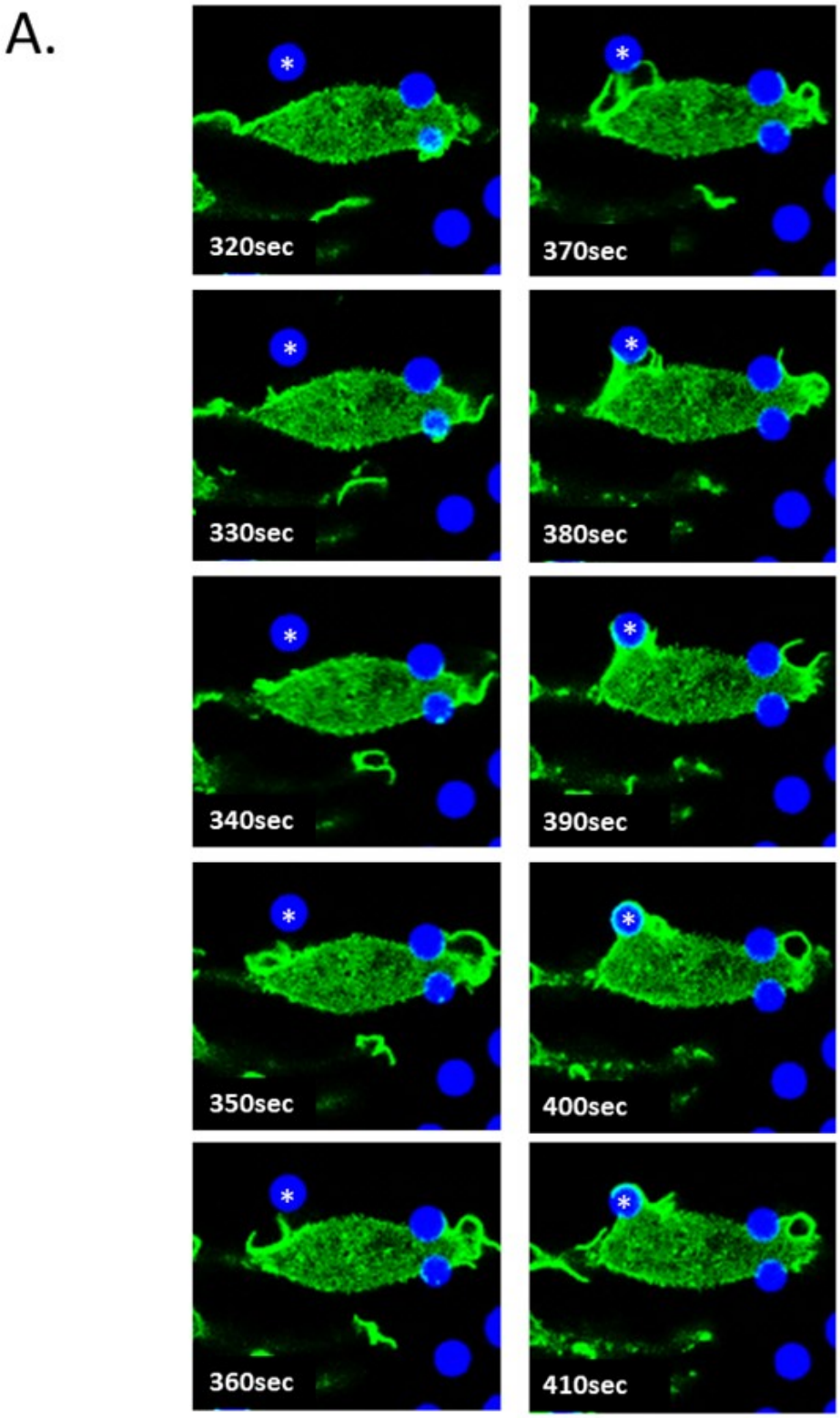
A.
320sec
370sec
330sec
380sec
340sec
390sec
350sec
400sec
360sec
410sec

FIGURE 6.5

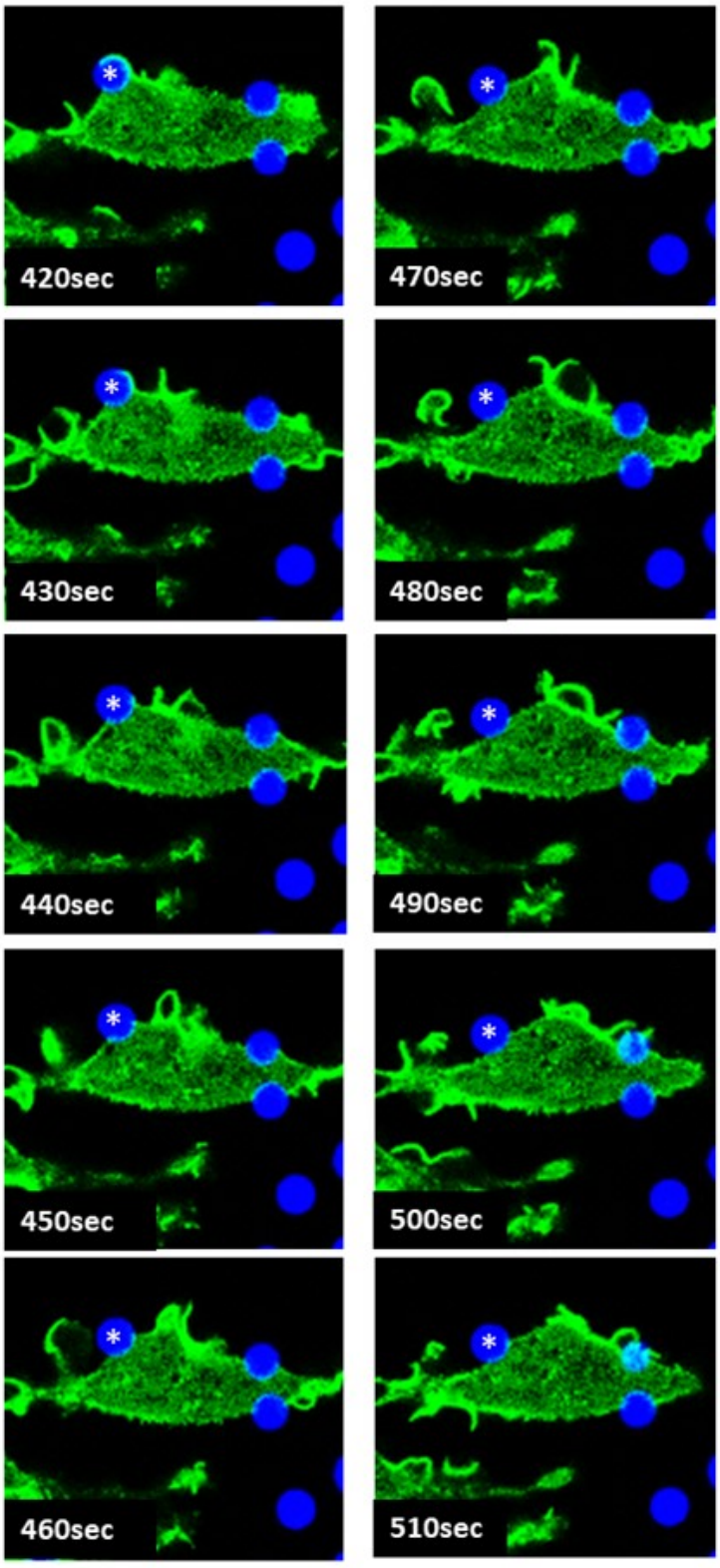
420sec
470sec
430sec
480sec
440sec
490sec
450sec
500sec
460sec
510sec

FIGURE 6.5

B.

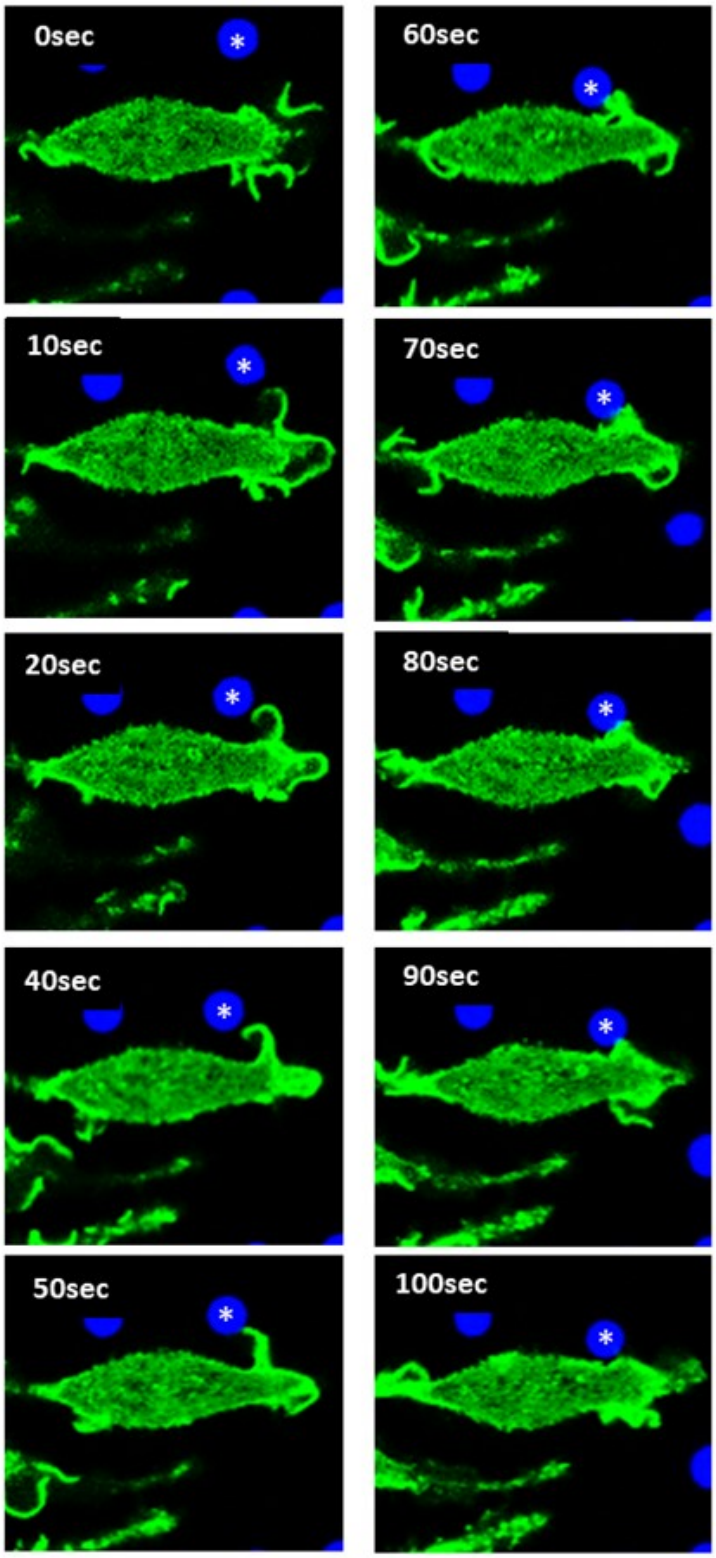
0sec
60sec
10sec
70sec
20sec
80sec
40sec
90sec
50sec
100sec

FIGURE 6.5

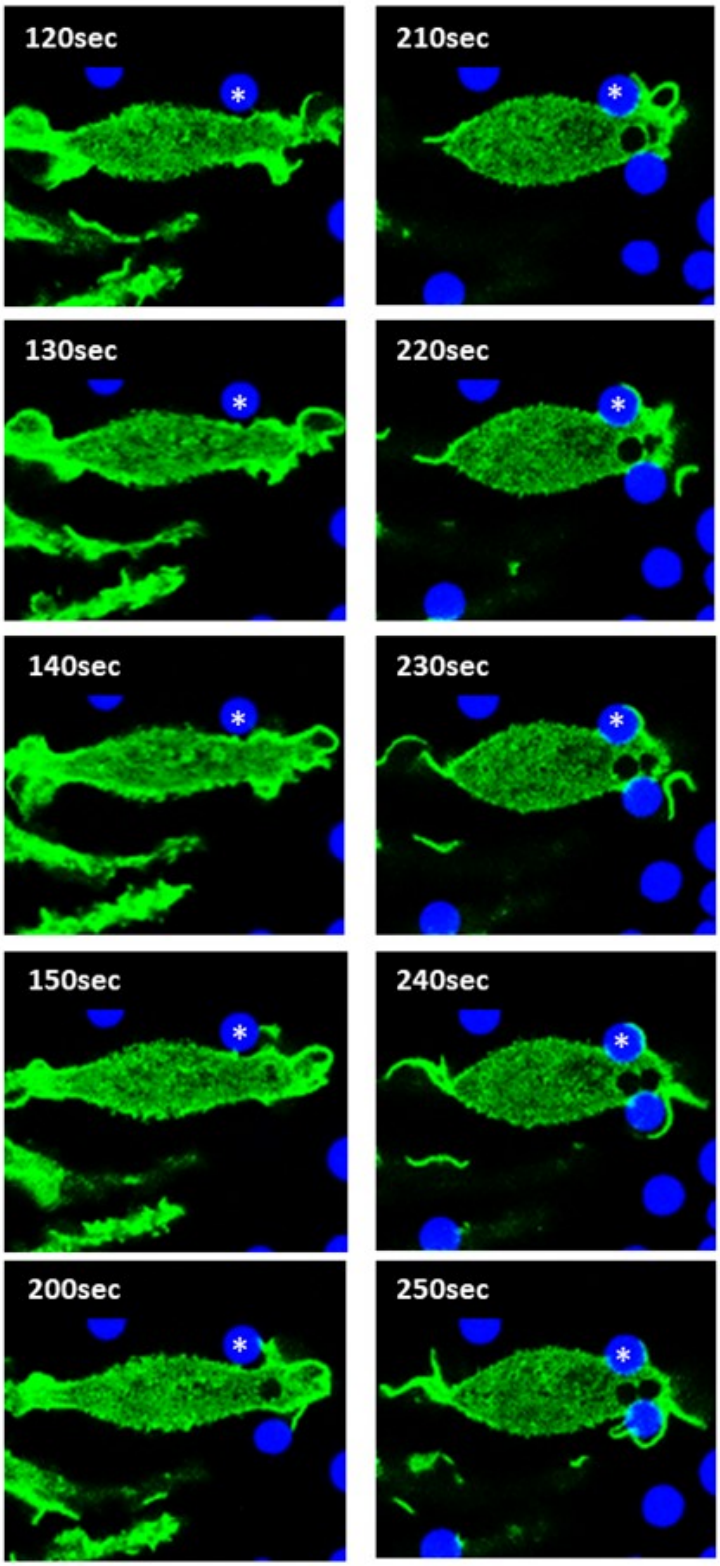
120sec
210sec
130sec
220sec
140sec
230sec
150sec
240sec
200sec
250sec

FIGURE 6.5

C.

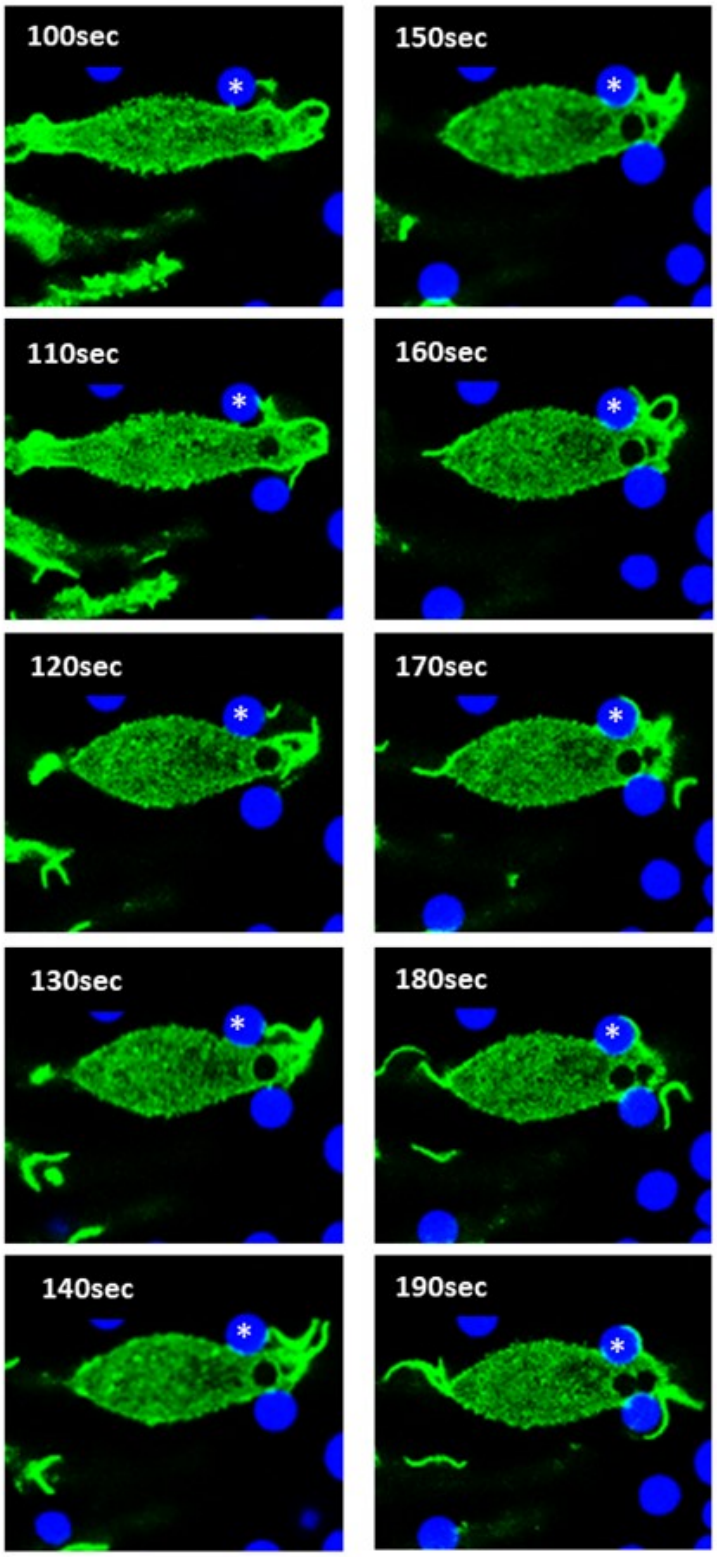
100sec
150sec
110sec
160sec
120sec
170sec
130sec
180sec
140sec
190sec

FIGURE 6.5

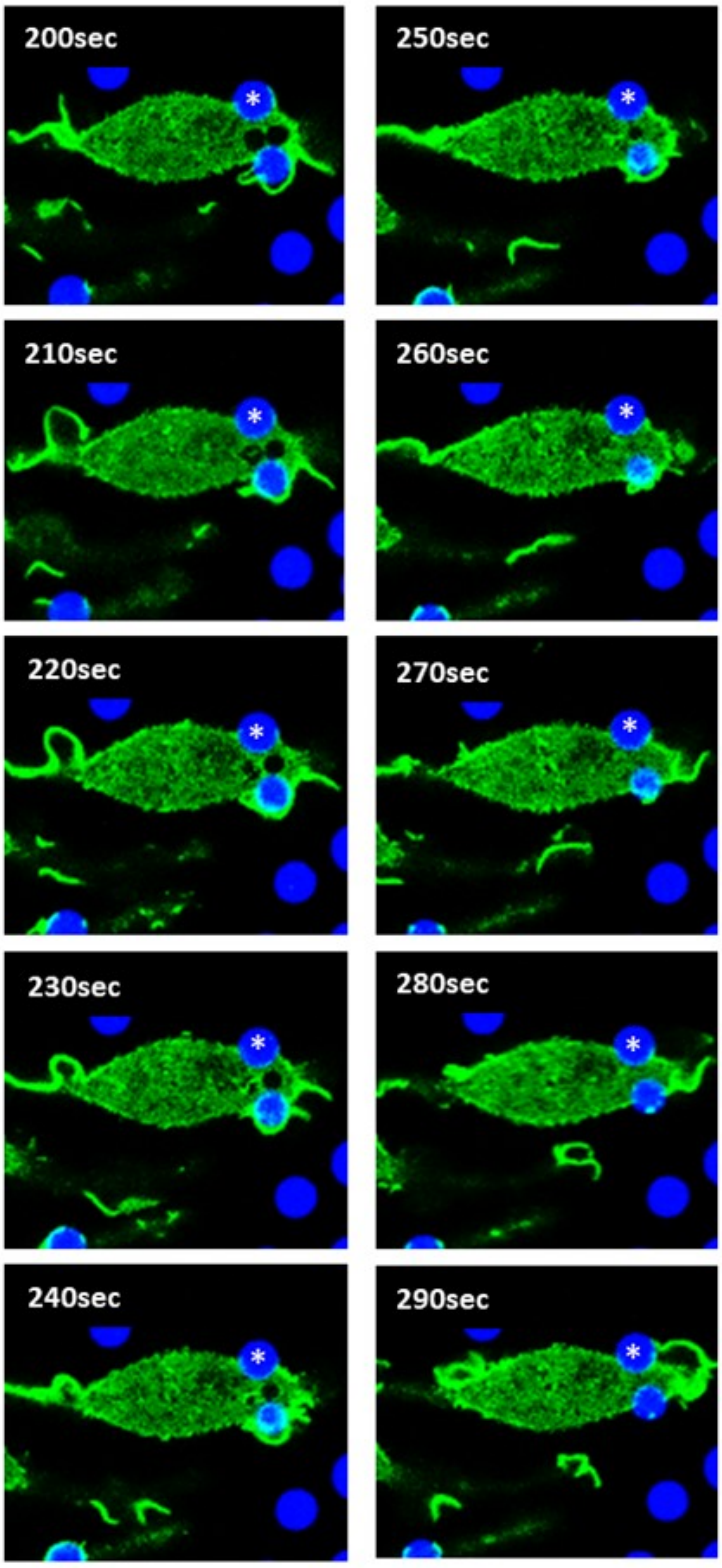
200sec
250sec
210sec
260sec
220sec
270sec
230sec
280sec
240sec
290sec

FIGURE 6.5

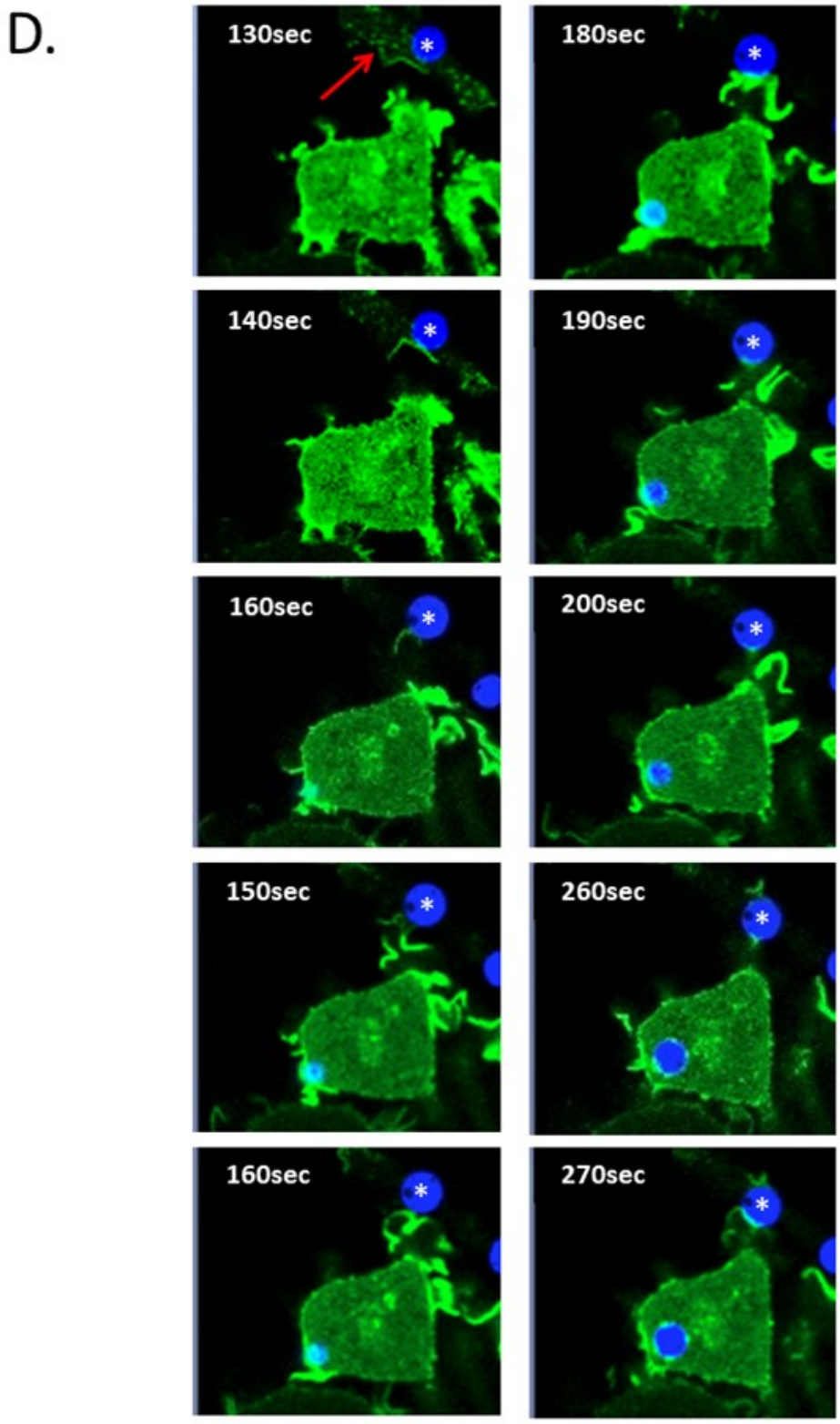
D.
130sec
180sec
140sec
190sec
160sec
200sec
150sec
260sec
160sec
270sec

FIGURE 6.5

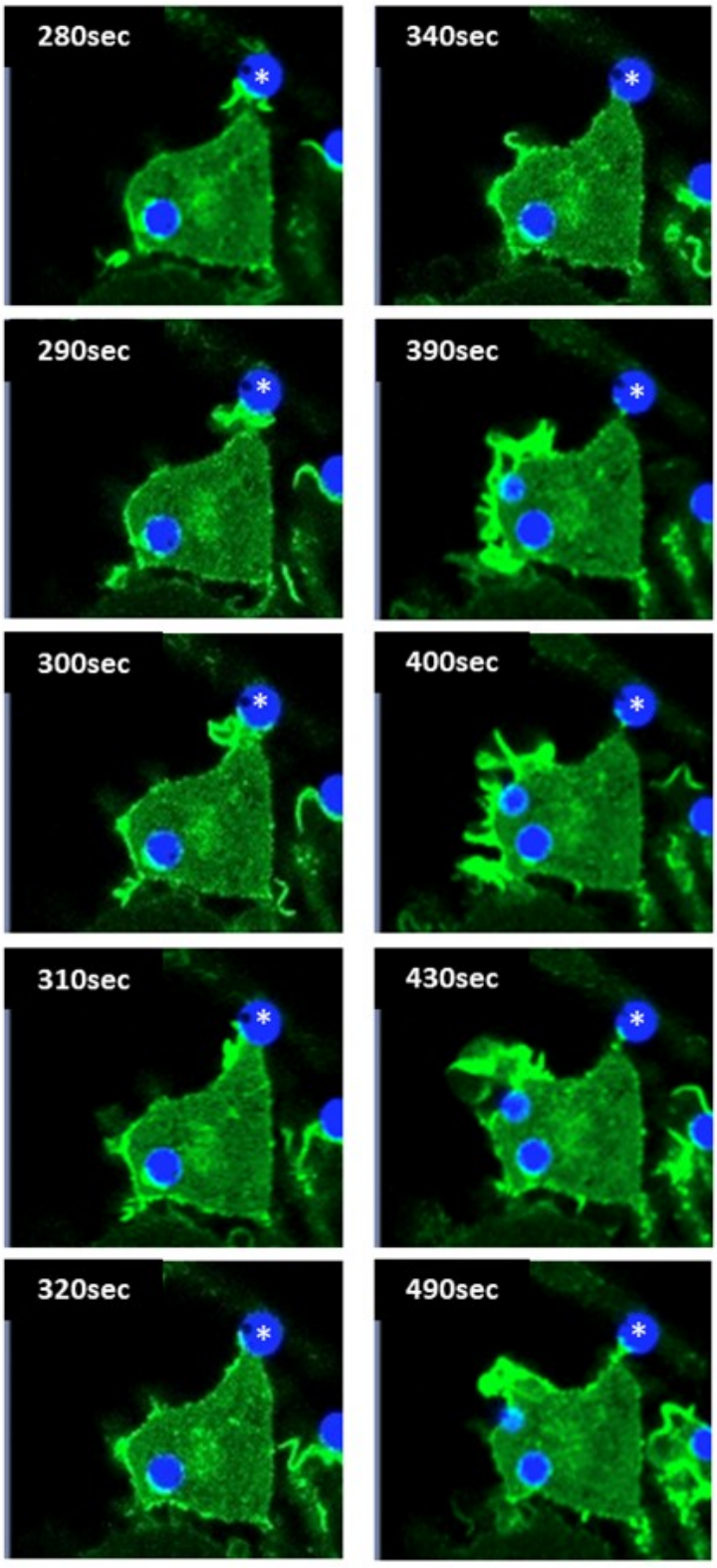
280sec
340sec
290sec
390sec
300sec
400sec
310sec
430sec
320sec
490sec

FIGURE 6.5 IpLITR 1.1b-mediated target interactions at 37 ^{o}C. RBL-2H3 cells ($3x10^5$) stably co-expressing IpLITR 1.1b and LifeAct-GFP were incubated at 37^{o}C with $9x10^5$ αHA mAb-coated 4.5 μm bright blue microspheres. Immediately after the addition of target beads, images were collected at 10 sec intervals for ~8 min using a Zeiss LSM 710 laser scanning confocal microscope (Objective 60x, 1.3 oil plan-Apochromat; Munich, Germany) and are shown for a series of representative phenotypes in A-D. In all time-stamps target beads are indicated with an asterisk.

FIGURE 6.6

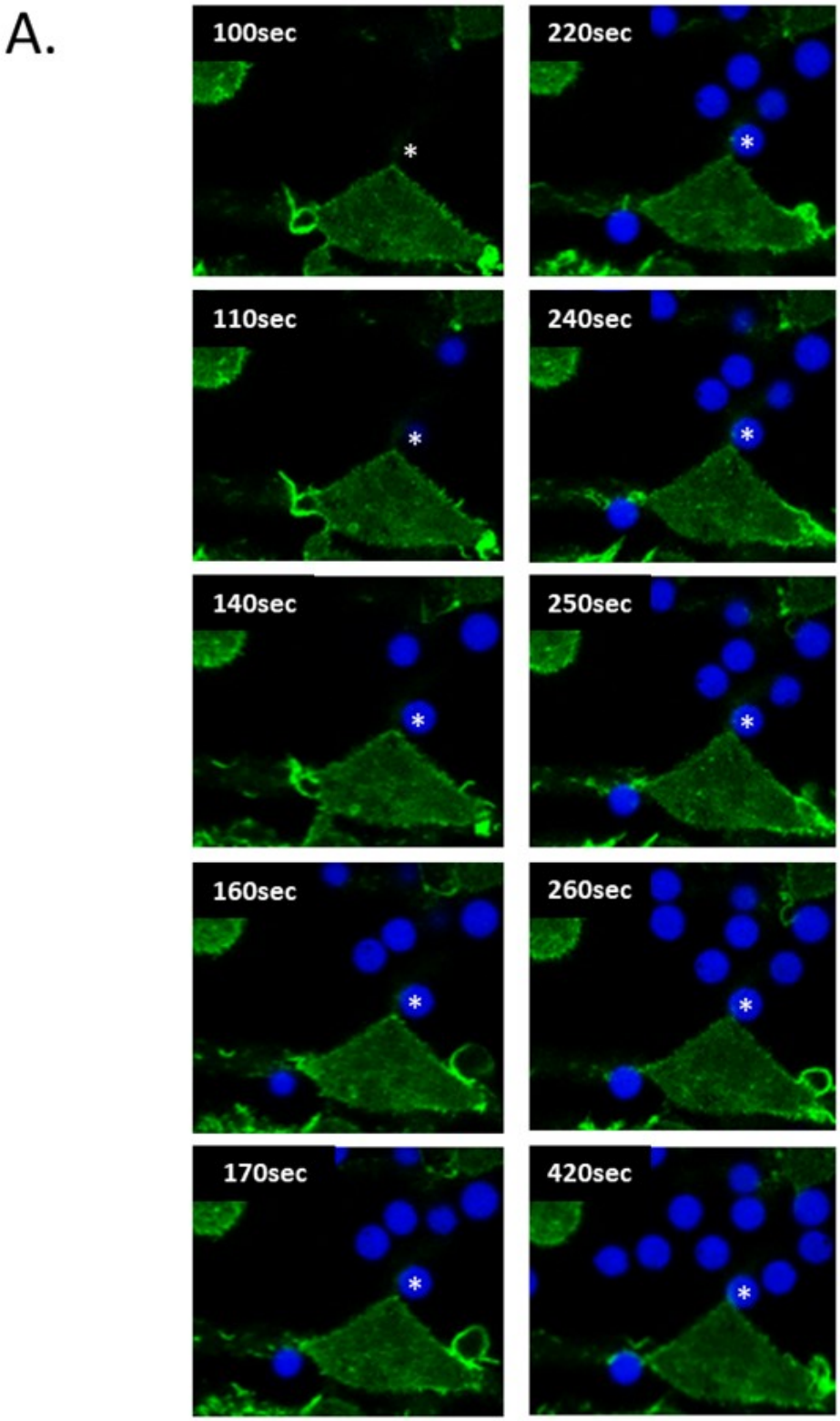
A.
100sec
220sec
110sec
240sec
140sec
250sec
160sec
260sec
170sec
420sec

FIGURE 6.6

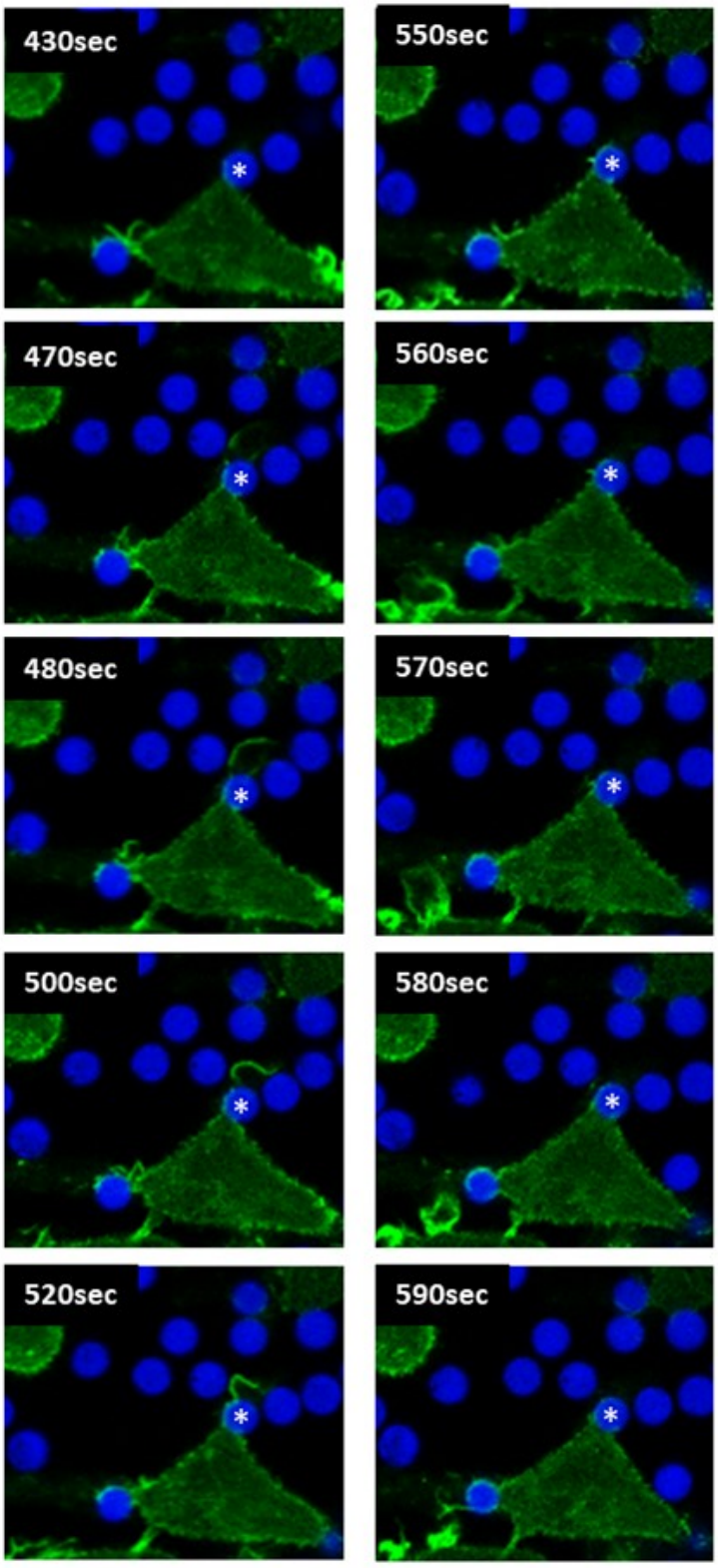
430sec
550sec
470sec
560sec
480sec
570sec
500sec
580sec
520sec
590sec

FIGURE 6.6

B.

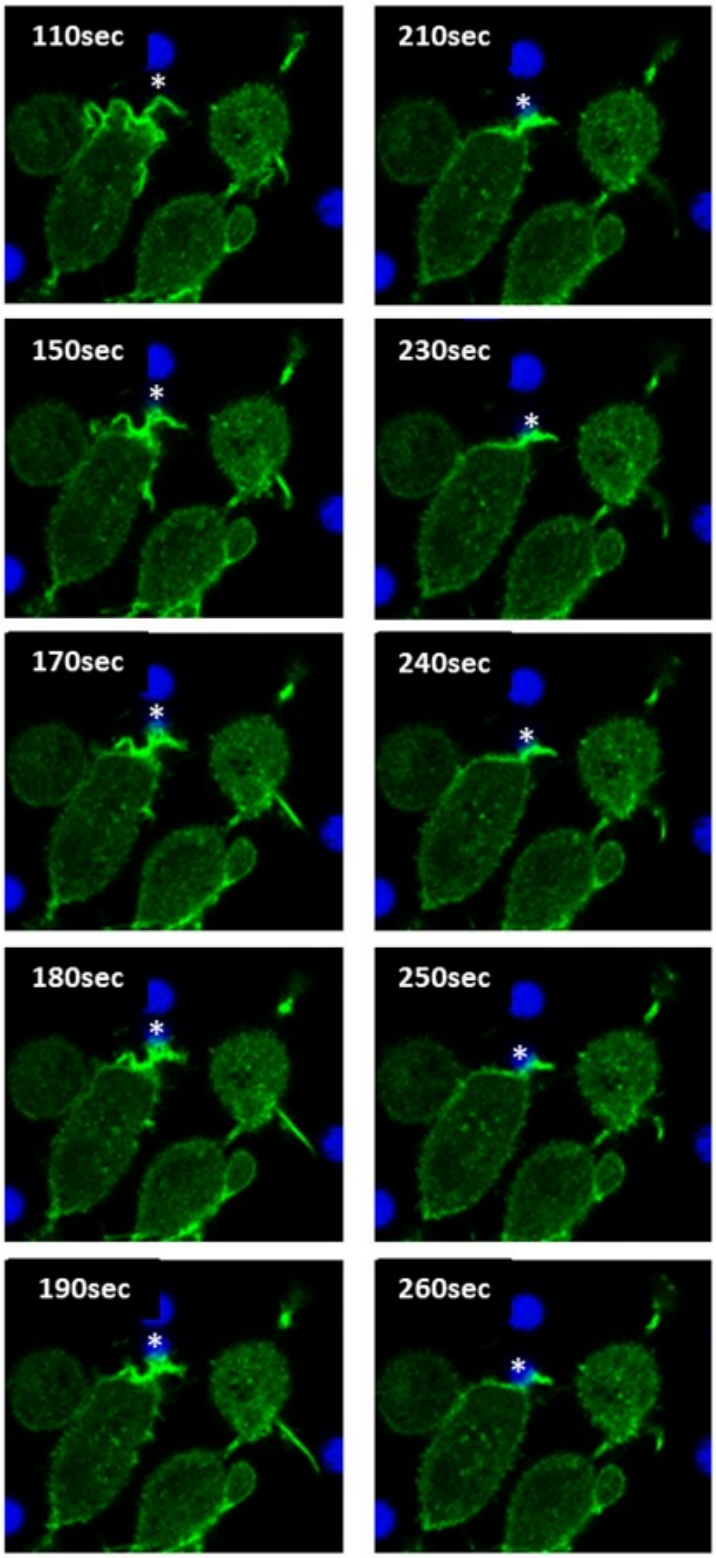
110sec
210sec
150sec
230sec
170sec
240sec
180sec
250sec
190sec
260sec

FIGURE 6.6

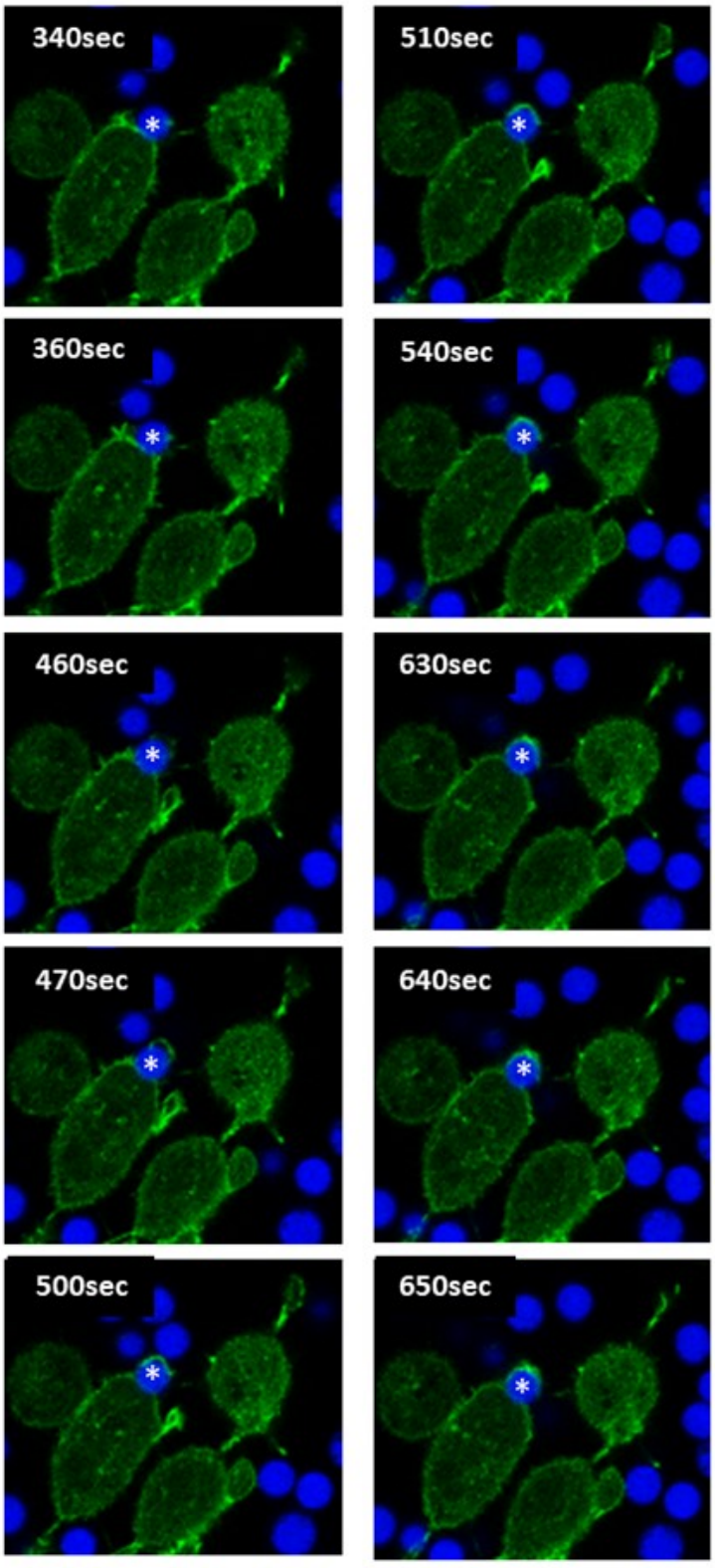
340sec
510sec
360sec
540sec
460sec
630sec
470sec
640sec
500sec
650sec

FIGURE 6.6

C.

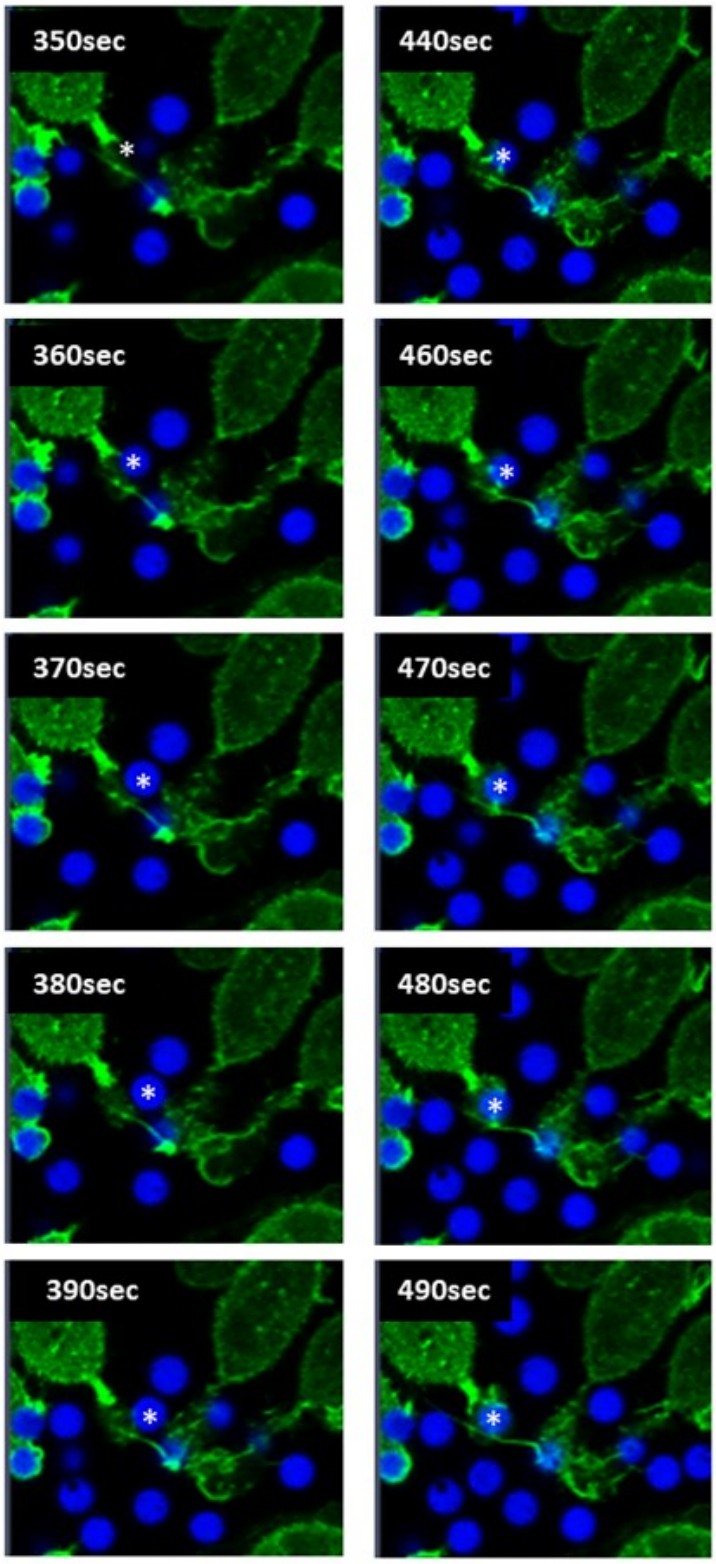
350sec
440sec
360sec
460sec
370sec
470sec
380sec
480sec
390sec
490sec

FIGURE 6.6

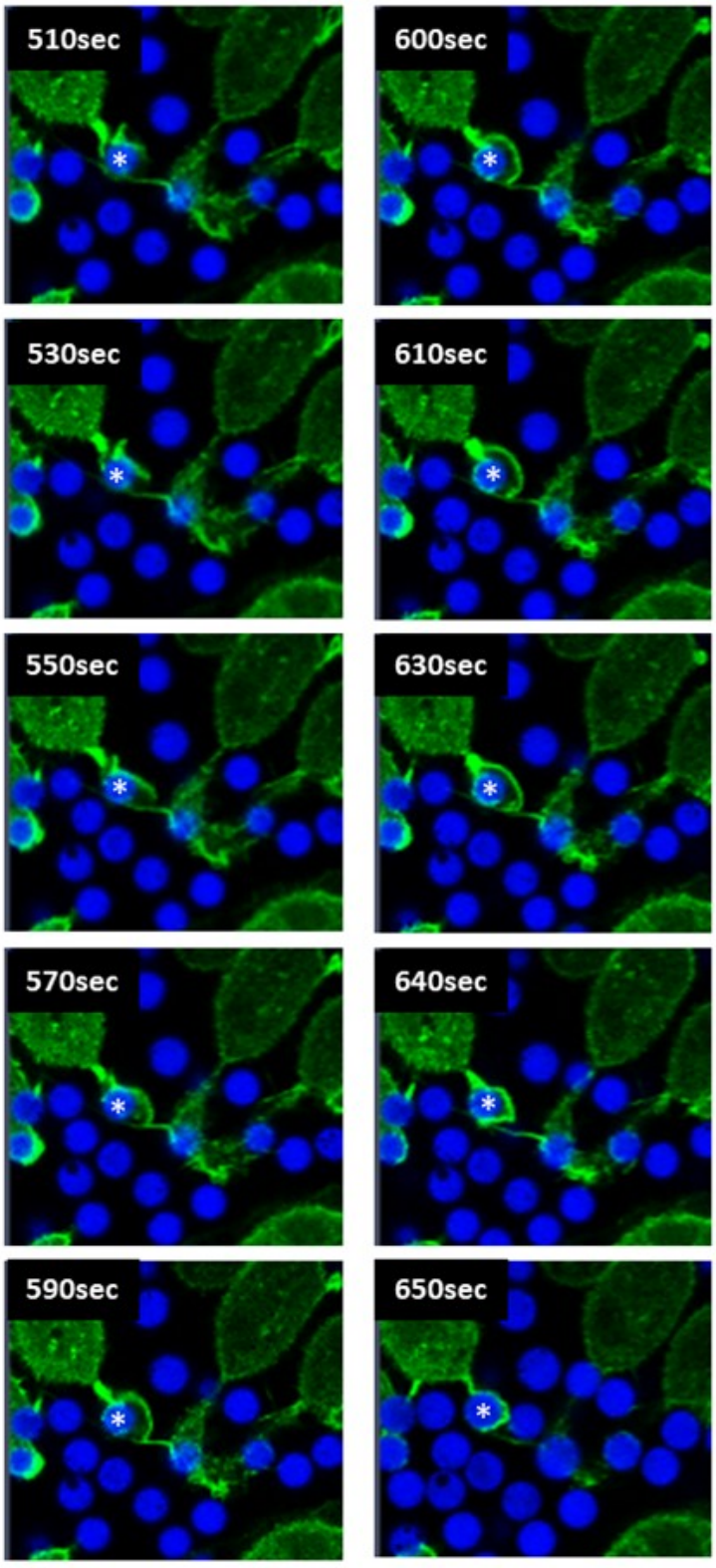
510sec
600sec
530sec
610sec
550sec
630sec
570sec
640sec
590sec
650sec

FIGURE 6.6

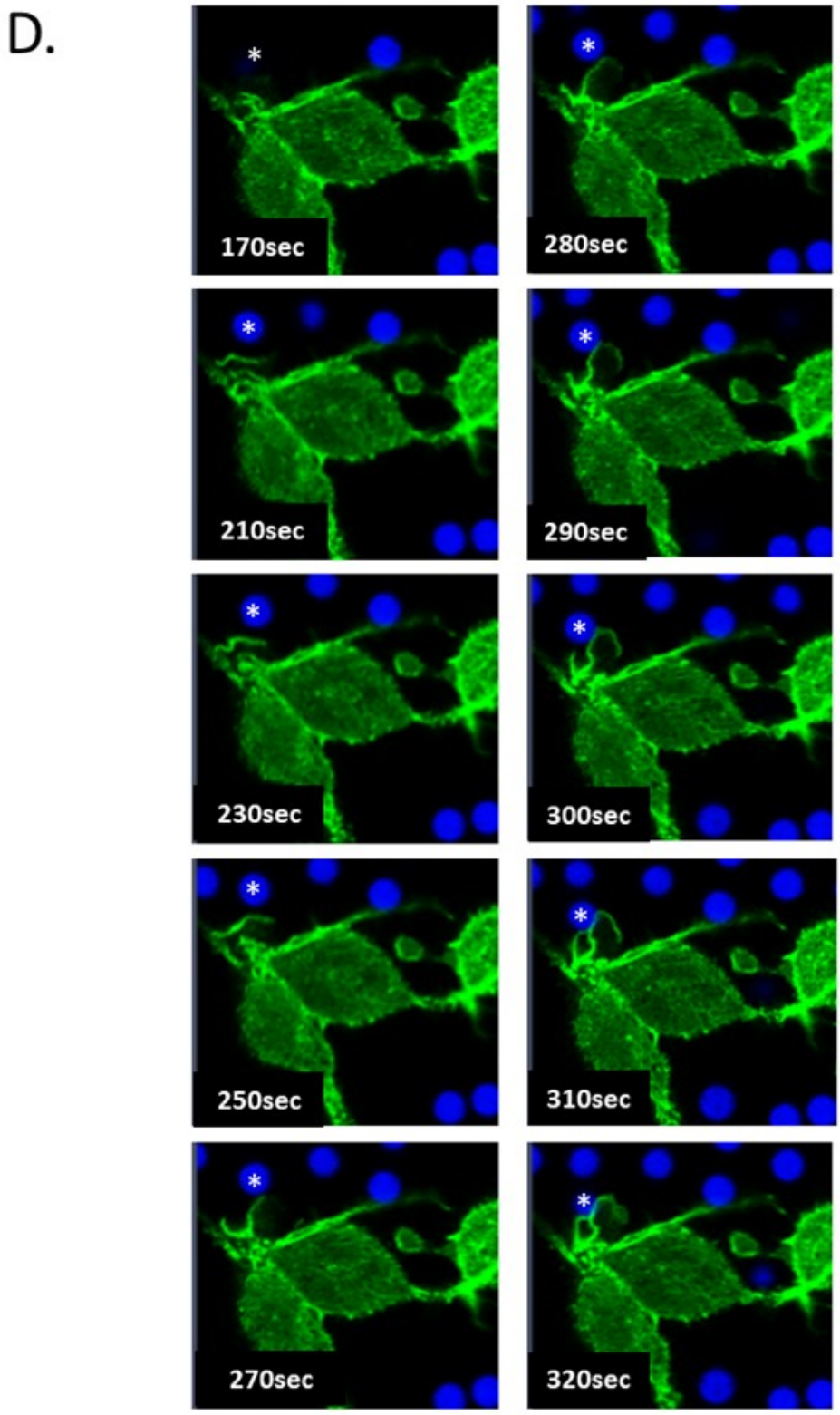
D.
170sec
280sec
210sec
290sec
230sec
300sec
250sec
310sec
270sec
320sec

FIGURE 6.6

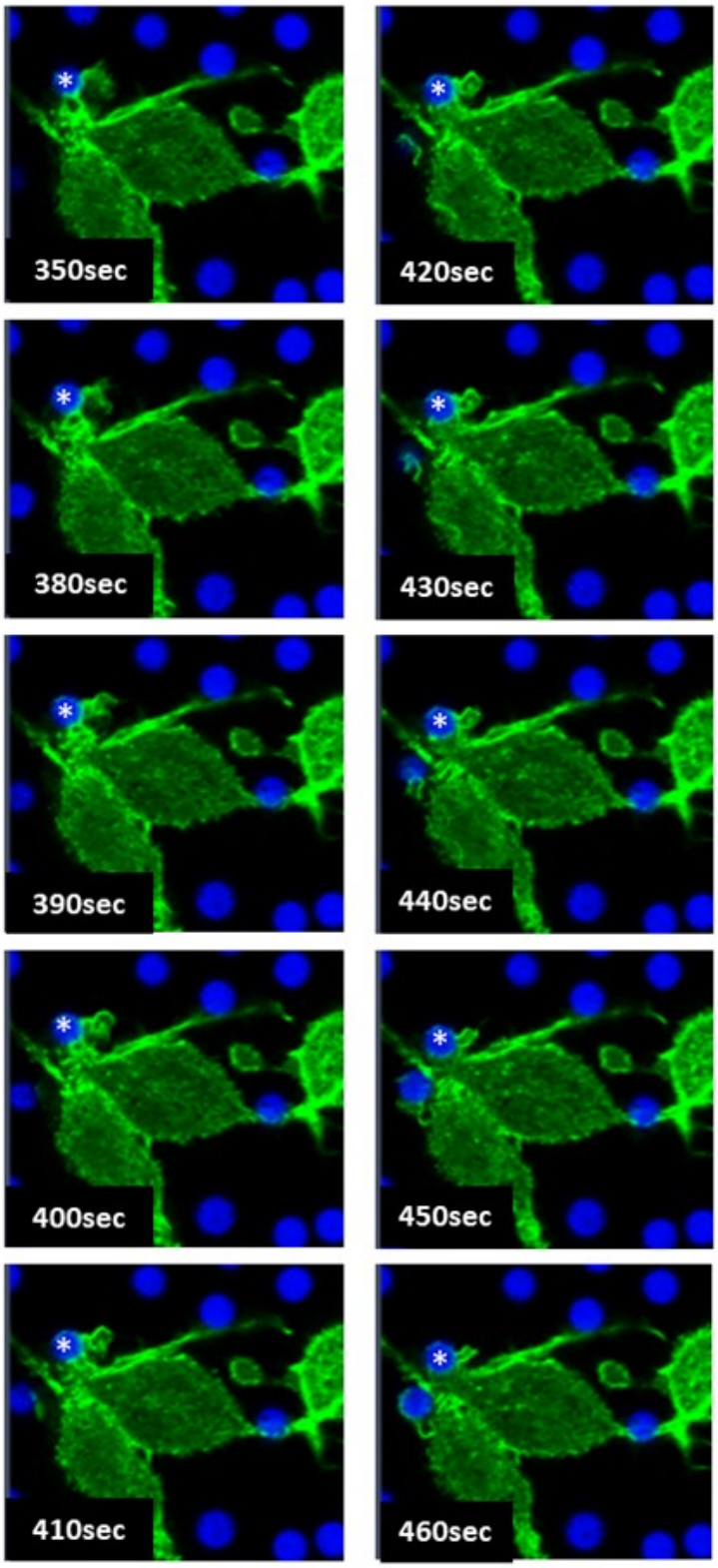
350sec
420sec
380sec
430sec
390sec
440sec
400sec
450sec
410sec
460sec

FIGURE 6.6

E.

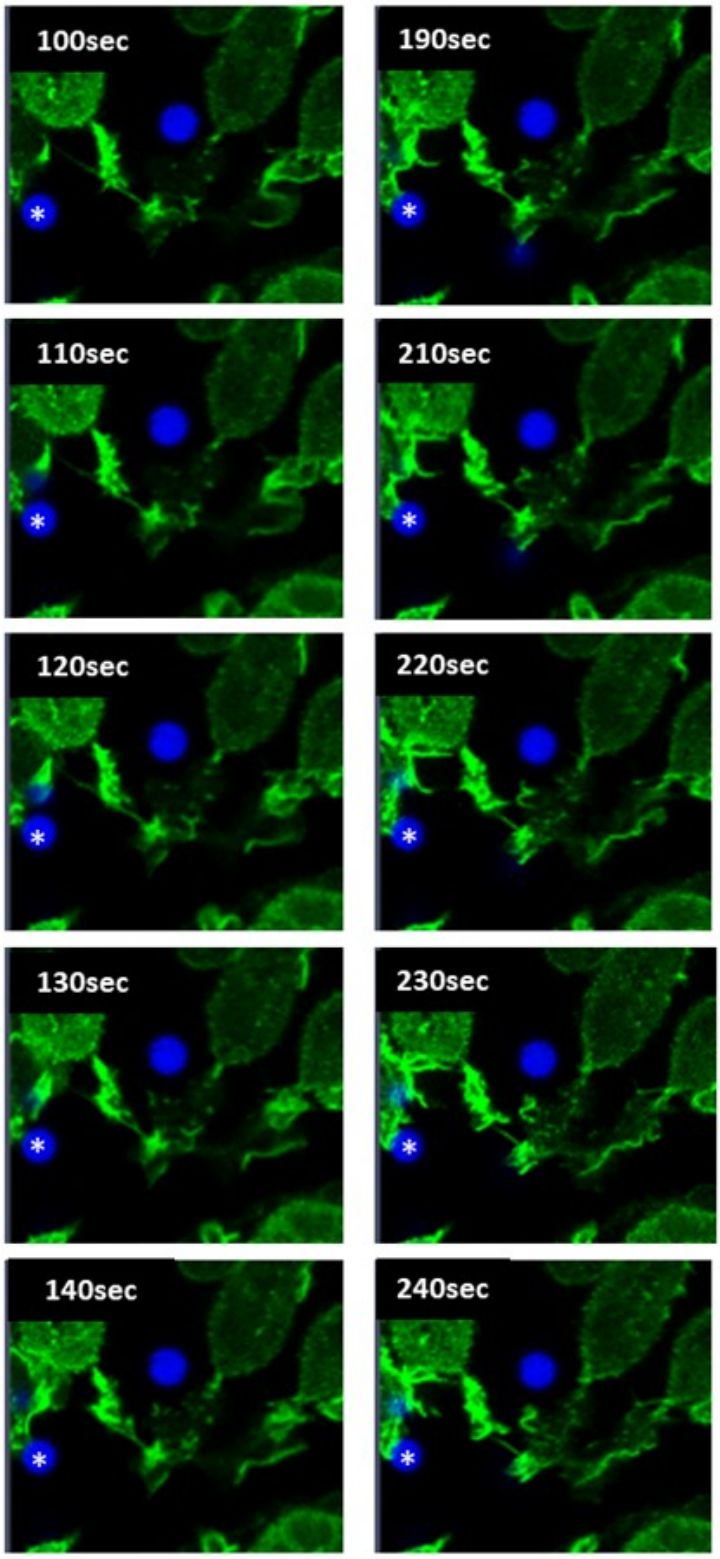
100sec
190sec
110sec
210sec
120sec
220sec
130sec
230sec
140sec
240sec

FIGURE 6.6

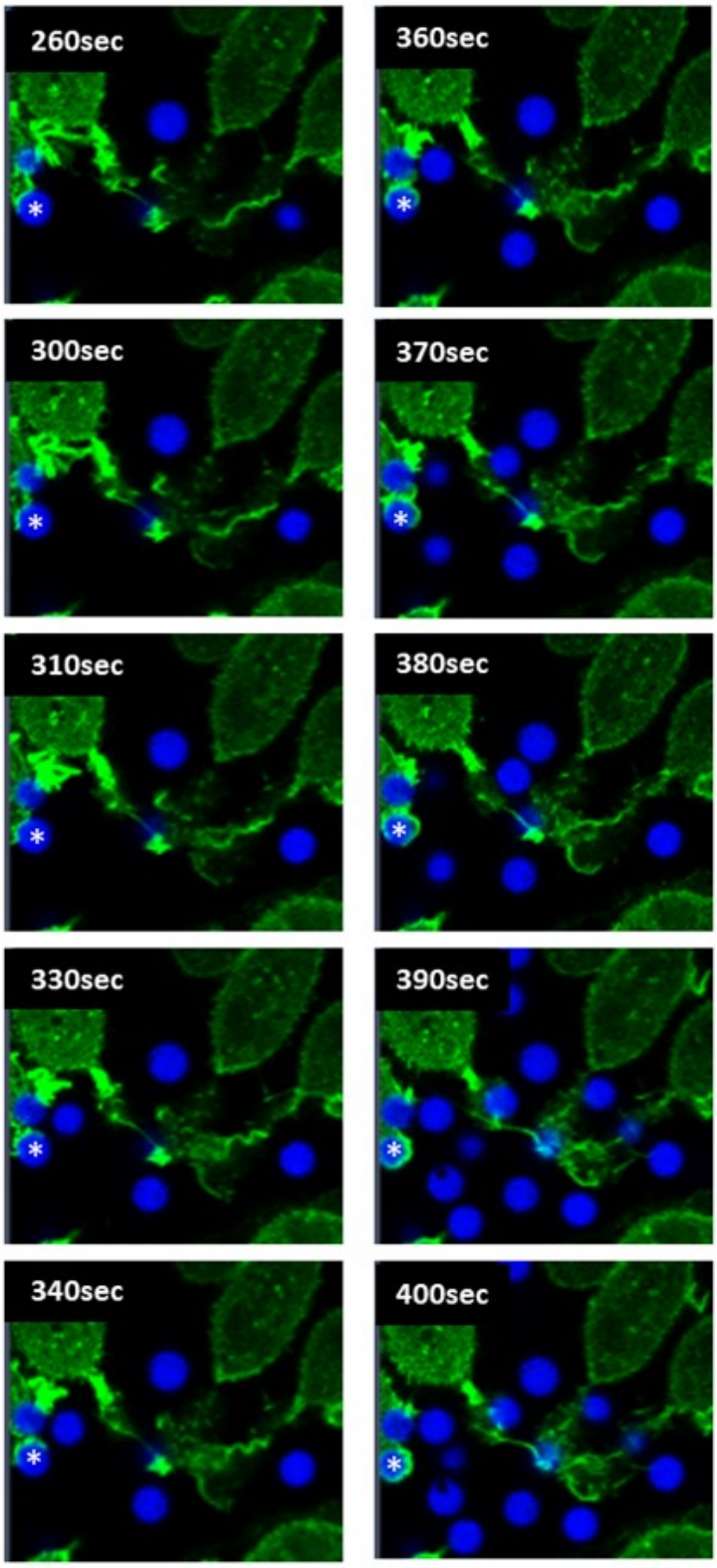
260sec
360sec
300sec
370sec
310sec
380sec
330sec
390sec
340sec
400sec

FIGURE 6.6 Examination of IpLITR 1.1b-mediated target interactions at 27 ^{o}C. RBL-2H3 cells ($3x10^{5}$) stably co-expressing IpLITR 1.1b and LifeAct-GFP were incubated at 27^{o}C with $9x10^{5}$ αHA mAb-coated 4.5 μm bright blue microspheres. Immediately after the addition of target beads, images were collected at 10 sec intervals for ~8 min using a Zeiss LSM 710 laser scanning confocal microscope (Objective 60x, 1.3 oil plan-Apochromat; Munich, Germany) and are shown for a series of representative phenotypes in A-E. Beads of interest are indicated with an asterisk.

FIGURE 6.7

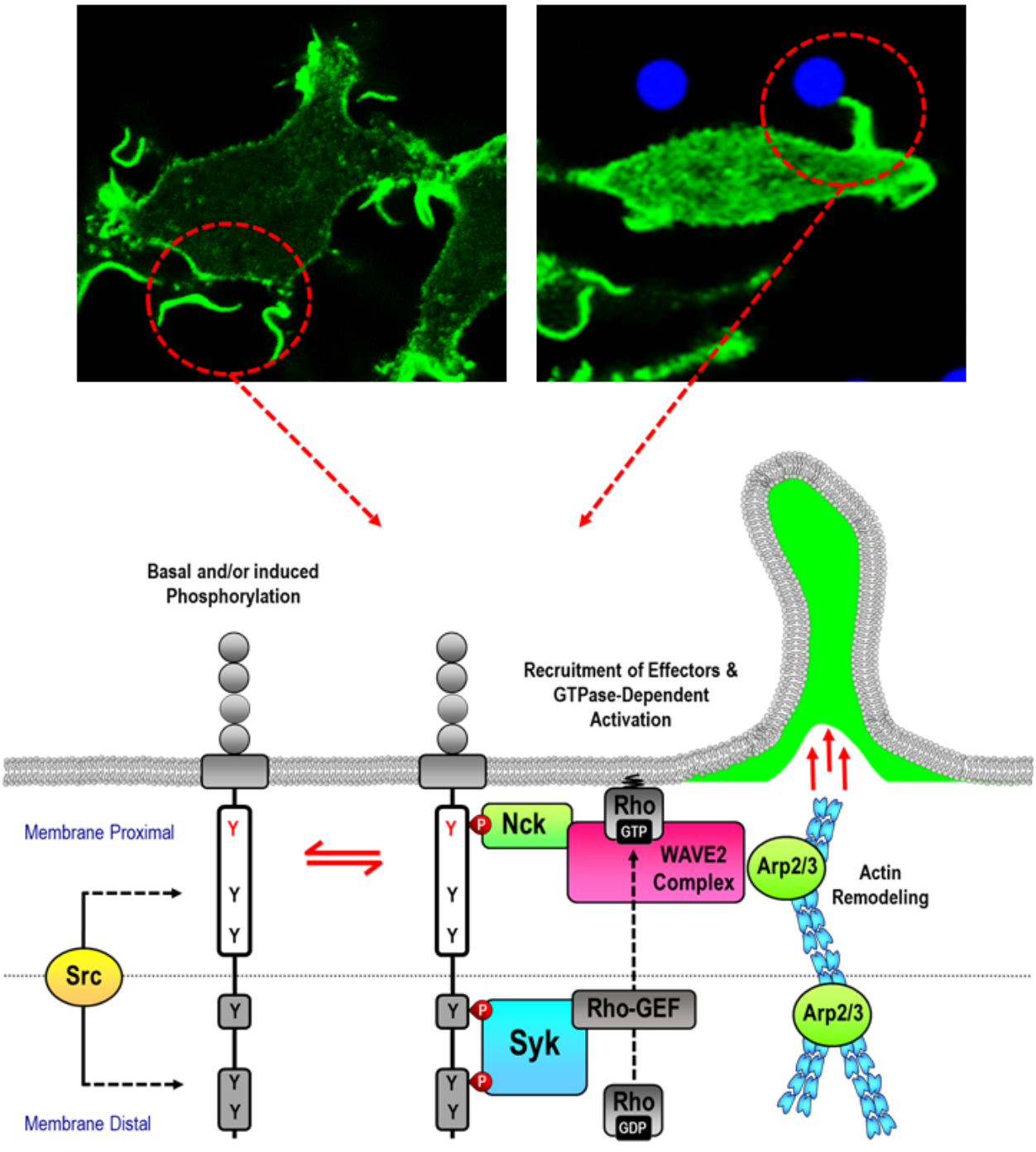
Basal and/or induced
Phosphorylation
Recruitment of Effectors &
GTPase-Dependent
Activation
Membrane Proximal
Membrane Distal
Src
Y
Y
Y
Y
Y
Y
Y
Y
Y
Y
Nck
Rho
GTP
WAVE2
Complex
Arp2/3
Actin
Remodeling
Arp2/3
Rho-GEF
Syk
Rho
GDP
P

FIGURE 6.7 Hypothesized mechanism of IpLITR 1.1b-mediated phagocytic target capture and tethering. Diagram representing hypothesized model of IpLITR 1.1b's mechanism for F-actin polymerization events associated with target capture/tethering phenotype. In this model Nck (proximal) and Syk (distal) are recruited to specific portions of IpLITR 1.1b's CYT to promote filopodia and/or tethering activities.

CHAPTER VII

EXAMINATION OF SYK AND NCK RECRUITMENT BY CATFISH LEUKOCYTE IMMUNE-TYPE RECEPTORS DURING FILOPODIA-MEDIATED TARGET CAPTURE AND ENGULFMENT

7.1 INTRODUCTION

Based on results obtained from Chapter VI the stable expression of IpLITR 1.1b but not IpLITR 2.6b/IpFcRγ-L, specifically triggers RBL-2H3 cells to induce filopodia formation. IpLITR 1.1b-mediated signaling also initiates secondary waves of actin polymerization events that are associated with the internalization and membrane tethering of extracellular targets. As discussed in the last chapter, I hypothesized that pre-association of IpLITR 1.1b with intracellular effectors capable of modulating the cytoskeletal machinery would allow for dynamic membrane remodeling events prior to the formation of stable receptor-ligand interactions [29,30,31]. Furthermore, the target acquisition and engulfment pathways facilitated by IpLITR 1.1b likely require the differential participation of its unique membrane proximal and distal CYT regions in the recruitment and activation of select intracellular effectors [46,47].

IpLITR 1.1b contains six tyrosine residues within its CYT region. The membrane proximal CYT region tyrosines (Y_{433}, Y_{453}, and Y_{463}) are not embedded within any known inhibitory or stimulatory signaling motifs (i.e ITIMS or ITAMs), whereas its membrane distal CYT region tyrosines (Y_{477}, Y_{499}, and Y_{503}) are positioned within two ITIM and one ITSM motif. Although the functional recruitment of signaling molecules to the CYT of IpLITR 1.1b has yet to be investigated, previous work done by our lab has led to some possible intracellular regulators as candidates. For example, IpLITR 1.1b may be recruiting Nck to assemble regulators of actin polymerization, including WAVE2 to the plasma membrane. This interaction may occur by

WAVE2 indirectly associating with IpLITR 1.1b using the adaptor protein Nck, which could possibly bind the proximal IpLITR 1.1b CYT region at the motif H-I-Y-D-E-V located at Y_{433} in [66]. This would bring key components of the actin polymerization machinery into proximity of stimulatory GEFs at the membrane; formulating the necessary tools for F-actin polymerization events to occur. Together, this would encompass the minimal machinery required for promoting local rearrangements of the actin cytoskeleton during target capture. Although direct recruitment of Nck to IpLITR 1.1b has yet to be confirmed, biochemical studies performed in our lab suggest that Nck may be recruited specifically to its proximal CYT region [192]. Alternatively, Syk may bind the distal CYT region of IpLITR 1.1b by interacting with phosphorylated tyrosines Y_{477} and Y_{499} that are positioned in two tandem ITIM motifs. As shown by others, certain spacing of tyrosines within consecutive ITIMs can accommodate the two Src homology 2 domains of Syk thus providing a unique docking site for this kinase [105]. If recruited to IpLITR 1.1b, I predict that Syk would then bind and activate an intracellular Rho-GEF that could then directly regulate one of the many known Rho GTPases that are responsible for controlling rapid actin-driven membrane dynamic remodeling through activation of Arp2/3 and the WAVE2 complex. Unfortunately, biochemical associations of Syk and Nck with IpLITR 1.1b do not confirm if these molecules are indeed relevant for IpLITR 1.1b-mediated responses, nor does it indicate at which phases of IpLITR 1.1b-mediated phagocytosis they may be associated with. However, this proposed mechanism provides the basic framework for further exploring a new mode of ITAM-independent phagocytosis facilitated by IpLITR 1.1b.

Based on the proposal that Syk and Nck are key players in the IpLITR 1.1b-mediated regulation of membrane dynamics, the primary focus of this chapter was to develop immunofluorescence-based imaging protocols to directly examine the recruitment of Syk and

Nck during IpLITR 1.1b-induced formation of filopodia and the capture and engulfment of targets. Specifically, I first wanted to determine whether Syk and Nck are present in constitutively generated filopodia-like structures in the absence of extracellular targets. Then using my bead-based phagocytosis protocol, plasma membrane-target interactions were used to qualitatively assess the dynamics of Syk and Nck accumulations during IpLITR 2.6b/IpFcRγ-L and IpLITR 1.1b-mediated activation of the phagocytic process. Results of this chapter demonstrate for the first time that Nck but not Syk colocalize with IpLITR 1.1b within constitutively generated filopodia structures. Furthermore, during the various phases of IpLITR 1.1b-mediated target binding, capture, and engulfment, both Syk and Nck were found to specifically accumulate at cell-target interfaces. Overall, these results provide a first look at the unique dynamics of IpLITR 1.1b-mediated molecular recruitments during F-actin-dependent membrane dynamics and provide new details regarding Syk and Nck recruitments during ITAM-dependent and independent phagocytic modes.

7.2 RESULTS

7.2.1 pSyk and Nck expression patterns in IpLITR-expressing RBL-2H3 cells

To examine the expression and potential colocalization of pSyk with IpLITRs, parental RBL-2H3 cells (Fig. 7.1A), IpLITR 2.6b/IpFcRγ-L-expressing (Fig. 7.1B), and IpLITR 1.1b-expressing RBL-2H3 stables (Fig. 7.1C) were co-stained with an αHA mouse mAb (red; to detect IpLITR expression) and an α-rabbit mAb specific for phosphorylated tyrosine's Y_{525}/Y_{526} Syk (green) followed by confocal imaging and colocalization analysis. In each staining experiment, three representative regions of three different cells were analyzed in areas that approximated the relative positions of their plasma membranes (see i-ix on Fig. 7.1A for an example, left panels). The z-stack images located at these specific regions were independently

analyzed using colocalization analysis software (Imaris 9.2.1). These z-stack images at each region were isolated from individual cells and then were used for colocalization analysis. For colocalization analysis, Pearsons correlation coefficient (PCC) was chosen as the measure within the selected regions, since it measures the correlation of localization between two intensities within a 3D volume and indicates whether the associations of two overlapping signals are greater than random chance. In general, a PCC value below 0.5 is deemed inconclusive on whether two stains are colocalized [260] while a PCC value of 1.0 indicates complete colocalization. As shown in Figure 7.1A, no IpLITR signal (red) is observed using αHA staining but a pSyk signal (green) was detected in the selected regions (i-ix). PCC values calculated for these parental cells ranged from 0.09 to 0.33 (Fig. 7.1D), indicating a negative result for colocalization. When IpLITR 2.6b/IpFcRγ-L-expressing cells were examined for receptor (red) and pSyk expression (green), both proteins were detected but based on the calculated PCC values (e.g. 0.06 to 0.40) in the defined areas (i.e. i-ix), these two proteins did not colocalize (Fig. 7.1D). Similar results were also obtained using IpLITR 1.1b-expressing cells, which showed no significant receptor and pSyk colocalization in all areas of the plasma membrane examined; including those that contained extended filopodia-like structures (Fig. 7.1C; i-ix and Fig. 7.1D).

When examining Nck expression patterns in parental RBL-2H3 cells and IpLITR stables (Fig. 7.2), it was once again shown that parental RBL-2H3 cells (Fig. 7.2A) and IpLITR 2.6b/IpFcRγ-L-expressing stables (Fig. 7.2B) did not feature significant colocalization values between αHA and α-Nck staining (Fig. 7.2D). In contrast, based on the areas analyzed in Figure 7.2C (i-ix), IpLITR 1.1b-expressing cells showed a dramatic increase in their PCC values for regions ii (0.84), iii (0.83), v (0.90), vi (0.88), viii (0.83), and ix (0.74). Importantly, these regions all contained filopodia-like structures unlike regions i, iv, and vii, which did not (Fig.

7.2C). On average, IpLITR 1.1b PCC values for Nck were significantly different from those values obtained for parental RBL-2H3 cells and IpLITR 2.6b/IpFcRγ-L as shown in the summary graph (Fig 7.3; black bars) whereas PCC values obtained for pSyk were not significantly different among all three cell-types (Fig. 7.3; white bars). A positive colocalization control experiment is provided in Figure 7.4. This control was generated by incubating IpLITR 1.1b-expressing cells with an αHA mouse mAb and then subsequently staining the cells with two different goat α-mouse IgG secondary antibodies; one conjugated to Alexa-488 probe while the other being conjugated with an Alexa-647 probe. Since both secondary antibodies have the same specificity (i.e. mouse IgG) these probes overlap perfectly with one another at positions of the IpLITR 1.1b (i.e. αHA staining). This control experiment shows consistent high-level PCC values (0.7-0.94) indicating a positive colocalization results in all areas examined (Fig 7.4).

7.2.2 pSyk recruitment patterns during IpLITR 2.6b/IpFcRγ-L-mediated regulation of phagocytosis

To examine pSyk recruitment specifically at the sites of IpLITR activation, an imaging based phagocytic assay was performed using both IpLITR 2.6b/IpFcRγ-L and IpLITR 1.1b-expressing RBL-2H3 cells. Here, αHA mAb opsonized beads were incubated with IpLITR-expressing cells that were subsequently stained for intracellular pSyk using α-rabbit conjugated Cy3 probe (red) and a fluorescent marker to identify extracellular exposed beads using a α-mouse IgG conjugated Cy5 probe (to detect the αHA mAb coated on the beads in the far-red fluorescent channel; coloration of blue changed post image capturing). The principle here is that internalized beads are protected by the plasma membrane and thus are not accessible to antibody staining. Therefore, any exposed surfaces of the beads that are not in close contact with the cell membrane or contained within the cell will be stained blue. Representative examples of pSyk

staining patterns during IpLITR 2.6b/IpFcRγ-L-mediated phagocytosis are shown in Figures 7.5 to 7.8. For each figure, shown are the confocal z-stack images (A), 3D reconstructed images (B), and a staining intensity histogram (C) that provides MFI intensities for pSyk (red) as well as the extracellular exposed areas of the selected beads (blue). Arrows in (B) and (C) indicate the areas of the image that were then analyzed to calculate the MFI. In each image the direction of analysis for the MFI values are indicated by the arrow over a specific distance across the image (C; x-axis = distance in μm).

In Figure 7.5A, an extracellular bead (blue; asterisk) appears loosely associated with the surface of an IpLITR 2.6b/IpFcRγ-L-expressing cell (green). This is evident by the fact that bead staining (blue ring) can be observed completely around the outer edges of the target (Fig 7.5A; top left image). This is also indicated by the high MFI values (~40,000 MFI) calculated in the blue channel (Fig 7.5C; blue line; 1.55 μm and 6.20 μm). While this target appears to be in contact with the cells surface (green), very little recruitment of pSyk is observed at the interface between this bead and the cell (Fig 7.5A; top right panel). This also correlates with relatively low MFI values in the red channel (~10, 000) calculated along the arrow (Fig 7.5C; red line). In Figure 7.6, what appears to be a partially engulfed bead (*) is identified since it has reduced bead-staining intensities (blue) specifically at the bead-cell contact site (Fig 7.6A). Conversely, at this interface, pSyk staining is clearly visible (Fig 7.6A and 7.6B) and the overall MFI for both bead (blue line) and pSyk (red line) are displayed in the histogram (Fig. 7.6C). Specifically, the extracellular exposed region of the bead has a relatively large MFI value of ~40,000 (Fig 7.6C; 1.55 μm), whereas at the bead-cell interface the bead staining intensity is lower (Fig 7.6C; 6.20 μm, ~10,000 MFI). This measured loss of bead staining at the bead-cell interface is accompanied by an increased intensity of pSyk accumulation at this site (Fig 7.6C; 6.20 μm, ~30,000). The

next figure shows an overall circular pSyk staining profile around what appears to be a completely engulfed bead (e.g. this bead displays no blue staining; Fig. 7.7A and 7.7B). The increased levels of pSyk staining (red line) are shown as two distinct peaks in Figure 7.7C (e.g. ~20, 000 MFI at 2.33 μm, and ~30,000 MFI at 6.20 μm) where no extracellular bead staining (blue line) is observed. Finally, in what also appears to be a completely engulfed target, neither extracellular bead staining (blue) nor pSyk staining (red) are observed at any relative position around the bead (Fig. 7.8A and 7.8B asterisk). This lack of staining is also clearly shown on the MFI histogram plot (Fig. 7.8C).

7.2.3 pSyk recruitment patterns during IpLITR 1.1b-mediated regulation of phagocytosis

Representative examples of IpLITR 1.1b-mediated pSyk recruitments during target capture and engulfment processes are shown in Figures 7.9 to 7.13. In the first example, two individual beads (*, ⊙) are each attached to F-actin (green) containing membrane structures at two different positions (Fig. 7.9A and 7.9B). At each of the cell-bead interfaces, pSyk staining (red) is observed, and these contact sites are also associated with low levels of extracellular bead staining (blue). For example, using the arrow to mark the MFI for bead and pSyk staining, each bead shows pSyk intensity peaks (Fig. 7.9C, red line) at each point of membrane-bead contact resulting in four distinct histogram peaks (e.g. at locations 1.40 μm, 5.58 μm, 11.16 μm, and 13.95 μm all have MFI values >20,000). These same positions also have relatively low bead staining intensities (Fig. 7.9C). Figure 7.10 shows two beads (* and ⊙) associated within what appears to be a continuous F-actin rich membranous extension (green) or filopodia-like structure. However, unlike the two beads shown in Figure 7.9, one of these beads (⊙) is completely surrounded by the membrane while the second bead (*) is only partially engulfed. Once again, at the membrane-target interface, reduced bead staining is evident at this position for bead (*), but

increased pSyk staining is observed at the same site (Fig. 7.10A and 7.10B). For the other target (⊙), no bead staining is observed but it is contained within a distinct ring of pSyk (Fig. 7.10A and 7.10B). The overall MFI profiles for these images are shown in Figure 7.10C, once again demonstrating the nature of pSyk patterning at the various bead-cell interfaces.

Another example of pSyk recruitment at the bead-cell interfaces of IpLITR 1.1b-expressing cells is shown in Figure 7.11. Here a bead (blue) is attached to the cell (green) in what appears to be a phagocytic cup-like structure (Fig. 7.11A). The side of the bead that contacts the cell is devoid of blue staining, but this interface does contain a clear ring of pSyk (Fig. 7.11A and 7.11B; red staining). An MFI profile staining histogram for this target-cell interaction is also provided in Figure 7.11C. A similar cell-bead phenotype is observed in Figure 7.12, showing multiple surface attached targets with underlying pSyk staining at the bead-cell interfaces. In this figure, two specific beads of interest are indicated by the symbols * and ⊙, and these where used to create the MFI intensity histogram (Fig. 7.12C). Lastly, shown in Figure 7.13 is the recruitment of pSyk to a bead that has undergone complete engulfment by an IpLITR 1.1b-expressing cell. This is suggested by a lack of extracellular bead staining (Fig 7.14A; top left image) as well as a significant localization of pSyk at that the same position (Fig 7.14C; top right image). MFI calculations across the bead (Fig. 7.13B) show a relatively large recruitment of pSyk at the location of the bead proximal to the cell (Fig. 7.13C; 2.33 μm, ~40,000 MFI). These values gradually diminish as the arrow approaches the membrane distal face of the bead (Fig 7.14C; 6.20 μm, ~20,000 MFI) and throughout the histogram, no extracellular bead (blue line) staining is observed. Overall, these results show that IpLITR 1.1b-expressing RBL-2H3 cells recruit pSyk during various the various stages of extracellular target capture and engulfment.

7.2.4 Nck recruitment patterns during IpLITR 2.6b/IpFcRγ-L-mediated regulation of phagocytosis

To examine Nck recruitment dynamics during IpLITR-mediated phagocytosis, a similar imaging-based phagocytic assay was performed as described above, however, for these experiments IpLITR-expressing cells were subsequently stained using an α-Nck rabbit mAb. Extracellular regions of the target beads were once again identified using an anti-mouse IgG conjugated Alexa-647 probe (to detect the αHA mAb coated on the beads in the blue fluorescent channel). The first representative example of Nck recruitment during IpLITR 2.6b/IpFcRγ-L-mediated phagocytosis is shown in Figure 7.14. Here, three different beads (*, ⊙, ❍) are selected for analysis. The first bead (*) is attached to the cell (green) by a phagocytic cup-like structure and Nck (red) is observed at the base of the bead-cell interface (Fig 7.15A). Most of this bead is stained blue indicating that its contact with the cell is likely recent, although Nck accumulation has begun to occur. A higher resolution of the Nck-containing structure formed at the bead-cell contact site is provided in the 3D rendered image (Fig. 7.14B) and the MFI histograms for F-actin (green line), bead (blue line), and Nck (red line) are shown for bead (*) in Figure 7.14C (top panel). The second bead (⊙) analyzed appears to have been completely internalized by the cell as indicated by the significant loss of bead (blue) staining (Fig 7.14A). This bead is also surrounded by a ring of Nck (red) stain (Fig 7.14A and 7.14B) as measured in its MFI histogram plot (Fig. 14C, middle panel). Lastly, the third bead (❍) is also engulfed showing no significant extracellular bead staining but with a relatively high overall intensity of Nck at the bead-cell interfaces (Fig. 7.14). Two additional representative examples showing the staining patterns for F-actin, bead, and Nck are provided in Figures 7.15 and 7.16.

7.2.5 Nck recruitment patterns during IpLITR 1.1b-mediated regulation of phagocytosis

Due to the dynamic plasma membrane structures (i.e. filopodia) formed by IpLITR 1.1b-expressing cells, both individual bead-cell contacts as well multiple contact events along filopodia-like structures for a given image were analyzed based on Nck (red), F-actin (green), and extracellular bead staining (blue). In Figure 7.17, three beads (*, ⊙, ❍) are imaged at a stage where they are all captured by an elongated F-actin (green) containing structure (Fig. 7.17A and 7.17B). While the majority of these beads remain exposed to the extracellular environment (blue), a reduction in blue fluorescence is observed at the sites where Nck staining intensities are the highest. This is easily seen in the z-stack (Fig. 7.17A) and 3D rendered images (Fig. 7.17) and is quantified using the MFI histogram (Fig. 7.17C). Each of the beads captured along this filopodia-like structure were also individually analyzed for relative Nck accumulations relative to the bead and F-actin stains (Fig. 7.17D). This once again shows that at the interface between the filopodia and the bead surface, all captured targets displayed their highest MFI for Nck at these positions. Another excellent representation of the dynamics of Nck recruitment during filopodia-mediated capture of beads is shown in Figure 7.18. Using the arrow as a guide, prior to target contact an F-actin and Nck-rich membrane extension contacts one bead (*) and then a second bead (⊙). Although a large portion of these beads are not surrounded by the cell membrane (blue stain), discrete pockets of Nck staining around the beads are observed (Fig. 7.18A and 7.18B). As quantified in the MFI histograms, three clear Nck peaks are featured at the contact positions 8.06 μm, 12.09 μm, and 15.12 μm (Fig. 7.18C) and each bead is also individually analyzed for their staining dynamics (Fig. 7.18D). Continuing with the theme of filopodia-mediated target capture by IpLITR 1.1b-expressing cells, Figures 7.19 and 7.20 provide two additional examples showing various Nck recruitment dynamics relative to F-actin

and extracellular bead positions along these uniquely IpLITR 1.1b generated structures. Finally, Figure 7.21 shows several beads secured on the surface of an IpLITR 1.1b-expressing cells, and two of these targets (* and ⊙) have been analyzed in detail.

7.3 DISUCSSION

The goal of this thesis chapter was to investigate the possible roles of two key F-actin polymerization effector proteins, Syk and Nck, during IpLITR 1.1b-induced filopodia formation and filopodia-mediated target capture and engulfment. First, I examined if pSyk and/or Nck colocalized with IpLITR expression in stably transfected RBL-2H3 cells in the absence of target microspheres. These experiments were performed by fluorescently co-labeling the surface expressed IpLITRs (using an αHA mAb) with the intracellular proteins pSyk and Nck. Then using confocal imaging and colocalization software, I calculated the likelihood that IpLITRs endogenously interacted with pSyk and/or Nck in different regions of the plasma membrane. Colocalization of protein-protein interactions was calculated using the Pearsons Correlation Coefficient (PCC) value, which has been used in a variety of other studies [261,262], indicating that this is an accepted method for detecting colocalization using fluorescent confocal imaging. For example, colocalization of Nck with the cytoskeletal structural protein paxillin in membrane protrusions was demonstrated using PCC colocalization analysis [261]. In my study, the positive control images consistently had high PCC values (>0.7) regardless of whether I calculated PCC values at the plasma membrane surface or at locations where filopodia-like structures were generated indicated that I could indeed detect the colocalization of proteins in stained images. Using this method, I showed that that Nck (PCC >0.7) colocalizes within membrane regions containing IpLITR 1.1b-generated filopodia structures but not at locations of the plasma membrane surface where filopodia where not produced. Importantly, unlike Nck, the pSyk PCC

values for IpLITR 1.1b-expressing cells were below the threshold for colocalization in IpLITR 1.1b-generated filopodia structures. Colocalization between IpLITR 1.1b and Nck was also supported by the fact that neither Nck nor pSyk produced significant PCC values (i.e. <0.5) when parental RBL-2H3 cells or IpLITR 2.6b/IpFcRγ-L-expressing cells were examined. Overall, the predicted interaction of Nck with IpLITR 1.1b in filopodia structures supports previous biochemical studies from our lab, which showed that Nck binds to the transmembrane proximal CYT region of IpLITR 1.1b [192]. This interaction likely occurs at the predicted Nck binding consensus motif located at Y_{433} (H-I-Y-D-E-V) [3]. Combined with my observations that IpLITR 1.1b and Nck colocalize in constitutively generated filopodia, stable interaction between IpLITR 1.1b and Nck is likely a key component of the mechanism required for the constitutive generation of dynamic F-actin containing filopodia by IpLITR 1.1b-expressing cells.

Nck and Syk have been identified as major regulatory proteins for F-actin polymerization events in a wide variety of cellular process [213]. Nck is an adaptor/scaffolding protein containing one SH2 and three SH3 binding domains which play important roles in receptor induced signaling events [213]. As a scaffolding protein devoid of enzymatic activity, Nck is important for connecting other intracellular signaling proteins together at sites of receptor activation via its SH3 binding domains and it known to have more than 60 binding partners [213]. Nck is involved in multiple receptor-induced phagocytic responses such as those initiated by FcR, CEACAM3, and CEACAM4 [3,7,109]. As a facilitator of signaling complex formation, Nck promotes the recruitment of signaling proteins in a receptor-specific manner to the plasma membrane to induce activation of the Arp2/3 complex, thereby causing localized F-actin polymerization events necessary for phagocytosis to occur. Interestingly, Nck has also been shown to be involved in both filopodia and invadopodia formations [246,263,264]. Filopodia are

extracellular membranous extensions used by cells for a variety of cellular processes including cell mobility, wound healing, and the capturing of extracellular targets [235,242,250,251]. As exploratory structures, filopodia are characterized by their abilities to extend into surrounding extracellular environments and act as sensory structures for cells by relaying extracellular information to the cell via certain receptors [235,237,238,242]. Invadopodium are a specialized type of extracellular extensions, which are associated with many metastatic cancers [244,264,265]. Functionally, invadopodium allow aggressive forms of cancerous cells to transverse across epithelial barriers by breaking down the extracellular matrices between layers and form secondary tumors [245,265]. Like its role in phagocytosis, Nck is important for facilitating multiple protein-protein interactions between F-actin polymerization machinery molecules to sites of filopodia formation thereby promoting the generation and extension of filopodia/invadopodium into the extracellular environment [109,261,263,265,266]. Unlike the scaffolding role of Nck, Syk-associated phagocytic responses rely on its enzymatic activity as a non-receptor tyrosine kinase to initiate downstream signaling events leading to F-actin polymerization and phagocytosis. Syk contains two SH2 domains, which it uses to bind tandem phosphorylated tyrosines within an ITAM located within the CYT region of many stimulatory receptor-types [104]. Syk also contains a kinase enzymatic domain for inducing phosphorylation of other intracellular proteins [267]. In general, tyrosines within the ITAM are phosphorylated via Src-family kinases at the initial stages of receptor activation post ligand-receptor interactions. This initial phosphorylation event then induces both the binding and activation of Syk to activated receptors [103,206,267]. The activated kinase domain of Syk then induces the phosphorylation of downstream signaling molecules which leads to the formation of signaling complexes at the sites of activated receptors on the membrane [267]. Newly phosphorylated

proteins then promote subsequent downstream signaling events and the formation of signaling complexes which results in the induction of F-actin polymerization [101,103,109,267]. Due to its vital signaling role in F-actin polymerization, Syk is required for many receptor-induced phagocytic responses including classical phagocytic receptors such as FcR and Dectin-1 [63,103,105,123] as well as non-classical phagocytic receptors such as MARCO, CD13, JEDI-10, CD44, and CEACAM3 [3,6,7,268–270]

The second main objective of this chapter was to examine the recruitment of pSyk and Nck at sites of receptor activation during the IpLITR-mediated phagocytic process. This was accomplished by first incubating either IpLITR 1.1b or IpLITR 2.6b/IpFcRγ-L-expressing cells with αHA mAb opsonized targets to engage and activate the receptors. Subsequently, beads were stained with a fluorescently-labelled secondary anti-mouse Ab to determine their relative associations with the plasma membrane. The presence of pSyk and Nck were detected after permeabilizing the cells and staining them commercially purchased antibodies specific for these intracellular molecules. Extracellular beads were readily detected in the blue fluorescent channel as their entire surface was accessible to the secondary antibody. However, as the target beads were bound and progressively surrounded by plasma membrane, these bead-membrane interfaces excluded secondary antibody staining, which diminished the observed staining at these specific locations. This was qualitatively assessed as a reduction in the mean fluorescence intensity (MFI) using imaging software. pSyk and Nck intracellular staining intensities were similarly examined using MFI to qualitatively measure their signal intensities at specified locations during the various stages of IpLITR-mediated phagocytosis. For these experiments, IpLITR staining was not directly measured but as previously described, these receptors are specifically engaged using the αHA mAb opsonized targets (i.e. bead-membrane contacts represent the sites of IpLITR

engagements and are a proxy for IpLITR-induced signaling events). A similar approach has also been used to track the recruitment and activation of other intracellular signaling effectors to various immune receptor-types. For example, the localization of the T-lymphocyte specific tyrosine kinase Lck in CD8+ T cells was identified by measuring MFI values along a cross sectional line during CD8+ T cell stimulation [271] and another example was shown in the previously mentioned Nck-paxillin colocalization study [261]. Here, authors also demonstrated the localization of Nck and paxillin to the leading edges of membrane protrusions by measuring signal intensities of both mCherry labelled Nck and YFP labelled paxillin. This was done by measuring GFP-Nck and YFP-paxillin signal intensities (i.e. MFI) and showed preferential localization of Nck/paxillin to regions within plasma membrane protrusions [261].

As anticipated, IpLITR 2.6b/IpFcRγ-L-expressing cells recruited both pSyk and Nck at the bead-cell interfaces. The patterning of these molecules observed through representative images of IpLITR 2.6b/IpFcRγ-L-expressing cells were consisted with the phases of the phagocytic process described previously in my thesis and mirrored that of other classical ITAM-induced response [2,85]. For instance, when a bead was loosely associated with the membrane, little to no Nck or pSyk was measured at this site. As the level of bead engagements progressed, the loss of bead staining correlated with the recruitment of pSyk and Nck at the bead-cell interface; a response expected to occur during receptor activation. Once the bead was completely engulfed, indicated by the total loss of bead staining, both pSyk and Nck staining were progressively reduced; indicating that IpLITR 2.6b/IpFcRγ-L-mediated signaling events were no longer required for F-actin mediated engulfment of the target. My observed pSyk and Nck recruitment patterns during the phagocytic process also correlate with the responses observed for other ITAM-induced phagocytic receptors such as FcR and CECAM3 [3,103,108]. IpLITR 1.1b-

expressing cells also showed recruitment of both pSyk and Nck at the bead-cell interfaces suggesting the recruitment/activation of these molecules in response to IpLITR 1.1b engagements. Recruitment of both Nck and pSyk was observed at beads positioned at the leading edge or on the surface of filopodia-like structures as well as on the exterior of cells, suggesting that these molecules may be important for the initial capturing phase as well as the tethering/engulfment phenotype elicited by IpLITR 1.1b-expressing cells. As mentioned above, if IpLITR 1.1b endogenously associates with Nck, then it is not surprising that it also localizes at regions of bead-cell interactions. Alternatively, it may also be possible that Nck binds newly activated IpLITR 1.1b receptors situated at the cell-bead contact sites and therefore may be a distinct Nck recruitment event from that of the constitutive association described above. The observed pSyk recruitment to IpLITR 1.1b at the sites of plasma membrane-bead interfaces is surprising since this receptor does not contain a classical ITAM within its CYT region. However, a unique mechanism might exist whereby the tandem SH2 domains of pSyk are accommodated by phosphorylated tryrosines within two tandem ITIMs present within the IpLITR 1.1b CYT. In chapter VI, I hypothesized that this interaction likely takes place at the tandem ITIMs located specifically at Y_{477} and Y_{499}. A similar mechanism has also been demonstrated for the ITIM-containing surface receptor PECAM-1 which has two ITIMs situated 22 amino acids apart, a distance that was shown to accommodate pSyk binding [105]. Interestingly, 22 amino acids separate the tyrosine residues located within the IpLITR 1.1b CYT ITIMs and therefore could act as a possible docking site for pSyk binding. Additionally, as previously shown in chapter IV, inhibition of Syk enzymatic properties reduced phagocytic activities of IpLITR 1.1b-expressing cells, reinforcing a possible role of pSyk in IpLITR 1.1b-mediated responses. Although I was unable to directly identify the position of the receptors at the bead-cell interface, the recruitment

of pSyk and Nck to these sites specifically was used as a proxy for receptor activation as pSyk and Nck staining was significantly localized at the bead-cell interaction sites. Overall these results provide further evidence in support of the hypothesis that Nck and pSyk are important regulators of IpLITR 1.1b-mediated generation of dynamic F-actin containing membranous protrusions (i.e. filopodia). These structures are constitutively produced by IpLITR 1.1b-expressing cells and can facilitate the binding, capture, and eventual engulfment of extracellular targets.

Data presented in this chapter provides new evidence regarding the proximal signaling events that occur during teleost immunoregulatory receptor-mediated phagocytosis and insights into the mechanism(s) associated with IpLITR 1.1b-induced cellular responses. My imaging, colocalization, and recruitment data clearly show interactions of a teleost ITIM containing receptor (i.e. IpLITR 1.1b) with intracellular effector proteins that are instrumental for regulating F-actin polymerization cellular responses. Specifically, my data suggests that IpLITR 1.1b endogenously colocalizes with Nck in filopodia-like plasma membrane structures and suggests that IpLITR 1.1b-Nck interactions play a pivotal role in the receptor-specific formation of filopodia. My data also shows that both pSyk and Nck are preferentially recruited at the sites of bead-cell interactions, providing the first evidence that an ITIM-containing immunoregulatory receptor can network with Nck and Syk to induce filopodia-mediated extracellular target binding, capture, and engulfment. Based on previous studies from our lab, it is likely that Nck binds to IpLITR 1.1b at a binding consensus motif located within its proximal region of its CYT, while pSyk likely binds to the tandem ITIMs within its distal region of its CYT [105]. The examination of IpLITR 1.1b and its unique ability to promote F-actin polymerization events demonstrates that functional plasticity within immunoregulatory signaling pathways had

emerged early in immunoregulatory receptor evolution. As such, IpLITR 1.1b-mediated formation of filopodia and their ability to interact with extracellular targets represents a unique model for further understanding F-actin dynamics during the control cellular effector responses. Therefore, this model will serve to broaden our understanding of how other vertebrate immunoregulatory receptor-types may network with intracellular signaling components to regulate effector responses such as the phagocytic process. An understanding that the unique composition of tyrosine residues within the CYT regions of immune receptors can form discrete signaling cassettes broadens our appreciation of immunoregulatory receptor signaling. The fact that IpLITR 1.1b, an ITIM containing and previously described inhibitory receptor, can also network with effectors of the F-actin polymerization machinery (e.g. Nck and Syk) shows that an individual IpLITR-type has variable and versatile immunoregulatory roles. Using imaging technologies, this thesis chapter provides new evidence for a unique pathway explaining how a putative inhibitory IpLITR-type can also trigger target capture and engulfment processes and an overall appreciation of immunoregulatory functional plasticity.

FIGURE 7.1

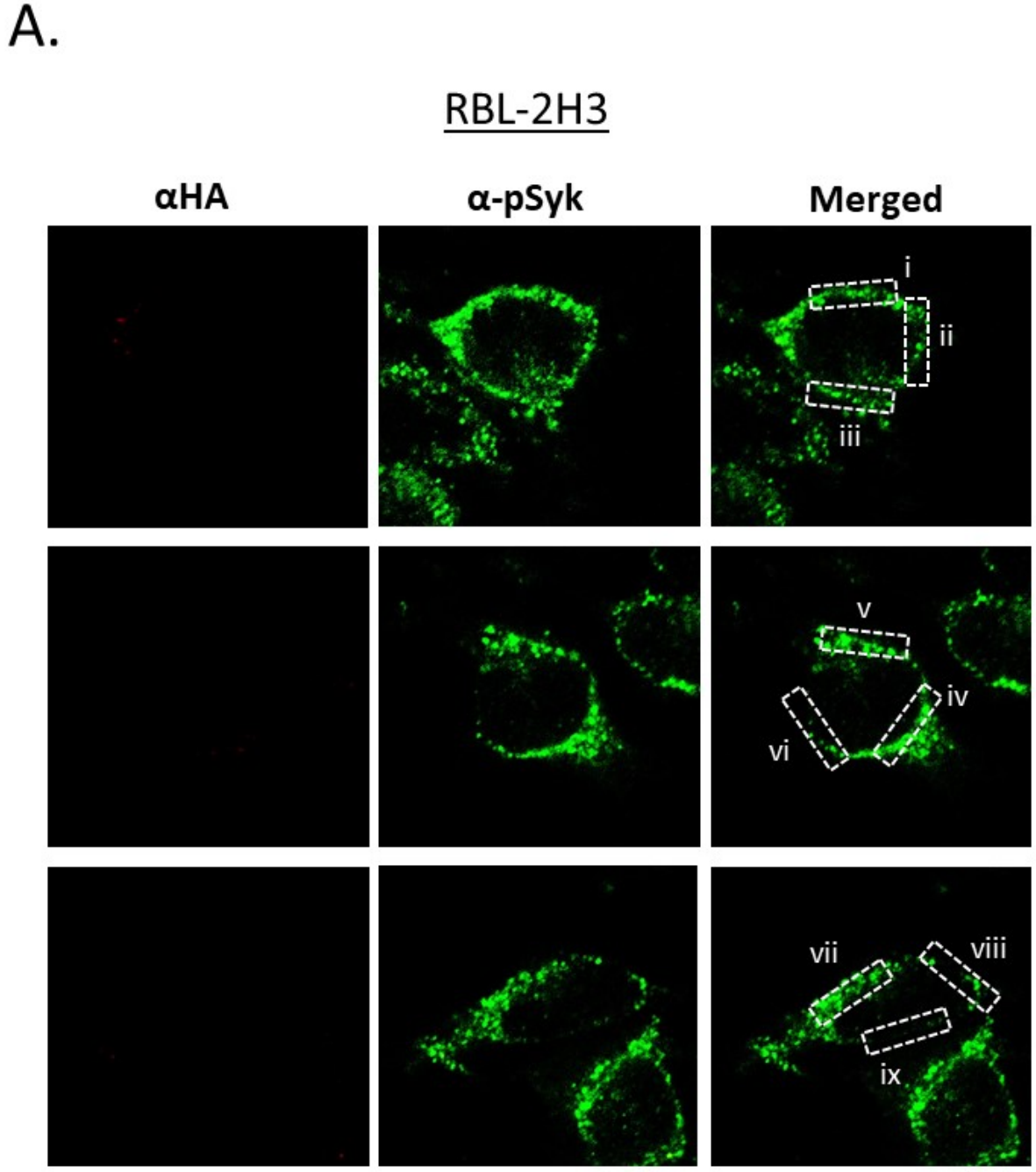

FIGURE 7.1

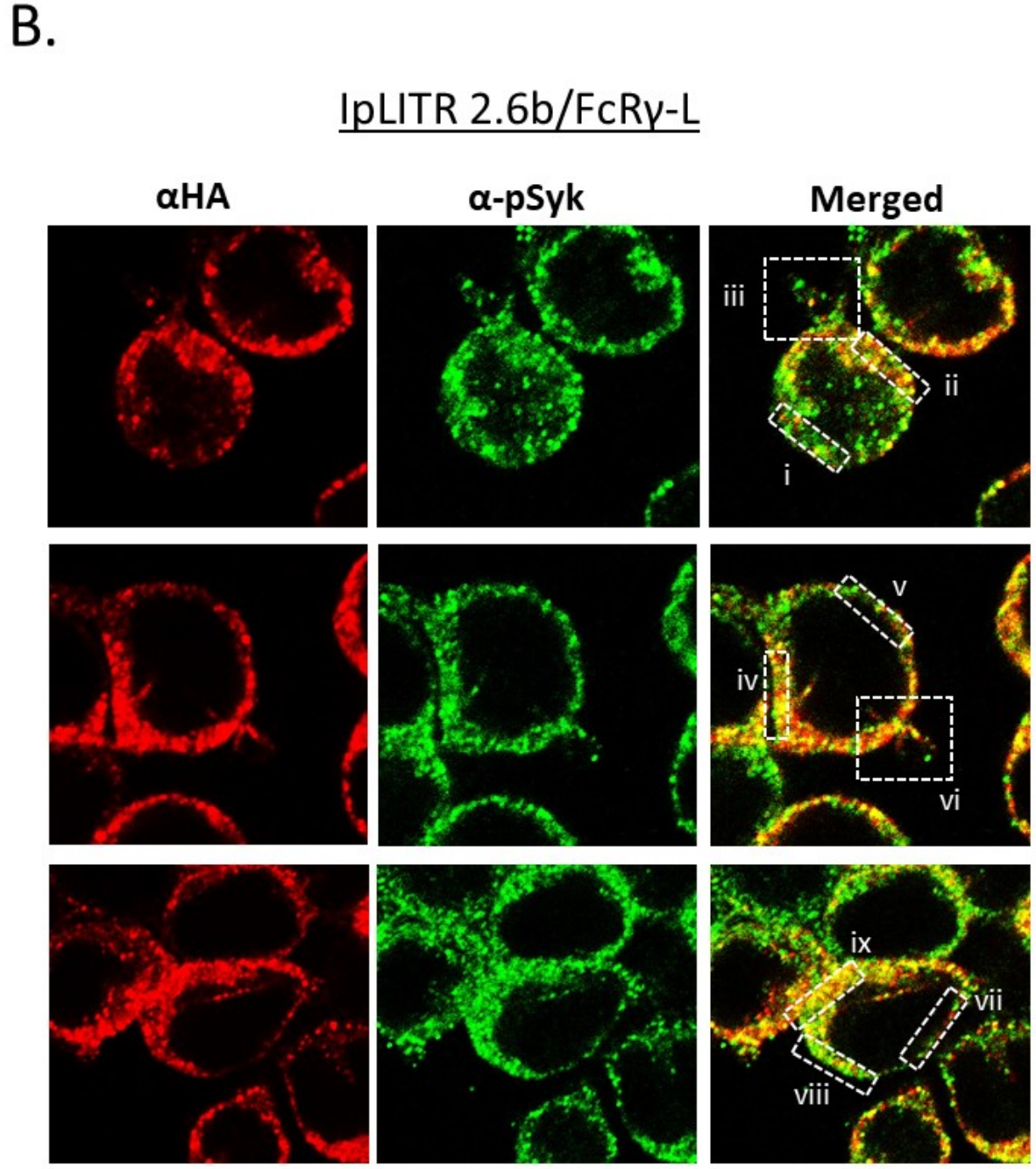

FIGURE 7.1

C.

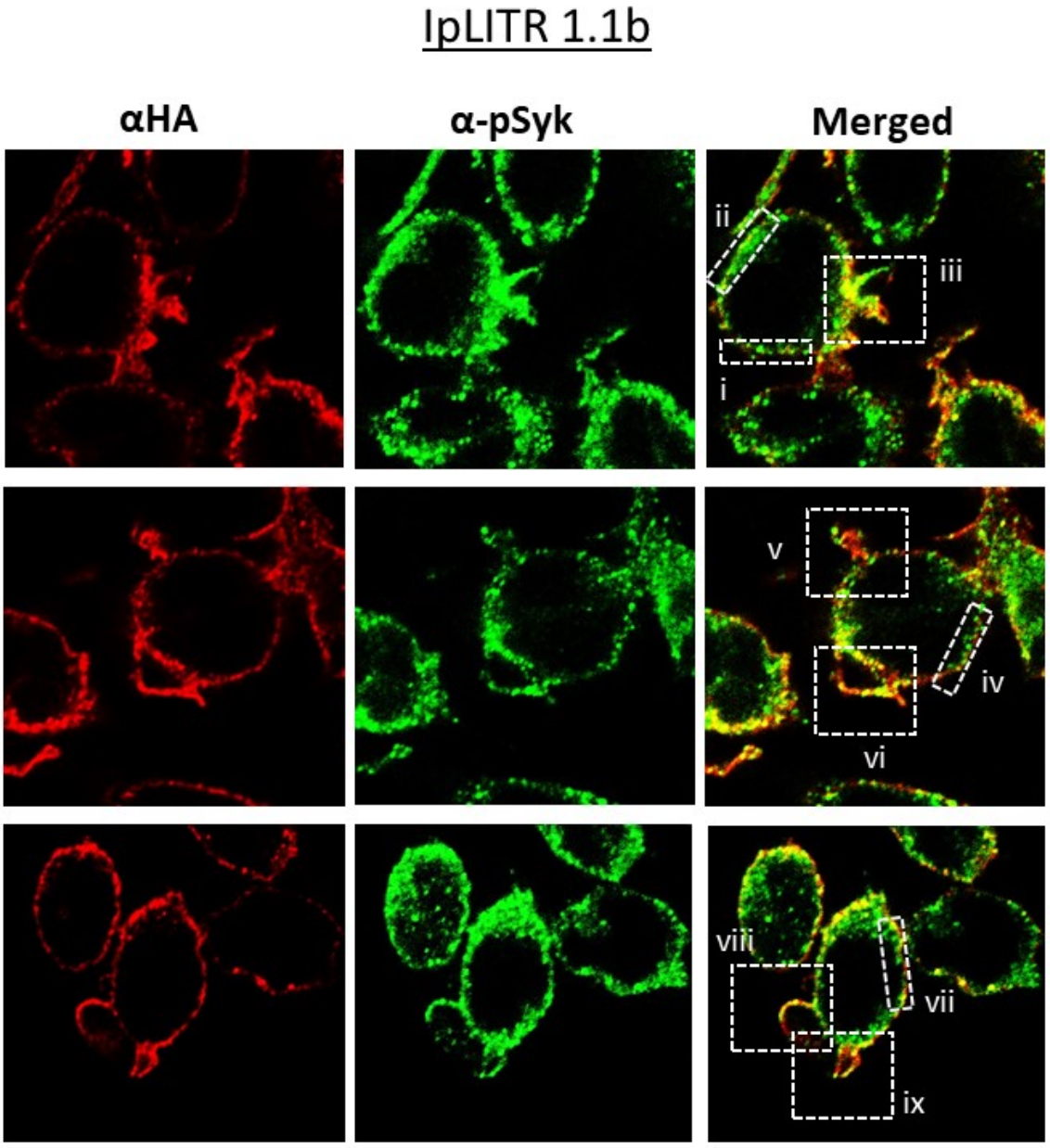

FIGURE 7.1

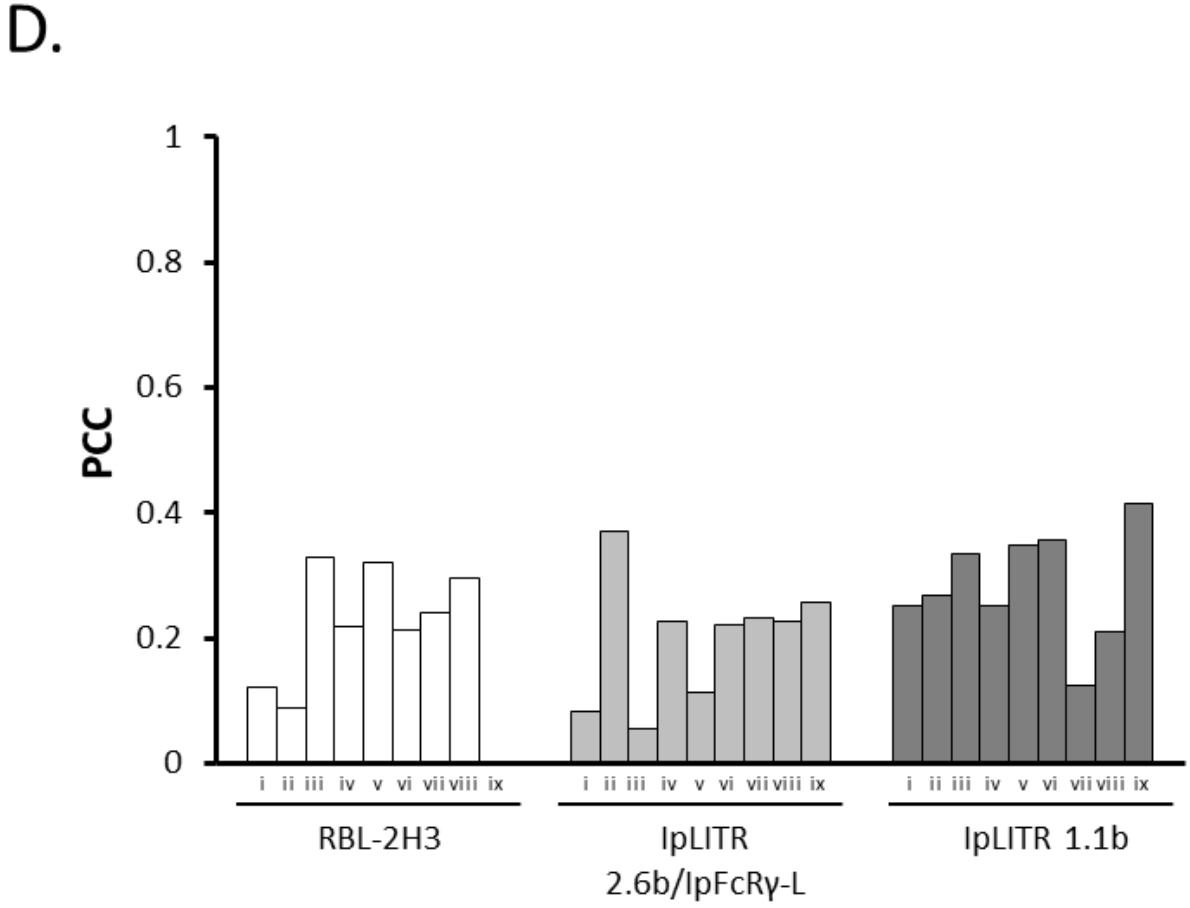
D.
PCC
1
0.8
0.6
0.4
0.2
0
i ii iii iv v vi vii viii ix
i ii iii iv v vi vii viii ix
i ii iii iv v vi vii viii ix
RBL-2H3
IpLITR 2.6b/IpFcRγ-L
IpLITR 1.1b

FIGURE 7.1 Colocalization of pSyk with surface expressed IpLITRs. $2x10^5$ cells of either parental RBL-2H3 (A) IpLITR 2.6b/IpFcRγ-L (B) or IpLITR 1.1b (C) –expressing cells were plated onto a coverslip and allowed to grow overnight. Next day cells were fixed with 4% PFA at 37°C. Visualization of IpLITR expression was completed by first staining for the HA-tag of IpLITRs using an αHA mAb and then subsequently staining of the receptors with a fluorescent secondary goat αmouse Alexa-647 (red) antibody. Cells were then permeabilized and stained with a rabbit α-pSyk mAb and then a secondary goat αrabbit Alexa-488 (green) to visualize the localization of pSyk in relation to localization of IpLITRs. Z-stack images were then obtained at 63x magnification using a Zeiss LSM 710 laser scanning confocal microscope. Colocalization analysis was then performed on obtained z-stack images using Imaris 9.2.1 at three isolated regions of the membrane (dashed box; i-ix) for three individual cells and PCC values were obtained for all cell-types for at each region tested (i-ix) (D).

FIGURE 7.2

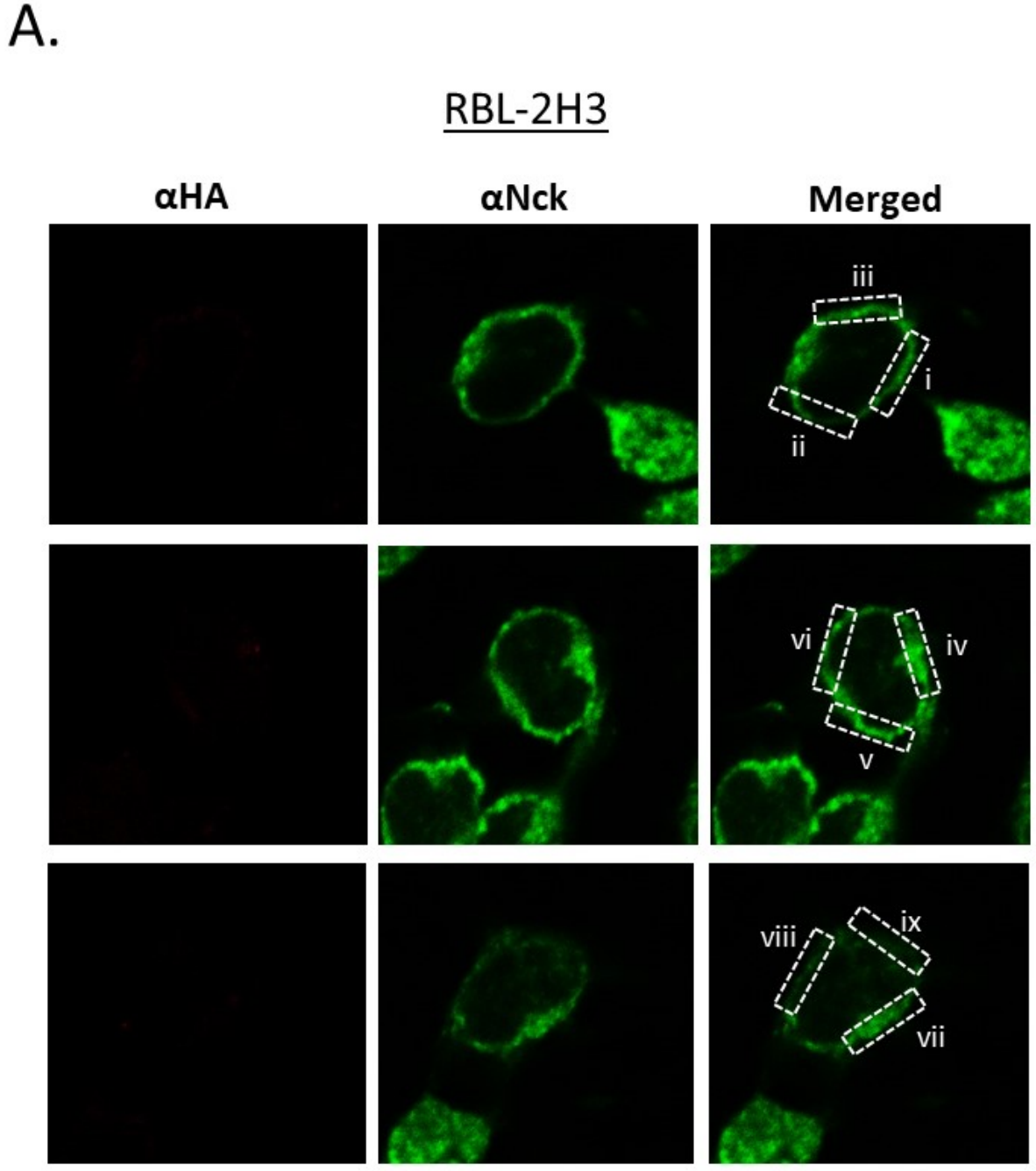

FIGURE 7.2

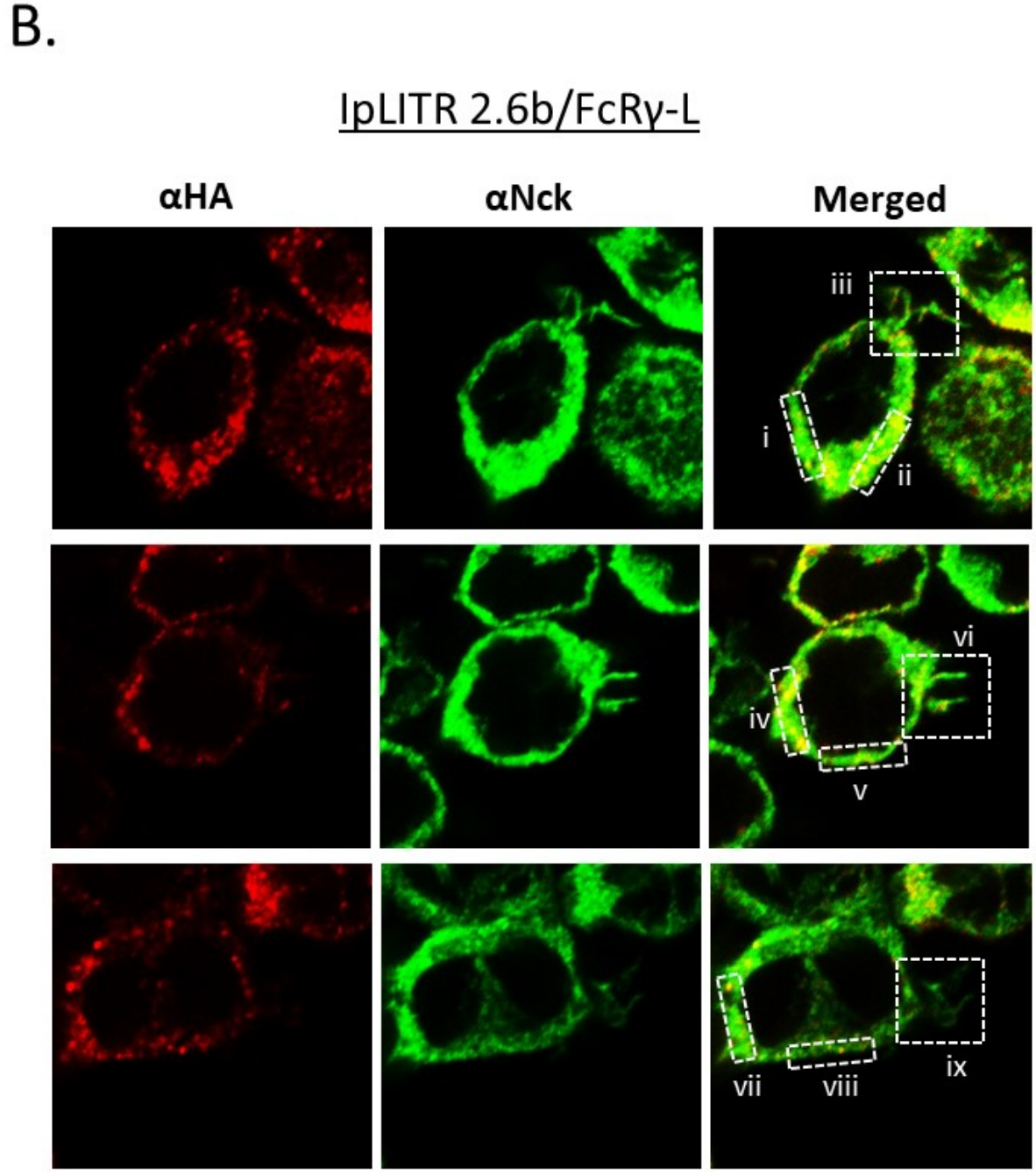

FIGURE 7.2

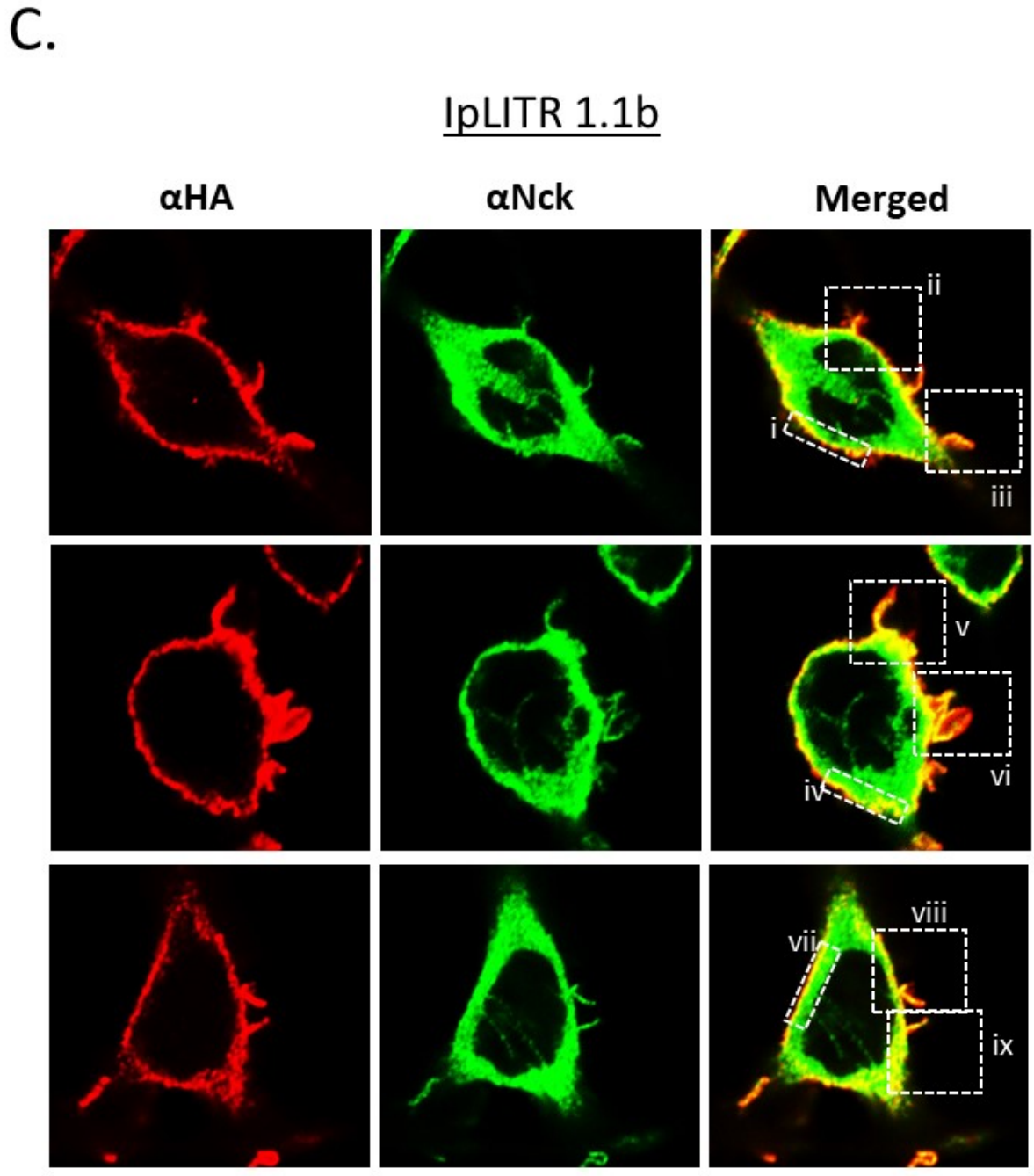

FIGURE 7.2

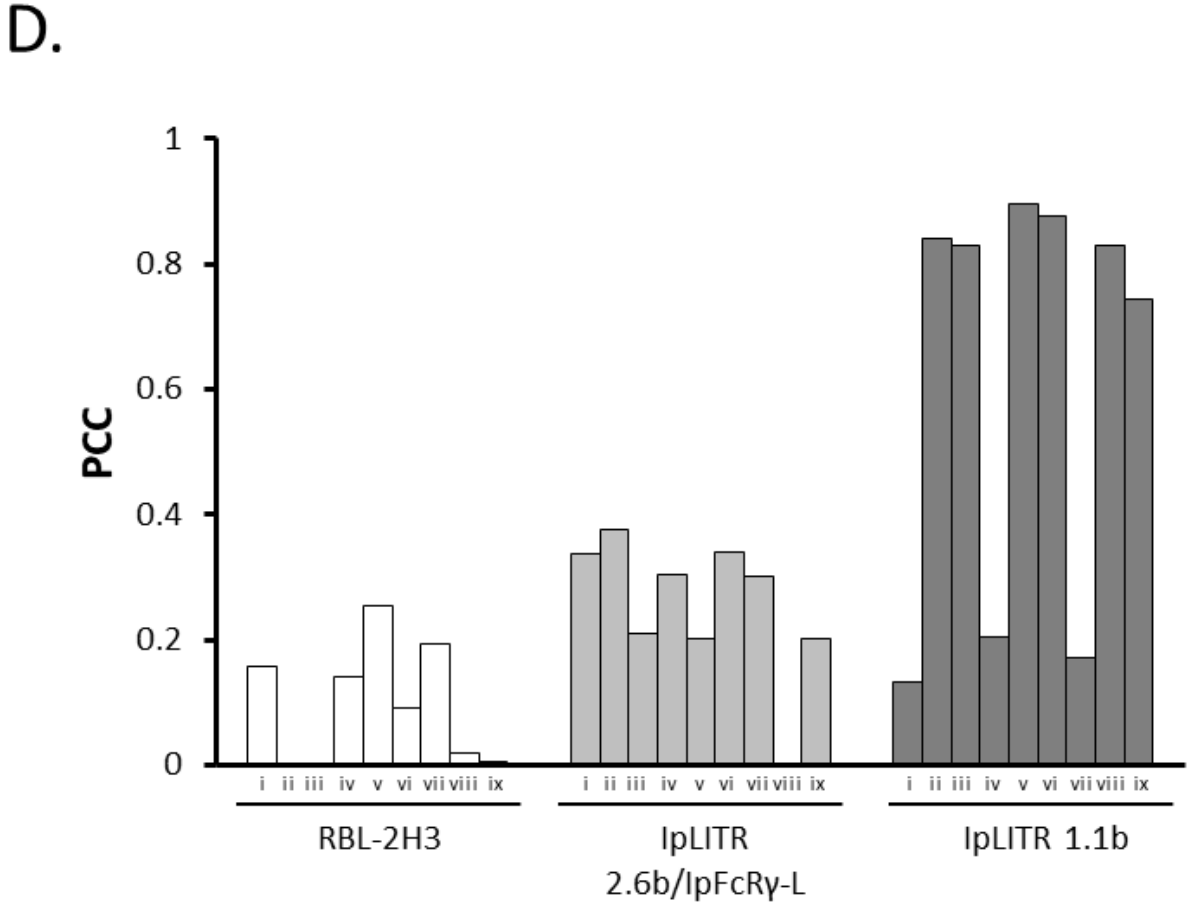
D.
PCC
1
0.8
0.6
0.4
0.2
0
i ii iii iv v vi vii viii ix
i ii iii iv v vi vii viii ix
i ii iii iv v vi vii viii ix
RBL-2H3
IpLITR 2.6b/IpFcRγ-L
IpLITR 1.1b

FIGURE 7.2 Colocalization of Nck with surface expressed IpLITRs. $2x10^5$ cells of either parental RBL-2H3 (A) IpLITR 2.6b/IpFcRγ-L (B) or IpLITR 1.1b (C) –expressing cells were plated onto a coverslip and allowed to grow overnight. Next day cells were fixed with 4% PFA at 37°C. Visualization of IpLITR expression was completed by first staining for the HA-tag of IpLITRs using an αHA mAb and the subsequent staining of the receptors with a fluorescent secondary goat αmouse Alexa-647 (red) antibody. Cells were then permeabilized and stained with a rabbit αNck mAb and then a secondary goat αrabbit Alexa-488 (green) to visualize the localization of Nck in relation to localization of IpLITRs. Z-stack images were then obtained at 63x magnification using a Zeiss LSM 710 laser scanning confocal microscope. Colocalization analysis was then performed on obtained z-stack images using Imaris 9.2.1 at three isolated regions of the membrane (dashed box; i-ix) for three individual cells and PCC values were obtained for all cell-types for at each region tested (i-ix) (D).

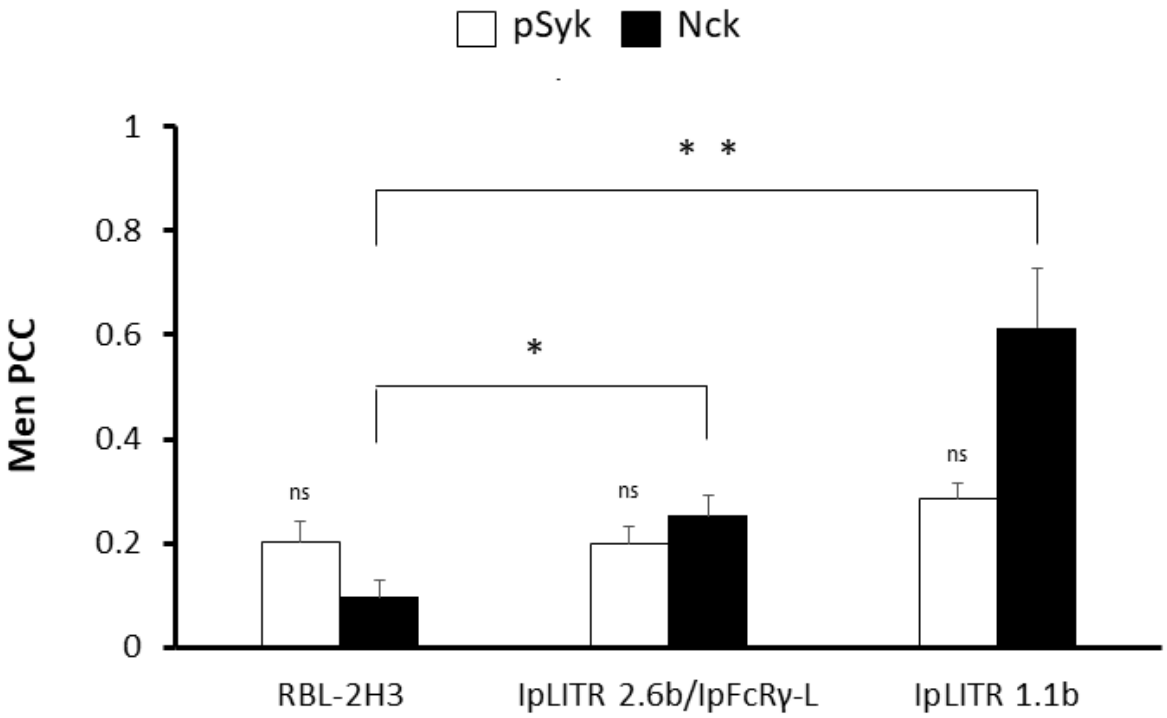

FIGURE 7.3 Averaged Pearson correlation coefficient of values for colocalization. Mean ±SEM values for each cell-type assessed across all regions analyzed for both pSyk (white bars) or Nck (black bars) colocalization with IpLITR expression. PCC values obtained using Imaris 9.2.1 for each selected region of interest. No statistical significance was found between all cell-types and pSyk colocalization when stained with a αHA mAb (ns). Statistical significance was calculated for Nck and αHA mAb staining between RBL-2H3 and IpLITR 2.6b/IpFcRγ-L (*) while IpLITR 1.1b had statistical significance when compared to both RBL-2H3 and IpLITR 2.6b 2.6b/IpFcRγ-L (**). Stats were done using a student t-test two tail paired variance and significance was determined by $p \leq 0.05$.

FIGURE 7.4

A.

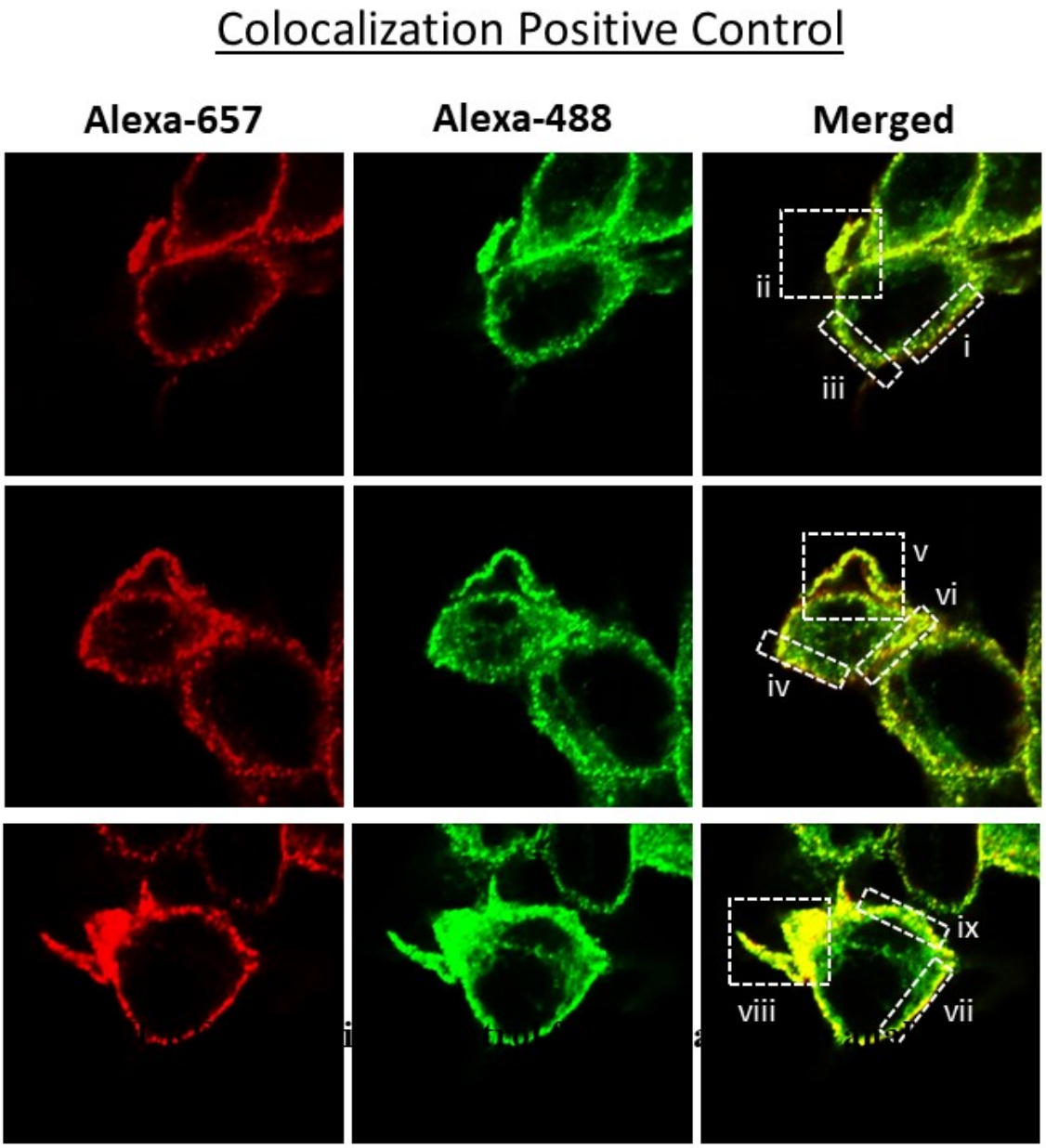
Colocalization Positive Control
Alexa-657
Alexa-488
Merged
ii
i
iii
v
vi
iv
ix
viii
vii

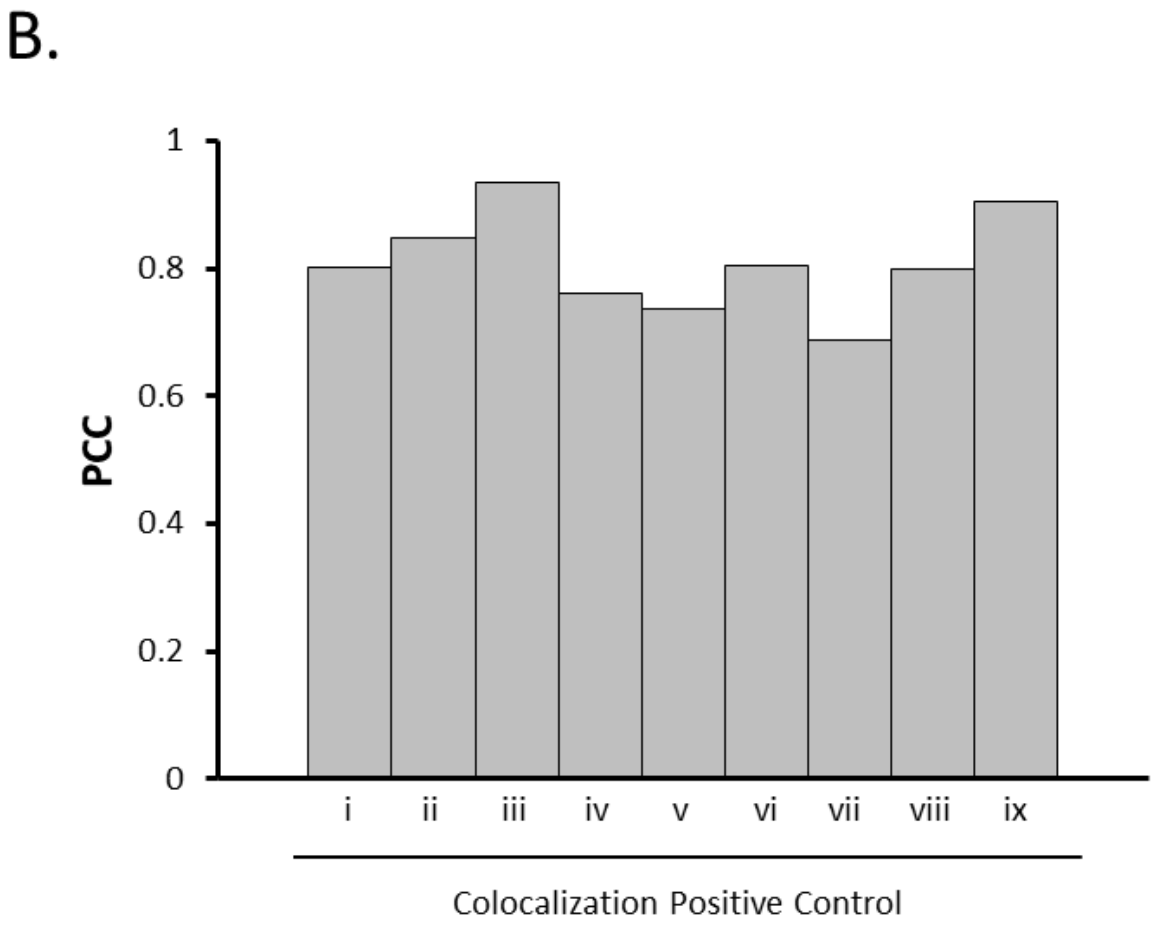

FIGURE 7.4 Positive control for colocalization analysis. IpLITR 1.1b-expressing cells were fixed using 4% PFA at 37x. After fixation surface IpLITR 1.1b was stained using a αHA mAb and subsequently was double stained using two secondary goat αmouse mAb antibodies one conjugated to Alexa-657 and the other conjugated to Alexa-488 fluorescence probe. Cells were then imaged using a Zeiss LSM 710 laser scanning confocal microscope (A) and colocalization analysis was then performed on obtained z-stack images using Imaris 9.2.1 at three separate regions (dashed box; i-ix) for three individual cells and Pearson Correlation Coefficient (PCC) were obtained for each region of interest (i-ix) (D).

FIGURE 7.5

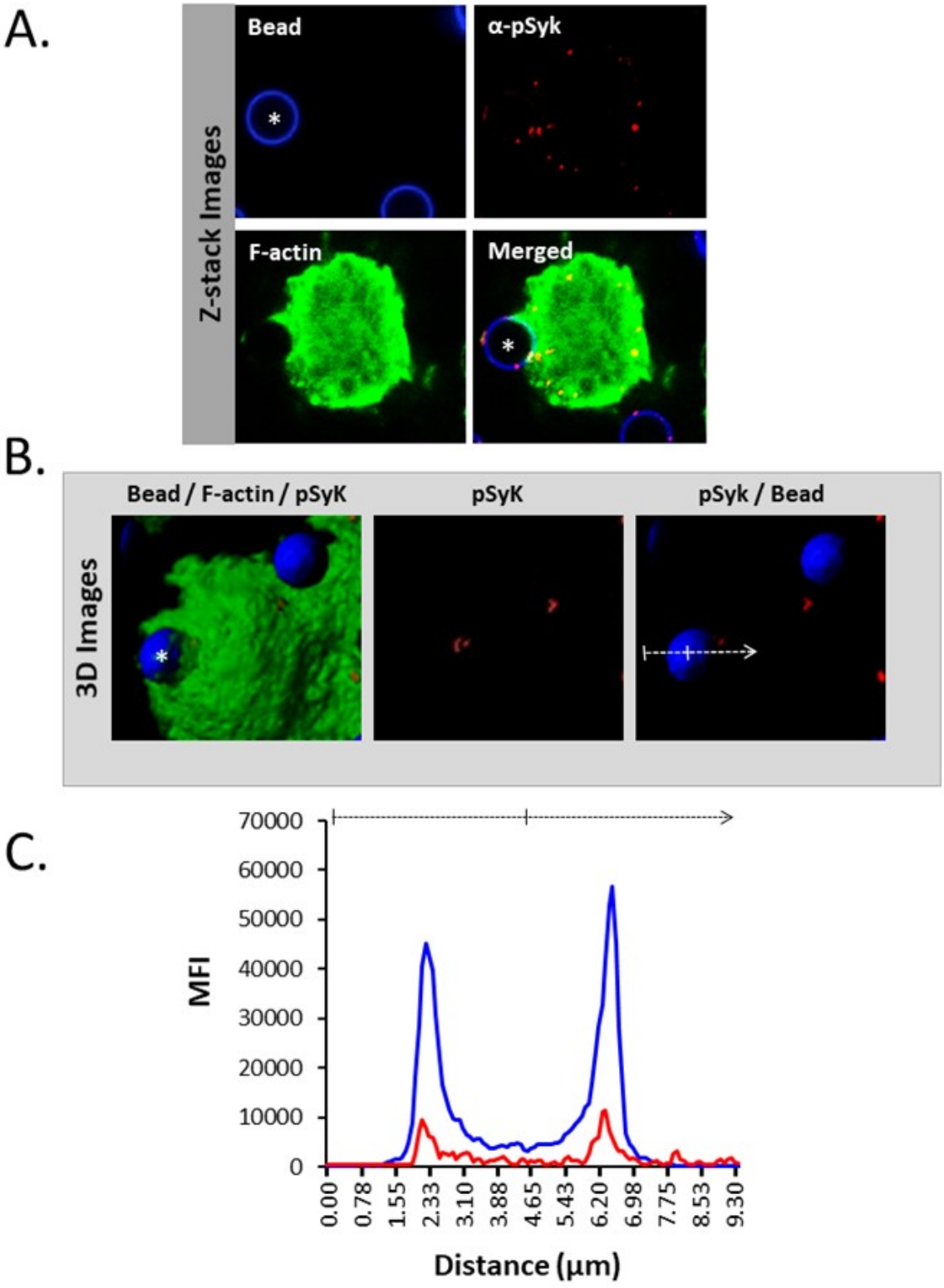
A.
Bead
α-pSyk
Z-stack Images
F-actin
Merged
B.
Bead / F-actin / pSyK
pSyK
pSyk / Bead
3D Images
C.
70000
60000
50000
40000
30000
20000
10000
0
MFI
0.00
0.78
1.55
2.33
3.10
3.88
4.65
5.43
6.20
6.98
7.75
8.53
9.30
Distance (µm)

FIGURE 7.6

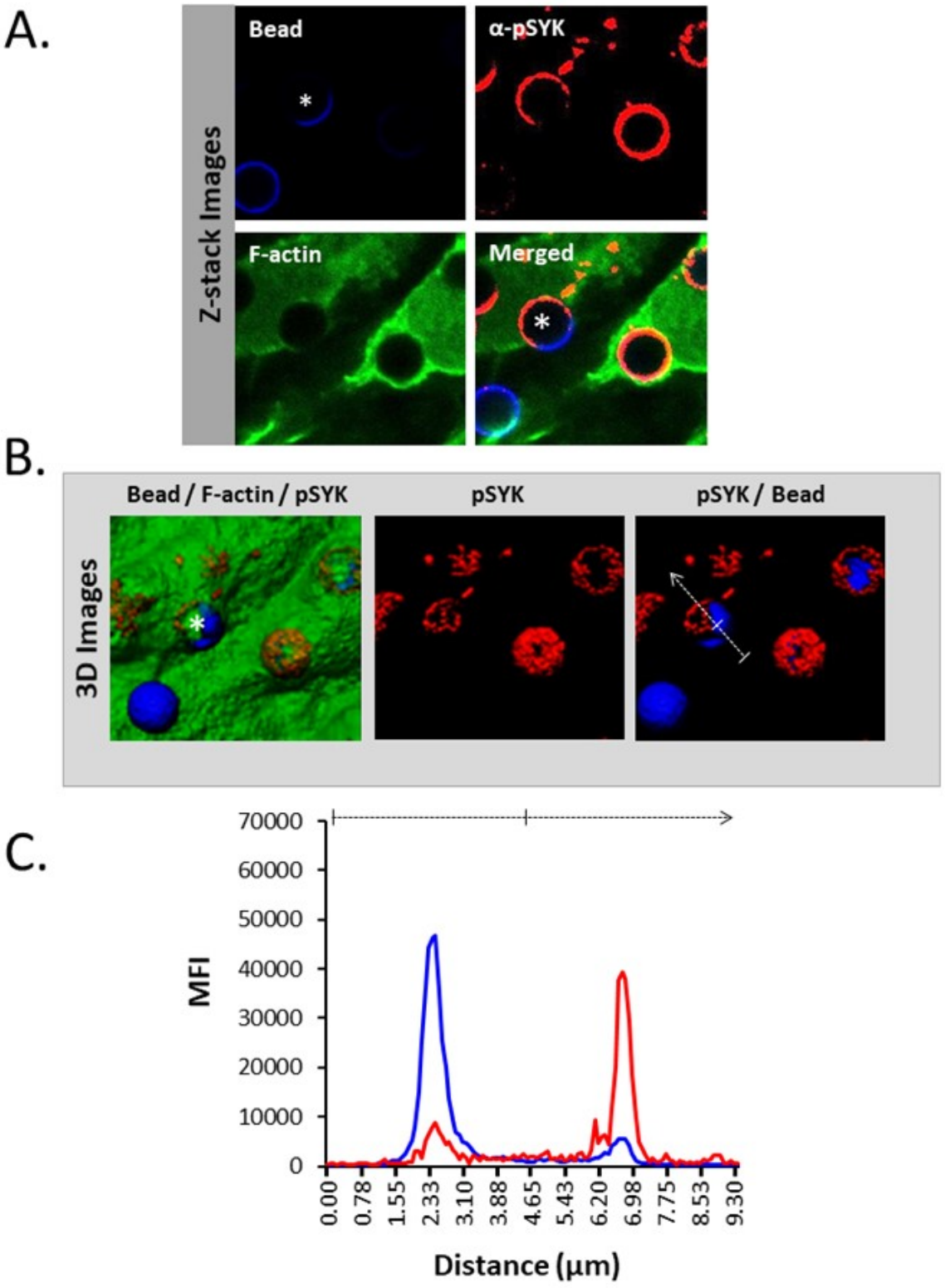
A.
Bead
α-pSYK
Z-stack Images
F-actin
Merged
B.
Bead / F-actin / pSYK
pSYK
pSYK / Bead
3D Images
C.
MFI
70000
60000
50000
40000
30000
20000
10000
0
0.00
0.78
1.55
2.33
3.10
3.88
4.65
5.43
6.20
6.98
7.75
8.53
9.30
Distance (µm)

FIGURE 7.7

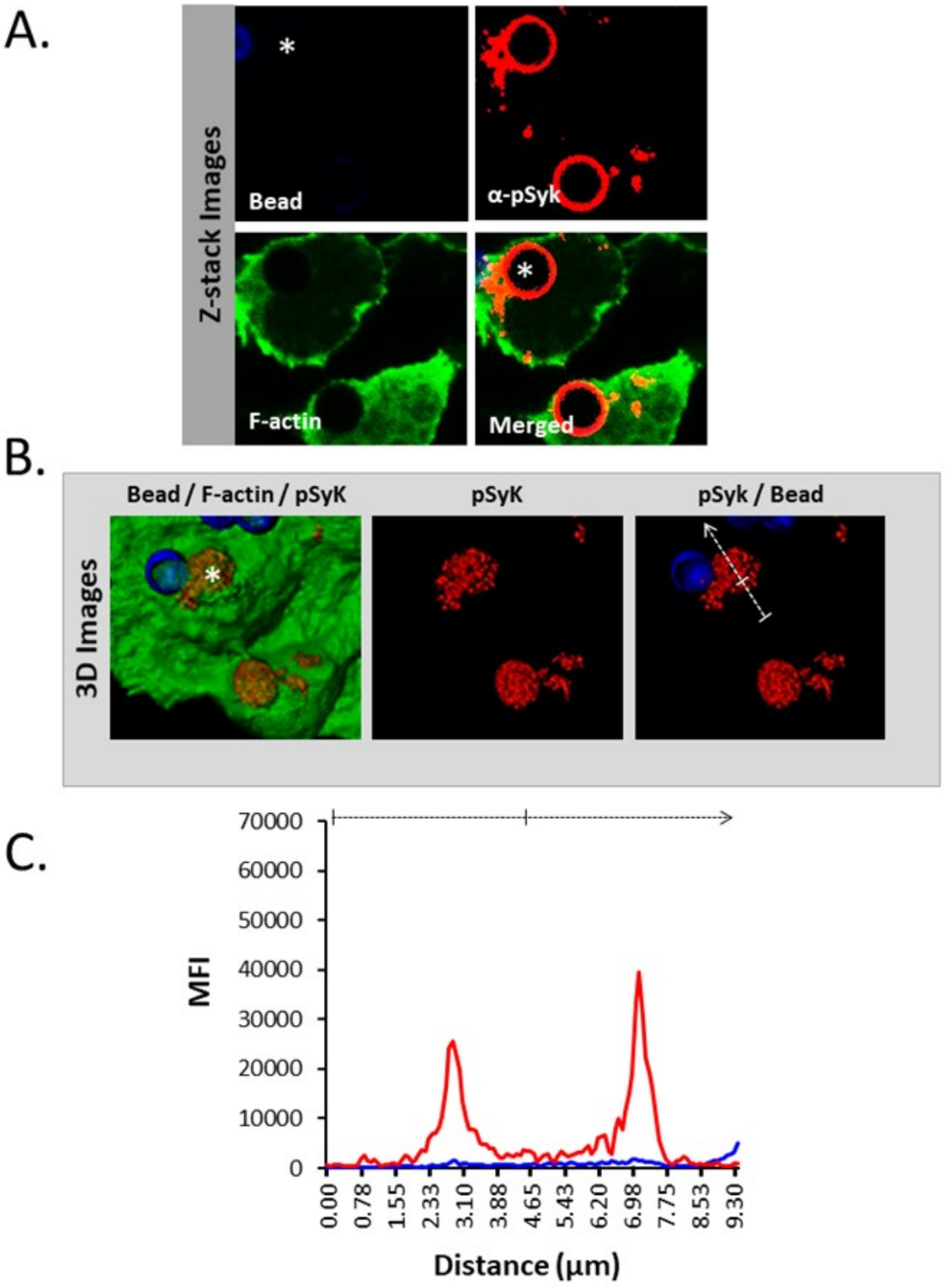
A.
Z-stack Images
Bead
α-pSyk
F-actin
Merged
B.
3D Images
Bead / F-actin / pSyK
pSyK
pSyk / Bead
C.
MFI
70000
60000
50000
40000
30000
20000
10000
0
0.00
0.78
1.55
2.33
3.10
3.88
4.65
5.43
6.20
6.98
7.75
8.53
9.30
Distance (µm)

FIGURE 7.8

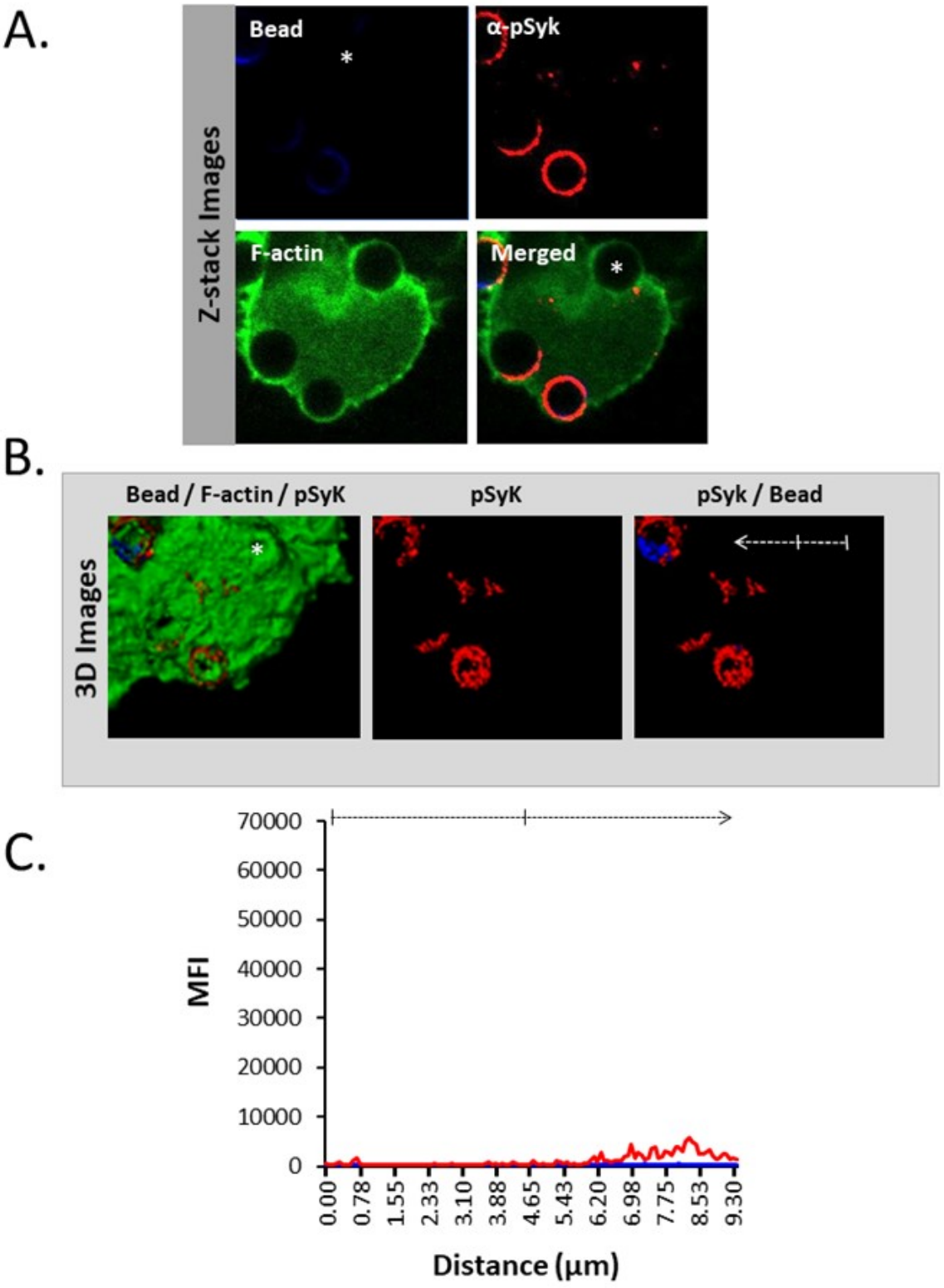
A.
Z-stack Images
Bead
α-pSyk
F-actin
Merged
B.
3D Images
Bead / F-actin / pSyK
pSyK
pSyk / Bead
C.
MFI
70000
60000
50000
40000
30000
20000
10000
0
0.00
0.78
1.55
2.33
3.10
3.88
4.65
5.43
6.20
6.98
7.75
8.53
9.30
Distance (µm)

FIGURE 7.5-7.8 Recruitment of pSyk during IpLITR 2.6b/IpFcRγ-L-mediated phagocytosis. Phagocytosis assays were performed by incubating $1x10^5$ IpLITR 2.6b/IpFcRγ-L-expressing cells stably transfected with LifeAct-GFP (green) with 4.5-μm non-fluorescent polystyrene beads ($3x10^5$) pre-opsonized with αHA mAb for 60 min at 37°C while adhered to coverslips. After bead incubation, cells were fixed with 4% PFA at 37°C. To asses the level of internalization of mAb beads, cells were incubated with a secondary goat αmouse Alexa-647. Post bead staining, cells were permeabilized and then stained for intracellular pSyk via first incubating with a rabbit α-pSyk mAb and then a secondary goat αrabbit Alexa-488. Z-stack images (A) were then obtained at a magnification of 63x using a Zeiss LSM 710 laser scanning confocal microscope, with beads of interested indicated by an asterisk. Post imaging collection, coloration for beads (blue), pSyk (red) and the cell (green) were artificially changed to better demonstrate the overall associations of all three colors via the imaging software Zen 2009. Representative z-stacks for individual cells chosen for further analysis were transformed into 3D renders to better visualize the spatial association of pSyk recruitment within the cells at bead-cell interfaces with beads used for further analysis indicated by an asterisk (B). Qualitative analysis was performed on shown z-stack images (from A) by collecting mean fluorescence intensities (MFI; y-axis) of both bead staining (blue line) and pSyk staining (red line) across the identified bead in the image shown (x-axis; distance; μm) using ImageJ 9.2.1 (C).

FIGURE 7.9

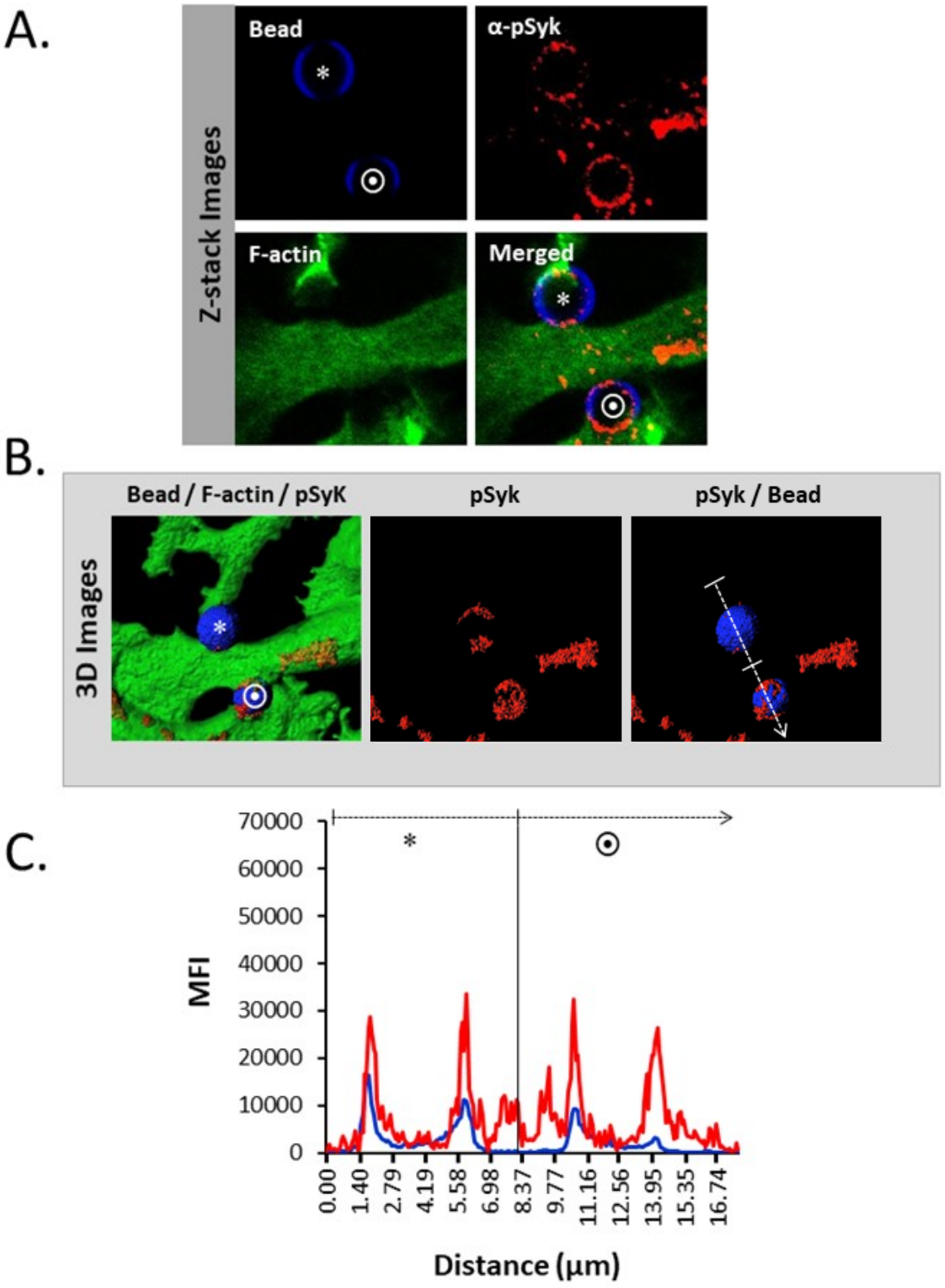
A.
Z-stack Images
Bead
α-pSyk
F-actin
Merged
B.
3D Images
Bead / F-actin / pSyK
pSyk
pSyk / Bead
C.
MFI
70000
60000
50000
40000
30000
20000
10000
0
0.00
1.40
2.79
4.19
5.58
6.98
8.37
9.77
11.16
12.56
13.95
15.35
16.74
Distance (µm)

FIGURE 7.10

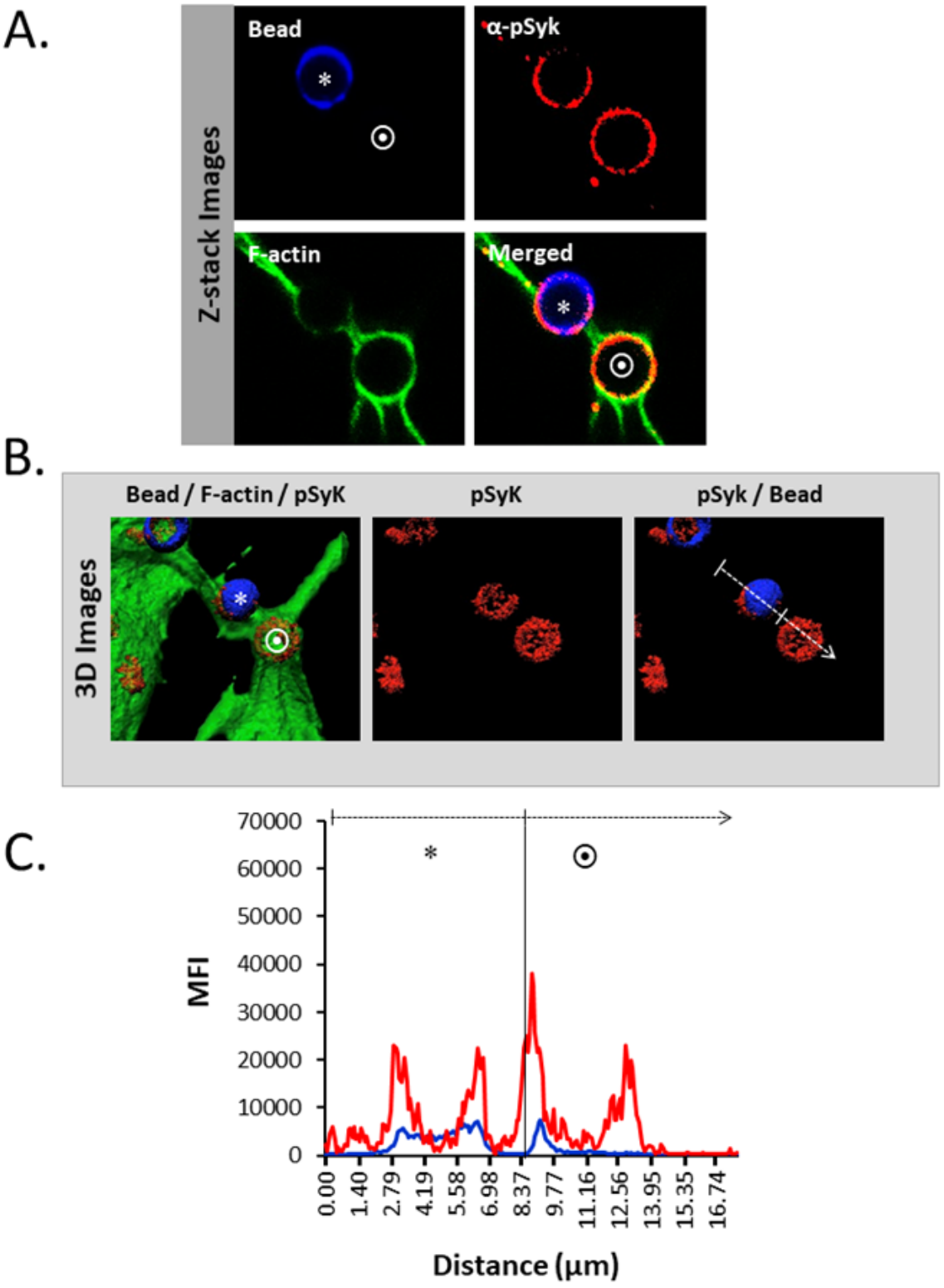
A.
Z-stack Images
Bead
α-pSyk
F-actin
Merged
B.
3D Images
Bead / F-actin / pSyK
pSyK
pSyk / Bead
C.
MFI
70000
60000
50000
40000
30000
20000
10000
0
0.00
1.40
2.79
4.19
5.58
6.98
8.37
9.77
11.16
12.56
13.95
15.35
16.74
Distance (µm)

FIGURE 7.11

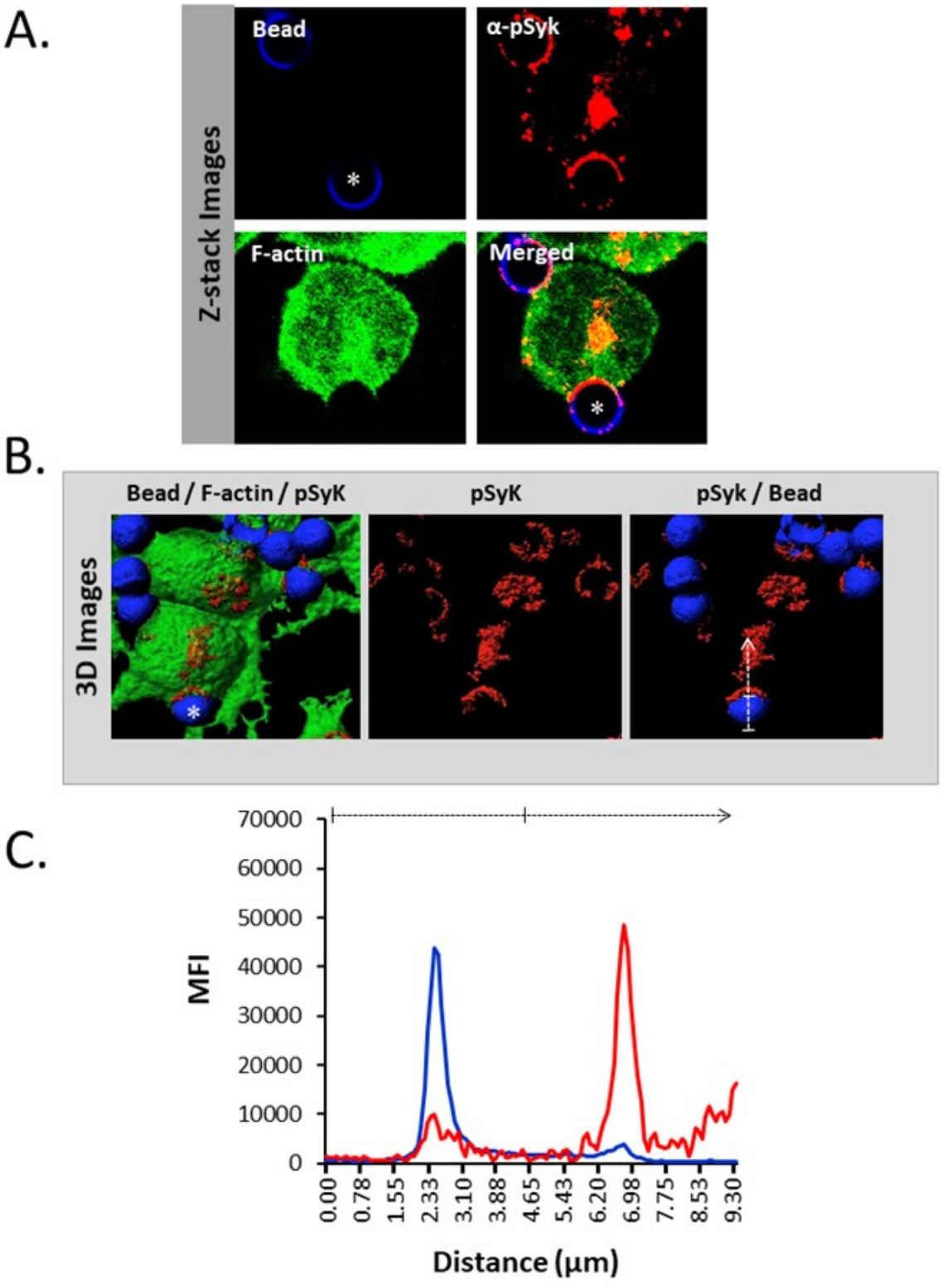
A.
Z-stack Images
Bead
α-pSyk
F-actin
Merged
B.
3D Images
Bead / F-actin / pSyK
pSyK
pSyk / Bead
C.
MFI
70000
60000
50000
40000
30000
20000
10000
0
0.00
0.78
1.55
2.33
3.10
3.88
4.65
5.43
6.20
6.98
7.75
8.53
9.30
Distance (µm)

FIGURE 7.12

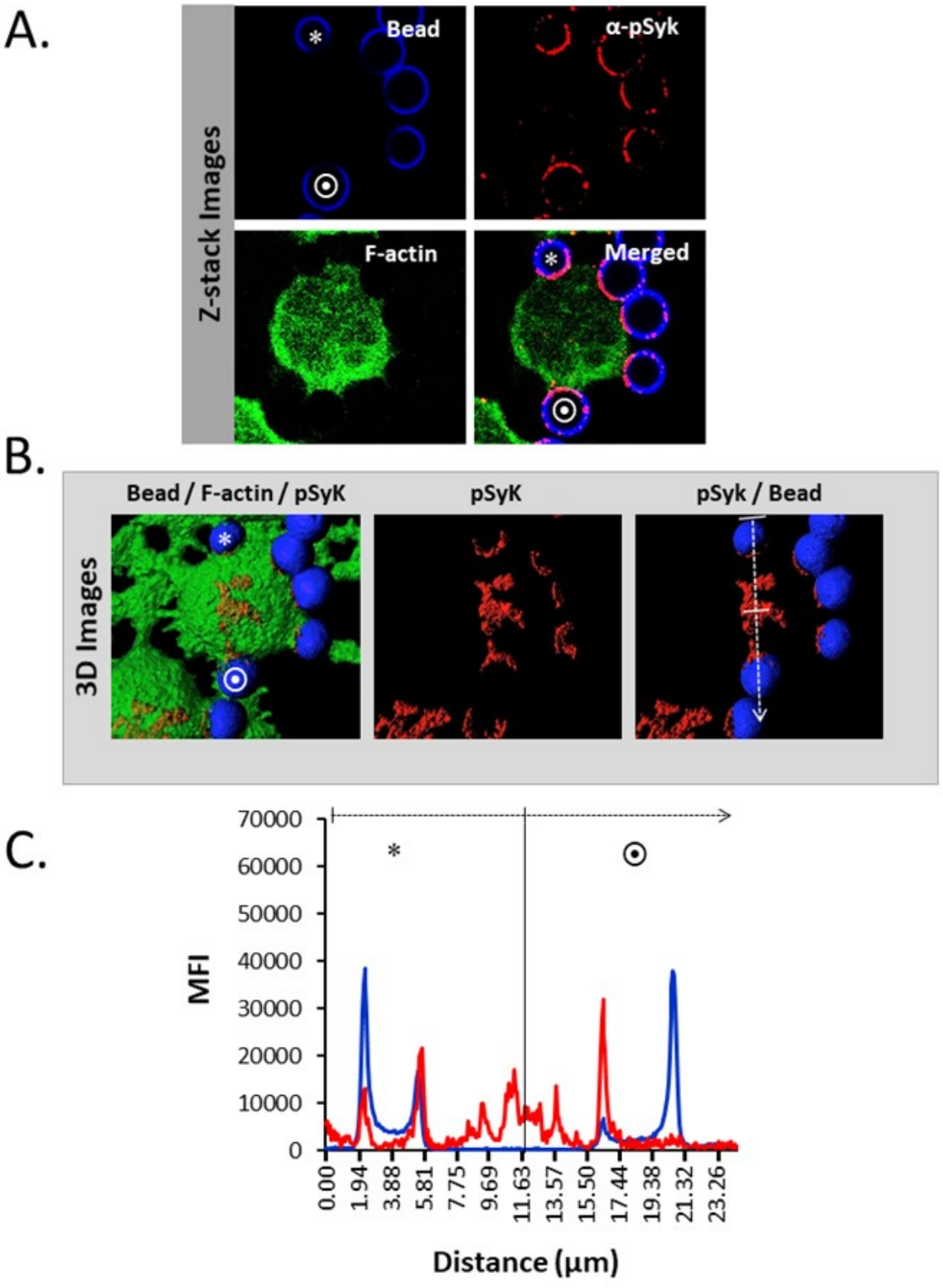
A.
Z-stack Images
Bead
α-pSyk
F-actin
Merged
B.
3D Images
Bead / F-actin / pSyK
pSyK
pSyk / Bead
C.
MFI
70000
60000
50000
40000
30000
20000
10000
0
0.00
1.94
3.88
5.81
7.75
9.69
11.63
13.57
15.50
17.44
19.38
21.32
23.26
Distance (µm)

FIGURE 7.13

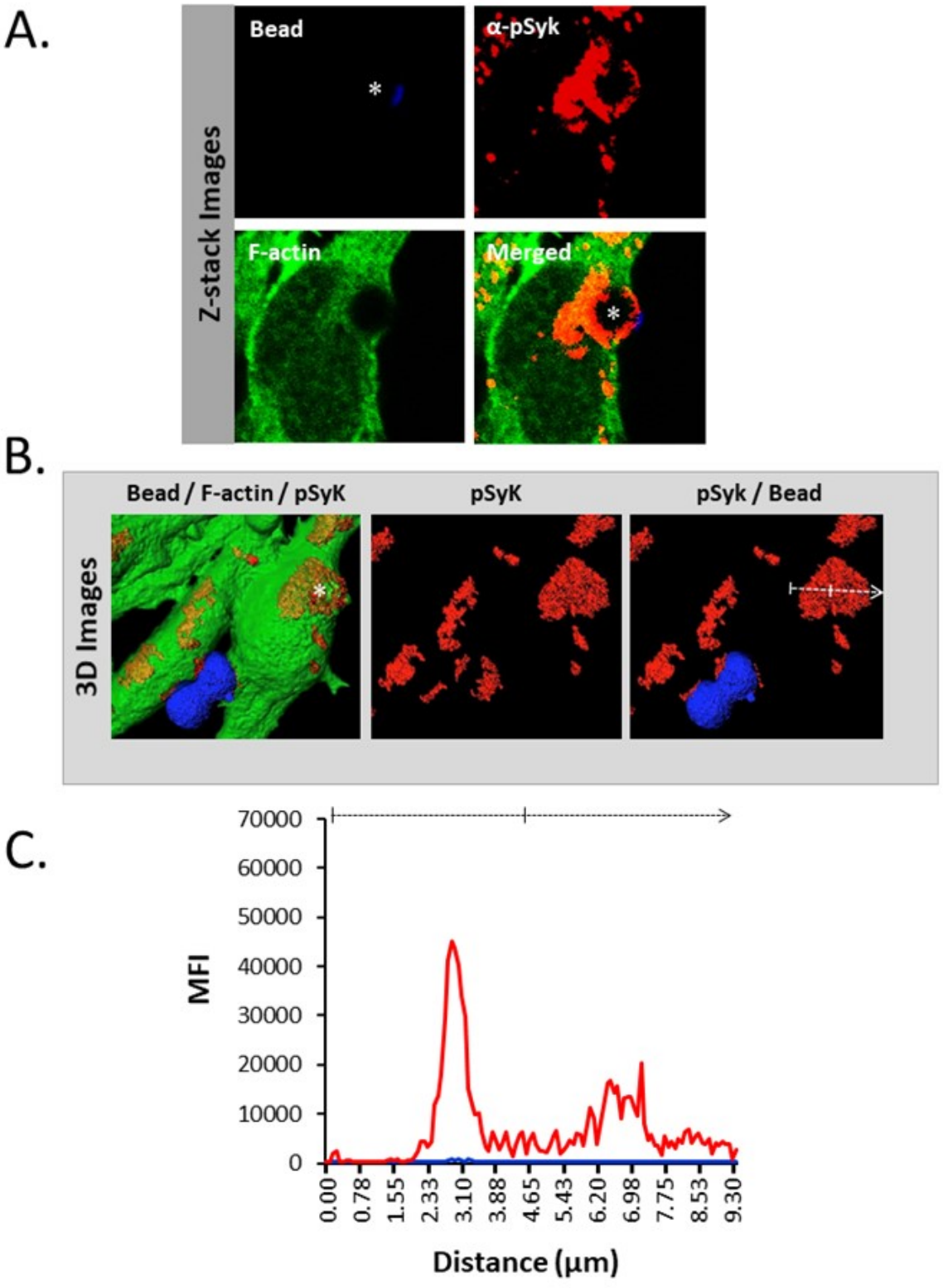
A.
Z-stack Images
Bead
α-pSyk
F-actin
Merged
B.
3D Images
Bead / F-actin / pSyK
pSyK
pSyk / Bead
C.
MFI
70000
60000
50000
40000
30000
20000
10000
0
0.00
0.78
1.55
2.33
3.10
3.88
4.65
5.43
6.20
6.98
7.75
8.53
9.30
Distance (µm)

FIGURE 7.9-7.13 Recruitment of pSyk during IpLITR 1.1b-mediated phagocytosis. Phagocytosis assays were performed by incubating $1x10^5$ IpLITR 1.1b-expressing cells stably transfected with LifeAct-GFP (green) with 4.5-μm non-fluorescent polystyrene beads ($3x10^5$) pre-opsonized with αHA mAb for 60 min at 37°C while adhered to coverslips. After bead incubation, cells were fixed with 4% PFA at 37°C. To asses the level of internalization of mAb beads, cells were incubated with a secondary goat αmouse Alexa-647. Post bead staining, cells were permeabilized and then stained for intracellular pSyk via first incubating with a rabbit α-pSyk mAb and then a secondary goat αrabbit Alexa-488. Z-stack images (A) were then obtained at a magnification of 63x using a Zeiss LSM 710 laser scanning confocal microscope, with beads of interested indicated by an asterisk. Post imaging collection, coloration for beads (blue), pSyk (red) and the cell (green) were artificially changed to better demonstrate the overall associations of all three colors via the imaging software Zen 2009. Representative z-stacks for individual cells chosen for further analysis were transformed into 3D renders to better visualize the spatial association of pSyk recruitment within the cells at bead-cell interfaces with beads used for further analysis indicated by an asterisk (B). Qualitative analysis was performed on shown z-stack images (from A) by collecting mean fluorescence intensities (MFI; y-axis) of both bead staining (blue line) and pSyk staining (red line) across the identified bead in the image shown (x-axis; distance; μm) using ImageJ 9.2.1 (C).

FIGURE 7.14

A.

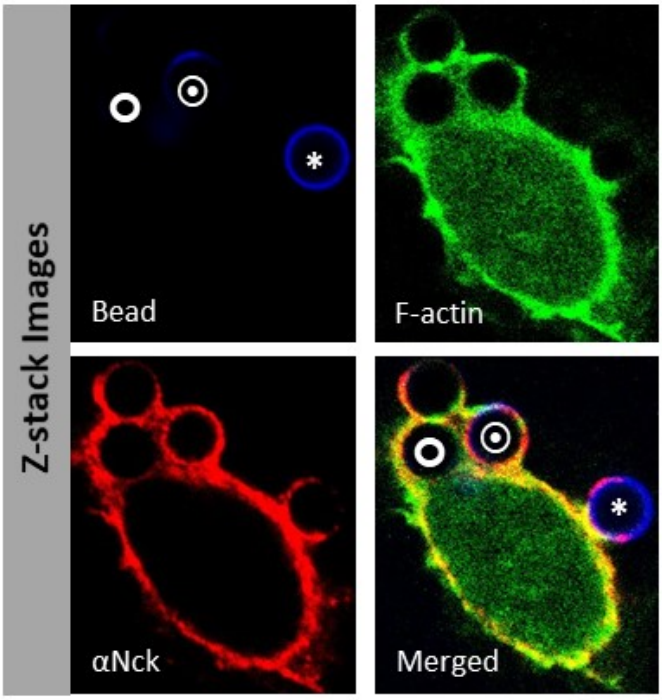

B.

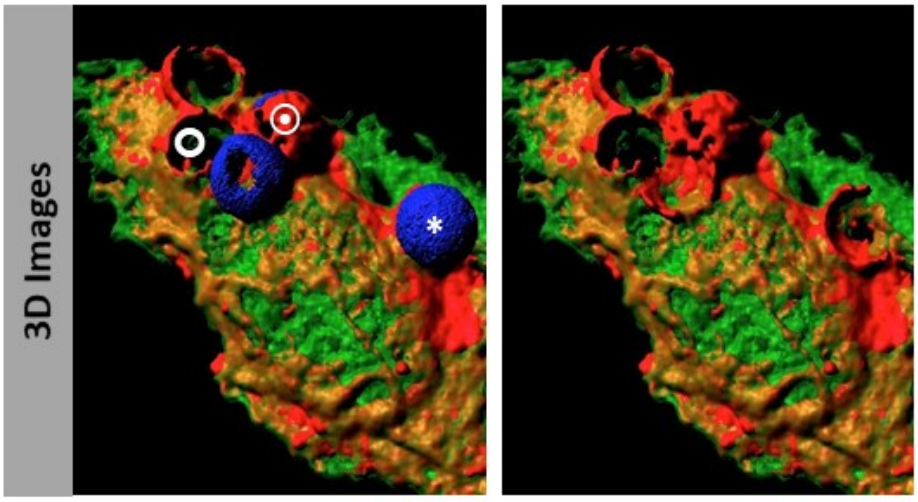

FIGURE 7.14

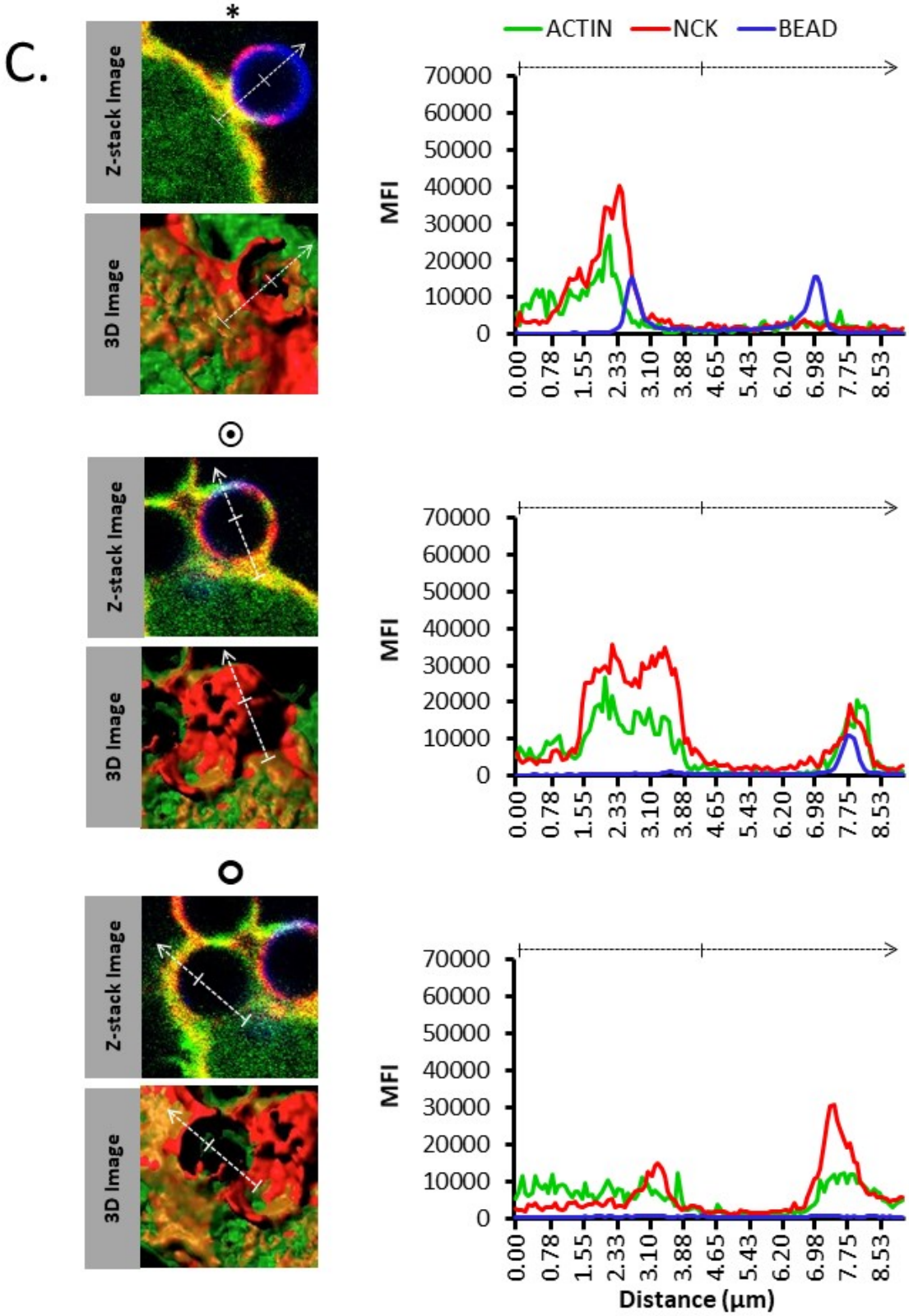
C.
*
Z-stack Image
3D Image
ACTIN
NCK
BEAD
MFI
70000
60000
50000
40000
30000
20000
10000
0
0.00
0.78
1.55
2.33
3.10
3.88
4.65
5.43
6.20
6.98
7.75
8.53
⊙
Z-stack Image
3D Image
MFI
O
Z-stack Image
3D Image
MFI
Distance (µm)

FIGURE 7.15

A.

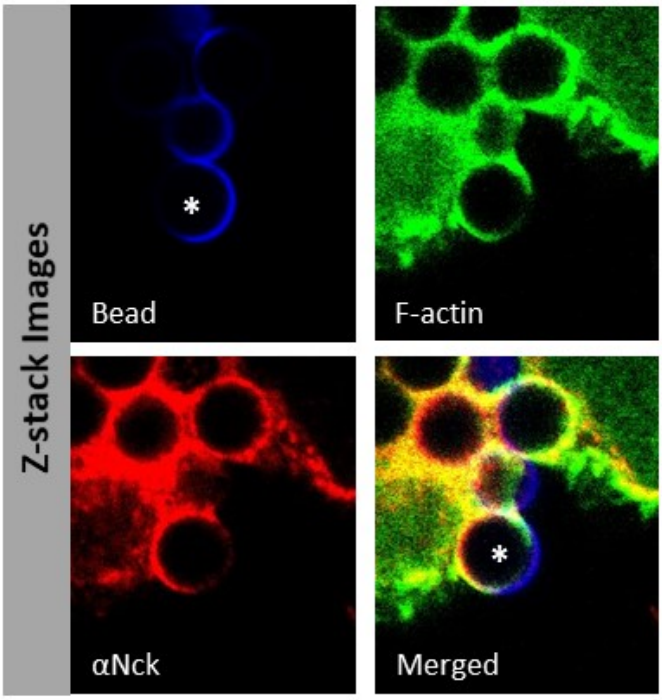

B.

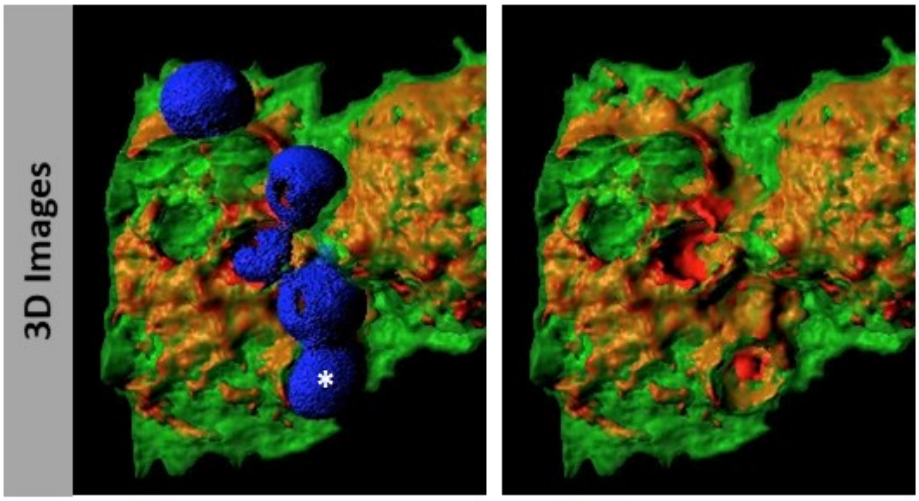

FIGURE 7.15

C.

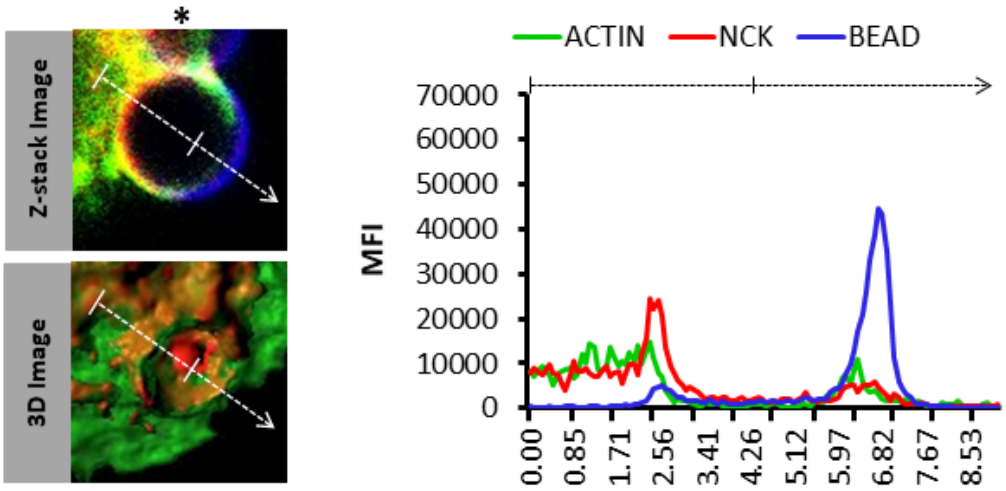
*
Z-stack Image
3D Image
ACTIN
NCK
BEAD
MFI
70000
60000
50000
40000
30000
20000
10000
0
0.00
0.85
1.71
2.56
3.41
4.26
5.12
5.97
6.82
7.67
8.53

FIGURE 7.16

A.

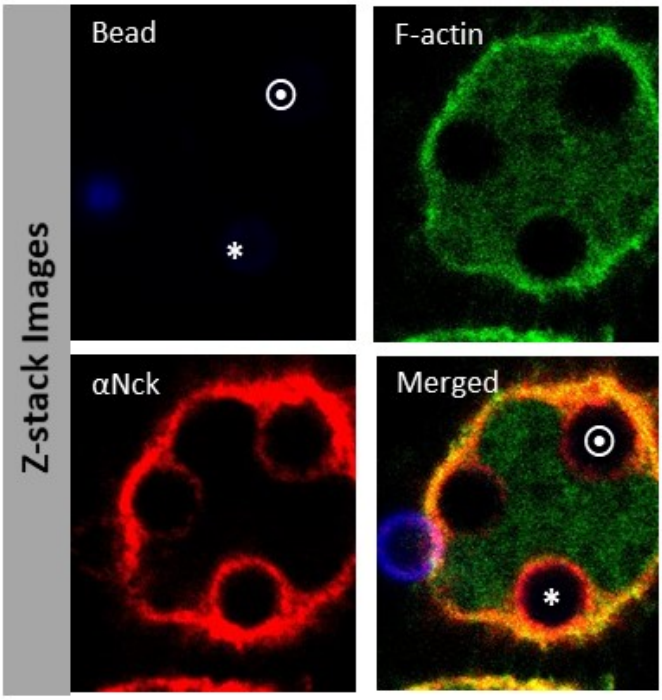

B.

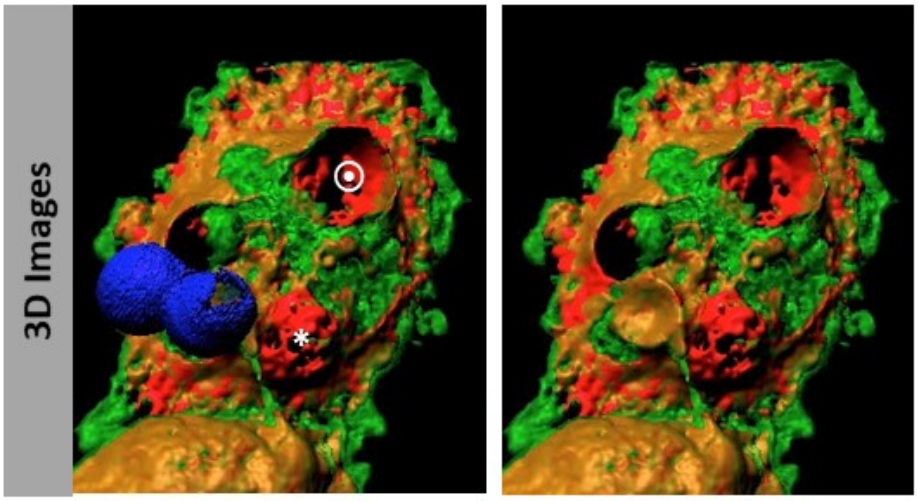

FIGURE 7.16

C.

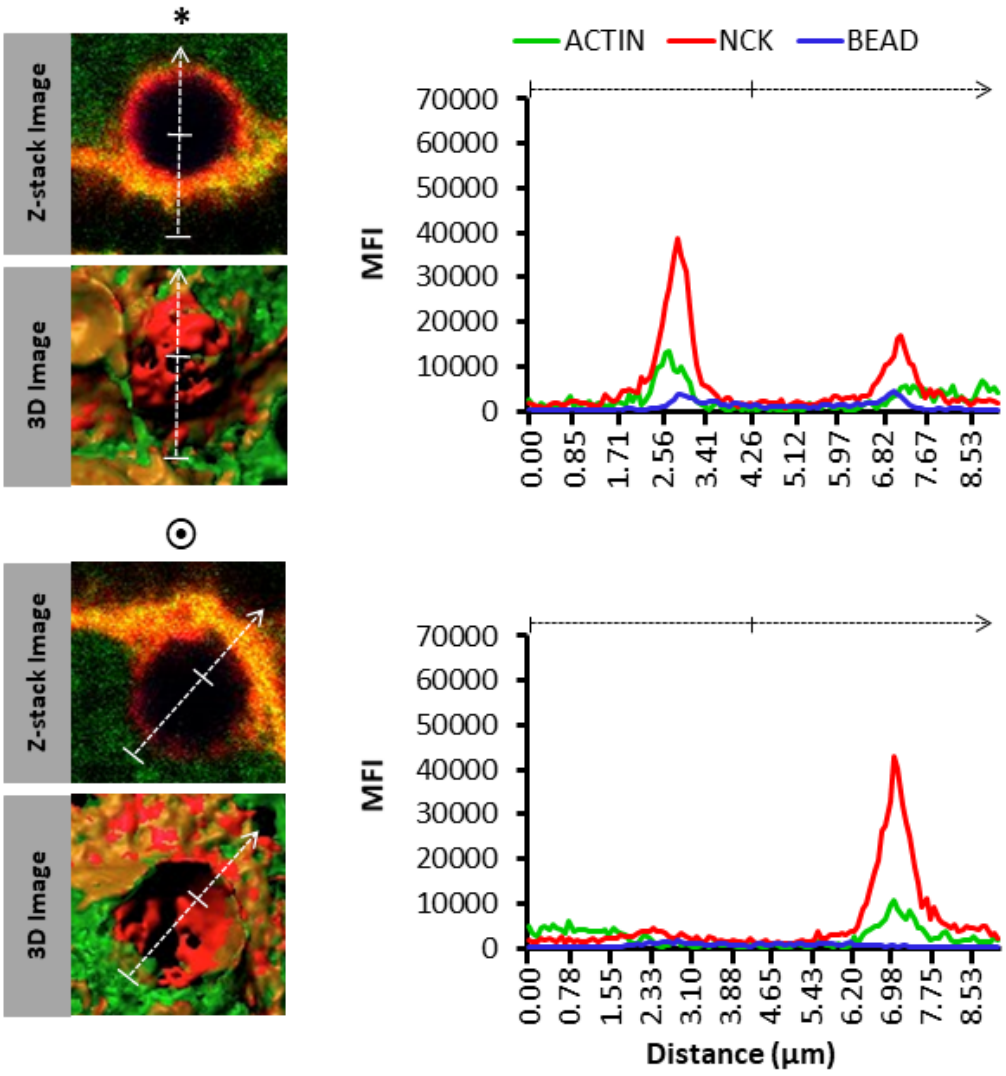
*
Z-stack Image
3D Image
⊙
Z-stack Image
3D Image
ACTIN
NCK
BEAD
MFI
70000
60000
50000
40000
30000
20000
10000
0
0.00
0.85
1.71
2.56
3.41
4.26
5.12
5.97
6.82
7.67
8.53
MFI
70000
60000
50000
40000
30000
20000
10000
0
0.00
0.78
1.55
2.33
3.10
3.88
4.65
5.43
6.20
6.98
7.75
8.53
Distance (µm)

FIGURE 7.14- 7.16 Recruitment of Nck during IpLITR 2.6b/IpFcRγ-L-mediated phagocytosis. Phagocytosis assays were performed by incubating $1x10^5$ IpLITR 2.6b/IpFcRγ-L-expressing cells stably transfected with LifeAct-GFP (green) with 4.5-μm non-fluorescent polystyrene beads ($3x10^5$) pre-opsonized with αHA mAb for 60 min at 37°C while adhered to coverslips. After bead incubation, cells were fixed with 4% PFA at 37°C. To asses the level of internalization of mAb beads, cells were incubated with a secondary goat αmouse Alexa-647. Post bead staining, cells were permeabilized and then stained for intracellular Nck via first incubating with a rabbit αNck mAb and then a secondary goat αrabbit Alexa-550. Z-stack images (A) were then obtained at a magnification of 63x using a Zeiss LSM 710 laser scanning confocal microscope, with beads of interested indicated by an asterisk. Post imaging collection, coloration for beads (blue), Nck (red) and the cell (green) were artificially changed to better demonstrate the overall associations of all three colors via the imaging software Zen 2009. Representative z-stacks for individual cells chosen for further analysis were transformed into 3D renders to better visualize the spatial association of Nck recruitment within the cells at bead-cell interfaces with beads used for further analysis indicated by an asterisk (B). Qualitative analysis was performed on shown z-stack images (from A) by collecting mean fluorescence intensities (MFI; y-axis) of both bead staining (blue line) and Nck staining (red line) across the identified bead in the image shown (x-axis; distance; μm) using ImageJ 9.2.1 (C).

FIGURE 7.17

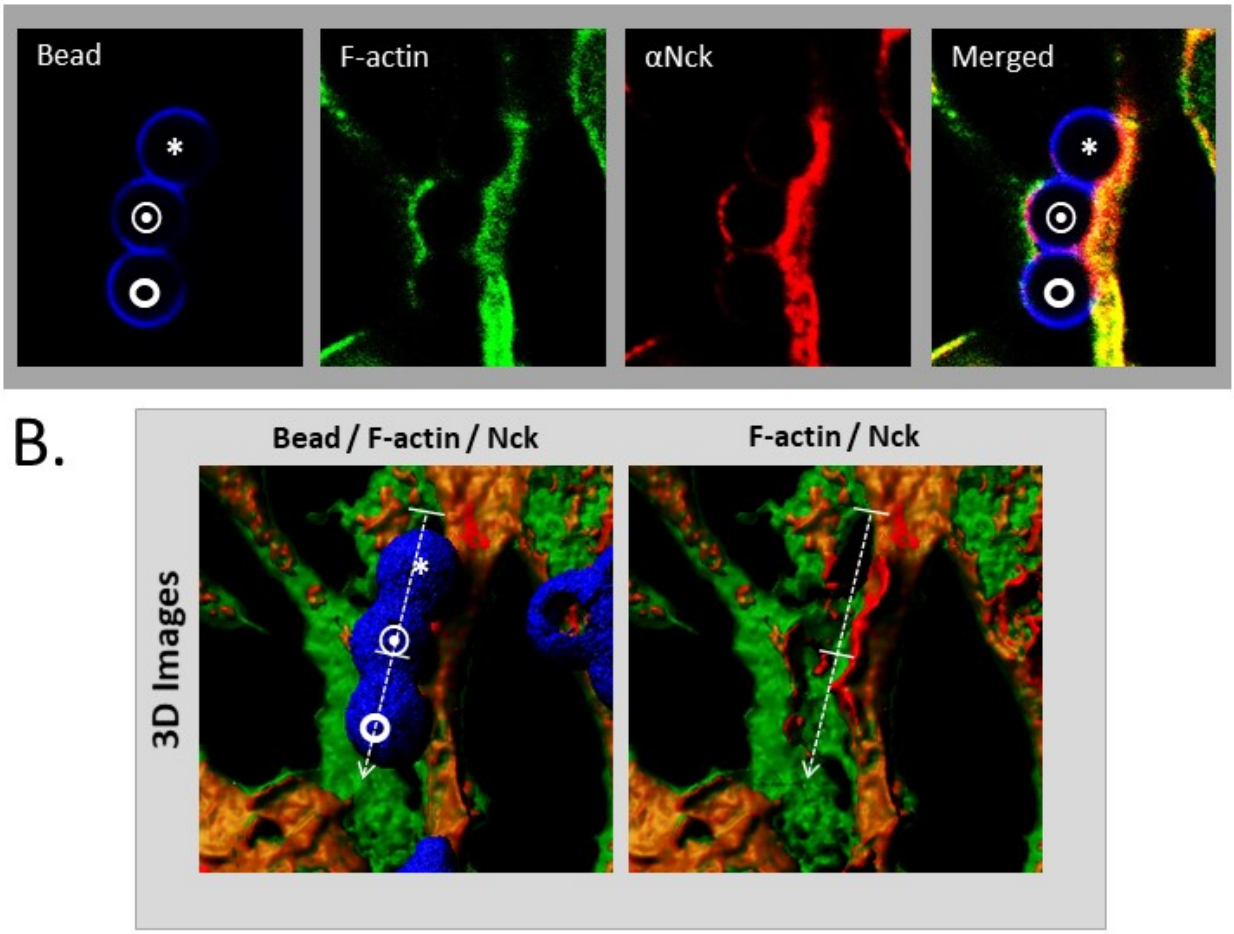
A.
Bead
F-actin
αNck
Merged
B.
Bead / F-actin / Nck
F-actin / Nck
3D Images
C.
ACTIN
NCK
BEAD
MFI
70000
60000
50000
40000
30000
20000
10000
0
0.00
1.01
2.02
3.02
4.03
5.04
6.05
7.05
8.06
9.07
10.08
11.09
12.09
13.10
14.11
15.12
16.12
17.13
18.14
Distance (µm)

FIGURE 7.17

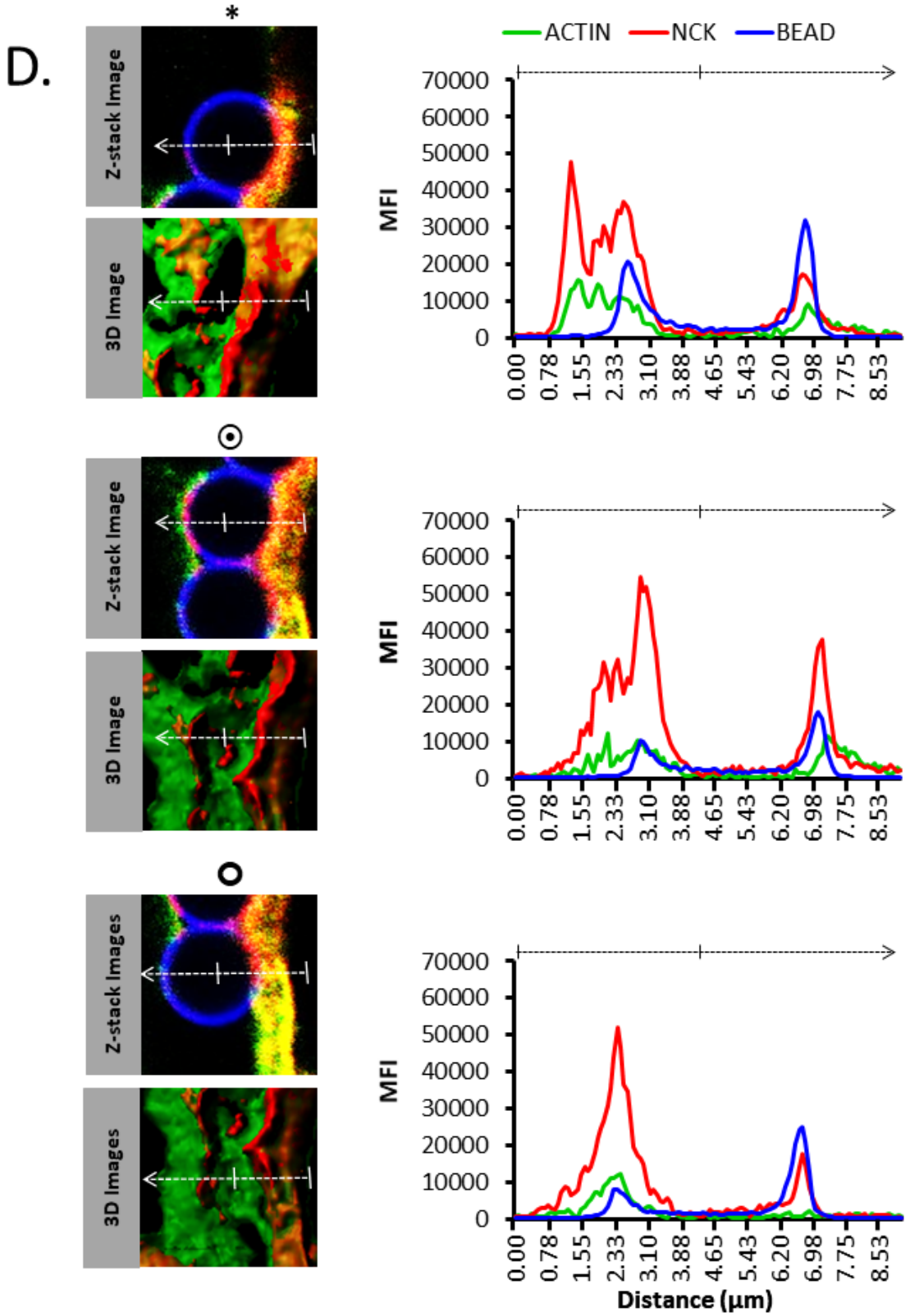
D.
*
Z-stack Image
3D Image
ACTIN
NCK
BEAD
MFI
70000
60000
50000
40000
30000
20000
10000
0
0.00
0.78
1.55
2.33
3.10
3.88
4.65
5.43
6.20
6.98
7.75
8.53
⊙
Z-stack Image
3D Image
MFI
O
Z-stack Images
3D Images
MFI
Distance (µm)

FIGURE 7.18

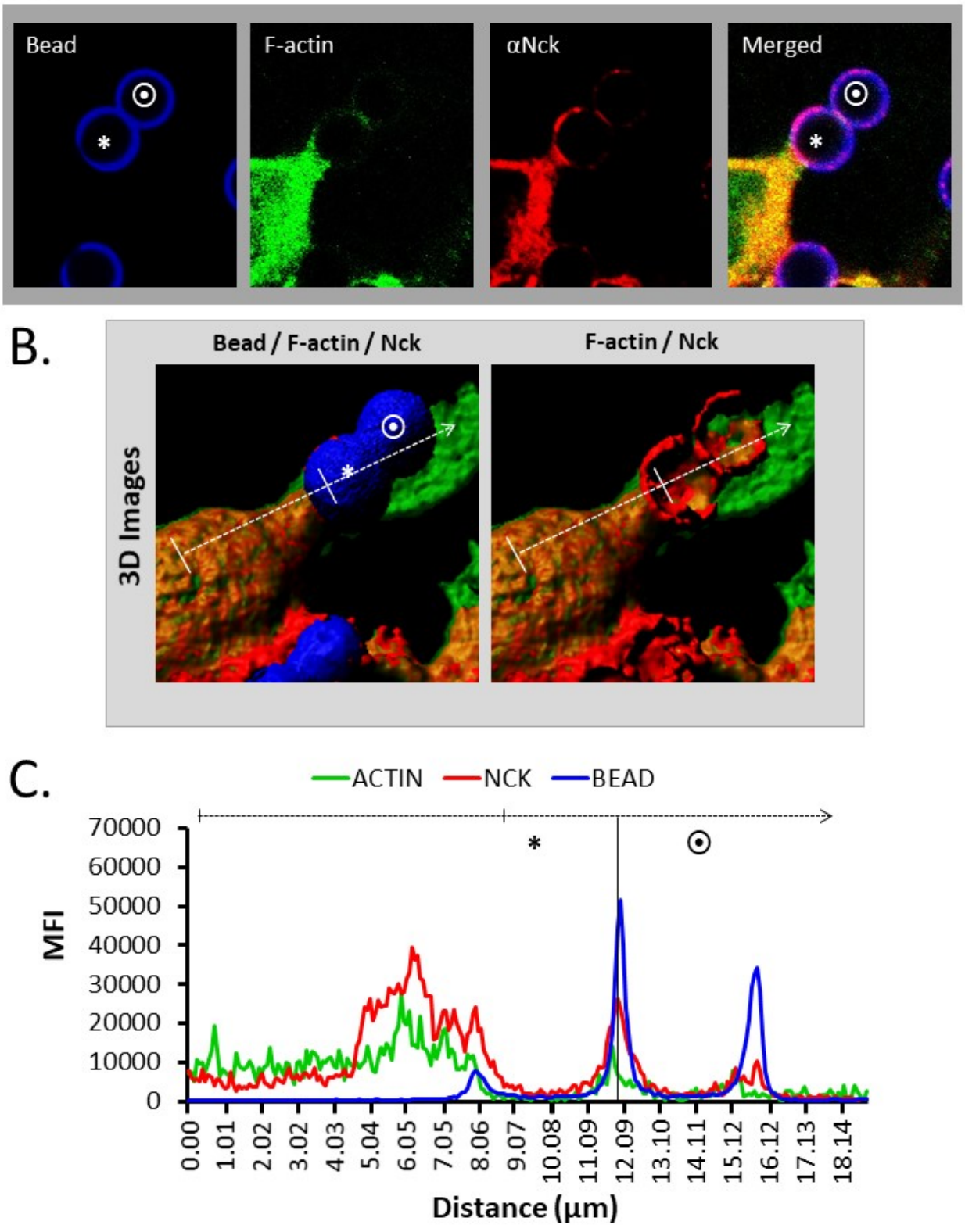
A.
Bead
F-actin
αNck
Merged
B.
Bead / F-actin / Nck
F-actin / Nck
3D Images
C.
ACTIN
NCK
BEAD
MFI
70000
60000
50000
40000
30000
20000
10000
0
0.00
1.01
2.02
3.02
4.03
5.04
6.05
7.05
8.06
9.07
10.08
11.09
12.09
13.10
14.11
15.12
16.12
17.13
18.14
Distance (µm)

FIGURE 7.18

D.

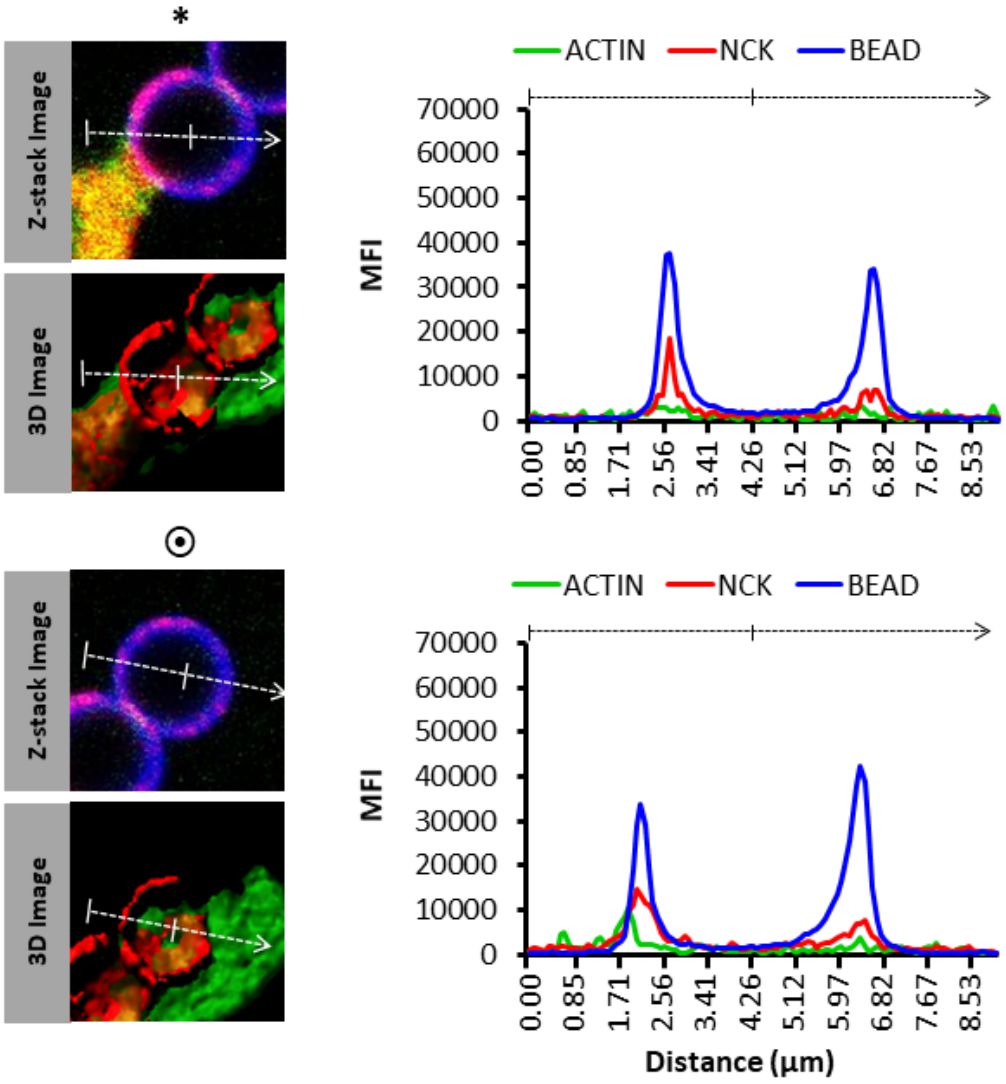
*
Z-stack Image
3D Image
ACTIN
NCK
BEAD
MFI
70000
60000
50000
40000
30000
20000
10000
0
0.00
0.85
1.71
2.56
3.41
4.26
5.12
5.97
6.82
7.67
8.53
⊙
Z-stack Image
3D Image
ACTIN
NCK
BEAD
MFI
70000
60000
50000
40000
30000
20000
10000
0
0.00
0.85
1.71
2.56
3.41
4.26
5.12
5.97
6.82
7.67
8.53
Distance (µm)

FIGURE 7.19

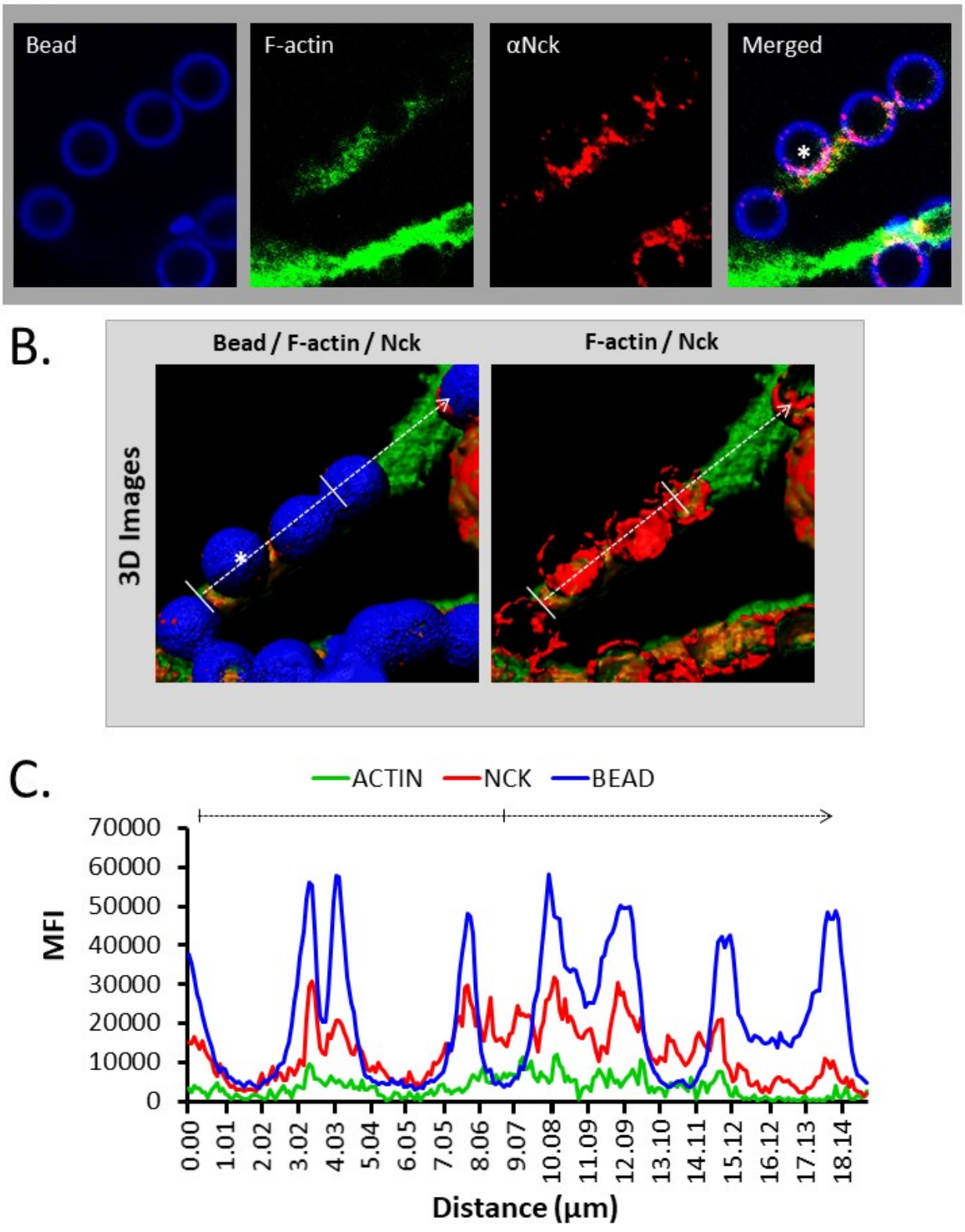
A.
Bead
F-actin
αNck
Merged
B.
Bead / F-actin / Nck
F-actin / Nck
3D Images
C.
ACTIN
NCK
BEAD
MFI
70000
60000
50000
40000
30000
20000
10000
0
0.00
1.01
2.02
3.02
4.03
5.04
6.05
7.05
8.06
9.07
10.08
11.09
12.09
13.10
14.11
15.12
16.12
17.13
18.14
Distance (µm)

FIGURE 7.19

D.

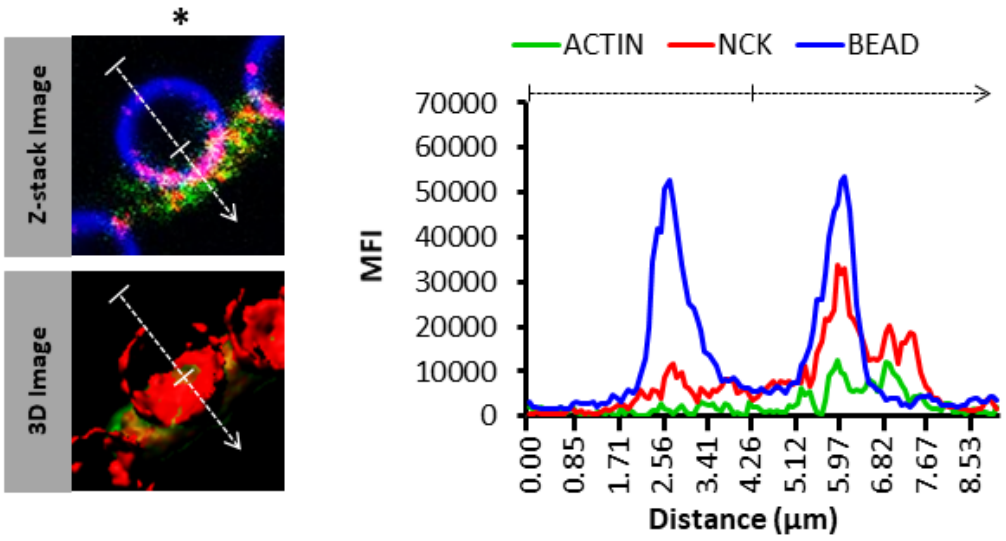
*
Z-stack Image
3D Image
ACTIN
NCK
BEAD
MFI
70000
60000
50000
40000
30000
20000
10000
0
0.00
0.85
1.71
2.56
3.41
4.26
5.12
5.97
6.82
7.67
8.53
Distance (µm)

FIGURE 7.20

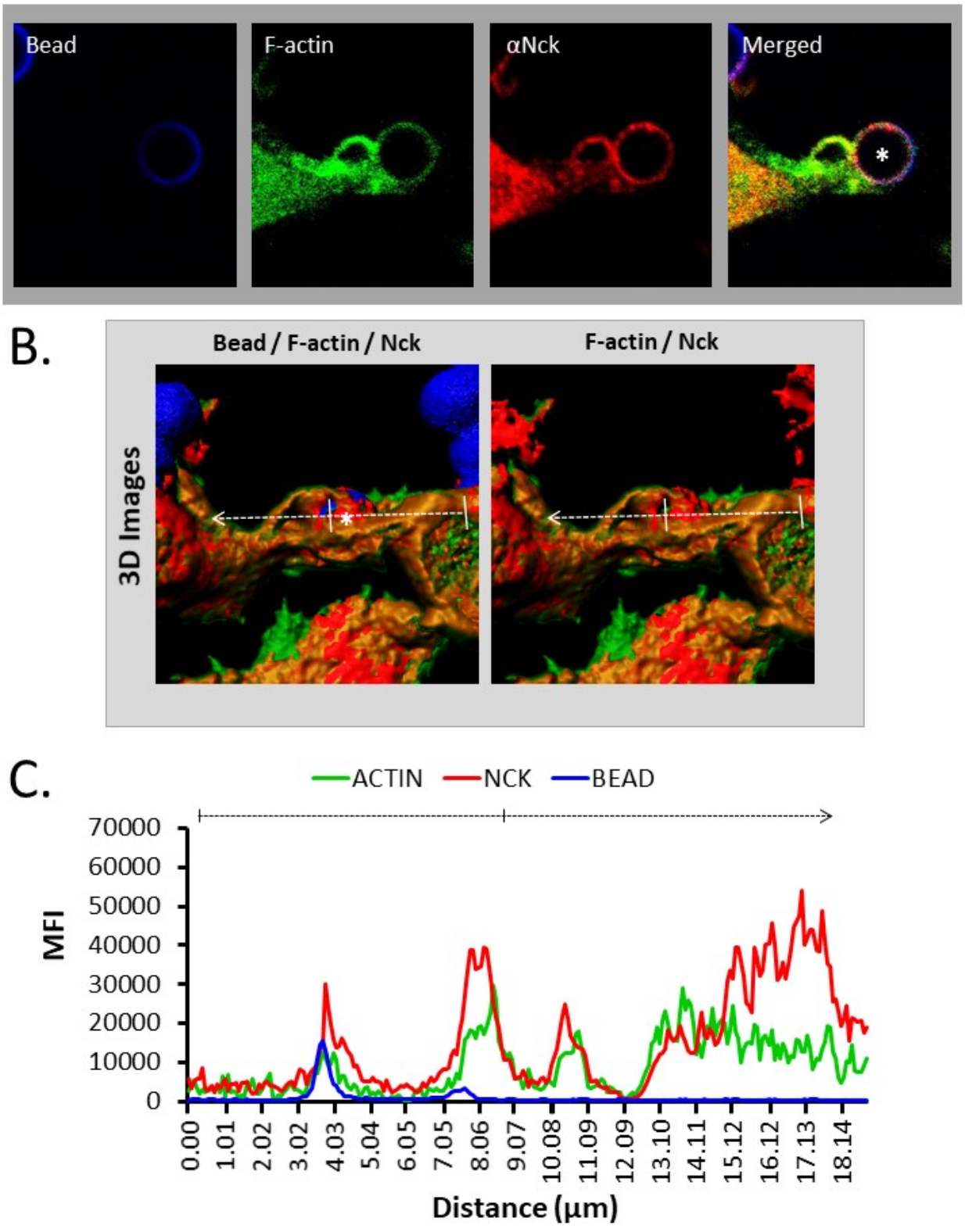
A.
Bead
F-actin
αNck
Merged
B.
Bead / F-actin / Nck
F-actin / Nck
3D Images
C.
ACTIN
NCK
BEAD
MFI
70000
60000
50000
40000
30000
20000
10000
0
0.00
1.01
2.02
3.02
4.03
5.04
6.05
7.05
8.06
9.07
10.08
11.09
12.09
13.10
14.11
15.12
16.12
17.13
18.14
Distance (µm)

FIGURE 7.20

D.

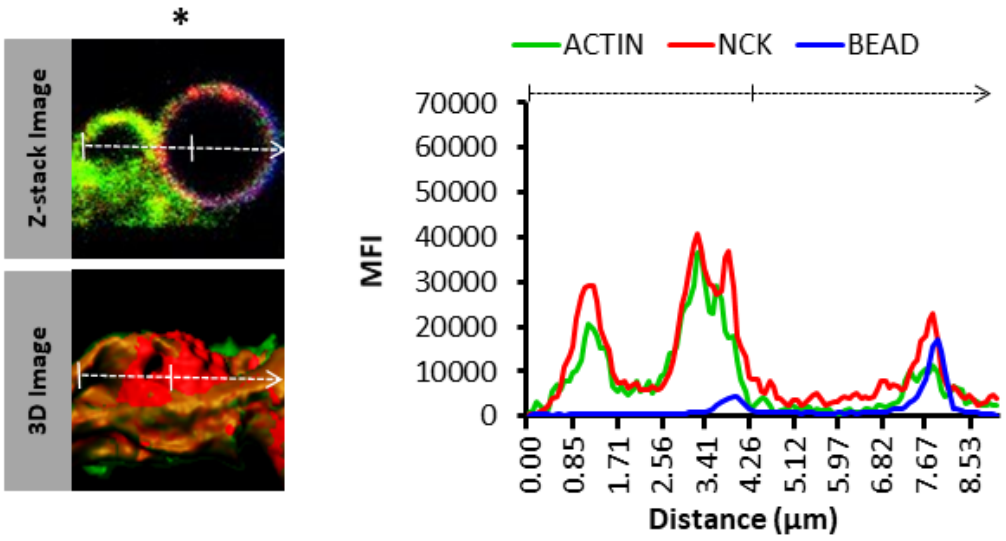
*
Z-stack Image
3D Image
ACTIN
NCK
BEAD
MFI
70000
60000
50000
40000
30000
20000
10000
0
0.00
0.85
1.71
2.56
3.41
4.26
5.12
5.97
6.82
7.67
8.53
Distance (µm)

FIGURE 7.21

A.

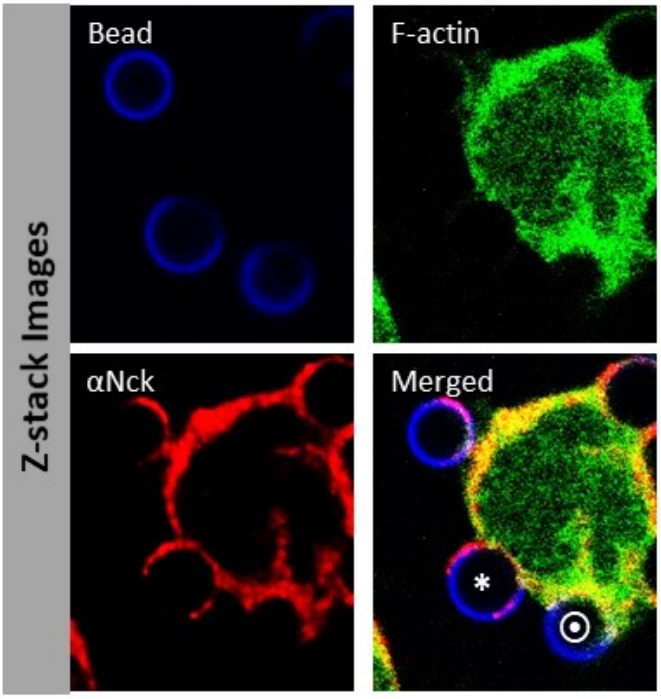

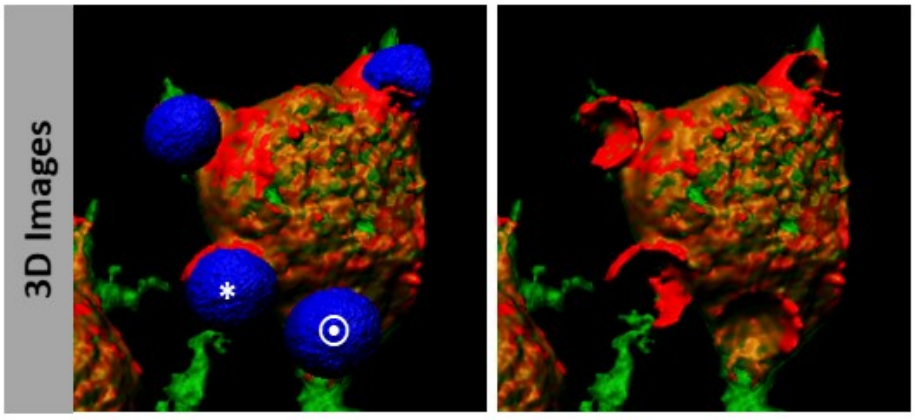

FIGURE 7.21

B.

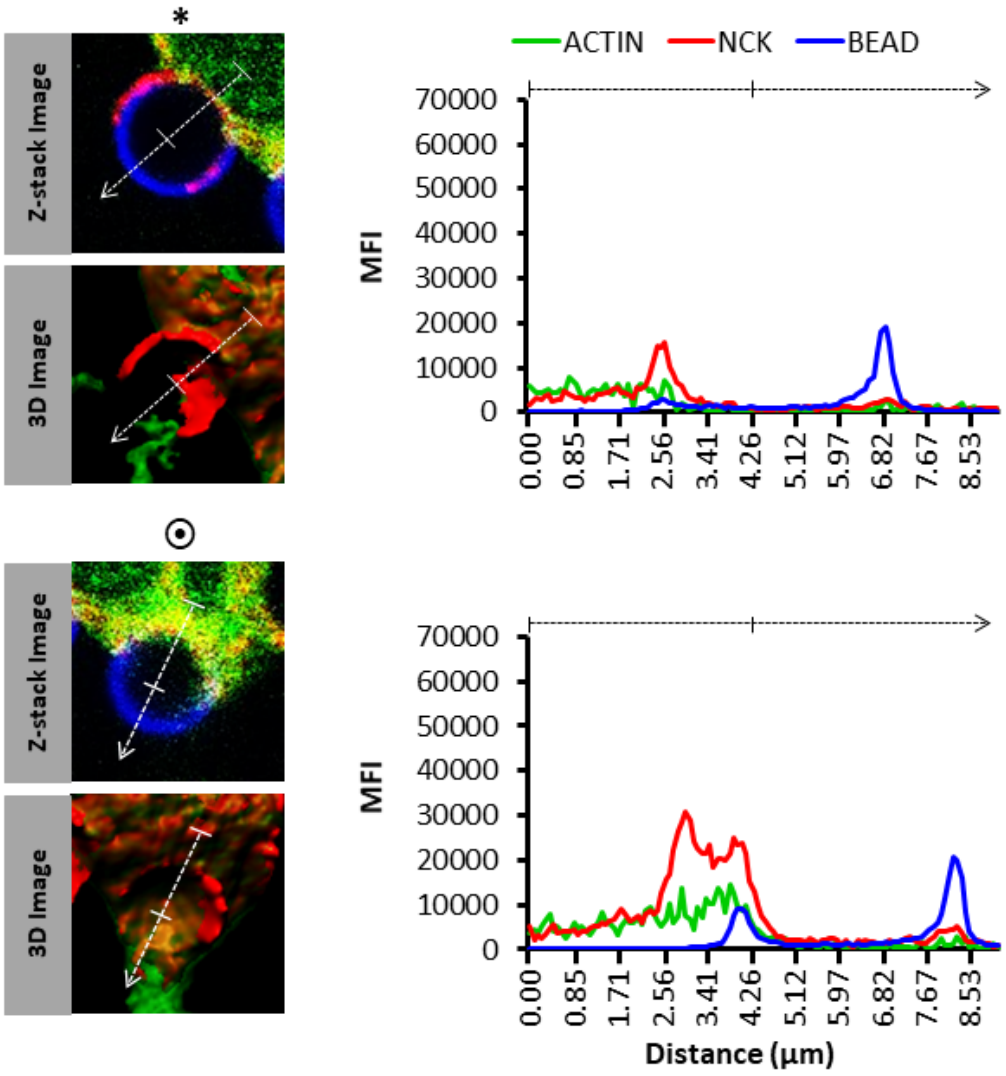
*
Z-stack Image
3D Image
ACTIN
NCK
BEAD
MFI
70000
60000
50000
40000
30000
20000
10000
0
0.00
0.85
1.71
2.56
3.41
4.26
5.12
5.97
6.82
7.67
8.53
⊙
Z-stack Image
3D Image
MFI
Distance (µm)

FIGURE 7.17-7.21 Recruitment of Nck during IpLITR 1.1b-mediated phagocytosis. Phagocytosis assays were performed by incubating $1x10^5$ IpLITR 1.1b-expressing cells stably transfected with LifeAct-GFP (green) with 4.5-μm non-fluorescent polystyrene beads ($3x10^5$) pre-opsonized with αHA mAb for 60 min at 37°C while adhered to coverslips. After bead incubation, cells were fixed with 4% PFA at 37°C. To asses the level of internalization of mAb beads, cells were incubated with a secondary goat αmouse Alexa-647. Post bead staining, cells were permeabilized and then stained for intracellular Nck via first incubating with a rabbit αNck mAb and then a secondary goat αrabbit Alexa-550. Z-stack images (A) were then obtained at a magnification of 63x using a Zeiss LSM 710 laser scanning confocal microscope, with beads of interested indicated by an asterisk. Post imaging collection, coloration for beads (blue), Nck (red) and the cell (green) were artificially changed to better demonstrate the overall associations of all three colors via the imaging software Zen 2009. Representative z-stacks for individual cells chosen for further analysis were transformed into 3D renders to better visualize the spatial association of Nck recruitment within the cells at bead-cell interfaces with beads used for further analysis indicated by an asterisk (B). Qualitative analysis was performed on shown z-stack images (from A) by collecting mean fluorescence intensities (MFI; y-axis) of both bead staining (blue line) and Nck staining (red line) across the identified bead in the image shown (x-axis; distance; μm) using ImageJ 9.2.1 (C).

CHAPTER VIII
GENERAL DICSUSSION

8.1 Summary of findings

Many comparative immunological studies have focused on the identification of immune genes in different animals, with only a small subset of these studies focused on the functional characterization of immunoregulatory proteins. The findings in this thesis demonstrate that IpLITRs can selectively engage distinct components of the phagocytic process and provides important new information regarding the target acquisition as well as internalization mechanisms involved in controlling phagocytic responses. This also offers new information regarding the directed ability of immunoregulatory receptor-types to initiate dynamic membrane structures and provides insights into an alternative ITAM-independent target capture pathway that is functionally distinct from classically described phagocytic pathways. My results also identify IpLITRs as an excellent model for investigating emergent concepts involved in the coordination of complex and highly-conserved effector responses, such as phagocytosis, during innate defense mechanisms that are often performed in a protease-rich inflammatory environment. The research provided here also appears to be the first to suggest that expression of a specific immunoregulatory receptor-type can promote the constitutive formation of filopodia. IpLITR 1.1b-mediated signaling also initiates secondary waves of actin polymerization events that are associated with the internalization and membrane tethering of extracellular targets, which I propose to be a distinct event from those involved in the constitutive filopodia generation pathway. Furthermore, target acquisition and engulfment pathways facilitated by IpLITR 1.1b likely require the differential participation of its membrane proximal and distal CYT regions for recruitment and activation of select intracellular effectors. Overall, my thesis research offers

novel information regarding the ability of immunoregulatory receptors to initiate filopodia formation and provides new insights into the temporal organization of cellular events surrounding the unique activation dynamics that regulate F-actin polymerization and membrane remodelling events during the binding, capture, and engulfment of targets.

Initially I developed assays to test the hypothesis that IpLITRs participated in both ITAM-dependent and ITAM-independent phagocytic signaling pathways. The results described in Chapter IV showed that IpLITR 1.1b facilitates phagocytosis through a distinct ITAM-independent mechanism and appeared to utilize membrane protrusions, or filipodia, during the early stages of phagocytosis for target capture, indicating that distinct modes of phagocytosis exist among IpLITR-types. The two classical modes of phagocytosis that have been extensively described in mammals involve either FcRs and CR3 [2]; with key receptor-mediated differences in the cellular mechanisms controlling target acquisition and engulfment. For example, stimulatory FcRs commonly associate with the adaptor protein FcRγ chain that encodes an ITAM in its CYT region. Following interactions with IgG-opsonized targets, FcR-FcRγ chain complexes oligomerize at the receptor-target interface to facilitate tyrosine phosphorylation of ITAMs by Src-family tryrosine kinases [101,272]. Phosphorylated ITAMs then bind the Syk, which serves as the main effector of FcR-mediated signaling events by directly binding and/or phosphorylating other intracellular components [103,209]. Select examples include class I PI3K [210,273,274], guanine nucleotide exchange factors GEF including Vav, and small Rho family GTPases such as Rac1 and Cdc42 [93,275]; the latter being important effectors controlling the formation of filamentous actin (F-actin) structures during generation of the phagocytic cup and extension of membranous pseudopods [5,114]. In comparison, CR3-mediated phagocytosis can occur in cells lacking Syk and is an ITAM-independent process [276]. However, CR3 activation

of phagocytosis is dependent on protein kinase C (PKC) activity [276] for the recruitment and activation of the small GTPase RhoA (but not Cdc42 and/or Rac1), which links CR3 engagement to local F-actin accumulation during phagocytosis [119,121]. Additional signaling proteins such as Talin, Rho-associated protein kinase, formin mDia, and myosin II are also known components of CR3 phagocytosis [113,122,211] that are not commonly associated with FcR-dependent phagocytosis.

Plasticity in phagocytic receptor functions is further appreciated by the recent report of the cellular activities of CEACAM3 [3,8]. CEACAM3 is a human-specific phagocytic receptor expressed by neutrophils that activates a unique short-circuited version of phagocytosis through a minimal set of molecules that effectively generate rapid actin-dependent pathogen internalization [3,8]. My data indicated IpLITR 1.1b-mediated phagocytosis was only effectively blocked in the presence of F-actin, Src, and Syk inhibitors. This may indicate that IpLITR 1.1b may exist in a primed state facilitating constitutive coupling to the F-actin machinery necessary for target acquisition and phagocytic cup formation. This could be due to constitutive association with mediators of actin dynamics, which would be like the novel phagocytic pathway described for CEACAM3. My results shown in Chapter IV I identify the control of actin-dependent filopodia and phagocytic cup formation by IpLITR 1.1b illustrates, for the first time, a unique ITAM-independent mechanism for the stimulation of phagocytosis by a non-mammalian immunoregulatory receptor.

In Chapter V, I showed trypsin selectively inhibited IpLITR 1.1b-mediated phagocytosis, which closely correlated with a reduction in the surface expression of this protein. IpLITR 1.1b-expressing cells trypsin treated rarely displayed fully internalized beads and had a reduction in the number of beads captured in phagocytic cups or at the ends of membranous filopodia. In fact,

most beads appeared to be located adjacent to the cell and not bound in membrane-based structures. This data suggested that extracellular proteases can selectively modulate the ability of IpLITR 1.1b to uniquely alter the remodeling of cellular membrane during the process of extracellular target capture and engulfment. My data also suggested that trypsin may not shed IpLITR 1.1 from the cell surface, but that trypsin may induce a conformational change in IpLITR 1.1b's structure that stimulates removal of the receptor from cell surface through regulated endocytosis. The *in vivo* role that trypsin may play in the translocation and regulation of IpLITR 1.1b-expression remains unknown; however, my results support an alternative perspective that trypsin may selectively modulate IpLITR 1.1b's functions by inducing signaling events from within the endomembrane system. This would be a similar effect identified for other immunoregulatory receptors in protease-rich environments. For example, when pathogens circumvent anatomical barriers, neutrophilic granulocytes are rapidly recruited to the site of infection where they release a variety of pro-inflammatory mediators and antimicrobial factors [277]. Neutrophil-derived serine proteases (NSPs) are potent antimicrobial agents that also have additional immunomodulatory functions [278,279]. NSPs are stored in azurophilic granules and consist predominantly of elastase, cathepsin G and proteinase 3; each of which display unique substrate specificity [278,280]. NSP-mediated proteolysis participates in complex physiological functions including the destruction of foreign microbes, tissue remodeling, and enzyme-mediated processing of select immune proteins [278,279]. NSPs can also directly target immunoregulatory receptor proteins including TLR4 [281] , CD14, CD43 [282], CD23 [283], complement receptor 1 [284,285], intercellular adhesion molecule 1, vascular cell-adhesion molecule 1 [286,287] and the cell surface-bound ligand binding chains of the IL-6 receptor [288]. This has varying effects on immune cell effector functions such as regulating cytokine secretion, cellular migration,

adhesion, complement activation, respiratory burst, and clearance of apoptotic cells during inflammation. Exogenously-derived pathogen proteases also serve important immunomodulatory roles as these enzymes can be used for immune-system evasion. For example, bacterial enzymes directly target antibody and complement proteins, which block the opsonization of microbes to inhibit engulfment by phagocytes [2,289] target intracellular signaling molecules belonging to the TLR pathway [290], and can digest surfactant protein-A [291]. These examples collectively indicate that host and pathogen proteases play vital roles in a wide variety of biological functions such as tissue homeostasis, inflammation, infections, and diseases.

Other families of cell surface receptors like IpLITRs display similar sensitivity specifically to trypsin. The most commonly examined trypsin-sensitive receptors belong to the protease activated receptor (PAR) family, which are seven-transmembrane domain G protein-coupled receptors that are directly activated by proteases-dependent cleavage events [292]. PAR2 is specifically triggered by trypsin [293], mast cell tryptase, and a few other mammalian serine proteases [292–299]. Activation of PAR2 has been linked with the release of pro-inflammatory mediators, leukocyte migration, expression of adhesion molecules (reviewed in [300]), and augments skin pigmentation by stimulating the phagocytic response of keratinocytes [301–303]. Furthermore, protease-activated PAR2 can transactivate other receptors including epidermal growth factor receptors (EGFRs; [304]) and TLR4 [290,305] during the coordinate control of inflammatory signaling cross-talk. Interestingly, transactivation of EGFRs by PAR2 also requires activation of membrane-bound matrix metalloproteinases (MMPs), which induce the release of membrane-anchored EGF receptor ligands [304]. Many of these MMPs are also involved in protease-mediated receptor shedding from the cell surface (reviewed in [306]). This has been increasingly recognized as a key regulatory mechanism since proteolytic shedding of

surface receptors often acts in a negative feedback fashion on receptor-mediated signaling events (reviewed in [307]). Several studies have previously shown that trypsin directly cleaves proteins from the cell surface, however, trypsin activity can also modify receptors without inducing their shedding or internalization. For example, the dectin-1 receptor is directly cleaved from the surface of macrophages by trypsin and this is associated with an inhibition of the internalization of zymosan particles [308]. Galectin-1 also exists as a trypsin-sensitive surface protein that is shed into the cellular supernatants following enzyme exposure [309]. Inactivation of the C5a receptor can also occur in response to various NSPs through the loss of the N-terminal binding portion of the receptor but not via cleavage of the entire ectodomain [34]. Uniquely, the chicken-specific TLR15 is activated by pathogen-derived proteases that, unlike host proteases, carry out a cleavage event that modifies the receptors structure required for TLR15-induced pro-inflammatory signaling events [310]. The trypsin-sensitivity of the mammalian MR and its associated reduced phagocytic activity parallels my own observations for IpLITR 1.1b. However, in contrast to my findings, the MR is proteolytically processed into a surface-expressed form that is smaller than the native protein [224]. The trypsin-generated MR is internalized and degraded, which supports my hypothesis that trypsin can provide a trigger for the regulated internalization of surface proteins. Overall, it appears that the catalytic activity of proteases plays important roles in the regulation of effector responses by directly and indirectly effecting immunoregulatory receptors.

In Chapter VI, I used live cell and SEM imaging techniques to identify if IpLITR 1.1b-expressing cells can uniquely generate actin-dense filopodia-like protrusions during the early stages of extracellular target interactions. My results support the hypothesis that F-actin-dense filopodia are generated by IpLITR 1.1b-expressing cells and can be used for target capture. At

depressed temperatures, although membrane structures had reduced mobility, IpLITR 1.1b-expressing cells still generated dynamic filopodia structures that continued to engage in sustained cell-target interactions. This was in stark contrast to the membrane dynamics observed for IpLITR 2.6/IpFcRγ-L-expressing cells that had no F-actin dynamics, or any membrane associated activity at lower temperatures. Results obtained from this work led me to conclude that IpLITR 1.1b-expression is important for the generation of filopodia-like structures prior to target associations. I therefore hypothesized IpLITR 1.1b may exist in a primed state that facilitates endogenous coupling to effectors of F-actin dynamics to constitutively trigger filopodia formation.

Across eukaryotes, the generation of filopodia during diverse cellular events have been reported to require several classes of protein kinases and kinase-associated molecular scaffolds, small Rho-family GTPases Rac1/2 and Cdc42, various cytoskeletal elements including components of the actin-polymerization machinery (e.g. myosins and formins), as well as the generation of membrane-embedded phosphatidylinositol 3,4,5-trisphosphate (PtdIns(3,4,5)P_3) [2,82,87,88,242,252,311,312]. Filopodia are regulated by mechanisms instigated by constitutive intracellular signaling events that appear to involve a number of conserved transduction molecules [235,242]. For example, the tyrosine kinase ableson murine leukemia mammalian oncogene-1 (c-Abl) is required for the promotion of filopodia during fibroblast cell spreading [246]. C-Abl induces filopodia production through the phosphorylation of the docking protein 1 scaffold and subsequent recruitment of Nck to docking protein 1 (Dok1) [246]. This causes increased localization of N-WASp to the plasma membrane, thereby inducing localized F-actin polymerization and subsequent filopodia production [246]. Filopodia formation also occurs via the recruitment of the inverse-BAR protein insulin receptor substrate protein of 53 kDa (IRSp53)

to the inner membrane leaflet [247–249]. Translocation of IRSp53to the plasma membrane is induced by the presence of Cdc42 whose interaction with IRSp53 recruits formins, WAVE2, and N-WASp into a growing effector complex required for actin nucleation [249,313]. Formin proteins enhance the assembly of actin during the progression of filopodia formation while fascins cause the bundling of F-actin into parallel structures that provides filopodia with their classical tubular structure [235,242]. Lastly, cellular motor proteins such as myosins are important for the transportation of additional proteins to the growing tip of filopodia, allowing their formation to continue farther into the extracellular milieu [242,250,251,312]. Overall, constitutively generated filopodia allow phagocytes to constantly probe their extracellular environments and these membranous probes may contain phagocytic receptors located along their edges; a process that depends on an unknown mechanism for the loading of phagocytic receptors into these distal protrusions [2,87,252]. Random phagocytic receptor-target interactions that may occur would enable the attachment of specific targets to the membrane facilitating their internalization.

An alternative mechanism for filopodia formation from that of constitutive generation is the activation of certain receptor-types via exogenous stimulation. For example, the exogenous addition of agonists for TLR4 and the calcium-sensing receptor (CaSR) (LPS and Ca^{2+} respectively) has been shown to increase the production of filopodia-like structures on immune cells suggesting that receptor-mediated responses to extracellular stimuli can be involved in forming filopodia [240,241,314]. Receptor-induced filopodia on cancerous cells use inducible pathways to produce filopodia which can facilitate invasion of surrounding tissues. These extensions, termed invadopodia, are formed by the exogenous addition of PDGF and EGF which showed to increase the level of invadopodia formation [244,245]. Invadopodia facilitate tumour

metastasis by first adhering to and then penetrating extracellular matrices as they contain specific matrix metalloproteinases at their extending tips that break down tissue barriers creating points of entry into tissues [244,245] . The generation of filopodia by cancerous cells has been shown to be in part regulated by FAK, Src, isoforms of PI3K, protein kinase C (PKC), and tyrosine kinase substrate 5 (TKS5) that function to regulate changes in lipid membrane composition and recruit signaling proteins to the site of invadopodia formation [244,245]. In particular, TKS5 acts as a scaffolding protein for a variety of proteins controlling F-actin polymerization; such as Nck, N-WASp, and the growth factor receptor-bound protein 2 (Grb2) [244]. Accumulation of these molecules allows for the activation of additional cytoskeletal regulatory proteins including the small Rho GTPases Ras-Rac 1/2 and Cdc42, as well as effectors of the Arp 2/3 complex [244,245]. Interestingly, my experiments demonstrate a possible third mechanism for filopodia formation as the stable expression of IpLITR 1.1b alone without exogenous stimulation initiated filopodia generation. Moreover, perhaps those events that have been identified as 'constitutively' induced filopodia are the result of endogenously activated receptors that have yet to be identified.

One possible mechanism for non-stimulated filopodia formation of IpLITR 1.1b-expressing cells may be the basal recruitment and activation of Nck to the proximal region of IpLITR 1.1bs CYT. Like CECAM3, IpLITR 1.1b may also recruit Nck in order to assemble regulators of actin polymerization, including WAVE2. In one predicted scenario, WAVE2 may indirectly associate with IpLITR 1.1b using the adaptor Nck that could bind the consensus sequence H-I-Y-D-E-V located at Y_{433} in the proximal IpLITR 1.1b CYT region [3]. The binding of Nck to IpLITR 1.1b could bring key initiators of the F-actin polymerization machinery into close proximity of stimulatory GEFs, inducing further downstream signaling events. Following

or during the recruitment of effectors of the actin cytoskeleton to the proximal CYT region of IpLITR 1.1b, I hypothesized that Syk may bind the distal CYT region of IpLITR 1.1b by interacting with phosphorylated tyrosines, Y_{477} and Y_{499}, positioned in two tandem ITIM motifs that could accommodate the two SH2 domains of Syk. This atypical mode of Syk recruitment to tandem ITIMs has already been demonstrated for PECAM-1 [105]. These tandem ITIMs located within the CYT region of PECAM-1 are spaced such that their tyrosine's are separated by 22 amino acids. Interestingly, this is also the same separation between Y_{477} and Y_{499} within IpLITR 1.1b distal region of its CYT and therefore might explain how Syk potentially interacts with the IpLITR 1.1b CYT. Once recruited to IpLITR 1.1b, I predict that Syk would bind and activate an intracellular Rho-GEF that could then directly regulate one of the many known Rho GTPases that are responsible for controlling rapid actin-driven filopodia through activation of Arp2/3 and the WAVE2 complex. Together, IpLITR 1.1b-mediated phagocytic activity would perhaps encompass the minimal machinery required (Nck, WAVE2, and Syk) for promoting local rearrangements of the actin cytoskeleton and would culminate in a PI3K-independent target capture pathway. A preliminary look at the possible recruitment of signaling effectors to IpLITR 1.1b by co-immunoprecipitation demonstrated that when phosphorylated, IpLITR 1.1b associated with Nck, Syk, and WAVE2 in RBL-2H3 cells [192]. These data link the CYT region of IpLITR 1.1b to endogenously available intracellular proteins that could regulate actin-dependent phagocytosis. This in part would be a similar situation to that identified for the human FcRL4, which like IpLITR 1.1b contains two ITIMs and an ITSM within its CYT. Studies of FcRL4 showed that its ITIMs and ITSM are endogenous phosphorylated in a ligand-independent manner which facilitated the recruitment of SHP-1/2 to its CYT region [315]. The recruitment of SHP-1/2 under these conditions was sufficient for inducing the dephosphorylation of Syk,

causing inhibition of BCR induced signaling [315]. Interestingly, the addition of the TLR9 agonist CpG to FcRL4-expressing cells induced translocation of FcRL4 intracellularly, which stimulated TLR9 signaling, suggesting a secondary stimulatory role post FcRL4 internalization [315]. Therefore, examples of immunoregulatory receptors engaging in intracellular signaling without receptor-ligation exist, which may explain how IpLITR 1.1b-expressiong alone can influence filopodia formation. Overall, my results suggest that IpLITR 1.1b may uniquely network with intracellular components requisite to produce F-actin containing filopodia-like structures.

In Chapter VII, I developed a confocal imaging-based assays to examine if Nck and/or pSyk constitutively associated with IpLITR 1.1b in filopodia (before the addition of targets) or at sites of receptor activation (target-cell interfaces). My colocalization analysis identified that Nck but not pSyk associated with IpLITR 1.1b in regions of filopodia formation. Nck as an adaptor protein can bind to a variety of intracellular signaling molecules to generate signaling complexes at the plasma membrane [213] and it has been shown to be an important regulatory factor of both filopodia/invadopodia formations [212,246,250,261,263–265,271]. Its importance in filopodia/invadopoia formations stems from its ability to actively associate with many other intracellular signaling proteins involved in F-actin polymerization (e.g. WAVE2, Grb2, Cdc42, Vav1, FAK, p21-kinase (PAK)), c-abl) [3,109,213,232,246,264,313] but also proteins responsible for generating the geometric shapes associated with filopodial structures (Dok1, IRSp53) [246,248,249]. Interestingly, Nck has also been shown to constitutively associate with other intracellular signaling molecules in resting cells. Specifically, Nck can endogenously associate with PAK in fibroblasts. Upon stimulation of fibroblasts via growth factors this constitutive complex is then transported to the membrane where it participates in F-actin

polymerization events [109]. PAK also has been identified as a regulatory factor in filopodia formation, and therefore perhaps the initial constitutive binding of PAK to Nck and then the engagement of Nck to IpLITR 1.1b may be a possible mechanism for IpLITR 1.1b-Nck induced filopodia formation. Nck can also constitutively interact with the GEF Vav1 in T cells as shown using Fo̅rster resonance energy transfer (FRET) analysis [271]. This occurred in resting T cells and was dependent on Nck interacting with the Vav1 proline-rich region as mutations within this region of Vav1 abrogated Nck-Vav1 interactions causing significantly altered F-actin polymerization [271]. Therefore, another possible mechanism by which IpLITR 1.1b-Nck could facilitate localized filopodia formation without prior receptor activation could be achieved via Nck binding to Vav1 and localizing it to sites of IpLITR 1.1b at the plasma membrane. Vav1 would be important then for the activation of small GTPases that would facilitate the activation of the F-actin nucleation effector WAVE2. One of the major factors surrounding the endogenous associations of Nck with IpLITR 1.1b is that Nck requires tyrosine phosphorylation to bind to receptors. Therefore, my IpLITR 1.1b-Nck data would suggest that IpLITR 1.1b is phosphorylated in the absence of ligand binding. Interestingly, as mentioned earlier, recent examination of the human FcRL4 protein has demonstrated that immunoregulatory receptors can be phosphorylated without prior activation and more importantly this ligand-independent phosphorylation can be used to regulate receptor signaling. Specifically, FcRL4 was shown to be endogenously phosphorylated on its CYT at two ITIM motifs and a ITSM and that FcRL4 bound and used SHP-1/2 for inhibitory signaling [315]. Such a mechanism in the case of IpLITR 1.1b would then allow constitutive associations of Nck with its own CYT and thereby would allow for the induction of filopodia.

In Chapter VII, I also showed that IpLITR 1.1b recruits Nck and pSyk to target-cell interfaces in a similar manner as predicted for IpLITR 2.6b/IpFcRγ-L, suggesting that Nck and pSyk are likely involved in IpLITR 1.1b activation. The requirement of pSyk kinase activity for phagocytosis is well documented, as its importance has been shown for both classical [101,209,218] and non-classical phagocytic receptors [6,63,268,269]. The importance of Syk in F-actin polymerization events is due to its ability to generate downstream signaling events via phosphorylation of other intracellular proteins. Such examples of Syk-induced phosphorylation include Vav1, Nck, SLP-76/LAT, PI3K, and PKC just to name a few [267]. Syk binds directly to phosphorylated receptors by situating itself right at the region where F-actin polymerization occurs. In the context of IpLITR 2.6b/IpFcRγ-L Syk is likely being recruited to its tandem ITAMs as has been described for many other ITAM-induced responses. For IpLITR 1.1b, based on my hypothesized model for how IpLITR 1.1b engages the F-actin polymerization machinery, the binding of pSyk is like occurring within the distal region of its CYT at the site of the tandem ITIMs. Nck has also been shown to be important for the induction of phagocytosis for ITAM-induced responses such as FcR-mediated phagocytosis [108,110]. During FcR-mediated phagocytosis, Nck is part of a large signaling complex consisting of Vav, profilin, Ena/vasodilator-stimulated phosphoprotein (VASP) and WASP, which are important for phagocytic cup formation as disruption of this complex abrogates formation of this structure [3,7]. As mentioned previously, Nck is also an important factor for CEACAM3-mediated phagocytosis but also recently has been identified to be involved in CEACAM4-mediated phagocytosis as well [3,7].

Taken together, these data support my proposed model in Chapter VII, whereby Nck and Syk bind to IpLITR 1.1b to promote F-actin polymerization events leading to the capture and

engulfment of extracellular targets. Furthermore, this data provides evidence that the generation of filopodia by the constitutive association of IpLITR 1.1b and Nck is a distinct signaling event from that of IpLITR 1.1b activation post ligand binding which likely involves both the recruitment of Nck and Syk. This data represents new insights into a possible mechanism for constitutive immunoregulatory receptor-induced filopodia formation. Furthermore, my work provides the first evidence that an ITIM-containing receptor is capable of inducing phagocytosis utilizing the classical stimulatory molecules Nck and Syk.

8.2 Future directions

8.2.1 Constitutive mechanism of IpLITR 1.1b-mediated filopodia formation

Although my work identified Nck as a possible molecule associated with IpLITR 1.1b-mediated filopodia formation many other experiments could be done to further this research. For example, is the colocalization of IpLITR 1.1b and Nck really occurring? What other types of molecules are involved in the constitutive associations? Is receptor micro-clustering facilitating the coordination of the filopodia formation? To address my first question, I would want to further confirm that the associations between IpLITR 1.1b and Nck are important for filopodia formation. To do this I would conduct site-directed mutagenesis targeting the predicted binding site of Nck at position Y_{433} on IpLITR 1.1b's CYT. I would generate a mutated variant of IpLITR 1.1b which would change the predicted Nck binding tyrosine (Y_{433}) to a phenylalanine (F), which should inhibit its binding to IpLITR 1.1b. I would then express this construct in RBL-2H3 cells and visualize both non-stimulated and stimulated IpLITR 1.1b-F_{433} mutant in real time to determine if their abilities to generate filopodia and filopodia-target interactions are abrogated. Alternatively, I would also perform immunoprecipitation studies whereby either IpLITR 1.1b wild type (WT) or IpLITR 1.1b-F_{433} construct would be immunoprecipitated from RBL-2H3

cells and then tested for the presence of IpLITR 1.1b-Nck interactions prior to cell stimulation. If IpLITR 1.1b does endogenously associated with Nck to facilitate filopodia formation I would suspect that IpLITR 1.1b WT but not IpLITR-F_{433} should co-immunoprecipitate with Nck, thereby identifying their engagements in a ligand-independent manner. Also, it would be very interesting to see if IpLITR 1.1b and Nck interactions could be observed in real time during filopodia formation. To do this, I would generate an IpLITR 1.1b-WT GFP-tagged construct along with a Nck-RFP tagged protein and co express them in RBL-2H3 cells. In doing so I could observe in real-time using my previously established LCI protocols the interactions of IpLITR 1.1b and Nck in filopodia, reinforcing my previous data and the hypothesis that these interactions are important for filopodia formation. Following the same line of experiments, I would want to test these same parameters but for other signaling molecules that may be involved such as WAVE2, PAK and Vav1 as these all have been shown to constitutively bind Nck in other receptor systems. These studies would further elucidate unique mechanisms by which immunoregulatory receptors can engage in F-actin polymerization events. To determine if perhaps micro clusters of IpLITR 1.1b are facilitating filopodia formation I could generate a IpLITR 1.1b WT-RFP expressing construct and co-stably express it with the LifeAct-GFP probe. I could then look at receptor movement and localization prior to the generation of filopodia to identify if perhaps receptor aggregation creates F-actin foci that eventually evolve into filopodia-like structures. These studies together would further our understanding of not only how IpLITR 1.1b facilitates F-actin polymerization events for filopodia formation but more importantly they would provide greater insights into novel mechanisms associated with immunoregulatory receptor signaling capabilities and the regulation of membrane dynamics as whole.

8.2.2 Roles of Nck and Syk recruitment to IpLITR 1.1b during phagocytosis

As described in my results, it appears that upon receptor activation both Nck and Syk are recruited to sites of IpLITR 1.1b post ligand binding. This was demonstrated by both confocal imaging as well as through qualitative analysis using specialized imaging software. However, to identify definitively that these recruitments are occurring, I would like to perform the same experiments using RBL-2H3 cells expressing CYT region mutants of IpLITR 1.1b. As mentioned above, I would like to generate an IpLITR 1.1b-F_{433} mutant, which should abolish Nck binding, but I would also like to generate an IpLITR 1.1b-F_{477}/F_{499} mutant to test the hypothesis that Syk is recruited to the tandem ITIMs within the distal region of IpLITRs 1.1b CYT. These studies would not only further the notion that ITIM-containing receptors can engage with stimulatory signaling molecules but would also give greater insights into mechanisms of functional plasticity across vertebrates. The use of these newly expressing IpLITR 1.1b mutant variants in RBL-2H3 cells would allow me to look at these specific sites as the recruitment regions for Nck and Syk by demonstrating whether the mutated CYT variants lose Nck/Syk recruitment capabilities using my immunoflurosence bead-molecule phagocytosis assay as previously described (Chapter VII). This study would further my hypothesis that Nck and Syk are directly recruited to IpLITR 1.1b I could also further assess Nck and Syk recruitment during IpLITR 1.1b-mediated phagocytosis in real time. This would be accomplished by generating IpLITR 1.1b-WT, IpLITR 1.1b-F_{433} (as mentioned above) and IpLITR 1.1b- F_{477}/F_{499} GFP-tagged constructs and co-expressing them with RFP-tagged Nck or RFP-tagged Syk and visualizing their localizations using LCI. If Nck and/or Syk recruitment is important for IpLITR 1.1b-mediated phagocytosis, I would suspect that IpLITR 1.1b-WT-expressing cells would recruit RFP-Nck or RFP-Syk to sites of bead-cell interactions, and therefore localize with the

IpLITR 1.1b-WT GFP constructs. If these interactions do occur, then I would suspect to see no localization of IpLITR-F_{433} GFP or IpLITR 1.1b- F_{477}/F_{499} GFP with either Nck or Syk respectively. This loss of binding of Nck or Syk would also be accompanied by the loss of the ability of IpLITR 1.1b-expressing cells to facilitate either target tethering or engulfment, which I could observe using both static and LCI imaging techniques. These results would confirm the utilization of Nck and Syk in IpLITR 1.1b-mediated F-actin polymerization events and support my hypothesized mechanism.

8.2.3 Identification of IpLITR ligands

One of the most important questions yet to be answered for IpLITRs as a receptor family is the identification of their endogenous ligands. Answering of this question is important for addressing not only the *in vivo* roles that IpLITRs play in regulating immunological responses but to identify if IpLITRs represent functional orthologs to other mammal receptors. If identified, functional studies in fish-specific systems could be done to further characterize the endogenous role that IpLITRs play in teleost immunity. Sequence alignments and structural analysis of the D1 and D2 domains of IpLITRs suggest a relationship to the LILR receptor family, and key MHC-I binding residues have been identified in similar positions within the D1 domain of some IpLITR sub-types [190]. This data suggestions that in part, IpLITRs may be important for self/non-self recognition via MHC-I interactions, however no binding studies have been successfully performed. Other members of the IgSF have been shown to bind completely unexpected ligands as has been demonstrated for the members of the FcRL receptors. For example, some FcRLs have been shown to bind IgA or IgG (FcRL4 and FcRL5 respectively) [315,316] while other FcRLs have shown to bind MHC-II molecules (FcRL6) as well as the poxvirus immunoevasin protein (FcRL5) [317] . The CHIRAB1 IgY FcR in chickens

interestingly shares more structural similarities to the MHC binding LILR receptor family rather than mammalian FcRs [318]. These are just a few examples that demonstrate the diversity in ligand recognition among IgSF members and therefore predicting IpLITR ligands is difficult.

One means by which ligands for IpLITRs could be identified is generating Fc-fusion proteins containing the EC domains of IpLITRs, which are fused to the Fc portion of IgG isotype. Once IpLITR-Fc chimerics are developed they could be used to screen for cell-associated or exogenous molecules (fish and microbial) using screening arrays. This would be a broad initial screening study to identify where possible IpLITR ligands may exist. Once IpLITR-Fc binding has been confirmed, pull down assays along with mass spectrometry could be used to identify specifically what type(s) of molecule(s) are capable of binding to IpLITR EC domains. Another approach that could be used is the generation of a BWZ reporter assay. This assay has been used to identify binding partners of other receptor-types with unknown ligands, such as the studies that identified chicken IgY receptors [319]. This could be done by using IpLITRs EC domains as bait for possible cell-surface expressed ligands or exogenous molecules. The transfection of IpLITRs connected to a BWZ reporter cell could be incubated with various other cell-types or exogenous extracts which once engaged in the expressed IpLITR EC domains would activate the receptors causing BWZ fluoresence, there by indicating receptor-ligand binding had occurred. From these studies one could generate a cDNA library and identified ligands subsequently could be tested by expression in an easily transfectable cell line such as HEK29T or AD293 and then incubated with IpLITR EC domain containing cells. cDNAs could be sequenced and the ligand possible identified.

8.4 Final Summary

The characterization of IpLITRs offers new insights into the regulation of innate immune cell effector responses and these fish proteins represent an alternative vertebrate innate immune receptor model system for examining innate immune processes. Classically, immunoregulatory receptors are categorized as being inhibitory or stimulatory based on key structural features of their CYT regions. However recent studies, including those presented in this thesis, are beginning to bring to light that perhaps this binary system is far more complex. Initially our lab identified that IpLITR 1.1b could promote phagocytosis when expressed in a myeloid cell line, however the mechanism underlying this unique function was not characterized. Therefore, my thesis research was focused on examining how an ITIM-containing receptor can promote a cellular response such as phagocytosis. Furthermore, I examined the mechanisms underlying the unique ability of IpLITR 1.1b to constitutively induce filopodia formation that were involved in the active capture, tethering, and engulfment of extracellular targets. This work sets the stage for an understanding of the fundamentals of immunoregulatory receptor-mediated control of F-acting dynamics required for plasma membrane remodelling. As such, my work provides new information in support of the hypothesis that certain immunoregulatory receptor types may specifically promote filopodia formations to propel them beyond the surface of the cell, thus increasing the likelihood that they will engage distant targets. This information broadens our appreciation of receptor-mediated target interactions and in principle shows that IpLITR 1.1b and its unique signaling capabilities can network with the minimal proximal signalling components to trigger filopodia formations. Overall, my work has provided the mechanistic basics required for further exploring how certain immunoregulatory receptor-types influence plasma membrane dynamics during target capture and engulfment events

REFERENCES

1 Wcisel DJ, Ota T, Litman GW, Yoder JA: Spotted Gar and the Evolution of Innate Immune Receptors. J Exp Zool Part B Mol Dev Evol 2017;328:666–684.

2 Flannagan RS, Jaumouillé V, Grinstein S: The Cell Biology of Phagocytosis. Annu Rev Pathol Mech Dis 2012;7:61–98.

3 Pils S, Kopp K, Peterson L, Delgado Tascón J, Nyffenegger-Jann NJ, Hauck CR: The adaptor molecule Nck localizes the WAVE complex to promote actin polymerization during CEACAM3-mediated phagocytosis of bacteria. PLoS One 2012;7:e32808.

4 Massol P, Montcourrier P, Guillemot J-C, Chavrier P: Fc receptor-mediated phagocytosis requires CDC42 and Rac1. EMBO J 1998;17:6219–6229.

5 May RC, Caron E, Hall A, Machesky LM: Involvement of the Arp2/3 complex in phagocytosis mediated by FcγR or CR3. Nat Cell Biol 2000;2:246–248.

6 Kraal G, van der Laan LJ, Elomaa O, Tryggvason K: The macrophage receptor MARCO. Microbes Infect 2000;2:313–6.

7 Delgado Tasco´n J, Adrian J, Kopp K, Scholz P, Tschan MP, Kuespert K, et al.: The granulocyte orphan receptor CEACAM4 is able to trigger phagocytosis of bacteria. J Leukoc Biol 2015;97:521–531.

8 Schmitter T, Pils S, Sakk V, Frank R, Fischer K-D, Hauck CR: The granulocyte receptor carcinoembryonic antigen-related cell adhesion molecule 3 (CEACAM3) directly associates with Vav to promote phagocytosis of human pathogens. J Immunol

2007;178:3797–805.

9 Ainsworth AJ: Fish granulocytes: Morphology, distribution, and function. Annu Rev Fish Dis 1992;2:123–148.

10 Cortes HD, Montgomery BC, Verheijen K, García-García E, Stafford JL: Examination of the stimulatory signaling potential of a channel catfish leukocyte immune-type receptor and associated adaptor. Dev Comp Immunol 2012;36:62–73.

11 Cortes HD, Lillico DMEE, Zwozdesky MA, Pemberton JG, O'Brien A, Montgomery BCSS, et al.: Induction of Phagocytosis and Intracellular Signaling by an Inhibitory Channel Catfish Leukocyte Immune-Type Receptor: Evidence for Immunoregulatory Receptor Functional Plasticity in Teleosts. J Innate Immun 2014;6:435–455.

12 Montgomery BC, Cortes HD, Burshtyn DN, Stafford JL: Channel catfish leukocyte immune-type receptor mediated inhibition of cellular cytotoxicity is facilitated by SHP-1-dependent and -independent mechanisms. Dev Comp Immunol 2012;37:151–63.

13 Montgomery BCS, Mewes J, Davidson C, Burshtyn DN, Stafford JL: Cell surface expression of channel catfish leukocyte immune-type receptors (IpLITRs) and recruitment of both Src homology 2 domain-containing protein tyrosine phosphatase (SHP)-1 and SHP-2. Dev Comp Immunol 2009;33:570–582.

14 Li J, Barreda DR, Zhang Y-A, Boshra H, Gelman AE, LaPatra S, et al.: B lymphocytes from early vertebrates have potent phagocytic and microbicidal abilities. Nat Immunol 2006;7:1116–1124.

15 Zhang Y-A, Salinas I, Li J, Parra D, Bjork S, Xu Z, et al.: IgT, a primitive

immunoglobulin class specialized in mucosal immunity. Nat Immunol 2010;11:827–835.

16 Stafford JL, Bengtén E, Du Pasquier L, Miller NW, Wilson M: Channel catfish leukocyte immune-type receptors contain a putative MHC class I binding site. Immunogenetics 2007;59:77–91.

17 Yoder JA: Form, function and phylogenetics of NITRs in bony fish. Dev Comp Immunol 2009;33:135–144.

18 Pancer Z, Saha NR, Kasamatsu J, Suzuki T, Amemiya CT, Kasahara M, et al.: Variable lymphocyte receptors in hagfish. Proc Natl Acad Sci 2005;102:9224–9229.

19 Alder MN, Rogozin IB, Iyer LM, Glazko G V, Cooper MD, Pancer Z: Diversity and Function of Adaptive Immune Receptors in a Jawless Vertebrate. Science (80-) 2005;310:1970–1973.

20 Pancer Z, Amemiya CT, Ehrhardt GRA, Ceitlin J, Larry Gartland G, Cooper MD: Somatic diversification of variable lymphocyte receptors in the agnathan sea lamprey. Nature 2004;430:174–180.

21 Iwasaki A, Medzhitov R: Control of adaptive immunity by the innate immune system. Nat Immunol 2015;16:343–353.

22 Riera Romo M, Pérez-Martínez D, Castillo Ferrer C: Innate immunity in vertebrates: an overview. Immunology 2016;148:125–139.

23 Salinas I: The Mucosal Immune System of Teleost Fish. Biology (Basel) 2015;4:525–539.

24 Ángeles Esteban M, Cerezuela R: Fish mucosal immunity: skin. Mucosal Heal Aquac 2015;67–92.

25 Uribe C, Folch H, Enriquez R, Moran G: Innate and adaptive immunity in teleost fish: a review. Vet Med (Praha);56:2011–486.

26 Xu Z, Parra D, Gómez D, Salinas I, Zhang Y-A, von Gersdorff Jørgensen L, et al.: Teleost skin, an ancient mucosal surface that elicits gut-like immune responses. Proc Natl Acad Sci U S A 2013;110:13097–102.

27 Brinchmann MF: Immune relevant molecules identified in the skin mucus of fish using -omics technologies. Mol Biosyst 2016;12:2056–63.

28 Rakers S, Niklasson L, Steinhagen D, Kruse C, Schauber J, Sundell K, et al.: Antimicrobial Peptides (AMPs) from Fish Epidermis: Perspectives for Investigative Dermatology. J Invest Dermatol 2013;133:1140–1149.

29 Egesten A, Blom M, Calafat J, Janssen H, Knol EF: Eosinophil granulocyte interaction with serum-opsonized particles: binding and degranulation are enhanced by tumor necrosis factor alpha. Int Arch Allergy Immunol 1998;115:121–8.

30 Odaka T, Suetake H, Maeda T, Miyadai T: Teleost Basophils Have IgM-Dependent and Dual Ig-Independent Degranulation Systems. J Immunol 2018;200:2767–2776.

31 Flerova EA, Balabanova L V: [Ultrastructure of granulocytes of bony fishes (orders Salmoniformes, Cypriniformes, Perciformes)]. Zh Evol Biokhim Fiziol;49:162–71.

32 Meseguer J, López-Ruiz A, Angeles Esteban M: Cytochemical characterization of leucocytes from the seawater teleost, gilthead seabream (Sparus aurata L.). Histochemistry 1994 [cited 2018 Jun 27];102:37–44.

33 Sepulcre M, Pelegrín P, Mulero V, Meseguer J: Characterisation of gilthead seabream

acidophilic granulocytes by a monoclonal antibody unequivocally points to their involvement in fish phagocytic response. Cell Tissue Res 2002;308:97–102.

34 van den Berg CW, Tambourgi D V, Clark HW, Hoong SJ, Spiller OB, McGreal EP: Mechanism of neutrophil dysfunction: neutrophil serine proteases cleave and inactivate the C5a receptor. J Immunol 2014;192:1787–95.

35 Havixbeck J, Barreda D: Neutrophil Development, Migration, and Function in Teleost Fish. Biology (Basel) 2015;4:715–734.

36 Havixbeck JJ, Rieger AM, Wong ME, Hodgkinson JW, Barreda DR: Neutrophil contributions to the induction and regulation of the acute inflammatory response in teleost fish. J Leukoc Biol 2016;99:241–252.

37 Rieger AM, Konowalchuk JD, Grayfer L, Katzenback BA, Havixbeck JJ, Kiemele MD, et al.: Fish and Mammalian Phagocytes Differentially Regulate Pro-Inflammatory and Homeostatic Responses In Vivo. PLoS One 2012;7:e47070.

38 Havixbeck JJ, Rieger AM, Churchill LJ, Barreda DR: Neutrophils exert protection in early Aeromonas veronii infections through the clearance of both bacteria and dying macrophages. Fish Shellfish Immunol 2017;63:18–30.

39 Ellett F, Elks PM, Robertson AL, Ogryzko N V., Renshaw SA: Defining the phenotype of neutrophils following reverse migration in zebrafish. J Leukoc Biol 2015;98:975–981.

40 Palić D, Andreasen CB, Ostojić J, Tell RM, Roth JA: Zebrafish (Danio rerio) whole kidney assays to measure neutrophil extracellular trap release and degranulation of primary granules. J Immunol Methods 2007;319:87–97.

41 Wen L, Zhao M, Chi H, Sun L: Histones and chymotrypsin-like elastases play significant roles in the antimicrobial activity of tongue sole neutrophil extracellular traps. Fish Shellfish Immunol 2018;72:470–476.

42 Chi H, Sun L: Neutrophils of Scophthalmus maximus produce extracellular traps that capture bacteria and inhibit bacterial infection. Dev Comp Immunol 2016;56:7–12.

43 Zhao M, Chi H, Sun L: Neutrophil Extracellular Traps of Cynoglossus semilaevis: Production Characteristics and Antibacterial Effect. Front Immunol 2017;8:290.

44 Chiesa S, Mingueneau M, Fuseri N, Malissen B, Raulet DH, Malissen M, et al.: Multiplicity and plasticity of natural killer cell signaling pathways. Blood 2006;107:2364–2372.

45 Halle S, Halle O, Förster R: Mechanisms and Dynamics of T Cell-Mediated Cytotoxicity In Vivo. Trends Immunol 2017;38:432–443.

46 Praveen K, Leary III JH, Evans DL, Jaso-Friedmann L: Nonspecific cytotoxic cells of teleosts are armed with multiple granzymes and other components of the granule exocytosis pathway. Mol Immunol 2006;43:1152–1162.

47 Bishop GR, Taylor S, Jaso-Friedmann L, Evans DL: Mechanisms of nonspecific cytotoxic cell regulation of apoptosis: cytokine-like activity of Fas ligand. Fish Shellfish Immunol 2002;13:47–67.

48 Fischer U, Koppang EO, Nakanishi T: Teleost T and NK cell immunity. Fish Shellfish Immunol 2013;35:197–206.

49 Reimers K, Abu Qarn M, Allmeling C, Bucan V, Vogt PM: Identification of the non-

specific cytotoxic cell receptor protein 1 (NCCRP1) in regenerating axolotl limbs. J Comp Physiol B 2006;176:599–605.

50 Oumouna M, Jaso-Friedmann L, Evans DL: Flow cytometry-based assay for determination of teleost cytotoxic cell lysis of target cells. Cytometry 2001;45:259–66.

51 Oumouna M, Jaso-Friedmann L, Evans DL: Activation of nonspecific cytotoxic cells (NCC) with synthetic oligodeoxynucleotides and bacterial genomic DNA: binding, specificity and identification of unique immunostimulatory motifs. Dev Comp Immunol 2002;26:257–69.

52 Taylor EB, Moulana M, Stuge TB, Quiniou SMA, Bengten E, Wilson M: A Leukocyte Immune-Type Receptor Subset Is a Marker of Antiviral Cytotoxic Cells in Channel Catfish, *Ictalurus punctatus*. J Immunol 2016;196:2677–2689.

53 Hogan RJ, Stuge TB, Clem LW, Miller NW, Chinchar VG: Anti-viral cytotoxic cells in the channel catfish (Ictalurus punctatus). Dev Comp Immunol;20:115–27.

54 Caligiuri MA: Human natural killer cells. Blood 2008;112:461–469.

55 Yoshida SH, Stuge TB, Miller NW, Clem LW: Phylogeny of lymphocyte heterogeneity: cytotoxic activity of channel catfish peripheral blood leukocytes dircted against allogeneic targets. Dev Comp Immunol 1995;19:71–77.

56 Quiniou MA, Bengten E, Wilson Erin Taylor MB, Moulana M, Stuge TB: Ictalurus punctatus Channel Catfish, Is a Marker of Antiviral Cytotoxic Cells in A Leukocyte Immune-Type Receptor Subset 2018; DOI: 10.4049/jimmunol.1502166

57 Huang Y, Zheng Q, Niu J, Tang J, Wang B, Abarike ED, et al.: NK-lysin from

Oreochromis niloticus improves antimicrobial defence against bacterial pathogens. Fish Shellfish Immunol 2018;72:259–265.

58 Dotiwala F, Mulik S, Polidoro RB, Ansara JA, Burleigh BA, Walch M, et al.: Killer lymphocytes use granulysin, perforin and granzymes to kill intracellular parasites. Nat Med 2016;22:210–216.

59 Pereiro P, Romero A, Díaz-Rosales P, Estepa A, Figueras A, Novoa B: Nucleated Teleost Erythrocytes Play an Nk-Lysin- and Autophagy-Dependent Role in Antiviral Immunity. Front Immunol 2017;8:1458.

60 Walters MN, Papadimitriou JM: Phagocytosis: a review. CRC Crit Rev Toxicol 1978 [cited 2018 Jun 26];5:377–421.

61 Greenberg S: Diversity in phagocytic signalling. J Cell Sci 2001 [cited 2017 Dec 13];114:1039–40.

62 Caron E, Hall A: Identification of two distinct mechanisms of phagocytosis controlled by different Rho GTPases. Science 1998;282:1717–21.

63 Herre J, Marshall ASJ, Caron E, Edwards AD, Williams DL, Schweighoffer E, et al.: Dectin-1 uses novel mechanisms for yeast phagocytosis in macrophages. Blood 2004;104:4038–45.

64 Esteban MA, Meseguer J: Factors influencing phagocytic response of macrophages from the sea bass (Dicentrarchus labrax L.): an ultrastructural and quantitative study. Anat Rec 1997 [cited 2018 Jun 28];248:533–41.

65 Esteban M, Cuesta A, Chaves-Pozo E, Meseguer J: Phagocytosis in Teleosts. Implications

of the New Cells Involved. Biology (Basel) 2015;4:907–922.

66 Rieger AM, Hall BE, Barreda DR: Macrophage activation differentially modulates particle binding, phagocytosis and downstream antimicrobial mechanisms. Dev Comp Immunol 2010;34:1144–59.

67 Grayfer L, Hodgkinson JW, Belosevic M: Antimicrobial responses of teleost phagocytes and innate immune evasion strategies of intracellular bacteria. Dev Comp Immunol 2014;43:223–242.

68 Hodgkinson J, Grayfer L, Belosevic M: Biology of Bony Fish Macrophages. Biology (Basel) 2015;4:881–906.

69 Zhao X, Liu L, Hegazy AM, Wang H, Li JJ, Zheng F, et al.: Mannose receptor mediated phagocytosis of bacteria in macrophages of blunt snout bream (Megalobrama amblycephala) in a Ca2+-dependent manner. Fish Shellfish Immunol 2015;43:357–363.

70 Pettersen EF, Ingerslev H-C, Stavang V, Egenberg M, Wergeland HI: A highly phagocytic cell line TO from Atlantic salmon is CD83 positive and M-CSFR negative, indicating a dendritic-like cell type. Fish Shellfish Immunol 2008;25:809–19.

71 Castillo-Briceño P, Sepulcre MP, Chaves-Pozo E, Meseguer J, García-Ayala A, Mulero V: Collagen regulates the activation of professional phagocytes of the teleost fish gilthead seabream. Mol Immunol 2009;46:1409–1415.

72 Øverland HS, Pettersen EF, Rønneseth A, Wergeland HI: Phagocytosis by B-cells and neutrophils in Atlantic salmon (Salmo salar L.) and Atlantic cod (Gadus morhua L.). Fish Shellfish Immunol 2010;28:193–204.

73 Page DM, Wittamer V, Bertrand JY, Lewis KL, Pratt DN, Delgado N, et al.: An evolutionarily conserved program of B-cell development and activation in zebrafish. Blood 2013;122:e1-11.

74 Sunyer JO: Evolutionary and functional relationships of B cells from fish and mammals: insights into their novel roles in phagocytosis and presentation of particulate antigen. Infect Disord Drug Targets 2012;12:200–12.

75 Yutin N, Wolf MY, Wolf YI, Koonin E V: The origins of phagocytosis and eukaryogenesis. Biol Direct 2009;4:9.

76 Csaba G: Is there a hormonal regulation of phagocytosis at unicellular and multicellular levels? A critical review. Acta Microbiol Immunol Hung 2017;64:357–372.

77 Zachar I, Szilágyi A, Számadó S, Szathmáry E: Farming the mitochondrial ancestor as a model of endosymbiotic establishment by natural selection. Proc Natl Acad Sci U S A 2018;115:E1504–E1510.

78 Stuart LM, Ezekowitz RAB: Phagocytosis: Elegant Complexity. Immunity 2005;22:539–550.

79 Underhill DM, Goodridge HS: Information processing during phagocytosis. Nat Rev Immunol 2012;12:492–502.

80 Rabinovitch M: Professional and non-professional phagocytes: an introduction. Trends Cell Biol 1995;5:85–7.

81 Rabinovitch M: Professional and non-professional phagocytes: an introduction. Trends Cell Biol 1995;5:85–7.

82 Freeman SA, Grinstein S: Phagocytosis: receptors, signal integration, and the cytoskeleton. Immunol Rev 2014;262:193–215.

83 Brown GD: Dectin-1: a signalling non-TLR pattern-recognition receptor. Nat Rev Immunol 2006;6:33–43.

84 Richards DM, Endres RG: The mechanism of phagocytosis: two stages of engulfment. Biophys J 2014;107:1542–53.

85 Gordon S: Phagocytosis: An Immunobiologic Process. Immunity 2016;44:463–475.

86 Aderem A, Underhill DM: MECHANISMS OF PHAGOCYTOSIS IN MACROPHAGES. Annu Rev Immunol 1999;17:593–623.

87 Flannagan RS, Harrison RE, Yip CM, Jaqaman K, Grinstein S: Dynamic macrophage "probing" is required for the efficient capture of phagocytic targets. J Cell Biol 2010;191:1205–18.

88 Horsthemke M, Bachg AC, Groll K, Moyzio S, Müther B, Hemkemeyer SA, et al.: Multiple roles of filopodial dynamics in particle capture and phagocytosis and phenotypes of Cdc42 and Myo10 deletion. J Biol Chem 2017;292:7258–7273.

89 Davidson AJ, Wood W: Unravelling the Actin Cytoskeleton: A New Competitive Edge? Trends Cell Biol 2016;26:569–76.

90 Lee SH, Dominguez R: Regulation of actin cytoskeleton dynamics in cells. Mol Cells 2010;29:311–25.

91 Bezanilla M, Gladfelter AS, Kovar DR, Lee W-L: Cytoskeletal dynamics: a view from the membrane. J Cell Biol 2015;209:329–37.

92 Stricker J, Falzone T, Gardel ML: Mechanics of the F-actin cytoskeleton. J Biomech 2010;43:9–14.

93 Patel JC, Hall A, Caron E: Vav Regulates Activation of Rac but Not Cdc42 during FcγR-mediated Phagocytosis. Mol Biol Cell 2002;13:1215–1226.

94 Utomo A, Cullere X, Glogauer M, Swat W, Mayadas TN: Vav proteins in neutrophils are required for FcgammaR-mediated signaling to Rac GTPases and nicotinamide adenine dinucleotide phosphate oxidase component p40(phox). J Immunol 2006;177:6388–97.

95 Uribe-Querol E, Rosales C: Control of Phagocytosis by Microbial Pathogens. Front Immunol 2017;8:1368.

96 Gordon S: Phagocytosis: An Immunobiologic Process 2016; DOI: 10.1016/j.immuni.2016.02.026

97 Vidarsson G, Dekkers G, Rispens T: IgG subclasses and allotypes: from structure to effector functions. Front Immunol 2014;5:520.

98 Daëron M: F c receptor biology. Annu Rev Immunol 1997;15:203–234.

99 Jaumouillé V, Grinstein S: Receptor mobility, the cytoskeleton, and particle binding during phagocytosis. Curr Opin Cell Biol 2011;23:22–29.

100 Underhill DM, Goodridge HS: The many faces of ITAMs. Trends Immunol 2007;28:66–73.

101 Johnson SA, Pleiman CM, Pao L, Schneringer J, Hippen K, Cambier JC: Phosphorylated immunoreceptor signaling motifs (ITAMs) exhibit unique abilities to bind and activate Lyn and Syk tyrosine kinases. J Immunol 1995;155:4596–603.

102 Billadeau DD, Leibson PJ: ITAMs versus ITIMs: striking a balance during cell regulation. J Clin Invest 2002;109:161–8.

103 Crowley MT, Costello PS, Fitzer-Attas CJ, Turner M, Meng F, Lowell C, et al.: A critical role for Syk in signal transduction and phagocytosis mediated by Fcgamma receptors on macrophages. J Exp Med 1997;186:1027–39.

104 Mócsai A, Ruland J, Tybulewicz VLJ: The SYK tyrosine kinase: a crucial player in diverse biological functions. Nat Rev Immunol 2010;10:387–402.

105 Wang J, Wu Y, Hu H, Wang W, Lu Y, Mao H, et al.: Syk protein tyrosine kinase involves PECAM-1 signaling through tandem immunotyrosine inhibitory motifs in human THP-1 macrophages. Cell Immunol 2011;272:39–44.

106 Park H, Ishihara D, Cox D: Regulation of tyrosine phosphorylation in macrophage phagocytosis and chemotaxis. Arch Biochem Biophys 2011;510:101–11.

107 Hamerman JA, Ni M, Killebrew JR, Chu C-L, Lowell CA: The expanding roles of ITAM adapters FcRgamma and DAP12 in myeloid cells. Immunol Rev 2009;232:42–58.

108 Coppolino MG, Krause M, Hagendorff P, Monner DA, Trimble W, Grinstein S, et al.: Evidence for a molecular complex consisting of Fyb/SLAP, SLP-76, Nck, VASP and WASP that links the actin cytoskeleton to Fcgamma receptor signalling during phagocytosis. J Cell Sci 2001 [cited 2018 Jun 30];114:4307–18.

109 Izadi KD, Erdreich-Epstein A, Liu Y, Durden DL: Characterization of Cbl-Nck and Nck-Pak1 Interactions in Myeloid FcγRII Signaling. Exp Cell Res 1998;245:330–342.

110 Dart AE, Donnelly SK, Holden DW, Way M, Caron E: Nck and Cdc42 co-operate to

recruit N-WASP to promote FcγR-mediated phagocytosis. J Cell Sci 2012;125:2825–2830.

111 Freeman SA, Grinstein S: Phagocytosis: receptors, signal integration, and the cytoskeleton. Immunol Rev 2014;262:193–215.

112 Gu H, Botelho RJ, Yu M, Grinstein S, Neel BG: Critical role for scaffolding adapter Gab2 in Fc gamma R-mediated phagocytosis. J Cell Biol 2003;161:1151–61.

113 Olazabal IM, Caron E, May RC, Schilling K, Knecht DA, Machesky LM: Rho-kinase and myosin-II control phagocytic cup formation during CR, but not FcgammaR, phagocytosis. Curr Biol 2002;12:1413–18.

114 Park H, Cox D: Cdc42 Regulates Fc $_{\gamma}$ Receptor-mediated Phagocytosis through the Activation and Phosphorylation of Wiskott-Aldrich Syndrome Protein (WASP) and Neural-WASP. Mol Biol Cell 2009;20:4500–4508.

115 Daniels AB, Worth RG, Dickstein RJ, Dickstein JS, Kim-Han T-H, Kim M-K, et al.: Analysis of FcγRIIA Cytoplasmic Tail Requirements in Signaling for Serotonin Secretion: Evidence for an ITAM-Dependent, PI3K-Dependent Pathway. Scand J Immunol 2010;71:232–239.

116 Zhang Y, Hoppe AD, Swanson JA: Coordination of Fc receptor signaling regulates cellular commitment to phagocytosis. Proc Natl Acad Sci U S A 2010;107:19332–7.

117 Getahun A, Cambier JC: Of ITIMs, ITAMs, and ITAMis: revisiting immunoglobulin Fc receptor signaling. Immunol Rev 2015;268:66–73.

118 Brown EJ: Complement receptors, adhesion, and phagocytosis. Infect Agents Dis 1992

[cited 2018 Sep 9];1:63–70.

119 Wiedemann A, Patel JC, Lim J, Tsun A, van Kooyk Y, Caron E: Two distinct cytoplasmic regions of the beta2 integrin chain regulate RhoA function during phagocytosis. J Cell Biol 2006;172:1069–79.

120 Lefort CT, Hyun Y-M, Schultz JB, Law F-Y, Waugh RE, Knauf PA, et al.: Outside-in signal transmission by conformational changes in integrin Mac-1. J Immunol 2009;183:6460–8.

121 Colucci-Guyon E, Niedergang F, Wallar BJ, Peng J, Alberts AS, Chavrier P: A Role for Mammalian Diaphanous-Related Formins in Complement Receptor (CR3)-Mediated Phagocytosis in Macrophages. Curr Biol 2005;15:2007–2012.

122 Lewkowicz E, Herit F, Le Clainche C, Bourdoncle P, Perez F, Niedergang F: The microtubule-binding protein CLIP-170 coordinates mDia1 and actin reorganization during CR3-mediated phagocytosis. J Cell Biol 2008;183:1287–98.

123 Plato A, Willment JA, Brown GD: C-type lectin-like receptors of the dectin-1 cluster: ligands and signaling pathways. Int Rev Immunol 2013;32:134–56.

124 Deng Z, Ma S, Zhou H, Zang A, Fang Y, Li T, et al.: Tyrosine phosphatase SHP-2 mediates C-type lectin receptor-induced activation of the kinase Syk and anti-fungal TH17 responses. Nat Immunol 2015;16:642–52.

125 Elliott MR, Koster KM, Murphy PS: Efferocytosis Signaling in the Regulation of Macrophage Inflammatory Responses. J Immunol 2017;198:1387–1394.

126 Green DR, Oguin TH, Martinez J: The clearance of dying cells: table for two. Cell Death

Differ 2016;23:915–26.

127 Segawa K, Nagata S: An Apoptotic ‘Eat Me’ Signal: Phosphatidylserine Exposure. Trends Cell Biol 2015;25:639–650.

128 Park D, Tosello-Trampont A-C, Elliott MR, Lu M, Haney LB, Ma Z, et al.: BAI1 is an engulfment receptor for apoptotic cells upstream of the ELMO/Dock180/Rac module. Nature 2007;450:430–4.

129 Miyanishi M, Tada K, Koike M, Uchiyama Y, Kitamura T, Nagata S: Identification of Tim4 as a phosphatidylserine receptor. Nature 2007;450:435–439.

130 Kobayashi N, Karisola P, Peña-Cruz V, Dorfman DM, Jinushi M, Umetsu SE, et al.: TIM-1 and TIM-4 glycoproteins bind phosphatidylserine and mediate uptake of apoptotic cells. Immunity 2007;27:927–40.

131 Park D, Hochreiter-Hufford A, Ravichandran KS: The Phosphatidylserine Receptor TIM-4 Does Not Mediate Direct Signaling. Curr Biol 2009;19:346–351.

132 Scott RS, McMahon EJ, Pop SM, Reap EA, Caricchio R, Cohen PL, et al.: Phagocytosis and clearance of apoptotic cells is mediated by MER. Nature 2001;411:207–211.

133 Seitz HM, Camenisch TD, Lemke G, Earp HS, Matsushima GK: Macrophages and dendritic cells use different Axl/Mertk/Tyro3 receptors in clearance of apoptotic cells. J Immunol 2007 [cited 2018 Sep 9];178:5635–42.

134 Tian L, Choi S-C, Murakami Y, Allen J, Morse III HC, Qi C-F, et al.: p85α recruitment by the CD300f phosphatidylserine receptor mediates apoptotic cell clearance required for autoimmunity suppression. Nat Commun 2014;5:3146.

135 Voss OH, Tian L, Murakami Y, Coligan JE, Krzewski K: Emerging role of CD300 receptors in regulating myeloid cell efferocytosis. Mol Cell Oncol 2015;2:e964625.

136 Voss OH, Tian L, Murakami Y, Coligan JE, Krzewski K: Emerging role of CD300 receptors in regulating myeloid cell efferocytosis. Mol Cell Oncol 2015;2:e964625.

137 Somersan S, Bhardwaj N: Tethering and tickling: a new role for the phosphatidylserine receptor. J Cell Biol 2001;155:501–4.

138 Hisatomi T, Sakamoto T, Sonoda K-H, Tsutsumi C, Qiao H, Enaida H, et al.: Clearance of apoptotic photoreceptors: elimination of apoptotic debris into the subretinal space and macrophage-mediated phagocytosis via phosphatidylserine receptor and integrin alphavbeta3. Am J Pathol 2003;162:1869–79.

139 Vandivier RW, Henson PM, Douglas IS: Burying the dead: the impact of failed apoptotic cell removal (efferocytosis) on chronic inflammatory lung disease. Chest 2006;129:1673–82.

140 Hoffmann PR, deCathelineau AM, Ogden CA, Leverrier Y, Bratton DL, Daleke DL, et al.: Phosphatidylserine (PS) induces PS receptor–mediated macropinocytosis and promotes clearance of apoptotic cells. J Cell Biol 2001;155:649–660.

141 Kearns MT, Dalal S, Horstmann SA, Richens TR, Tanaka T, Doe JM, et al.: Vascular endothelial growth factor enhances macrophage clearance of apoptotic cells. Am J Physiol Lung Cell Mol Physiol 2012;302:L711-8.

142 Braun-Nesje R, Kaplan G, Seljelid R: Rainbow trout macrophages in vitro: morphology and phagocytic activity. Dev Comp Immunol 1982;6:281–91.

143 Wang R, Neumann N., Shen Q, Belosevic M: Establishment and characterization of a macrophage cell line from the goldfish. Fish Shellfish Immunol 1995;5:329–346.

144 Neumann NF, Stafford JL, Barreda D, Ainsworth AJ, Belosevic M: Antimicrobial mechanisms of fish phagocytes and their role in host defense. Dev Comp Immunol;25:807–25.

145 Johnson E, Smith P: Attachment and phagocytosis by salmon macrophages of agarose beads coated with human C3b and C3bi. Dev Comp Immunol 1984;8:623–30.

146 Jørgensen JB, Robertsen B: Yeast beta-glucan stimulates respiratory burst activity of Atlantic salmon (Salmo salar L.) macrophages. Dev Comp Immunol;19:43–57.

147 Kemenade, Groeneveld, Rens, Rombout: characterization of macrophages and neutrophilic granulocytes from pronephros of carp (Cyprinus carpio). J Exp Biol 1994;187:143–58.

148 Kordon AO, Abdelhamed H, Ahmed H, Park JY, Karsi A, Pinchuk LM: Phagocytic and Bactericidal Properties of Channel Catfish Peritoneal Macrophages Exposed to Edwardsiella ictaluri Live Attenuated Vaccine and Wild-Type Strains. Front Microbiol 2017;8:2638.

149 Kordon AO, Abdelhamed H, Ahmed H, Park JY, Karsi A, Pinchuk LM: Phagocytic and Bactericidal Properties of Channel Catfish Peritoneal Macrophages Exposed to Edwardsiella ictaluri Live Attenuated Vaccine and Wild-Type Strains. Front Microbiol 2017;8:2638.

150 Hohn C, Lee S-R, Pinchuk LM, Petrie-Hanson L: Zebrafish Kidney Phagocytes Utilize

Macropinocytosis and Ca2+-Dependent Endocytic Mechanisms. PLoS One 2009;4:e4314.

151 Hodgkinson J, Grayfer L, Belosevic M: Biology of Bony Fish Macrophages. Biology (Basel) 2015;4:881–906.

152 Grayfer L, Kerimoglu B, Yaparla A, Hodgkinson JW, Xie J, Belosevic M: Mechanisms of Fish Macrophage Antimicrobial Immunity. Front Immunol 2018;9:1105.

153 Hodgkinson JW, Fibke C, Belosevic M: Recombinant IL-4/13A and IL-4/13B induce arginase activity and down-regulate nitric oxide response of primary goldfish (Carassius auratus L.) macrophages. Dev Comp Immunol 2017;67:377–384.

154 Hodgkinson JW, Fibke C, Belosevic M: Recombinant IL-4/13A and IL-4/13B induce arginase activity and down-regulate nitric oxide response of primary goldfish (Carassius auratus L.) macrophages. Dev Comp Immunol 2017;67:377–384.

155 Mathias JR, Dodd ME, Walters KB, Yoo SK, Ranheim EA, Huttenlocher A: Characterization of zebrafish larval inflammatory macrophages. Dev Comp Immunol 2009;33:1212–1217.

156 Sever L, Vo NTK, Bols NC, Dixon B: Expression of tapasin in rainbow trout tissues and cell lines and up regulation in a monocyte/macrophage cell line (RTS11) by a viral mimic and viral infection. Dev Comp Immunol 2014;44:86–93.

157 Saunders HL, Oko AL, Scott AN, Fan CW, Magor BG: The cellular context of AID expressing cells in fish lymphoid tissues. Dev Comp Immunol 2010;34:669–676.

158 Yang H, Biermann MH, Brauner JM, Liu Y, Zhao Y, Herrmann M: New Insights into Neutrophil Extracellular Traps: Mechanisms of Formation and Role in Inflammation.

Front Immunol 2016;7:302.

159 Katzenback BA, Belosevic M: Isolation and functional characterization of neutrophil-like cells, from goldfish (Carassius auratus L.) kidney. Dev Comp Immunol 2009;33:601–611.

160 Hodgkinson JW, Ge J-Q, Katzenback BA, Havixbeck JJ, Barreda DR, Stafford JL, et al.: Development of an in vitro model system to study the interactions between Mycobacterium marinum and teleost neutrophils. Dev Comp Immunol 2015;53:349–357.

161 Sohnle PG, Chusid MJ: The effect of temperature on the chemiluminescence response of neutrophils from rainbow trout and man. J Comp Pathol 1983;93:493–7.

162 Waterstrat PR, Ainsworth AJ, Capley G: In vitro responses of channel catfish, Ictalurus punctatus, neutrophils to Edwardsiella ictaluri. Dev Comp Immunol 1991;15:53–63.

163 Ainsworth AJ, Chen DX: Differences in the phagocytosis of four bacteria by channel catfish neutrophils. Dev Comp Immunol 1990 [cited 2018 Sep 9];14:201–9.

164 Ainsworth AJ, Dexiang C, Waterstrat PR, Greenway T: Effect of temperature on the immune system of channel catfish (Ictalurus punctatus)--I. Leucocyte distribution and phagocyte function in the anterior kidney at 10 degrees C. Comp Biochem Physiol A Comp Physiol 1991;100:907–12.

165 Pijanowski L, Golbach L, Kolaczkowska E, Scheer M, Verburg-van Kemenade BML, Chadzinska M: Carp neutrophilic granulocytes form extracellular traps via ROS-dependent and independent pathways. Fish Shellfish Immunol 2013;34:1244–1252.

166 Palić D, Ostojić J, Andreasen CB, Roth JA: Fish cast NETs: Neutrophil extracellular traps are released from fish neutrophils. Dev Comp Immunol 2007;31:805–816.

167 Barreda DR, Neely HR, Flajnik MF: Evolution of Myeloid Cells. Microbiol Spectr 2016;4. DOI: 10.1128/microbiolspec.MCHD-0007-2015

168 Mildner A, Jung S: Development and function of dendritic cell subsets. Immunity 2014;40:642–56.

169 Banchereau J, Briere F, Caux C, Davoust J, Lebecque S, Liu Y-J, et al.: Immunobiology of Dendritic Cells. Annu Rev Immunol 2000;18:767–811.

170 Author L, Ganassin RC, Bols NC: A Stromal Cell Line from Rainbow Trout Spleen, RTS34st, That Supports the Growth of Rainbow Trout Macrophages and Produces Conditioned Medium with Mitogenic Effects on. 1999.

171 Bassity E, Clark TG: Functional Identification of Dendritic Cells in the Teleost Model, Rainbow Trout (Oncorhynchus mykiss). PLoS One 2012;7:e33196.

172 Lugo-Villarino G, Balla KM, Stachura DL, Bañuelos K, Werneck MBF, Traver D: Identification of dendritic antigen-presenting cells in the zebrafish. Proc Natl Acad Sci U S A 2010;107:15850–5.

173 Movat HZ, Weiser WJ, Glynn MF, Mustard JF: Platelet phagocytosis and aggregation DOI: 10.1083/jcb.27.3.531

174 Nagasawa T, Nakayasu C, Rieger AM, Barreda DR, Somamoto T, Nakao M: Phagocytosis by Thrombocytes is a Conserved Innate Immune Mechanism in Lower Vertebrates. Front Immunol 2014;5:445.

175 Zhang X-J, Wang P, Zhang N, Chen D-D, Nie P, Li J-L, et al.: B Cell Functions Can Be Modulated by Antimicrobial Peptides in Rainbow Trout Oncorhynchus mykiss: Novel

Insights into the Innate Nature of B Cells in Fish. Front Immunol 2017;8:388.

176 Zhu L -y., Lin A -f., Shao T, Nie L, Dong W -r., Xiang L -x., et al.: B Cells in Teleost Fish Act as Pivotal Initiating APCs in Priming Adaptive Immunity: An Evolutionary Perspective on the Origin of the B-1 Cell Subset and B7 Molecules. J Immunol 2014;192:2699–2714.

177 Popi AF, Longo-Maugéri IM, Mariano M: An Overview of B-1 Cells as Antigen-Presenting Cells. Front Immunol 2016;7:138.

178 Secombes CJ, Fletcher TC: The role of phagocytes in the protective mechanisms of fish. Annu Rev Fish Dis 1992;2:53–71.

179 Mikrou A, Marioli D, Papanastasiou AD, Zarkadis IK: CR3 complement receptor: Cloning and characterization in rainbow trout. Fish Shellfish Immunol 2009;26:19–28.

180 Castro R, Jouneau L, Pham H-P, Bouchez O, Giudicelli V, Lefranc M-P, et al.: Teleost Fish Mount Complex Clonal IgM and IgT Responses in Spleen upon Systemic Viral Infection. PLoS Pathog 2013;9:e1003098.

181 Shen L, Stuge TB, Evenhuis JP, Bengtén E, Wilson M, Chinchar VG, et al.: Channel catfish NK-like cells are armed with IgM via a putative FcmicroR. Dev Comp Immunol 2003;27:699–714.

182 Stafford JL, Wilson M, Nayak D, Quiniou SM, Clem LW, Miller NW, et al.: Identification and characterization of a FcR homolog in an ectothermic vertebrate, the channel catfish (Ictalurus punctatus). J Immunol 2006

183 Kang BK, Schlesinger LS: Characterization of mannose receptor-dependent phagocytosis

mediated by Mycobacterium tuberculosis lipoarabinomannan. Infect Immun 1998

184 Aderem A, Underhill DM: MECHANISMS OF PHAGOCYTOSIS IN MACROPHAGES. Annu Rev Immunol 1999;17:593–623.

185 Poynter SJ, Monjo AL, Micheli G, DeWitte-Orr SJ: Scavengers for bacteria: Rainbow trout have two functional variants of MARCO that bind to gram-negative and –positive bacteria. Dev Comp Immunol 2017;77:95–105.

186 Zhang L, Nie L, Cai S-Y, Chen J, Chen J: Role of a macrophage receptor with collagenous structure (MARCO) in regulating monocyte/macrophage functions in ayu, Plecoglossus altivelis. Fish Shellfish Immunol 2018;74:141–151.

187 Montgomery BC, Cortes HD, Mewes-Ares J, Verheijen K, Stafford JL: Teleost IgSF immunoregulatory receptors. Dev Comp Immunol 2011;35:1223–1237.

188 Farré D, Martínez-Vicente P, Engel P, Angulo A: Immunoglobulin superfamily members encoded by viruses and their multiple roles in immune evasion. Eur J Immunol 2017;47:780–796.

189 Akula S, Mohammadamin S, Hellman L: Fc Receptors for Immunoglobulins and Their Appearance during Vertebrate Evolution. PLoS One 2014;9:e96903.

190 Stafford JL, Bengtén E, Du Pasquier L, McIntosh RD, Quiniou SM, Clem LW, et al.: A novel family of diversified immunoregulatory receptors in teleosts is homologous to both mammalian Fc receptors and molecules encoded within the leukocyte receptor complex. Immunogenetics 2006;58:758–73.

191 Mewes J, Verheijen K, Montgomery BCS, Stafford JL: Stimulatory catfish leukocyte

immune-type receptors (IpLITRs) demonstrate a unique ability to associate with adaptor signaling proteins and participate in the formation of homo- and heterodimers. Mol Immunol 2009;47:318–331.

192 Zwozdesky MA, Fei C, Lillico DME, Stafford JL: Imaging flow cytometry and GST pulldown assays provide new insights into channel catfish leukocyte immune-type receptor-mediated phagocytic pathways. Dev Comp Immunol 2017;67:126–138.

193 Lillico DME, Zwozdesky MA, Pemberton JG, Deutscher JM, Jones LO, Chang JP, et al.: Teleost leukocyte immune-type receptors activate distinct phagocytic modes for target acquisition and engulfment. J Leukoc Biol 2015;98:235–48.

194 Riedl J, Crevenna AH, Kessenbrock K, Yu JH, Neukirchen D, Bista M, et al.: Lifeact: a versatile marker to visualize F-actin. Nat Methods 2008;5:605–7.

195 Cho YK, Shusta E V.: Antibody library screens using detergent-solubilized mammalian cell lysates as antigen sources. Protein Eng Des Sel 2010;23:567–577.

196 Nation JL: A new method using hexamethyldisilazane for preparation of soft insect tissues for scanning electron microscopy. Stain Technol 1983.

197 Braet F, De Zanger R, Wisse E: Drying cells for SEM, AFM and TEM by hexamethyldisilazane: a study on hepatic endothelial cells. J Microsc 1997

198 Lillico DME, Pemberton JG, Stafford JL: Trypsin differentially modulates the surface expression and function of channel catfish leukocyte immune-type receptors. Dev Comp Immunol 2016;65:231–244.

199 Lillico DME, Pemberton JG, Stafford JL: Selective Regulation of Cytoskeletal Dynamics

and Filopodia Formation by Teleost Leukocyte Immune-Type Receptors Differentially Contributes to Target Capture During the Phagocytic Process. Front Immunol 2018;9:1144.

200 Allen LA, Aderem A: Molecular definition of distinct cytoskeletal structures involved in complement- and Fc receptor-mediated phagocytosis in macrophages. J Exp Med 1996;184:627–37.

201 Rougerie P, Miskolci V, Cox D: Generation of membrane structures during phagocytosis and chemotaxis of macrophages: role and regulation of the actin cytoskeleton. Immunol Rev 2013;256:222–39.

202 Rotty JD, Wu C, Bear JE: New insights into the regulation and cellular functions of the ARP2/3 complex. Nat Rev Mol Cell Biol 2012;14:7–12.

203 Kaplan G: Differences in the mode of phagocytosis with Fc and C3 receptors in macrophages. Scand J Immunol 1977;6:797–807.

204 Daëron M, Malbec O, Latour S, Bonnerot C, Segal DM, Fridman WH: Distinct intracytoplasmic sequences are required for endocytosis and phagocytosis via murine Fc gamma RII in mast cells. Int Immunol 1993;5:1393–401.

205 Pierini L, Holowka D, Baird B: Fc epsilon RI-mediated association of 6-micron beads with RBL-2H3 mast cells results in exclusion of signaling proteins from the forming phagosome and abrogation of normal downstream signaling. J Cell Biol 1996;134:1427–39.

206 García-García E, Brown EJ, Rosales C: Transmembrane mutations to FcgammaRIIA alter

its association with lipid rafts: implications for receptor signaling. J Immunol 2007;178:3048–58.

207 Lu J, Marjon KD, Marnell LL, Wang R, Mold C, Du Clos TW, et al.: Recognition and functional activation of the human IgA receptor (Fc RI) by C-reactive protein. Proc Natl Acad Sci 2011;108:4974–4979.

208 Mankovich AR, Lee C-Y, Heinrich V: Differential effects of serum heat treatment on chemotaxis and phagocytosis by human neutrophils. PLoS One 2013;8:e54735.

209 Kiefer F, Brumell J, Al-Alawi N, Latour S, Cheng A, Veillette A, et al.: The Syk protein tyrosine kinase is essential for Fcgamma receptor signaling in macrophages and neutrophils. Mol Cell Biol 1998;18:4209–20.

210 Ninomiya N, Hazeki K, Fukui Y, Seya T, Okada T, Hazeki O, et al.: Involvement of phosphatidylinositol 3-kinase in Fc gamma receptor signaling. J Biol Chem;269:22732–7.

211 Lim J, Wiedemann A, Tzircotis G, Monkley SJ, Critchley DR, Caron E: An essential role for talin during alpha(M)beta(2)-mediated phagocytosis. Mol Biol Cell 2007;18:976–85.

212 Li W, Fan J, Woodley DT: Nck/Dock: an adapter between cell surface receptors and the actin cytoskeleton. Oncogene 2001;20:6403–17.

213 Buday L, Wunderlich L, Tamás P: The Nck family of adapter proteins: regulators of actin cytoskeleton. Cell Signal 2002;14:723–31.

214 Blasutig IM, New LA, Thanabalasuriar A, Dayarathna TK, Goudreault M, Quaggin SE, et al.: Phosphorylated YDXV Motifs and Nck SH2/SH3 Adaptors Act Cooperatively To Induce Actin Reorganization. Mol Cell Biol 2008;28:2035–2046.

215 Mendoza MC: Phosphoregulation of the WAVE regulatory complex and signal integration. Semin Cell Dev Biol 2013;24:272–9.

216 Somersan S, Bhardwaj N: Tethering and tickling: a new role for the phosphatidylserine receptor. J Cell Biol 2001;155:501–4.

217 Thomas L, Bielemeier A, Lambert PA, Darveau RP, Marshall LJ, Devitt A: The N-terminus of CD14 acts to bind apoptotic cells and confers rapid-tethering capabilities on non-myeloid cells. PLoS One 2013;8:e70691.

218 Cooney DS, Phee H, Jacob A, Coggeshall KM: Signal transduction by human-restricted Fc gamma RIIa involves three distinct cytoplasmic kinase families leading to phagocytosis. J Immunol 2001;167:844–54.

219 Unkeless JC: The presence of two Fc receptors on mouse macrophages: evidence from a variant cell line and differential trypsin sensitivity. J Exp Med 1977;145:931–45.

220 Huizinga TWJ, van der Schoot CE, Jost C, Klaassen R, Kleijer M, von dem Borne AEGK, et al.: The Pi-linked receptor FcRIII is released on stimulation of neutrophils. Nature 1988;333:667–669.

221 Dransfield I, Buckle AM, Savill JS, McDowall A, Haslett C, Hogg N: Neutrophil apoptosis is associated with a reduction in CD16 (Fc gamma RIII) expression. J Immunol 1994;153:1254–63.

222 Homburg CH, de Haas M, von dem Borne AE, Verhoeven AJ, Reutelingsperger CP, Roos D: Human neutrophils lose their surface Fc gamma RIII and acquire Annexin V binding sites during apoptosis in vitro. Blood 1995;85:532–40.

223 Middelhoven PJ, Van Buul JD, Hordijk PL, Roos D: Different proteolytic mechanisms involved in FcgammaRIIIb shedding from human neutrophils. Clin Exp Immunol 2001;125:169–175.

224 Shepherd VL, Abdolrasulnia R, Stephenson J, Crenshaw C: Modulation of mannose receptor activity by proteolysis. Biochem J 1990;270:771–6.

225 Vandivier RW, Fadok VA, Hoffmann PR, Bratton DL, Penvari C, Brown KK, et al.: Elastase-mediated phosphatidylserine receptor cleavage impairs apoptotic cell clearance in cystic fibrosis and bronchiectasis. J Clin Invest 2002;109:661–670.

226 Zhang S, Yeap X-Y, Grigoryeva L, Dehn S, DeBerge M, Tye M, et al.: Cardiomyocytes induce macrophage receptor shedding to suppress phagocytosis. J Mol Cell Cardiol 2015;87:171–179.

227 Fei C, Pemberton J, Lillico D, Zwozdesky M, Stafford J: Biochemical and Functional Insights into the Integrated Regulation of Innate Immune Cell Responses by Teleost Leukocyte Immune-Type Receptors. Biology (Basel) 2016;5:13.

228 Unkeless JC, Eisen HN: Binding of monomeric immunoglobulins to Fc receptors of mouse macrophages. J Exp Med 1975;142:1520–33.

229 Mingari MC, Moretta L, Moretta A, Ferrarini M, Preud'homme JL: Fc-receptors for IgG and IgM immunoglobulins on human T lymphocytes: mode of re-expression after proteolysis or interaction with immune complexes. J Immunol 1978;121:767–70.

230 Olsen J V, Ong S-E, Mann M: Trypsin cleaves exclusively C-terminal to arginine and lysine residues. Mol Cell Proteomics 2004;3:608–14.

231 Marth JD, Grewal PK: Mammalian glycosylation in immunity. Nat Rev Immunol 2008;8:874–887.

232 Hall AB, Gakidis MAM, Glogauer M, Wilsbacher JL, Gao S, Swat W, et al.: Requirements for Vav guanine nucleotide exchange factors and Rho GTPases in FcgammaR- and complement-mediated phagocytosis. Immunity 2006;24:305–16.

233 Agramonte-Hevia J, González-Arenas A, Barrera D, Velasco-Velázquez M: Gram-negative bacteria and phagocytic cell interaction mediated by complement receptor 3. FEMS Immunol Med Microbiol 2002;34:255–66.

234 Dambuza IM, Brown GD: C-type lectins in immunity: recent developments. Curr Opin Immunol 2015;32:21–27.

235 Bornschlögl T: How filopodia pull: what we know about the mechanics and dynamics of filopodia. Cytoskeleton (Hoboken) 2013;70:590–603.

236 Nemethova M, Auinger S, Small JV: Building the actin cytoskeleton: filopodia contribute to the construction of contractile bundles in the lamella. J Cell Biol 2008;180:1233–44.

237 Kress H, Stelzer EHK, Holzer D, Buss F, Griffiths G, Rohrbach A: Filopodia act as phagocytic tentacles and pull with discrete steps and a load-dependent velocity. Proc Natl Acad Sci U S A 2007;104:11633–8.

238 Vonna L, Wiedemann A, Aepfelbacher M, Sackmann E: Micromechanics of filopodia mediated capture of pathogens by macrophages. Eur Biophys J 2007;36:145–51.

239 Koerten HK, Ploem JS, Daems WT: Ingestion of latex beads by filopodia of adherent mouse peritoneal macrophages. A scanning electron microscopical and reflection contrast

microscopical study. Exp Cell Res 1980;128:470–5.

240 Williams LM, Ridley AJ: Lipopolysaccharide induces actin reorganization and tyrosine phosphorylation of Pyk2 and paxillin in monocytes and macrophages. J Immunol 2000 [cited 2017 Dec 11];164:2028–36.

241 Patel PC, Harrison RE: Membrane ruffles capture C3bi-opsonized particles in activated macrophages. Mol Biol Cell 2008;19:4628–39.

242 Mattila PK, Lappalainen P: Filopodia: molecular architecture and cellular functions. Nat Rev Mol Cell Biol 2008;9:446–454.

243 Liu C, Wu C, Yang Q, Gao J, Li L, Yang D, et al.: Macrophages Mediate the Repair of Brain Vascular Rupture through Direct Physical Adhesion and Mechanical Traction. Immunity 2016;44:1162–1176.

244 Murphy DA, Courtneidge SA: The “ins” and “outs” of podosomes and invadopodia: characteristics, formation and function. Nat Rev Mol Cell Biol 2011;12:413–26.

245 Stylli SS, Kaye AH, Lock P: Invadopodia: at the cutting edge of tumour invasion. J Clin Neurosci 2008;15:725–37.

246 Woodring PJ, Meisenhelder J, Johnson SA, Zhou G-L, Field J, Shah K, et al.: c-Abl phosphorylates Dok1 to promote filopodia during cell spreading. J Cell Biol 2004;165:493–503.

247 Zhao H, Pykäläinen A, Lappalainen P: I-BAR domain proteins: linking actin and plasma membrane dynamics. Curr Opin Cell Biol 2011;23:14–21.

248 Ahmed S, Goh WI, Bu W: I-BAR domains, IRSp53 and filopodium formation. Semin

Cell Dev Biol 2010;21:350–356.

249 Nakagawa H, Miki H, Nozumi M, Takenawa T, Miyamoto S, Wehland J, et al.: IRSp53 is colocalised with WAVE2 at the tips of protruding lamellipodia and filopodia independently of Mena. J Cell Sci 2003;116:2577–83.

250 Jacquemet G, Hamidi H, Ivaska J: Filopodia in cell adhesion, 3D migration and cancer cell invasion. Curr Opin Cell Biol 2015;36:23–31.

251 Sayyad WA, Amin L, Fabris P, Ercolini E, Torre V: The role of myosin-II in force generation of DRG filopodia and lamellipodia. Sci Rep 2015;5:7842.

252 Naj X, Hoffmann A-K, Himmel M, Linder S: The Formins FMNL1 and mDia1 Regulate Coiling Phagocytosis of Borrelia burgdorferi by Primary Human Macrophages. Infect Immun 2013;81:1683–1695.

253 Erwig L-P, Henson PM: Clearance of apoptotic cells by phagocytes. Cell Death Differ 2008;15:243–250.

254 Wang T, Ma D: Warm up and cool down! Oncotarget 2015;6:30449–50.

255 Rutishauser U, Sachs L: RECEPTOR MOBILITY AND THE BINDING OF CELLS TO LECTIN-COATED FIBERS DOI: 10.1083/jcb.66.1.76

256 Ueda MJ, Ito T, Okada TS, Ohnishi SI: A correlation between membrane fluidity and the critical temperature for cell adhesion. J Cell Biol 1976;71:670–4.

257 Kinchen JM, Ravichandran KS: Journey to the grave: signaling events regulating removal of apoptotic cells. J Cell Sci 2007;120:2143–9.

258 Flannagan RS, Canton J, Furuya W, Glogauer M, Grinstein S: The phosphatidylserine

receptor TIM4 utilizes integrins as coreceptors to effect phagocytosis. Mol Biol Cell 2014;25:1511–1522.

259 Hoffmann PR, deCathelineau AM, Ogden CA, Leverrier Y, Bratton DL, Daleke DL, et al.: Phosphatidylserine (PS) induces PS receptor-mediated macropinocytosis and promotes clearance of apoptotic cells. J Cell Biol 2001;155:649–59.

260 Pike JA, Styles IB, Rappoport JZ, Heath JK: Quantifying receptor trafficking and colocalization with confocal microscopy. Methods 2017;115:42–54.

261 Chaki SP, Barhoumi R, Berginski ME, Sreenivasappa H, Trache A, Gomez SM, et al.: Nck enables directional cell migration through the coordination of polarized membrane protrusion with adhesion dynamics. J Cell Sci 2013;126:1637–1649.

262 Svennersten K, Hallén-Grufman K, de Verdier PJ, Wiklund NP, Poljakovic M: Localization of P2X receptor subtypes 2, 3 and 7 in human urinary bladder. BMC Urol 2015;15:81.

263 Morris DC, Popp JL, Tang LK, Gibbs HC, Schmitt E, Chaki SP, et al.: Nck deficiency is associated with delayed breast carcinoma progression and reduced metastasis. Mol Biol Cell 2017;28:3500–3516.

264 Oser M, Dovas A, Cox D, Condeelis J: Nck1 and Grb2 localization patterns can distinguish invadopodia from podosomes. Eur J Cell Biol 2011;90:181–188.

265 Yamaguchi H, Lorenz M, Kempiak S, Sarmiento C, Coniglio S, Symons M, et al.: Molecular mechanisms of invadopodium formation. J Cell Biol 2005;168:441–452.

266 Stylli SS, I STT, Verhagen AM, Xu SS, Pass I, Courtneidge SA, et al.: Nck adaptor

proteins link Tks5 to invadopodia actin regulation and ECM degradation. J Cell Sci 2009;122:2727–2740.

267 Mócsai A, Ruland J, Tybulewicz VLJ: The SYK tyrosine kinase: a crucial player in diverse biological functions. Nat Rev Immunol 2010;10:387–402.

268 Licona-Limón I, Garay-Canales CA, Muñoz-Paleta O, Ortega E: CD13 mediates phagocytosis in human monocytic cells. J Leukoc Biol 2015;98:85–98.

269 Scheib JL, Sullivan CS, Carter BD: Jedi-1 and MEGF10 Signal Engulfment of Apoptotic Neurons through the Tyrosine Kinase Syk. J Neurosci 2012;32:13022–13031.

270 Sung YM, Xu X, Sun J, Mueller D, Sentissi K, Johnson P, et al.: Tumor Suppressor Function of Syk in Human MCF10A In Vitro and Normal Mouse Mammary Epithelium In Vivo. PLoS One 2009;4:e7445.

271 Lettau M, Pieper J, Janssen O: Nck adapter proteins: functional versatility in T cells. Cell Commun Signal 2009;7:1.

272 Ghazizadeh S, Bolen JB, Fleit HB: Tyrosine phosphorylation and association of Syk with Fc gamma RII in monocytic THP-1 cells. Biochem J 1995;305 (Pt 2):669–74.

273 Marshall JG, Booth JW, Stambolic V, Mak T, Balla T, Schreiber AD, et al.: Restricted accumulation of phosphatidylinositol 3-kinase products in a plasmalemmal subdomain during Fc gamma receptor-mediated phagocytosis. J Cell Biol 2001;153:1369–80.

274 Araki N, Johnson MT, Swanson JA: A role for phosphoinositide 3-kinase in the completion of macropinocytosis and phagocytosis by macrophages. J Cell Biol 1996;135:1249–60.

275 Hoppe AD, Swanson JA: Cdc42, Rac1, and Rac2 Display Distinct Patterns of Activation during Phagocytosis. Mol Biol Cell 2004;15:3509–3519.

276 Lutz MA, Correll PH: Activation of CR3-mediated phagocytosis by MSP requires the RON receptor, tyrosine kinase activity, phosphatidylinositol 3-kinase, and protein kinase C zeta. J Leukoc Biol 2003;73:802–14.

277 Kobayashi SD, Voyich JM, Burlak C, DeLeo FR: Neutrophils in the innate immune response. Arch Immunol Ther Exp (Warsz) [cited 2018 Jul 7];53:505–17.

278 Losso JN: The Biochemical and Functional Food Properties of the Bowman-Birk Inhibitor. Crit Rev Food Sci Nutr 2008;48:94–118.

279 Segal AW: HOW NEUTROPHILS KILL MICROBES. Annu Rev Immunol 2005;23:197–223.

280 Korkmaz B, Horwitz MS, Jenne DE, Gauthier F: Neutrophil Elastase, Proteinase 3, and Cathepsin G as Therapeutic Targets in Human Diseases. Pharmacol Rev 2010;62:726–759.

281 Devaney JM, Greene CM, Taggart CC, Carroll TP, O'Neill SJ, McElvaney NG: Neutrophil elastase up-regulates interleukin-8 via toll-like receptor 4. FEBS Lett 2003;544:129–32.

282 Remold-O'Donnell E, Parent D: Specific sensitivity of CD43 to neutrophil elastase. Blood 1995;86:2395–402.

283 BRIGNONE C, MUNOZ O, BATOZ M, ROUQUETTE-JAZDANIAN A, COUSIN J-L: Proteases produced by activated neutrophils are able to release soluble CD23 fragments

endowed with proinflammatory effects. FASEB J 2001;15:2027–2029.

284 Hamacher J, Sadallah S, Schifferli JA, Villard J, Nicod LP: Soluble complement receptor type 1 (CD35) in bronchoalveolar lavage of inflammatory lung diseases. Eur Respir J 1998;11:112–9.

285 Sadallah S, Hess C, Miot S, Spertini O, Lutz H, Schifferli J-A: Elastase and metalloproteinase activities regulate soluble complement receptor 1 release. Eur J Immunol 1999;29:3754–3761.

286 Champagne B, Tremblay P, Cantin A, St Pierre Y: Proteolytic cleavage of ICAM-1 by human neutrophil elastase. J Immunol 1998;161:6398–405.

287 Lévesque JP, Takamatsu Y, Nilsson SK, Haylock DN, Simmons PJ: Vascular cell adhesion molecule-1 (CD106) is cleaved by neutrophil proteases in the bone marrow following hematopoietic progenitor cell mobilization by granulocyte colony-stimulating factor. Blood 2001;98:1289–97.

288 Bank U, Küpper B, Ansorge S: Inactivation of Interleukin-6 by Neutrophil Proteases at Sites of Inflammation; in : Cellular Peptidases in Immune Functions and Diseases 2. Boston, Kluwer Academic Publishers, 2000, pp 431–437.

289 Potempa M, Potempa J: Protease-dependent mechanisms of complement evasion by bacterial pathogens. Biol Chem 2012;393:873–88.

290 Chi L, Li Y, Stehno-Bittel L, Gao J, Morrison DC, Stechschulte DJ, et al.: Interleukin-6 production by endothelial cells via stimulation of protease-activated receptors is amplified by endotoxin and tumor necrosis factor-alpha. J Interferon Cytokine Res 2001;21:231–40.

291 Kuang Z, Hao Y, Walling BE, Jeffries JL, Ohman DE, Lau GW: Pseudomonas aeruginosa Elastase Provides an Escape from Phagocytosis by Degrading the Pulmonary Surfactant Protein-A. PLoS One 2011;6:e27091.

292 Mackie EJ, Pagel CN, Smith R, de Niese MR, Song SJ, Pike RN: Protease-activated receptors: a means of converting extracellular proteolysis into intracellular signals. IUBMB Life 2002;53:277–81.

293 Nystedt S, Emilsson K, Wahlestedt C, Sundelin J: Molecular cloning of a potential proteinase activated receptor. Proc Natl Acad Sci U S A 1994;91:9208–12.

294 Camerer E, Kataoka H, Kahn M, Lease K, Coughlin SR: Genetic evidence that protease-activated receptors mediate factor Xa signaling in endothelial cells. J Biol Chem 2002;277:16081–7.

295 Mirza H, Schmidt VA, Derian CK, Jesty J, Bahou WF: Mitogenic responses mediated through the proteinase-activated receptor-2 are induced by expressed forms of mast cell alpha- or beta-tryptases. Blood 1997;90:3914–22.

296 Molino M, Barnathan ES, Numerof R, Clark J, Dreyer M, Cumashi A, et al.: Interactions of mast cell tryptase with thrombin receptors and PAR-2. J Biol Chem 1997;272:4043–9.

297 Corvera CU, Déry O, McConalogue K, Böhm SK, Khitin LM, Caughey GH, et al.: Mast cell tryptase regulates rat colonic myocytes through proteinase-activated receptor 2. J Clin Invest 1997;100:1383–93.

298 Takeuchi T, Harris JL, Huang W, Yan KW, Coughlin SR, Craik CS: Cellular localization of membrane-type serine protease 1 and identification of protease-activated receptor-2 and

single-chain urokinase-type plasminogen activator as substrates. J Biol Chem 2000;275:26333–42.

299 Smith R, Jenkins A, Lourbakos A, Thompson P, Ramakrishnan V, Tomlinson J, et al.: Evidence for the activation of PAR-2 by the sperm protease, acrosin: expression of the receptor on oocytes. FEBS Lett 2000;484:285–90.

300 Shpacovitch V, Feld M, Hollenberg MD, Luger TA, Steinhoff M: Role of protease-activated receptors in inflammatory responses, innate and adaptive immunity. J Leukoc Biol 2008;83:1309–1322.

301 D'Andrea MR, Derian CK, Leturcq D, Baker SM, Brunmark A, Ling P, et al.: Characterization of protease-activated receptor-2 immunoreactivity in normal human tissues. J Histochem Cytochem 1998;46:157–64.

302 Lourbakos A, Potempa J, Travis J, D'Andrea MR, Andrade-Gordon P, Santulli R, et al.: Arginine-specific protease from Porphyromonas gingivalis activates protease-activated receptors on human oral epithelial cells and induces interleukin-6 secretion. Infect Immun 2001;69:5121–30.

303 Cocks TM, Fong B, Chow JM, Anderson GP, Frauman AG, Goldie RG, et al.: A protective role for protease-activated receptors in the airways. Nature 1999;398:156–160.

304 Darmoul D, Gratio V, Devaud H, Laburthe M: Protease-activated receptor 2 in colon cancer: trypsin-induced MAPK phosphorylation and cell proliferation are mediated by epidermal growth factor receptor transactivation. J Biol Chem 2004;279:20927–34.

305 Rallabhandi P, Nhu QM, Toshchakov VY, Piao W, Medvedev AE, Hollenberg MD, et al.:

Analysis of proteinase-activated receptor 2 and TLR4 signal transduction: a novel paradigm for receptor cooperativity. J Biol Chem 2008;283:24314–25.

306 Weber S, Saftig P: Ectodomain shedding and ADAMs in development. Development 2012;139:3693–3709.

307 Hayashida K, Bartlett AH, Chen Y, Park PW: Molecular and Cellular Mechanisms of Ectodomain Shedding. Anat Rec Adv Integr Anat Evol Biol 2010;293:925–937.

308 Kadish JL, Choi CC, Czop JK: Phagocytosis of unopsonized zymosan particles by trypsin-sensitive and beta-glucan-inhibitable receptors on bone marrow-derived murine macrophages. Immunol Res 1986;5:129–38.

309 Cho M, Cummings RD: Galectin-1, a beta-galactoside-binding lectin in Chinese hamster ovary cells. II. Localization and biosynthesis. J Biol Chem 1995;270:5207–12.

310 de Zoete MR, Bouwman LI, Keestra AM, van Putten JPM: Cleavage and activation of a Toll-like receptor by microbial proteases. Proc Natl Acad Sci 2011;108:4968–4973.

311 Castellano F, Montcourrier P, Guillemot JC, Gouin E, Machesky L, Cossart P, et al.: Inducible recruitment of Cdc42 or WASP to a cell-surface receptor triggers actin polymerization and filopodium formation. Curr Biol 1999;9:351–60.

312 Bohil AB, Robertson BW, Cheney RE: Myosin-X is a molecular motor that functions in filopodia formation. Proc Natl Acad Sci 2006;103:12411–12416.

313 Goh WI, Lim KB, Sudhaharan T, Sem KP, Bu W, Chou AM, et al.: mDia1 and WAVE2 proteins interact directly with IRSp53 in filopodia and are involved in filopodium formation. J Biol Chem 2012;287:4702–14.

314 Canton J, Schlam D, Breuer C, Gütschow M, Glogauer M, Grinstein S: Calcium-sensing receptors signal constitutive macropinocytosis and facilitate the uptake of NOD2 ligands in macrophages. Nat Commun 2016;7:11284.

315 Sohn HW, Krueger PD, Davis RS, Pierce SK: FcRL4 acts as an adaptive to innate molecular switch dampening BCR signaling and enhancing TLR signaling. Blood 2011;118:6332–6341.

316 Haga CL, Ehrhardt GRA, Boohaker RJ, Davis RS, Cooper MD: Fc receptor-like 5 inhibits B cell activation via SHP-1 tyrosine phosphatase recruitment. Proc Natl Acad Sci 2007;104:9770–9775.

317 Li FJ, Won WJ, Becker EJ, Easlick JL, Tabengwa EM, Li R, et al.: Emerging roles for the FCRL family members in lymphocyte biology and disease. Curr Top Microbiol Immunol 2014;382:29–50.

318 Taylor AI, Beavil RL, Sutton BJ, Calvert RA: A monomeric chicken IgY receptor binds IgY with 2:1 stoichiometry. J Biol Chem 2009;284:24168–75.

319 Taylor AI, Beavil RL, Sutton BJ, Calvert RA: A monomeric chicken IgY receptor binds IgY with 2:1 stoichiometry. J Biol Chem 2009;284:24168–75.